

Dissertation zur Erlangung des Doktorgrades
der Fakultät für Chemie und Pharmazie
der Ludwig-Maximilians-Universität München

Towards the Asymmetric Synthesis of
Tetrodotoxin
And
The Design of Glutamate- and Lipid-
based Photopharmaceuticals

David Benjamin Konrad
aus Weißenhorn

2018

Erklärung

Diese Dissertation wurde im Sinne von § 7 der Promotionsordnung vom 28. November 2011 von Herrn Prof. Dr. Dirk Trauner betreut.

Eidesstattliche Versicherung

Diese Dissertation wurde eigenständig und ohne unerlaubte Hilfe erarbeitet.

München, den 22.05.2018

.....

David Konrad

Dissertation eingereicht am:	22. Mai 2018
1. Prüfer:	Prof. Dr. Dirk Trauner
2. Prüfer:	Prof. Dr. Anja Hoffmann-Röder
Mündliche Prüfung am:	26. Juli 2018

Dedication

To my family

Acknowledgements

First and foremost, I want to thank Prof. Dr. Dirk Trauner for welcoming me into his group as a doctoral student and providing the ideal environment for the work on complex natural products and my growth as a scientist. It was a pleasure to work with as much independence as you entrusted to me. I appreciate that you included me into many collaborations which have given me the opportunity to network around the world and to accustom myself with research in countless disciplines. At last, I want to extend my thanks to you for your strong and continuous support. You have sent countless letters of recommendations on my behalf since I pursued my Bachelors thesis in your group and it is thanks to you that I have become the scientist that I am today.

I want to thank Prof. Dr. Anja Hoffmann-Röder, who kindly agreed to act as my second advisor and the members of my committee Prof. Dr. Ivan Huc, Prof. Dr. Konstantin Karaghiosoff, Dr. Dorian Didier and Prof. Dr. Paul Knochel.

Throughout my time in the Trauner group, it was filled with great chemists and people. Thanks to all for the good advice and the time well spent together. I especially want to thank Johannes, Philipp, James and Marthe for our continuous and pleasant collaborations and our native speaker Ben who inexhaustibly corrected my English writings. I also want to thank Eddie and Mario, who have been close friends to me for both my undergraduate and graduate studies.

To my friends and colleagues in the UV lab Daniel, Ben, Felix, Nils, Ahmed, Henry and Pascal: It was a great pleasure to work beside you over the past years. I am very happy that we managed continuously foster a pleasant working environment for ourselves which made it very enjoyable to go to work in the morning. Thanks for taking up with my army of interns that was a constant part of our lab.

I would like to thank my hardworking Bachelor students, research interns and Master students Ivi, Simon, Alex, Caren, Kuno, Ed, Dana, Beccy, Max, Nathalie and Bilal. You have greatly supported my research by optimizing reactions, finding alternative synthetic routes, preparing building blocks, evaluating protecting group strategies and synthesizing natural products. I am very proud with what you have achieved and all the work you have invested in your training.

You were a constant source of motivation for me and I have learned many lessons about teaching from you.

Thanks to the the Trauner group staff members: Carrie, Luis, Heike, Aleks and Martin. I greatly appreciate that you kept the group and our research at the LMU running – even after the official move to the NYU.

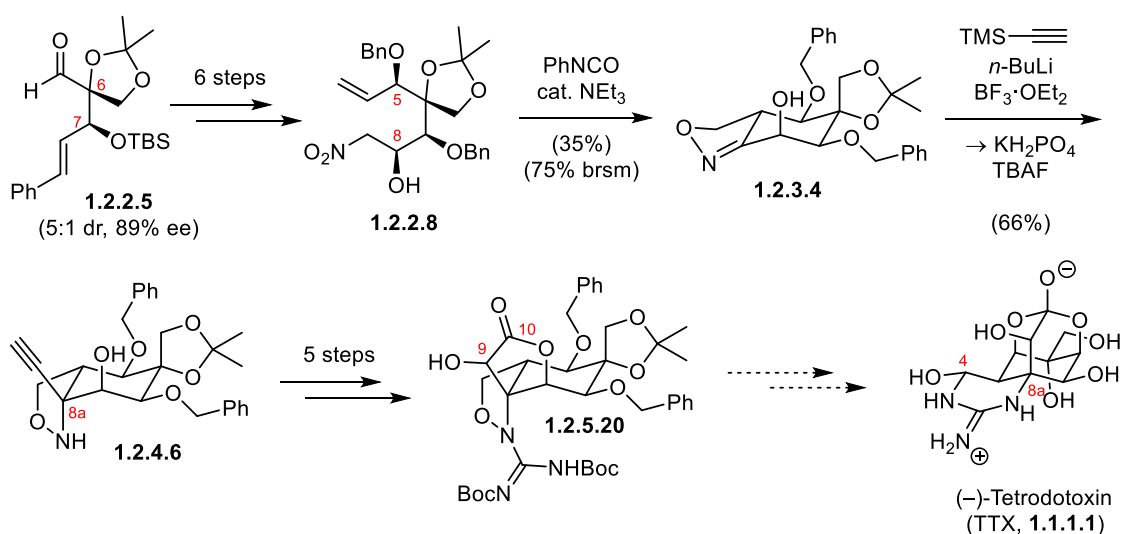
I would like to extend my regards to the staff of the analytical departments. The NMR facilities that were run by David Stephenson and Claudia Ober were essential to my research as well as the mass spectrometry facilities that were run by Werner Spahl and Sonja Kosak. Thanks to Giulio, Carrie and Daniel for servicing the NMR machine on the 4th floor and Felix Kalfa for servicing the IR spectrometer. In addition, I would like to thank Peter Mayer for recording and solving my X-Ray structures.

Last and most importantly, I would like to thank my family. Thank you, Eva, for enduring my long working hours that even extended into my spare time and my parental leave – and for still marrying me. Thanks for our daughter Leonie, who is one of the biggest joys of my life. Thanks for your endless support and for providing the balance that I needed in my life to succeed with my dissertation. I could not have done it without you! I also want to thank my parents, who supported me throughout my life and made it possible for me to move to Munich and pursue my studies in chemistry. To all my friends who I rarely had time for during these last years, thanks for still make time for me.

Abstracts

Chapter 1: Towards the Asymmetric Synthesis of Tetrodotoxin

Tetrodotoxin (TTX, **1.1.1.1**) (Scheme 1) is well-known as the poison of the puffer fish. The high toxicity is a result of its ability to selectively block voltage-gated sodium channels (Nav1.1-1.9). Its structure is characterized by a densely functionalized dioxadamantane with an exocyclic six-membered guanidine hemiaminal heterocycle and nine stereogenic centers. This synthetically challenging architecture has made TTX a popular target in natural product synthesis. Our retrosynthetic analysis is based on the premise that the latent C4 aldehyde and the C8a α -tertiary amine may arise from an isoxazolidine. This isoxazolidine enables two reliable key retrons: a nitrile oxide 1,3-dipolar cycloaddition and an ethynyl anion addition into the resulting oxime. The initial C6 and C7 stereocenters were set through a Kiyooka aldol reaction and provided **1.2.2.5** (Scheme 1) with 5:1 dr and 89% ee. With this foundation, a fully functionalized linear nitro alkene **1.2.2.8** was diastereoselectively synthesized using an alkynyl anion addition and a Henry reaction into the corresponding aldehydes. The Huisgen 1,3-dipolar cycloaddition afforded the bicycle **1.2.3.4** containing the full cyclohexane oxygenation pattern and the ethynyl lithium addition into the oxazoline set the α -tertiary amine stereocenter and installed the full carbon skeleton (**1.2.4.6**) in a total of 11 steps. Elaboration of the α -hydroxy ester and guanidine elements in 5 additional steps provided our most advanced building block **1.2.5.20**. Finalization of TTX (**1.1.1.1**) is envisaged to proceed via a reductive deprotection, primary alcohol oxidation and acid-mediated deprotection – isomerization sequence.

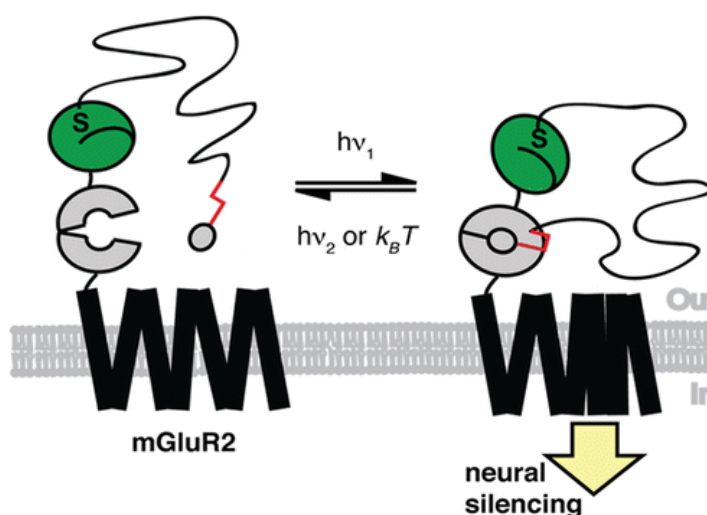


Scheme 1. Established Route towards Tetrodotoxin.

Chapter 2: The Design of Glutamate- and Lipid-based Photopharmaceuticals

Part 2.1 Glutamate-based Photopharmaceuticals

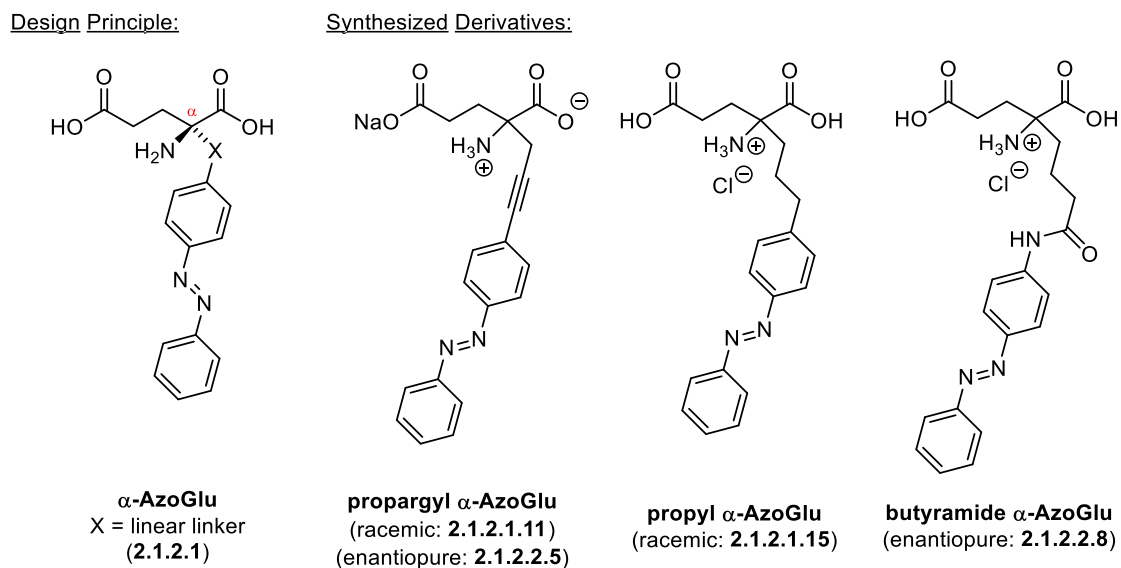
The in-depth study of the functions of metabotropic glutamate receptors (mGluRs) requires the availability of appropriate biochemical tools. Photopharmaceuticals are excellent tools to study biological functions, since they can be switched ON and OFF with the spatiotemporal precision of light. Therefore, we have developed a new generation of photoswitchable orthogonal remotely tethered ligands (PORTLs). These PORTLs contain benzylguanines that are linked to a photochromic glutamate-derived ligand via a long flexible linker and are named BGAGs. The benzylguanines allows for the attachment of the BGAGs to the mGluR2 using SNAP-tags which creates a light-sensitive SNAG-mGluR2 (Scheme 2). For this study, we have prepared BGAGs with varying PEG-linker lengths (0, 4, 8 and 12 ethylene glycol units) and designed the visible light-controlled BGAG₁₂₍₄₆₀₎. BGAG₁₂₍₄₆₀₎ is essential for continuing our research with the mechanistic evaluation of photoswitchable group II and III mGluRs and to establish dual optical control. More importantly, to pursue experiments in complex tissues and animals, it is essential to use non-hazardous, tissue-penetrating visible light for photoswitching.



Scheme 2. SNAG-mGluR2 enables control over neuronal functions with light.

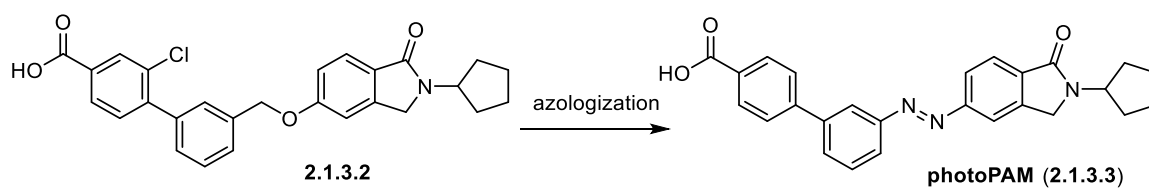
To complement our SNAG-mGluR2 methodology which activates GPCR function with light, we investigated the incorporation of azobenzene on the glutamate α -position with varying linker lengths to design photoswitchable mGluR2 antagonists (α -AzoGlu, 2.1.2.1, Scheme 3). We developed a racemic route that allowed us to access the propargyl- and propyl-linked α -AzoGlu

derivatives **2.1.2.1.11** and **2.1.2.1.15**. To evaluate the efficiency of enantiomerically pure antagonist structures, we further devised a stereoselective synthesis which afforded the propargyl- and butyramide-linked α -AzoGlu variants **2.1.2.2.5** and **2.1.2.2.8**.



Scheme 3. Designing α -AzoGlu derivatives with varying linkers.

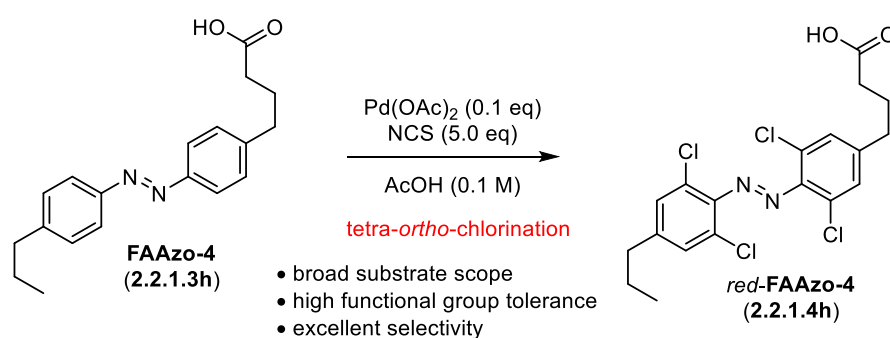
To comprehend the full extent of the physiological mGluR2 function, it is crucial to study the role of the allosteric binding site. In this context, we designed a photoswitchable mGluR2 positive allosteric modulator (**photoPAM**, **2.1.3.3**) based on the azologization of the phenol-derived benzylether functionality of the established PAM **2.3.1.2** (Scheme 4).



Scheme 4. Azologization of **2.1.3.2** to **photoPAM (2.1.3.3)**.

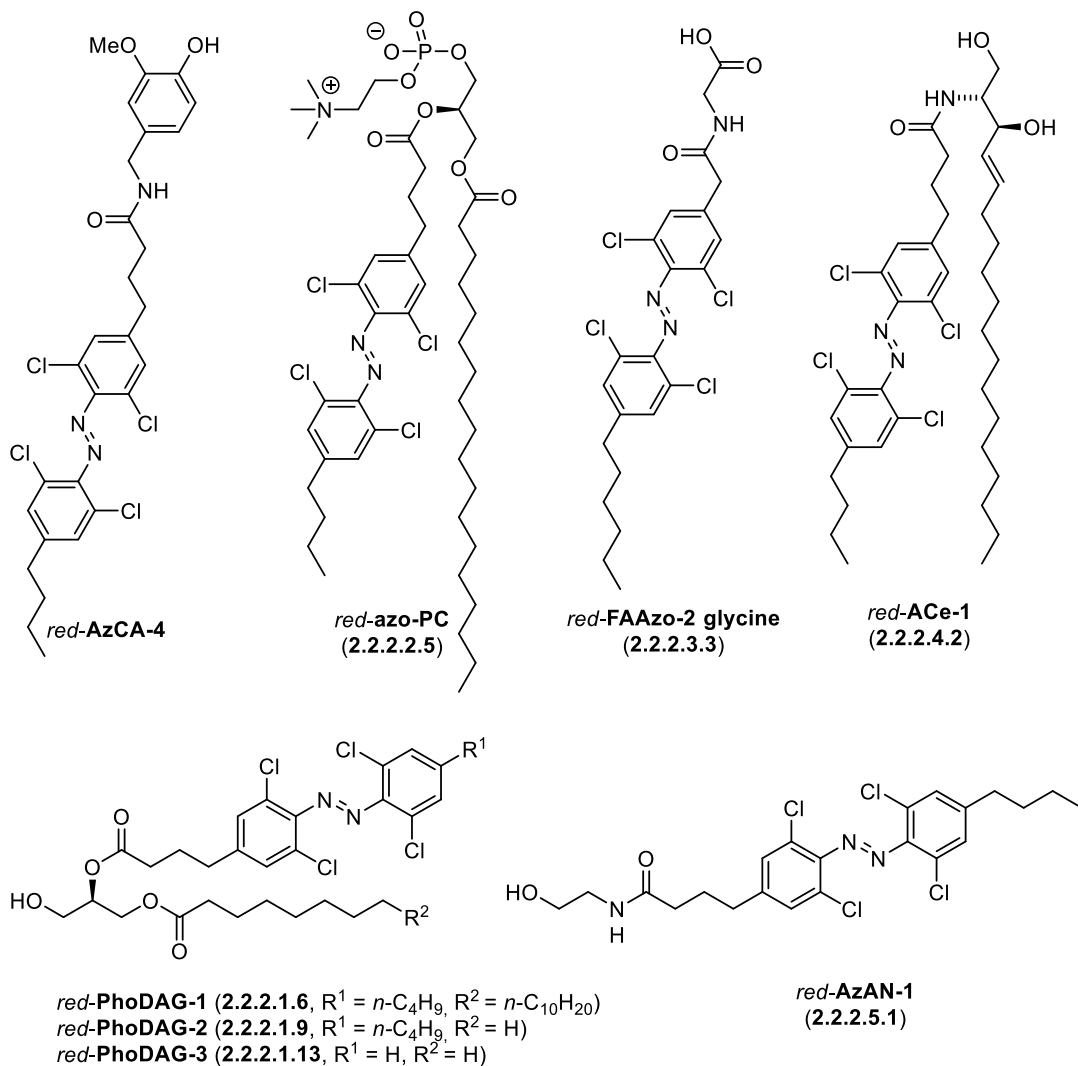
Part 2.2 Lipid-based Photopharmaceuticals

Azobenzenes are photoswitches that can be cycled between their *trans*- and *cis*-configuration with light. They can be incorporated into pharmaceuticals to generate photopharmaceuticals that allow for the control of biological functions with the spatiotemporal precision of light. For the use of photopharmaceuticals in animals, it is crucial to use tissue-penetrating red light. However, the use of standard methods for red-shifting photoswitchable ligands is often accompanied by the loss of efficiency or function. We have addressed this longstanding problem by developing a general methodology to install the tetra-*ortho*-chloro substitution pattern on azobenzenes via a palladium-catalyzed C–H chlorination (Scheme 5).



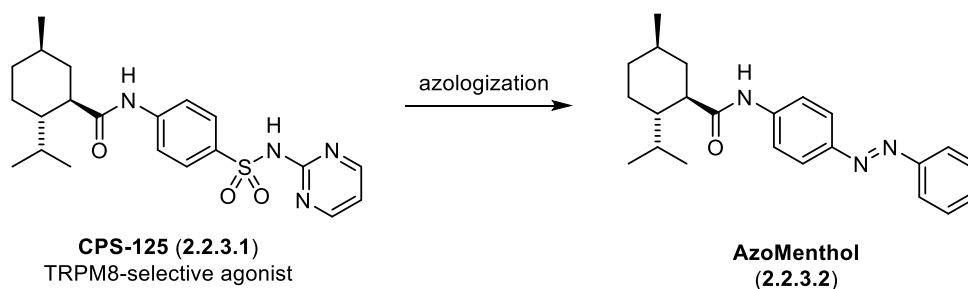
Scheme 5. Tetra-*ortho*-chlorination of pre-existing azobenzenes.

We applied this method to an established photochromic ligand **AzCA-4** to generate *red-AzCA-4* (Scheme 6). *Red-AzCA-4*, like its parent compound, enables the optical control of the vanilloid receptor 1 (TRPV1), which is involved in pain signaling and body temperature regulation. Therefore, we showed that the minimal changes to the structure and the size of the molecule through tetra-*ortho*-chloro substitution does not hinder the biological function of this lipid-based photopharmaceutical. To demonstrate the generality of this concept and to enable the application of our chemical tools in animals, we synthesized a library of red-shifted lipid-based photochromic ligands (Scheme 6). This library includes the diacylglycerol derivatives *red-PhoDAG-1-3* (2.2.2.1.6, 2.2.2.1.9 and 2.2.2.1.13), the phosphatidylcholine derivative *red-azo-PC* (2.2.2.2.5), the fatty acid-amino acid hybrid *red-FAAzo-2-glycine* (2.2.2.3.3), the ceramide derivative *red-ACe-1* (2.2.2.4.2) and the anandamide derivative *red-AzAN-1* (2.2.2.5.1).



Scheme 6. Red-shifted photoswitchable lipid library.

For the optical control of the cold-sensing TRPM8 channel, we designed **AzoMenthol** (2.2.3.2) by azologization of the TRPM8-selective agonist **CPS-125** (2.2.3.1) (Scheme 7). The synthesis of **AzoMenthol** (2.2.3.2) was performed in 3 steps from (–)-menthol in good yields.



Scheme 7. Design of **AzoMenthol** (2.2.3.2).

Publications

Parts of this work were published in peer-reviewed scientific journals and on scientific conferences. In addition, manuscripts based on results of this work are currently being prepared or under review.

Scientific publications of results presented in this work:

“Synthesis of Redshifted Azobenzene Photoswitches via Late-Stage Functionalization” – D. B. Konrad, J. A. Frank, D. Trauner*, *Chem. Eur. J.* **2016**, *22*, 4364–4368.

“Orthogonal Optical Control of a G Protein-Coupled Receptor with a SNAP-Tethered Photochromic Ligand” – J. Broichhagen, A. Damijonaitis, J. Levitz, K. R. Sokol, P. Leippe, D. Konrad, E. Y. Isacoff*, D. Trauner*, *ACS Cent. Sci.* **2015**, *1*, 383–393.

“Light-Controlled Lipid Interaction and Membrane Organization in Photolipid Bilayer Membranes” – P. Urban, S. D. Pritzl, D. B. Konrad, J. A. Frank, C. Pernpeintner, C. R. Roeske, D. Trauner*, T. Lohmüller*, *under review*.

“Concise Asymmetric Synthesis of Kweichowenol A” – D. B. Konrad, B. Kicin, D. Trauner*, *under review*.

“Chemical Syntheses and Biochemical Properties of the Tetrodotoxin Natural Product Family” – D. B. Konrad, D. Trauner*, *in preparation*.

Additional scientific publications:

“PhoDAGs Enable Optical Control of Diacylglycerol-Sensitive Transient Receptor Potential Channels” – T. Leinders-Zufall, U. Storch, K. Bleyemehl, M. Mederos y Schnitzler, J. A. Frank, D. B. Konrad, D. Trauner, T. Gudermann, F. Zufall*, *Cell Chem. Biol.* **2017**, *25*, 215–223.

“Dual optical control and mechanistic insights into photoswitchable group II and III metabotropic glutamate receptors” – J. Levitz, J. Broichhagen, P. Leippe, D. Konrad, D. Trauner*, E. Y. Isacoff*, *Proc. Natl. Acad. Sci.* **2017**, *114*, 3546–3554.

“Selective Lithiation, Magnesiumation and Zincation of Unsymmetrical Azobenzenes Using Continuous Flow” – M. Ketels, D. B. Konrad, K. Karaghiosoff, D. Trauner, P. Knochel*, *Org. Lett.* **2017**, *19*, 1666–1669.

“Optical Control of GIRK Channels Using Visible Light” – J. B. Trads, J. Burgstaller, L. Laprell, D. B. Konrad, L. de la Rosa de la Osa, C. D. Weaver, H. Baier, D. Trauner*, D. M. Barber*, *Org. Biomol. Chem.* **2017**, *15*, 76–81.

“Experimental and Computational Design of Highly Red-shifted Azobenzenes” – D. B. Konrad, G. Savasci, C. Ochsenfeld*, D. Trauner*, A. Ali*, *in preparation*.

Scientific Conferences:

- 1) “Towards an Asymmetric Synthesis of (-)-Tetrodotoxin” – D. B. Konrad, D. Trauner. **26th ISHC Congress**, Regensburg Germany.
- 2) “Optical Control of TRPV1 using Red-shifted Photoswitches” – D. B. Konrad, J. A. Frank, D. Trauner. **International Symposium on the Regulation of Cell Functions by Transient Receptor Potential Channels 2016**, Herrsching, Germany.
- 3) “Red-shifting Photopharmaceuticals via Late-stage Functionalization.” – D. B. Konrad, J. A. Frank, D. Trauner. **2016 Symposium on Chemical Biology**, Geneva, Switzerland.

Abbreviations

Alloc	allyloxycarbonyl
aq.	aqueous
atm	atmosphere(s)
ATR	attenuated total reflection
BAIB	(diacetoxyiodo)benzene
Boc	<i>tert</i> -butyloxycarbonyl
BOM	benzyloxymethyl
br	broad (NMR, IR)
CAM	ceric ammonium molybdate
CAN	ceric ammonium nitrate
CBS	Corey-Bakshi-Shibata
Cbz	carboxybenzyl
CDI	carbonyldiimidazole
COSY	homonuclear correlation spectroscopy
CSA	camphorsulfonic acid
d	doublet (NMR)
DBU	1,8-diazabicyclo(5.4.0)undec-7-ene
DCB	dichlorobenzene
DCC	<i>N,N'</i> -dicyclohexylcarbodiimide
DIBAL-H	diisobutylaluminum hydride
DMA	<i>N,N</i> -dimethylacetamide
DMAP	4-dimethylaminopyridine
DMF	<i>N,N</i> -dimethylformamide
DMP	Dess-Martin periodinane
DMSO	dimethyl sulfoxide
dr	diastereomeric ratio
ee	enantiomeric excess
ED	effective dose
EDC	1-ethyl-3-(3-dimethylaminopropyl)carbodiimide
EI	electron ionization (MS)
ESI	electrospray ionization (MS)
GPCR	G-protein-coupled receptor

h	heptet (NMR)
h	hour(s)
HBTU	(2-(1H-benzotriazol-1-yl)-1,1,3,3-tetramethyluronium hexafluorophosphate
HG-II	Hoveyda-Grubbs catalyst, 2 nd generation
HMBC	heteronuclear multiple-bond correlation spectroscopy
HMDS	bis(trimethylsilyl)amine
HMPA	hexamethylphosphoramide
HPLC	high performance liquid chromatography
HSQC	heteronuclear single-quantum correlation spectroscopy
IBX	2-iodoxybenzoic acid
IR	infrared spectroscopy
IPP	isopentenyl pyrophosphate
LD	lethal dose
LDA	lithium diisopropylamide
m	medium (IR)
m	multiplet (NMR)
M	mol/L
<i>m</i> -CPBA	<i>meta</i> -chloroperoxybenzoic acid
mGluR	metabotropic glutamate receptor
min	minute(s)
MOM	methoxymethyl
<i>m</i> _p	melting point
Ms	methanesulfonyl
MS	mass spectrometry
Nav	voltage-gated sodium channels
NMR	nuclear magnetic resonance
NBS	<i>N</i> -bromosuccinimide
NCS	<i>N</i> -chlorosuccinimide
NMI	1-methylimidazole
NMO	<i>N</i> -methylmorpholine- <i>N</i> -oxide
NOESY	nuclear Overhauser effect spectroscopy
PAM	positive allosteric modulator
PB	phosphate buffer
PBS	phosphate-buffered saline

Pd/C	palladium on charcoal
PDC	pyridinium dichromate
PEG	polyethylene glycol
PMB	<i>para</i> -methoxybenzyl
PORTL	photoswitchable orthogonal remotely tethered ligands
PPTS	pyridinium <i>para</i> -toluenesulfonate
PSTBP	puffer fish saxitoxin and tetrodotoxin binding protein
q	quartet (NMR)
quint	quintet (NMR)
rt	room temperature
s	singlet (NMR)
s	strong (IR)
six	sixtet (NMR)
SAR	structure activity relationship
sat.	saturated
sec	second(s)
<i>spp.</i>	Species
t	triplet (NMR)
TBAB	tetrabutylammonium bromide
TBAF	tetrabutylammonium fluoride
TBS	<i>tert</i> -butyldimethylsilyl
TBTU	2-(1H-benzotriazole-1-yl)-1,1,3,3-tetramethylammonium tetrafluoroborate
TEMPO	2,2,6,6-tetramethyl-1-piperidinyloxy
TES	triethylsilyl
TFA	trifluoroacetic acid
TFAA	trifluoroacetic anhydride
THF	tetrahydrofuran
TMG	1,1,3,3-tetramethylguanidine
TMS	trimethylsilyl
TPAP	tetrapropylammonium perruthenate
Ts	toluenesulfonyl
TS	transition state
TTX	Tetrodotoxin
UV-Vis	ultraviolet-visible

VGSC	voltage-gated sodium channels
vs	very strong (IR)
vw	very weak (IR)
w	weak (IR)

Table of Contents

ERKLÄRUNG	FEHLER! TEXTMARKE NICHT DEFINIERT.
DEDICATION	II
ACKNOWLEDGEMENTS	III
ABSTRACTS	V
PUBLICATIONS	X
ABBREVIATIONS	XII
TABLE OF CONTENTS	XVI
1 TOWARDS THE ASYMMETRIC SYNTHESIS OF TETRODOTOXIN	2
1.1 INTRODUCTION	2
1.1.1 <i>Tetodotoxin – A Brief Overview</i>	2
1.1.2 <i>Binding of Tetrodotoxin to Voltage-Gated Sodium Channels</i>	3
1.1.3 <i>The Distribution and Origin of Tetrodotoxin</i>	4
1.1.4 <i>The Tetrodotoxin Natural Product Family</i>	6
1.1.5 <i>Biological Activities of Tetrodotoxin Derivatives</i>	10
1.1.6 <i>Biosynthetic Hypotheses</i>	13
1.1.7 <i>Synthetic Approaches towards Tetrodotoxin</i>	16
1.2 RESULTS AND DISCUSSION	30
1.2.1 <i>Retrosynthetic Analysis of Tetrodotoxin</i>	30
1.2.2 <i>Establishing the Oxygenation Pattern on a Linear Precursor</i>	30
1.2.3 <i>The Huisgen 1,3-dipolar Cycloaddition</i>	33
1.2.4 <i>Setting the α-Tertiary Amine</i>	37
1.2.5 <i>Installation of the α-Hydroxy Acid and Guanidylation</i>	39
1.2.6 <i>Endgame: Manipulating the N-O Bond and Protecting Groups</i>	45
1.3 CONCLUSION AND OUTLOOK	47
1.3.1 <i>Summary</i>	47
1.3.2 <i>Outlook</i>	49
2 THE DESIGN OF GLUTAMATE- AND LIPID-BASED PHOTOPHARMACEUTICALS	53
2.1 GLUTAMATE-BASED PHOTOPHARMACEUTICALS	53
2.1.1 <i>Orthogonal Optical Control of a G Protein-Coupled Receptor with a SNAP-Tethered Photochromic Ligand</i>	53
2.1.2 <i>The Designing of Photoswitchable mGluR2 Antagonists</i>	109
2.1.3 <i>A Photoswitchable Positive Allosteric Modulator for the mGluR2</i>	113
2.2 LIPID-BASED PHOTOPHARMACEUTICALS	115

2.2.1	<i>Synthesis of Redshifted Azobenzene Photoswitches by Late-Stage Functionalization</i>	115
2.2.2	<i>Red-shifting Lipid-based Photopharmaceuticals</i>	161
2.2.3	<i>The Designing of a Photoswitchable TRPM8 Agonist</i>	168
3	EXPERIMENTAL SECTION	170
3.1	MATERIAL AND METHODS	170
3.1.1	<i>Equipment and Instruments</i>	170
3.1.2	<i>Methods</i>	171
3.1.3	<i>Chemicals</i>	172
3.2	EXPERIMENTAL PROCEDURES	173
3.2.1	<i>Experimental Procedures – Chapter 1</i>	173
3.2.2	<i>Experimental Procedures – Chapter 2</i>	222
4	APPENDIX	265
4.1	NMR-SPECTRA	265
4.1.1	<i>NMR-Spectra – Chapter 1</i>	265
4.1.2	<i>NMR-Spectra – Chapter 2</i>	309
4.2	X-RAY DATA	345
4.3	UV-VIS DATA	349
5	REFERENCES	361

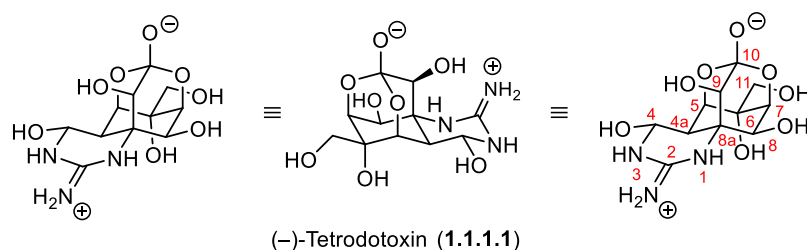
Chapter 1 – Towards the *Asymmetric* Synthesis of
Tetrodotoxin

1 Towards the Asymmetric Synthesis of Tetrodotoxin

1.1 Introduction

1.1.1 Tetodotoxin – A Brief Overview

Tetrodotoxin (TTX) (**1.1.1.1**, Scheme 1.1.1.1) is well known as the deadly neurotoxin of the pufferfish, which is regarded as a speciality in the Japanese cuisine renowned for its refined taste. It is produced by bacteria such as *Vibrionaceae*¹ and accumulated by immune hosts as a defensive agent.² For humans, it is regarded as the one of the most lethal non-proteinaceous toxins with low molecular weight ($LD_{50} = 10.2 \mu\text{g/kg}$).³ Intoxication inhibits the production and propagation of action potentials and thereby blocks the nervous signaling pathways in the body,⁴ leading to paralysis associated with respiratory failure. The origin of its toxicity is the selective blocking of voltage-gated sodium channels Nav1.1-1.9 with a preference for Nav1.1-1.4 and Nav1.6-1.7, which are thus categorized as TTX-sensitive voltage-gated sodium channels. These biochemical properties have made the natural product a valuable tool in biochemical research.



Scheme 1.1.1.1. The structure of TTX.

The name tetrodotoxin is derived from tetraodontiformes, an order that includes the pufferfish, and was introduced by Tahara in 1911 who was working on isolation procedures.⁵ The first pure, crystalline sample was isolated by Yokoo in 1950.⁶ However, the structure was only elucidated more than a decade later by the independent findings of Woodward,⁷ Goto⁸ and Tsuda⁹ due to the unique TTX structure compared to the majority of alkaloid natural products. After confirmation of the structure via X-Ray crystallography,¹⁰ the stage was set for Kishi and co-workers who established the first synthetic route towards this unusual natural molecule in 1972.¹¹⁻¹⁴ Over the past four decades, countless further attempts¹⁵ to devise the shortest and most elegant synthesis have been reported making tetrodotoxin a classic target in total synthesis.¹⁶

1.1.2 Binding of Tetrodotoxin to Voltage-Gated Sodium Channels

In mammalian brains, Nav proteins¹⁷ are composed of a complex containing a 260 kDa α -subunit with at least one 33-36 kDa auxiliary β 1, β 2 or β 3 subunits.¹⁸ The α -subunit folds into four homologous domains (Figure 1.1.2.1), each consisting of six α -helical transmembrane segments. Segment 4 contains a positively charged amino acid residue at every third position which functions as a voltage sensor. Segments 5 and 6 of each domain form the ion-selectivity filter which is comprised of a conserved DEKA amino acid sequence and located at the extracellular end of the pore.

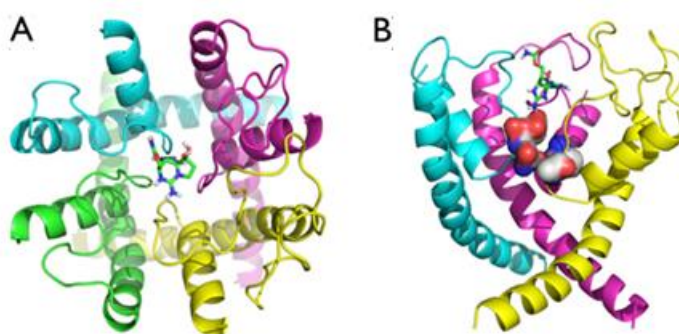


Figure 1.1.2.1. Homology model-derived images of saxitoxin bound rNav1.4.¹⁷ The pore is shown from the top (A) as well as the side (B) and the four domains of the pore are depicted in green (domain I), cyan (domain II), magenta (domain III) and yellow (domain IV). The DEKA selectivity filter is highlighted in (B) as space-filling models.

TTX (**1.1.1.1**) blocks the voltage-gated sodium channels (VGSCs) by binding to the selectivity filter at the extracellular entrance.¹⁹ This results in reduced membrane permeability to sodium ions and thereby the effective threshold of the required excitatory signal is increased, causing a reduced excitability of postsynaptic neurons. Binding of TTX (**1.1.1.1**) to the skeletal muscle Nav1.4 is facilitated by the formation of six H-bonds from the guanidine and the hydroxy groups on C4 and C11 to the three acidic residues of the channel: D181 (domain III) and E180 (domain I and domain II) (Figure 1.1.2.2 A). In addition, the C9 hydroxy group forms a transient H-bond with the side chain of E177 (domain II) inside the filter (Figure 1.1.2.2 B). This binding model is in accordance with the observation that the C4, C9 and C11 alcohols of TTX (**1.1.1.1**) are important for binding to the channel and that their removal results in a reduction of affinity by two orders of magnitude.²⁰ Y178 (domain I) resides in close contact with TTX (Figure 1.1.2.2 C) and is essential for TTX specificity.²¹

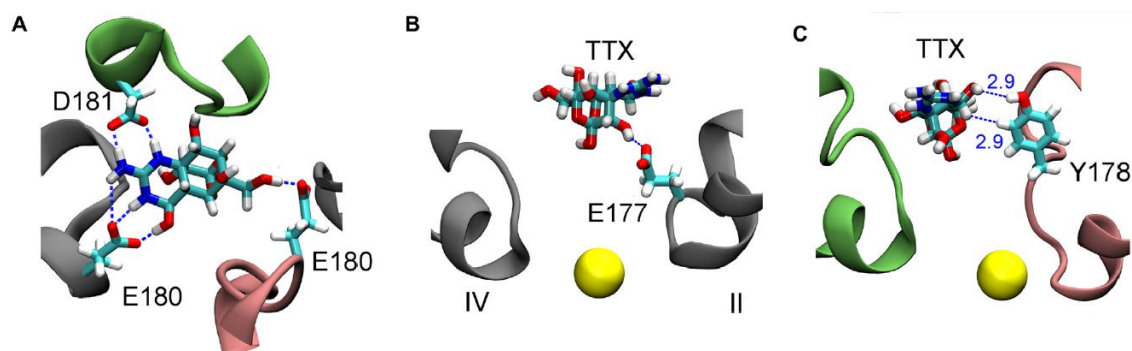


Figure 1.1.2.2. TTX (1.1.1.1)-position relative to the filter of Nav1.4; determined by 50 ns unbiased MD simulation. The four domains of the pore are depicted in red (domain I), grey (domain II), green (domain III) and grey (domain IV).¹⁹

In contrast to the mammalian Nav1.4, the bacterial NavAb is not affected by TTX due to a modified selectivity filter.²² The DEKA-ring of the Nav1.4 is replaced by an EEEE-ring in the bacterial NavAb pore. The higher negative charge density of the NavAb filter results in an enhanced affinity for sodium ions which thereby outcompete TTX (1.1.1.1) for binding.¹⁹ A predominant mechanism to establish TTX-resistance in animals is the mutation of the aromatic tyrosine residue that is located in close proximity to the bound TTX (1.1.1.1) for asparagine or cysteine in pore loop region of the Nav1.4 domain I.²³⁻²⁴ Another element that contributes to the resistance are TTX-binding proteins. The glycoprotein puffer fish saxitoxin and tetrodotoxin binding protein (PSTBP) is regarded as the major TTX-binding protein. It is a carrier protein that transports TTX (1.1.1.1) among tissues such as the liver, the ovary and the skin which thereby diminishes the concentration of free TTX (1.1.1.1) in the plasma.²⁵⁻²⁷

1.1.3 The Distribution and Origin of Tetrodotoxin

TTX (1.1.1.1) is found in a variety of phylogenetically unrelated terrestrial and aquatic species (Figure 1.1.3.1) such as pufferfish, horseshoe crabs, blue-ringed octopuses, newts, frogs, gobies, xanthid crabs, gastropods, starfish, flatworms, ribbon worms, annelids, arrow worms, red calcareous algae, dinoflagellates or bacteria.²⁸⁻²⁹ For many species, TTX (1.1.1.1) serves as a defensive agent and is concentrated in the skin.³⁰⁻³¹ During spawning season, the marine pufferfish increasingly transfer the neurotoxin to their eggs as protection for the offspring.³² This could be linked to the occurrence that TTX also serves as a pheromone of female pufferfish (*fugu niphobles*) to attract males.³³ To avoid this defensive mechanism and prey on the rough-skinned newts, the common garter snake has evolved a resistance against intoxication.³⁴⁻³⁵ The

blue-ringed octopus uses TTX as a hunting tool to paralyze its prey.³⁶ Therefore, it is located in their posterior salivary glands and transmitted through the saliva by biting the victim.



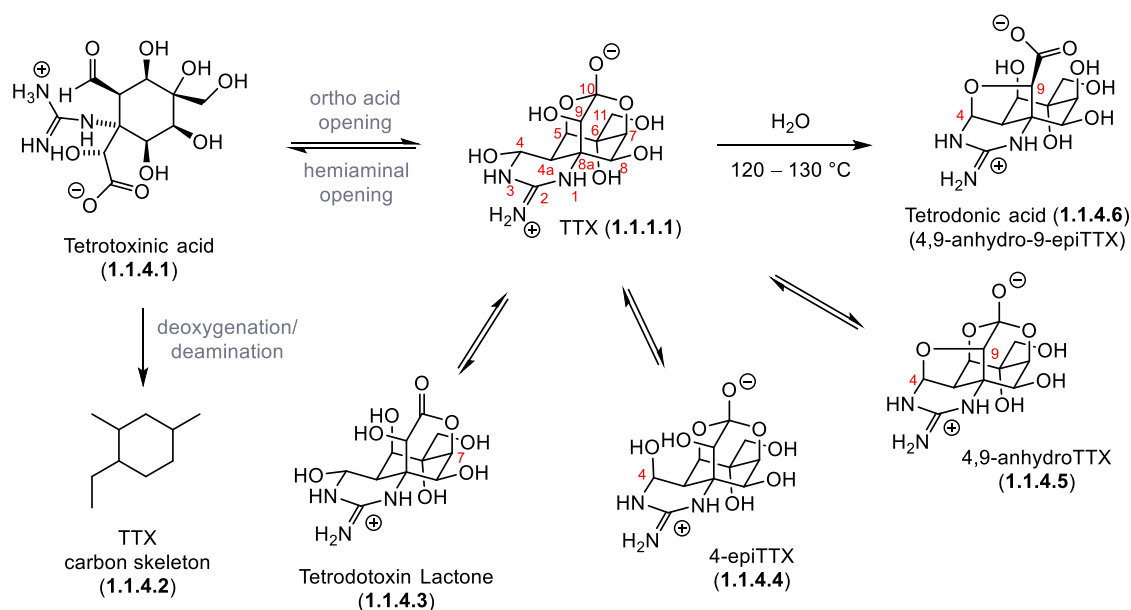
Figure 1.1.3.1. Pufferfish (*Arothron hispidus*)³⁷, Horseshoe Crab (*Tachypleus gigas*)³⁸, Blue-Ringed Octopus (*Hapalochlaena maculosa*)³⁹, California Newt (*Taricha torosa*)⁴⁰, Limosa Harlequin Frog (*Atelopus limosus*)⁴¹ and Common Garter Snake (*Thamnophis sirtalis*)⁴².

It is worth noting that TTX-bearing species are distributed worldwide in diverse terrestrial, marine, fresh water and brackish water environments. For instance, TTX-containing newts were found in North America⁴³ (*Notophthalmus viridescens* and *Taricha torosa*), Japan⁴⁴ (*Cynops pyrrhogaster*), Germany⁴⁵ (*Triturus* spp.) and Italy⁴⁶ (*Triturus alpestris*). The geographical distribution of this potent neurotoxin in evolutionary diverse animals led to three hypotheses regarding its biochemical origin: exogenous TTX sources, endogenous TTX synthesis and symbiotic relationships with TTX-producing microorganisms. Many marine bacteria such as *Pseudomonas* spp. and *Vibrio* spp. are reported to produce TTX which could be accumulated through the food chain.⁴⁷⁻⁵⁰ This hypothesis is based on the effect that pufferfish (*Takifugu rubripes*) held in a TTX-free environment were non-toxic.⁵¹ In addition, the newt *Notophthalmus viridescens* is subject to considerable toxin level variations depending on their geographic origins and it has been shown that these species lose their toxicity when fed with a TTX-free diet.⁵² Examples that support the endogenous origin are the newt *Taricha granulosa* and the toad *Atelopus oxyrhynchus* which increase their toxicity when kept in captivity without an external TTX source.^{30, 53-54} Bacterial symbiosis is a common phenomenon in marine animals and in many cases, bacterial secondary metabolites were found in the host animal species.⁵⁵ The symbiosis-

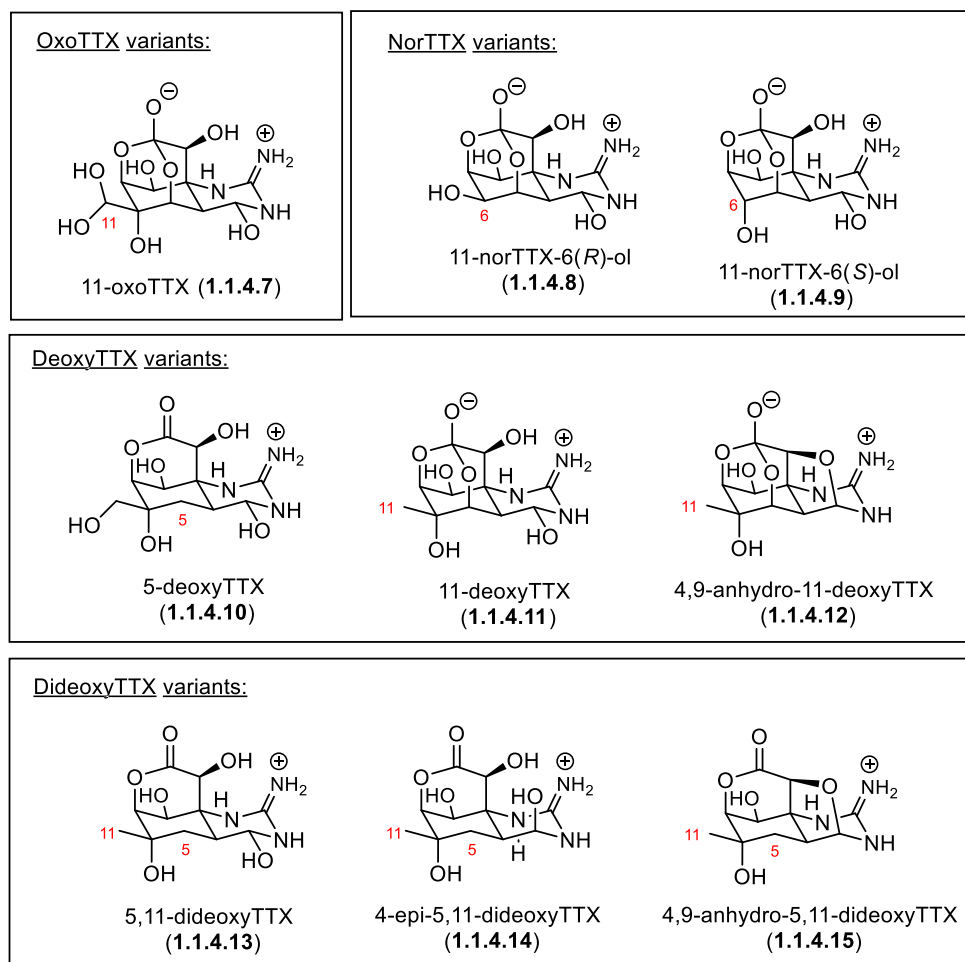
based hypothesis is supported by the occurrence that TTX producing *Vibrio spp.* were cultured from the intestine of a Xanthid crab (*Atergatis floridus*).⁴⁹

1.1.4 The Tetrodotoxin Natural Product Family

Tetrodotoxin (**1.1.1.1**, Scheme 1.1.4.1) is the most prominent member of a vast natural product family.²⁹ Its structure (**1.1.1.1**) is characterized by a highly functionalized dioxadamantane core with an exocyclic six-membered guanidine hemiaminal heterocycle. Disconnecting the spontaneously forming C4 *N,O*-acetal and C10 ortho acid leads to tetrotoxinic acid (**1.1.4.1**) which is known to exist in solution.⁵⁶ This aminopolyol (**1.1.4.1**) contains 7 stereogenic centers, including an α -tertiary amine, an α -hydroxy acid and a range of 1,2-diol moieties. Stripping the molecule (**1.1.1.1**) down to the basic carbon skeleton **1.1.4.2** emphasizes the simplicity of the backbone which stands in sharp contrast to the high density of functional groups on TTX (**1.1.1.1**). Many members of the TTX natural product family are TTX (**1.1.1.1**) isomers and/or in equilibrium with the neurotoxin (Scheme 1.1.4.1). Opening of the C10 ortho acid functionality, for instance, produces almost exclusively the C7 lactone form of tetrodotoxin (**1.1.4.3**).⁸ In acidic solution, the epimerization of the C4 hemiaminal provides 4-epiTTX (**1.1.4.4**), whereas condensation of the C9 alcohol with the hemiaminal produces 4,9-anhydroTTX (**1.1.4.5**) which contains an aminal functionality.⁵⁷ Heating TTX (**1.1.1.1**) to 120 °C – 130 °C in water epimerizes the C9 stereocenter which facilitates opening of the C10 ortho acid and formation of an ether bridge between C4 and C9 to give tetrodonic acid (4,9-anhydro-9-epiTTX, **1.1.4.6**).^{8-9, 56} The analogues 4-epiTTX (**1.1.4.4**), 4,9-anhydroTTX (**1.1.4.5**) and tetrodonic acid (**1.1.4.6**) are often isolated together with TTX (**1.1.1.1**) from natural sources⁵⁸ such as the newt species⁵⁹⁻⁶⁰ *Cynops ensicauda* or the frog species *Brachycephalus ephippium*⁶¹⁻⁶².



In addition to the TTX isomers (Scheme 1.1.4.1), a range of oxidized (oxoTTX), demethylated (norTTX) and deoxygenated (deoxyTTX) analogues are commonly isolated from natural sources (Scheme 1.1.4.2). The oxidized 11-oxoTTX (**1.1.4.7**) was found in pufferfish (*Arothron nigropunctatus*)⁶¹, newt (*Taricha* spp.)⁴², frog (*Brachycephalus ephippium*)^{61, 63}, gastropod (*Nassarius* spp.)^{43, 64} and xanthid crab (*Atergatis floridus*)⁶⁵ species. Both diastereomers of 11-norTTX (**1.1.4.8** and **1.1.4.9**) were isolated from the sea slug *Pleurobranchaea maculata*⁶⁶ and the pufferfish *Lagocephalus sceleratus*⁶⁷⁻⁶⁸. Only the 11-norTTX-6(R)-ol isomer (**1.1.4.8**) was isolated from the crab *Atergatis floridus*⁶⁹ and newt *Cynops ensicauda*⁶⁰ whereas solely the 11-norTTX-6(S)-ol isomer (**1.1.4.9**) was isolated from the frog *Brachycephalus ephippium*⁶² and the newt *Arothron nigropunctatus*⁷⁰. Monodeoxygenated 11-deoxyTTX (**1.1.4.11**) and its interconvertible isomer 4,9-anhydro-11-deoxyTTX (**1.1.4.12**) were isolated from the newt *Cynops ensicauda*. The 11-deoxyTTX was also found in frog (*Brachycephalus ephippium*)³¹ and pufferfish (*Fugu niphobles*)⁷¹ sources where it was detected together with 5-deoxyTTX (**1.1.4.10**). Dideoxygenated 5,11-dideoxyTTX (**1.1.4.13**) stems from the pufferfish *Takifugu poecilonotus*⁷² as well as the flatworm *planocerid* sp. ¹⁷²⁻⁷³ and is in equilibrium with 4-epi-5,11-dideoxyTTX (**1.1.4.14**) and 4,9-anhydro-5,11-dideoxyTTX (**1.1.4.15**) which was determined as part of their chemical synthesis.⁷⁴

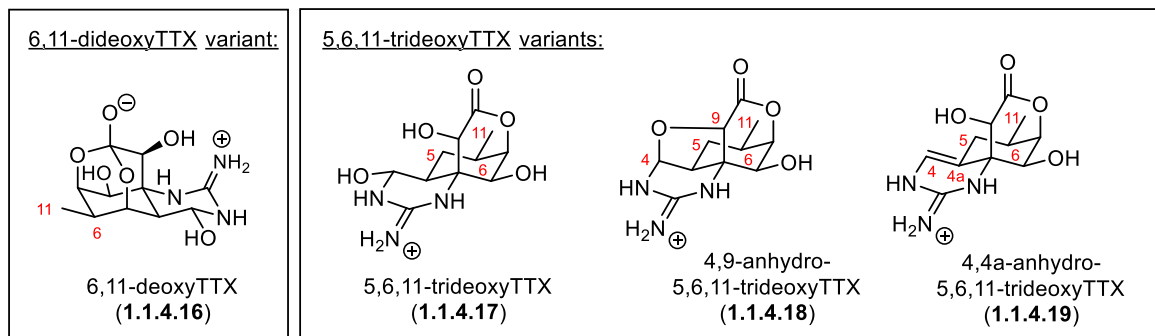


Scheme 1.1.4.2. Oxidized (oxoTTX), deoxygenated (deoxyTTX) and demethylated (norTTX) TTX derivatives.

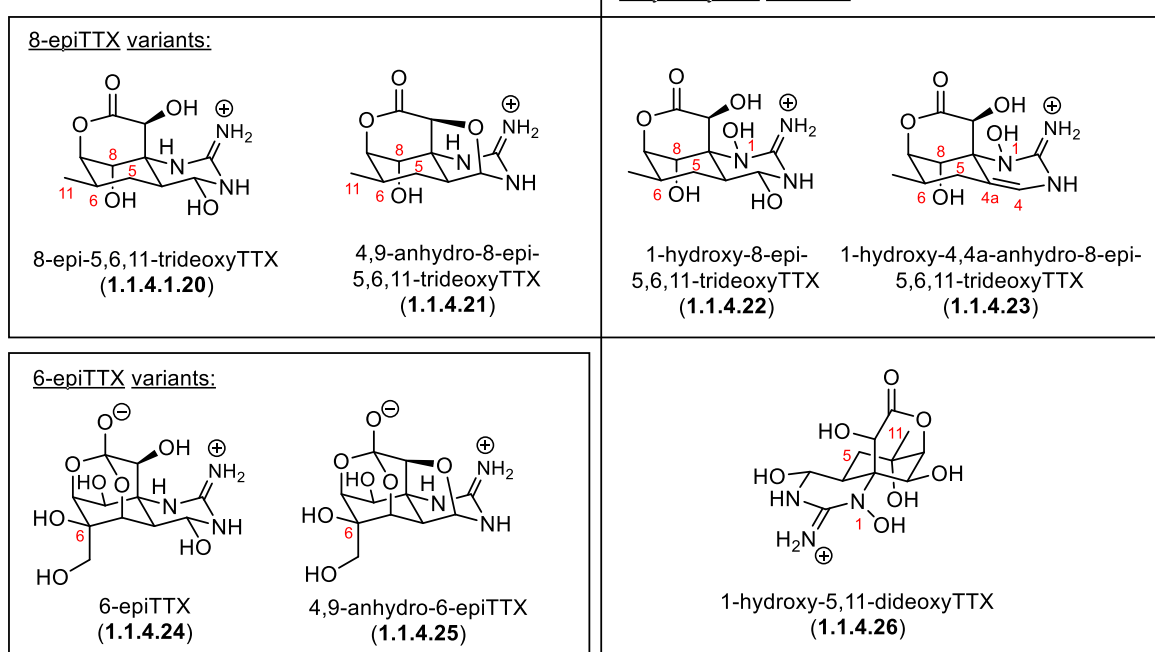
It is hypothesized that the biosynthesis of TTX and its analogues is dependent on the host species. This theory is supported by the fact that many members of the family are only isolated from specific hosts. As a consequence, a wealth of TTX-derived structures was found with a high level of diversity regarding the substitution pattern on the natural product core structure. The biosynthetic differences could be highlighted by comparing the isolated TTX derivatives from pufferfish and newt species (Scheme 1.1.4.3). The 6,11-dideoxy and 5,6,11-trideoxyTTX species that incorporate the (*R*)-configuration at C8, for example, were not found in newts but observed in pufferfish. They include 6,11-dideoxyTTX (1.1.4.16) from *Fugu niphobles*⁷¹, 5,6,11-trideoxyTTX (1.1.4.17), 4,9-anhydro-5,6,11-trideoxyTTX (1.1.4.18), and 4,4a-anhydro-5,6,11-trideoxyTTX (1.1.4.19) from *Fugu poecilonotus*.⁵⁹ 8-EpiTTX, 1-hydroxyTTX and 6-epiTTX variants were only isolated from newts. *Cynops ensicauda popei*⁵⁹ was the source of 8-epi-5,6,11-trideoxyTTX (1.1.4.20), 4,9-anhydro-8-epi-5,6,11-trideoxyTTX (1.1.4.21), 1-hydroxy-8-epi-5,6,11-trideoxyTTX (1.1.4.22), 1-hydroxy-4,4a-anhydro-5,6,11-trideoxy-TTX (1.1.4.23) and 6-epiTTX

(1.1.4.24). *Cynops pyrrhogaster*⁴⁴ was the source of 4,9-anhydro-6-epiTTX (1.1.4.25) and *Taricha granulosa*⁷⁵ was the source of 1-hydroxy-5,11-dideoxyTTX (1.1.4.26).

Pufferfish-specific analogues:

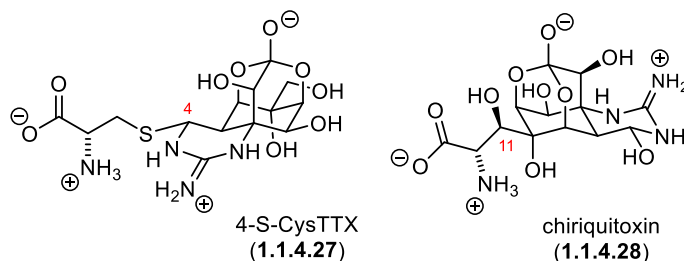


Newts-specific analogues:



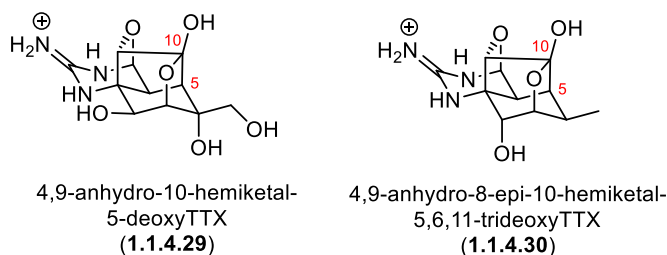
Scheme 1.1.4.3. Comparison of TTX analogues in pufferfish and newt species.

Two members of the natural product family have amino acid structures incorporated: 4-S-CysTTX (1.1.4.27) from the puffer fish *Fugu Pardalis*⁷⁶⁻⁷⁷ and chiriquitoxin (1.1.4.28) from the toad *Atelopus chiriquiensis*⁷⁷⁻⁷⁹ (Scheme 1.1.4.4). 4-S-CysTTX was isolated from the puffer fish liver and it was experimentally validated that it could be prepared through a reaction of 4,9-anhydroTTX (1.1.4.5) with cysteine in aqueous solutions (pH 8.0). This has led to the hypothesis that it is a metabolic product which is formed non-enzymatically.



Scheme 1.1.4.4. Amino acid-containing TTX derivatives.

The latest additions to the TTX family were the C5, C10 carbon-carbon bonded 4,9-anhydro-10-hemiketal-5-deoxyTTX (1.1.4.29) and 4,9-anhydro-8-epi-10-hemiketal-5,6,11-trideoxyTTX (1.1.4.30) that were isolated from the newt *Cynops ensicauda popei*.⁸⁰ Their isolation has led to the hypothesis that the biosynthesis of TTX (1.1.1.1) in newts proceeds through C5, C10 carbon-carbon bonded species and that 4,9-anhydro-10-hemiketal-5-deoxyTTX (1.1.4.29) is the direct precursor to 4,9-anhydroTTX (1.1.4.5).



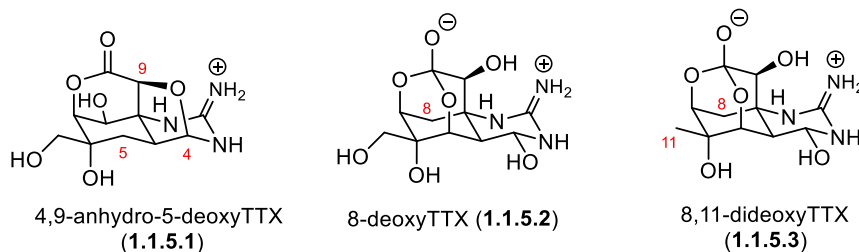
Scheme 1.1.4.5. C5, C10-bonded TTX derivatives.

The isolation of new members of the TTX natural product family strongly contributes to the elucidation of the species-specific biosynthesis of TTX (Chapter 1.1.6) and is therefore still in the focus of modern research.⁸¹

1.1.5 Biological Activities of Tetrodotoxin Derivatives

Many studies were conducted to determine biological activities of natural and unnatural TTX derivatives on VGSCs using different methodologies. The efficiencies of the sodium channel blockers were typically reported in comparison to TTX and therefore allowed for the deduction of relative activities and activity trends. In general, structure activity relationship (SAR)-based studies of TTX derivatives have shown that a high binding affinity to the VGSCs is established through hydrogen bonds from the guanidine moiety as well as the C4, C6, C8, C9, C10 and C11 hydroxy groups.⁸²⁻⁹⁰

The inhibitory activity of members of the TTX natural product family to the cytotoxicity of ouabain and veratridine in mouse neuroblastoma cells (Neuro-2a) were evaluated and reported in median effective doses (ED_{50}). These studies were conducted to determine the importance of the C5, C8 and C11 hydroxy groups and thus included the synthetic derivatives 4,9-anhydro-5-deoxyTTX (**1.1.5.1**), 8-deoxyTTX (**1.1.5.2**) and 8,11-dideoxyTTX (**1.1.5.3**) (Scheme 1.1.5.1).^{82, 90} Removal of the C5-hydroxy group (5-deoxyTTX, **1.1.4.10**, $ED_{50} = 1.4 \pm 0.8 \mu\text{M}$) from TTX (**1.1.1.1**, $ED_{50} = 3.4 \pm 1.8 \text{ nM}$) interferes with the formation of the ortho acid structure and led to approx. 500-fold decrease in inhibition.⁸² A more significant decrease in activity was observed through formation of 4,9-anhydro-5-deoxyTTX (**1.1.5.1**, $ED_{50} = 9.6 \pm 5.2 \mu\text{M}$) which is attributed to the loss of the C4, C5, C9 and C11 hydrogen bonding partners to the sodium channels. A less pronounced effect was observed in 8-deoxyTTX (**1.1.5.2**, $ED_{50} = 0.25 \pm 0.12 \mu\text{M}$) which suffered from approx. 100 fold decrease in inhibition in comparison to TTX (**1.1.1.1**). In separate study that used the same methodology, the activity of TTX (**1.1.1.1**, $ED_{50} = 4.6 \pm 0.70 \text{ nM}$) was compared to that of 11-deoxyTTX (**1.1.4.11**, $ED_{50} = 270 \pm 74 \text{ nM}$) and 8,11-dideoxytetrodotoxin (**1.1.5.3**, $ED_{50} = 9.3 \pm 3.3 \mu\text{M}$).⁹⁰



Scheme 1.1.5.1. Synthetic TTX derivatives.

Another approach to categorize the ability of the TTX natural product family members to block voltage-gated sodium channels is through their toxicity. Therefore, lethal dose (LD)-values (intraperitoneal injection into mice) could serve a tool to rank the relative bioactivity of the TTX derivatives.⁹¹ DeoxyTTX derivatives, in general, are less toxic than TTX (**1.1.1.1**, $LD_{50} = 10 \mu\text{g/Kg}$). For example, 11-deoxyTTX (**1.1.4.11**, $LD_{50} = 70 \mu\text{g/Kg}$) is less active by a factor of 7 and the toxicity decreases with a decreasing number of hydroxy moieties: 6,11-dideoxyTTX (**1.1.4.16**, $LD_{50} = 420 \mu\text{g/Kg}$) and 5,6,11-trideoxyTTX (**1.1.4.17**, $LD_{\text{min}} = 750 \mu\text{g/Kg}$).⁹¹⁻⁹² The loss of efficacy by retaining the C6 and C11 hydroxy groups but epimerizing the C6 stereocenter in 6-epiTTX (**1.1.4.24**, $LD_{50} = 60 \mu\text{g/Kg}$) could be explained by partial interference with their hydrogen bonds to the sodium channel as compared to TTX (**1.1.1.1**). This phenomenon was

also observed in 4-epiTTX (**1.1.4.4**, LD₅₀ = 64 µg/Kg). The toxicity loss by removing both hydrogen bonds from the C4 and C9 hydroxy groups through the formation of 4,9-anhydroTTX (**1.1.4.5**, LD₅₀ = 490 µg/Kg) is in the range of the dideoxy-variant 6,11-dideoxyTTX (**1.1.4.16**). Comparable activities to TTX (**1.1.1.1**) are observed for the derivatives with higher levels of functionality such as chiriquitoxin (**1.1.4.28**, LD₅₀ = 13 µg/Kg)⁹³ and 11-oxoTTX (**1.1.4.7**, LD₅₀ = 16 µg/Kg).

To get a deeper insight into the binding of TTX derivatives to their targets, a study was conducted to evaluate the affinity to rat brain membrane, which contains a high abundance of sodium channels.⁸³ Therefore, equilibrium dissociation constants (K₀) were determined by the ability of the tested structures to inhibit the binding of [³H]saxitoxin. TTX (**1.1.1.1**, K₀ = 1.8 ± 0.1 nM) was compared to demethylated derivatives 11-norTTX-6(S)-ol (**1.1.4.9**, K₀ = 23 ± 1 nM) and 11-norTTX-6(R)-ol (**1.1.4.8**, K₀ = 31 ± 3 nM). This result clearly states that the loss of one hydroxymethyl group is associated with a loss in affinity, whereas retaining the position of the C6 hydroxy moiety results in a stronger binding mode. Removal of the C11 hydroxy group (11-deoxyTTX, **1.1.4.11**, K₀ = 37 ± 2 nM), epimerization of a hydroxy-containing carbon (6-epiTTX, **1.1.4.24**, K₀ = 39 ± 3 nM and 4-epiTTX, **1.1.4.4**, K₀ = 68 ± 10 nM) or formation of 4,9-anhydroTTX (**1.1.4.5**, K₀ = 180 ± 11 nM) lead to a substantial decrease in affinity.

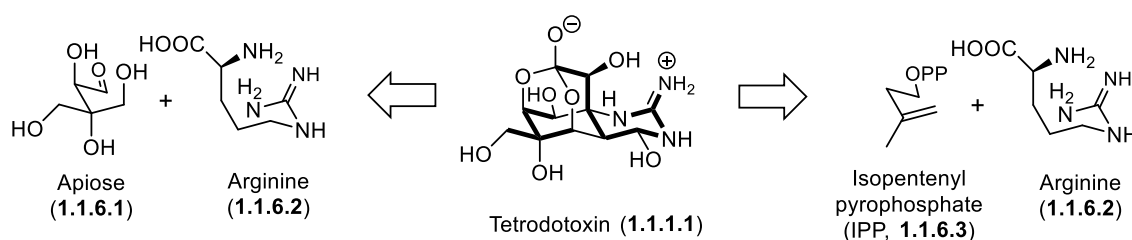
Two exceptional cases are the oxidized and more functionalized derivatives 11-oxoTTX (**1.1.4.7**, K₀ = 1.5 ± 0.2 nM) and chiriquitoxin (**1.1.4.28**, K₀ = 1.0 ± 0.1 nM), respectively, which are better inhibitors of [³H]saxitoxin binding to rat brain synaptic membranes than TTX (**1.1.1.1**).⁸³ In addition to the observation that the oxidized derivative (**1.1.4.7**) has a higher binding affinity, it was shown that 11-oxoTTX (**1.1.4.7**, ED₅₀ = 0.7 nM) is a more potent blocker of the VGSC than TTX (**1.1.1.1**, ED₅₀ = 4.1 nM) in voltage-clamp experiments on frog skeletal muscle fibers.⁸⁹ Chiriquitoxin (**1.1.4.28**), in contrast to TTX (**1.1.1.1**), is also known to interfere with the outwardly rectifying potassium channels.⁹³

To compare the activity of 4,9-anhydroTTX (**1.1.4.5**) and TTX (**1.1.1.1**), their blocking efficacies were tested on Nav isoforms expressed in *Xenopus laevis* oocytes.²⁰ Half maximal inhibitory concentrations (IC₅₀ in nM) were obtained for TTX (**1.1.1.1**): 7.8 ± 1.3 (Nav1.2), 2.8 ± 2.3 (Nav1.3), 4.5 ± 1.0 (Nav1.4), 1970 ± 565 (Nav1.5), 3.8 ± 1.5 (Nav1.6), 5.5 ± 1.4 (Nav1.7), and 1330 ± 459 (Nav1.8); as well as 4,9-anhydroTTX (**1.1.4.5**): 1260 ± 121 (Nav1.2), 341 ± 36 (Nav1.3), 988 ± 62 (Nav1.4), 78500 ± 11600 (Nav1.5), 7.8 ± 2.3 (Nav1.6), 1270 ± 251 (Nav1.7), and >30000 (Nav1.8). 4,9-AnhydroTTX (**1.1.4.5**) is

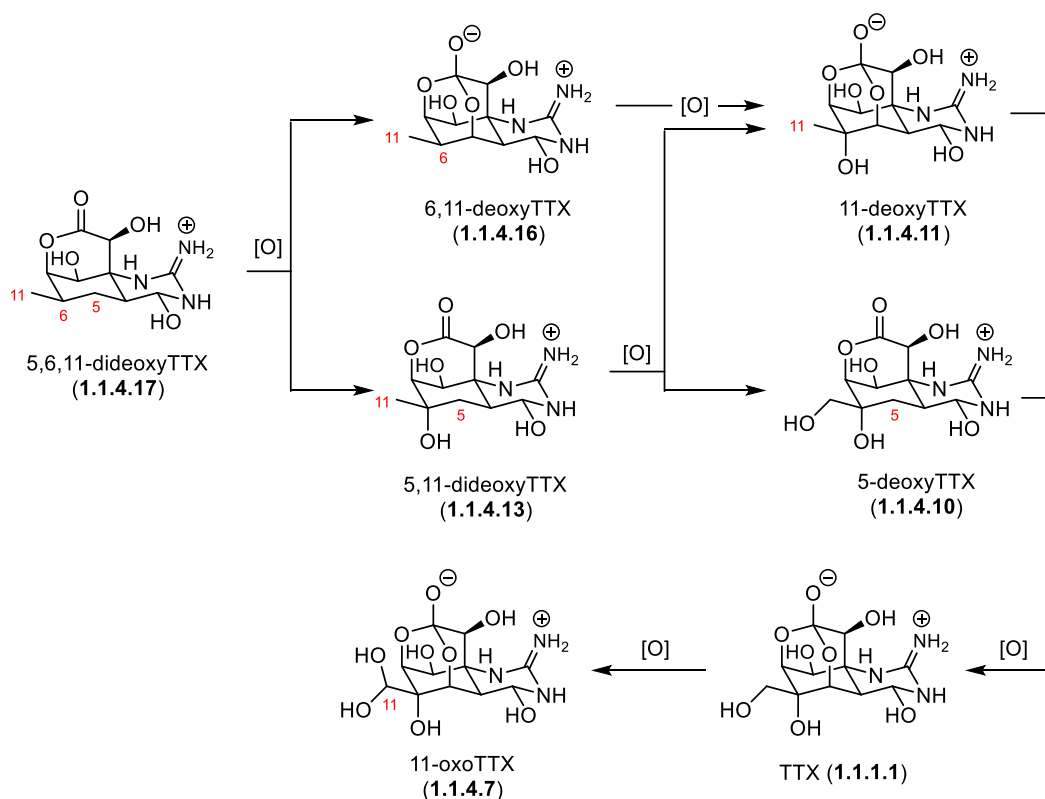
substantially less active than TTX (**1.1.1.1**) for the Nav isoforms 1.2-1.5, 1.7 and 1.8, but has a comparable activity for the isoform 1.6. Therefore, 4,9-anhydroTTX (**1.1.4.5**) is a highly selective blocker of the Nav1.6 with a 40-160 fold increased efficacy with regard to the other Nav channel isoforms.⁹⁴

1.1.6 Biosynthetic Hypotheses

To date, many hypotheses for the biosynthesis of TTX (**1.1.1.1**) were discussed based on structural features of the TTX natural product family members.⁹⁵ An early proposal suggested that TTX could be traced back to a C5-branched sugar such as apiose (**1.1.6.1**) and amino acid arginine (**1.1.6.2**) (Scheme 1.1.6.1).⁷⁵ This hypothesis accounts for the full oxygenation pattern as well as the guanidine moiety. However, the isolation of many deoxyTTX derivatives suggests that the TTX core is built from less oxygenated precursors such as isopentenyl pyrophosphate (IPP, **1.1.6.3**) followed by late-stage oxidations.⁹⁶

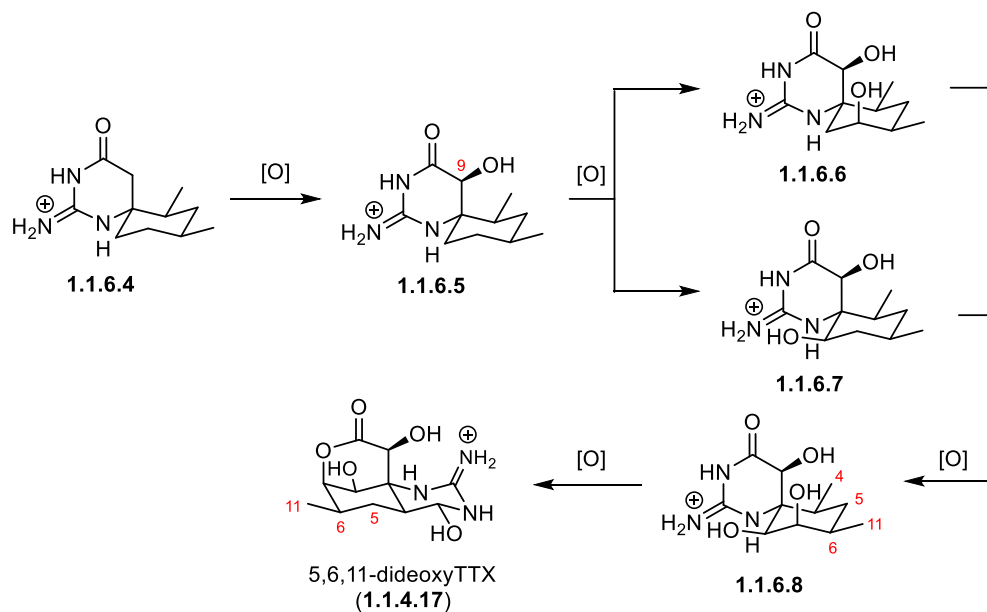


It is reasonable to assume that the biosynthesis of TTX (**1.1.1.1**) in marine and terrestrial taxa follows different pathways,^{45, 53} based on the structural differences between members of the TTX natural product family that stem from pufferfish and newt sources (see Chapter 1.1.4). The isolation of mixtures of 5-deoxyTTX (**1.1.4.10**), 11-deoxyTTX (**1.1.4.11**), 5,11-dideoxyTTX (**1.1.4.13**), 6,11-dideoxyTTX (**1.1.4.16**) and 5,6,11-trideoxyTTX (**1.1.4.17**) in the pufferfish hints to a stepwise biosynthetic late-stage oxidation to from 5,6,11-trideoxyTTX (**1.1.4.17**) to TTX (**1.1.1.1**) (Scheme 1.1.6.2).⁷² This hypothesis is further supported by the occurrence of the oxidized 11-oxoTTX (**1.1.4.7**).^{61, 72}



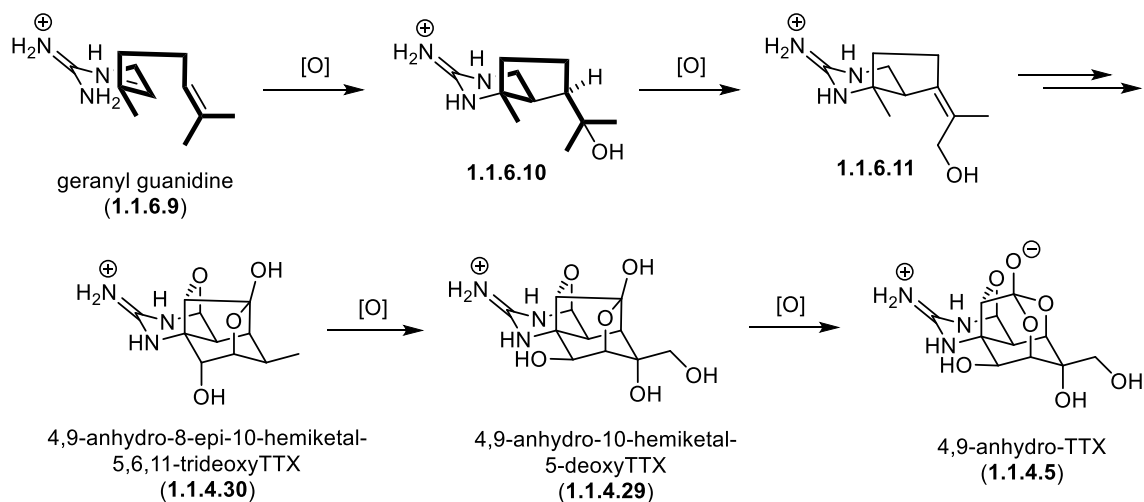
Scheme 1.1.6.2. Proposed biosynthetic late-stage oxidation of 5,6,11-trideoxyTTX (1.1.4.17).

A new perspective on the early stages of the TTX (1.1.1.1) biosynthesis in marine species arose through the isolation of spirocyclic guanidinyllactams (1.1.6.4 – 1.1.6.8) from the pufferfish *Tetraodon biocellatus* (Scheme 1.1.6.3).⁹⁷ The guanidylated carbon skeleton 1.1.6.4 is thereby sequentially oxidized to 5,6,11-trideoxyTTX (1.1.4.17). Isolated intermediates include C9 hydroxylated cyclohexane 1.1.6.5 which could be further oxidized to 1.1.6.8 via 1.1.6.6 and 1.1.6.7. Oxidation of the C4 position (1.1.6.8) followed by lactam hydrolysis and esterification leads to 5,6,11-trideoxyTTX (1.1.4.17).



Scheme 1.1.6.3. Proposed oxidative biosynthesis pathway in pufferfish.

Determining the biosynthetic building blocks of TTX in newts was attempted by feeding [2- ^{14}C]-acetate, [^{14}C (U)]-glucose, [guanido- ^{14}C]-arginine and [ureido- ^{14}C]-citrulline to *Taricha torosa* and *Taricha granulosa*, but did not lead to incorporation of the radioactive segments.⁹⁸ The structural features of TTX derivatives that stem from newt sources suggest a biosynthesis through a terpene pathway. This hypothesis was supported by the isolation of cyclic guanidine-containing monoterpenes, (**1.1.6.10** and **1.1.6.11**) from the toxic Japanese sword-tail newt (*Cynops ensicauda popei*) (Scheme 1.1.6.4).⁹⁹ Oxidative cyclization of geranyl guanidine (**1.1.6.9**) may afford **1.1.6.10** which could be further oxidized to **1.1.6.11**.



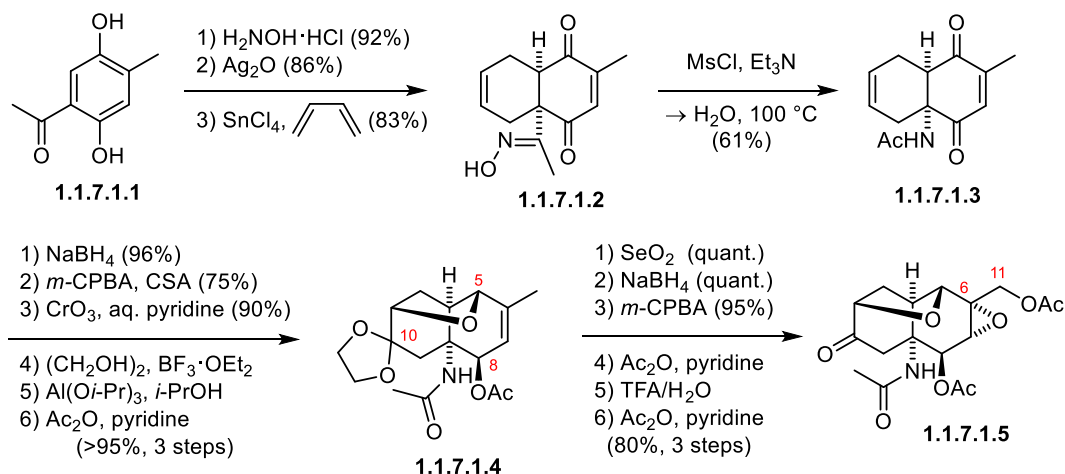
Scheme 1.1.6.4. Proposed terpene-based biosynthesis pathway newts.

These findings are further corroborated by the identification of the C5, C10 carbon-carbon bonded 4,9-anhydro-8-epi-10-hemiketal-5,6,11-trideoxyTTX (**1.1.4.30**) and 4,9-anhydro-10-hemiketal-5-deoxyTTX (**1.1.4.29**).⁸⁰ These more elaborate TTX derivatives were also isolated from *Cynops ensicauda popei* and are therefore likely products from biosynthetic oxidations of **1.1.6.11**. In theory, 4,9-anhydro-10-hemiketal-5-deoxyTTX (**1.1.4.29**) could be converted 4,9-anhydroTTX (**1.1.4.5**) by a Baeyer-Villiger-type monooxygenase.⁸⁰

1.1.7 Synthetic Approaches towards Tetrodotoxin

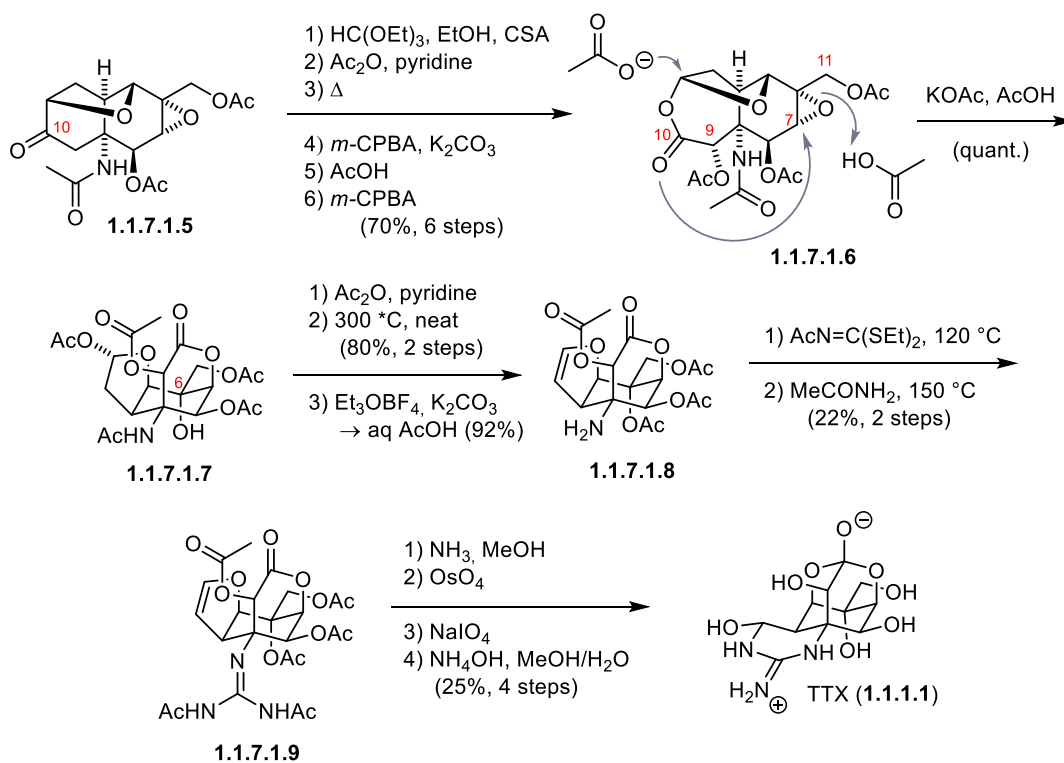
1.1.7.1 The Kishi Synthesis of Tetrodotoxin

The first synthesis of TTX (**1.1.1.1**) was established by Kishi and co-workers in 1972 (Scheme 1.1.7.1.1 and 1.1.7.1.2).¹² Their synthesis commenced by the formation of a *cis*-decalin (**1.1.7.1.2**) through a SnCl₄-mediated Diels-Alder reaction between butadiene and a *para*-quinone (Scheme 1.1.7.1.1). The *para*-quinone was generated through oxime-formation of **1.1.7.1.1** with hydroxylamine followed by oxidation with Ag₂O.^{14, 100} A Beckmann rearrangement of the ketoxime **1.1.7.1.2** then provided the α -tertiary amine motif (**1.1.7.1.3**).¹³ For the introduction of the TTX oxygenation pattern, Kishi and co-workers exploited the effect that reagents/reactants approach from the convex face of the bicyclic *cis*-decalin structure.^{11, 13} In this context, the C5 stereocenter (**1.1.7.1.4**) was set through NaBH₄ reduction and the resulting hydroxy group was in an ideal position to open the epoxide that was formed through a Prilezhaev oxidation. The liberated C10 alcohol was oxidized and protected as a dioxolane. A selective Meerwein-Ponndorf-Verley reduction set the C8 hydroxy group **1.1.7.1.4**. The C11 alcohol (**1.1.7.1.5**) was introduced by a Riley oxidation – reduction sequence and the C6 oxygen atom (**1.1.7.1.5**) was set through a Prilezhaev epoxidation. C10 acetal deprotection was followed by an acetylation procedure and provided **1.1.7.1.5**.



Scheme 1.1.7.1.1. Kishi synthesis of TTX (1.1.1.1) – Part 1.

To install the C9 hydroxy group (1.1.7.1.6), a Rubottom-type oxidation was used which required the formation of an enol ether (Scheme 1.1.7.1.2). This was achieved by formation of a diethyl ketal from the C10 ketone (1.1.7.1.5) and after addition of the hydrolyzed C11 acetate group, one ethanol group was thermally extruded. Epoxidation of the generated enol ether and hydrolysis with AcOH provided the C9 acetate (1.1.7.1.6).

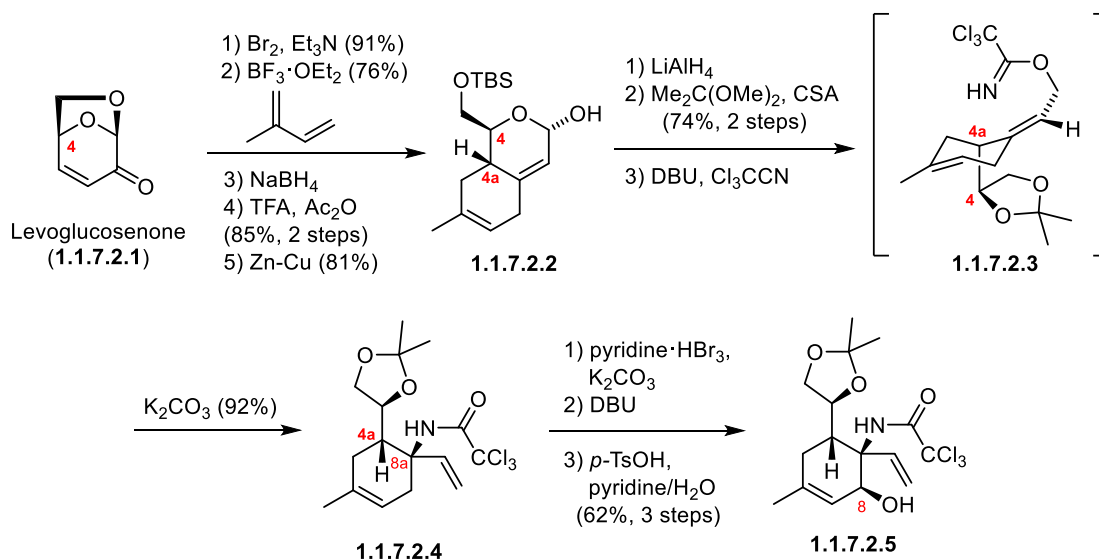


Scheme 1.1.7.1.2. Kishi synthesis of TTX (1.1.1.1) – Part 2.

The C10 ketone was oxidized to an ester group through a Baeyer-Villiger reaction which set the stage for a cascade cyclization. This cascade was initiated through an attack of an acetate anion onto the acetal moiety (**1.1.7.1.6**), which liberated the C10 carboxylate. The carboxylate group was ideally positioned to open the epoxide at the C7 position and provided **1.1.7.1.7** with the desired C7 stereoconfiguration. Acetylation of the C6 alcohol enabled the thermal elimination of the acetate within the tetrahydrofuran ring to give the corresponding dihydrofuran (**1.1.7.1.8**). Cleavage of the amide bond was achieved using Meerwein's salt and gave amine **1.1.7.1.8** which was subjected to newly developed guanidylolation methodology to afford guanidine **1.1.7.1.9**.¹² To finalize TTX (**1.1.1.1**), the dihydrofuran was oxidatively cleaved followed by a global acetate deprotection which provided the natural product in a total of 31 steps from 5-acetyltoluhydroquinone.

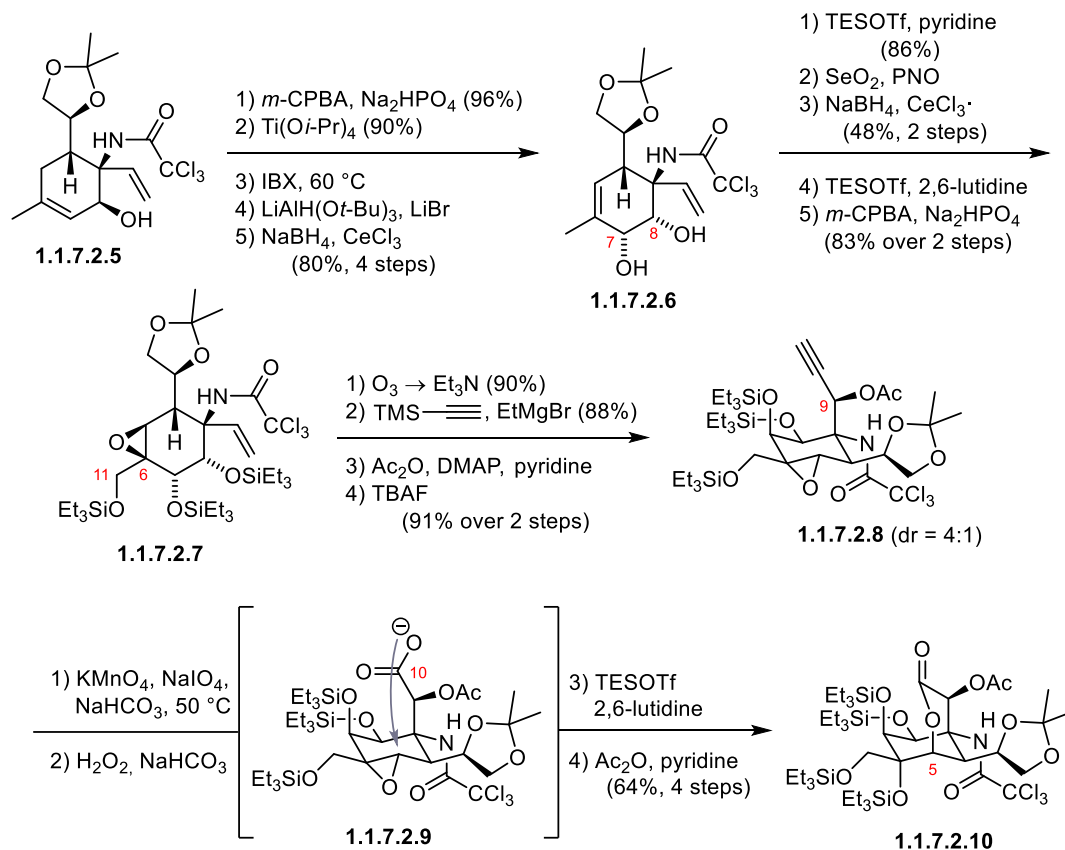
1.1.7.2 The Isobe Synthesis of Tetrodotoxin

Isobe and co-workers have developed the first asymmetric synthesis of TTX (**1.1.1.1**) in 2003 which furnished the natural product in 77 steps from the chiral starting material 2-acetoxy glucal.¹⁰¹⁻¹⁰² To increase the utility of their synthesis, they devised an improved version in 2004 starting from levoglucosenone (**1.1.7.2.1**) (Scheme 1.1.7.2.1, 1.1.7.2.2 and 1.1.7.2.3).¹⁰³⁻¹⁰⁴ As part of their synthesis, the C4 stereocenter of levoglucosenone (**1.1.7.2.1**) was used to direct the Diels-Alder cycloaddition and provide the six-membered core carboxycle of TTX (**1.1.1.1**) with the desired C4a configuration (**1.1.7.2.2**) (Scheme 1.1.7.2.1).¹⁰⁵ Redox and protecting group manipulations provided **1.1.7.2.3**, which underwent an Overman rearrangement and set the C8a α -tertiary amine (**1.1.7.2.4**). Thereafter, the oxygenation pattern of TTX (**1.1.1.1**) was installed on the cyclohexene core (**1.1.7.2.4**) which could be diastereoselectively directed through the C8a and C4a stereocenters. A hydroxy group at C8 was installed by dibromination of the alkene group followed by DBU-mediated S_N2' substitution of the allylic bromine by a nucleophilic attack of the trichloroacetamide oxygen atom.^{74, 106} The resulting oxazoline was hydrolyzed to provide allylic alcohol **1.1.7.2.5**.



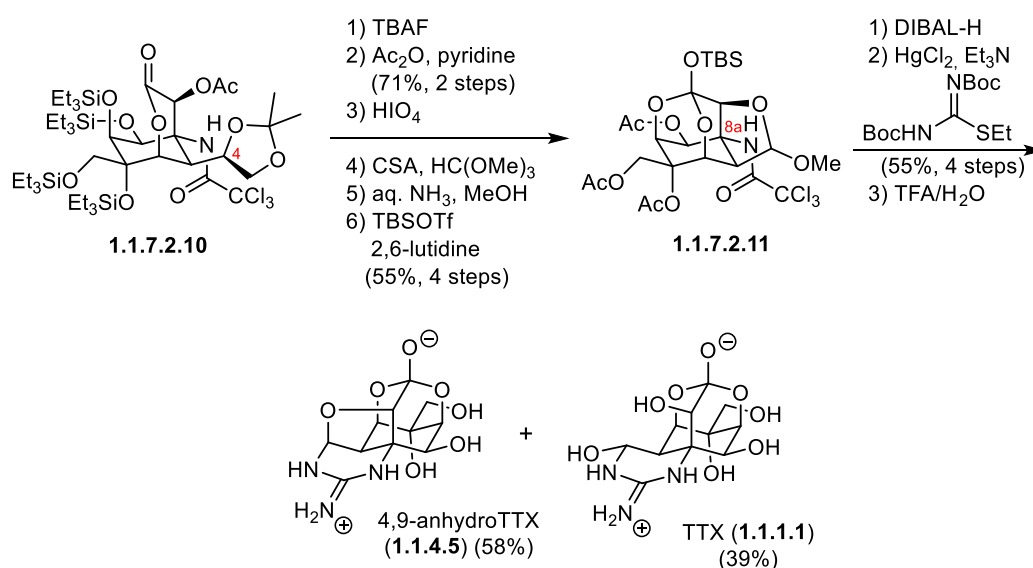
Scheme 1.1.7.2.1. Elaboration of levoglucosenone (**1.1.7.2.1**) into aminoalcohol **1.1.7.2.5**.

Prilezhaev epoxidation and epoxide-opening via elimination provided an allylic 1,2-diol which was oxidized to the corresponding diketone and subjected to a 2-step reduction sequence to give the desired stereoconfigurations of the C7 and C8 hydroxy groups (**1.1.7.2.6**, Scheme 1.1.7.2.2).¹⁰⁷ A Riley oxidation – reduction sequence provided the C11 hydroxy moiety, whereas the C6 oxygen was diastereoselectively installed through a Prilezhaev oxidation to give **1.1.7.2.7**. The C9 stereocenter was introduced by ozonolysis of the vinyl group followed by Cram chelate-mediated ethynylmagnesium bromide addition into the resulting aldehyde (**1.1.7.2.8**). Oxidative cleavage of the terminal alkyne using sequential oxidations with $\text{KMnO}_4/\text{NaIO}_4$ and H_2O_2 provided the corresponding C10 carboxylate (**1.1.7.2.9**) which nucleophilically opened the epoxide and set the C5 stereocenter (**1.1.7.2.10**).



Scheme 1.1.7.2.2. Installation of the TTX oxygenation pattern.

To finalize TTX (**1.1.1.1**, Scheme 1.1.7.2.3) the 1,2-diol moiety at C4 was oxidatively cleaved to the corresponding aldehyde and the C8a α -tertiary amine was transformed into a guanidine using a modified Kishi guanidylation. Global deprotection furnished TTX (**1.1.1.1**) and 4,9-anhydroTTX (**1.1.4.5**) in 39 steps from levoglucosenone (**1.1.7.2.1**).

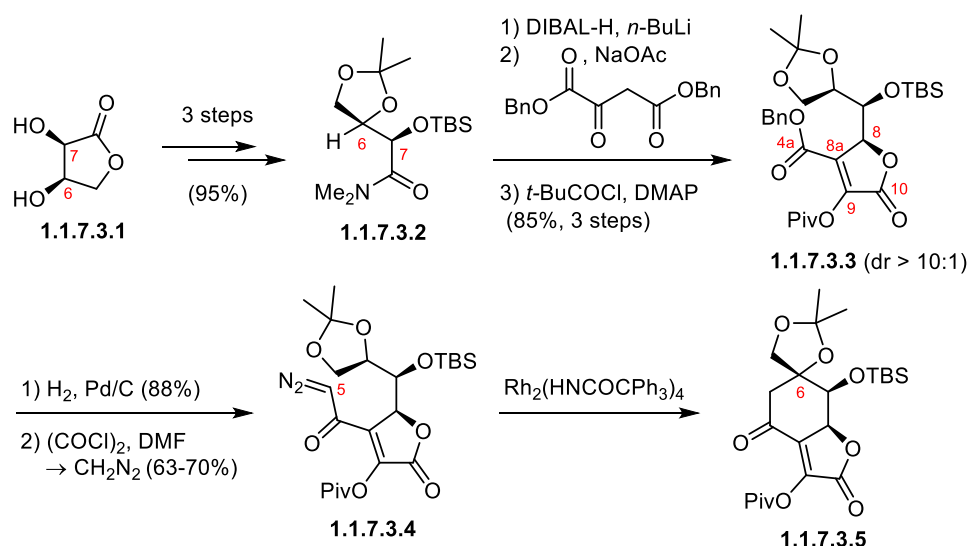


Scheme 1.1.7.2.3. Finalizing TTX (1.1.1.1) and 4,9-anhydroTTX (1.1.4.5) from 1.1.7.2.10.

Based on their general synthetic approach towards TTX (1.1.1.1), Isobe and co-workers have modified their synthesis to prepare 11-deoxyTTX (1.1.4.11)¹⁰⁷, 5,11-dideoxyTTX (1.1.4.13)⁷⁴, chiriquitoxin (1.1.4.28)¹⁰⁸, 5-deoxyTTX (1.1.4.10)⁸², 8-deoxyTTX (1.1.5.2)⁸², 8,11-dideoxyTTX (1.1.5.3)¹⁰⁹⁻¹¹⁰ and 5,6,11-trideoxyTTX (1.1.4.17)¹¹¹.

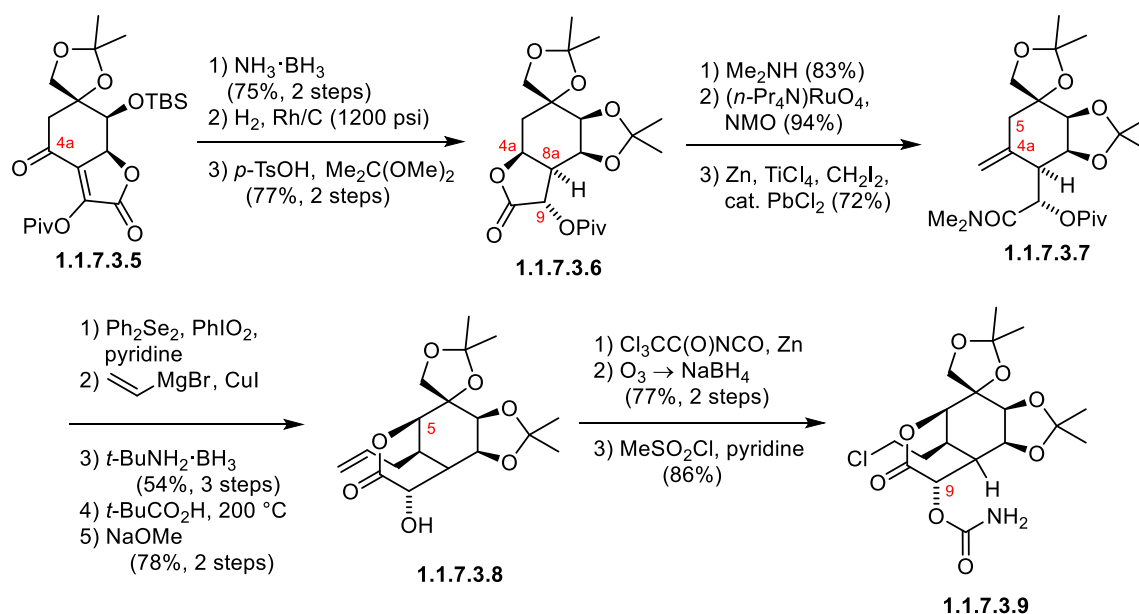
1.1.7.3 The DuBois Synthesis of Tetrodotoxin

DuBois and co-workers have demonstrated the utility of their carbene/nitrene C–H insertion methodologies by establishing an asymmetric synthesis of TTX (1.1.1.1) from enantiomerically pure D-erythronic acid γ -lactone (1.1.7.3.1, Scheme 1.1.7.3.1).¹¹²⁻¹¹³ D-erythronic acid γ -lactone (1.1.7.3.1) contains two stereocenters that correspond to the C6 and C7 of TTX (1.1.1.1) and was converted to amide 1.1.7.3.2 in a 3-step amide formation – protecting group manipulation sequence. An aldol reaction with dibenzyl oxaloacetate was used as an opening step to set the C8 stereocenter and provide the C9, C10 structural elements as well as the C4a and C8a carbon atoms (1.1.7.3.3). A homologation appended diazomethane (1.1.7.3.4) which was used in the rhodium-catalyzed carbene C–H insertion to close cyclohexane core (1.1.7.3.5).

**Scheme 1.1.7.3.1.** Establishing the cyclohexane core of TTX (1.1.1.1).

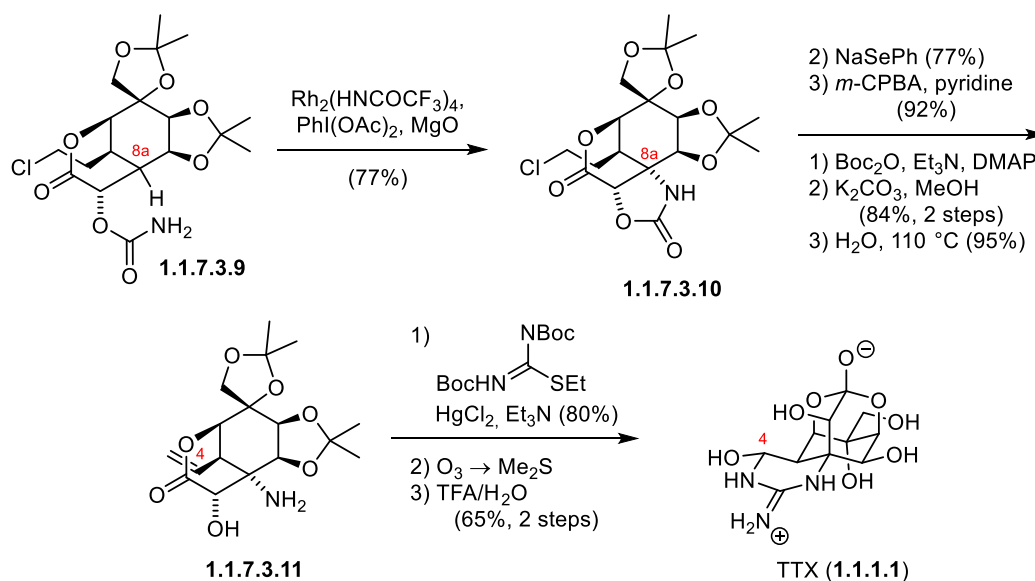
Reduction of the C4a carbonyl to the corresponding hydroxy group enabled the subsequent hydrogenation which proceeded from the convex face of the bicycle and set the C8a and C9 stereocenters (1.1.7.3.6) (Scheme 1.1.7.3.2). After acetonide protection (1.1.7.3.6), the lactone

structure was opened with dimethylamine and the liberated C4a alcohol was oxidized to a ketone using a Ley oxidation. This C4a ketone was transformed into an exo-methylene via a Tebbe olefination (1.1.7.3.7) which in turn enabled a Riley oxidation of the C5 methylene to a ketone. The exo-methylene was converted into an allyl group through a metal-mediated vinyl addition (1.1.7.3.8) and a reduction of the C5 ketone was performed. Acid-mediated lactone formation onto the resulting C5 alcohol (1.1.7.3.8) set the precursor for the key C–H nitrene insertion. This step relied on the installation of a carbamate group on the C9 alcohol followed by transformation of the allyl group into an ethyl chloride (1.1.7.3.9).



Scheme 1.1.7.3.2. Preparing the nitrene C–H insertion precursor 1.1.7.3.9.

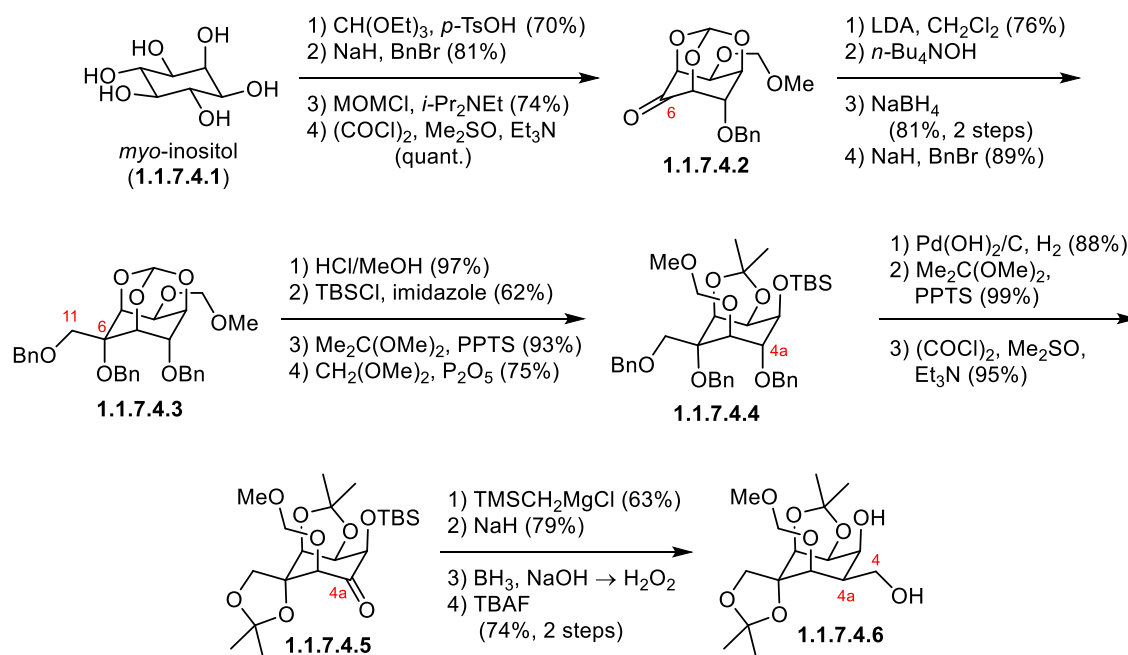
A binuclear rhodium complex catalyzed the carbamate nitrene inserted into the C8a C–H bond and provided an α -tertiary amine (1.1.7.3.10) (Scheme 1.1.7.3.3). The ethyl chloride group was transformed into the C4a vinyl group via a Grieco-type elimination and the amine was deprotected using a 3-step sequence (1.1.7.3.11). Kishi guanidylation of the primary amine, ozonolysis of the vinyl group to liberate the C4a aldehyde and acid-mediated global deprotection provided TTX (1.1.1) in a total of 30 steps from D-erythronic acid γ -lactone (1.1.7.3.1).



Scheme 1.1.7.3.3. Finalizing TTX (1.1.1.1) from carbamate 1.1.7.3.9.

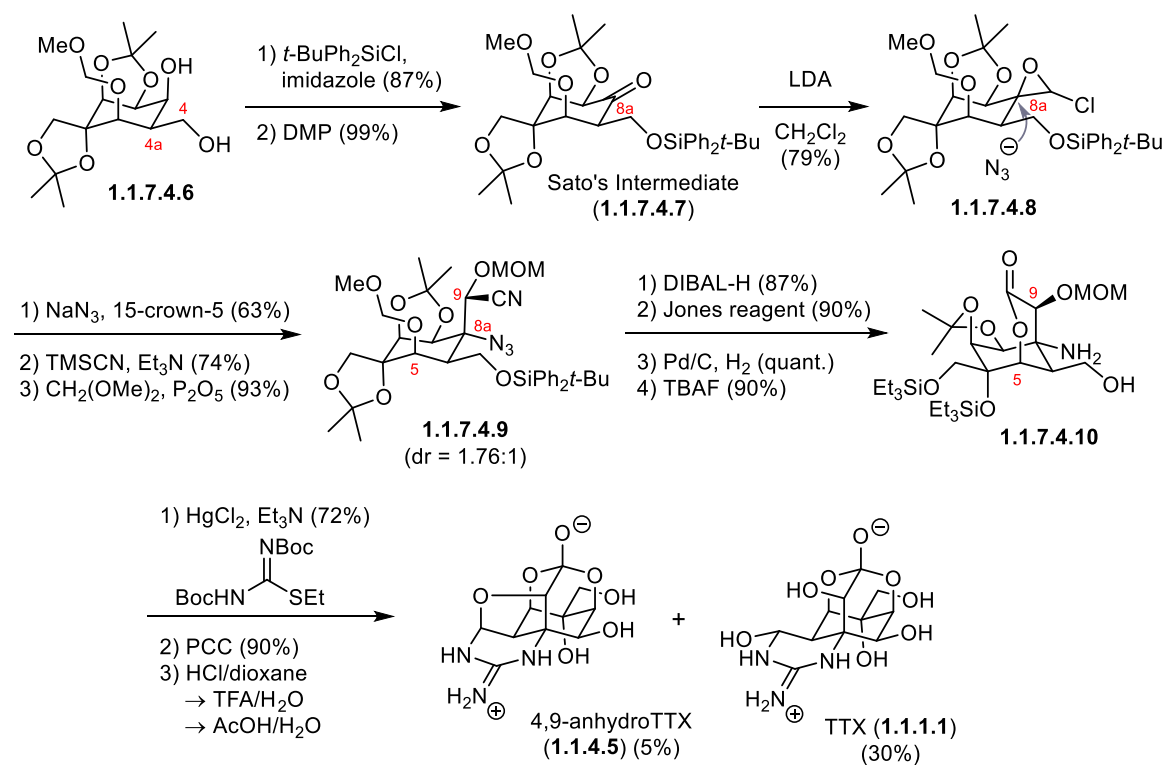
1.1.7.4 The Sato Synthesis of Tetrodotoxin

The approach of Sato and co-workers focused on converting polyhydroxylated sugar derivatives into TTX (1.1.1.1).¹¹⁴⁻¹¹⁶ Their first-generation strategy employed *myo*-inositol (1.1.7.4.1, Scheme 1.1.7.4.1) as a chiral starting material and used selective protecting group manipulations to focus a reaction to the desired hydroxy groups.¹¹⁶ The application of an ortho ester, benzyl and MOM groups provided a free alcohol at the C6 position (1.1.7.4.2) which was oxidized to the ketone using Swern conditions. Installation of a chloro epoxide and base-mediated epoxide-opening provided an α -hydroxy aldehyde which was reduced to the desired C6, C11 1,2-diol (1.1.7.4.3). A 6-step deprotection – protection sequence afforded the free C4a hydroxy group which was subjected to a Swern oxidation (1.1.7.4.5). The resulting ketone (1.1.7.4.5) was converted into an exo-methylene through a Petterson olefination and further modified to give the primary C4 alcohol via a hydroboration – oxidation procedure (1.1.7.4.6).



Scheme 1.1.7.4.1. Conversion of *myo*-inositol (1.1.7.4.1) to diol 1.1.7.4.6.

Protection of the primary alcohol with *t*-BuPh₂SiCl enabled the selective oxidation of the C8a alcohol to the ketone (Sato's intermediate, 1.1.7.4.7) (Scheme 1.1.7.4.2) which was reacted with lithium dichloromethide to give the chloro epoxide 1.1.7.4.8. Opening of the epoxide (1.1.7.4.8) with sodium azide set the C8a α -tertiary azide (1.1.7.4.9). A hydrocyanation diastereoselectively (*dr* = 1.76:1) set the C9-alcohol and introduced the C10 carbon atom. The nitrile 1.1.7.4.9 was reacted to the corresponding C5-bonded lactone by DIBAL-H reduction and Jones oxidation. Hydrogenation of the azide gave the α -tertiary amine 1.1.7.4.10 and was followed by Kishi guanidylation as well as oxidation of the C4 alcohol. Global acid-mediated deprotection finalized TTX (1.1.1.1) in a total of 32 steps from *myo*-inositol. Sato and co-workers have established two additional formal synthesis of TTX (1.1.1.1) which intercepted Sato's intermediate (1.1.7.4.7) and started from D-glucose.¹¹⁴⁻¹¹⁶

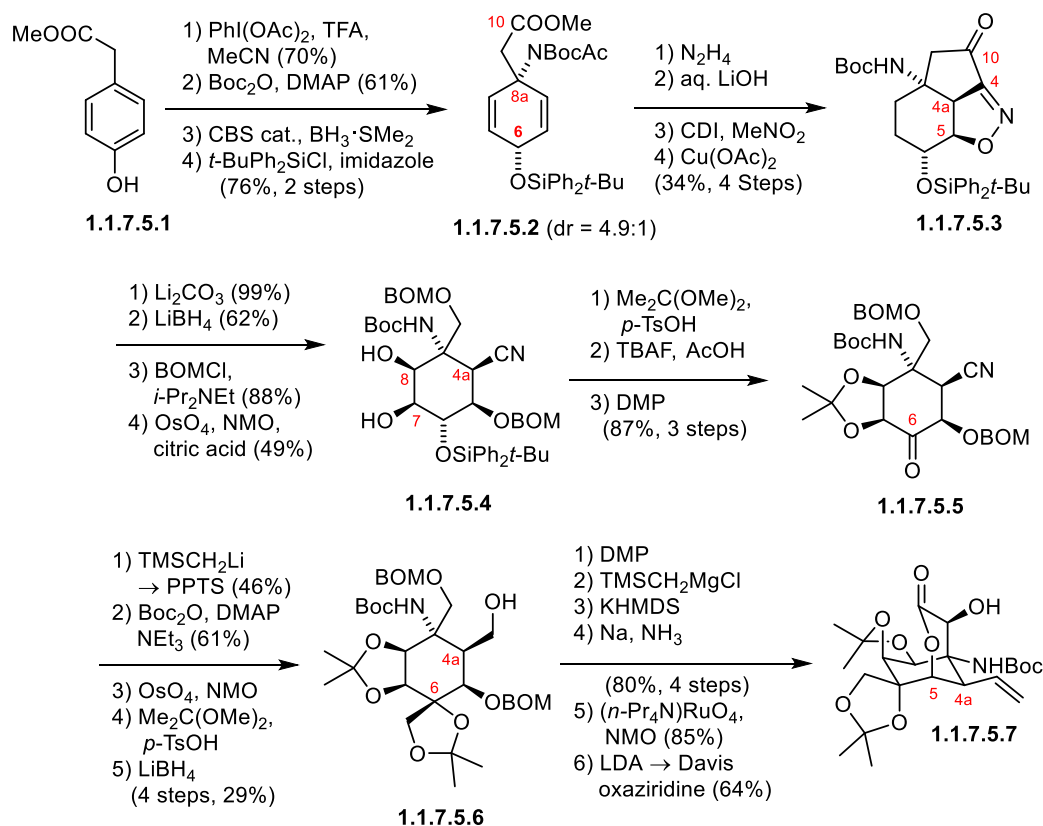


Scheme 1.1.7.4.2. Finalizing TTX (1.1.1.1) via Sato's intermediate (1.1.7.4.7).

1.1.7.5 The Ciufolini Synthesis of Tetrodotoxin

Ciufolini and co-workers established a formal synthesis of TTX (1.1.1.1) intercepting DuBois' intermediate 1.1.7.5.7 (Scheme 1.1.7.5.1).¹¹⁷⁻¹¹⁹ Their approach was based on an oxidative dearomative amidation methodology that provided the racemic α -tertiary amine (1.1.7.5.2) in the first step of the synthesis.¹²⁰ A CBS reduction set a C6 hydroxy stereocenter (1.1.7.5.2, dr = 4.9:1) which was necessary to perform the following steps with good diastereoselectivity. Thereafter, nitromethane was appended to the C10 ester and directly subjected to a 1,3-dipolar cycloaddition to install the C4 carbon and the C5 oxygen with the desired selectivity (1.1.7.5.3). The C10, C4 carbon-carbon bond was cleaved through a base-mediated rearrangement that provided a C4a nitrile and C5 alcohol (1.1.7.5.4) and regenerated the C10 acid. After reduction of the acid an BOM-protection, an Upjohn dihydroxylation afforded the C7, C8 1,2-diol 1.1.7.5.4. The C6 alcohol was oxidized to the ketone 1.1.7.5.5 and a Petterson olefination – Upjohn dihydroxylation sequence provided the C6, C11 1,2-diol (1.1.7.5.6). Protecting group manipulations helped to direct the reactivity towards the C4a nitrile and convert it to a vinyl group through a reduction – Dess-Martin oxidation – Patterson olefination approach. To finalize DuBois' intermediate 1.1.7.5.7, the C10 alcohol was subjected to a Ley oxidation which afforded the C5 bonded lactone (1.1.7.5.7). The generated bicyclic structure enabled the diastereoselective

installation of the C9 alcohol via Davis oxidation. Using this approach, TTX (**1.1.1.1**) could be prepared in a total of 30 steps.

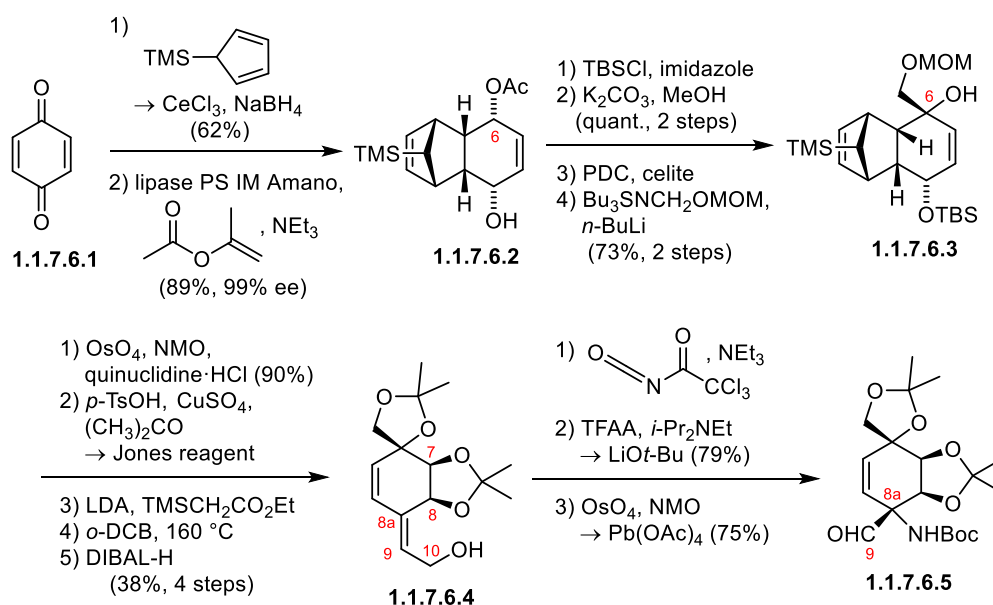


Scheme 1.1.7.5.1. Ciufolini's approach to TTX.

1.1.7.6 The Fukuyama Synthesis of Tetrodotoxin

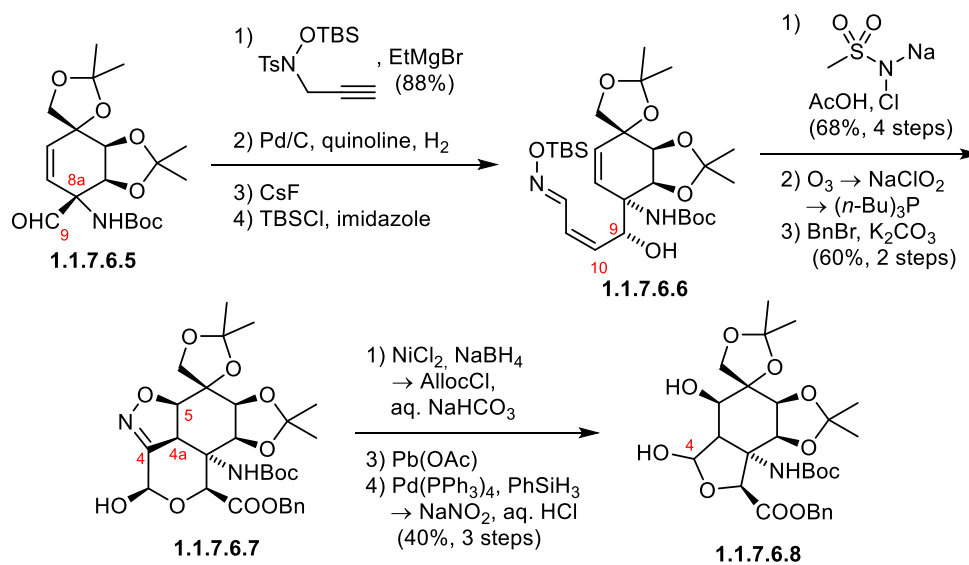
In their pursuit of TTX (**1.1.1.1**), Fukuyama and co-workers followed a strategy to form a reversible bicycle and use the bias of reactions to proceed from the convex face of this system to install the oxygenation pattern¹²¹. *Para*-benzoquinone (**1.1.7.6.1**) was reacted in a Diels-Alder reaction with 5-TMS-cyclopentadiene followed by reduction of the ketones to provide a 1,4-diol-substituted *cis*-fused bicycle (**1.1.7.6.2**). An enzymatic resolution was used to separate the enantiomers and the route was continued with the C6 acetate **1.1.7.6.2**. The C11 hydroxymethyl group was diastereoselectively appended through metal-mediated addition into the corresponding ketone (**1.1.7.6.3**) and the C7, C8 alkene was reacted in an Upjohn dihydroxylation to a 1,2-diol (**1.1.7.6.4**). To implement the C9, C10 segment, the C8a alcohol was oxidized and substituted via a Peterson olefination. 5-TMS-cyclohexadiene was then thermally extruded to liberate an alkene and the C10 ester was reduced to the alcohol **1.1.7.6.4**. The C10

alcohol was substituted with a carbamate unit, which underwent an Ichikawa rearrangement through a reaction with TFAA to give the C8a α -tertiary amine and a vinyl unit (**1.1.7.6.5**).



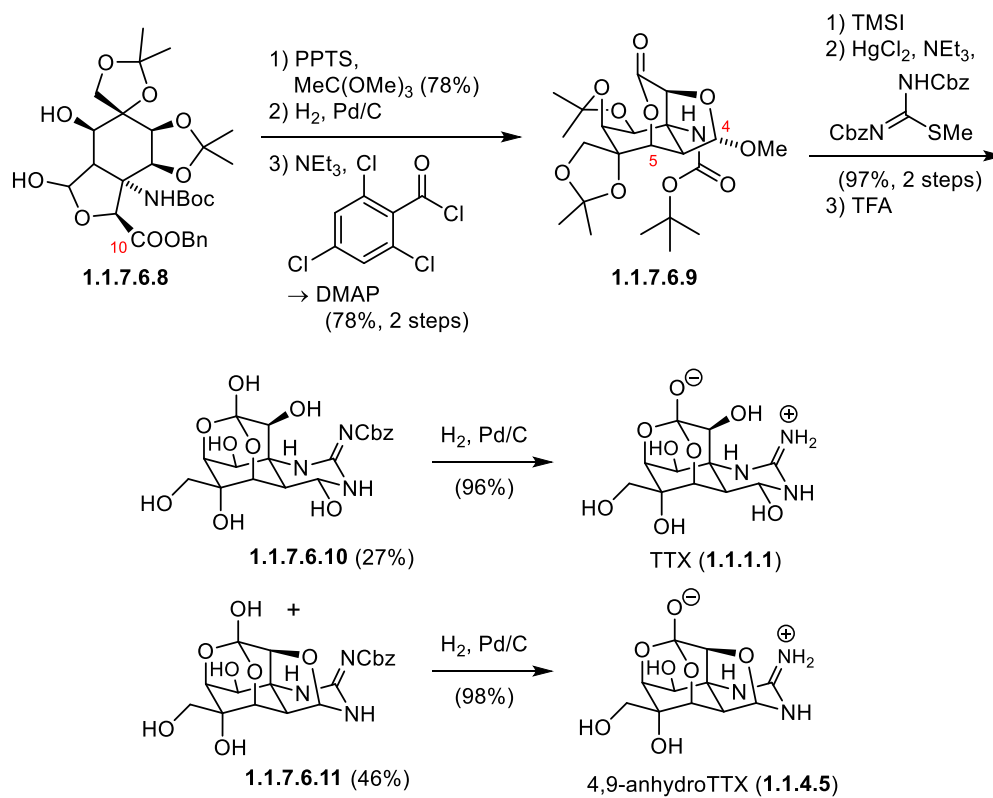
Scheme 1.1.7.6.1. Enantioselective synthesis of **1.1.7.6.5** from *para*-benzoquinone (**1.1.7.6.1**).

Oxidative alkene cleavage afforded the C9 aldehyde (**1.1.7.6.5**, Scheme 1.1.7.6.1) which was subjected to a metal-mediated alkynyl addition (Scheme 1.1.7.6.2). The addition followed a Cram chelate transition state and provided the desired stereoconfiguration of the C9 hydroxy group (**1.1.7.6.6**). The internal alkyne was partially hydrogenation to the *cis*-alkene which enabled a 1,3-dipolar cycloaddition onto cyclohexene by generation of a nitrile oxide from the protected hydroxylamine. This Huisgen cycloaddition resulted in a tricycle and diastereoselectively set the C5 carbon-oxygen bond as well as the C4a carbon-carbon bond (**1.1.7.6.7**). Oxidation state adjustments on the the tricyclic structure were performed through an ozonolysis and full reduction of the isoxazoline. The resulting 1,2-aminolactol was oxidatively cleaved and the amine was extruded from the aminal to provide the C4 lactol (**1.1.7.6.8**)



Scheme 1.1.7.6.2. Establishing the full carbon skeleton (**1.1.7.6.8**).

After debenzoylation to the C10 acid, a Yamaguchi esterification gave the six-membered lactone **1.1.7.6.9** by coupling with the C5 alcohol. The guanidine was installed using Kishi conditions which was followed by treatment with TFA to provide a mixture of Cbz-TTX (**1.1.7.6.10**) and Cbz-4,9-anhydroTTX (**1.1.7.6.11**). Removal of the Cbz group finalized TTX (**1.1.1.1**) and 4,9-anhydroTTX (**1.1.4.5**). It is worth noting that Fukuyama and co-workers have additionally synthesized 11-norTTX-6(*R*)-ol (**1.1.4.8**) through a modified version of this route.

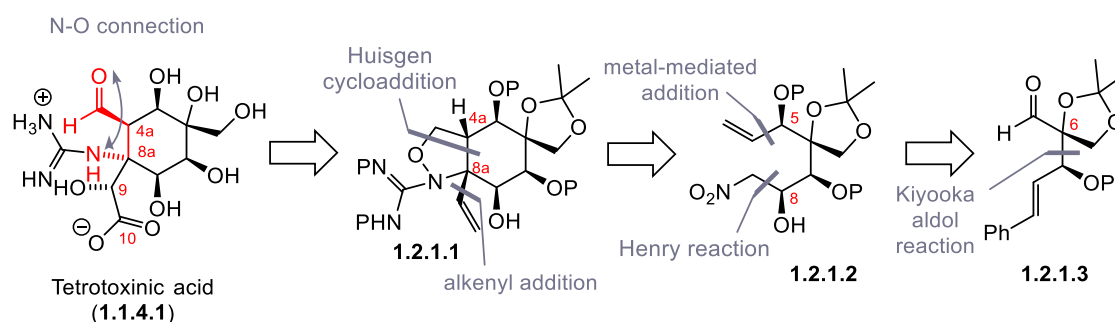


Scheme 1.1.7.6.3. Finalizing TTX (1.1.1.1) and 4,9-anhydroTTX (1.1.4.5).

1.2 Results and Discussion

1.2.1 Retrosynthetic Analysis of Tetrodotoxin

Tetrotoxinic acid (**1.1.4.1**) is in equilibrium with tetrodotoxin (**1.1.1.1**) and its isomers (Scheme 1.1.4.1, Chapter 1.1.4).⁵⁶ It is known to exist in solutions but cyclizes to the isolated natural products in solid form. Therefore, it serves as an excellent precursor to tetrodotoxin (**1.1.1.1**). Our retrosynthetic analysis of tetrodotoxinic acid (**1.1.4.1**) is based upon the premise that the latent C4 aldehyde and the C8a α -tertiary amine may arise from an isoxazolidine (**1.2.1.1**, Scheme 1.2.1.1). This isoxazolidine moiety (**1.2.1.1**) enables two reliable key retrons: a Huisgen 1,3-dipolar cycloaddition and a vinyl anion addition into the resulting oxime. Following these disconnections leads to a linear, densely functionalized nitro alkene (**1.2.1.2**). The oxygenation pattern of intermediate **1.2.1.2** could be built by exploiting acyclic stereocontrol. This approach is conceptual different to the previous syntheses of tetrodotoxin (**1.1.1.1**) (Chapter 1.1.7) and is envisaged to enable a rapid stereoselective construction of the fully functionalized cyclohexane core.

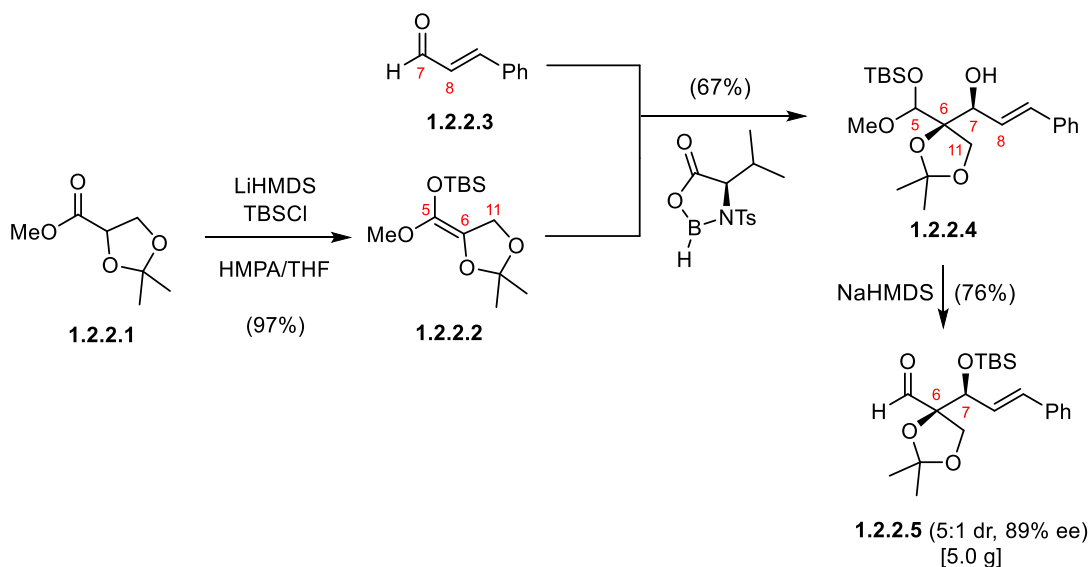


The C5 and C8 secondary alcohols (**1.2.1.2**) could be diastereoselectively installed through an ethynylmagnesium addition into an aldehyde and a Henry reaction, respectively, leading to **1.2.1.3**. The enantiomer of the TBS-protected aldehyde (**ent-1.2.1.3**) was previously prepared by Kalesse and co-workers via a enantio- and diastereoselective Kiyooka aldol reaction.¹²²

1.2.2 Establishing the Oxygenation Pattern on a Linear Precursor

We began the synthesis of TTX (**1.1.1.1**) with the preparation of the *tert*-butyldimethylsilyl (TBS) ketene acetal **1.2.2.2** from commercially available acetonide ester **1.2.2.1** (Scheme 1.2.2.1). The linear propyl chain of TBS ketene acetal **1.2.2.2** is incorporated as the C5, C6 and C11 carbons of

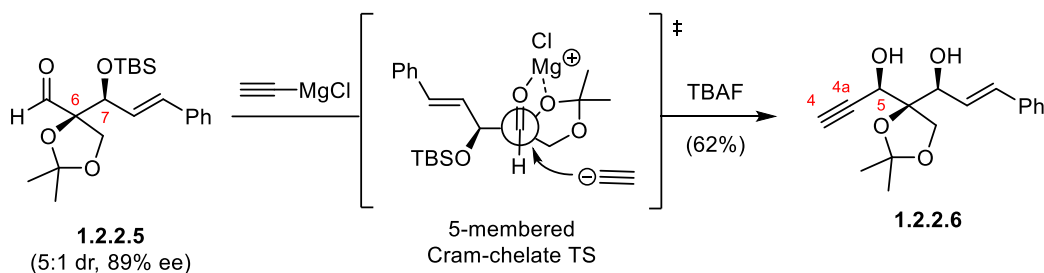
the target natural product (**1.1.1.1**). A Kiyooka aldol reaction is powerful key opening step as it is known to set quaternary stereocenters with excellent enantioselectivity and diastereoselectivity by using disubstituted TBS ketene acetals as nucleophiles.¹²³ In contrast to the trimethylsilyl (TMS) ketene acetal nucleophiles in Mukaiyama aldol reactions, the use of their TBS variants enables the *in situ* reduction of the latent ester group of **1.2.2.2** to the corresponding mixed *tert*-butyldimethylsilanol methanol acetal (**1.2.2.4**) via a hydride transfer from the chiral oxazaborolidinone reagent to the reaction intermediate. Using **1.2.2.2** as a nucleophile in Kiyooka aldol reactions was pioneered by Kalesse and co-workers who demonstrated that **ent-1.2.2.5** could be prepared on small scale.¹²² We devised a modified procedure for the multigram scale synthesis of aldehyde **1.2.2.5**. The reaction with cinnamaldehyde (**1.2.2.3**) appended the C7 and C8 carbons of TTX (**1.1.1.1**) and set the C6 tertiary alcohol and the C7 secondary alcohol stereocenters with 5:1 dr (**1.2.2.4**). Mosher ester analysis (Chapter 1.2.3) and X-Ray crystallography determined that the reaction afforded the desired enantiomer with 89% ee. A base-mediated silyl-transfer from the C5 acetal (**1.2.2.4**) to the C7 alcohol furnished aldehyde **1.2.2.5** on a 5 g scale in good overall yields.



Scheme 1.2.2.1. Modified procedure for the multigram scale synthesis of aldehyde **1.2.2.5**.

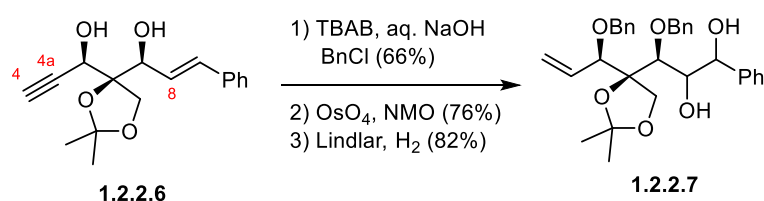
The C4 and C4a carbon atoms (**1.2.2.6**, Scheme 1.2.2.2) were installed through a metal-mediated ethynylmagnesium chloride addition into the corresponding aldehyde. This reaction proceeded through a 5-membered Cram chelate transition state¹²⁴ and provided the C5 secondary alcohol stereocenter with a 3.5:1 dr. After full conversion of aldehyde **1.2.2.5**, TBAF was added to the reaction in the same pot to provide the 1,3-diol **1.2.2.6**. The diastereomers were separated via

column chromatography to provide 62% of a single diastereomer of diol **1.2.2.6** from aldehyde **1.2.2.5**.



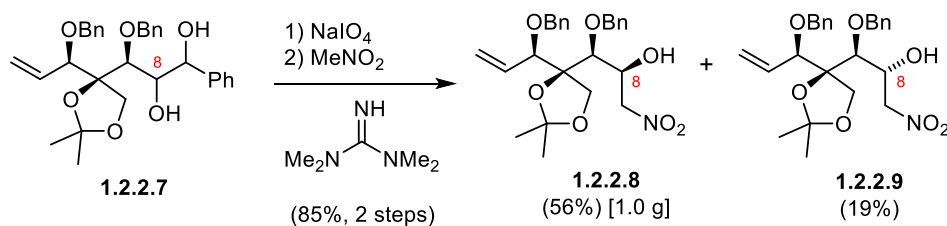
Scheme 1.2.2.2. Cram chelate-controlled ethynyl Grignard addition.

To liberate the C8 aldehyde for the Henry reaction and establish the nitro alkene precursor (**1.2.2.8**) for the Huisgen cycloaddition, the protection of the 1,3-diol (**1.2.2.6**) and the adjustment of the alkyne and styrene oxidation states were necessary. Preliminary protecting groups studies showed that benzylation provided the requisite stability and steric flexibility to enable the Henry reaction and subsequent 1,3-dipolar cycloaddition. The benzyl groups were installed in moderate yields (Scheme 1.2.2.3) and followed by an Upjohn dihydroxylation. Lindlar hydrogenation provided the terminal alkene **1.2.2.7** in good overall yields. To avoid the Lindlar hydrogenation step, we evaluated the addition of vinylmagnesium chloride to aldehyde **1.2.2.5** followed by benzylation of the 1,3-diol and regioselective dihydroxylation. Although the vinyl addition and benzylation procedure provided similar results to the reported ethynyl addition procedure, a regioselective styrene dihydroxylation in the presence of a mono-substituted alkene was not feasible.



Scheme 1.2.2.3. Protecting group and oxidation state adjustments to 1,2-diol **1.2.2.7**.

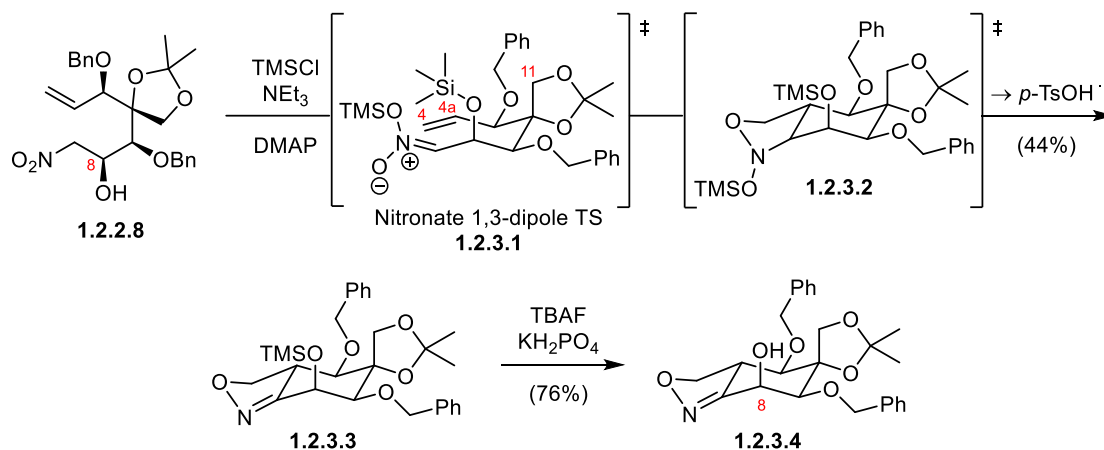
The 1,2-diol **1.2.2.7** (Scheme 1.2.2.4) was oxidatively cleaved to the corresponding C8 aldehyde and directly subjected to a gram scale TMG-mediated Henry reaction. The desired nitro alkene **1.2.2.8** was obtained as a 3:1 mixture with its C8 diastereomer **1.2.2.9** in good yields. The mixture could be separated using preparative reverse-phase HPLC purification.



Scheme 1.2.2.4. Diastereoselective Henry reaction.

1.2.3 The Huisgen 1,3-dipolar Cycloaddition

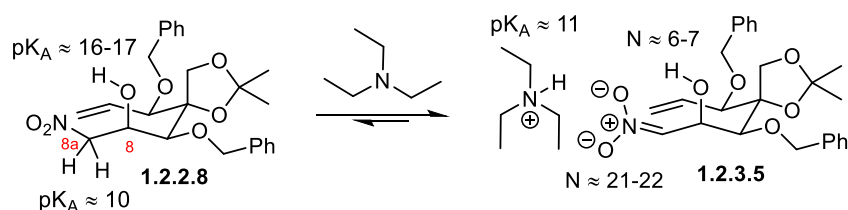
With the fully functionalized nitro alkene **1.2.2.8** in hand, we focused our attention towards establishing a procedure for the 1,3-dipolar cycloaddition (Scheme 1.2.3.1). *In situ* protection of the C8-hydroxy group and formation of a TMS-nitronate prompted the desired 1,3-dipolar cycloaddition with the C4, C4a alkene dipolarophile.¹²⁵ The reaction proceeded through a six-membered transition state (**1.2.3.1**) to give the intermediate **1.2.3.2** which eliminated TMSOH upon treatment with acid and provided the desired TMS-oxazoline **1.2.3.3**. It is worth noting, that a 3:1 mixture between **1.2.2.8** and **1.2.2.9** could be subjected to the reaction and exclusively provided the cyclization product **1.2.3.3**. TBAF-mediated TMS-deprotection afforded C8 hydroxy oxazolindine **1.2.3.4** that contained the central cyclohexane core of TTX (**1.1.1.1**) with the full oxygenation pattern.



Scheme 1.2.3.1. TMS-mediated nitronate 1,3-dipolar cycloaddition.

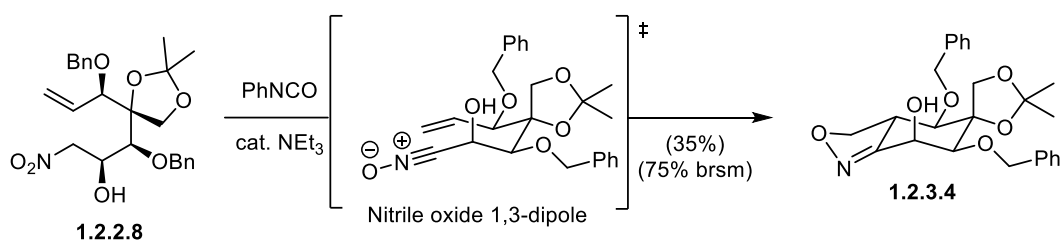
The drawback of using the TMSCl-mediated nitronate 1,3-dipolar cycloaddition, however, was that even the optimized conditions (Scheme 1.2.3.1) gave inconsistent yields in the range of 17%-46% with decomposition of the remaining starting material **1.2.2.8**. We hypothesized that a 1,3-diaxial interaction between the C11 methylene group and the C8 TMS group hinders the

formation of the six-membered transition state (**1.2.3.1**). In addition, a 1,3-allylic strain between the C8 TMS group and the TMS-nitronate (**1.2.3.1**) could interfere with the cycloaddition reaction. The use of a more flexible and less bulky C8 protecting group and the formation of a nitrile oxide 1,3-dipole could help to avoid these unfavorable interactions and improve the reaction yields. Attempts to substitute the C8 alcohol (**1.2.2.8**) with benzyl and *para*-methoxybenzyl (PMB) protecting groups did not provide the corresponding products. Therefore, our attempts focused on performing the Huisgen reaction in the presence of the free C8 alcohol. In theory (Scheme 1.2.3.2), the use of an amine base such as triethylamine (triethylammonium: $pK_A \approx 11$) could almost exclusively deprotonate the C8a protons (nitroethane: $pK_A \approx 10$) in the presence of the secondary C8 alcohol (secondary alcohols: $pK_A \approx 16-17$).¹²⁶⁻¹²⁷ After deprotonation, the nitroethane-derived anions ($N \approx 21-22$) are stronger nucleophiles than secondary alcohols ($N \approx 6-7$) or secondary alkoxides ($N \approx 17-18$) according to the Mayr scale.¹²⁸⁻¹³⁰ As a consequence, a selective dehydration of the C8a nitro group to the corresponding nitrile oxide could be facilitated by using triethylamine as a base without affecting the secondary alcohol.



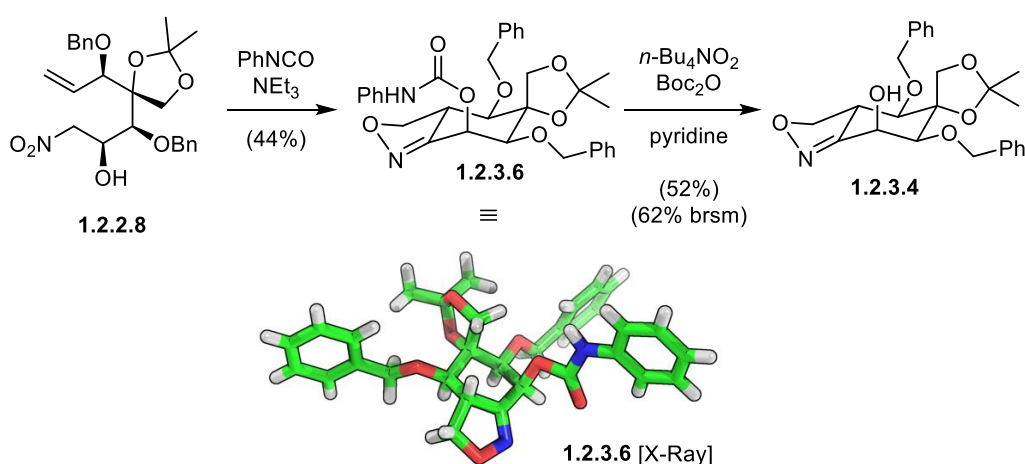
Scheme 1.2.3.2. pK_A and nucleophilicity of the cycloaddition precursor functionalities (**1.2.2.8**).

Based on our considerations, we subjected nitro alkene **1.2.2.8** (Scheme 1.2.3.3) to phenyl isocyanate and catalytic amounts of triethylamine. The reaction proceeded smoothly and after 43 h, the desired oxazoline **1.2.3.4** was obtained in 35% yield along with 53% recovered starting material. Due to the fact that the bulk of the starting material could be reisolated and that the reaction provides reliable yields without the need for further deprotection steps, this approach is a substantial improvement over the TMS-nitronate cycloaddition (Scheme 1.2.3.1).

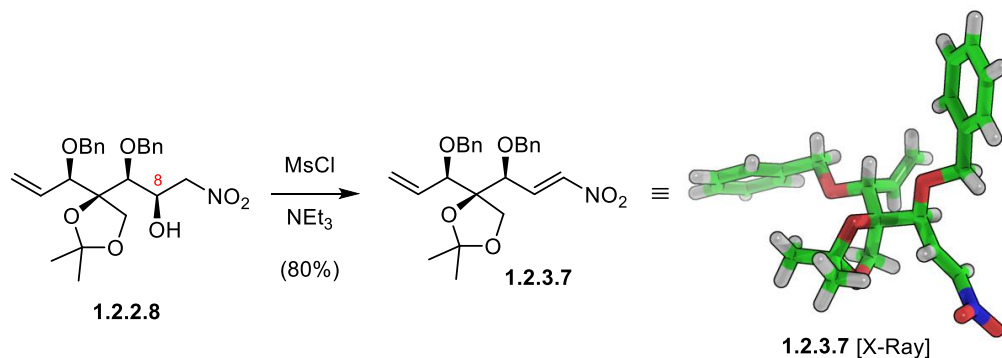


Scheme 1.2.3.3. Nitrile oxide 1,3-dipolar cycloaddition.

We found that prolonging the reaction beyond 43 h gradually transformed the product alcohol **1.2.3.4** to the C8 phenyl carbamate **1.2.3.6** (Scheme 1.2.3.4). Extending the reaction time to 142 h, for example, afforded **1.2.3.6** in 44% yield. After full conversion of nitro alkene **1.2.2.8** to **1.2.3.6**, the carbamate group could be removed to afford the corresponding alcohol **1.2.3.4**. However, the low overall yield of this 2-step sequence limits its utility for large scale cycloadditions. On the basis of these experiments, we could confirm the stereochemical configuration of our cycloaddition product through an X-Ray structure of the crystalline **1.2.3.6**.

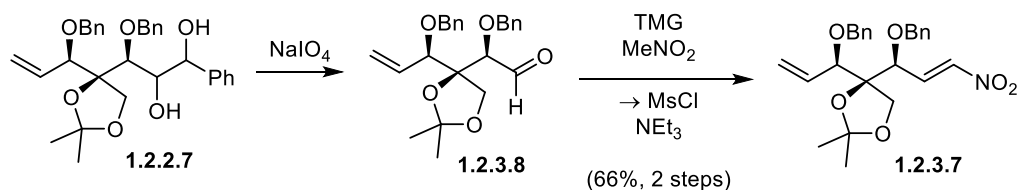
**Scheme 1.2.3.4.** Cycloaddition to carbamate **1.2.3.6** and deprotection alcohol **1.2.3.4**.

After finding a feasible route to access the oxazoline **1.2.3.4** and confirming its stereochemical configuration, we aimed to epimerize and recycle the Henry reaction byproduct **1.2.2.9**. Therefore, the C8 hydroxy group was eliminated to the crystalline α , β -unsaturated nitro alkene **1.2.3.7** (Scheme 1.2.3.4) and its structure was confirmed through X-Ray crystallography.



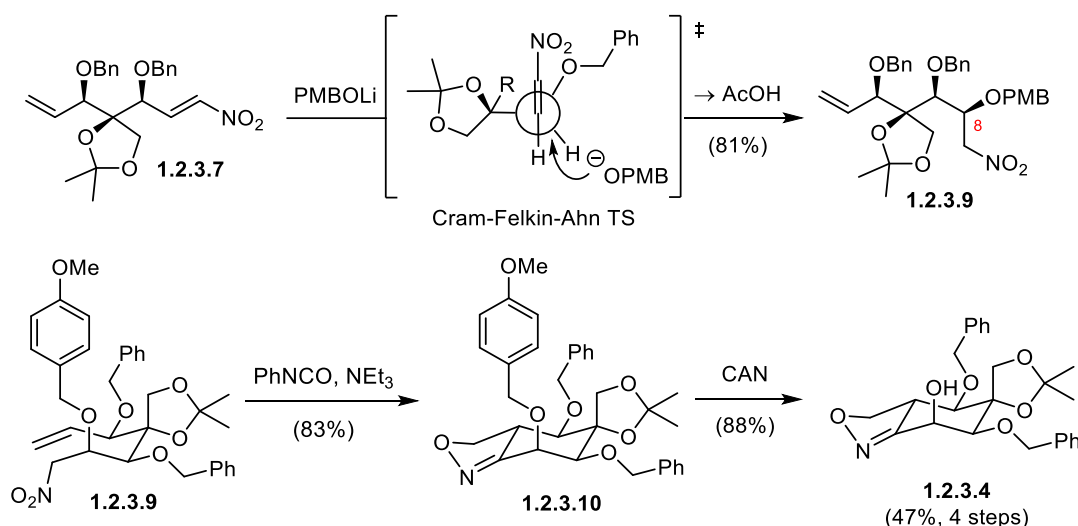
Scheme 1.2.3.5. Elimination of the C8 alcohol.

As an alternative to recycling the C8-(*R*)-configured nitro alkene **1.2.2.8**, the α , β -unsaturated nitro alkene **1.2.3.7** could be directly synthesized from diol **1.2.2.7** (Scheme 1.2.3.6). Oxidative diol cleavage afforded aldehyde **1.2.3.8**, which was directly subjected to a one-pot Henry condensation. The Michael system **1.2.3.7** was thereby obtained in 66% over 2 steps from diol **1.2.2.7**.

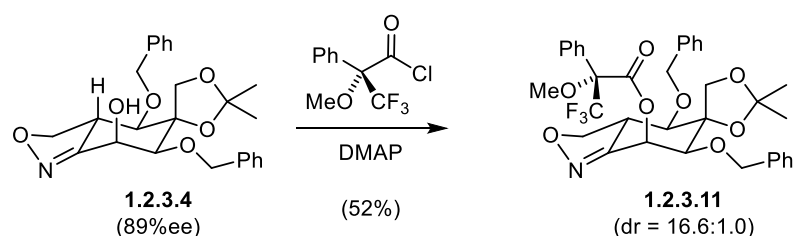


Scheme 1.2.3.6. Two-step procedure from diol **1.2.2.7** to α , β -unsaturated nitro alkene **1.2.3.7**

A Michael addition of PMBOLi into the α , β -unsaturated nitro alkene **1.2.3.7** was guided by a Cram-Felkin-Ahn transition state (Scheme 1.2.3.7) and exclusively afforded the desired (*S*)-configuration at C8. With the PMB alcohol **1.2.3.9** in hand, we confirmed our hypothesis that the yields of the cycloaddition could be improved by generating a nitrile oxide with a flexible and slim protecting group at the C8 position. Using PhNCO and NEt₃ provided 83% of PMB-substituted cyclohexane **1.2.3.10**, which was deprotected in good yields. In total, cyclohexanol **1.2.3.4** was obtained by recycling the C8-(*R*)-configured nitro alkene **1.2.2.9** in 47% yield over four steps or by direct synthesis from the diol **1.2.2.7** in 39% yield over five steps.

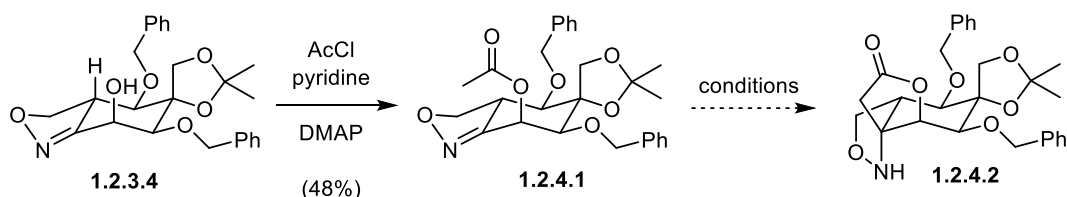


In order to analyze the enantiopurity of our cycloaddition product and the enantioselectivity of the Kiyooka aldol reaction, we prepared Mosher ester **1.2.3.11** by coupling alcohol **1.2.3.4** with (*S*)- α -methoxy- α -(trifluoromethyl)phenylacetyl chloride (Scheme 1.2.3.8). According to ^{19}F -NMR analysis, a 16.6:1.0 diastereomeric ratio was observed which corresponds to 89%ee for alcohol **1.2.3.4**.



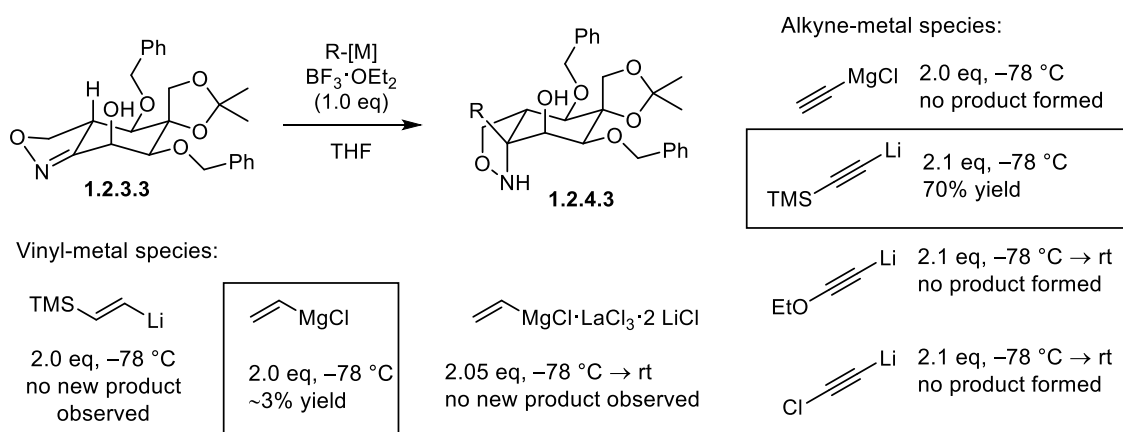
1.2.4 Setting the α -Tertiary Amine

Our attempts to convert the oxazoline **1.2.3.4** into an α -tertiary amine-containing oxazolidine focused on two approaches: a Mannich reaction (Scheme 1.2.4.1) and a metal-mediated ethynyl/vinyl addition into the ketoxime functionality (Scheme 1.2.4.2). For the evaluation of a Mannich-type reaction, alcohol **1.2.3.4** (Scheme 1.2.4.1) was acetylated to give acetate **1.2.4.1**. A series of acidic and basic conditions were explored with acetate **1.2.4.1** before attempting to combine of Lewis acids and Brønsted bases. However, the desired product lactone **1.2.4.2** could not be obtained.



Scheme 1.2.4.1. Exploring a Mannich reaction to the α -tertiary amine **1.2.4.2**.

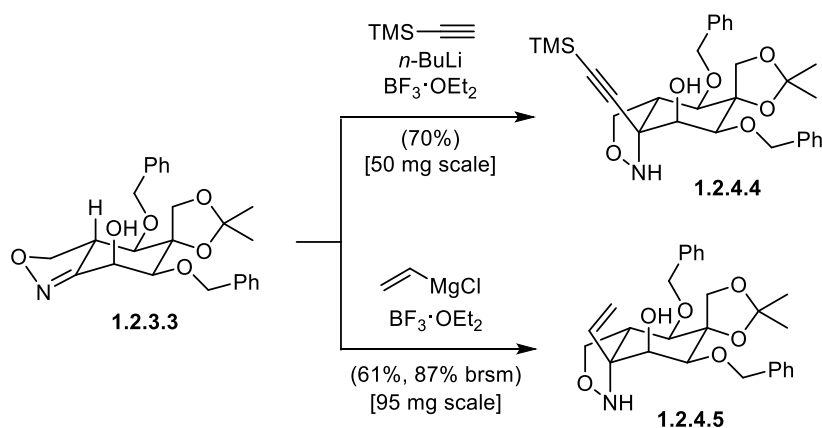
Next, the addition of a variety of vinyl/ethynyl metal species to oxazoline **1.2.3.4** was tested in the presence of the Lewis acid boron trifluoride (Scheme 1.2.4.2). We found that the success of the reaction did not only rely on the hybridization of the carbanion species and the metal counterion, but also on distant substitutions of the carbon fragment and minor electronic differences. For example, the use of ethynyl magnesium chloride, ethoxyethynyl lithium and chloroethynyl lithium did not provide the desired product. The addition of lithium TMS-acetylene on the other hand afforded the corresponding α -tertiary amine **1.2.4.3** in good yields. Vinyl species, such as (*E*)-(2-(trimethylsilyl)vinyl)lithium and $\text{LaCl}_3 \cdot 2\text{LiCl}$ -complexed vinylmagnesium chloride could not add into the ketoxime, but traces of product **1.2.4.3** were observed by performing the reaction with vinylmagnesium chloride.



Scheme 1.2.4.2. Exploring a metal-mediated addition into the ketoxime.

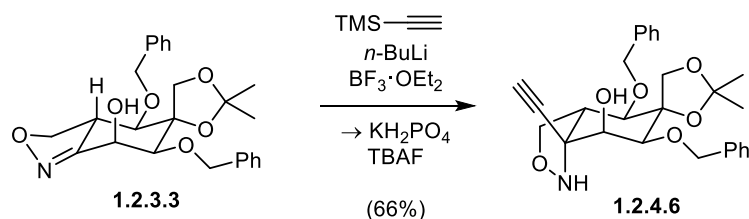
The great success of our metal-species screening (Scheme 1.2.4.2) has yielded procedures to prepare two version of the α -tertiary amine (**1.2.4.4** and **1.2.4.5**) with the desired diastereoselectivity. We reasoned that the stereochemical outcome of the reaction was the result of the strong bias for nucleophiles to approach from the convex face of the bicyclic structure (**1.2.3.4**) and the ability of the C8 hydroxy group act as a directing group.¹³¹ To enable a reliable preparation of these building blocks, the reactions were evaluated on a larger scales (50-

100 mg). The TMS-ethynyl lithium addition proceeded smoothly with 50 mg of the starting material **1.2.3.4** and afforded 70% of the oxazolidine **1.2.4.4** without the need to modify the reaction conditions. A good yield of the allyl amine **1.2.4.5** required to use 20 equivalents of vinylmagnesium chloride and to carefully adjust the temperature from $-70\text{ }^{\circ}\text{C}$ to $-50\text{ }^{\circ}\text{C}$ during the reaction. This approach provided 61% of the desired vinyl addition product **1.2.4.5** along with 30% recovered starting material **1.2.3.4** on a 95 mg scale.



Scheme 1.2.4.3. Optimized and scalable syntheses of the α -tertiary amines.

To avoid an additional TMS-deprotection step, we devised a one-pot procedure to directly synthesize terminal alkyne **1.2.4.6** (Scheme 1.2.4.4). This was achieved by addition of phosphate-buffered TBAF to the reaction mixture after full conversion of oxazoline **1.2.3.4** with lithium TMS-acetylene.

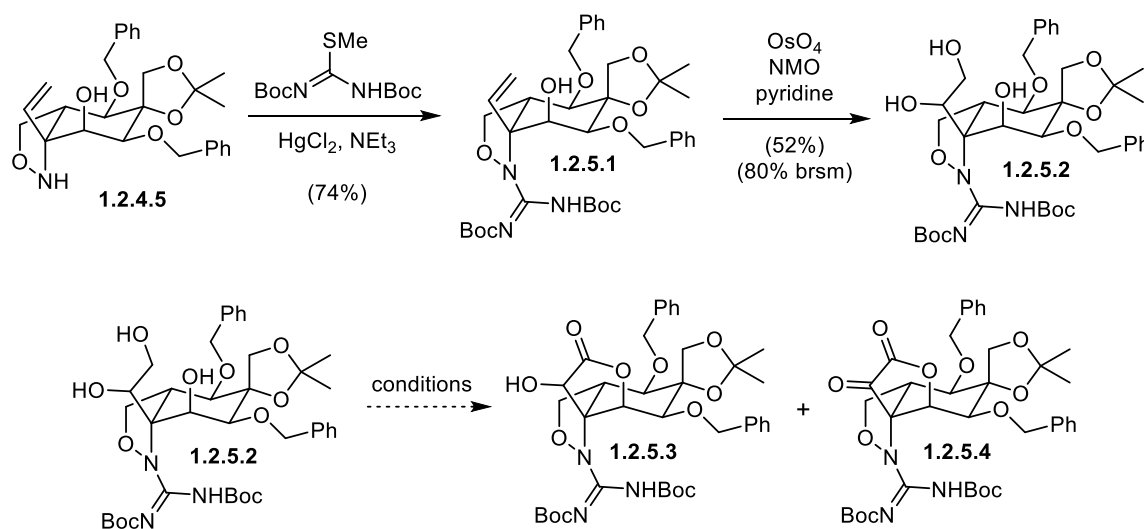


Scheme 1.2.4.4. One-pot alkyne-addition – TMS deprotection.

1.2.5 Installation of the α -Hydroxy Acid and Guanidylation

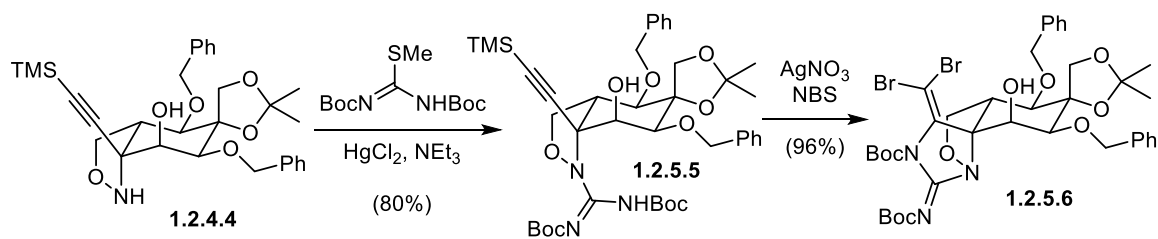
After successful diastereoselective preparation of the α -tertiary amine functionality, the next steps entailed the oxidation of the vinyl (**1.2.4.5**) or alkynyl (**1.2.4.4** and **1.2.4.6**) groups to the corresponding α -hydroxy ester and the installation of the guanidine moiety. Subjecting alkene **1.2.4.5** to Kishi guanidylation conditions (Scheme 1.2.5.1) provided the guanidinyloxazolidine

1.2.5.1 in good yields. A subsequent Upjohn dihydroxylation procedure that relied on the addition of pyridine as a co-solvent afforded C8, C9, C10 triol (**1.2.5.2**) in 52% yield along with 35% recovered starting material (**1.2.5.1**). An extensive study to oxidize triol **1.2.5.2** did not yield α -hydroxy ester **1.2.5.3** or α -keto ester **1.2.5.4**. Evaluated conditions included conditions such as PtO_2/O_2 , IBX, TEMBO/BAIB and TPAP/NMO.



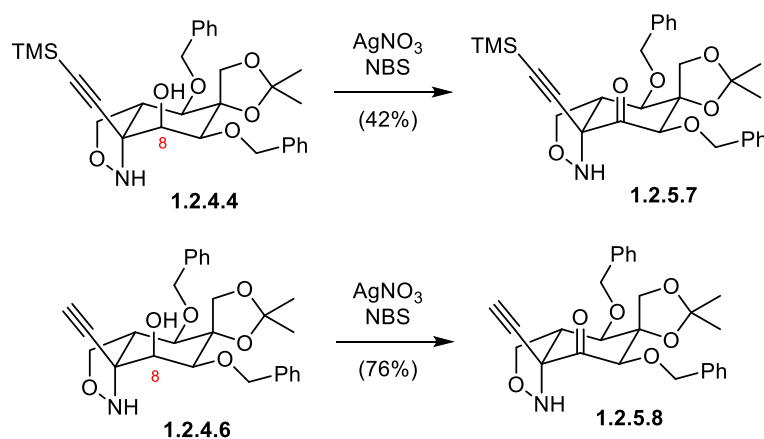
Scheme 1.2.5.1. Kishi guanidylation – oxidation sequence.

Due to the apparent difficulties to synthesize the α -hydroxy ester **1.2.5.3** from the guanidyl alkene **1.2.5.1**, we chose to evaluate the oxidation of the alkyne group (Scheme 1.2.5.2). The desired oxidation precursor **1.2.5.5** was prepared by Kishi guanidylation of oxazolidine **1.2.4.4** in good yields. Although we studied many conditions including KMnO_4 -, OsO_4 - and AgNO_3 -based reactions, we were unable to selectively oxidize the TMS-alkyne moiety (**1.2.5.5**) into an α -hydroxy ester **1.2.5.3** or α -keto ester **1.2.5.4**. It is well established that the silyl group of TMS-alkynes can be substituted for a bromide by using AgNO_3 and NBS.¹³² In general, these bromoalkynes are reliably oxidized to the α -keto ester or α -keto acid groups using KMnO_4 .¹³² Applying these conditions to TMS-alkyne **1.2.5.5** effected a bromo-cyclization¹³³ of the alkyne and gave a dibromo guanidyl enamine **1.2.5.6**. Although this was an unexpected result, the guanidinylenamine was a promising intermediate for oxidative or hydrolytic procedures. However, reagents such as OsO_4 , *p*-TsOH or HgCl_2 did not provide the desired products (**1.2.5.3** or **1.2.5.4**).



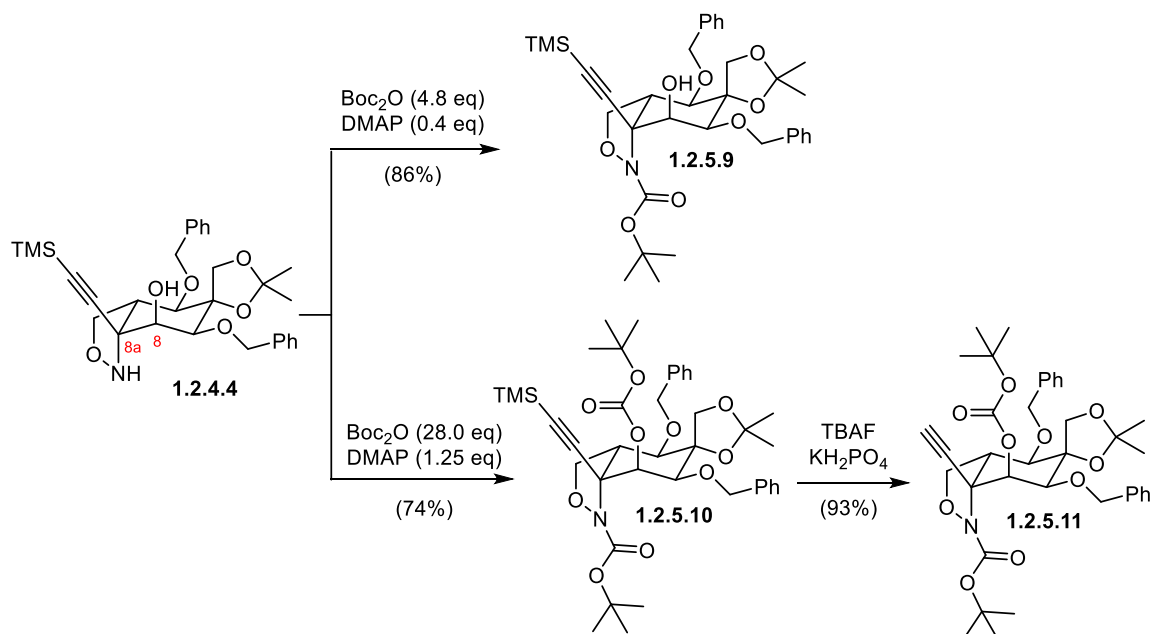
Scheme 1.2.5.2. Kishi guanidylation – cyclization.

Based on the failed attempts to oxidize triol **1.2.5.2**, TMS-alkyne **1.2.5.5** and guanidinylenamine **1.2.5.6** with well-established protocols, we hypothesized that our reactions were either hindered by the steric environment of the substrate or a specific functional group was not tolerated. To evaluate whether the guanidine interfered with the oxidation reactions, we focused on oxidizing the unsubstituted oxazolidinones **1.2.4.4** and **1.2.4.6**. Again, we observed decomposition of our substrates with the majority of oxidation procedures. Using AgNO_3 and NBS in an attempted TMS-bromine or hydrogen-bromine exchange,¹³² we observed a selective oxidation of the C8 alcohol to the ketone (**1.2.5.7** and **1.2.5.8**, Scheme 1.2.5.3).



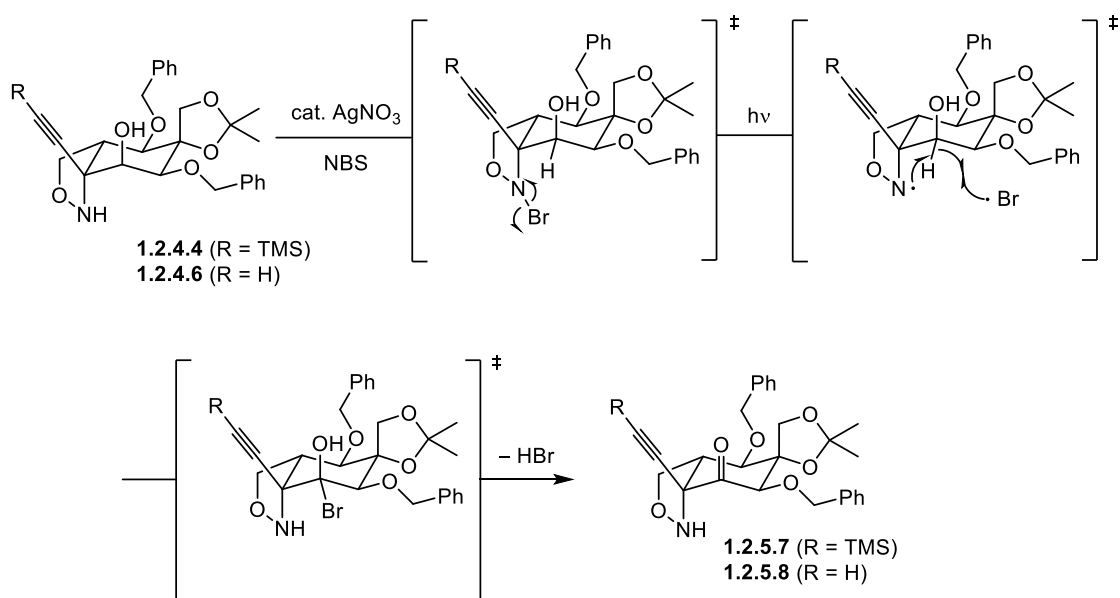
Scheme 1.2.5.3. Selective C8 alcohol oxidation to the ketone.

To further avoid any interference from the C8a hydroxylamine and/or C8 alcohol, we prepared protected version of our substrate **1.2.4.4**. By controlling the amounts of Boc_2O and DMAP used in the reaction, we afforded a mono-Boc substitution (**1.2.5.9**) with an unsubstituted C8 hydroxy group or a double Boc-substitution (**1.2.5.10**) in good yields. To remove the steric bulk around the alkyne, the TMS group (**1.2.5.10**) was removed to provide the terminal alkyne **1.2.5.11**.



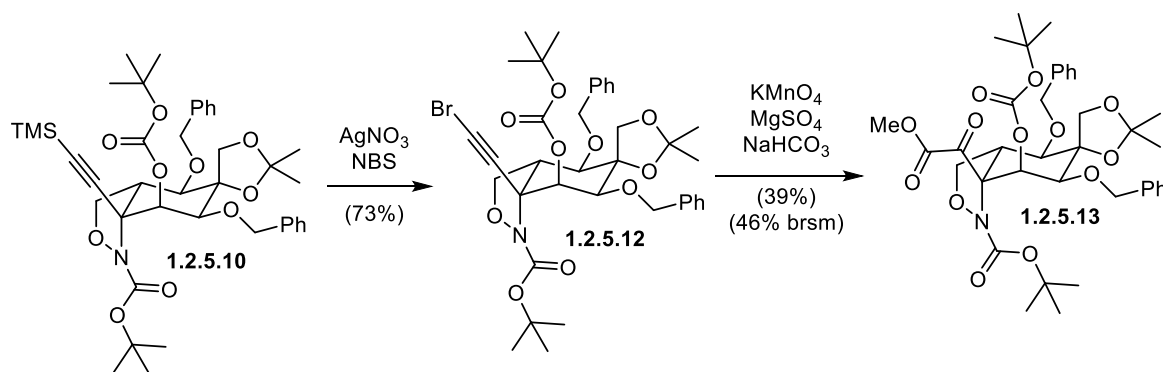
Scheme 1.2.5.4. Protecting group manipulations on aminoalcohol **1.2.4.4**.

With cyclohexanol **1.2.5.9** in hand, we tested if our newly discovered AgNO_3/NBS -mediated alcohol oxidation conditions are general or require the availability of the free C8a amine group. We found that subjecting the mono-Boc protected amino alcohol **1.2.5.9** to NBS in the presence of catalytic amounts of AgNO_3 did neither afford the C8 ketone nor the corresponding bromoalkyne. Therefore, it is reasonable to assume that the amine plays a crucial role for the oxidation reaction which could be explained by a Hoffmann-Löffler-Freytag-type mechanism (Scheme 1.2.5.5).



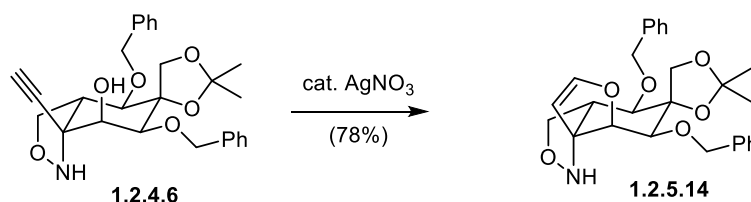
Scheme 1.2.5.5. Hoffmann-Löffler-Freytag-type mechanism for alcohol (**1.2.4.4** and **1.2.4.6**) oxidation.

After protection of the amine and alcohol functionalities (**1.2.5.10**), the TMS-bromine exchange was indeed feasible and provided bromide **1.2.5.12** in good yields (Scheme 1.2.5.6). The obtained substrate **1.2.5.12** reacted with KMnO_4 to give the desired α -keto ester moiety **1.2.5.13**. This successful reaction showed that the steric environment of the alkyne group does not hinder the oxidation reaction and confirmed our hypothesis that the guanidine as well as the free amine and alcohol groups interfered with the attempted reactions. However, the yield of **1.2.5.13** substantially dropped from 39% to 14% when the procedure was scaled from 8 mg to 16 mg. The limited scalability of this reaction does not allow for the preparation of the necessary product quantities to continue our synthesis and we focused our attention to an alternative approach.



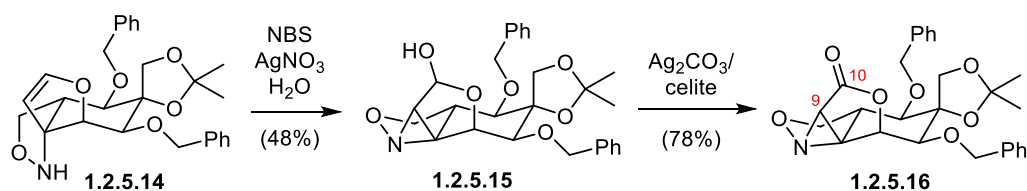
Scheme 1.2.5.6. Two-step oxidation of the TMS-alkyne **1.2.5.10** to α -keto ester **1.2.5.13**.

We reasoned that the low yields of the conversion of bromoalkyne **1.2.5.12** to α -keto ester **1.2.5.13** (Scheme 1.2.5.6) was a result of the low alkyne reactivity. Therefore, we planned to transform the alkyne **1.2.4.6** into a more reactive group, such as an enol ether moiety in dihydrofuran **1.2.5.14**. This was achieved through an AgNO_3 -catalyzed hydroalkoxylation in good yields (Scheme 1.2.5.7).



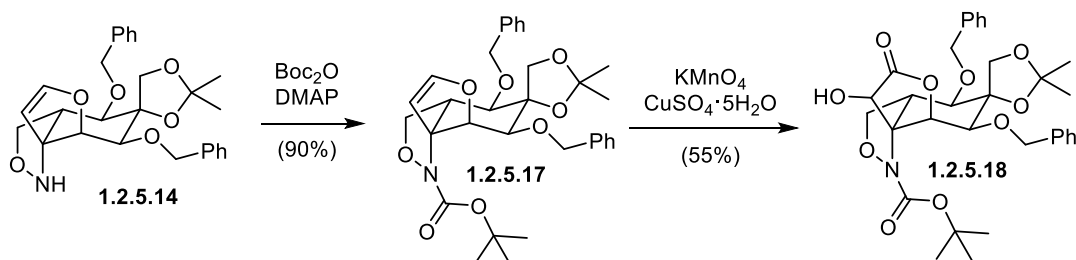
Scheme 1.2.5.7. Cyclization of hydroalkyne **1.2.4.6** to dihydrofuran **1.2.5.14**.

We were intrigued by the realization that AgNO_3 and NBS in combination with an unsubstituted oxazolidine could produce a nitrogen-centered radical (Scheme 1.2.5.5). With an appropriate substrate, the formation of this radical species could lead to a productive pathway and enable an alternative oxidation reaction. Therefore, dihydrofuran **1.2.5.14** was subjected to NBS with stoichiometric amounts of AgNO_3 and H_2O as co-solvent to allow for the direct substitution of a potentially formed bromide for a hydroxy group (Scheme 1.2.5.8). Indeed, the nitrogen radical reacted with the alkene moiety and provided aziridine lactol **1.2.5.15** which was converted to the corresponding lactone **1.2.5.16** through a Fetizon reaction.



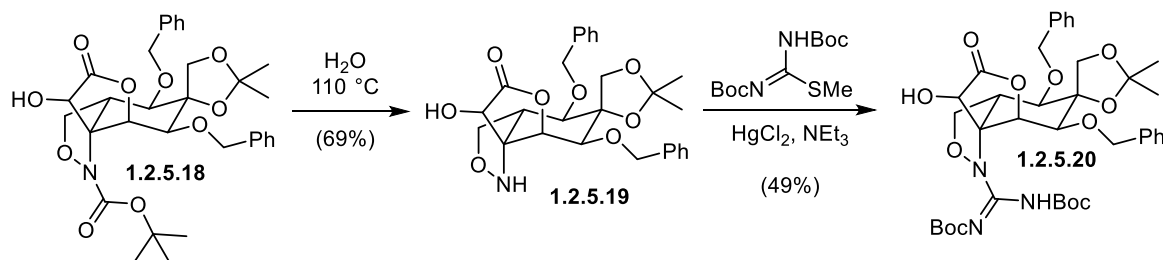
Scheme 1.2.5.8. Oxidative aziridination of **1.2.5.14** to lactone **1.2.5.16** via lactol **1.2.5.15**.

With the desired oxidation state at C9 and C10 (**1.2.5.16**) in hand, we evaluated common procedures to open the aziridine. However, a substitution of the aziridine at the C9 position was not feasible with an oxygen nucleophile. We have further studied conditions to oxidize the oxygen-substituted alkene group **1.2.5.14**, but did not afford the corresponding α -hydroxy ester or α -keto ester functionalities. In accordance with the results from the attempted alkyne oxidation (Scheme 1.2.5.2 – Scheme 1.2.5.6) we reasoned that in order to exclusively direct an oxidation to the alkene functionality (**1.2.5.14**) the oxazolidine nitrogen needs to be protected. Substitution of the oxazolidine (**1.2.5.14**) with Boc_2O proceeded smoothly to give the dihydrofuran **1.2.5.17** in excellent yields. This highly optimized substrate **1.2.5.17** contained a substituted C8 alcohol, a Boc-protected oxazolidine and a reactive alkene group. We tested oxidation conditions for the direct ketohydroxylation and found that the heterogenous $\text{KMnO}_4/\text{CuSO}_4$ reagent provided the highest yields of the desired α -hydroxy ester **1.2.5.18**.



Scheme 1.2.5.9. Ketohydroxylation of alkene **1.2.5.17**.

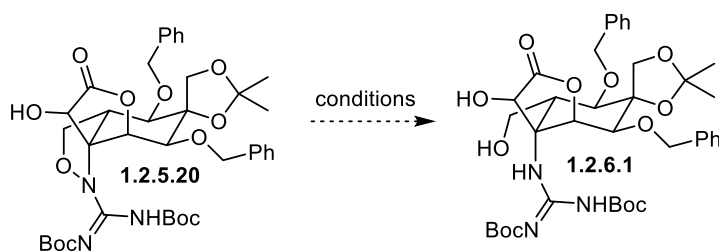
To install the guanidine group, the *tert*-butyl carbamate was first removed by boiling the α -hydroxy ester **1.2.5.18** in H₂O. The resulting oxazolidine **1.2.5.19** was subjected to a Kishi guanidylolation and gave the corresponding guanidine **1.2.5.20** in acceptable yields.



Scheme 1.2.5.10. Guanidine synthesis in the presence of the α -hydroxy ester.

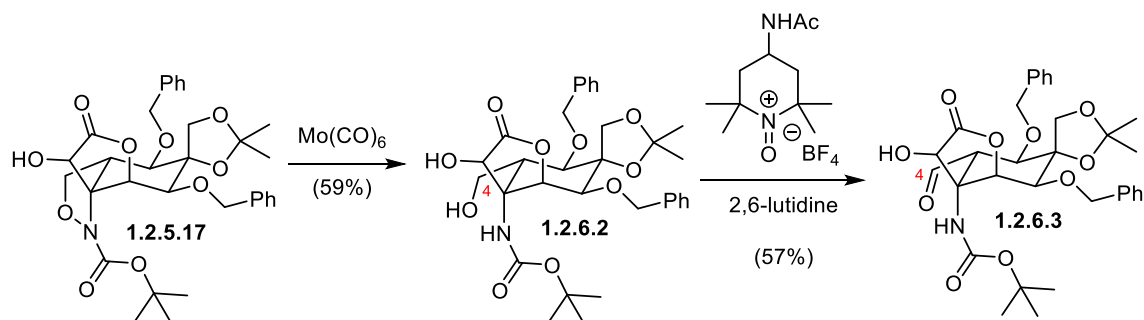
1.2.6 Endgame: Manipulating the N-O Bond and Protecting Groups

Finalizing TTX (**1.1.1.1**) relies on the reductive cleavage of the N-O bond, oxidation of the resulting primary alcohol, reductive removal of the benzyl groups and an acid-mediated deprotection – isomerization sequence. We first focused our attention on the reductive N-O bond cleavage and the oxidation of the resulting primary C4 alcohol. Subjecting the guanidine **1.2.5.20** to many reductive conditions, however, did not provide the corresponding alcohol **1.2.6.1**.



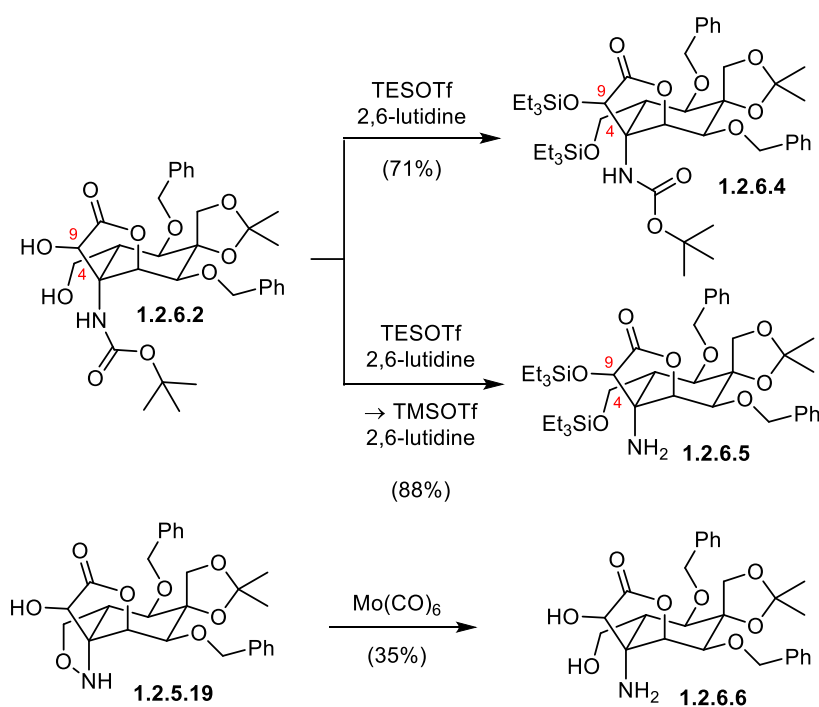
Scheme 1.2.6.1. Reductive N-O bond cleavage.

Due to the potential interference of the guanidine moiety, we continued our study with Boc-oxazolidine **1.2.5.18**. Using Mo(CO)₆ as a reducing agent provided the alcoholamine **1.2.6.2** which was selectively oxidized to the C4 aldehyde **1.2.6.3** using Bobbit's salt. This successful sequence afforded **1.2.6.3** which strongly supports the feasibility of our approach.



Scheme 1.2.6.2. N-O bond cleavage and selective primary alcohol oxidation to aldehyde **1.2.6.3**.

The obtained substrate **1.2.6.3** could not be further converted to either to an acetal-protected version of the aldehyde or the free aminoaldehyde by cleavage of the carbamate group. Therefore, we synthesized substrates with an alternative protecting group substitution profile to find an optimal candidate for the following guanidylation – C4 alcohol oxidation sequence. For example, TES-protection of the C4 and C9 alcohols (**1.2.6.2**) (Scheme 1.2.6.3) proceeded to give TES carbamate **1.2.6.4**. By addition of TMSOTf into the reaction mixture after full conversion of the diol **1.2.6.2**, we devised a one-pot procedure for the TES-protection – carbamate deprotection and afforded amine **1.2.6.5** in good yields. A free C4, C9 1,3-diol C8a amine **1.2.6.6** was obtained by applying the $\text{Mo}(\text{CO})_6$ -mediated reduction to oxazolidine **1.2.5.19**.

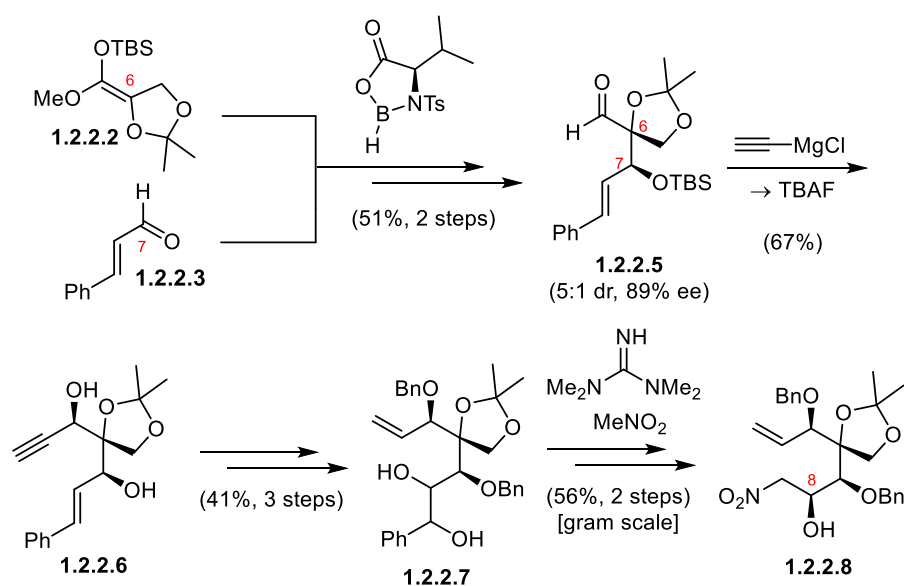


Scheme 1.2.6.3. Establishing different protecting group substitution profiles on **1.2.6.2**.

1.3 Conclusion and Outlook

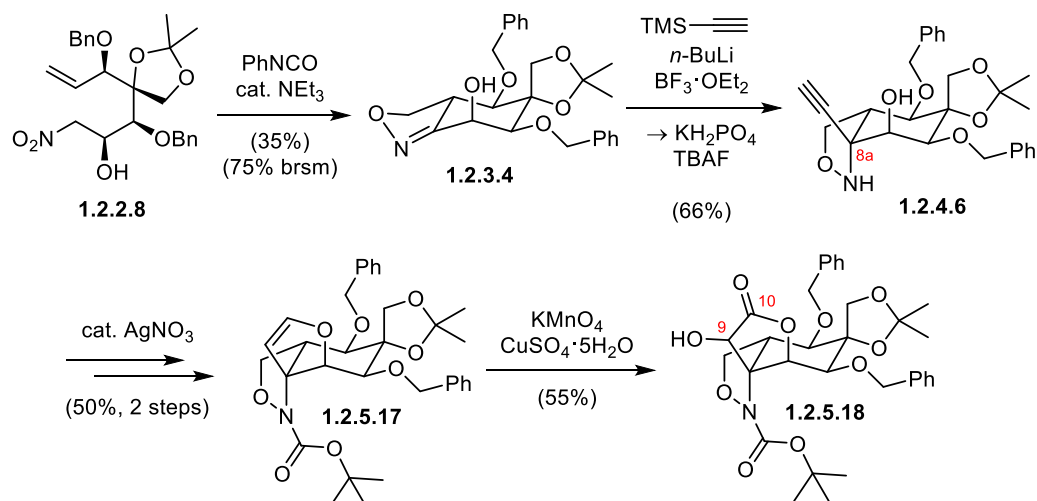
1.3.1 Summary

In summary, we have established a 16-step route to late-stage building blocks **1.2.5.20**, **1.2.6.3**, **1.2.6.6** as part of our synthesis of TTX (**1.1.1.1**). The oxygenation pattern on the cyclohexane was built by exploiting acyclic stereocontrol. This approach is conceptual different to the previous syntheses of tetrodotoxin (Chapter 1.1.7) and has enabled a rapid 9-step stereoselective construction of a fully functionalized cyclization precursor **1.2.2.8** (Scheme 1.3.1.1). The C6 tertiary alcohol and C7 secondary alcohol stereocenters were set in through a Kiyooka aldol reaction which provided aldehyde **1.2.2.5** with 5:1 dr and 89% ee. The C5 secondary alcohol was installed through a Cram chelate-controlled ethynyl magnesium chloride addition, whereas the C8 secondary alcohol was the result of a diastereoselective Henry reaction.



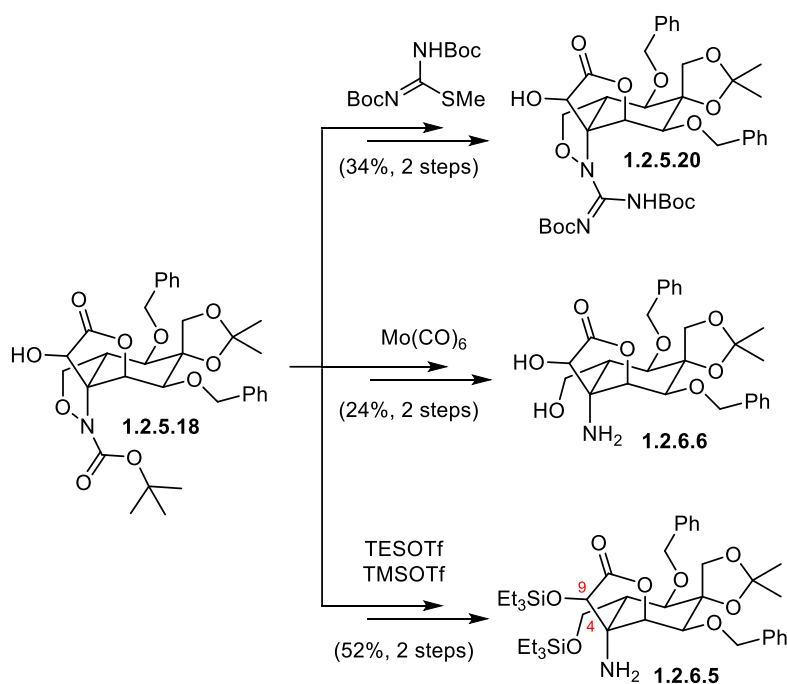
Scheme 1.3.1.1. Synthesis of the oxygenation pattern on a linear precursor.

The key nitrile oxide 1,3-dipolar cycloaddition proceeded with excellent diastereoselectivity and provided the bicycle **1.2.3.4** (Scheme 1.3.1.2). To install the α -tertiary amine and provide the full carbon skeleton of TTX (**1.1.1.1**), lithium TMS-alkyne was added from the sterically more accessible convex face of the bicycle into the oxazoline (**1.2.3.4**) and provided oxazolidine **1.2.4.6**. The synthesis of α -hydroxy ester (**1.2.5.18**) was achieved in a total of 14 steps through an AgNO_3 -catalyzed alkyne cyclization followed by KMnO_4 -mediated ketohydroxylation.



Scheme 1.3.1.2. Setting the α -tertiary amine and α -hydroxy ester functionalities.

To evaluate the late-stage redox adjustments, deprotection and isomerization procedures (see Chapter 1.3.2), we prepared the three substrates: guanidinyloxazolidine **1.2.5.20**, diolamine **1.2.6.6** and amine **1.2.6.5** (Scheme 1.3.1.3). These compounds were prepared in two steps from α -hydroxy ester **1.2.5.18**, which amounts to a total of 16 steps from a commercial precursor (**1.2.2.1**). This rapid construction of the full carbon skeleton and heteroatom substitution pattern (**1.2.5.20**) is a result of our strategic disconnections. These disconnections are in strong contrast to previous approaches (Chapter 1.1.7) which have relied on 28 steps or more to finalize the natural product (**1.1.1.1**).

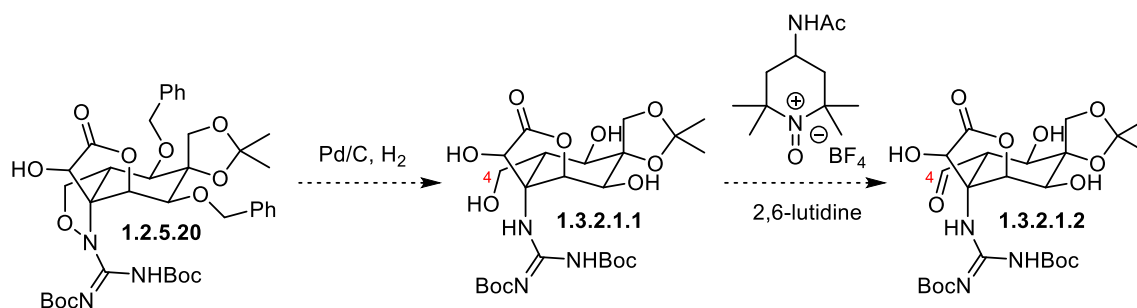


Scheme 1.3.1.3. Synthesizing late-stage substrates for redox adjustment and deprotection studies.

1.3.2 Outlook

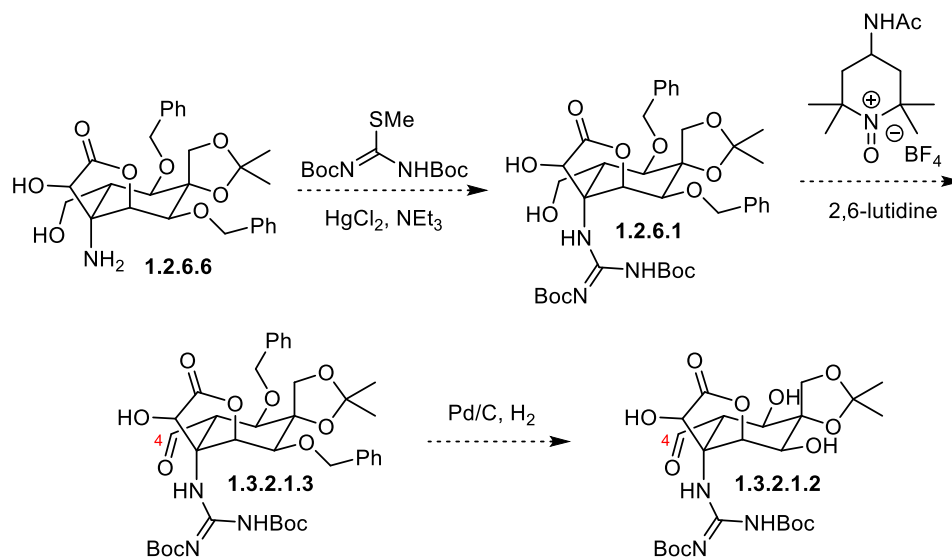
1.3.2.1 Oxidation State Adjustments and Deprotection

To finalize TTX (**1.1.1.1**), we are planning to pursue two approaches that are based on the most advanced substrates: guanidine **1.2.5.20** and diolamine **1.2.6.6**. Ideally, the benzyl groups and the N-O bond of guanidinyloxazolidine **1.2.5.20** could be cleaved through a heterogeneous hydrogenation procedure.¹³⁴ A selective primary alcohol oxidation, such as the Bobbit reaction,¹³⁵ could selectively oxidize the C4 alcohol of tetraol **1.3.2.1.1** and establish the isomerization precursor **1.3.2.1.2**.



Scheme 1.3.2.1.1. Hydrogenation – primary alcohol oxidation sequence to **1.3.2.1.2**.

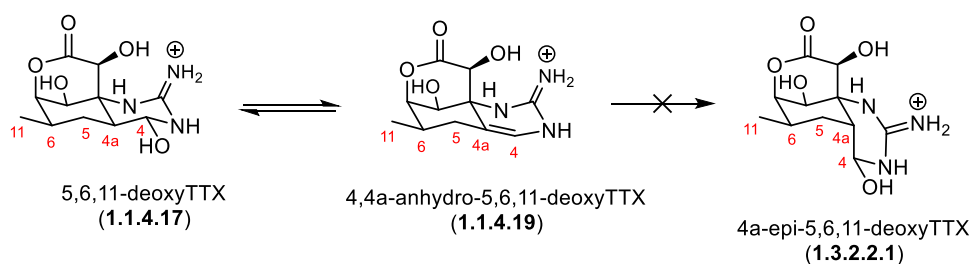
Since we have evaluated many hydrogenation procedures for the preparation of **1.3.2.1.2** without success, an alternative plan was formed which relies on the oxidation state adjustments on diolamine **1.2.6.6** followed by late-stage benzyl group cleavage. The Kishi guanidylation could selectively target the amine without affecting the free alcohol groups (**1.2.6.1**).¹¹⁶ A selective primary alcohol oxidation, such as the Bobbit reaction, could be used to install the C4 aldehyde oxidation state (**1.3.2.1.3**).¹³⁵ This approach would allow us to use a more diverse set of conditions for the benzyl group cleavage (**1.3.2.1.2**), such as oxidation reagents and Lewis acids, without focusing solely on reductive hydrogenations.



Scheme 1.3.2.1.2. Guanidylation – primary alcohol oxidation – hydrogenation sequence.

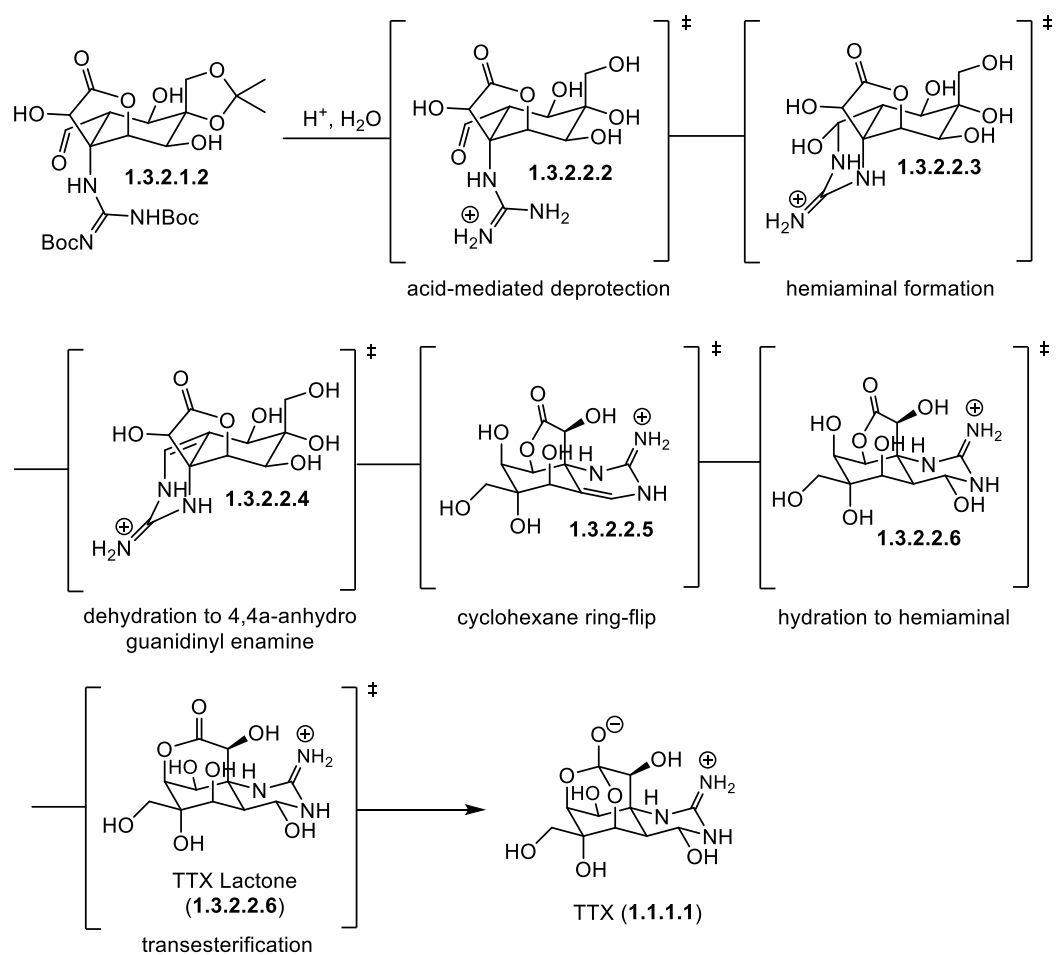
1.3.2.2 Isomerization Cascade

Finalizing TTX (**1.1.1.1**) from **1.3.2.1.2** requires the cleavage of the guanidine Boc-groups, hydrolysis of the acetonide moiety, isomerization of the C4a stereocenter and transesterification of the C10 ester group from the C8 alcohol to form a C5, C7-bridged ortho acid. We hypothesize that these steps could be performed by treatment of **1.3.2.1.2** with an aqueous acid. These conditions are known to reliably cleave Boc groups and mediated acetonide hydrolysis and we envisage that this procedure could also affect the desired isomerization cascade.¹¹² We base our hypothesis on the observed thermodynamic stability of TTX (**1.1.1.1**) and its derivatives (Chapter 1.1.4). For instance, stable 4,4a-anhydro-5,6,11-trideoxyTTX (**1.1.4.19**) exists and is in equilibrium with 5,6,11-deoxyTTX (**1.1.4.17**) but the isomerization product 4a-epi-5,6,11-deoxyTTX (**1.3.2.2.1**, Scheme 1.3.2.2.1) has not been isolated. Therefore, it is reasonable to assume that the bicyclic framework of TTX (**1.1.1.1**) is thermodynamically favorable.



Scheme 1.3.2.2.1. Isomerization pathways of 5,6,11-deoxyTTX (**1.1.4.17**).

It was shown by the opening of the C5, C7 ortho acid of TTX (1.1.1.1) to the corresponding carboxylic acid in boiling H₂O as part of the formation of tetrodonic acid (1.1.4.6) that a cleavage of the ester bond is a facile process and even proceeds under neutral conditions. The C5, C7 ortho acid of TTX (1.1.1.1), the C7 lactone of TTX lactone (1.1.4.3) and C10 acid of tetrotoxinic acid are the only observed connectivities of the C10 group and it is thus likely that the ortho acid forms from by transesterification of the C8 ester (1.3.2.1.2). Based on these considerations, we propose that an acid-mediated deprotection to 1.3.2.2.2 is followed by a cyclohexane ring-flip to 1.3.2.2.5 which is aided by the formation of a 4,4a-anhydro guandiy enamine 1.3.2.2.4 via the hemiaminal 1.3.2.2.3. Hydration of the guanidiny enamine 1.3.2.2.5 to the hemiaminal 1.3.2.2.6 and transesterification via TTX lactone 1.1.4.3 is envisaged to furnish TTX (1.1.1.1).



Scheme 1.3.2.2.2. Proposed acid mediated deprotection – isomerization cascade.

Chapter 2 – The Design of Lipid- and Glutamate-
based Photopharmaceuticals

2 The Design of Glutamate- and Lipid-based Photopharmaceuticals

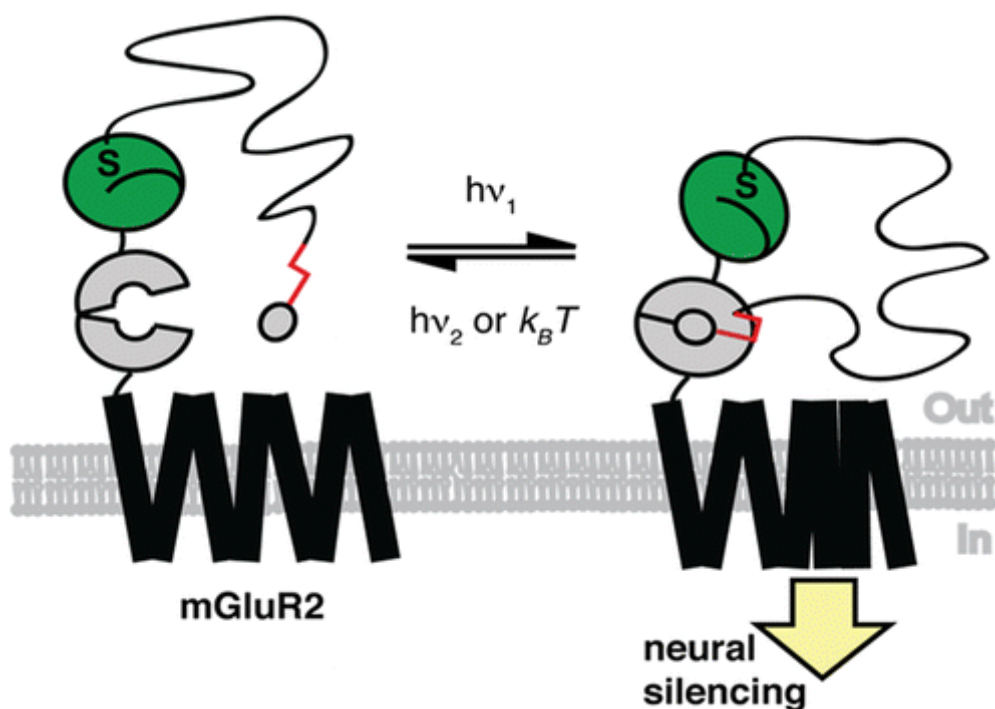
2.1 Glutamate-based Photopharmaceuticals

2.1.1 Orthogonal Optical Control of a G Protein-Coupled Receptor with a SNAP-Tethered Photochromic Ligand

Reprinted with permission from:

Johannes Broichhagen, Arunas Damijonaitis, Joshua Levitz, Kevin R. Sokol, Philipp Leippe, David Konrad, Ehud Y. Isacoff, and Dirk Trauner, *ACS Cent. Sci.* **2015**, *1*, 383–393.

Copyright © 2015 American Chemical Society



The author David B. Konrad contributed to: the design and chemical synthesis of the red-shifted PORTL BGAG₁₂₍₄₆₀₎.

This is an open access article published under an ACS AuthorChoice License, which permits copying and redistribution of the article or any adaptations for non-commercial purposes.



ACS
central
science

Research Article

http://pubs.acs.org/journal/acscii

Orthogonal Optical Control of a G Protein-Coupled Receptor with a SNAP-Tethered Photochromic Ligand

Johannes Broichhagen,^{†,‡,§} Arunas Damijonaitis,^{†,‡,§} Joshua Levitz,^{§,||} Kevin R. Sokol,^{†,‡} Philipp Leippe,^{†,‡} David Konrad,^{†,‡} Ehud Y. Isacoff,^{||,⊥,#} and Dirk Trauner^{*,†,‡}

[†]Department of Chemistry, Ludwig-Maximilians-Universität München, Butenandtstrasse 5-13, 81377 München, Germany

[‡]Munich Center for Integrated Protein Science, Butenandtstrasse 5-13, 81377 München, Germany

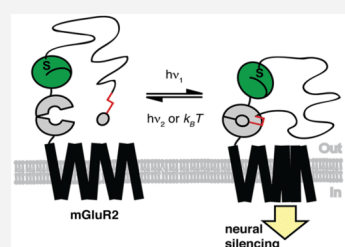
^{||}Department of Molecular and Cell Biology, University of California, Berkeley, California 94720, United States

[⊥]Helen Wills Neuroscience Institute, University of California, Berkeley, California 94720, United States

[#]Physical Bioscience Division, Lawrence Berkeley National Laboratory, Berkeley, California 94720, United States

Supporting Information

ABSTRACT: The covalent attachment of synthetic photoswitches is a general approach to impart light sensitivity onto native receptors. It mimics the logic of natural photoreceptors and significantly expands the reach of optogenetics. Here we describe a novel photoswitch design—the photo-switchable orthogonal remotely tethered ligand (PORTL)—that combines the genetically encoded SNAP-tag with photochromic ligands connected to a benzylguanine via a long flexible linker. We use the method to convert the G protein-coupled receptor mGluR2, a metabotropic glutamate receptor, into a photoreceptor (SNAG-mGluR2) that provides efficient optical control over the neuronal functions of mGluR2: presynaptic inhibition and control of excitability. The PORTL approach enables multiplexed optical control of different native receptors using distinct bioconjugation methods. It should be broadly applicable since SNAP-tags have proven to be reliable, many SNAP-tagged receptors are already available, and photochromic ligands on a long leash are readily designed and synthesized.



INTRODUCTION

The ability to covalently link synthetic molecules with proteins has significantly increased the power of molecular biology and has provided new therapeutic approaches via antibody drug conjugates. In recent years, chemical biologists have developed methods that not only can be used *in vitro* and in cell cultures but also can be applied *in vivo*, even in large animals and, potentially, in humans.¹

Important issues in bioconjugation are the speed, selectivity, and orthogonality of the reaction and the extent to which the target protein needs to be modified to enable covalent attachment. Engineered cysteines have proved popular since they represent a minimal change in the protein structure and reliably react with certain electrophiles, such as maleimides.¹ More selective methods depend on the expansion of the genetic code² and otherwise inert molecules that specifically react with protein motifs.³ These include self-labeling “tags”, such as the SNAP-tag,⁴ the CLIP-tag,⁵ or the Halo-tag,⁶ and amino acid sequences that can be modified using external enzymes.⁷

Bioconjugation has also played an important role in photopharmacology, which is an effort to control biological activity with synthetic photoswitches.⁸ While soluble photochromic ligands (PCLs) are diffusion limited, photoswitchable tethered ligands (PTLs) covalently attach to an engineered site in the target protein. This places the ligand in the vicinity of its

binding pocket, so that light maneuvers it in and out of a position where it can bind.⁹ The PTL approach allows for precise targeting since the bioconjugation motif, which is usually an engineered cysteine for maleimide conjugation, can be genetically encoded and selectively expressed in cells of interest. By contrast, PCLs act on native receptors, making for easier use, especially in therapeutic settings, albeit with less precision.

Although PTLs have proven to be powerful for controlling neural signaling and animal behavior,¹⁰ they have faced the disadvantages of cysteine/maleimide chemistry. Maleimides hydrolyze under physiological conditions and conjugate to glutathione, making them incompatible with the intracellular environment. Moreover, both in the cell and on the cell surface, they are likely to react with accessible native cysteines that are not at the designed PTL anchoring site. Although attachment to the introduced cysteine can be enhanced by affinity labeling due to increased times of proximity when the ligand binds in the binding pocket,¹¹ the susceptibility of maleimides to unwanted nucleophiles, including water, makes them less than ideal for applications in photopharmacology.

Received: July 18, 2015

Published: October 16, 2015

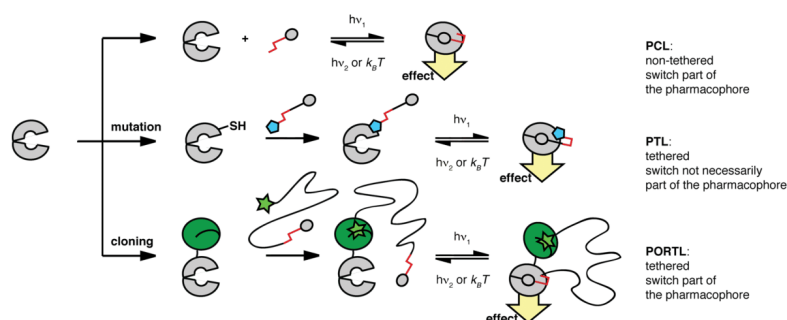


Figure 1. PORTL concept. A photochromic ligand (PCL) is freely diffusible, and the switch is part of the pharmacophore (top). This is not necessarily the case in a photoswitchable tethered ligand (PTL) (middle). The photoswitchable orthogonal remotely tethered ligand approach (PORTL, bottom) combines the switch as part of the pharmacophore with a long, flexible tether that allows for anchoring on a remote site.

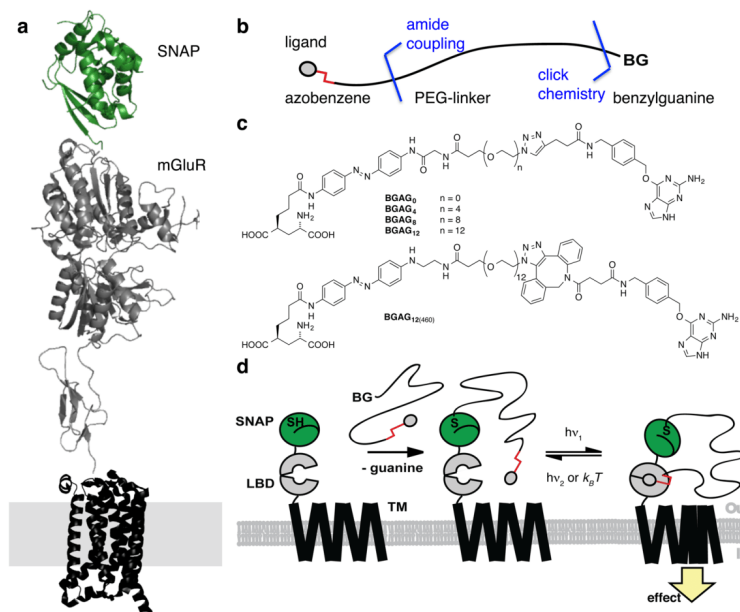


Figure 2. Concept and Design of PORTL compounds for SNAP-tag conjugation. (a) Model of a SNAP-mGluR subunit showing the relative dimensions of the domains (SNAP pdb, 3kzy; mGluR3-LBD pdb, 2e4u; mGluRS-7TM pdb, 4o09). The mGluR extracellular domains are shown in gray, and the transmembrane domains are shown in black, while the SNAP-tag is shown in green. (b) Schematic design of a photoswitchable orthogonal remotely tethered ligand (PORTL) using amide coupling and click chemistry to ensure synthetic modularity. (c) PORTL consisting of a ligand connected to an azobenzene flexible linker (PEG-chain) of various length and a benzylguanine (BG). Only one regioisomer is shown in BGAG₁₂₍₄₆₀₎. Depending on the substitution pattern on the azobenzene the switching wavelength can be tuned. (d) Schematic showing the logic of PORTL-mediated reversible activation and deactivation of a target receptor with two orthogonal wavelengths of light.

A solution to these challenges could be the introduction of electrophiles that react with very high selectivity and yet are stable toward water. Under normal circumstances, this requires a larger protein tag, moving the site of attachment far away

from the ligand-binding site, typically in the range of several nanometers. Although tethers with photoswitches placed in series could be designed, multiple isomerization states of the tether and the spread of conformations of the long entropic

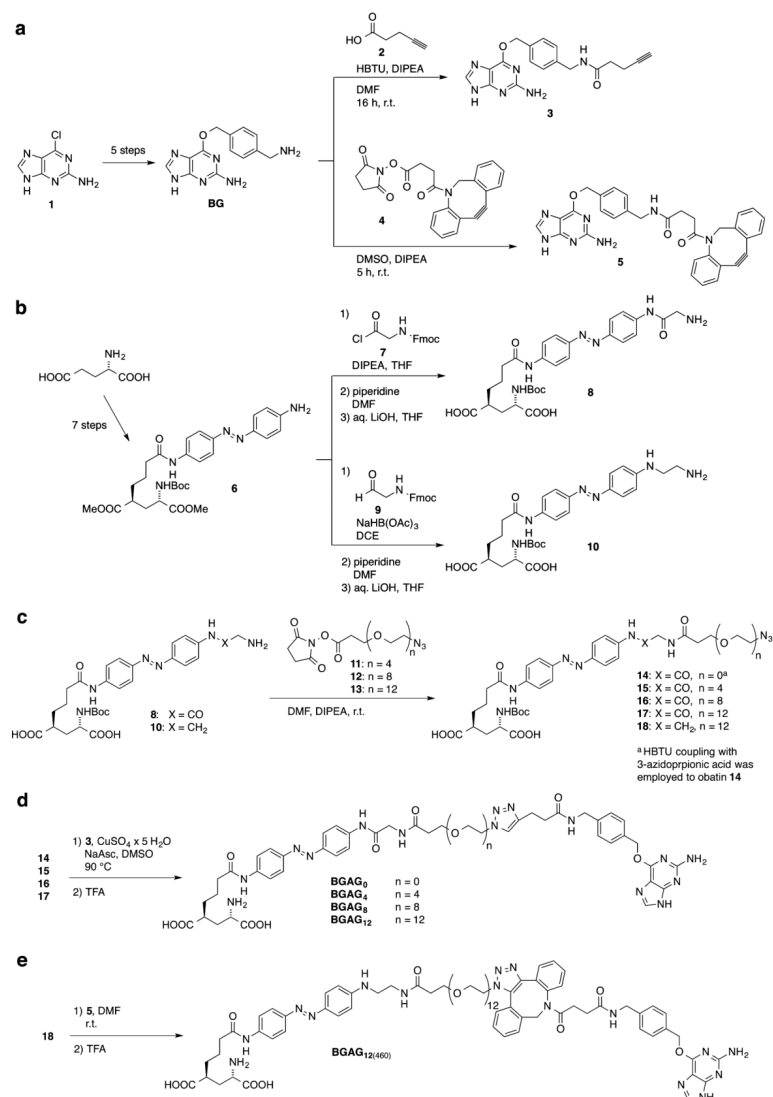


Figure 3. Synthesis of BGAGs. (a) Synthesis of BG-alkynes **3** and **5** for click chemistry. (b) Diversification of previously described **6** to give blue azobenzene glutamate **8** and red-shifted azobenzene glutamate **10**. (c) PEG-chain installation. (d) Cu(I)-catalyzed alkyne azide click to obtain BGAGs. (e) Strain promoted alkyne azide click to obtain BGAG₁₂₍₄₆₀₎.

spring¹² could complicate control and prevent clean changes in biological activity upon irradiation.

Here we introduce a new concept, termed PORTL (photoswitchable orthogonal remotely tethered ligand), that

overcomes the limitations of maleimide chemistry and lays to rest concerns about off-target attachment (Figure 1). Like a PTL, a PORTL consists of a bioconjugation handle, a photoswitchable group, and a ligand. In this case, however,

the switch does not primarily impact the overall length, pointing angle, and flexibility of the tether, but rather the pharmacology of the tethered ligand. As such, the switch becomes an integral part of the pharmacophore and the change in biological activity is designed to result not from a change in the relative position of the ligand with respect to its binding site but, rather, from a change in the efficacy of the ligand, as it does in a PCL. Therefore, the tether can be long and flexible, allowing for the use of larger bioconjugation motifs, such as a SNAP-tag, which provide an anchoring site at a more remote location with respect to the ligand-binding site. The SNAP-tag is a modified DNA repair enzyme that functions as a self-labeling domain by selectively and quickly reacting with benzylguanine (BG) electrophiles.⁴ It enables specific and efficient labeling with BG fluorophores in cultured cells and in brain slice.¹³ Importantly, unlike maleimides, BGs are essentially inert toward water, regular cysteines, and glutathione, making them ideal for labeling in physiological systems that include extracellular and intracellular targets.^{4b,14}

We demonstrate the validity of the PORTL concept by fusing the class C G protein-coupled receptor (GPCR), mGluR2, with a SNAP-tag and endowing it with a synthetic azobenzene photoswitch through benzylguanine chemistry. The resulting photoreceptor, termed SNAG-mGluR2 (SNAP-tagged-azobenzene-glutamate receptor), permits rapid, repeatable, high-efficacy photoagonism of mGluR2 with thermally bistable and fast relaxing photoswitches. SNAG-mGluR2 allows for optical manipulation of neuronal excitability and synaptic transmission in hippocampal neurons. We also show that the SNAG approach may be combined with the cysteine attachment of a conventional PTL to allow for orthogonal optical control of two glutamate receptors within the same cell, paving the way for other multiplexing strategies.

RESULTS

Design of PORTL Photoswitches for Metabotropic Glutamate Receptors. mGluRs are class C GPCRs that mediate many aspects of glutamatergic signaling in the brain and serve as drug targets for a number of neurological disorders.¹⁵ The defining structural feature of class C GPCRs is a large, bilobed extracellular ligand-binding domain (LBD) that assembles as a dimer and mediates receptor activation. We previously developed photoswitchable versions of mGluR2, -3, and -6, termed "LimGluRs", via cysteine conjugation of *D*-maleimide-azobenzene glutamate ("D-MAG") molecules to the LBD near the glutamate binding site.^{10g,16} This work indicated that mGluRs are amenable to agonism by azobenzene-conjugated glutamate compounds. In addition, previous work has shown that *N*-terminal SNAP-tagged mGluRs retain normal function and may be efficiently labeled in living cells.¹⁷ In order to take advantage of the many attractive properties of the SNAP-tag linkage relative to that of cysteine-maleimide, we sought to optically control the LBD of mGluR2 via PORTL conjugation to a genetically encoded SNAP-tag fused to the LBD.

To design a new family of photoswitches we first analyzed SNAP and mGluR crystal structures to determine the dimensions required to permit a compound conjugated to an *N*-terminal SNAP-tag via a BG group at one end to reach the orthosteric binding site within the mGluR LBD via a glutamate at the other end (Figure 2a). We decided to place the central photoswitchable azobenzene unit close to the glutamate ligand based on the logic that the ability of the glutamate moiety to

dock in the binding pocket and activate mGluR2 would be altered by photoisomerization of the azobenzene, as achieved earlier for soluble photochromic ligands¹⁸ rather than a length-dependent change in the ability to reach the binding site. Furthermore, we hypothesized that a long, flexible polyethylene glycol linker between the BG and azobenzene units would span the necessary distance between the SNAP domain and the mGluR2 LBD and permit the glutamate moiety to reach the binding site (Figure 2b).

Based on our previous work, which indicated that agonism of mGluR2 via glutamate-azobenzene molecules requires 4' *D* stereochemistry, which we refer to as "D-MAG",^{10g} we decided to maintain this feature in our new SNAP-tag photoswitches. We opted to construct the linker between BG and azobenzene out of monodisperse PEG-polymers of different sizes. PEG polymers do not strongly adhere to protein surfaces and are known to be conformationally very flexible.¹ To allow this system to be adopted for other pharmacophores in the future, we designed the synthetic chemistry to be flexible as well, using amide bond formation and click chemistry for rapid assembly. Alkyne-azide click chemistry has been extensively used for bioorthogonal reactions and can be employed in the presence of benzylguanines.¹⁹ Both the Cu(I)-catalyzed click chemistry or the cyclooctyne strain promoted version, which can be used *in vivo*, are available.

Together, these considerations led to the design of two families of benzylguanine-azoglutamates with either a diacyl azodianiline switch (BGAG_n), as used in the original set of D-MAGs for a 2-wavelength on/off bistable optical control of mGluRs,^{10g} or a red-shifted azobenzene switch (BGAG_{n(460)}), as used more recently for single wavelength single or two-photon control of an mGluR^{16,20} (Figure 2c). In these molecules, the first index denotes the number of ethylene glycol repeat units and the tether length, whereas the number in parentheses indicates the wavelength that results in maximum *cis*-azobenzene content upon irradiation.

Synthesis of Benzylguanines-Azobenzenes-Glutamates (BGAGs). Our synthesis of BGAGs started with guanine derivative **1**, which was converted into the known benzylguanine (BG) in 5 steps^{4a} (Figure 3a). Coupling with 4-pentynoic acid (**2**) then yielded BG-alkyne **3**. Alternatively, cyclooctyne **4** was linked to BG by amidation to obtain BG-DBCO **5**. On the ligand side, we utilized several steps from the reported synthesis of D-MAGs starting from *L*-glutamate^{10g} to synthesize glutamate azobenzene **6** via Frater-Seebach allylation.²¹ Acylation with glycine derivative **7**, followed by deprotection, gave primary amine **8**, whereas reductive amination with aldehyde **9**²² and deprotection yielded diamine **10** (Figure 3b). Coupling of both **8** and **10** with bifunctional PEG-O-Su esters of varying length yielded azides **15**–**18** (whereas **14** was obtained by HBTU-mediated coupling) that were ready for click chemistry (Figure 3c).

BGAGs with a "regular" azobenzene switch were synthesized by Cu(I) catalyzed azide alkyne click chemistry, followed by deprotection, which yielded BGAG_{0,4,8,12} (Figure 3d). It should be noted that high temperatures and high catalyst loadings were needed to drive the click-reaction to completion and that the red-shifted version could not be obtained from **18** and **3** under these conditions. Therefore, strain promoted reaction of **18** with **5**, followed by deprotection of the amino acid moiety, was used instead, which gave the red-shifted photoswitch BGAG₁₂₍₄₆₀₎. The purity of all BGAGs was assessed by ¹H

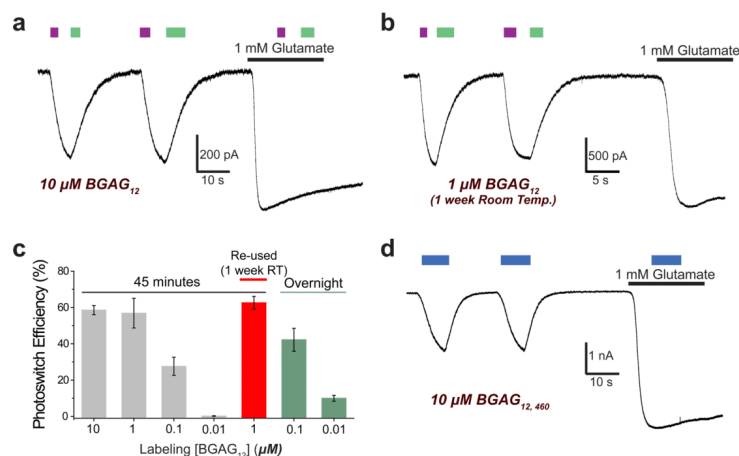


Figure 4. Optical control of SNAG-mGluR2 in HEK293T cells coexpressing SNAP-mGluR2 and GIRK. (a) Representative patch-clamp trace demonstrating the reversible optical control of SNAG-mGluR2 (SNAP-mGluR2 + BGAG₁₂₍₄₆₀₎). Photoactivation is achieved with a brief pulse of UV light ($\lambda = 380$ nm, purple) and reversed by a brief pulse of green light ($\lambda = 500$ nm, green). Application of saturating 1 mM glutamate gives full activation and prevents further photoswitching. (b) Representative trace showing photoactivation of SNAG-mGluR2 using 1 μ M BGAG₁₂ after it was incubated for 1 week in aqueous buffer. (c) Summary of the efficiency of photoactivation of SNAG-mGluR2 (compared to 1 mM glutamate) following different BGAG₁₂ labeling conditions. Error bars represent SEM. (d) Representative trace showing photoactivation of SNAG₄₆₀-mGluR2 (SNAP-mGluR2 + BGAG₁₂₍₄₆₀₎) with blue light ($\lambda = 445$ nm). Relaxation occurs spontaneously in the dark.

NMR, HR-MS, and HPLC (see Supporting Information and Figure S1).

Optical Control of SNAG-mGluR2 in HEK293T Cells.

After synthesizing the set of BGAG molecules, we next sought to test whether they could be efficiently conjugated to SNAP-mGluR2 and used to optically manipulate mGluR2 function (Figure 2d). We first expressed a GFP-fusion construct (SNAP-mGluR2-GFP) in HEK293T cells and saw efficient labeling with a BG-conjugated Alexa dye that was limited to the cell surface (Figure S2), as previously reported.^{17b,17c} This indicated that charged, BG-conjugated compounds are unlikely to cross the membrane and will, thus, primarily target receptors on the cell surface. Furthermore, *in vitro* studies showed, unlike maleimides, no dependence of SNAP labeling on the presence of a reducing or oxidizing environment (Figure S3).

We next tested the ability of BGAGs to photoactivate SNAP-mGluR2 using whole cell patch-clamp electrophysiology in HEK293T cells cotransfected with the G protein-activated inward rectifier potassium (GIRK) channel. Cells expressing SNAP-mGluR2 were initially incubated with 10 μ M BGAG₁₂ for 45 min at 37 °C. Following extensive washing to remove excess, nonattached photoswitches, photoisomerization to the *cis* configuration with a brief (<1 s) bout of illumination at 380 nm produced robust photoactivation that persisted in the dark and was reversed by a brief (~1 s) bout of illumination at 500 nm to isomerize the azobenzene back to the *trans* state (Figures 4a, S2a). mGluR2 photoactivation via BGAG₁₂ was highly reproducible. In the photoswitch “off” state (i.e., in the dark or following illumination at 500 nm), responses to the native neurotransmitter ligand glutamate were intact. Photocurrents were abolished at high glutamate concentrations, suggesting that BGAG₁₂ does not function as a partial agonist (Figure 4a).

Light responses were ~60% of the responses to saturating glutamate ($59.3 \pm 2.8\%$, $n = 10$ cells), consistent with both efficient conjugation and receptor activation. Importantly, cells expressing wild type mGluR2 (i.e., with no SNAP-tag) and incubated with BGAG₁₂ showed no light responses (Figure S4b), confirming that there is no BGAG conjugation in the absence of a SNAP-tag by performing the wash-in and wash-out protocol in the same manner as for SNAP-mGluR2. Given the successful optical control of mGluR2, we termed the tool that combines SNAP-mGluR2 and BGAG “SNAG-mGluR2”. SNAG-mGluR2 showed similar photocurrent efficacy and kinetics to the previously reported LimGluR2.^{10b} SNAG-mGluR2 photoactivation was fully blocked by the competitive mGluR2 antagonist LY341495, without altering the baseline current, supporting the interpretation that BGAG₁₂ activates mGluR2 via its native, orthosteric binding site and does not significantly activate in the *trans* configuration of the azobenzene (Figure S4c). The apparent affinity for glutamate of SNAG-mGluR2 was comparable to that of SNAP-mGluR2 not labeled by BGAG₁₂ and, indeed, of wild type mGluR2 (Figure S4d), indicating that normal mGluR2 function is maintained.

We next tested different labeling conditions of BGAG₁₂ and found that 45 min incubation with ≥ 1 μ M BGAG₁₂ showed optimal labeling (Figure S5a,b). However, photocurrents were still observed with 100 nM labeling for 45 min (Figure S5c) and could even be observed with concentrations as low as 10 nM with overnight labeling (Figure S5d–f). Remarkably, the labeling solution could be reused for multiple experiments for 1 week following dilution in aqueous buffer at room temperature, without a decline in efficacy of optical activation (Figure 4b,c). This result is in stark contrast to maleimide-based MAG

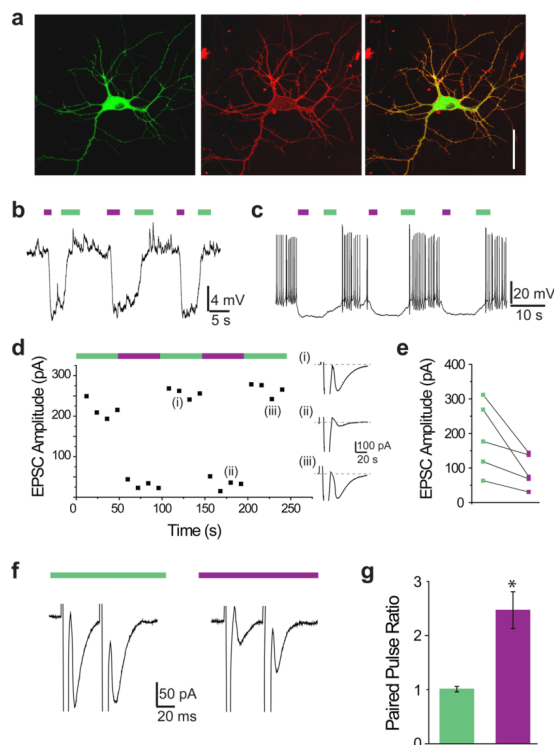


Figure 5. Optical control of SNAG-mGluR2 in hippocampal neurons. (a) Representative confocal images showing the expression of SNAP-mGluR2-GFP (left) and its labeling with BG-Alexa-647 (middle) in hippocampal neurons. In the merge (right) of the two images it is clear that dye labeling occurs on the surface of the neuron only. (b, c) Representative recording showing SNAG-mGluR2 mediated hyperpolarization (b) and silencing (c) of hippocampal neurons in whole cell patch-clamp recordings. Violet bars indicate 380 nm illumination, and green bars indicate 500 nm illumination. (d) Time course of autaptic EPSC amplitude for a representative neuron showing rapid, reversible inhibition of synaptic transmission by SNAG-mGluR2. (i), (ii), and (iii) show individual traces associated with data points. (e) Summary of SNAG-mGluR2 mediated optical synaptic inhibition by 380 nm light in all cells tested. (f) Representative recording showing an increase in paired pulse ratio in response to SNAG-mGluR2 activation using an interstimulus interval of 50 ms. (g) Summary of paired pulse ratio in 500 nm (green) or 380 nm (violet) for the same cell as in panel f.

photoswitches, which typically need to be applied at concentrations up to 100–200 μM ^{10,11} and are hydrolyzed in water with a half-life in the range of minutes to hours.¹

To further explore the mechanism of photoswitching in SNAG-mGluR2, we synthesized a PCL version of BGAG₁₂ where the BG group was omitted (“AG₁₂”; Figure S6a). AG₁₂ photoagonized SNAP-mGluR2 with the same directionality as BGAG₁₂ (Figure S6b), supporting the hypothesis that photoswitching is based on the relative efficacy of the azobenzene-glutamate moiety in *cis* versus *trans*, rather than a length or geometry-dependent change in the ability to reach the binding site. We also tested BGAG variants ranging in length from 0 to 8 PEG repeats and found comparable photoactivation of SNAG-mGluR2 to BGAG₁₂ for all versions (Figure S7), suggesting similar effective concentrations of the ligand near the binding pocket.

We next tested the red-shifted version of BGAG₁₂, BGAG_{12(460)}}, to see if we could develop a SNAG-mGluR2 variant that is controlled with a single wavelength of visible light. Following labeling with 10 μM BGAG_{12(460)}}, photoactivation of SNAP-mGluR2 was achieved reproducibly in response to illumination with blue light (420–470 nm bandpass) (Figure 4d). Relaxation occurred rapidly in the dark following illumination, as expected, and the photoactivation was $\sim 35\%$ relative to saturating glutamate ($34.9 \pm 4.2\%$, $n = 18$ cells). We termed the combination of SNAP-mGluR2 and BGAG_{12(460)}} “SNAG₄₆₀-mGluR2”.

Having developed multiple versions of SNAG-mGluR2 that were able to efficiently photoactivate mGluR2, we next wondered if this toolset could be used to optically manipulate mGluR2 in its native neuronal setting.

Optical Manipulation of Excitability and Synaptic Transmission via SNAG-mGluR2 in Hippocampal Neu-

rons. mGluR2, like other neuronal $G_{i/o}$ -coupled GPCRs, primarily signals either somatodendritically, to hyperpolarize membranes through the activation of GIRK channels, or presynaptically, to inhibit neurotransmitter release by a number of mechanisms, including inhibition of voltage-gated calcium channels.^{15a} We hypothesized that SNAG-mGluR2 would efficiently gate both of those canonical functions in neurons.

We first expressed SNAP-mGluR2-GFP in dissociated hippocampal neurons and labeled with BG-Alexa-647 to determine if SNAP-BG conjugation could occur efficiently in neuronal cultures, which are considerably denser than HEK 293T cell cultures. We observed strong SNAP-mGluR2-GFP expression and surface labeling with Alexa-647 (Figure 5a), indicating that the SNAP tethering approach is suitable to neurons. Importantly, untransfected cells did not show BG-Alexa-647 fluorescence (Figure S8), confirming the specificity of the labeling chemistry. Next, instead of labeling with BG-Alexa-647, we labeled with BGAG₁₂ and observed rapid membrane hyperpolarization (~2–8 mV) in response to illumination at 380 nm, which was reversed by illumination at 500 nm (Figure 5b). When the neurons were at depolarized potentials that induced firing, the light-induced hyperpolarization was sufficient to inhibit the action potentials (Figure 5c).

To test for presynaptic inhibition, we cultured hippocampal neurons at low density to promote the formation of autapses, i.e., synapses between the axon and dendrites of the same neuron. In autaptic neurons, photoactivation of SNAG-mGluR2 reversibly decreased excitatory postsynaptic current (EPSC) amplitude by up to 70% (average = $48.3 \pm 7.3\%$, $n = 5$ cells) (Figure 5d,e). Optical inhibition of EPSC amplitude was accompanied by an increase in paired pulse ratio (Figure 5f,g) and a decrease in synaptic depression during high frequency trains (Figure S9), consistent with a presynaptic reduction in the probability of transmitter release. Together, these observations demonstrate that the SNAG system is well suited for neuronal cells and that SNAG-mGluR2 itself is a powerful tool for optical manipulation of neuronal inhibition via native mGluR2-mediated mechanisms that control neural firing and transmitter release.

Dual Optical Control of SNAG-mGluR2 and LiGluR via Orthogonal Photoswitch Labeling. A major goal in physiology is to be able to independently manipulate different receptors within the same preparation using different wavelengths of light. This type of experiment could be extremely powerful for deciphering the different roles, and potential crosstalk, of different signaling pathways within a cell or neural circuit. With this goal in mind, we wondered if SNAG-mGluR2 could be used in conjunction with a previous generation photoswitchable receptor to provide individual optical control of two receptors within the same cell. We turned to LiGluR, a GluK2 ionotropic glutamate receptor that is photoactivated by molecules of the maleimide-azobenzene-glutamate (MAG) family through cysteine-maleimide linkage.^{18a,23} To test this, we coexpressed SNAP-mGluR2 along with its GIRK channel effector and LiGluR (GluK2-L439C) in HEK293T cells. We labeled the cells with BGAG₁₂ for 30 min, and then with L-MAG₀₄₆₀, a blue light-activated, spontaneously relaxing version of MAG with similar spectral properties to BGAG₁₂₍₄₆₀₎.²⁰ Due to the spectral and light sensitivity differences between the two photoswitches, we were able to independently and sequentially activate SNAG-mGluR2 and LiGluR (Figure 6a, see Methods). Photoactivation of SNAG-mGluR2 with dim illumination at 380 nm induced slow inward photocurrents, which were

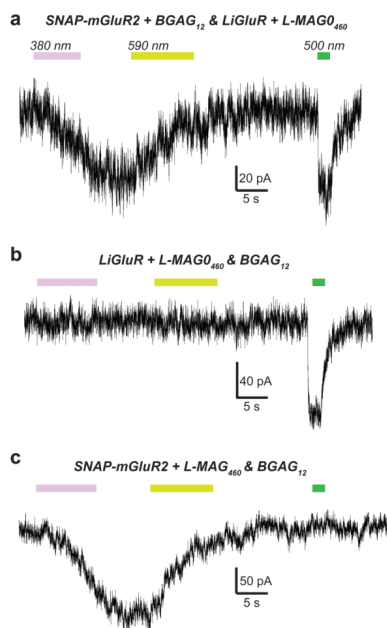


Figure 6. Dual optical control of SNAG-mGluR2 and LiGluR in HEK 293T cells via orthogonal labeling of BGAG₁₂ and MAG₄₆₀. (a–c) Representative traces showing the responses to dim 380 nm light (<math><0.005 \text{ mW/mm}^2</math>; purple bars), 590 nm light ($\sim 1 \text{ mW/mm}^2</math>; yellow bars), and 500 nm light ($\sim 1 \text{ mW/mm}^2</math>; green bars) in cells treated with BGAG₁₂ and L-MAG₀₄₆₀. Cells expressing both SNAP-mGluR2 and LiGluR show a slow SNAG-mGluR2-mediated response to 380 nm light that is reversed by 590 nm light and a fast LiGluR-mediated response to 500 nm light (a). In the absence of SNAP-mGluR2, the slow response to 380 nm is not seen (b), and in the absence of LiGluR, the fast response to 500 nm is not seen (c), confirming the origins of each current.$$

deactivated by illumination at 590 nm, as shown above. 590 nm yellow light was used to ensure orthogonality to L-MAG₀₄₆₀. In contrast, photoactivation of LiGluR-L-MAG₀₄₆₀ by illumination at 500 nm induced rapid, spontaneously relaxing photocurrents, as shown earlier.²⁰ When only one of the receptors was expressed, only its characteristic photoresponse was seen. In the case of SNAG-mGluR2 this was a slow ON, slow OFF photocurrent induced by illumination at 380 and 500 nm, respectively, whereas in the case of LiGluR-L-MAG₀₄₆₀ this was a rapid, spontaneously relaxing photocurrent, which was triggered by illumination at 500 nm, which turned off spontaneously in the dark (Figure 6b,c). Although a SNAP-tag does react slowly with maleimides (Figure S3), this can be circumvented by first labeling with BGAG to saturation before applying MAG compounds. Together these experiments show that the PORTL approach based on conjugation of BGAGs to SNAP-tagged receptors allows for independent, dual optical control within the same preparation, a major step forward for chemical optogenetics.

DISCUSSION

Photoswitchable tethered ligands (PTLs) provide a powerful component of the optogenetic arsenal for biophysical, synaptic, neural circuit, behavioral, and disease treatment applications.^{8,23} Unlike opsin-based approaches, which rely on the exogenous expression of non-native light-gated membrane proteins, PTLs offer target-specific control of native signaling proteins through the bioconjugation of synthetic light-controlled compounds. They allow one to study the physiological roles of individual proteins with a high subtype specificity and spatiotemporal and genetic precision compared to classical pharmacological or genetic techniques. Until the present, PTL anchoring to the signaling protein of interest has been almost exclusively based on the covalent attachment of a maleimide group on the PTL to an engineered cysteine positioned near the pore or ligand binding pocket of the protein.²⁴ Even on extracellular parts of proteins, where most native cysteines are disulfide bonded and not subject to attack by a maleimide, there are many free cysteines where PTLs will attach. As a result, the specificity of action of cysteine-reactive PTLs relies not on unique targeting but on the insensitivity of other proteins to the minor repositioning of tethered ligands.^{10a,18a,25} Still, there would be a major advantage if protein attachment could be bio-orthogonal and so highly specific. Maleimide-cysteine attachment has proven viable in small animals, such as zebrafish, and easily accessible tissues, such as the outer retina of mouse. However, maleimides may be inefficient in larger systems due to slow diffusion and competition with hydrolysis, and is restricted to the extracellular environment, since inside the cell competition for the target cysteine by glutathione at millimolar concentrations would be forbidding. In addition, attachment to a native accessible cysteine, such as in enzyme active sites, could be deadly. Our goal was to create a new orthogonal and efficient strategy for specific PTL attachment that is easy to generalize. We present a solution to these challenges in the form of a second generation PTL, termed PORTL, an approach built around the conjugation of BG-labeled photoswitches to genetically encoded SNAP-tags.

The PORTL approach takes advantage of the fact that the SNAP-tag reacts with BGs in a very efficient and selective way that is fully orthogonal to native chemical reactions.⁴ Unlike first-generation PTLs, which need to be tethered near the site of ligand binding,^{10a,6,18a,25,26} PORTL tethers the photoswitch farther away, on a separate domain, providing a useful separation between the attachment point and functional headgroup of the compound by a long linker. In principle, the photoswitch could also be attached to a separate transmembrane protein, an antibody, or a membrane anchor. This physical separation is expected to place the ligand headgroup of a PORTL at a relatively lower local concentration than a conventional PTL. The headgroup would then be photoswitched between active and inactive states like a photochromic ligand, and should be inactive ideally in the dark. Aspects of this logic were previously applied to a photoswitchable ligand attached via a long flexible tether to a GABA_A receptor, although in that case the ligand was a potentiator, not an agonist, the ligand was active in the dark, and the attachment was to an introduced cysteine.²⁷ A further feature to our design is that the predicted relatively low local concentration of PORTL headgroups may help ensure the lack of basal modulation of receptor activity by the relaxed state of the photoswitch.

With these considerations in mind, we designed and synthesized benzylguanine-azoglutamate (BGAG) PORTL compounds that may be attached to a SNAP-tagged version of the class C GPCR mGluR2 to produce the chemical optogenetic tool termed "SNAG-mGluR2". SNAG-mGluR2 permits the high-efficacy, rapid, repeatable photoactivation of mGluR2 with a 2-color, bistable BGAG (SNAG-mGluR2) or a 1-color, spontaneously relaxing BGAG_{12(460)}} (SNAG₄₆₀-mGluR2). In both cases, SNAG-mGluR2 remains inactive in the dark and is activated in the high-energy state in response to either near UV (~380 nm, BGAG_n) or visible light (~460 nm, BGAG_{12(460)}}). Consistent with our predictions about the mechanism of PORTL photoactivation, untethered photoswitches that mimic the azobenzene-glutamate part of BGAG showed the same directionality of photoswitching on mGluR2, suggesting that the efficacy of the photoswitchable ligand is higher in *cis* than *trans* and independent of the tether. Importantly, since it maintains the entire full-length sequence of mGluR2, SNAG-mGluR2 should also retain all native signaling properties ranging from ligand binding to G protein coupling to downstream regulation. Consistent with this, SNAG-mGluR2 permitted efficient optical manipulation of two distinct native downstream targets of mGluR2 in neurons: a somato-dendritic control of excitability and a presynaptic control of synaptic transmission.

In line with the attractive properties of SNAP-tag conjugation, BGAG photosensitizes SNAP-mGluR2 at concentrations 100–1000× lower than typically used for maleimide-based PTLs, minimizing potential activation of glutamate receptors during photoswitch incubation. Furthermore, owing to its insensitivity to hydrolysis by water, BGAG remains reactive over not minutes but days, and stocks diluted in aqueous buffer may be reused without a loss of labeling efficiency. Taken together, these properties should make the PORTL approach ideally suited for labeling in intact tissue or *in vivo*, as was recently shown for fluorophore conjugation to a SNAP-tag in the nervous system of mouse.^{13b}

Another major advantage of the PORTL approach is its modularity, which will allow it to be widely applicable to many protein targets with a variety of photoswitches. The SNAP-tag is well characterized and has been used extensively to label fusion proteins with fluorophores or to create semisynthetic probes for the sensing of small molecules.^{13a} Like GFP, the SNAP-tag can be fused to proteins of interest without significantly altering their activity. Indeed, several SNAP-tagged transmembrane class A, class B, and class C GPCRs, including all of the mGluRs,^{17a,28} have been described, and many of these are commercially available.

To facilitate the application of this approach to a wide range of target proteins, we designed our synthetic strategy to be as modular and efficient as possible, taking advantage of the power of click chemistry. Building on existing pharmacology and the growing repertoire of PCLs, PORTL compounds may be synthesized with different headgroups for many other target proteins of interest. These compounds may include photoswitchable agonists, antagonists, or allosteric modulators. Relative to the challenge of finding optimal cysteine residues for maleimide-based photoswitch conjugation with first-generation PTLs, the PORTL system will greatly facilitate the design and implementation of new photosensitive proteins. For instance, voltage-gated potassium channels^{10a} and nicotinic acetylcholine receptors,²⁹ which had been previously out under optical control using maleimides, could be amenable to the

PORTL approach. In addition, the PORTL system with the SNAP-tag will enable the optical control of intracellular targets because, unlike maleimide, the benzylguanine-labeling motif is unaffected by the reducing environment of the cell.

Finally, a major breakthrough in this study that is made possible by the PORTL system is the demonstration of the ability to orthogonally optically manipulate SNAP-mGluR2 and the maleimide-based LiGluR in the same cell. The ability to separately label and manipulate multiple receptor populations may be especially useful for probing crosstalk between proteins at the molecular, cellular, or circuit level. In the future, combination of SNAP-tethered photoswitches with PORTL compounds targeting the orthogonal SNAP-variant CLIP⁵ or the unrelated Halo tag⁶ may greatly expand the ability to optically control multiple receptor populations independently in the same preparation. Tuning of the spectral properties of the azobenzene photoswitch will further facilitate the ability to complex multiple tools within the same preparation. Overall, the PORTL approach brings us closer toward the overarching goal of obtaining the ability to individually and precisely photoactivate or inhibit the fundamental signaling molecules of the brain in concert in behaving animals. Even in the absence of optical control, tethered pharmacology (which PORTL represents) holds great promise as a means to precisely control biological function.

METHODS

Chemical Synthesis and Availability of Photoswitches. Details on the chemical synthesis of BGAGs and their precursors and characterization data can be found in the [Supporting Information](#). BGAGs are available for academic use from the Trauner laboratory upon request.

HEK293T and Hippocampal Neuron Electrophysiology. HEK293T cell recordings were performed as described previously.^{10g} Cells were seeded on 18 mm glass coverslips and transfected with 0.7 $\mu\text{g}/\text{well}$ SNAP-mGluR2 (and/or LiGluR: GluK2-L439C) and GIRK1-F137S DNA, along with 0.1 $\mu\text{g}/\text{well}$ tdTomato as a transfection marker, using Lipofectamine 2000 (Invitrogen). Whole-cell HEK cell recordings were performed 24–48 h later at room temperature (22–24 °C) using an Axopatch 200B headstage/amplifier (Molecular Devices) on an inverted microscope (Olympus IX series) or an EPC10 USB patch clamp amplifier (HEKA) and PatchMaster software (HEKA) on a Leica DM IL LED. Recordings were performed in high potassium (HK) extracellular solution containing (in mM) 120 KCl, 29 NaCl, 1 MgCl_2 , 2 CaCl_2 , 10 HEPES, pH 7.4. Glass pipettes of resistance between 4 and 8 $\text{M}\Omega$ were filled with intracellular solution containing (in mM) 140 KCl, 10 HEPES, 3 Na_2ATP , 0.2 Na_2GTP , 5 EGTA, 3 MgCl_2 , pH 7.4. Voltage-clamp recordings were typically performed at -60 mV. Drugs were purchased from Tocris, diluted in HK solution, and applied using a gravity-driven perfusion system. Data were analyzed with Clampfit (Molecular Devices) or IgorPro (v6.22, wavemetrics).

Prior to recording, cells were washed with extracellular labeling solution and labeled with BGAG variants at the reported concentrations for 45–50 min in an incubator at 37 °C. The extracellular labeling solution contained (in mM) 138 NaCl, 1.5 KCl, 1 MgCl_2 , 2 CaCl_2 , 10 HEPES, pH 7.4. For overnight labeling experiments, BGAG was diluted in HEK cell culture media (DMEM + 5% FBS). For experiments involving LiGluR, following BGAG incubation cells were incubated for 5 min at room temperature with 0.3 mg/mL concanavalin A to

prevent receptor desensitization followed by 50 μM L-MAG0₄₆₀ for 30 min at room temperature. Illumination was mediated by Xe-lamp (DG4, Sutter) in combination with excitation filters. Neutral density filters (Omegafilters) were used to vary the light intensity.

Dissociated hippocampal neuron cultures were prepared from postnatal P0 or P1 mice on 12 mm glass coverslips as previously described.^{10g} Neurons were transfected with SNAP-mGluR2 (1.5 $\mu\text{g}/\text{well}$) and tdTomato (0.25 $\mu\text{g}/\text{well}$ as a transfection marker) using the calcium phosphate method at DIV9. Whole cell patch clamp experiments were performed 3–6 days after transfection (DIV 12–15). Labeling was performed using the same protocol as HEK cells except BGAG was diluted in extracellular recording solution containing (in mM) 138 NaCl, 1.5 KCl, 1.2 MgCl_2 , 2.5 CaCl_2 , 10 glucose, 5 HEPES, pH 7.4. Glass pipettes of resistance 4–8 $\text{M}\Omega$ were filled with an intracellular solution containing (in mM) 140 K-gluconate, 10 NaCl, 5 EGTA, 2 MgCl_2 , 1 CaCl_2 , 10 HEPES, 2 MgATP , and 0.3 Na_2GTP , pH 7.2. Autaptic neurons were voltage clamped at -60 mV, and a 2–3 ms voltage step to +20 mV was used to evoke a spike followed (~ 3 –5 ms later) by an EPSC. Stimulation was performed once every 12 s to prevent rundown.

Confocal imaging of SNAP-mGluR2-GFP and Alexa dye-labeled constructs was performed on a Zeiss LSM780 Axio Examiner. Dye labeling was performed in appropriate extracellular solutions for 45 min at 1 μM in an incubator at 37 °C, followed by extensive washing before imaging.

ASSOCIATED CONTENT

Supporting Information

The Supporting Information is available free of charge on the ACS Publications website at DOI: 10.1021/acscentsci.5b00260.

Preparation of BGAGs, characterization by NMR, HRMS, and HPLC, and supporting figures (PDF)

AUTHOR INFORMATION

Corresponding Author

*E-mail: Dirk.Trauner@lmu.de.

Author Contributions

[§]J.B., A.D., and J.L.: equal contribution.

Notes

The authors declare no competing financial interest.

ACKNOWLEDGMENTS

We gratefully acknowledge S. Nadal for synthetic work and L. de la Osa de la Rosa for technical assistance. We thank Prof. Dr. J.-P. Pin for providing plasmids encoding for SNAP-tagged mGluRs. The work was supported by a Studienstiftung des deutschen Volkes PhD fellowship (J.B.), the International Max Planck Research School for Molecular and Cellular Life Sciences (IMPRS-LS) (A.D.), the National Institutes of Health Nanomedicine Developmental Center for the Optical Control of Biological Function (2PN2EY018241) (E.Y.I. and D.T.), the National Science Foundation EAGER Award (IOS-1451027) (E.Y.I.), and an Advanced Grant from the European Research Commission (268795) (D.T.).

REFERENCES

- (1) Hermanson, G. T. *Bioconjugate Techniques*, 3rd ed.; Academic Press: 2013.

- (2) (a) Wang, L.; Schultz, P. G. Expanding the genetic code. *Angew. Chem., Int. Ed.* **2004**, *44* (1), 34–66. (b) Tsai, Y. H.; Essig, S.; James, J. R.; Lang, K.; Chin, J. W. Selective, rapid and optically switchable regulation of protein function in live mammalian cells. *Nat. Chem.* **2015**, *7* (7), 554–561.
- (3) Hinner, M. J.; Johnsson, K. How to obtain labeled proteins and what to do with them. *Curr. Opin. Biotechnol.* **2010**, *21* (6), 766–776.
- (4) (a) Keppler, A.; Gendreizig, S.; Gronemeyer, T.; Pick, H.; Vogel, H.; Johnsson, K. A general method for the covalent labeling of fusion proteins with small molecules in vivo. *Nat. Biotechnol.* **2002**, *21* (1), 86–89. (b) Keppler, A.; Kindermann, M.; Gendreizig, S.; Pick, H.; Vogel, H.; Johnsson, K. Labeling of fusion proteins of O⁶-alkylguanine-DNA alkyltransferase with small molecules in vivo and in vitro. *Methods* **2004**, *32* (4), 437–444.
- (5) Gautier, A.; Juillerat, A.; Heinis, C.; Correa, I. R., Jr.; Kindermann, M.; Beauvais, F.; Johnsson, K. An engineered protein tag for multiprotein labeling in living cells. *Chem. Biol.* **2008**, *15* (2), 128–136.
- (6) Los, G. V.; Encell, L. P.; McDougall, M. G.; Hartzell, D. D.; Karassina, N.; Zimprich, C.; Wood, M. G.; Learish, R.; Ohana, R. F.; Uhr, M.; Simpson, D.; Mendez, J.; Zimmerman, K.; Otto, P.; Vidugiris, G.; Zhu, J.; Darzins, A.; Klauert, D. H.; Bulleit, R. F.; Wood, K. V. HaloTag: a novel protein labeling technology for cell imaging and protein analysis. *ACS Chem. Biol.* **2008**, *3* (6), 373–382.
- (7) (a) Chen, I.; Howarth, M.; Lin, W.; Ting, A. Y. Site-specific labeling of cell surface proteins with biophysical probes using biotin ligase. *Nat. Methods* **2005**, *2* (2), 99–104. (b) Spicer, C. D.; Davis, B. G. Selective chemical protein modification. *Nat. Commun.* **2014**, *5*, 4740.
- (8) (a) Fehrentz, T.; Schonberger, M.; Trauner, D. Optochemical genetics. *Angew. Chem., Int. Ed.* **2011**, *50* (51), 12156–12182. (b) Broichhagen, J.; Frank, J. A.; Trauner, D. A Roadmap to Success in Photopharmacology. *Acc. Chem. Res.* **2015**, *48*, 1947–1960.
- (9) Broichhagen, J.; Trauner, D. The in vivo chemistry of photochromic tethered ligands. *Curr. Opin. Chem. Biol.* **2014**, *21*, 121–127.
- (10) (a) Banghart, M.; Borges, K.; Isacoff, E.; Trauner, D.; Kramer, R. H. Light-activated ion channels for remote control of neuronal firing. *Nat. Neurosci.* **2004**, *7* (12), 1381–1386. (b) Szobota, S.; Gorostiza, P.; Del Bene, F.; Wyart, C.; Fortin, D. L.; Kolstad, K. D.; Tulyathan, O.; Volgraf, M.; Numano, R.; Aaron, H. L.; Scott, E. K.; Kramer, R. H.; Flannery, J.; Baier, H.; Trauner, D.; Isacoff, E. Y. Remote control of neuronal activity with a light-gated glutamate receptor. *Neuron* **2007**, *54* (4), 535–545. (c) Wyart, C.; Del Bene, F.; Warp, E.; Scott, E. K.; Trauner, D.; Baier, H.; Isacoff, E. Y. Optogenetic dissection of a behavioural module in the vertebrate spinal cord. *Nature* **2009**, *461* (7262), 407–410. (d) Janovjak, H.; Szobota, S.; Wyart, C.; Trauner, D.; Isacoff, E. Y. A light-gated, potassium-selective glutamate receptor for the optical inhibition of neuronal firing. *Nat. Neurosci.* **2010**, *13* (8), 1027–1032. (e) Caporale, N.; Kolstad, K. D.; Lee, T.; Tochitsky, I.; Dalkara, D.; Trauner, D.; Kramer, R.; Dan, Y.; Isacoff, E. Y.; Flannery, J. G. LiGluR restores visual responses in rodent models of inherited blindness. *Mol. Ther.* **2011**, *19* (7), 1212–1219. (f) Kauwe, G.; Isacoff, E. Y. Rapid feedback regulation of synaptic efficacy during high-frequency activity at the *Drosophila* larval neuromuscular junction. *Proc. Natl. Acad. Sci. U. S. A.* **2013**, *110* (22), 9142–9147. (g) Levitz, J.; Pantoja, C.; Gaub, B.; Janovjak, H.; Reiner, A.; Hoagland, A.; Schoppik, D.; Kane, B.; Stawski, P.; Schier, A. F.; Trauner, D.; Isacoff, E. Y. Optical control of metabotropic glutamate receptors. *Nat. Neurosci.* **2013**, *16* (4), 507–516. (h) Gaub, B. M.; Berry, M. H.; Holt, A. E.; Reiner, A.; Kienzler, M. A.; Dolgova, N.; Nikonov, S.; Aguirre, G. D.; Beltran, W. A.; Flannery, J. G.; Isacoff, E. Y. Restoration of visual function by expression of a light-gated mammalian ion channel in retinal ganglion cells or ON-bipolar cells. *Proc. Natl. Acad. Sci. U. S. A.* **2014**, *111* (51), E5574–E5583.
- (11) Gorostiza, P.; Volgraf, M.; Numano, R.; Szobota, S.; Trauner, D.; Isacoff, E. Y. Mechanisms of photoswitch conjugation and light activation of an ionotropic glutamate receptor. *Proc. Natl. Acad. Sci. U. S. A.* **2007**, *104* (26), 10865–10870.
- (12) Schafer, L. V.; Muller, E. M.; Gaub, H. E.; Grubmüller, H. Elastic properties of photoswitchable azobenzene polymers from molecular dynamics simulations. *Angew. Chem., Int. Ed.* **2007**, *46* (13), 2232–2237.
- (13) (a) Reymond, L.; Lukinavicius, G.; Umezawa, K.; Maurel, D.; Brun, M. A.; Masharina, A.; Bojkowska, K.; Mollwitz, B.; Schena, A.; Griss, R.; Johnsson, K. Visualizing biochemical activities in living cells through chemistry. *Chimia* **2011**, *65* (11), 868–871. (b) Yang, G.; de Castro Reis, F.; Sundukova, M.; Pimpinella, S.; Asaro, A.; Castaldi, L.; Batti, L.; Bilbao, D.; Reymond, L.; Johnsson, K.; Heppenstall, P. A. Genetic targeting of chemical indicators in vivo. *Nat. Methods* **2015**, *12* (2), 137–139.
- (14) (a) Juillerat, A.; Gronemeyer, T.; Keppler, A.; Gendreizig, S.; Pick, H.; Vogel, H.; Johnsson, K. Directed evolution of O⁶-alkylguanine-DNA alkyltransferase for efficient labeling of fusion proteins with small molecules in vivo. *Chem. Biol.* **2003**, *10* (4), 313–317. (b) Bojkowska, K.; Santoni de Sio, F.; Barde, I.; Offner, S.; Verp, S.; Heinis, C.; Johnsson, K.; Trono, D. Measuring in vivo protein half-life. *Chem. Biol.* **2011**, *18* (6), 805–815.
- (15) (a) Conn, P. J.; Pin, J. P. Pharmacology and functions of metabotropic glutamate receptors. *Annu. Rev. Pharmacol. Toxicol.* **1997**, *37*, 205–237. (b) Niswender, C. M.; Conn, P. J. Metabotropic glutamate receptors: physiology, pharmacology, and disease. *Annu. Rev. Pharmacol. Toxicol.* **2010**, *50*, 295–322.
- (16) Carroll, E. C.; Berlin, S.; Levitz, J.; Kienzler, M. A.; Yuan, Z.; Madsen, D.; Larsen, D. S.; Isacoff, E. Y. Two-photon brightness of azobenzene photoswitches designed for glutamate receptor optogenetics. *Proc. Natl. Acad. Sci. U. S. A.* **2015**, *112* (7), E776–785.
- (17) (a) Doumazane, E.; Scholler, P.; Zwier, J. M.; Trinquet, E.; Rondard, P.; Pin, J. P. A new approach to analyze cell surface protein complexes reveals specific heterodimeric metabotropic glutamate receptors. *FASEB J.* **2011**, *25* (1), 66–77. (b) Doumazane, E.; Scholler, P.; Fabre, L.; Zwier, J. M.; Trinquet, E.; Pin, J. P.; Rondard, P. Illuminating the activation mechanisms and allosteric properties of metabotropic glutamate receptors. *Proc. Natl. Acad. Sci. U. S. A.* **2013**, *110* (15), E1416–E1425. (c) Vafabakhsh, R.; Levitz, J.; Isacoff, E. Y. Conformational Dynamics of a Class C GPCR. *Nature* **2015**, *524*, 497–501.
- (18) (a) Volgraf, M.; Gorostiza, P.; Numano, R.; Kramer, R. H.; Isacoff, E. Y.; Trauner, D. Allosteric control of an ionotropic glutamate receptor with an optical switch. *Nat. Chem. Biol.* **2006**, *2* (1), 47–52. (b) Broichhagen, J.; Jurastow, I.; Iwan, K.; Kummer, W.; Trauner, D. Optical control of acetylcholinesterase with a tacrine switch. *Angew. Chem., Int. Ed.* **2014**, *53* (29), 7657–7660. (c) Stawski, P.; Sumser, M.; Trauner, D. A photochromic agonist of AMPA receptors. *Angew. Chem., Int. Ed.* **2012**, *51* (23), 5748–5751. (d) Stein, M.; Middendorp, S. J.; Carta, V.; Pejo, E.; Raines, D. E.; Forman, S. A.; Sigel, E.; Trauner, D. Azo-propofols: photochromic potentiators of GABA(A) receptors. *Angew. Chem., Int. Ed.* **2012**, *51* (42), 10500–10504. (e) Stein, M.; Breit, A.; Fehrentz, T.; Gudermann, T.; Trauner, D. Optical control of TRPV1 channels. *Angew. Chem., Int. Ed.* **2013**, *52* (37), 9845–9848. (f) Schönberger, M.; Trauner, D. A photochromic agonist for mu-opioid receptors. *Angew. Chem., Int. Ed.* **2014**, *53* (12), 3264–3267. (g) Schönberger, M.; Althaus, M.; Fronius, M.; Clauss, W.; Trauner, D. Controlling epithelial sodium channels with light using photoswitchable amilorides. *Nat. Chem.* **2014**, *6* (8), 712–719. (h) Broichhagen, J.; Schönberger, M.; Cork, S. C.; Frank, J. A.; Marchetti, P.; Bugliani, M.; Shapiro, A. M.; Trapp, S.; Rutter, G. A.; Hodson, D. J.; Trauner, D. Optical control of insulin release using a photoswitchable sulfonylurea. *Nat. Commun.* **2014**, *5*, 5116. (i) Damijonaitis, A.; Broichhagen, J.; Urushima, T.; Hull, K.; Nagpal, J.; Laprell, L.; Schönberger, M.; Woodmansee, D. H.; Rafiq, A.; Sumser, M. P.; Kummer, W.; Gottschalk, A.; Trauner, D. AzoCholine enables optical control of alpha 7 nicotinic acetylcholine receptors in neural networks. *ACS Chem. Neurosci.* **2015**, *6* (5), 701–707.
- (19) (a) Prescher, J. A.; Bertozzi, C. R. Chemistry in living systems. *Nat. Chem. Biol.* **2005**, *1* (1), 13–21. (b) Hong, V.; Steinmetz, N. F.; Manchester, M.; Finn, M. G. Labeling live cells by copper-catalyzed alkyne-azide click chemistry. *Bioconjugate Chem.* **2010**, *21* (10),

1912–1916. (c) Song, X.; Wang, C.; Han, Z.; Xu, Y.; Xiao, Y. Terminal alkyne substituted O6-benzylguanine for versatile and effective syntheses of fluorescent labels to genetically encoded SNAP-tags. *RSC Adv.* **2015**, *5*, 23646–23649.

(20) Kienzler, M. A.; Reiner, A.; Trautman, E.; Yoo, S.; Trauner, D.; Isacoff, E. Y. A red-shifted, fast-relaxing azobenzene photoswitch for visible light control of an ionotropic glutamate receptor. *J. Am. Chem. Soc.* **2013**, *135* (47), 17683–17686.

(21) Hanessian, S.; Margarita, R. 1,3-asymmetric induction in dianionic allylation reactions of amino acid derivatives-synthesis of functionally useful enantiopure glutamates, pipercolates and pyroglutamates. *Tetrahedron Lett.* **1998**, *39* (33), 5887–5890.

(22) Chen, J. J.; Aduda, V. DMSO-aided o-iodoxybenzoic acid (IBX) oxidation of Fmoc-protected amino alcohols. *Synth. Commun.* **2007**, *37* (19–21), 3493–3499.

(23) Reiner, A.; Levitz, J.; Isacoff, E. Y. Controlling ionotropic and metabotropic glutamate receptors with light: principles and potential. *Curr. Opin. Pharmacol.* **2015**, *20*, 135–143.

(24) Lemoine, D.; Habermacher, C.; Martz, A.; Mery, P. F.; Bouquier, N.; Diverchy, F.; Taly, A.; Rassendren, F.; Specht, A.; Grutter, T. Optical control of an ion channel gate. *Proc. Natl. Acad. Sci. U. S. A.* **2013**, *110* (51), 20813–20818.

(25) Lin, W. C.; Davenport, C. M.; Mourot, A.; Vytla, D.; Smith, C. M.; Medeiros, K. A.; Chambers, J. J.; Kramer, R. H. Engineering a light-regulated GABAA receptor for optical control of neural inhibition. *ACS Chem. Biol.* **2014**, *9* (7), 1414–1419.

(26) (a) Fortin, D. L.; Banghart, M. R.; Dunn, T. W.; Borges, K.; Wagenaar, D. A.; Gaudry, Q.; Karakossian, M. H.; Otis, T. S.; Kristan, W. B.; Trauner, D.; Kramer, R. H. Photochemical control of endogenous ion channels and cellular excitability. *Nat. Methods* **2008**, *5* (4), 331–338. (b) Sandoz, G.; Levitz, J.; Kramer, R. H.; Isacoff, E. Y. Optical control of endogenous proteins with a photoswitchable conditional subunit reveals a role for TREK1 in GABA(B) signaling. *Neuron* **2012**, *74* (6), 1005–1014.

(27) Yue, L.; Pawlowski, M.; Dellal, S. S.; Xie, A.; Feng, F.; Otis, T. S.; Bruzik, K. S.; Qian, H.; Pepperberg, D. R. Robust photoregulation of GABA(A) receptors by allosteric modulation with a propofol analogue. *Nat. Commun.* **2012**, *3*, 1095.

(28) Maurel, D.; Comps-Agrar, L.; Brock, C.; Rives, M. L.; Bourrier, E.; Ayoub, M. A.; Bazin, H.; Tinel, N.; Durroux, T.; Prezeau, L.; Trinquet, E.; Pin, J. P. Cell-surface protein-protein interaction analysis with time-resolved FRET and snap-tag technologies: application to GPCR oligomerization. *Nat. Methods* **2008**, *5* (6), 561–567.

(29) Tochitsky, I.; Banghart, M. R.; Mourot, A.; Yao, J. Z.; Gaub, B.; Kramer, R. H.; Trauner, D. Optochemical control of genetically engineered neuronal nicotinic acetylcholine receptors. *Nat. Chem.* **2012**, *4* (2), 105–111.

Supplementary Material for:**Orthogonal Optical Control of a G Protein-Coupled Receptor
with a SNAP-Tethered Photochromic Ligand**

Johannes Broichhagen,^{†,‡,§} Arunas Damijonaitis,^{†,‡,§} Joshua Levitz,^{§,||} Kevin R. Sokol,^{†,‡} Philipp
Leippe,^{†,‡} David Konrad,^{†,‡} Ehud Y. Isacoff,^{||,⊥,#} and Dirk Trauner^{*,†,‡}

[†]Department of Chemistry, Ludwig-Maximilians-Universität München, Butenandtstrasse 5-13, 81377 München, Germany

[‡]Munich Center for Integrated Protein Science, Butenandtstrasse 5-13, 81377 München, Germany

^{||}Department of Molecular and Cell Biology, University of California, Berkeley, California 94720, United States

[⊥]Helen Wills Neuroscience Institute, University of California, Berkeley, California 94720, United States

[#]Physical Bioscience Division, Lawrence Berkeley National Laboratory, Berkeley, California 94720, United States

Corresponding Author

*E-mail: Dirk.Trauner@lmu.de.

Author Contributions [§]J.B., A.D., and J.L.: equal contribution.

Contents

1	Experimental	5
1.1	General.....	5
1.2	Synthesis of BGAGs	6
1.2.1	<i>N</i> -(4-(((2-Amino-9 <i>H</i> -purin-6-yl)oxy)methyl)benzyl)pent-4-ynamide (3)	7
1.2.2	<i>N</i> -(4-(((2-Amino-9 <i>H</i> -purin-6-yl)oxy)methyl)benzyl)-4-(11,12-dehydrodibenzo[<i>b,f</i>]azocin-5(6 <i>H</i>)-yl)-4-oxobutanamide (5)	8
1.2.3	(2 <i>S</i> ,4 <i>S</i>)-2-(4-((4-((<i>E</i>)-(4-(2-Aminoacetamido)phenyl)diazenyl)phenyl)amino)-4-oxobutyl)-4-((<i>tert</i> -butoxycarbonyl)amino)pentanedioic acid (6)	9
1.2.4	(2 <i>S</i> ,4 <i>S</i>)-2-(4-((4-((<i>E</i>)-(4-(2-(3-azidopropanamido)acetamido)phenyl)diazenyl)phenyl)-amino)-4-oxobutyl)-4-((<i>tert</i> -butoxycarbonyl)amino)pentanedioic acid (14).....	10
1.2.5	(2 <i>S</i> ,4 <i>S</i>)-2-Amino-4-(4-((4-((<i>E</i>)-(4-(2-(3-(4-(3-((4-((2-amino-9 <i>H</i> -purin-6-yl)oxy)methyl)benzyl)amino)-3-oxopropyl)-1 <i>H</i> -1,2,3-triazol-1-yl)propanamido)acetamido)-phenyl)diazenyl)phenyl)amino)-4-oxobutyl)pentanedioic acid, BGAG ₀	11
1.2.6	(2 <i>S</i> ,4 <i>S</i>)-2-(4-((4-((<i>E</i>)-(4-(1-Azido-15-oxo-3,6,9,12-tetraoxa-16-azaoctadecan-18-yl)amino)phenyl)diazenyl)phenyl)amino)-4-oxobutyl)-4-((<i>tert</i> -butoxycarbonyl)-amino)pentanedioic acid (15)	12
1.2.7	(2 <i>S</i> ,4 <i>S</i>)-2-Amino-4-(4-((4-((<i>E</i>)-(4-(1-(4-(3-((4-((2-amino-9 <i>H</i> -purin-6-yl)oxy)methyl)-benzyl)amino)-3-oxopropyl)-1 <i>H</i> -1,2,3-triazol-1-yl)-15-oxo-3,6,9,12-tetraoxa-16-aza-octadecan-18-amido)phenyl)diazenyl)phenyl)amino)-4-oxobutyl)-pentanedioic acid, BGAG ₄	13
1.2.8	(2 <i>S</i> ,4 <i>S</i>)-2-(4-((4-((<i>E</i>)-(4-(1-Azido-27-oxo-3,6,9,12,15,18,21,24-octa-28-azatriacontan-30-yl)amino)phenyl)diazenyl)-phenyl)amino)4-oxobutyl)-4-((<i>tert</i> -butoxycarbonyl)-amino)pentanedioic acid (16)	14
1.2.9	(2 <i>S</i> ,4 <i>S</i>)-2-Amino-4-(4-((4-((<i>E</i>)-(4-(1-(4-(3-((4-((2-amino-9 <i>H</i> -purin-6-yl)oxy)methyl)-benzyl)amino)-3-oxopropyl)-1 <i>H</i> -1,2,3-triazol-1-yl)-27-oxo-3,6,9,12,15,18,21,24-octa-28-azatriacontan-30-amido)phenyl)diazenyl)phenyl)amino)-4-oxobutyl)pentane-dioic acid, BGAG ₈ ...	15
1.2.10	(2 <i>S</i> ,4 <i>S</i>)-2-(4-((4-((<i>E</i>)-(4-(1-Azido-39-oxo-3,6,9,12,15,18,21,24,27,30,33,36-dodecaoxa-40-azadotetracontan-42-amido)phenyl)diazenyl)phenyl)amino)-4-oxobutyl)-4-((<i>tert</i> -butoxycarbonyl)amino)pentanedioic acid (17).....	16
1.2.11	(2 <i>S</i> ,4 <i>S</i>)-2-Amino-4-(4-((4-((<i>E</i>)-(4-(1-(4-(3-((4-((2-amino-9 <i>H</i> -purin-6-yl)oxy)methyl)benzyl)amino)-3-oxopropyl)-1 <i>H</i> -1,2,3-triazol-1-yl)-39-oxo-3,6,9,12,15,18,21,24,27,30,33,36-dodecaoxa-40-azadotetracontan-42-amido)phenyl)diazenyl)phenyl)amino)-4-oxobutyl)pentanedioic acid, BGAG ₁₂	17
1.2.12	(2 <i>S</i> ,4 <i>S</i>)-2-(4-((4-((<i>E</i>)-(4-(2-aminoethyl)amino)phenyl)diazenyl)phenyl)amino)-4-oxobutyl)-4-((<i>tert</i> -butoxycarbonyl)amino)pentanedioic acid (10)	18

1.2.13	(2S,4S)-2-(4-((E)-4-((1-azido-39-oxo-3,6,9,12,15,18,21,24,27,30,33,36-dodecaoxa-40-azadotetracontan-42-yl)amino)phenyl)diazenyl)phenyl)amino)-4-oxobutyl)-4-((tert-butoxycarbonyl)amino)pentanedioic acid, (18).....	20
1.2.14	(2S,4S)-2-amino-4-(4-((E)-4-((1-8-(4-((2-amino-9H-purin-6-yl)oxy)methyl)benzyl)amino)-4-oxobutanoyl)-8,9-dihydro-1H-dibenzo[b,f][1,2,3]triazolo[4,5-d]azo-cin-1-yl)-39-oxo-3,6,9,12,15,18,21,24,27,30,33,36-dodecaoxa-40-azadotetracontan-42-yl)amino)phenyl)diazenyl)phenyl)amino)-4-oxobutyl)pentanedioic acid, BGAG _{12,460}	21
1.2.15	(2S,4S)-2-Amino-4-(4-oxo-4-((E)-4-(38-oxo-2,5,8,11,14,17,20,23,26,29,32,35-dodecaoxa-39-azahentetracontan-41-amido)phenyl)diazenyl)phenyl)amino)butyl)-pentanedioic acid, D-AG ₁₂	22
1.2.16	(2S,4S)-2-Amino-4-(4-oxo-4-((E)-4-(38-oxo-2,5,8,11,14,17,20,23,26,29,32,35-dodecaoxa-39-azahentetracontan-41-yl)amino)phenyl)diazenyl)phenyl)amino)-butyl)pentanedioic acid, D-AG ₁₂₍₄₄₅₎	23
2	Spectral data	24
2.1	N-(4-(((2-Amino-9H-purin-6-yl)oxy)methyl)benzyl)pent-4-ynamide (3)	24
2.2	(2S,4S)-2-(4-((E)-4-(2-(3-azidopropanamido)acetamido)phenyl)diazenyl)phenyl)- amino)-4-oxobutyl)-4-((tert-butoxycarbonyl)amino)pentanedioic acid (14)	25
2.3	(2S,4S)-2-amino-4-(4-((E)-4-(2-(3-(4-3-(((2-amino-9H-purin-6-yl)oxy)methyl)benzyl)amino)-3-oxopropyl)-1H-1,2,3-triazol-1-yl)propanamido)acetamido)phenyl)diazenyl)phenyl)amino)-4-oxobutyl)pentanedioic acid, BGAG ₀	26
2.4	(2S,4S)-2-Amino-4-(4-((E)-4-(1-(4-(3-(((2-amino-9H-purin-6-yl)oxy)methyl)benzyl)amino)-3-oxopropyl)-1H-1,2,3-triazol-1-yl)-15-oxo-3,6,9,12-tetraoxa-16-azaoctadecan-18-amido)phenyl)diazenyl)phenyl)amino)-4-oxobutyl)-pentanedioic acid, BGAG ₄	27
2.5	(2S,4S)-2-Amino-4-(4-((E)-4-(1-(4-(3-(((2-amino-9H-purin-6-yl)oxy)methyl)benzyl)amino)-3-oxopropyl)-1H-1,2,3-triazol-1-yl)-27-oxo-3,6,9,12,15,18,21,24-octaoxa-28-azatriacontan-30-amido)phenyl)diazenyl)phenyl)amino)-4-oxobutyl)pentanedioic acid, BGAG ₈	28
2.6	(2S,4S)-2-Amino-4-(4-((E)-4-(1-(4-(3-(((2-amino-9H-purin-6-yl)oxy)methyl)benzyl)amino)-3-oxopropyl)-1H-1,2,3-triazol-1-yl)-39-oxo-3,6,9,12,15,18,21,24,27,30,33,36-dodecaoxa-40-azadotetracontan-42-amido)phenyl)diazenyl)phenyl)amino)-4-oxobutyl)pentanedioic acid, BGAG ₁₂	29
2.7	(2S,4S)-2-amino-4-(4-oxo-4-((E)-4-(38-oxo-2,5,8,11,14,17,20,23,26,29,32,35-dodecaoxa-39-azahentetracontan-41-amido)phenyl)diazenyl)phenyl)amino)butyl)pentanedioic acid, D-AG ₁₂	31
2.8	Dimethyl (2S,4S)-2-(4-((E)-4-((2-aminoethyl)amino)phenyl)diazenyl) phenyl)amino)-4-oxobutyl)-4-((tert-butoxycarbonyl)amino) pentanedioate.....	32
2.9	(2S,4S)-2-(4-((E)-4-((2-aminoethyl)amino)phenyl)diazenyl)phenyl)amino)-4-oxobutyl)-4-((tert-butoxycarbonyl)amino)pentanedioic acid, (10).....	33
2.10	(2S,4S)-2-Amino-4-(4-oxo-4-((E)-4-(38-oxo-2,5,8,11,14,17,20,23,26,29,32,35-dodecaoxa-39-azahentetracontan-41-yl)amino)phenyl)diazenyl)phenyl)-amino)butyl)pentanedioic acid, D-AG _{12,445}	34
3	Supporting Figures	35

4	References	44
---	------------------	----

1 Experimental

1.1 General

Solvents for chromatography and reactions were purchased HPLC grade (except DMF was purchased from Acros, 99.8 %, extra dry over molecular sieves) or distilled over an appropriate drying reagent prior to use. If necessary, solvents were degassed either by freeze-pump-thaw or by bubbling N₂ through the vigorously stirred solution for several minutes. Unless otherwise stated, all other reagents were used without further purification from commercial sources.

Flash column chromatography was carried out on silica gel 60 (0.040–0.063 mm) purchased from Merck. Reactions and chromatography fractions were monitored by thin layer chromatography (TLC) on Merck silica gel 60 F254 glass plates. The plates were visualized under UV light at 254 nm.

NMR spectra were recorded in deuterated solvents on a BRUKER Avance III HD 400 (equipped with a CryoProbe™) instruments and calibrated to residual solvent peaks (¹H/¹³C in ppm): DMSO-d₆ (2.50/39.52), Me₃OD-d₄ (3.31/49.00). Multiplicities are abbreviated as follows: s = singlet, d = doublet, t = triplet, q = quartet, br = broad, m = multiplet. Spectra are reported based on appearance, not on theoretical multiplicities derived from structural information.

High-resolution electrospray (ESI) mass spectra were obtained on a Varian MAT 711 MS instrument operating in either positive or negative ionization modes.

LC-MS was performed on an Agilent 1260 Infinity HPLC System, MS-Agilent 1100 Series, Type: 1946D, Model: SL, equipped with a Agilent Zorbax Eclipse Plus C18 (100 x 4.6 mm, particle size 3.5 micron) RP column with a constant flow-rate of 2 mL/min, if not stated otherwise. Retention times (*t_R*) are given in minutes (min).

HPLC was performed on a Varian Prep Star HPLC System, Model SD-1 equipped with Varian Dynamax columns (RP-Analytical: Microsorb 60 C18, 250 x 4.6 mm, particle size 8 μm; RP-SemiPrep: Microsorb 60 C18, 250 x 21.4 mm, particle size 8 μm; RP-Prep: Microsorb 60 C18, 250 x 41.4 mm, particle size 8 μm). Prior to injection, samples were filtered through a syringe filter (Chromafil Xtra GF100/25, pore size 1 μm).

1.2 Synthesis of BGAGs

A. General procedure for attachment of the Azide-functionalized PEG-linker

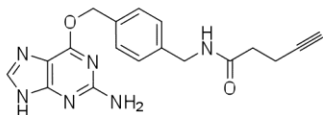
In a schlenk flask, **8** or *N*-Boc-*D*-redAGO **10** (1.1 equiv.), Azido-(PEG)_{*n*}-NHS-ester (Baseclick, *n* = 4 (**11**, #BCL-001), *n* = 8 (**12**, #BCL-032), *n* = 12 (**13**, #BCL-033); 1.0 equiv.) and DIPEA (2.0 equiv.) were added to degassed, anhydrous DMF (0.5 mL) under N₂-atmosphere. The reaction mixture was stirred at r.t. while reaction progress was monitored by LCMS. Upon completion, the crude reaction mixture was purified by C18 reverse phase (RP) flash column chromatography (100/0 → 60/40 = 1 mM HCl/MeCN) or by RP-HPLC (MeCN/H₂O/formic acid = 10/90/0.1 → 80/20/0.1 over 42 min). The product containing fractions were combined, concentrated *in vacuo* and freeze-dried to obtain the desired product.

B. General procedure for click reaction

In a schlenk flask, the reaction mixture was prepared with the corresponding azide (1.0 equiv.) and BG-alkyne (**SI2.1**) (1.1 eq) in degassed DMSO (2–4 mL) under N₂-atmosphere. Stock solutions of sodium ascorbate (NaAsc, 131 mM) and copper-(II)-sulfate pentahydrate (105 mM) were prepared separately in degassed water. 50 μL of each stock solution were mixed under N₂ to preform the catalytically active Cu^I species and quickly transferred to the reaction mixture. The resulting reaction mixture was heated to 90 °C and reaction progress was monitored by LCMS. Upon completion, the crude product was purified by RP flash column chromatography (100/0 → 60/40 = 1 mM HCl/MeCN) or RP-HPLC (MeCN/H₂O/formic acid = 10/90/0.1 → 80/20/0.1 over 42 min). The product containing fractions were combined, concentrated *in vacuo* and freeze-dried to obtain the desired product.

C. General procedure for Boc-deprotection:

In a falcon tube, neat TFA (250 μL) was added to the Boc-protected molecule and stirred at r.t. for 10 min. Diethylether (50 mL) was added and the resulting suspension was centrifuged (4000 rpm, 20 min, 4 °C). The supernatant was discarded, the solid was washed again with diethylether and finally dried under high vacuum to obtain the desired product.

1.2.1 N-(4-(((2-Amino-9H-purin-6-yl)oxy)methyl)benzyl)pent-4-ynamide (3)

6-((4-(Aminomethyl)benzyl)oxy)-9H-purin-2-amine¹ (**BG**) (382 mg, 1.41 mmol, 1.2 equiv.), 4-pentynoic acid (**2**) (115 mg, 1.17 mmol, 1.0 equiv.), HBTU (489 mg, 1.29 mmol, 1.1 equiv.) and DIPEA (302 mg, 2.34 mmol, 409 μ L, 2.0 equiv.) were dissolved in DMF (5 mL). Reaction progress was monitored by LCMS and after completion, the crude reaction mixture was subjected to RP-HPLC (MeCN/H₂O/FA = 10/90/0.1 \rightarrow 80/20/0.1 over 40 min). The product containing fractions were combined, concentrated *in vacuo* and dried under high vacuum to obtain the product BG-alkyne (**3**) (178 mg, 0.508 mmol) as a white powder in 43% yield.

NMR spectroscopy revealed two rotamers, proven by heating the NMR sample to 50 °C and merging of the spectroscopic signals (data not shown). Peaks are reported for the major rotamer.

¹H NMR (400 MHz, DMSO-d₆): δ [ppm] = 8.45–8.34 (m, 1H), 8.13 (s, 1H), 8.10 (s, 1H), 7.47 (d, J = 8.4 Hz, 2H), 7.29 (d, J = 8.4 Hz, 2H), 6.59 (br s, 2H), 5.48 (s, 2H), 4.32–4.21 (m, 2H), 2.78 (m, 1H), 2.43–2.28 (m, 4H).

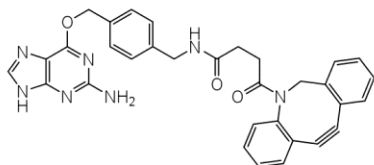
¹³C NMR (101 MHz, DMSO-d₆): δ [ppm] = 170.3, 159.2, 159.1, 155.0, 141.0, 139.5, 134.7, 128.7, 127.3, 126.4, 83.8, 71.4, 67.2, 41.9, 34.2, 14.3.

HRMS (ESI): calc. for C₁₈H₁₉N₆O₂⁺ (M+H)⁺: 351.1564, found: 351.1562.

UV/Vis (LCMS): $\lambda_{\text{max}1}$ = 196 nm, $\lambda_{\text{max}2}$ = 212 nm, $\lambda_{\text{max}3}$ = 287 nm.

t_{R} (LCMS; MeCN/H₂O/formic acid = 10/90/0.1 \rightarrow 90/10/0.1 over 7 min) = 1.955 min.

1.2.2 N-(4-(((2-Amino-9H-purin-6-yl)oxy)methyl)benzyl)benzyl)-4-(11,12-dehydrodibenzo[b,f]azocin-5(6H)-yl)-4-oxobutanamide (5)



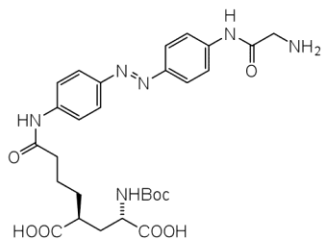
6-((4-(Aminomethyl)benzyl)oxy)-9H-purin-2-amine¹ (**BG**) (6.7 mg, 24.9 μmol , 1.0 equiv.), DBCO-NHS-ester (Jena Bioscience, CLK-A133-25, **4**) (10.0 mg, 24.9 μmol , 1.0 equiv.) and DIPEA (6.4 mg, 49.8 μmol , 8.7 μL , 2.0 equiv.) were dissolved in DMSO (0.5 mL). Reaction progress was monitored by LCMS and after completion the crude reaction mixture was subjected to RP-HPLC (MeCN/H₂O/FA = 5/95/0.1 \rightarrow 80/20/0.1 over 40 min). The product containing fractions were combined, concentrated *in vacuo* and dried under high vacuum to obtain **5** (1.0 mg, 1.79 μmol) in 7% yield. The low yield can be attributed to residual water in the used DMSO as the corresponding DBCO-acid was obtained as the main product.

HRMS (ESI): calc. for C₃₂H₂₈N₇O₃⁺ [M+H]⁺: 558.2248, found: 558.2254.

UV/Vis (LCMS): λ_{max} = 290 nm.

t_R (LCMS; MeCN/H₂O/formic acid = 10/90/0.1 \rightarrow 90/10/0.1 over 7 min) = 3.118 min.

1.2.3 (2S,4S)-2-(4-((4-((E)-(4-(2-Aminoacetamido)phenyl)diazenyl)phenyl)amino)-4-oxobutyl)-4-((tert-butoxycarbonyl)amino)pentanedioic acid (6)



6 was prepared according to a literature procedure and analytical data matched the one reported.²

¹H-NMR (400 MHz, DMSO-d₆) δ [ppm] = 10.29 (s, 1H), 7.93–7.75 (m, 9H), 6.60 (d, *J* = 7.8 Hz, 1H), 3.90 (q, *J* = 8.1 Hz, 1H), 3.78 (s, 2H), 2.44–2.25 (m, 3H), 1.88–1.42 (m, 6H), 1.36 (s, 9H).

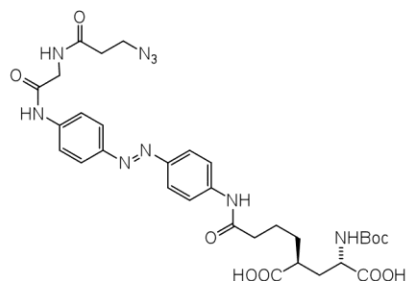
¹³C NMR (101 MHz, DMSO-d₆) δ [ppm] = 176.3, 174.0, 171.5, 165.9, 155.1, 148.0, 147.4, 142.2, 140.9, 123.5, 123.4, 119.4, 119.2, 77.9, 55.0, 52.0, 41.6, 40.1, 36.5, 30.9, 28.2, 23.0.

HRMS (ESI): calc. for C₂₈H₃₇N₆O₈⁺ [M+H]⁺: 585.2667, found: 585.2673.

UV/VIS (LCMS): λ_{max} (π → π*) = 368 nm.

t_R (LCMS, MeCN/H₂O/formic acid = 90/10/0.1 → 10/90/0.1 over 7 min) = 2.418 min.

1.2.4 (2S,4S)-2-4-((4-((E)-4-(2-(3-azidopropanamido)acetamido)phenyl)diazenyl)phenyl)-amino)-4-oxobutyl)-4-((tert-butoxycarbonyl)amino)pentanedioic acid (14**)**



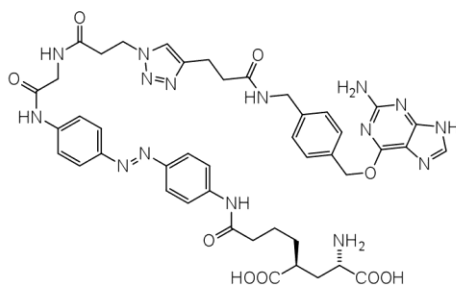
A schlenk flask was charged with **8** (10 mg, 17 μ mol, 1.0 equiv.), HBTU (7.2 mg, 19 μ mol, 1.1 equiv.) and 3-azidopropionic acid³ (3.0 mg, 16 μ mol, 1.5 equiv.) under a N₂-atmosphere. Degassed, anhydrous DMF (1 mL) was added and the reaction mixture was cooled to 0 °C before DIPEA (6.0 μ L, 34 μ mol, 2.0 equiv.) was added dropwise. The reaction mixture was allowed to warm to r.t. and reaction progress was monitored by LCMS. Upon completion, the crude reaction mixture was purified by RP-HPLC (10/90/0.1 \rightarrow 80/20/0.1 = MeCN/H₂O/formic acid over 45 min). The product containing fractions were combined, concentrated *in vacuo* and freeze-dried to obtain 10 mg (15 μ mol) of **14** as a yellow solid in 88% yield.

¹H NMR (400 MHz, DMSO-d₆) δ [ppm] = 10.34 (s, 1H), 10.25 (s, 1H), 8.43 (t, *J* = 5.8 Hz, 1H), 7.98–7.71 (m, 8H), 3.96 (d, *J* = 5.7 Hz, 2H), 3.89 (t, *J* = 7.3 Hz, 1H), 3.53 (t, *J* = 6.4 Hz, 2H), 2.67 (s, 1H), 2.43–2.23 (m, 4H), 1.86–1.42 (m, 6H), 1.36 (s, 9H).

HRMS (ESI): calc. for C₃₁H₃₈N₉O₉ [M-H]⁻: 680.2798, found: 680.2798.

t_R (RP-HPLC, MeCN/H₂O/formic acid = 10/90/0.1 \rightarrow 80/20/0.1 over 42 min) = 26.2 min (*trans*)

1.2.5 (2S,4S)-2-Amino-4-(4-((4-((E)-4-(2-(3-(4-(3-(4-(3-(((2-amino-9H-purin-6-yl)oxy)methyl)benzyl)amino)-3-oxopropyl)-1H-1,2,3-triazol-1-yl)propanamido)acetamido)-phenyl)diazenyl)phenyl)amino)-4-oxobutyl)pentanedioic acid, BGAG₀



BGAG₀ was prepared according to general procedures B and C.

Amounts:

3 (5.8 mg, 17 μ mol, 1.1 equiv.)

14 (10 mg, 15 μ mol, 1.0 equiv.)

yield: 3.3 mg (3.5 μ mol, 23% over two steps), yellow solid.

¹H NMR (400 MHz, DMSO-d₆) δ 10.52 (s, 1H), 10.33 (s, 1H), 10.27 (s, 1H), 8.51–8.24 (m, 3H), 7.96–7.59 (m, 8H), 7.52 (dd, *J* = 8.9, 3.1 Hz, 1H), 7.41 (m, 2H), 7.23 (t, *J* = 9.0 Hz, 3H), 7.18–7.06 (m, 1H), 6.98 (s, 1H), 6.82 (t, *J* = 7.4 Hz, 1H), 6.29 (br s, 2H), 5.42 (br s, 2H), 4.52 (t, *J* = 7.0 Hz, 2H), 4.27 (t, *J* = 4.9 Hz, 2H), 3.94 (d, *J* = 5.7 Hz, 2H), 3.60 (s, 1H), 3.16 (d, *J* = 4.0 Hz, 1H), 2.90–2.83 (m, 2H), 2.79 (t, *J* = 6.8 Hz, 2H), 2.67 (p, *J* = 1.7 Hz, 1H), 2.41–2.31 (m, 3H), 1.88–1.33 (m, 6H).

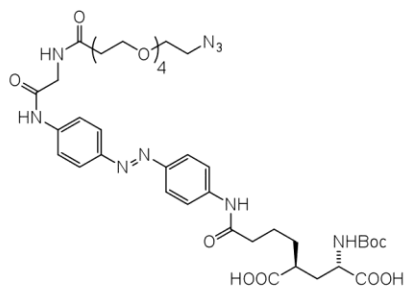
HRMS (ESI): calc. for C₄₄H₄₈N₁₅O₉⁻ [M-H]⁻: 930.3765, found: 930.3770.

t_R (RP-HPLC, MeCN/H₂O/formic acid = 10/90/0.1 → 80/20/0.1 over 42 min) = 18.4 min (*trans*, before Boc-deprotection).

UV/VIS (LCMS): λ_{\max} ($\pi \rightarrow \pi^*$) = 368 nm.

t_R (LCMS, MeCN/H₂O/formic acid = 90/10/0.1 → 10/90/0.1 over 10 min, flow: 1 ml/min) = 3.960 min.

1.2.6 (2S,4S)-2-((4-((E)-4-((1-Azido-15-oxo-3,6,9,12-tetraoxa-16-azaoctadecan-18-yl)amino)phenyl)diazenyl)phenyl)amino)-4-oxobutyl)-4-((tert-butoxycarbonyl)amino)pentanedioic acid (15)



15 was prepared according to general procedure A.

Amounts:

N₃-PEG₄-NHS-ester (#BCL-001, 8.6 mg, 22 μmol, 1.1 equiv.)

8 (14.3 mg, 24 μmol, 1.0 equiv.)

DIPEA (7.7 μL, 44 μmol, 2.0 equiv.)

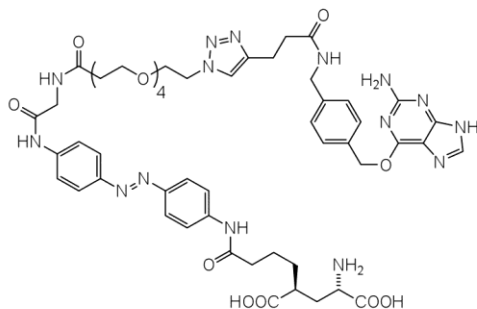
yield: 18.0 mg (21 μmol, 86%), yellow solid.

HRMS (ESI): calc. for C₃₉H₅₄N₉O₁₃⁻ [M-H]⁻: 856.3847, found: 856.3844.

UV/VIS (LCMS): λ_{max} (π → π*) = 368 nm.

t_R (LCMS, MeCN/H₂O/formic acid = 90/10/0.1 → 10/90/0.1 over 10 min) = 5.130 min.

1.2.7 (2S,4S)-2-Amino-4-(4-((4-((E)-4-(1-(4-(3-((4-((2-amino-9H-purin-6-yl)oxy)methyl)-benzyl)amino)-3-oxopropyl)-1H-1,2,3-triazol-1-yl)-15-oxo-3,6,9,12-tetraoxa-16-azaoctadecan-18-amido)phenyl)diazenyl)phenyl)amino)-4-oxobutyl)-pentanedioic acid, BGAG₄



BGAG₄ was prepared according to general procedures B and C.

Amounts:

3 (7.8 mg, 23 μ mol, 1.1 equiv.)

15 (18 mg, 21 μ mol, 1.0 equiv)

yield: 5.1 mg (5 μ mol, 24% over two steps).

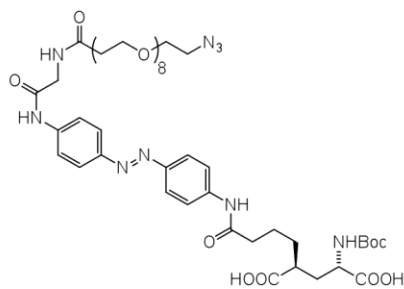
¹H NMR (400 MHz, DMSO-*d*₆) δ [ppm] = 10.58 (s, 1H), 10.33 (s, 1H), 10.30 (s, 1H), 8.37 (t, *J* = 6.2 Hz, 2H), 8.28 (t, *J* = 5.8 Hz, 2H), 7.89–7.69 (m, 12H), 7.23 (d, *J* = 7.9 Hz, 2H), 7.14 (d, *J* = 7.9 Hz, 2H), 6.28 (s, 2H), 4.44 (t, *J* = 5.1 Hz, 4H), 4.23 (d, *J* = 5.9 Hz, 2H), 3.93 (d, *J* = 5.7 Hz, 2H), 3.77 (t, *J* = 5.3 Hz, 3H), 3.62 (t, *J* = 6.5 Hz, 2H), 3.54–3.44 (m, 12H), 2.86 (t, *J* = 7.6 Hz, 2H), 2.45–2.30 (m, 5H), 1.97–1.72 (m, 3H), 1.70–1.39 (m, 6H).

HRMS (ESI): calc. for C₅₂H₆₆N₁₅O₁₃⁺ [M+H]⁺: 1108.4959, found: 1108.4943.

UV/VIS (LCMS): λ_{\max} ($\pi \rightarrow \pi^*$) = 368 nm.

*t*_R (LCMS, MeCN/H₂O/formic acid = 90/10/0.1 \rightarrow 10/90/0.1 over 10 min) = 2.927 min.

1.2.8 (2S,4S)-2-(4-((4-((E)-4-((1-Azido-27-oxo-3,6,9,12,15,18,21,24-octaoxa-28-azatriacontan-30-yl)amino)phenyl)diazanyl)-phenyl)amino)4-oxobutyl)-4-((tert-butoxycarbonyl)-amino)pentanedioic acid (16)



16 was prepared according to general procedure A.

Amounts:

N₃-PEG₈-NHS-ester (#BCL-032, 10.0 mg, 17.7 μmol, 1.0 equiv.)

8 (11.4 mg, 19.5 μmol, 1.1 equiv.)

DIPEA (6.2 μL, 35.4 μmol, 2.0 equiv.)

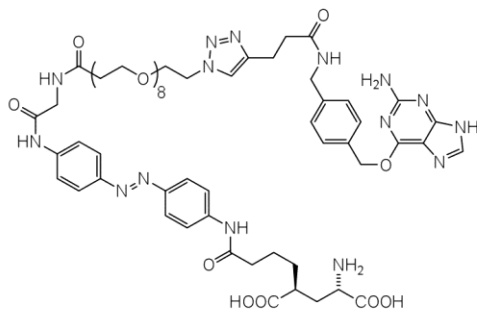
yield: 18.0 mg (17 μmol, 89%), yellow solid.

HRMS (ESI): calc. for C₄₇H₆₉N₉O₁₇²⁻ [M-2H]²⁻: 515.7411, found: 515.7407.

UV/VIS (LCMS): λ_{max} (π → π*) = 368 nm.

t_R (LCMS, MeCN/H₂O/formic acid = 90/10/0.1 → 10/90/0.1 over 10 min) = 4.998 min.

1.2.9 (2S,4S)-2-Amino-4-(4-((4-((E)-4-(1-(4-(3-((4-((2-amino-9H-purin-6-yl)oxy)methyl)-benzyl)amino)-3-oxopropyl)-1H-1,2,3-triazol-1-yl)-27-oxo-3,6,9,12,15,18,21,24-octa-oxa-28-azatriacontan-30-amido)phenyl)diazenyl)phenyl)amino)-4-oxobutyl)pentane-dioic acid, BGAG₈



BGAG₈ was prepared according to general procedures B and C.

Amounts:

3 (7.1 mg, 21 μmol, 1.2 equiv.)

16 (18 mg, 17 μmol, 1.0 equiv.)

yield: 9.6 mg (7.5 μmol, 44% over two steps), yellow solid.

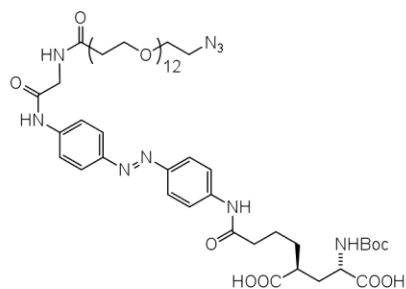
¹H NMR (400 MHz, DMSO-d₆) δ 10.91 (s, 1H), 10.32 (s, 1H), 10.29 (s, 1H), 8.43–8.20 (m, 5H), 8.09 (s, 1H), 7.89–7.72 (m, 10H), 7.23 (d, *J* = 7.7 Hz, 2H), 7.14 (d, *J* = 7.7 Hz, 2H), 6.55 (s, 2H), 4.73 (s, 1H), 4.50–4.39 (m, 4H), 4.23 (d, *J* = 6.3 Hz, 2H), 3.93 (d, *J* = 5.8 Hz, 2H), 3.77 (t, *J* = 5.3 Hz, 2H), 3.62 (t, *J* = 6.6 Hz, 2H), 3.49 (d, *J* = 4.6 Hz, 2H), 2.86 (t, *J* = 7.7 Hz, 2H), 2.46–2.31 (m, 6H), 2.10–1.96 (m, 1H), 1.85 (dt, *J* = 14.2, 7.0 Hz, 1H), 1.58 (d, *J* = 6.3 Hz, 5H).

HRMS (ESI): calc. for C₆₀H₈₂N₁₅O₁₇⁺ [M+H]⁺: 1284.6008, found: 1284.6004.

UV/VIS (LCMS): λ_{max} (π → π*) = 368 nm.

t_R (LCMS, MeCN/H₂O/formic acid = 90/10/0.1 → 10/90/0.1 over 10 min) = 3.059 min.

1.2.10 (2S,4S)-2-(4-((4-((E)-4-(1-Azido-39-oxo-3,6,9,12,15,18,21,24,27,30,33,36-dodecaoxa-40-azadotetracontan-42-amido)phenyl)diazenyl)phenyl)amino)-4-oxobutyl)-4-((tert-butoxycarbonyl)amino)pentanedioic acid (17)



17 was prepared according to general procedure A.

Amounts:

N₃-PEG₁₂-NHS-Ester (Baseclick #BCL-033, 10.0 mg, 13.5 μmol, 1.0 equiv.)

8 (8.7 mg, 14.8 μmol, 1.1 equiv.)

DIPEA (3.5 mg, 27.0 μmol, 4.7 μL, 2.0 equiv.)

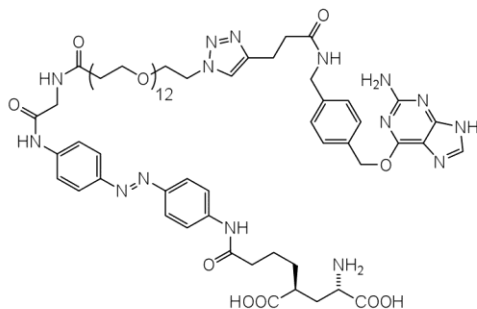
yield: 13.0 mg (10.8 μmol, 80%), yellow solid.

HRMS (ESI): calc. for C₅₅H₈₅N₉O₂₁²⁻ [M-2H]²⁻: 603.7936, found: 603.7937.

UV/Vis (LCMS): λ_{max} (π → π*) = 368 nm.

t_R (LCMS; MeCN/H₂O/formic acid = 10/90/0.1 → 90/10/0.1 over 7 min) = 3.232 min.

1.2.11 (2S,4S)-2-Amino-4-(4-((4-((E)-4-(1-(4-(3-((4-(((2-amino-9H-purin-6-yl)oxy)methyl)benzyl)amino)-3-oxopropyl)-1H-1,2,3-triazol-1-yl)-39-oxo-3,6,9,12,15,18,21,24,27,30,33,36-dodecaoxa-40-azadotetracontan-42-amido)phenyl)diazenyl)phenyl)amino)-4-oxobutyl)pentanedioic acid, BGAG₁₂



BGAG₁₂ was prepared according to general procedures B and C.

Amounts:

3 (4.2 mg, 11.9 μmol , 1.2 equiv.)

17 (12.0 mg, 9.9 μmol , 1.0 equiv.)

yield: 6.8 mg (7.06 μmol , 65% over two steps), orange solid.

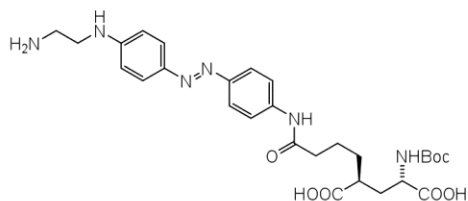
¹H NMR (400 MHz, DMSO-*d*₆): δ [ppm] = 10.30 (s, 1H), 10.26 (s, 1H), 8.47 (br s, 1H), 8.81 (t, *J* = 6.0 Hz, 1H), 8.36–8.16 (m, 3H), 7.93–7.68 (m, 8H), 7.48 (d, *J* = 6.0 Hz, 2H), 7.24 (d, *J* = 6.0 Hz, 2H), 6.88–6.74 (m, 1H), 5.53 (br s, 2H), 4.44 (t, *J* = 5.2 Hz, 2H), 4.27 (d, *J* = 6.0 Hz, 2H), 3.94 (d, *J* = 5.6 Hz, 2H), 3.87–3.78 (m, 1H), 3.76 (t, *J* = 5.2 Hz, 2H), 3.63 (t, *J* = 6.8 Hz, 2H), 3.56–3.41 (m, 44H), 2.86 (t, *J* = 8.0 Hz, 2H), 2.62–2.55 (m, 2H), 2.46–2.28 (m, 7H), 2.16–1.91 (m, 2H), 1.90–1.74 (m, 1H), 1.66–1.51 (m, 4H), 1.48–1.28 (m, 2H).

HRMS (ESI): calc. for C₆₈H₉₉N₁₅O₂₁²⁺[M+2H]²⁺: 730.8565, found: 730.8564.

UV/Vis (LCMS): λ_{max} ($\pi \rightarrow \pi^*$) = 369 nm.

t_R (LCMS; MeCN/H₂O/formic acid = 10/90/0.1 \rightarrow 90/10/0.1 over 7 min) = 2.463 min.

1.2.12 (2S,4S)-2-(4-((4-((E)-4-((2-aminoethyl)amino)phenyl)diazenyl)phenyl)amino)-4-oxobutyl)-4-((tert-butoxycarbonyl)amino)pentanedioic acid (10)



Dimethyl (2S,4S)-2-(4-((4-((E)-4-aminophenyl)diazenyl)phenyl)amino)-4-oxobutyl)-4-((tert-butoxycarbonyl)amino)pentanedioate² (200 mg, 0.360 mmol, 1.0 equiv.) and Fmoc-2-aminoacetaldehyde⁴ (101 mg, 0.360 mmol, 1.0 equiv.) were dissolved in DCE (10 mL) and one drop of acetic acid was added. Sodium triacetoxyborohydride (270 mg, 1.28 mmol, 3.6 equiv.) was added portionwise and the reaction mixture was stirred at r.t. for 4.5 h. The reaction mixture was quenched and subsequently washed with sat. aq. NaHCO₃ (3x) before the organic layer was concentrated *in vacuo*. The residue was redissolved in DMF (47.5 mL), piperidine (2.5 mL) was added and the deprotecting reaction was stirred overnight. The reaction mixture was concentrated *in vacuo*, the residue was redissolved in EtOAc, washed with sat. aq. NaHCO₃ (2x) and brine (sat.) before the organic layer was dried over MgSO₄. The solvent was removed *in vacuo* before purification by flash column chromatography (90/10/1 = DCM/MeOH/TEA) followed by RP column chromatography (100/0 → 60/40 = 1mM HCl/MeCN). The product containing fractions were combined, concentrated *in vacuo* and freeze-dried to obtain the intermediate bis-methylester dimethyl (2S,4S)-2-(4-((4-((E)-4-((2-aminoethyl)amino)phenyl)diazenyl)phenyl)amino)-4-oxobutyl)-4-((tert-butoxycarbonyl)amino) pentanedioate as its red-orange HCl salt (84 mg, 0.13 mmol) in 36% yield over 2 steps.

¹H-NMR (400 MHz, MeOD-d₄) δ [ppm] = 7.82–7.66 (m, 6H), 6.80 (d, *J* = 8.9 Hz, 2H), 4.16 (dd, *J* = 8.4, 6.2 Hz, 1H), 3.71–3.65 (m, 6H), 3.55 (t, *J* = 6.1 Hz, 2H), 3.18 (t, *J* = 6.8 Hz, 2H), 2.52 (p, *J* = 6.9 Hz, 1H), 2.44–2.35 (m, 2H), 2.01–1.90 (m, 2H), 1.73–1.57 (m, 3H), 1.42 (s, 9H), 1.29 (q, *J* = 6.6, 5.9 Hz, 1H).

¹³C-NMR (101 MHz, MeOH-d₄) δ [ppm] = 177.3, 174.3, 174.0, 157.9, 152.8, 149.7, 145.6, 141.5, 126.5, 123.7, 121.2, 113.7, 80.7, 53.4, 52.7, 52.4, 43.5, 41.7, 39.8, 37.6, 34.8, 32.6, 28.7, 24.2.

HRMS (ESI): calc. for C₃₀H₄₃O₇N₆⁺ [M+H]⁺: 599.3188, found: 599.3191.

UV/VIS (LCMS): λ_{max} = 412 nm.

t_R (LCMS, MeCN/H₂O/formic acid = 90/10/0.1 → 10/90/0.1 over 7 min) = 2.915 min.

In a round bottom flask, dimethyl (2S,4S)-2-(4-((4-((E)-4-((2-aminoethyl)amino)phenyl)diazenyl)phenyl)amino)-4-oxobutyl)-4-((tert-butoxycarbonyl)amino) pentanedioate (84 mg, 0.13 mmol, 1.0 equiv.) was dissolved in a mixture of H₂O (3.7 mL) and THF (7.3 mL) before lithium hydroxide (78 mg, 3.3 mmol, 25 equiv.) was added as a solid at 0 °C in one portion. The reaction was stirred for 2 h at 0 °C,

before it was neutralized by addition of formic acid (0.12 mL, 3.3 mmol, 25 equiv.). The THF was removed *in vacuo* before the aqueous phase was subjected to RP column chromatography (100/0 → 75/25 = 1 mM HCl/MeCN). The product containing fractions were combined, concentrated *in vacuo* and freeze-dried to obtain **10** as its red HCl salt (33.5 mg, 55 μmol) in 43% yield.

¹H-NMR (400 MHz, DMSO-d₆) δ [ppm] 10.18 (s, 1H), 7.80–7.64 (m, 6H), 6.82 (s, 1H), 6.75 (d, *J* = 8.6 Hz, 2H), 6.51 (d, *J* = 7.7 Hz, 1H), 3.91 (q, *J* = 8.2 Hz, 1H), 3.46–3.36 (m, 2H), 3.02 (t, *J* = 6.3 Hz, 2H), 2.47–2.37 (m, 1H), 2.32 (t, *J* = 7.2 Hz, 2H), 1.72–1.44 (m, 5H), 1.37 (s, 9H), 1.34 (s, 1H).

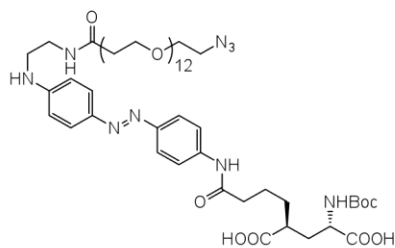
¹³C-NMR (101 MHz, DMSO-d₆) δ [ppm] = 176.9, 174.7, 171.8, 155.3, 151.5, 148.2, 143.8, 141.3, 125.2, 123.0, 119.7, 112.4, 78.2, 52.9, 42.4, 40.7, 38.3, 37.0, 35.8, 31.6, 28.7, 23.6.

HRMS (ESI): calc. for C₂₈H₃₉O₇N₆⁺ [M+H]⁺: 571.2875, found: 571.2877.

UV/VIS (LCMS): λ_{max} = 412 nm.

t_R (LCMS, MeCN/H₂O/formic acid = 90/10/0.1 → 10/90/0.1 over 7 min) = 2.438 min.

1.2.13 (2S,4S)-2-(4-((4-((E)-4-((1-azido-39-oxo-3,6,9,12,15,18,21,24,27,30,33,36-dodecaoxa-40-azadotetracontan-42-yl)amino)phenyl)diazenyl)phenyl)amino)-4-oxobutyl)-4-((tert-butoxycarbonyl)amino)pentanedioic acid, (18)



18 was prepared according to general procedure A.

Amounts:

N₃-PEG₁₂-NHS-Ester (Baseclick #BCL-033, 10.0 mg, 13.5 μmol, 1.0 equiv.)

10 (8.5 mg, 14.9 μmol, 1.1 equiv.)

DIPEA (3.5 mg, 27.0 μmol, 4.7 μL, 2.0 equiv.)

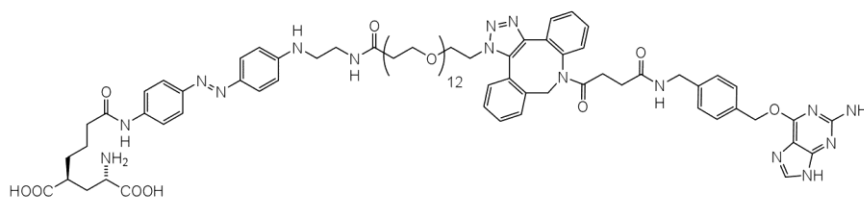
yield: 14.0 mg (11.7 μmol, 87%), red-orange solid.

HRMS (ESI): calc. for C₅₅H₈₇N₉O₂₀²⁻ [M-2H]²⁻: 596.8039, found: 596.8035.

UV/Vis (LCMS): λ_{max} = 412 nm.

t_R (LCMS; MeCN/H₂O/formic acid = 10/90/0.1 → 90/10/0.1 over 10 min) = 5.117 min.

1.2.14 (2S,4S)-2-amino-4-(4-((4-((E)-4-((1-(8-(4-((4-(((2-amino-9H-purin-6-yl)oxy)methyl)-benzyl)amino)-4-oxobutanoyl)-8,9-dihydro-1H-dibenzo[b,f][1,2,3]triazolo[4,5-d]azocin-1-yl)-39-oxo-3,6,9,12,15,18,21,24,27,30,33,36-dodecaoxa-40-azadotetracontan-42-yl)amino)phenyl)diazenyl)phenyl)amino)-4-oxobutyl)pentanedioic acid, BGAG_{12,460}



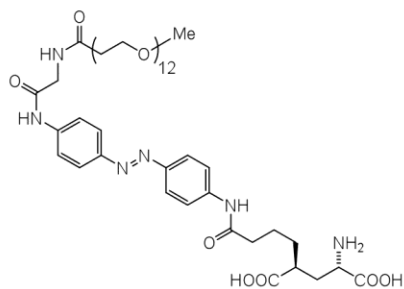
In a round bottom flask, **5** (1.0 mg, 1.79 μmol) and **18** (2.1 mg, 1.79 μmol) were combined and dissolved in MeOH. After stirring at r.t. for 30 min all starting material was consumed according to LCMS and all volatiles were removed *in vacuo* to obtain the crude protected triazole. The solid was treated with 0.35 mL neat TFA for 10 min at r.t. before Et₂O was added and the suspension was subjected to sedimentation (4,000 rpm, r.t., 20 min) to collect a deep-red solid, which was washed again with Et₂O and dried under HV to obtain 1.2 mg (1.03 μmol) **BGAG₁₂₍₄₆₀₎** in 58% yield (over 2 steps).

HRMS (ESI): calc. for C₈₂H₁₁₀N₁₆O₂₁²⁺ (M+2H)²⁺: 827.4010, found: 827.4015.

UV/Vis (LCMS): λ_{max} = 413 nm.

t_R (LCMS; MeCN/H₂O/formic acid = 10/90/0.1 \rightarrow 90/10/0.1 over 7 min) = 2.601 min.

1.2.15 (2S,4S)-2-Amino-4-(4-oxo-4-((4-((E)-(4-(38-oxo-2,5,8,11,14,17,20,23,26,29,32,35-dodecaoxa-39-azahentetracontan-41-amido)phenyl)diazanyl)phenyl)amino)butyl)-pentanedioic acid, D-AG₁₂



D-AG₁₂ was prepared according to general procedures A and C.

Amounts:

Methyl-PEG₁₂-NHS-ester (Thermo Scientific #22685, 9.7 mg, 14 μmol, 1.0 equiv.)

8 (9.1 mg, 16 μmol, 1.1 equiv.)

DIPEA (4.9 μL, 28 μmol, 2 equiv.)

yield: 8.0 mg (7.6 μmol, 54% over two steps), orange solid.

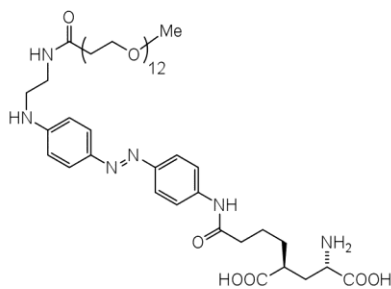
¹H-NMR (400 MHz, DMSO-*d*₆) δ [ppm] = 10.31 (s, 1H), 10.27 (s, 1H), 8.27 (t, *J* = 5.8 Hz, 1H), 7.88–7.76 (m, 8H), 3.93 (d, *J* = 5.7 Hz, 2H), 3.63 (t, *J* = 6.5 Hz, 5H), 3.50 (s, 45H), 3.23 (s, 4H), 2.61 (s, 1H), 2.43 (t, *J* = 6.5 Hz, 5H), 2.36 (t, *J* = 7.0 Hz, 2H), 1.83 (s, 1H), 1.60 (p, *J* = 11.4, 10.7 Hz, 3H), 1.48–1.39 (m, 1H).

HRMS (ESI): calc. for C₄₉H₇₉N₆NaO₁₉²⁺ [M+Na+H]²⁺: 539.2643, found: 539.2639.

UV/VIS (LCMS): λ_{max} (π → π*) = 368 nm.

t_R (LCMS, MeCN/H₂O/formic acid = 90/10/0.1 → 10/90/0.1 over 10 min) = 3.346 min.

1.2.16 (2S,4S)-2-Amino-4-(4-oxo-4-((4-((E)-4-((38-oxo-2,5,8,11,14,17,20,23,26,29,32,35-dodecaoxa-39-azahentetracontan-41-yl)amino)phenyl)diazenyl)phenyl)amino)-butyl)pentanedioic acid, D-AG₁₂₍₄₄₅₎



D-AG₁₂₍₄₄₅₎ was prepared according to general procedures A and C.

Amounts:

Methyl-PEG12-NHS-ester (Thermo Scientific, #22685, 9.8 mg, 14 μ mol, 1.0 equiv.)

18 (9.0 mg, 16 μ mol, 1.1 equiv.)

yield: 12 mg, (12 μ mol, 73% over two steps), red solid.

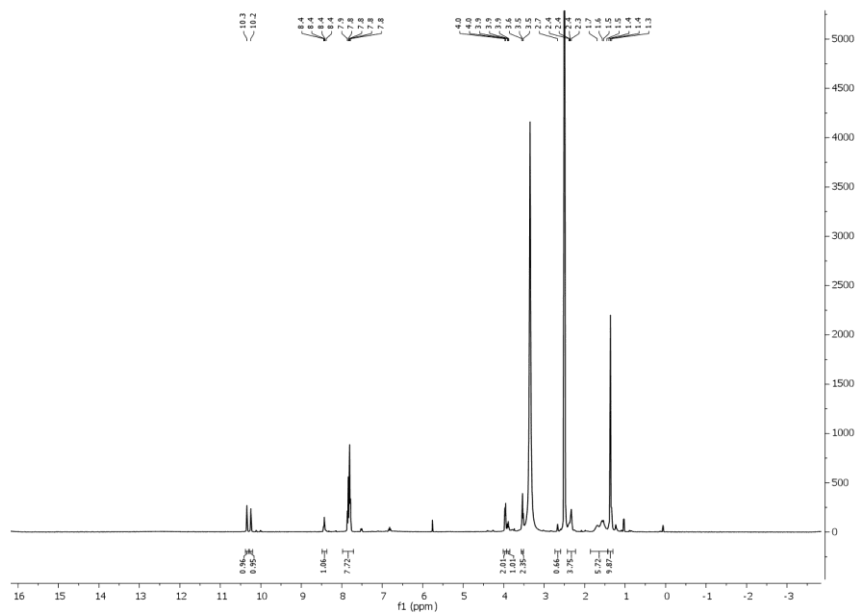
¹H NMR (400 MHz, DMSO-d₆) δ [ppm] = 10.17 (s, 1H), 8.03 (t, J = 5.5 Hz, 1H), 7.71 (dt, J = 12.6, 9.1 Hz, 6H), 6.70 (d, J = 8.8 Hz, 2H), 6.62 (s, 1H), 3.62 (dt, J = 18.7, 7.1 Hz, 4H), 3.49 (d, J = 3.0 Hz, 50H), 2.60 (q, J = 7.3 Hz, 1H), 2.34 (q, J = 6.6 Hz, 5H), 1.95–1.74 (m, 2H), 1.68–1.37 (m, 5H).

HRMS (ESI): calc. for C₄₉H₈₁N₆NaO₁₈²⁺ [M+Na+H]⁺: 532.2747, found: 532.2743.

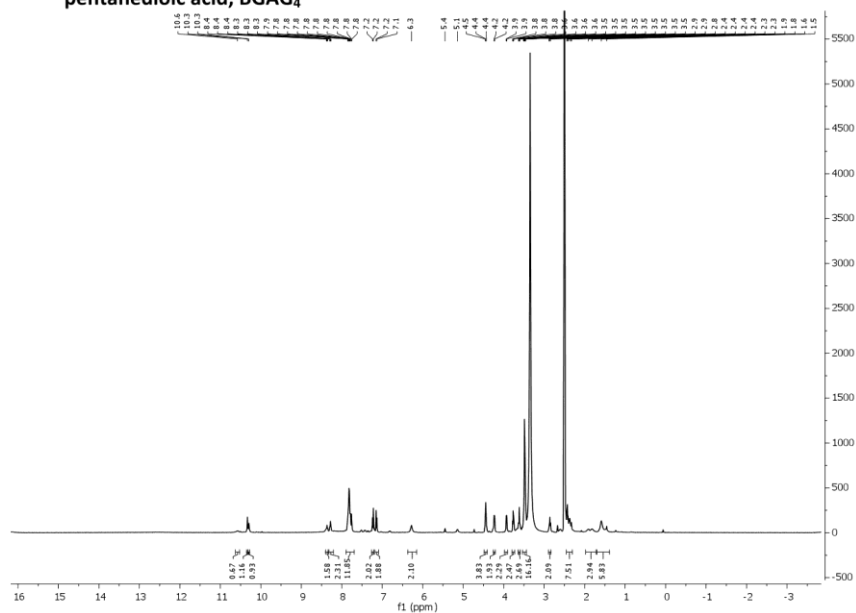
UV/VIS (LCMS): λ_{max} = 412 nm.

t_{R} (LCMS, MeCN/H₂O/formic acid = 90/10/0.1 \rightarrow 10/90/0.1 over 10 min) = 3.397 min.

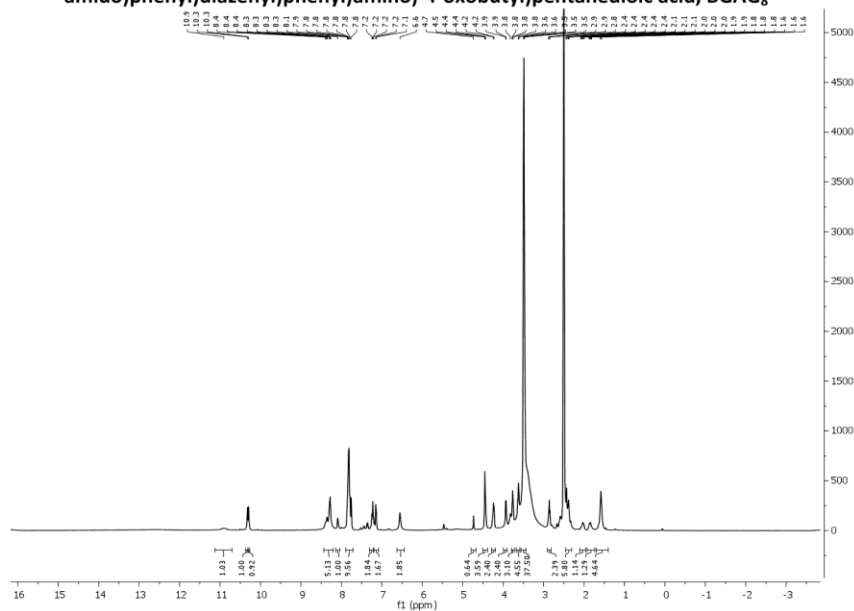
2.2 (2S,4S)-2-(4-((4-((E)-4-(2-(3-azidopropanamido)acetamido)phenyl)diazenyl)phenyl)-amino)-4-oxobutyl)-4-((tert-butoxycarbonyl)amino)pentanedioic acid (14)



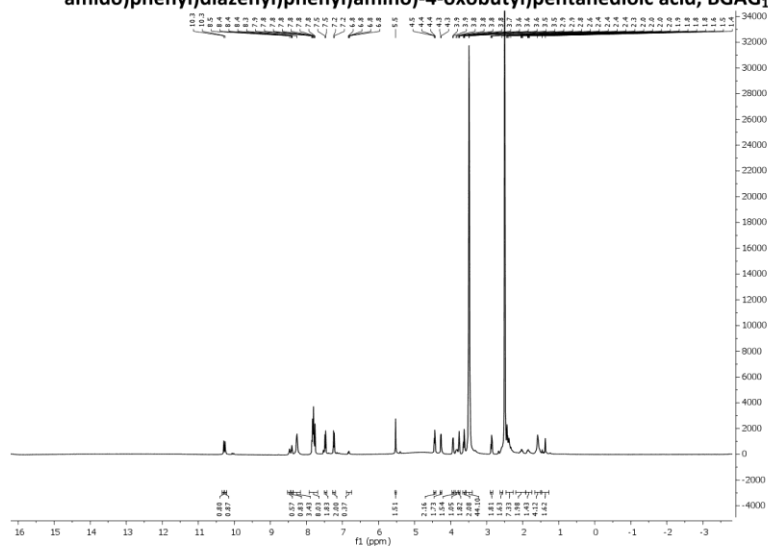
2.4 (2S,4S)-2-Amino-4-(4-((E)-4-(1-(4-(3-(((2-amino-9H-purin-6-yl)oxy)methyl)benzyl)amino)-3-oxopropyl)-1H-1,2,3-triazol-1-yl)-15-oxo-3,6,9,12-tetraoxa-16-azaoctadecan-18-amido)phenyl)diazenyl)phenyl)amino)-4-oxobutyl)-pentanedioic acid, BGAG₄

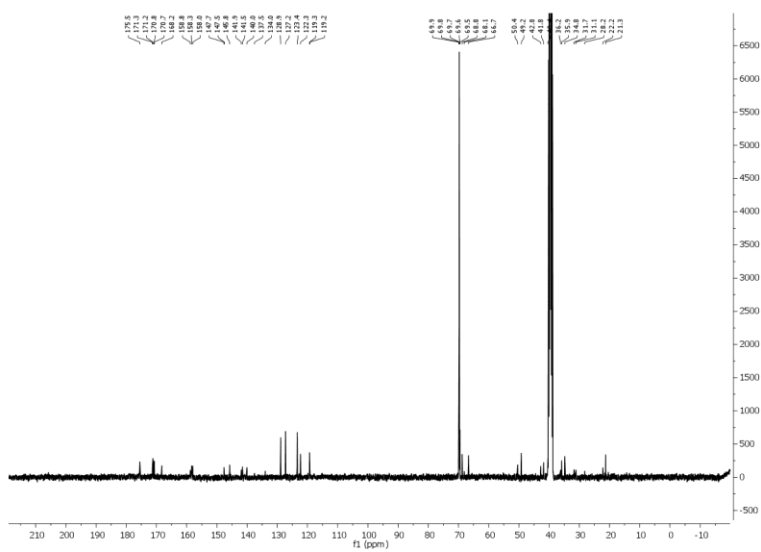


2.5 (2S,4S)-2-Amino-4-(4-((E)-4-(1-(4-(3-(((2-amino-9H-purin-6-yl)oxy)methyl)benzyl)amino)-3-oxopropyl)-1H-1,2,3-triazol-1-yl)-27-oxo-3,6,9,12,15,18,21,24-octaoxa-28-azatriacontan-30-amido)phenyl)diazenyl)phenyl)amino)-4-oxobutyl)pentanedioic acid, BGAG₈

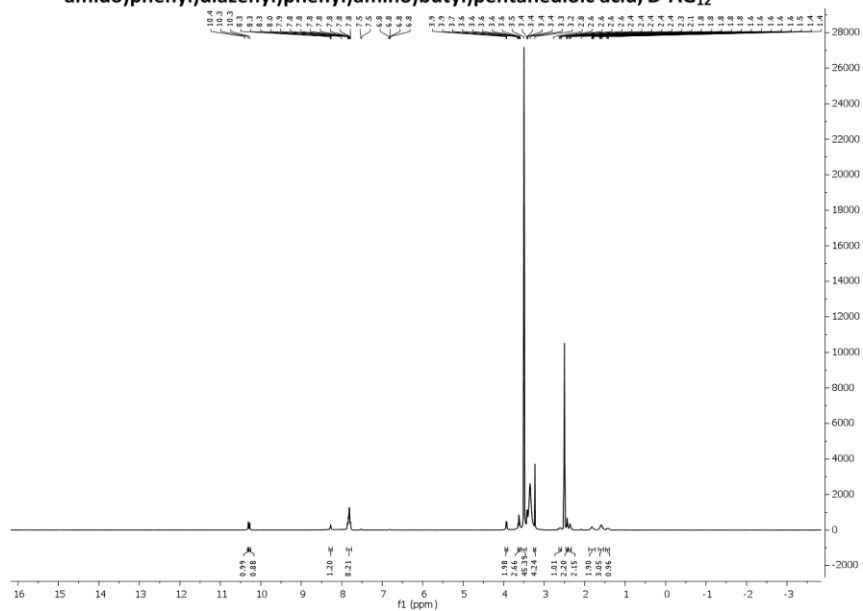


2.6 (2S,4S)-2-Amino-4-(4-((E)-4-(1-(4-(3-(((2-amino-9H-purin-6-yl)oxy)methyl)benzyl)amino)-3-oxopropyl)-1H-1,2,3-triazol-1-yl)-39-oxo-3,6,9,12,15,18,21,24,27,30,33,36-dodecaoxa-40-azadotetracontan-42-amido)phenyl)diazanyl)phenyl)amino)-4-oxobutyl)pentanedioic acid, BGAG₁₂

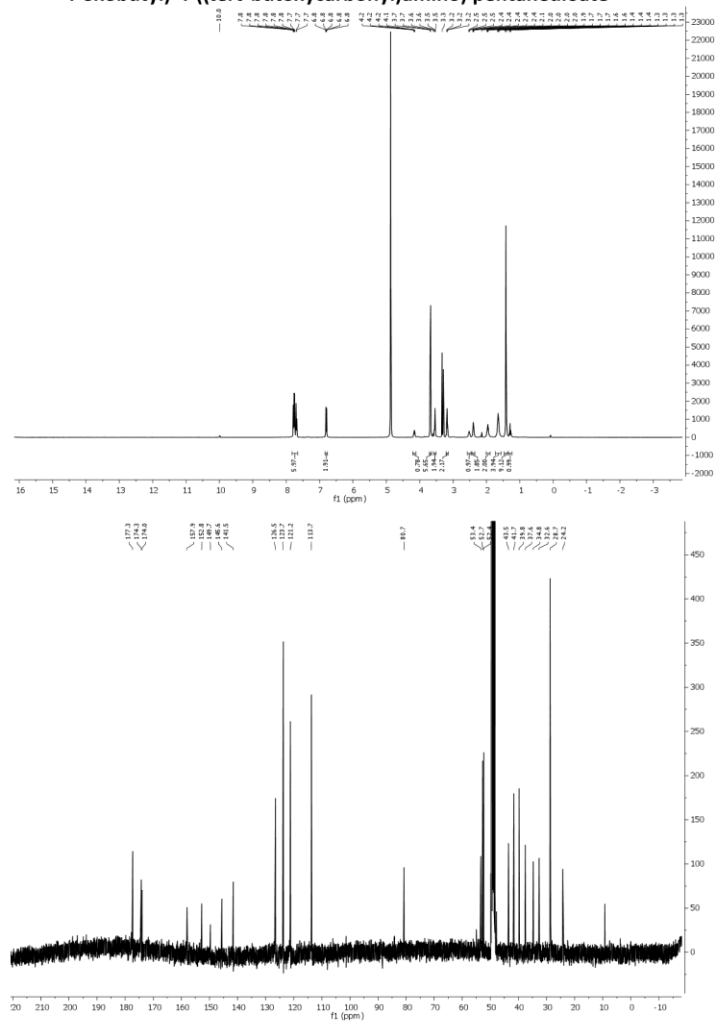




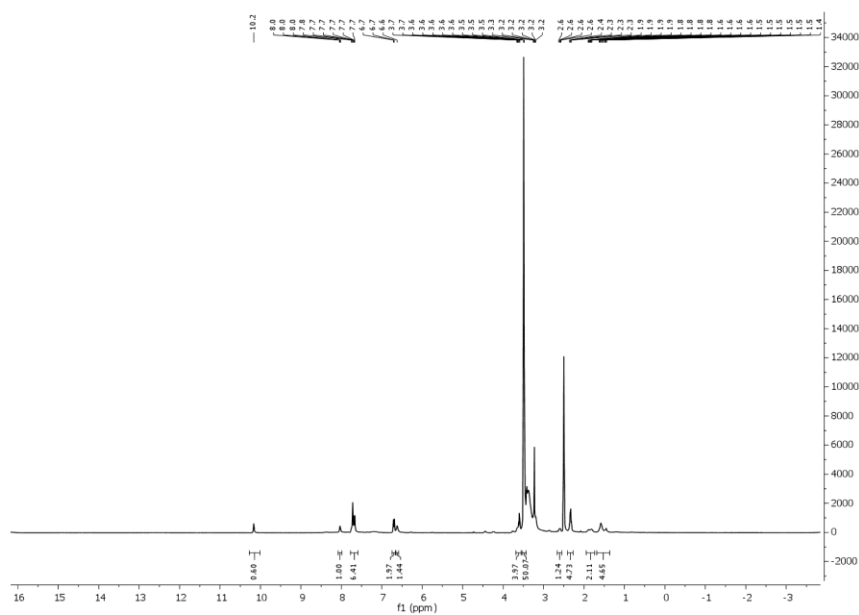
2.7 (2S,4S)-2-amino-4-(4-oxo-4-((E)-4-(38-oxo-2,5,8,11,14,17,20,23,26,29,32,35-dodecaoxa-39-azahentetracontan-41-amido)phenyl)diazenyl)phenyl)amino)butyl)pentanedioic acid, D-AG₁₂



2.8 Dimethyl (2S,4S)-2-(4-((4-((E)-4-((2-aminoethyl)amino)phenyl)diazenyl) phenyl)amino)-4-oxobutyl)-4-((tert-butoxycarbonyl)amino) pentanedioate



2.10 (2S,4S)-2-Amino-4-(4-oxo-4-((4-((E)-4-((38-oxo-2,5,8,11,14,17,20,23,26,29,32,35-dodecaoxa-39-azahentetracontan-41-yl)amino)phenyl)diazanyl)phenyl)-amino)butyl)pentanedioic acid, D-AG_{12,445}



3 Supporting Figures

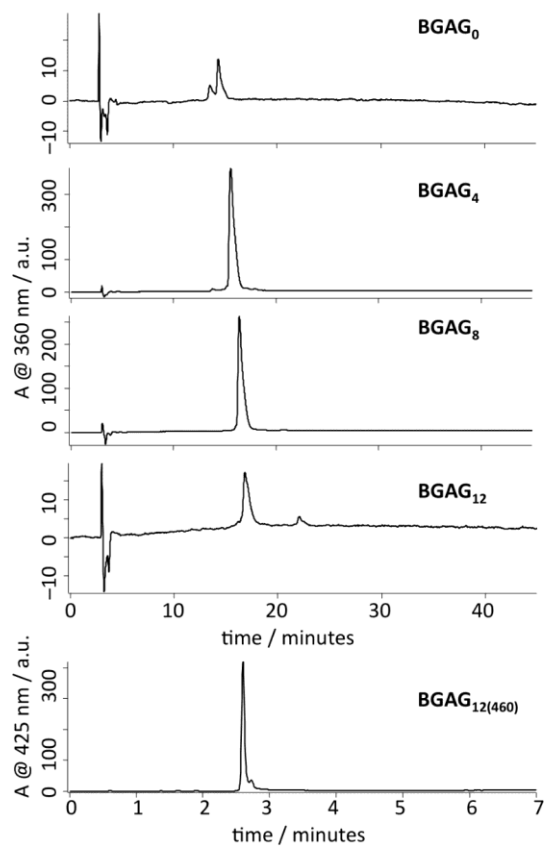


Figure S1: HPLC traces of the **BGAG** library demonstrating its purity.

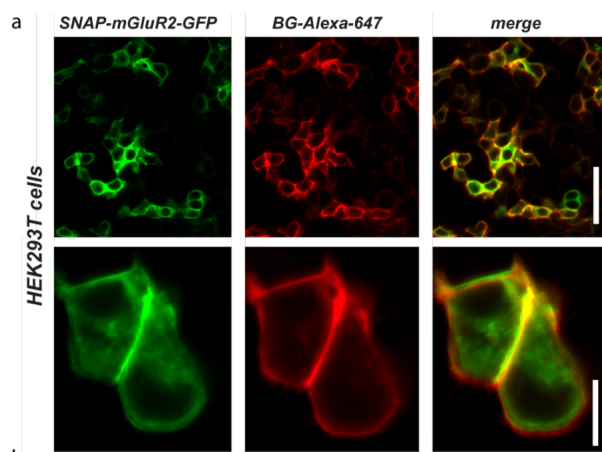


Figure S2: Expression and fluorophore labeling with benzylguanine-Alexa-647 (BG-Alexa-647) of SNAP-mGluR2-GFP in HEK293T cells. First column: GFP fluorescence. Second column: BG-Alexa-647 fluorescence. Third column: merge. Scale bars represents 50 μ M (top) and 10 μ M (bottom) .

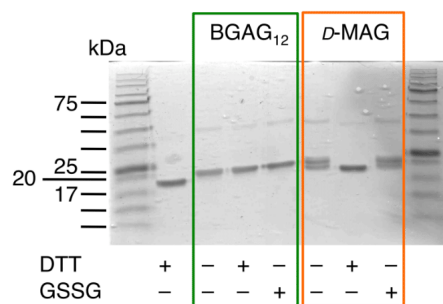


Figure S3: SDS-PAGE after *in vitro* SNAP-tag labeling (New England Biolabs, #P9312S) with **BGAG₁₂** and *D*-MAG. Reductive (dithiothreitol, DTT), oxidative (oxidized glutathione, GSSG) or neutral conditions (no additive) were employed according to the manufacturer's instructions. **BGAG₁₂** reacts with the SNAP-tag under each condition, while *D*-MAG reacts only under oxidative and neutral conditions (although slower as indicated by the unlabelled SNAP-tag band) and is unreactive towards the SNAP-tag under reductive conditions.

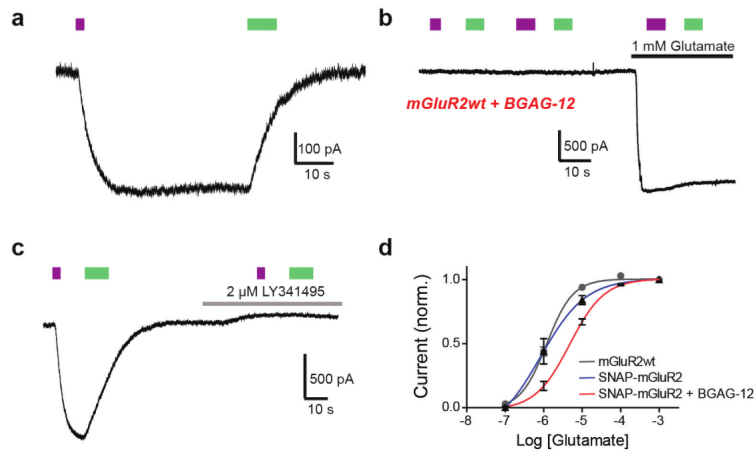


Figure S4: Further characterization of SNAG-mGluR2. **a)** Representative patch-clamp recording demonstrates reversible, bistable optical control of SNAG-mGluR2 with BGAG₁₂ (*i.e.* SNAG-mGluR2). SNAG-mGluR2 is activated by a brief pulse of UV light ($\lambda = 380$ nm, gray) and deactivated with a brief pulse of green light ($\lambda = 500$ nm, green). Black bar represents no light. **b)** When wild type mGluR2 (mGluR2wt) is incubated with BGAG₁₂, no photoresponse is seen after wash-out but application of 1 mM glutamate still produces a large inward current. **c)** Photoactivation of SNAG-mGluR2 is fully blocked by the competitive mGluR2 antagonist LY341495. **d)** Glutamate concentration-response curves for mGluR2wt and SNAG-mGluR2 with or without BGAG₁₂ labeling. Glutamate titration was performed in the dark for all conditions.

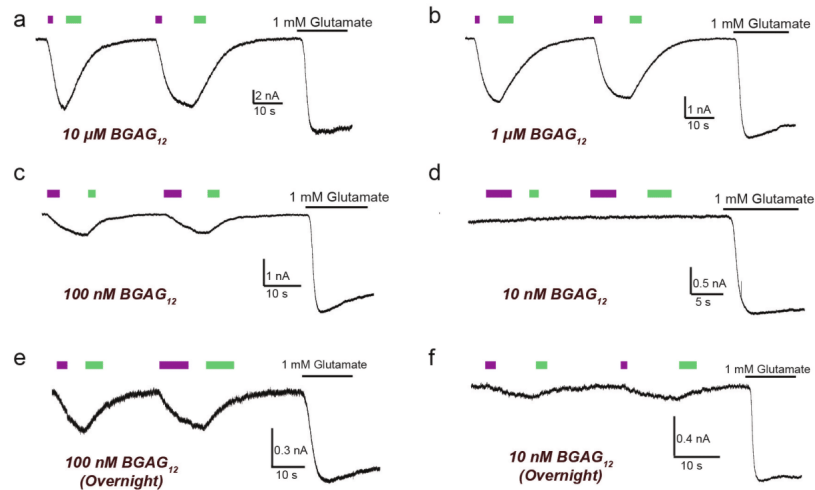


Figure S5: Summary of labeling conditions for **BGAG₁₂** on SNAP-mGluR2 in HEK293T cells. **a-d)** Representative traces showing photoactivation of SNAP-mGluR2 following incubation with BGAG₁₂ for 45 minutes in standard extracellular solution at various concentrations. Purple bars indicate 380 nm light and green bars indicate 500 nm light. **e-f)** Representative trace showing photoactivation of SNAP-mGluR2 following overnight labeling with 100 nM (**e**) or 10 nM (**f**) BGAG₁₂.

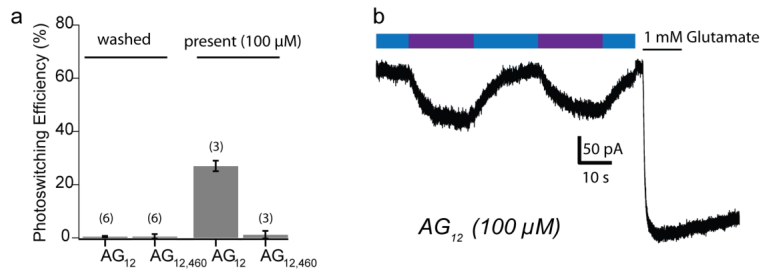


Figure S6: Optical control of SNAG-mGluR2 with AGs in HEK 293T cells. **a)** Summary of photoswitch efficiency relative to 1 mM glutamate for AG₁₂ and AG_{12,460} either treated as **BGAG**₁₂ (incubated for 1 h (10 μM) then washed) or with the photoswitch present (washed in (100 μM)). Error bars represent SEM; the numbers of cells tested are in parentheses. **b)** Representative patch-clamp recording demonstrates the reversible optical control of SNAG-mGluR2 with AG₁₂. SNAG-mGluR2 is activated with a UV light ($\lambda = 380$ nm, violet) and deactivated with blue light ($\lambda = 440$ nm, blue). Application of saturating 1 mM glutamate gives full activation and prevents further photoactivation in all cases.

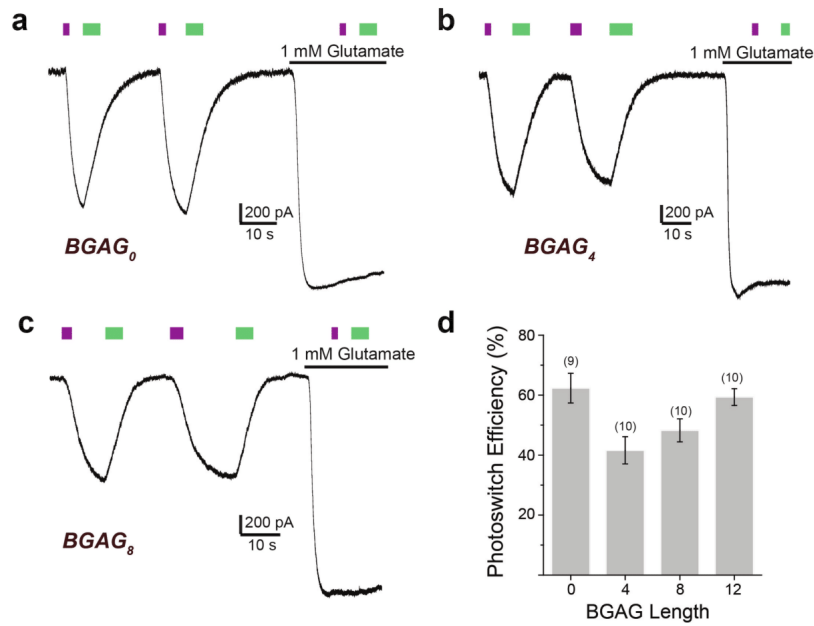


Figure S7: Optical control of SNAG-mGluR2 with variable length BGAGs in HEK 293T cells. **a-c)** Representative patch-clamp recording demonstrates the reversible optical control of SNAG-mGluR2 with either $BGAG_0$ (**a**), $BGAG_4$ (**b**), or $BGAG_8$ (**c**). SNAG-mGluR2 is activated with a brief pulse of UV light ($\lambda = 390$ nm, gray) and deactivated with a brief pulse of green light ($\lambda = 500$ nm, green). Application of saturating 1 mM glutamate gives full activation and prevents further photoactivation in all cases. **d)** Summary of photoswitch efficiency relative to 1 mM glutamate for all BGAG variants. Error bars represent SEM; the numbers of cells tested are in parentheses.

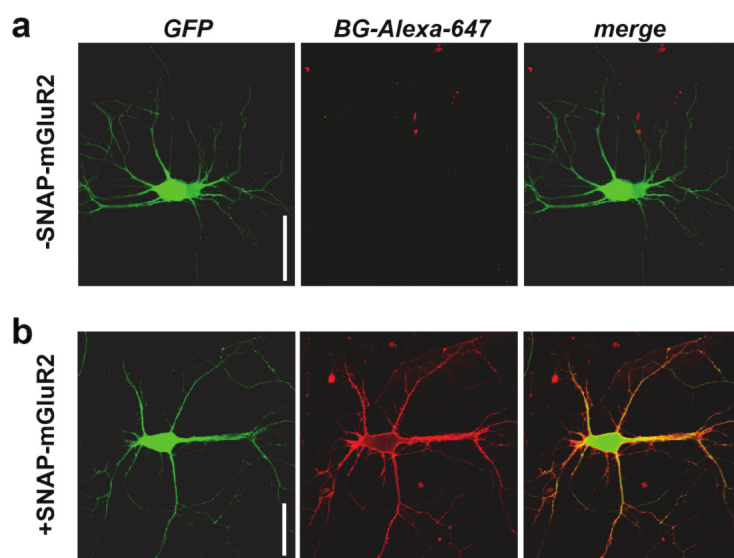


Figure S8: BG-Alexa-647 labeling controls for hippocampal neurons. **a-b)** Representative images showing BG-Alexa-647 labeling of GFP-expressing neurons in the absence (**a**) or presence (**b**) of SNAP-mGluR2 coexpression.

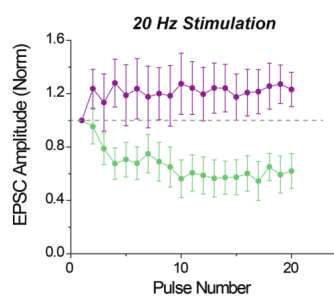


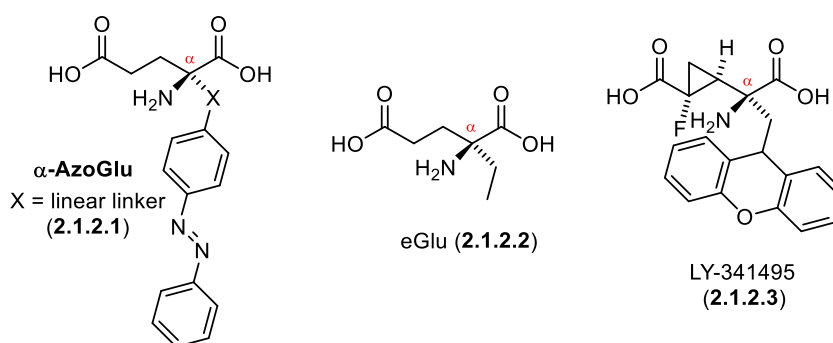
Figure S9: SNAG-mGluR2 mediated optical modulation of short term plasticity. Summary of response to high frequency (20 Hz) stimulation of a SNAG-mGluR2-expressing neuron in the presence of 380 nm (violet) or 500 nm (green) illumination. EPSC amplitude is normalized to the amplitude of the first pulse within the train.

4 References

1. Keppler, A. *et al.* A general method for the covalent labeling of fusion proteins with small molecules in vivo. *Nat. Biotechnol.* **21**, 86–89 (2003).
2. Levitz, J. *et al.* Optical control of metabotropic glutamate receptors. *Nat. Neurosci.* **16**, 507–16 (2013).
3. Di Antonio, M. *et al.* Selective RNA versus DNA G-quadruplex targeting by situ click chemistry. *Angew. Chemie - Int. Ed.* **51**, 11073–11078 (2012).
4. Chen, J. J. & Aduda, V. DMSO-Aided *o*-Iodoxybenzoic Acid (IBX) Oxidation of Fmoc-Protected Amino Alcohols. *Synth. Commun.* **37**, 3493–3499 (2007).

2.1.2 The Designing of Photoswitchable mGluR2 Antagonists

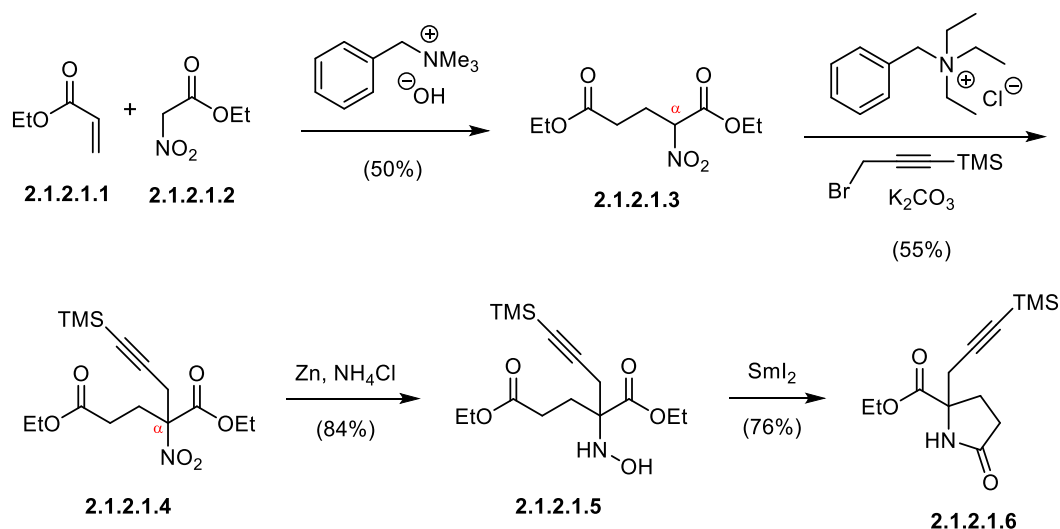
To complement our method to activate mGluR2 functions by implementing a light-sensitive SNAG-mGluR2, we further investigated azobenzene substitutions on glutamate to design a photoswitchable antagonist. Our study was based on the discovery that α -substituted glutamates blocked the orthosteric binding site.¹³⁶⁻¹³⁷ For example, eGlu (**2.1.2.2**, $K_i = 27 \pm 2 \mu\text{M}$) and LY-341495 (**2.1.2.3**, $K_i = 9 \pm 1 \text{ nM}$) (Scheme 2.1.2.1) have shown to inhibit [³H]-LY354740 binding to cloned rat mGluR2 and function as antagonists. The realization that bulky substructures such as a xanthene (LY-341495, **2.1.2.3**) are well-tolerated at the α -position of glutamate-based inhibitors is a strong indication that a *cis*- or *trans*-azobenzene moiety could be installed without a substantial loss of bioactivity. Therefore, we are planning to design our antagonist library α -AzoGlu (**2.1.2.1**) by using glutamate as a functional basis and appended an azobenzene group at the α -position with varying linker lengths and modifications.



Scheme 2.1.2.1. The design of photoswitchable antagonists based on eGlu and LY-341495.

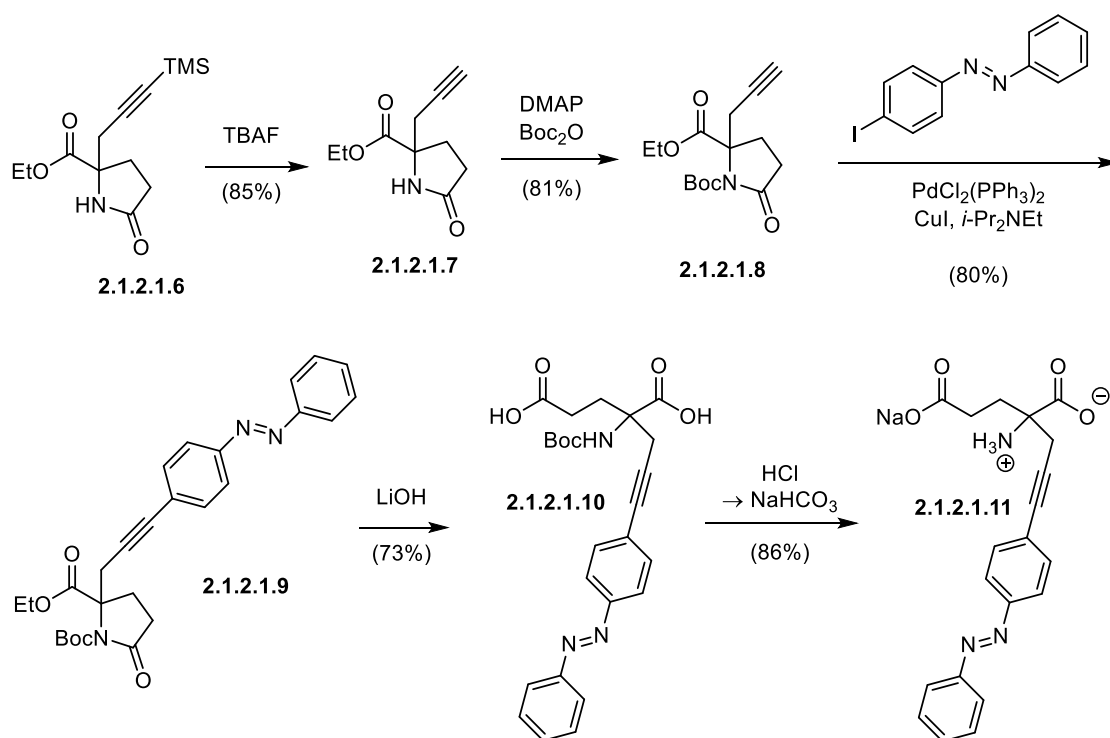
2.1.2.1 A Racemic Approach to Photoswitchable α -substituted Glutamates

Our first strategy to implement a synthetic handle at the glutamate α -position was based on the formation of a nitroglutamate (**2.1.2.1.3**) followed by nucleophilic C-C bond formation and reduction. This approach provides racemic α -substituted glutamate derivative. Nitroglutamate **2.1.2.1.3** was prepared through a phase-transfer catalyzed Michael reaction of nitroester **2.1.2.1.2** with ethyl acrylate **2.1.2.1.1**. The α -position was substituted with TMS propargyl bromide which established an alkyne handle (**2.1.2.1.4**). Reduction of the nitro group to the amine (**2.1.2.1.6**) relied on a 2-step sequence with hydroxylamine **2.1.2.1.5** as an intermediate. The SmI_2 -mediated reduction of this hydroxylamine **2.1.2.1.5** led to a cyclization of the amine onto the distant carboxylic ester group and formed lactam **2.1.2.1.6**.



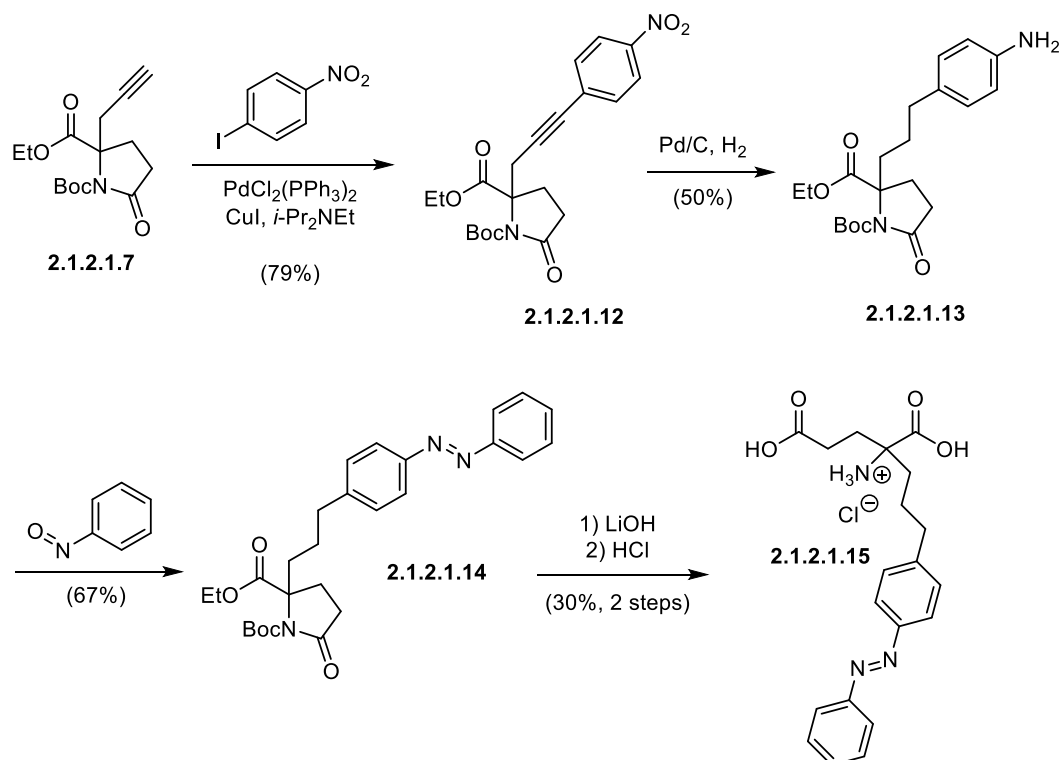
Scheme 2.1.2.1.1. Synthesis of the α -propargyl glutamate 2.1.2.1.6.

Removal of the TMS group (2.1.2.1.7) and attachment of a *tert*-butyloxycarbonyl on the amide provided the terminal alkyne 2.1.2.1.8 in good yields. Sonogashira coupling appended the 4-iodoazobenzene onto the propargyl linker (2.1.2.1.9) and was followed by a 2-step basic ester/lactam hydrolysis (2.1.2.1.10) – acidic Boc removal to give the propargyl-linked α -AzoGlu 2.1.2.1.11.



Scheme 2.1.2.1.2. Appending the azobenzene structure and finalizing the α -AzoGlu derivative 2.1.2.1.11.

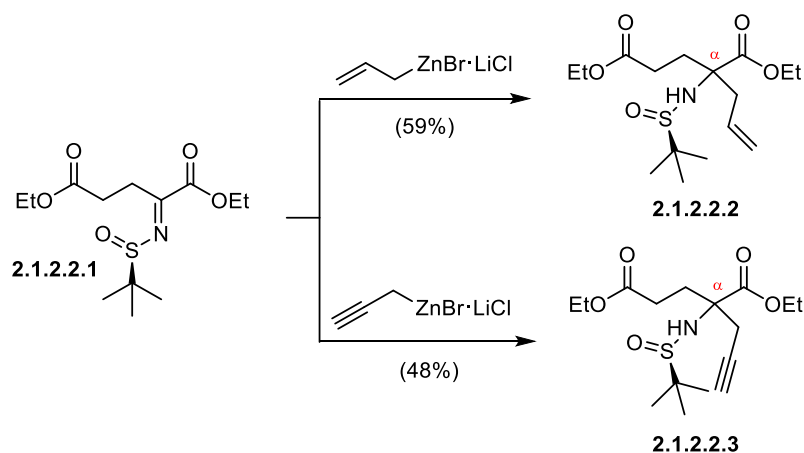
For the synthesis of the propyl-linked α -AzoGlu derivative **2.1.2.1.15**, a Sonogashira coupling was performed between alkyne **2.1.2.1.7** and 4-iodonitrobenzene (**2.1.2.1.12**, Scheme 2.1.2.1.3). Both the nitro group and the alkyne were hydrogenatively reduced to give propyl-substituted aniline **2.1.2.1.13** which was subjected to a Baeyer-Mills reaction to install the azobenzene photoswitch (**2.1.2.1.14**). A 2-step deprotection sequence afforded the propyl-linked α -AzoGlu **2.1.2.1.15**.



Scheme 2.1.2.1.3. Implementing a propyl linker to give α -AzoGlu derivative **2.1.2.1.15**.

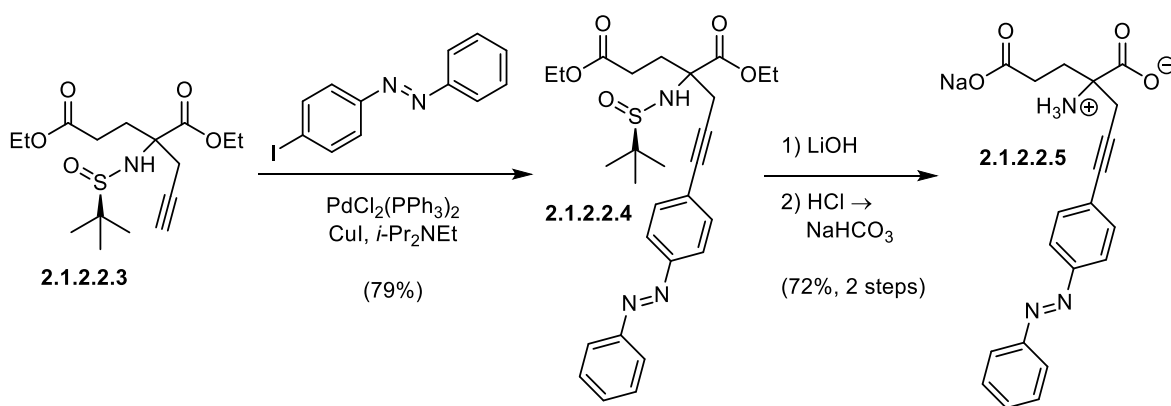
2.1.2.2 A Stereoselective Approach to Photoswitchable α -substituted Glutamates

In order to asymmetrically set the glutamate stereocenter and implement more diverse α -substitution patterns, we evaluated an alternative route towards α -AzoGlu (**2.1.2.1**) derivatives. We utilized a diastereoselective approach by condensing Ellman's chiral *tert*-butyl sulfinylamide onto diethyl α -ketoglutarate and studied the addition of organometallic nucleophiles into the sulfinylimine (Scheme 2.1.2.2.1).¹³⁸ In addition to propargylzinc substitution (**2.1.2.2.3**) we optimized a reaction with allylzinc bromide to give a single diastereomer of **2.1.2.2.2** in good yields. Although we performed our experiments with complete stereoselectivity and obtained a single enantiomer of **2.1.2.2.2** and **2.1.2.2.3**, we have not yet determined the absolute stereochemical configuration.



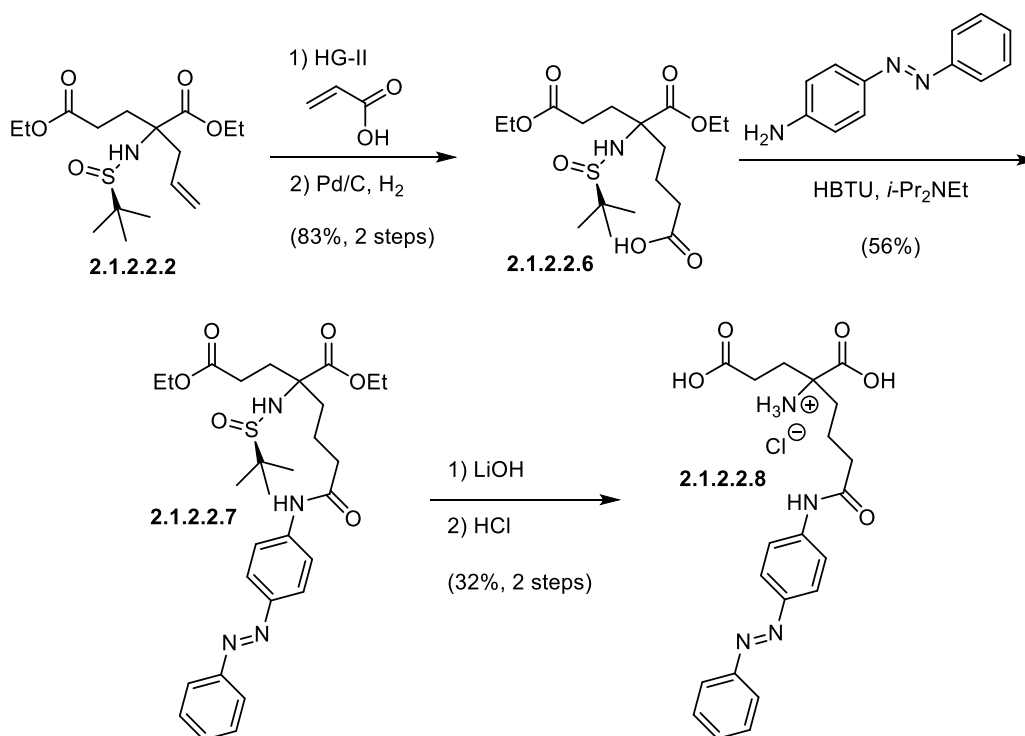
Scheme 2.1.2.2.1. Diastereoselective installation of the α -substitution on glutamate.

With propargyl glutamate **2.1.2.2.3** in hand, we pursued the synthesis of enantiomerically pure propargyl-linked α -AzoGlu **2.1.2.2.5** in a 3-step sequence (Scheme 2.1.2.2.2). Sonogashira reaction with 4-iodoazobenzene provided the photoswitchable intermediate **2.1.2.2.4** which was deprotected to **2.1.2.2.5** by sequential reactions with LiOH and HCl.



Scheme 2.1.2.2.2. Finalizing the enantiomerically pure propargyl-linked α -AzoGlu **2.1.2.2.5**.

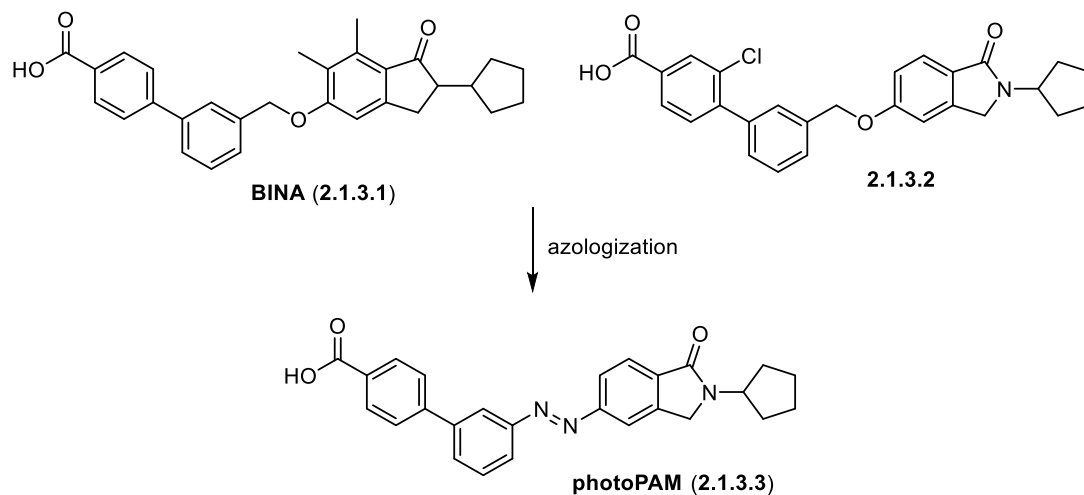
Based on the α -allyl glutamate **2.1.2.2.2**, we synthesized butyramide-linked α -AzoGlu **2.1.2.2.8** (Scheme 2.1.2.2.3). The allyl group was converted into a butyric acid (**2.1.2.2.6**) by metathesis with acrylic acid and Pd/C-mediated hydrogenation. An amide coupling reaction with 4-aminoazobenzene appended the photoswitch portion of the molecule (**2.1.2.2.7**). The 2-step deprotection relied on a LiOH-mediated ester hydrolysis and a HCl-mediated sulfonamide cleavage to afford butyramide-linked α -AzoGlu **2.1.2.2.8**.



Scheme 2.1.2.2.3. Finalizing the enantiomerically pure butyramide-linked α -AzoGlu 2.1.2.2.8.

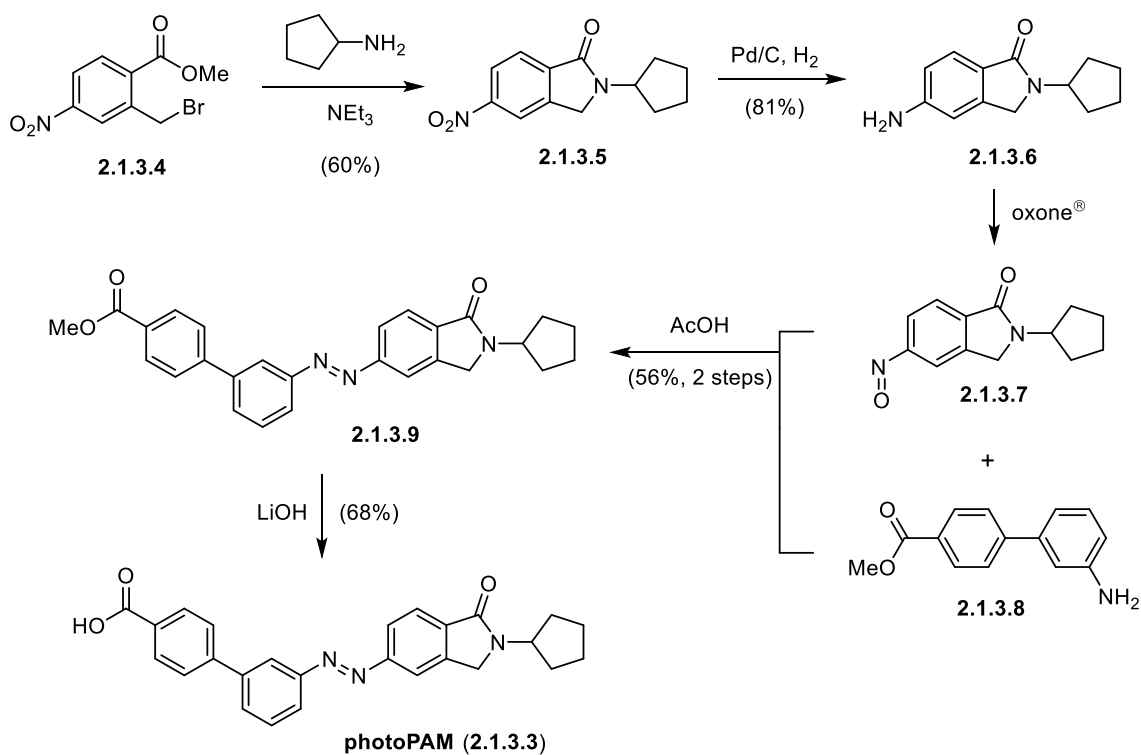
2.1.3 A Photoswitchable Positive Allosteric Modulator for the mGluR2

The development of glutamate-based photopharmaceuticals (Chapter 2.1.1 and 2.1.2) allows us to evaluate the effect of activating or blocking the mGluR2 orthosteric binding pocket on target cells or target organisms. However, to comprehend the full extent of the physiological mGluR2 function, it is crucial to include the role of the allosteric binding site into the study. The medicinal significance of moderating the mGluR2 activity through this pathway was established by the development of a series of positive allosteric modulators (PAMs).¹³⁹ These studies provided evidence for the potential to treat several disorders of the central nervous system including drug dependence and anxiety by targeting the allosteric pocket. In this context, a photoswitchable PAM (photoPAM) of the mGluR2 would serve as an excellent tool to study the GPCR function by allowing the control of receptor modulation with the spatiotemporal precision of light. Our design of a photoPAM (2.1.3.3, Scheme 2.1.3.1) is based on the azologization¹⁴⁰ of the phenol-derived benzylether functionality of the established PAMs BINA (2.3.1.1) and 2.3.1.2.¹⁴¹⁻¹⁴³



Scheme 2.1.3.1. Azologization of BINA (2.1.3.1) and 2.1.3.2 to photoPAM (2.1.3.3).

To synthesize **photoPAM** (2.1.3.3), the commercially available benzyl bromide **2.1.3.4** was substituted with cyclopentylamine. The resulting nitroarene **2.1.3.5** was hydrogenatively reduced to aniline **2.1.3.6** and selectively oxidized to the nitrosoarene **2.1.3.7**. This nitrosoarene **2.1.3.7** was coupled with the commercially obtained aniline **2.1.3.8** in a Baeyer-Mills reaction and gave the azobenzene derivative **2.1.3.9**. Hydrolysis of the methyl ester (**2.1.3.9**) with LiOH provided **photoPAM** (2.1.3.3) in good yields.



Scheme 2.1.3.2. Synthesis of photoPAM (2.1.3.3).

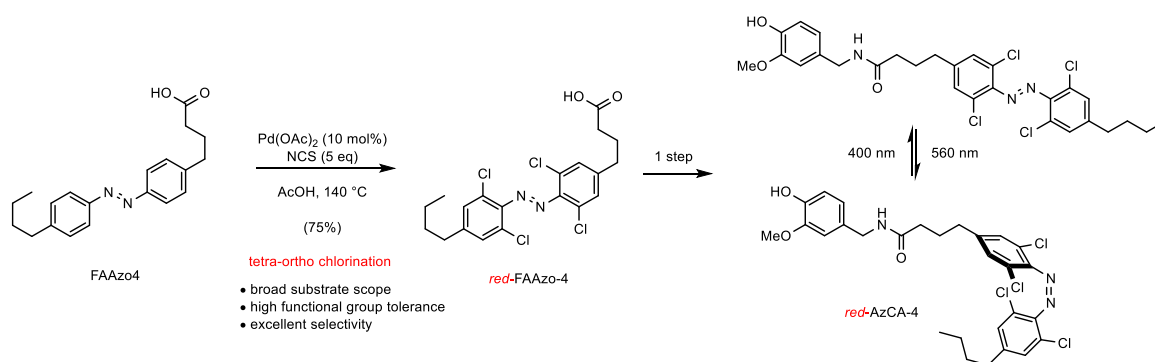
2.2 Lipid-based Photopharmaceuticals

2.2.1 Synthesis of Redshifted Azobenzene Photoswitches by Late-Stage Functionalization

Reprinted with permission from:

David B. Konrad, James A. Frank, Dirk Trauner, *Chem. Eur. J.* **2016**, *2*, 43644368.

Copyright © 2016 WILEY-VCH Verlag GmbH & Co. KGaA, Weinheim



The author David B. Konrad contributed to: the design of the study, the development of the methodology, the chemical synthesis, the UV/Vis experiments and the writing of the manuscript.

Photopharmacology
Synthesis of Redshifted Azobenzene Photoswitches by Late-Stage Functionalization
David B. Konrad, James A. Frank, and Dirk Trauner^{*[a]}

Abstract: Azobenzenes are versatile photoswitches that can be cycled between their *trans*- and *cis*-configuration with light. The wavelengths required for this isomerization are substantially shifted from the UV to the visible range through tetra-*ortho*-chlorination. These halogenated azobenzenes display unique photoswitching characteristics, but their syntheses remain limited and inefficient. A new general method for the synthesis of tetra-*ortho*-chloro azobenzenes has been developed, which relies on direct palladium(II)-catalyzed C–H activation of pre-existing standard azobenzenes. This late-stage functionalization has a broad substrate scope and can be used to create a variety of useful building blocks for the construction of more elaborate redshifted photopharmaceuticals. This method is used to prepare *red-AzCA-4*, a photoswitchable vanilloid that enables optical control of the cation channel TRPV1 with visible light.

Azobenzenes are small, readily accessible, and robust photoswitches.^[1] These properties make them excellent building blocks for incorporation into photopharmaceuticals that can be used to control biological functions with the spatial and temporal precision of light.^[2] With this approach, significant advances have been made, for instance, in the field of vision restoration, whereby blind mice regained light sensitivity on treatment with a photoswitchable ion channel blocker.^[3] For irradiation in complex animal tissues like the retina, it is desirable to use non-hazardous visible light to reduce tissue damage. For regular azobenzenes, photoswitching relies on UV (360 nm) and blue light (440 nm) and this high-energy irradiation can be harmful to living tissue on prolonged application.^[4,5] Therefore, significant efforts have been made to develop new azobenzenes with redshifted absorption spectra that enable isomerization with visible light.^[5,6]

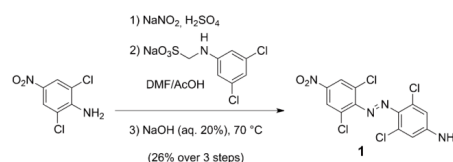
Tetra-*ortho*-substitution with heteroatoms is widely known to shift the absorption wavelengths of azobenzenes towards the visible range.^[7,8] A remarkable example is the tetra-*ortho*-chloro azobenzene [1,2-bis(2,6-dichlorophenyl)diazene]. It un-

dergoes isomerization to the *cis* configuration at a wavelength of 560 nm (green light), which is a shift over a range of 200 nm when compared to the parent azobenzene.^[9] To date, however, only one tetra-*ortho*-chlorinated azobenzene building block, **1**, has been reported to enable optical control of protein function (Scheme 1).^[8,9] This may result from the lack of a general synthetic procedure for the installation of this substitution pattern. As a consequence, many of the established photochromic ligands (PCLs) and photochromic tethered ligands (PTLs) still rely on irradiation with UV light.^[10] Therefore, the development of a reliable and general method for the preparation of the tetra-*ortho*-chloro-substituted azobenzenes is highly desirable. Herein, we describe a new methodology for the preparation of tetra-*ortho*-chloro azobenzenes, which enables the synthesis of a variety of new azobenzene building blocks that can be used for the construction of more advanced redshifted photopharmaceuticals.^[10]

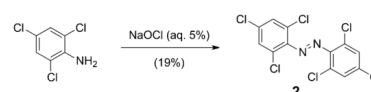
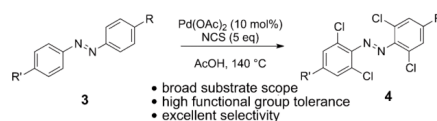
It is reasonable to assume that the low yields reported in the azo-coupling reaction affording **1** (Woolley and co-workers, Scheme 1)^[8] and the oxidative aniline dimerization affording **2** (Warren and co-workers, Scheme 1)^[11] result from the steric re-

Previous approaches:

Woolley, 2013: Azo-coupling reaction



Warren, 2012: Oxidative aniline dimerization


This work: Late-stage C–H chlorination

 Scheme 1. Synthetic approaches towards tetra-*ortho*-chloro azobenzenes.

[a] D. B. Konrad, J. A. Frank, Prof. Dr. D. Trauner
 Department of Chemistry
 Ludwig-Maximilians-Universität München
 81377 Munich (Germany)
 E-mail: dirk.trauner@lmu.de

Supporting information and ORCID(s) from the author(s) for this article is available on the WWW under <http://dx.doi.org/10.1002/chem.201505061>.

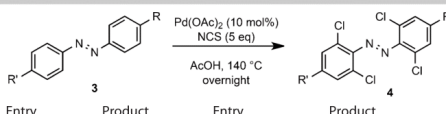
pulsion between the *ortho*-chloro groups that shield the reacting sites. To circumvent this, a late-stage functionalization is desirable whereby chlorination is carried out after the construction of the azobenzene core. A suitable method for the direct functionalization of arenes is palladium-catalyzed C–H functionalization.^[12] In 1970, Fahey described that azobenzenes can undergo palladium-mediated C–H chlorination reactions in the presence of chlorine gas.^[13,14] However, these experiments yielded an intractable mixture of mono-, di-, tri-, and tetra-substituted azobenzenes.^[13] Presumably, the diazene unit coordinates to the palladium catalyst in this reaction and guides the chlorination towards the *ortho* positions.^[12,13] Encouraged by these findings, we aimed to utilize a modern variant of aromatic C–H activation to achieve this transformation with synthetically useful yields and selectivity.^[12]

Over the past decade, palladium-catalyzed C–H activation guided by intramolecular ligands has evolved as a popular tool for the functionalization of arenes.^[12,15] This can be attributed to the numerous functional groups that can be introduced with this method, including halogen atoms,^[16,17] acetoxy groups,^[18,19] acyl groups,^[20] or alkoxy groups,^[21] by using various directing groups.^[22] Many of the reported approaches have focused on mono-*ortho*-substitution of azobenzenes.^[17,19–21,23] To date, only a limited number of selective di- and tri-substitution methodologies have been reported.^[20]

To facilitate a selective tetra-halogenation, we chose to evaluate the conditions reported by Sanford and co-workers as part of their C–H halogenation reaction.^[24] Subjecting 4-fluoroazobenzene (**3a**) to 10 mol% Pd(OAc)₂ and 5 equivalents *N*-chlorosuccinimide (NCS) in MeCN at 120 °C afforded a mixture of substituted azobenzenes. We hypothesized that the increasing steric bulk surrounding the diazene upon sequential chlorinations interfered with palladium coordination during later C–H insertions. Increasing the temperature to 140 °C and using the less volatile solvent AcOH enabled full conversion to the tetra-*ortho*-chloro azobenzene (Table 1, entry 1) within 15 h (for details on the optimization, see Tables 1 and 2 in the Supporting Information).

We then subjected a variety of commonly used azobenzene building blocks to our reaction conditions. As summarized in Table 1, this reaction could be applied to a broad range of substrates. *Para*-halogen atoms in general were well tolerated (Table 1, entries 1–3), with the best yields obtained for 4-iodoazobenzene (**4c**). The 4-bromo (**4b**) and 4-fluoro (**4a**) compounds were prepared in slightly lower but still acceptable yields. These halogenated derivatives are especially valuable building blocks, as they can be further decorated through cross-coupling reactions.^[25] Although the 4-aminoazobenzene could not be cleanly chlorinated, the corresponding nitroazobenzene (**4d**) underwent the reaction in 57% yield and is an effective precursor to the aniline. In addition, we showed that bifunctional azobenzenes containing two useful functional groups, such as 4-iodo-4'-nitroazobenzene (**4e**) and 4,4'-dibromoazobenzene (**4f**), could be successfully chlorinated by using our method. Nitrile groups (**4g**) were not as well tolerated, but could still be synthesized in modest yields. Oxygen-containing azobenzenes were also well tolerated (Table 1, entries 8–11).

Table 1. Substrates used in this study.

Entry	Product	Entry	Product
			
1	4a (58%)	8	4h, red-FAAzo-4 (75%)
2	4b (57%)	9	4i (66%)
3	4c (69%)	10	4j (52%)
4	4d (57%)	11	4k (48%)
5	4e (34%)	12 ^[a]	4l (60%)
6	4f (64%)	13 ^[a]	4m (55%)
7	4g (29%)	14 ^[a]	4n (61%)

[a] Unacetylated starting materials were used.

Esters (**4i**), carboxylic acids (**4h** and **4k**) and aldehydes (**4j**) did not interfere with the reaction and we observed no competing chlorinations at sites other than the desired *ortho* positions.

Next, we subjected an alkylamine-functionalized azobenzene to the chlorination conditions (Table 1, entry 12). In the case of **3l**, we observed that the amine was protected by acetylation which prevented its interference in the tetra-*ortho*-chlorination and afforded **4l**. Other nucleophilic substituents, such as a benzylic alcohol (**3m**), were analogously acetylated and converted into the corresponding tetra-*ortho*-chloro azobenzene esters (**4m**). Finally, we tested a nitro group in combination with an ethyl alcohol substituent on the azobenzene (**3n**), which gave the desired product **4n** in good yield (Table 1, entry 14).

We next applied this synthetic methodology to an established photochromic ligand **AzCA-4**, which enables optical control of the vanilloid receptor 1 (TRPV1).^[26] TRPV1 is a non-selective cation channel expressed in the sensory neurons of the dorsal root and trigeminal ganglia, where it plays an important role in nociception and inflammatory pain.^[27] **AzCA-4** is a "regular" azobenzene that is inactive towards TRPV1 in its dark-adapted *trans* configuration, but increases in efficacy upon isomerization to *cis* with UV-A (365 nm) light.^[26] We prepared the second-generation photoswitchable TRPV1 agonist, **red-AzCA-4**, by the coupling of our readily available redshifted photoswitchable fatty acid **red-FAAzo-4** (**4h**; Table 1, entry 8) with vanillylamine in 57% yield (Figure 1a).

The activation wavelength of **red-AzCA-4** was significantly shifted by 200 nm towards the visible range. Thus, **red-AzCA-4** could be isomerized to its active *cis* form with green light (Figure 1b). The maximum *cis* content was achieved under irradiation at $\lambda = 560$ nm (green light) and the maximum *trans* content with $\lambda = 400$ nm (violet light). We tested the utility of **red-AzCA-4** as a photoswitchable vanilloid in HEK293T cells expressing TRPV1-YFP.^[28] Like its parent compound, **red-AzCA-4** possessed an increased efficacy towards the ion channel in its *cis* configuration, which was generated upon irradiation with green light (Figure 1c). Application of **red-AzCA-4** (500 nM) under $\lambda = 400$ nm light produced only a small inward current, which could be greatly potentiated by irradiation at $\lambda = 560$ nm (Figure 1d). Interestingly, **red-AzCA-4** could still be photoactivated with UV-A light ($\lambda = 350$ nm; Figure 1e), in accordance with its UV/Vis spectrum.^[9] The full action spectrum of **red-AzCA-4** operating on TRPV1 is shown in Figure 1f.

In conclusion, we have developed a new synthetic methodology for the convenient synthesis of tetra-*ortho*-chloro azobenzenes. This approach has enabled the synthesis of a collection of redshifted azobenzene building blocks through late-stage functionalization of pre-existing azobenzenes. By red-shifting **AzCA-4**, we showed that these enhanced photoswitches can be directly inserted into already-existing photopharmaceuticals, enabling the use of longer-wavelength light to control protein function. This simple and general method will enable rapid access to a plethora of redshifted PCLs and PTLs better suited for application in living animals and humans.

Experimental Section

Synthesis of red-FAAzo-4 (**4h**; typical procedure for tetra-*ortho*-chlorination): (*E*)-4-[4-((4-butylphenyl)diazanyl)phenyl]butanoic acid (**FAAzo-4**, **3h**; 300 mg, 0.925 mmol, 1.0 equiv), NCS (617 mg, 4.62 mmol, 5.0 equiv), and Pd(OAc)₂ (20.8 mg, 0.0925 mmol, 0.10 equiv) were dissolved in AcOH (15.4 mL) under N₂ atmosphere in a 30 mL pressure tube. The tube was sealed and the reaction was heated to 140 °C for 12 h 45 min, during which time the color turned from light to dark red. After cooling to room temperature, the solvent was removed under reduced pressure and the mixture was transferred to a separating funnel with CH₂Cl₂ (180 mL), saturated aqueous NaCl (40 mL), and phosphate buffer (pH 7, 40 mL). The organic layer was separated, dried over Na₂SO₄, and concentrated under reduced pressure. Purification by flash column chromatography (46.1 g SiO₂, CH₂Cl₂/AcOH = 199:1) afforded (*E*)-4-[4-((4-butyl-2,6-dichlorophenyl)diazanyl)-3,5-dichlorophenyl]butanoic acid (**red-FAAzo-4**, **4h**; 322 mg, 0.696 mmol, 75%) as a red-brown gum.

Whole-cell electrophysiology in HEK293T cells: HEK293T cells (obtained from the Leibniz-Institute DSMZ: #305) were incubated at 37 °C (10% CO₂) in Dulbecco's Modified Eagle Medium (DMEM) with 10% fetal bovine serum (FBS) and were split at 80–90% confluency. For cell detachment, the medium was removed and the cells were washed with calcium-free phosphate-buffered saline (PBS) buffer and treated with trypsin for 2 min at 37 °C. The detached cells were diluted in growth medium and plated on acid-etched coverslips coated with poly-L-lysine in a 24-well plate. 50 000 cells were added to each well in 500 μ L standard growth medium along with the DNA (per coverslip: 500 ng TRPV1-YFP)^[28] and JetPRIME[®] transfection reagents according to the manufacturer's instructions (per coverslip: 50 μ L JetPRIME[®] buffer, 0.5 μ L JetPRIME[®] transfection reagent). The transfection medium was exchanged for normal growth media 4 h after transfection and electrophysiological experiments were carried out 20–40 h later. Whole-cell patch clamp experiments were performed by using a standard electrophysiology setup equipped with a HEKA Patch Clamp EPC10 USB amplifier and PatchMaster software (HEKA Elektronik). Micropipettes were generated from "Science Products GB200-F-8P with filament" pipettes using a Narishige PC-10 vertical puller. The patch pipette resistance varied between 5–9 M Ω . The bath solution contained (in mM): 140 NaCl, 5 KCl, 5 HEPES, 1 MgCl₂, 5 glucose (adjusted to pH 7.4 with 3 M NaOH). The pipette solution contained: 100 mM K-gluconate, 40 mM KCl, 5 mM HEPES, 5 mM MgATP, 1 mM MgCl (adjusted to pH 7.2 with 1 M KOH). The cells were first visualized to contain TRPV1-YFP by irradiation at $\lambda = 480$ nm by using a Polychrome V (Till Photonics) monochromator. All cells had a leak current below 100 pA upon breaking at -60 mV. All voltage clamp measurements were carried out at a holding potential of -60 mV. The compounds were applied by puff pipette by using a "Toohey Spritzer pressure system II" at 25 psi. The puff pipette resistance varied between 3–5 M Ω . All experiments were performed at room temperature.

Compound switching: For electrophysiology in HEK293T cells, compound switching was achieved by using a Polychrome V (Till Photonics) monochromator. The light beam was guided by a fiber-optic cable through the microscope objective and operated by the amplifier and PatchMaster software (HEKA Elektronik). Irradiation during UV/Vis experiments was performed by pointing the fiber into the cuvette from above.

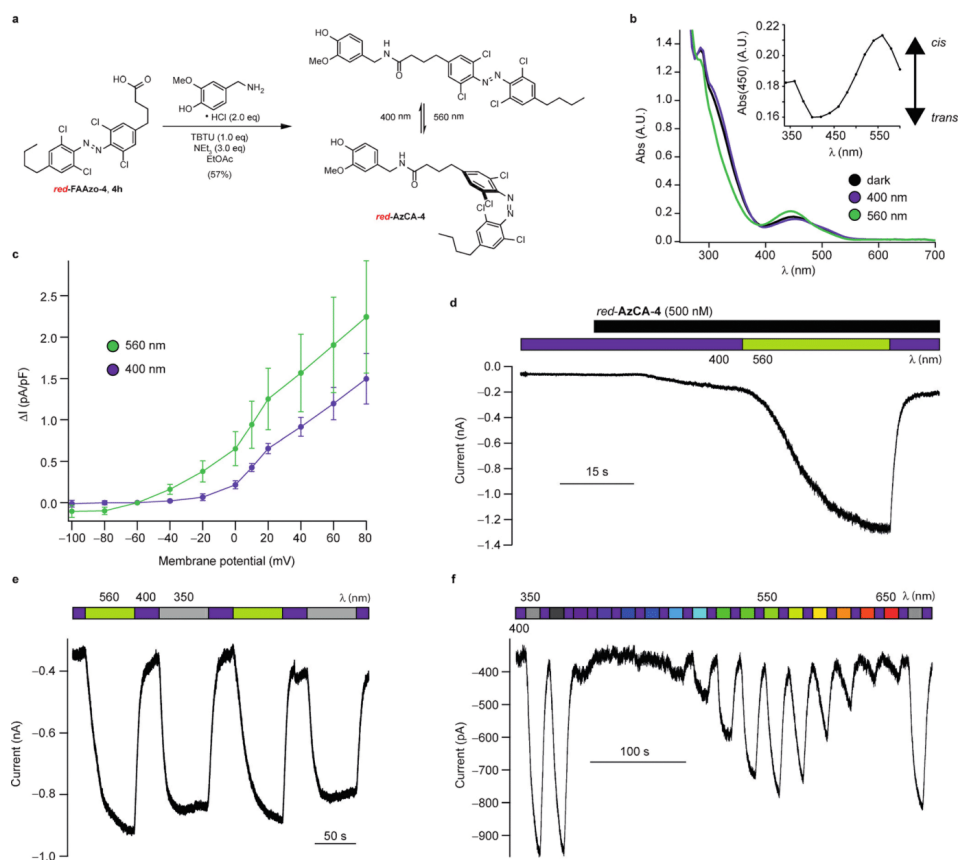


Figure 1. *red-AzCA-4* enabled control of TRPV1 with redshifted activation: a) *red-AzCA-4* was synthesized from *red-FAAzo-4* (4 h). b) Absorption spectra of *red-AzCA-4* in its dark-adapted, violet-adapted ($\lambda = 400$ nm) and green-adapted ($\lambda = 560$ nm) states. The highest *trans* content was achieved under $\lambda = 400$ nm irradiation, whereas the greatest *cis* content was achieved with $\lambda = 560$ nm light. In HEK293T cells transiently expressing TRPV1-YFP: c) the current–voltage plot showed that *red-AzCA-4* (500 nM) was a more potent TRPV1-agonist in its *cis* configuration ($n = 3$), displayed as the change in current from the baseline holding potential (-60 mV, pA/pF) as a function of the IV holding potential (mV). Error bars are displayed as \pm s.e.m. d) The application of *red-AzCA-4* (500 nM) under violet light produced only a small inward current, which was reversibly potentiated with green light. e) TRPV1 could be repeatedly cycled ON and OFF with UV-A (350 nm)/green (560 nm) and violet light (400 nm), respectively, as was also shown by f) an action spectrum. Holding potential = -60 mV.

Acknowledgements

We gratefully acknowledge financial support from the Deutsche Forschungsgemeinschaft (TRR152). D.B.K. is grateful to the Friedrich-Ebert-Stiftung for a PhD scholarship. Additionally, the authors would like to acknowledge Dana Kaubitzsch, Nils Winter, Katharina Hüll, and David Barber for experimental assistance, as well as Benjamin Williams, Felix Hartrampf, and Nicolas Armanino for helpful discussions.

Keywords: azobenzene · C–H activation · halogenation · ion channels · photopharmacology

- [1] H. M. D. Bandara, S. C. Burdette, *Chem. Soc. Rev.* **2012**, *41*, 1809–1825.
- [2] a) A. A. Beharry, G. A. Woolley, *Chem. Soc. Rev.* **2011**, *40*, 4422–4437; b) W. Szymański, J. M. Beierle, H. A. V. Kistemaker, W. A. Velema, B. L. Feringa, *Chem. Rev.* **2013**, *113*, 6114–6178.
- [3] A. Polosukhina, J. Litt, I. Tochitsky, J. Nemargut, Y. Sychev, I. De Kouchkovsky, T. Huang, K. Borges, D. Trauner, R. N. Van Gelder, R. H. Kramer, *Neuron* **2012**, *75*, 271–282.
- [4] T. Fehrentz, M. Schönberger, D. Trauner, *Angew. Chem. Int. Ed.* **2011**, *50*, 12156–12182; *Angew. Chem.* **2011**, *123*, 12362–12390.

- [5] M. A. Kienzler, A. Reiner, E. Trautman, S. Yoo, D. Trauner, E. Y. Isacoff, *J. Am. Chem. Soc.* **2013**, *135*, 17683–17686.
- [6] a) J. Broichhagen, J. A. Frank, N. R. Johnston, R. K. Mitchell, K. Smid, P. Marchetti, M. Bugliani, G. A. Rutter, D. Trauner, D. J. Hodson, *Chem. Commun.* **2015**, *51*, 6018–6021; b) J. Broichhagen, A. Damijonaitis, J. Levitz, K. R. Sokol, P. Leippe, D. Konrad, E. Y. Isacoff, D. Trauner, *ACS Cent. Sci.* **2015**, *1*, 383–393; c) M. Dong, A. Babalhavaeji, S. Samanta, A. A. Beharry, G. A. Woolley, *Acc. Chem. Res.* **2015**, *48*, 2662–2670.
- [7] a) D. Bléger, J. Schwarz, A. M. Brouwer, S. Hecht, *J. Am. Chem. Soc.* **2012**, *134*, 20597–20600; b) C. Knie, M. Utecht, F. Zhao, H. Kulla, S. Kovalenko, A. M. Brouwer, P. Saalfrank, S. Hecht, D. Bléger, *Chem. Eur. J.* **2014**, *20*, 16492–16501; c) S. Samanta, T. M. McCormick, S. K. Schmidt, D. S. Seferos, G. A. Woolley, *Chem. Commun.* **2013**, *49*, 10314–10316.
- [8] S. Samanta, A. A. Beharry, O. Sadovski, T. M. McCormick, A. Babalhavaeji, V. Tropepe, G. A. Woolley, *J. Am. Chem. Soc.* **2013**, *135*, 9777–9784.
- [9] A. Rullo, A. Reiner, A. Reiter, D. Trauner, E. Y. Isacoff, G. A. Woolley, *Chem. Commun.* **2014**, *50*, 14613–14615.
- [10] J. Broichhagen, J. A. Frank, D. Trauner, *Acc. Chem. Res.* **2015**, *48*, 1947–1960.
- [11] R. T. Gephart, D. L. Huang, M. J. B. Aguilera, G. Schmidt, A. Shahu, T. H. Warren, *Angew. Chem. Int. Ed.* **2012**, *51*, 6488–6492; *Angew. Chem.* **2012**, *124*, 6594–6598.
- [12] T. W. Lyons, M. S. Sanford, *Chem. Rev.* **2010**, *110*, 1147–1169.
- [13] D. R. Fahey, *J. Chem. Soc. D* **1970**, 417a.
- [14] D. R. Fahey, *J. Organomet. Chem.* **1971**, *27*, 283–292.
- [15] a) O. S. Andrienko, V. S. Goncharov, V. S. Raida, *Russ. J. Org. Chem.* **1996**, *32*, 89; b) K. M. Engle, T.-S. Mei, M. Wasa, J.-Q. Yu, *Acc. Chem. Res.* **2012**, *45*, 788–802.
- [16] a) X. Sun, G. Shan, Y. Sun, Y. Rao, *Angew. Chem. Int. Ed.* **2013**, *52*, 4440–4444; *Angew. Chem.* **2013**, *125*, 4536–4540; b) X.-T. Ma, S.-K. Tian, *Adv. Synth. Catal.* **2013**, *355*, 337–340.
- [17] D. Kalyani, A. R. Dick, W. Q. Anani, M. S. Sanford, *Tetrahedron* **2006**, *62*, 11483–11498.
- [18] A. K. Cook, M. H. Emmert, M. S. Sanford, *Org. Lett.* **2013**, *15*, 5428–5431.
- [19] A. R. Dick, K. L. Hull, M. S. Sanford, *J. Am. Chem. Soc.* **2004**, *126*, 2300–2301.
- [20] H. Song, D. Chen, C. Pi, X. Cui, Y. Wu, *J. Org. Chem.* **2014**, *79*, 2955–2962.
- [21] Z. Yin, X. Jiang, P. Sun, *J. Org. Chem.* **2013**, *78*, 10002–10007.
- [22] a) T.-S. Mei, R. Giri, N. Mangel, J.-Q. Yu, *Angew. Chem. Int. Ed.* **2008**, *47*, 5215–5219; *Angew. Chem.* **2008**, *120*, 5293–5297; b) J.-J. Li, T.-S. Mei, J.-Q. Yu, *Angew. Chem. Int. Ed.* **2008**, *47*, 6452–6455; *Angew. Chem.* **2008**, *120*, 6552–6555; c) T.-S. Mei, D.-H. Wang, J.-Q. Yu, *Org. Lett.* **2010**, *12*, 3140–3143.
- [23] H. Li, P. Li, L. Wang, *Org. Lett.* **2013**, *15*, 620–623.
- [24] D. Kalyani, A. R. Dick, W. Q. Anani, M. S. Sanford, *Org. Lett.* **2006**, *8*, 2523–2526.
- [25] M. Volgraf, P. Gorostiza, S. Szobota, M. R. Helix, E. Y. Isacoff, D. Trauner, *J. Am. Chem. Soc.* **2007**, *129*, 260–261.
- [26] J. A. Frank, M. Moroni, R. Moshourab, M. Sumser, G. R. Lewin, D. Trauner, *Nat. Commun.* **2015**, *6*, 7118.
- [27] a) M. J. Caterina, M. A. Schumacher, M. Tominaga, T. A. Rosen, J. D. Levine, D. Julius, *Nature* **1997**, *389*, 816–824; b) A. Szallasi, D. N. Cortright, C. A. Blum, S. R. Eid, *Nat. Rev. Drug Discovery* **2007**, *6*, 357–372.
- [28] N. Hellwig, N. Albrecht, C. Harteneck, G. Schultz, M. Schaefer, *J. Cell Sci.* **2005**, *118*, 917–928.

Received: December 16, 2015
Published online on February 17, 2016

CHEMISTRY

A **European** Journal

Supporting Information

Synthesis of Redshifted Azobenzene Photoswitches by Late-Stage Functionalization

David B. Konrad, James A. Frank, and Dirk Trauner^{*[a]}

chem_201505061_sm_miscellaneous_information.pdf

Table of Contents

1. General Experimental Details.....	S2
1.1 Chemicals.....	S2
1.2 Methods.....	S2
1.3 Equipment and Instruments.....	S3
2. Experimental Procedures.....	S4
3. NMR Data.....	S19
3.1 Photoisomerization Experiments.....	S19
3.2 NMR Spectra.....	S20
4. UV-Vis Spectra.....	S35
5. Optimization Table.....	S39
6. References.....	S41

1. General Experimental Details

1.1 Chemicals

All chemicals were purchased from Sigma Aldrich, Fisher Scientific, TCI Europe or Alfa Aesar. Solvents were purchased in technical grade quality and were distilled under reduced pressure prior use. Dry solvents were purchased from commercial sources. NEt_3 was distilled from CaH_2 . Phosphate buffer (pH 7) refers to mixture of Na_2HPO_4 (19.59 g) and KH_2PO_4 (9.36 g), which was diluted to a volume of 1 L with deionized water.

1.2 Methods

Unless otherwise noted, all reactions were magnetically stirred, performed under inert gas (N_2) atmosphere and were carried out in glassware that was evacuated and dried by heating with a heat-gun (550 °C). For reactions at elevated temperature oil baths and electric heating plates were used. Stated reaction temperatures refer to the external bath temperature. For transfer of reagents or solvents, cannulas and syringes were used which were flooded with inert gas before use.

Drying over Na_2SO_4 involves stirring the solution with the anhydrous salt for several minutes followed by a filtration through a glass frit and subsequent rinsing of the filter cake with additional solvent.

Purification by column chromatography (CC) was performed under elevated pressure (flash CC) on Geduran[®] Si60 silica gel (40 – 63 μm) from Merck KGaA. After CC, the concentrated fractions were filtered once through a glass frit to remove residual silica.

For monitoring reactions, analyzing fractions of CC and measuring R_f values silica gel F_{254} TLC plates from Merck KGaA were used. To visualize the analytes, TLC plates were irradiated with UV-light.

Reaction yields refer to spectroscopically pure isolated amounts of compounds.

1.3 Equipment and Instruments

Nuclear Magnetic Resonance spectroscopy (NMR) ^1H -NMR, ^{13}C -NMR, COSY, HSQC and HMBC spectra were recorded at 25 °C on a Varian VNMRs 400, INOVA 400 or Bruker AVANCE III HD 400 MHz with cryoprobe. Chemical shifts are reported in ppm (δ) relative to tetramethylsilane (TMS) with the solvent resonance as internal standard (for the corresponding data see: H. E. Gottlieb, V. Kotlyar, A. Nudelman, *J. Org. Chem.* **1997**, *62*, 7512-7515). All NMR spectra were analyzed using MesreNova 9.0 software developed by the Mestrelab Research S. L. company. The signals derived from the ^1H -NMR spectra are reported with chemical shift, multiplicity (s = singlet, d = doublet, t = triplet, q = quartet, m = multiplet or a combination of these descriptions), coupling constant (Hz), integration and assignment. Data for ^{13}C -NMR are reported with chemical shift and assignment. Additionally to ^1H - and ^{13}C -NMR measurements, 2D-NMR techniques such as homonuclear correlation spectroscopy (COSY), heteronuclear single quantum coherence (HSQC), heteronuclear multiple bond coherence (HMBC) and nuclear Overhauser effect spectroscopy (NOESY) were used to assist the compound identification process. Note that the atom numbering of the signal assignment does not correspond to IUPAC rules.

Mass Spectrometry (MS) High resolution MS spectra were recorded by the LMU mass spectrometry service on the following spectrometers (ionization mode): Thermo Finnigan MAT 95 (GC/EI or DEP/EI) and Thermo Finnigan LTQ FT (ESI).

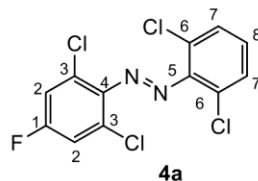
IR spectroscopy IR spectra of solids and liquids were recorded on a PerkinElmer Spectrum BX II FT-IR device. The neat substance was directly applied as thin film on the ATR unit. The IR data are reported as measured wavenumbers followed by the corresponding relative band intensities in brackets. The abbreviations vs (very strong), s (strong), m (medium) and w (weak), vw (very weak) and br (broad) stand for relative intensities.

UV-VIS spectroscopy UV-VIS spectra were recorded on a Varian 50 Scan UV-Visible Spectrophotometer. Illumination was provided by a TILL Photonics Polychrome 5000 monochromator. The experiments were conducted using a 50 μM solution of the compound in DMSO. The spectra were recorded after irradiation of the sample with the specified wavelength for 5 minutes. The absorption is plotted as arbitrary units (A.U.) as a function of wavelength λ (nm).

Melting Point (m_p) Melting points were determined on a B-450 melting point apparatus from BÜCHI Labortechnik AG. The values are uncorrected.

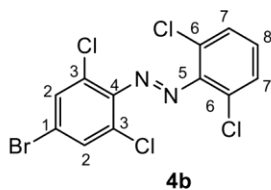
2. Experimental Procedures

(*E*)-1-(2,6-Dichloro-4-fluorophenyl)-2-(2,6-dichlorophenyl)diazene (**4a**)



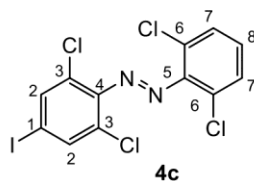
(*E*)-4-Fluoroazobenzene^[1] (**3a**, 20.0 mg, 0.100 mmol, 1.0 eq), NCS (66.8 mg, 0.500 mmol, 5.0 eq) and Pd(OAc)₂ (2.2 mg, 0.010 mmol, 0.10 eq) were dissolved in AcOH (1.00 mL) under a N₂-atmosphere in a 5 mL reaction tube. The tube was sealed with a glass stopper which was then secured with teflon tape and Parafilm[®]. The reaction was heated to 140 °C for 15 h 20 min during which time the color turned dark red. After cooling to room temperature, the solvent was evaporated and the mixture was transferred to a separatory funnel with CH₂Cl₂ (35 mL), sat. aq. NaCl (5 mL) and phosphate buffer (pH 7, 5 mL). The organic layer was separated, dried over Na₂SO₄ and concentrated under reduced pressure. Purification by flash column chromatography (3.42 g SiO₂, pentane) afforded (*E*)-1-(2,6-dichloro-4-fluorophenyl)-2-(2,6-dichlorophenyl)diazene (**4a**, 19.5 mg, 0.0577 mmol, 58%) as a red solid. ¹H-NMR analysis indicated that the sample contains a 7.9:1.0 mixture of *trans*- to *cis*-isomers.

R_f (pentane) = 0.28. **m_p** = 83.3 – 84.6 °C. **¹H-NMR** (400 MHz, C₆D₆): δ (ppm) = 6.86 (d, *J* = 8.1 Hz, 2H, H2), 6.52 (d, *J* = 8.0 Hz, 2H, H7), 6.33 (t, *J* = 8.1 Hz, 1H, H8). **¹³C-NMR** (101 MHz, C₆D₆): δ (ppm) = 162.48 (C1), 159.95 (C1), 148.15 (C5), 144.51 (C4), 144.46 (C4), 129.63 (C8), 129.41 (C7), 129.31 (C3), 129.20 (C3), 127.46 (C6), 117.26 (C2), 117.01 (C2). **¹⁹F-NMR** (376 MHz, C₆D₆): δ (ppm) = -109.35 (t, *J* = 8.0 Hz). **IR** (Diamond-ATR, neat): $\tilde{\nu}_{\text{max}}$ (cm⁻¹) = 3079 (vw), 2960 (vw), 2921 (vw), 2851 (vw), 1591 (m), 1576 (m), 1568 (m), 1458 (w), 1432 (s), 1406 (w), 1394 (m), 1261 (w), 1245 (m), 1202 (w), 1178 (w), 1154 (w), 1065 (m), 953 (m), 911 (w), 898 (vw), 857 (s), 810 (s), 775 (vs), 724 (m), 698 (m), 662 (w). **HRMS (EI)**: calc. for (C₁₂H₅N₂³⁵Cl₄F)⁺: 335.9191, found: 335.9175.

(E)-1-(4-Bromo-2,6-dichlorophenyl)-2-(2,6-dichlorophenyl)diazene (4b)

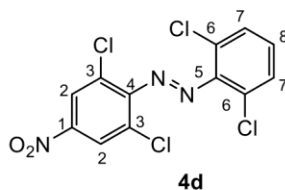
(*E*)-4-Bromoazobenzene^[2] (**3b**, 20.0 mg, 0.0766 mmol, 1.0 eq), NCS (51.1 mg, 0.383 mmol, 5.0 eq) and Pd(OAc)₂ (1.7 mg, 7.7 μmol, 0.10 eq) were dissolved in AcOH (0.77 mL) under a N₂-atmosphere in a 5 mL reaction tube. The tube was sealed with a glass stopper which was then secured with teflon tape and Parafilm[®]. The reaction was heated to 140 °C for 14 h 20 min during which time the color turned dark red. After cooling to room temperature, the solvent was removed under reduced pressure. Purification by flash column chromatography (5.1 g SiO₂, pentane) afforded (*E*)-1-(4-bromo-2,6-dichlorophenyl)-2-(2,6-dichlorophenyl)diazene (**4b**, 17.4 mg, 0.0436 mmol, 57%) as an orange-red solid. ¹H-NMR analysis indicated that the sample contains a 4.5:1.0 mixture of *trans*- to *cis*-isomers.

R_f (pentane) = 0.39. **m_p** = 123.2 – 125.9 °C. **¹H-NMR** (400 MHz, C₆D₆): δ (ppm) = 7.01 (s, 2H, H2), 6.85 (d, *J* = 8.0 Hz, 2H, H7), 6.33 (d, *J* = 7.8 Hz, 1H, H8). **¹³C-NMR** (101 MHz, C₆D₆): δ (ppm) = 148.00 (C5), 146.82 (C4), 132.18 (C2), 129.80 (C8), 129.46 (C7), 128.52 (C3), 127.59 (C6), 122.46 (C1). **IR** (Diamond-ATR, neat): $\tilde{\nu}_{\text{max}}$ (cm⁻¹) = 3075 (vw), 2921 (vw), 1927 (vw), 1723 (vw), 1563 (s), 1543 (m), 1501 (w), 1469 (vw), 1434 (s), 1378 (w), 1365 (m), 1264 (vw), 1197 (w), 1154 (vw), 1126 (w), 1096 (w), 1078 (vw), 916 (w), 854 (vs), 795 (s), 784 (s), 770 (vw), 758 (s), 727 (s), 688 (w), 672 (w). **HRMS (EI)**: calc. for (C₁₂H₅N₂³⁵Cl₄⁷⁹Br)⁺: 395.8390, found: 395.8376.

(E)-1-(2,6-Dichloro-4-iodophenyl)-2-(2,6-dichlorophenyl)diazene (4c)

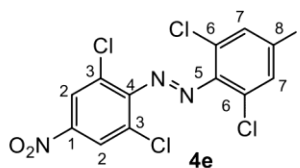
(E)-4-Iodoazobenzene^[3] (**3c**, 20.0 mg, 0.0659 mmol, 1.0 eq), NCS (43.3 mg, 0.325 mmol, 5.0 eq) and Pd(OAc)₂ (1.5 mg, 6.5 μmol, 0.10 eq) were dissolved in AcOH (0.65 mL) under a N₂-atmosphere in a 5 mL reaction tube. The tube was sealed with a glass stopper which was then secured with teflon tape and Parafilm[®]. The reaction was heated to 140 °C for 14 h 30 min during which time the color turned dark red. After cooling to room temperature, the solvent was evaporated and the mixture was transferred to a separatory funnel with CH₂Cl₂ (35 mL), sat. aq. NaCl (5 mL) and phosphate buffer (pH 7, 5 mL). The organic layer was separated, dried over Na₂SO₄ and concentrated under reduced pressure. Purification by flash column chromatography (3.42 g SiO₂, pentane) afforded (E)-1-(2,6-dichloro-4-iodophenyl)-2-(2,6-dichlorophenyl)diazene (**4c**, 20.1 mg, 0.0451 mmol, 68%) as a brown solid. ¹H-NMR analysis indicated that the sample contains a 4.9:1.0 mixture of *trans*- to *cis*-isomers.

R_f (pentane) = 0.45. **m_p** = 81.5 – 86.8 °C. **¹H-NMR** (400 MHz, C₆D₆): δ (ppm) = 7.24 (s, 2H, H2), 6.85 (d, *J* = 8.1 Hz, 2H, H7), 6.32 (t, *J* = 8.1 Hz, 1H, H8). **¹³C-NMR** (101 MHz, C₆D₆): δ (ppm) = 148.00 (C5), 147.47 (C4), 137.84 (C2), 129.79 (C8), 129.45 (C7), 128.24 (C3), 127.60 (C6), 93.56 (C1). **IR** (Diamond-ATR, neat): $\tilde{\nu}_{\max}$ (cm⁻¹) = 3070 (vw), 2922 (vw), 2851 (vw), 2279 (vw), 1730 (vw), 1556 (s), 1535 (m), 1473 (w), 1433 (s), 1414 (m), 1360 (m), 1262 (w), 1199 (w), 1160 (w), 1115 (w), 1069 (w), 1004 (vw), 916 (vw), 852 (s), 824 (w), 806 (s), 771 (vs), 733 (s), 686 (w), 671 (m). **HRMS (EI)**: calc. for (C₁₂H₅N₂³⁵Cl₄¹²⁷I)⁺: 443.8252, found: 443.8246.

(E)-1-(2,6-Dichloro-4-nitrophenyl)-2-(2,6-dichlorophenyl)diazene (4d)

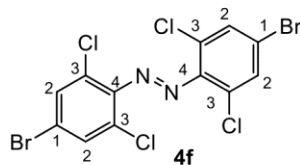
(*E*)-4-Nitroazobenzene^[41] (**3d**, 20.0 mg, 0.0880 mmol, 1.0 eq), NCS (58.8 mg, 0.440 mmol, 5.0 eq) and Pd(OAc)₂ (1.9 mg, 8.8 μmol, 0.10 eq) were dissolved in AcOH (0.88 mL) under a N₂-atmosphere in a 5 mL reaction tube. The tube was sealed with a glass stopper which was then secured with teflon tape and Parafilm[®]. The reaction was heated to 140 °C for 14 h 20 min during which time the color turned dark red. After cooling to room temperature, the solvent was evaporated and the mixture was transferred to a separatory funnel with CH₂Cl₂ (35 mL), sat. aq. NaCl (5 mL) and phosphate buffer (pH 7, 5 mL). The organic layer was separated, dried over Na₂SO₄ and concentrated under reduced pressure. Purification by flash column chromatography (3.42 g SiO₂, pentane) afforded (*E*)-1-(2,6-dichloro-4-nitrophenyl)-2-(2,6-dichlorophenyl)diazene (**4d**, 18.2 mg, 0.0499 mmol, 57%) as a red solid. ¹H-NMR analysis indicated that the sample contains an 18:1.0 mixture of *trans*- to *cis*-isomers.

R_f (pentane:Et₂O 19:1) = 0.63. **m_p** = 141.4 – 144.5 °C. **¹H-NMR** (400 MHz, C₆D₆): δ (ppm) = 7.58 (s, 2H, H2), 6.85 (d, *J* = 8.0 Hz, 2H, H7), 6.33 (t, *J* = 8.1 Hz, 1H, H8). **¹³C-NMR** (101 MHz, C₆D₆): δ (ppm) = 152.02 (C1), 147.22 (C5), 146.69 (C4), 130.61 (C8), 129.69 (C7), 127.22 (C3), 124.41 (C2). According to the HMBC spectrum, the C6 peak is obscured by the solvent peak. **IR** (Diamond-ATR, neat): $\tilde{\nu}_{\max}$ (cm⁻¹) = 3090 (w), 2955 (vw), 2923 (w), 2852 (vw), 2360 (vw), 1575 (vw), 1560 (vw), 1530 (s), 1469 (w), 1436 (m), 1386 (w), 1339 (vs), 1286 (m), 1260 (w), 1201 (w), 1186 (w), 1167 (w), 1146 (w), 1114 (w), 1069 (w), 1050 (w), 926 (w), 891 (s), 819 (s), 806 (s), 782 (vs), 739 (vs), 696 (m), 668 (w). **HRMS (EI)**: calc. for (C₁₂H₅O₂N₃³⁵Cl₄)⁺: 362.9136, found: 362.9129.

(E)-1-(2,6-Dichloro-4-iodophenyl)-2-(2,6-dichloro-4-nitrophenyl)diazene (4e)

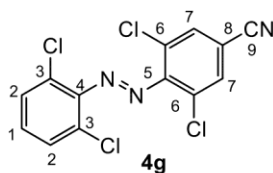
(E)-1-(4-Iodophenyl)-2-(4-nitrophenyl)diazene^[3] (**3e**, 23.1 mg, 0.0654 mmol, 1.0 eq), NCS (43.7 mg, 0.327 mmol, 5.0 eq) and Pd(OAc)₂ (1.5 mg, 6.5 μmol, 0.10 eq) were dissolved in AcOH (0.65 mL) under a N₂-atmosphere in a 5 mL reaction tube. The tube was sealed with a glass stopper which was then secured with teflon tape and Parafilm[®]. The reaction was heated to 140 °C for 13 h 30 min during which time the color turned dark red. After cooling to room temperature, the solvent was removed under reduced pressure. Purification by flash column chromatography (4.1 g SiO₂, pentane:CH₂Cl₂ = 19:1) afforded (E)-1-(2,6-dichloro-4-iodophenyl)-2-(2,6-dichloro-4-nitrophenyl)diazene (**4e**, 10.8 mg, 0.0220 mmol, 34%) as a brown solid. ¹H-NMR analysis indicated that the sample contains only the *trans*-isomer.

R_f (pentane:CH₂Cl₂ 9:1) = 0.34. **m_p** = 187.8 – 193.4 °C. **¹H-NMR (400 MHz, C₆D₆)**: δ (ppm) = 7.58 (s, 2H, H2), 7.24 (s, 2H, H7). **¹³C-NMR (101 MHz, C₆D₆)**: δ (ppm) = 150.40 (C1), 145.24 (C4), 145.01 (C5), 136.66 (C7), 127.16 (C6), 125.66 (C3), 122.93 (C2), 93.61 (C8). **IR** (Diamond-ATR, neat): $\tilde{\nu}_{\max}$ (cm⁻¹) = 3082 (w), 2957 (w), 2921 (w), 2851 (w), 2359 (vw), 1555 (m), 1530 (vs), 1385 (w), 1362 (w), 1339 (vs), 1260 (m), 1198 (w), 1182 (w), 1081 (m), 1018 (m), 927 (w), 890 (m), 856 (m), 823 (vs), 814 (vs), 737 (s), 679 (m). **HRMS (EI)**: calc. for (C₁₂H₄N₃O₂¹²⁷I³⁵Cl₄)⁺: 488.8102, found: 488.8099.

(E)-1,2-Bis(4-bromo-2,6-dichlorophenyl)diazene (4f)

(*E*)-1,2-Bis(4-bromophenyl)diazene^[5] (**3f**, 539 mg, 1.59 mmol, 1.0 eq), NCS (1.057 g, 7.93 mmol, 5.0 eq) and Pd(OAc)₂ (35.7 mg, 0.159 mmol, 0.10 eq) were dissolved in AcOH (15.9 mL) under a N₂-atmosphere in 50 mL pressure tube. The tube was sealed and the reaction was heated to 140 °C for 12 h 30 min during which time the color turned dark red. After cooling to room temperature, the solvent was removed under reduced pressure. Purification by flash column chromatography (36.9 g SiO₂, pentane) afforded (*E*)-1,2-bis(4-bromo-2,6-dichlorophenyl)diazene (**4f**, 484 mg, 1.01 mmol, 64%) as an orange solid. ¹H-NMR analysis indicated that the sample contains a 4.5:1.0 mixture of *trans*- to *cis*-isomers.

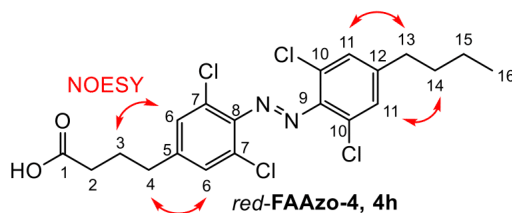
R_f (pentane:CH₂Cl₂ 19:1) = 0.55. **m_p** = 165.2 – 168.5 °C. **¹H-NMR (400 MHz, C₆D₆)**: δ (ppm) = 7.02 (s, 4H, H2). **¹³C-NMR (101 MHz, C₆D₆)**: δ (ppm) = 146.70 (C4), 132.25 (C2), 128.52 (C3), 122.68 (C1). **IR (Diamond-ATR, neat)**: $\tilde{\nu}_{\max}$ (cm⁻¹) = 3073 (vw), 2961 (vw), 2920 (vw), 2850 (vw), 1724 (vw), 1559 (s), 1542 (s), 1456 (w), 1368 (m), 1260 (m), 1193 (m), 1118 (m), 1080 (s), 1057 (m), 1019 (m), 964 (w), 852 (s), 838 (s), 816 (vs), 802 (vs), 740 (m), 700 (w), 682 (m). **HRMS (EI)**: calc. for (C₁₂H₄N₂⁷⁹Br₂³⁵Cl₄)⁺: 473.7495, found: 473.7488.

(E)-3,5-Dichloro-4-((2,6-dichlorophenyl)diazenyl)benzonitrile (4g)

(E)-4-(Phenyldiazenyl)benzonitrile^[6] (**3g**, 20.0 mg, 0.0965 mmol, 1.0 eq), NCS (64.4 mg, 0.483 mmol, 5.0 eq) and Pd(OAc)₂ (2.2 mg, 9.7 μmol, 0.10 eq) were dissolved in AcOH (0.97 mL) under a N₂-atmosphere in a 5 mL reaction tube. The tube was sealed with a glass stopper which was then secured with teflon tape and Parafilm[®]. The reaction was heated to 140 °C for 12 h during which time the color turned dark red. After cooling to room temperature, the solvent was evaporated and the mixture was transferred to a separatory funnel with CH₂Cl₂ (35 mL), sat. aq. NaCl (5 mL) and phosphate buffer (pH 7, 5 mL). The organic layer was separated, dried over Na₂SO₄ and concentrated under reduced pressure. Purification by flash column chromatography (4.1 g SiO₂, pentane:Et₂O = 49:1) afforded (E)-3,5-dichloro-4-((2,6-dichlorophenyl)diazenyl)benzonitrile (**4g**, 9.6 mg, 0.0267 mmol, 29%) as a brownish red solid. ¹H-NMR analysis indicated that the sample contains only the *trans*-isomer.

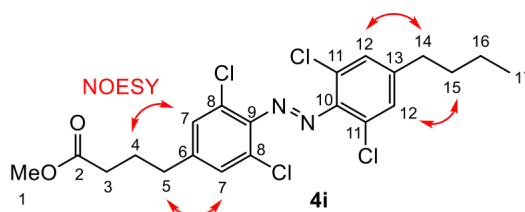
R_f (pentane:EtOAc 19:1) = 0.29. **m_p** = 131.3 – 135.2 °C. **¹H-NMR (400 MHz, C₆D₆)**: δ (ppm) = 6.83 (d, *J* = 8.1 Hz, 2H, H2), 6.59 (s, 2H, H7), 6.31 (t, *J* = 8.1 Hz, 1H, H1). **¹³C-NMR (101 MHz, C₆D₆)**: δ (ppm) = 150.78 (C5), 147.34 (C4), 132.33 (C7), 130.44 (C1), 129.63 (C2), 127.39 (C6), 115.89 (C9), 113.76 (C8). According to the HMBC spectrum, the C3 peak is obscured by the solvent peak. **IR** (Diamond-ATR, neat): $\tilde{\nu}_{\max}$ (cm⁻¹) = 3079 (vw), 2961 (vw), 2921 (vw), 2236 (vw), 1693 (vw), 1562 (w), 1538 (w), 1434 (m), 1378 (w), 1260 (m), 1200 (w), 1092 (m, br), 1017 (s), 876 (m), 789 (vs), 776 (vs), 742 (m), 732 (m). **HRMS (EI)**: calc. for (C₁₃H₅N₃³⁵Cl₄)⁺: 342.9238, found: 342.9232.

(E)-4-(4-((4-Butyl-2,6-dichlorophenyl)diazenyl)-3,5-dichlorophenyl)butanoic acid (*red*-FAAzo-4, 4h)



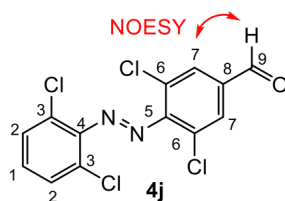
(*E*)-4-(4-((4-Butylphenyl)diazenyl)phenyl)butanoic acid^[7] (**FAAzo-4, 3h**, 300 mg, 0.925 mmol, 1.0 eq), NCS (617 mg, 4.62 mmol, 5.0 eq) and Pd(OAc)₂ (20.8 mg, 0.0925 mmol, 0.10 eq) were dissolved in AcOH (15.4 mL) under a N₂-atmosphere in a 30 mL pressure tube. The tube was sealed and reaction was heated to 140 °C for 12 h 45 min during which time the color turned dark red. After cooling to room temperature, the solvent was removed *in vacuo* and the mixture was transferred to a separatory funnel with CH₂Cl₂ (180 mL), sat. aq. NaCl (40 mL) and phosphate buffer (pH 7, 40 mL). The organic layer was separated, dried over Na₂SO₄ and concentrated under reduced pressure. Purification by flash column chromatography (46.1 g SiO₂, CH₂Cl₂:AcOH = 199:1) afforded (*E*)-4-(4-((4-butyl-2,6-dichlorophenyl)diazenyl)-3,5-dichlorophenyl)butanoic acid (*red*-**FAAzo-4, 4h**, 322 mg, 0.696 mmol, 75%) as a red-brown gum. ¹H-NMR analysis indicated that the sample contains a 4.4:1.0 mixture of *trans*- to *cis*-isomers.

R_f (CH₂Cl₂:AcOH 99:1) = 0.06. ¹H-NMR (400 MHz, C₆D₆): δ (ppm) = 6.91 (s, 2H, H11), 6.83 (s, 2H, H6), 2.01 (t, *J* = 7.5 Hz, 2H, H13), 1.91 (m, 4H, H4 and H2), 1.41 (p, *J* = 7.4 Hz, 2H, H3), 1.18 – 1.09 (m, 2H, H14), 1.09 – 0.99 (m, 2H, H15), 0.77 (t, *J* = 7.1 Hz, 3H, H16). ¹³C-NMR (101 MHz, C₆D₆): δ (ppm) = 179.70 (C1), 146.37 (C8), 145.96 (C9), 145.76 (C12), 144.09 (C5), 129.61 (C11), 129.54 (C6), 127.89 (C10), 34.85 (C13), 33.99 (C2), 33.17 (C4), 32.94 (C14), 25.54 (C3), 22.47 (C15), 14.01 (C16). According to the HMBC spectrum, the C7 peak is obscured by the solvent peak. **IR** (Diamond-ATR, neat): $\tilde{\nu}_{\text{max}}$ (cm⁻¹) = 2955 (m), 2928 (m), 2859 (w), 1705 (vs), 1589 (m), 1548 (m), 1531 (w), 1456 (m), 1436 (m), 1400 (s), 1339 (m), 1264 (m), 1103 (w), 1080 (w), 1050 (w), 927 (m), 891 (m), 857 (s), 806 (vs), 787 (s), 739 (s), 696 (m), 668 (m). **HRMS (ESI)**: calc. for (C₂₀H₁₉N₂O₂³⁵Cl₄)⁻ 459.0206, found: 459.0215.

Methyl (*E*)-4-(4-((4-butyl-2,6-dichlorophenyl)diazenyl)-3,5-dichlorophenyl)butanoate (**4i**)

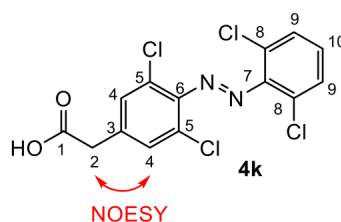
Methyl (*E*)-4-(4-((4-butylphenyl)diazenyl)phenyl)butanoate (**3i**, 20.0 mg, 0.0591 mmol, 1.0 eq), NCS (39.5 mg, 0.295 mmol, 5.0 eq) and Pd(OAc)₂ (1.3 mg, 5.9 μmol, 0.10 eq) were dissolved in AcOH (0.59 mL) under a N₂-atmosphere in a 5 mL reaction tube. The tube was sealed with a glass stopper which was then secured with teflon tape and Parafilm[®]. The reaction was heated to 140 °C for 14 h during which time the color turned dark red. After cooling to room temperature, the solvent was evaporated and the mixture was transferred to a separatory funnel with CH₂Cl₂ (35 mL), sat. aq. NaCl (5 mL) and phosphate buffer (pH 7, 5 mL). The organic layer was separated, dried over Na₂SO₄ and concentrated under reduced pressure. Purification by flash column chromatography (3.42 g SiO₂, pentane:Et₂O = 19:1) afforded methyl (*E*)-4-(4-((4-butyl-2,6-dichlorophenyl)diazenyl)-3,5-dichlorophenyl)butanoate (**4i**, 18.4 mg, 0.0386 mmol, 66%) as a dark red oil. ¹H-NMR analysis indicated that the sample contains a 4.0:1.0 mixture of *trans*- to *cis*-isomers.

R_f (pentane:Et₂O 9:1) = 0.29. **¹H-NMR (400 MHz, C₆D₆)**: δ (ppm) = 6.91 (s, 2H, H12), 6.85 (s, 2H, H7), 3.35 (s, 3H, H1), 1.99 (m, 4H, H5 and H14), 1.89 (t, *J* = 7.3 Hz, 2H, H3), 1.47 (p, *J* = 7.4 Hz, 2H, H4), 1.22 – 1.07 (m, 2H, H15), 1.03 (dt, *J* = 13.4, 7.0 Hz, 2H, H16), 0.77 (t, *J* = 7.2 Hz, 3H, H17). **¹³C-NMR (101 MHz, C₆D₆)**: δ (ppm) = 172.72 (C2), 146.30 (C9), 145.98 (C10), 145.72 (C13), 144.36 (C6), 129.60 (C7 or C12), 129.58 (C7 or C12), 127.88 (C8), 51.08 (C1), 34.84 (C14), 34.13 (C5), 33.06 (C3), 32.93 (C15), 25.90 (C4), 22.46 (C16), 14.01 (C17). According to the HMBC spectrum, C11 peak is obscured by the solvent peak. **IR (Diamond-ATR, neat)**: $\tilde{\nu}_{\max}$ (cm⁻¹) = 2954 (w), 2929 (w), 2860 (w), 2359 (vw), 1735 (vs), 1590 (m), 1549 (m), 1456 (m), 1436 (m), 1399 (s), 1378 (w), 1341 (w), 1250 (m), 1203 (s), 1174 (s), 1148 (m), 1103 (w), 1081 (w), 1054 (w), 1030 (w), 934 (w), 857 (s), 802 (vs), 739 (m). **HRMS (ED)**: calc. for (C₂₁H₂₂O₂N₂³⁵Cl₄)⁺: 474.0435, found: 474.0431.

(E)-3,5-Dichloro-4-((2,6-dichlorophenyl)diazenyl)benzaldehyde (4j)

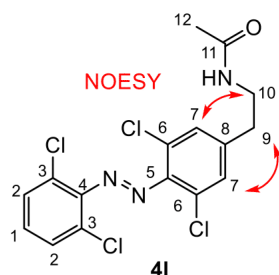
(*E*)-4-(Phenyldiazenyl)benzaldehyde^[81] (**3j**, 20.0 mg, 0.0951 mmol, 1.0 eq), NCS (63.5 mg, 0.475 mmol, 5.0 eq) and Pd(OAc)₂ (2.1 mg, 9.5 μmol, 0.10 eq) were dissolved in AcOH (0.95 mL) under a N₂-atmosphere in a 5 mL reaction tube. The tube was sealed with a glass stopper which was then secured with teflon tape and Parafilm[®]. The reaction was heated to 140 °C for 13 h during which time the color turned dark red. After cooling to room temperature, the solvent was removed under reduced. Purification by flash column chromatography (3.59 g SiO₂, pentane:Et₂O = 99:1) afforded (*E*)-3,5-dichloro-4-((2,6-dichlorophenyl)diazenyl)benzyl acetate (**4j**, 17.3 mg, 0.0497 mmol, 52%) as a red gum. ¹H-NMR analysis indicated that the sample contains a 15:1.0 mixture of *trans*- to *cis*-isomers.

R_f (pentane: Et₂O 9:1) = 0.35. **¹H-NMR** (400 MHz, C₆D₆): δ (ppm) = 9.05 (s, 1H, H9), 7.25 (s, 2H, H7), 6.86 (d, *J* = 8.1 Hz, 2H, H2), 6.33 (t, *J* = 8.1 Hz, 1H, H1). **¹³C-NMR** (101 MHz, C₆D₆): δ (ppm) = 187.87 (C9), 151.64 (C5), 147.52 (C4), 136.69 (C8), 130.30 (C1), 129.91 (C7), 129.61 (C2), 128.00 (C3), 127.68 (C6). **IR** (Diamond-ATR, neat): $\tilde{\nu}_{\max}$ (cm⁻¹) = 3359 (vw), 3056 (vw), 2956 (vw), 2920 (w), 2851 (w), 1695 (vs), 1663 (w), 1632 (w), 1560 (m), 1468 (w), 1435 (s), 1364 (s), 1261 (w), 1194 (s), 1100 (w), 1074 (w), 1053 (w), 1010 (w), 944 (w), 908 (w), 881 (m), 810 (vs), 794 (s), 773 (vs), 741 (s), 732 (s), 723 (s), 676 (m). **HRMS (EI)**: calc. for (C₁₃H₆N₂O³⁵Cl₄)⁺: 345.9234, found: 345.9231.

(E)-2-(3,5-Dichloro-4-((2,6-dichlorophenyl)diazenyl)phenyl)acetic acid (4k)

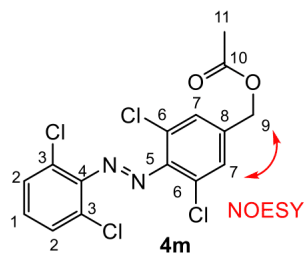
(E)-2-(4-(Phenyldiazenyl)phenyl)acetic acid^[9] (**3k**, 20.0 mg, 0.0832 mmol, 1.0 eq), NCS (55.6 mg, 0.416 mmol, 5.0 eq) and Pd(OAc)₂ (1.9 mg, 8.3 μmol, 0.10 eq) were dissolved in AcOH (0.83 mL) under a N₂-atmosphere in a 5 mL reaction tube. The tube was sealed with a glass stopper which was then secured with teflon tape and Parafilm[®]. The reaction was heated to 140 °C for 14 h during which time the color turned dark red. After cooling to room temperature, the solvent was evaporated and the mixture was transferred to a separatory funnel with CH₂Cl₂ (35 mL), sat. aq. NaCl (5 mL) and phosphate buffer (pH 7, 5 mL). The organic layer was separated, dried over Na₂SO₄ and concentrated under reduced pressure. Purification by flash column chromatography (3.76 g SiO₂, pentane:EtOAc:AcOH = 80:20:1) afforded (E)-2-(3,5-dichloro-4-((2,6-dichlorophenyl)diazenyl)phenyl)acetic acid (**4k**, 15.2 mg, 0.0402 mmol, 48%) as a red-brown hygroscopic solid. ¹H-NMR analysis indicated that the sample contains a 2.9:1.0 mixture of *trans*- to *cis*-isomers.

R_f (pentane:EtOAc:AcOH 90:9:1) = 0.60. **m_p** = 160.5 – 171.3 °C. **¹H-NMR (400 MHz, C₆D₆)**: δ (ppm) = 6.87 (d, *J* = 8.0 Hz, 2H, H₉), 6.87 (s, 2H, H₄), 6.32 (t, *J* = 8.0 Hz, 1H, H₁₀), 2.82 (s, 2H, H₂). **¹³C-NMR (101 MHz, C₆D₆)**: δ (ppm) = 173.23 (C₁), 148.23 (C₇), 146.89 (C₆), 136.07 (C₃), 130.61 (C₄), 129.58 (C₁₀), 129.41 (C₉), 129.16 (C₅), 127.59 (C₈), 39.09 (C₂). **IR** (Diamond-ATR, neat): $\tilde{\nu}_{\max}$ (cm⁻¹) = 3075 (w), 2924 (m), 2853 (w), 2633 (vw), 1709 (vs), 1592 (m), 1563 (m), 1553 (m), 1492 (w), 1435 (s), 1399 (s), 1200 (s, br), 1098 (m), 1028 (w), 941 (m), 909 (m), 857 (m), 800 (s), 776 (vs), 739 (m), 665 (m). **HRMS (ESI)**: calc. for (C₁₄H₉N₂O₂³⁵Cl₄)⁺: 376.9413, found: 376.9412.

(E)-N-(3,5-Dichloro-4-((2,6-dichlorophenyl)diazenyl)phenethyl)acetamide (4I)

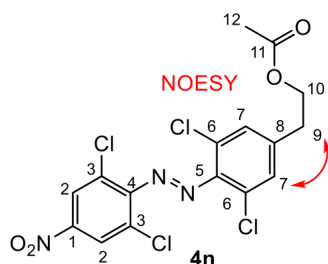
(E)-2-(4-(Phenyldiazenyl)phenyl)ethan-1-amine^[4] (**3I**, 20.0 mg, 0.0888 mmol, 1.0 eq), NCS (63.2 mg, 0.474 mmol, 5.3 eq) and Pd(OAc)₂ (2.1 mg, 9.5 μmol, 0.11 eq) were dissolved in AcOH (0.95 mL) under a N₂-atmosphere in a 5 mL reaction tube. The tube was sealed with a glass stopper which was then secured with teflon tape and Parafilm[®]. The reaction was heated to 140 °C for 13 h 30 min during which time the color turned dark red. After cooling to room temperature, the solvent was evaporated and the mixture was transferred to a separatory funnel with CH₂Cl₂ (35 mL), sat. aq. NaCl (5 mL) and phosphate buffer (pH 7, 5 mL). The organic layer was separated, dried over Na₂SO₄ and concentrated under reduced pressure. Purification by flash column chromatography (3.42 g SiO₂, CH₂Cl₂:NEt₃ = 199:1) afforded (E)-N-(3,5-dichloro-4-((2,6-dichlorophenyl)diazenyl)phenethyl)acetamide (**4I**, 21.5 mg, 0.0531 mmol, 60%) as a dark red oil. ¹H-NMR analysis indicated that the sample contains a 2.9:1.0 mixture of *trans*- to *cis*-isomers.

R_f (pentane:EtOAc 9:1) = 0.70. ¹H-NMR (400 MHz, C₆D₆): δ (ppm) = 6.87 (d, *J* = 8.2 Hz, 2H, H2), 6.80 (s, 2H, H7), 6.33 (t, *J* = 8.1 Hz, 1H, H1), 4.17 (s, 1H, NH), 2.88 (q, *J* = 6.6 Hz, 2H, H10), 2.18 (t, *J* = 6.7 Hz, 2H, H9), 1.45 (s, 3H, H12). ¹³C-NMR (101 MHz, C₆D₆): δ (ppm) = 168.77 (C11), 148.28 (C4), 146.28 (C5), 142.76 (C8), 130.00 (C7), 129.57 (C1), 129.42 (C2), 127.52 (C3), 40.25 (C10), 34.85 (C9), 22.79 (C12). According to the HMBC spectrum, the C6 peak is obscured by the solvent peak. **IR** (Diamond-ATR, neat): $\tilde{\nu}_{\max}$ (cm⁻¹) = 3288 (vw, br), 2956 (m), 2921 (vs), 2851 (m), 1650 (w), 1548 (w), 1462 (w), 1434 (w), 1377 (w), 1261 (w), 1097 (w), 1021 (w), 864 (vw), 802 (m), 730 (w). **HRMS (ESI)**: calc. for (C₁₆H₁₄ON₃³⁵Cl₄)⁺: 403.9885, found: 403.9892.

(E)-3,5-Dichloro-4-((2,6-dichlorophenyl)diazenyl)benzyl acetate (4m)

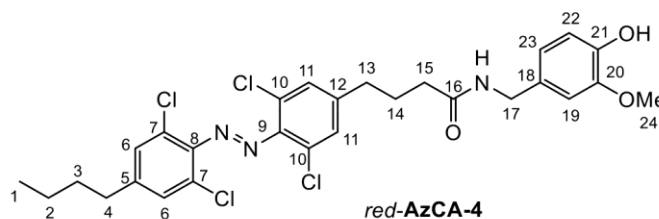
(E)-4-(Phenyldiazenyl)phenylmethanol^[10] (**3m**, 20.0 mg, 0.0942 mmol, 1.0 eq), NCS (62.3 mg, 0.471 mmol, 5.0 eq) and Pd(OAc)₂ (2.1 mg, 9.4 μmol, 0.10 eq) were dissolved in AcOH (0.94 mL) under a N₂-atmosphere in a 5 mL reaction tube. The tube was sealed with a glass stopper which was then secured with teflon tape and Parafilm®. The reaction was heated to 140 °C for 13 h 30 min during which time the color turned dark red. After cooling to room temperature, the solvent was evaporated and the mixture was transferred to a separatory funnel with CH₂Cl₂ (35 mL), sat. aq. NaCl (5 mL) and phosphate buffer (pH 7, 5 mL). The organic layer was separated, dried over Na₂SO₄ and concentrated under reduced pressure. Purification by flash column chromatography (3.59 g SiO₂, pentane:Et₂O = 9:1) afforded (E)-3,5-dichloro-4-((2,6-dichlorophenyl)diazenyl)benzyl acetate (**4m**, 20.4 mg, 0.0520 mmol, 55%) as a brownish red oil. ¹H-NMR analysis indicated that the sample contains a 3.0:1.0 mixture of *trans*- to *cis*-isomers.

R_f (pentane:EtOAc 9:1) = 0.47. **¹H-NMR** (400 MHz, C₆D₆): δ (ppm) = 6.97 (s, 2H, H7), 6.88 (d, *J* = 8.1 Hz, 2H, H2), 6.34 (t, *J* = 8.1 Hz, 1H, H1), 4.50 (s, 2H, H9), 1.58 (s, 3H, H11). **¹³C-NMR** (101 MHz, C₆D₆): δ (ppm) = 169.54 (C10), 148.12 (C4), 147.41 (C5), 138.97 (C8), 129.69 (C1), 129.44 (C2), 128.74 (C7), 127.61 (C3), 63.87 (C9), 20.18 (C11). According to the HMBC spectrum, the C6 peak is obscured by the solvent peak. **IR** (Diamond-ATR, neat): $\tilde{\nu}_{\text{max}}$ (cm⁻¹) = 2927 (vw), 1742 (vs), 1596 (w), 1562 (w), 1434 (s), 1402 (w), 1372 (m), 1220 (vs), 1098 (w), 1029 (m), 973 (w), 860 (m), 808 (s), 776 (vs), 738 (m), 668 (w). **HRMS (ESI)**: calc. for (C₁₅H₁₁O₂N₂³⁵Cl₄)⁺: 390.9569, found: 390.9569.

(E)-3,5-Dichloro-4-((2,6-dichloro-4-nitrophenyl)diazenyl)phenethyl acetate (4n)

(*E*)-2-(4-((4-Nitrophenyl)diazenyl)phenyl)ethan-1-ol (**3n**, 25.0 mg, 0.0922 mmol, 1.0 eq), NCS (61.5 mg, 0.461 mmol, 5.0 eq) and Pd(OAc)₂ (2.1 mg, 9.2 μmol, 0.10 eq) were dissolved in AcOH (0.92 mL) under a N₂-atmosphere in a 5 mL reaction tube. The tube was sealed with a glass stopper which was then secured with teflon tape and Parafilm[®]. The reaction was heated to 140 °C for 12 h 30 min during which time the color turned to dark red. After cooling to room temperature, the solvent was removed under reduced pressure. Purification by flash column chromatography (4.1 g SiO₂, pentane:Et₂O = 19:1) afforded (*E*)-3,5-dichloro-4-((2,6-dichloro-4-nitrophenyl)diazenyl)phenethyl acetate (**4n**, 25.4 mg, 0.0563 mmol, 61%) as a brown solid. ¹H-NMR analysis indicated that the sample contains a 2.7:1.0 mixture of *trans*- to *cis*-isomers.

R_f (pentane:EtOAc 9:1) = 0.43. **m_p** = 119.4 – 122.0 °C. **¹H-NMR (400 MHz, C₆D₆)**: δ (ppm) = 7.61 (s, 2H, H2), 6.83 (s, 2H, H7), 3.83 (t, *J* = 6.7 Hz, 2H, H10), 2.20 (t, *J* = 6.7 Hz, 2H, H9), 1.60 (s, 3H, H12). **¹³C-NMR (101 MHz, C₆D₆)**: δ (ppm) = 169.87 (C11), 152.22 (C1), 146.64 (C4), 145.49 (C5), 142.45 (C8), 130.32 (C7), 128.50 (C6), 127.16 (C3), 124.41 (C2), 63.43 (C10), 34.14 (C9), 20.32 (C12). **IR** (Diamond-ATR, neat): $\tilde{\nu}_{\max}$ (cm⁻¹) = 3089 (w), 2956 (vw), 2919 (vw), 2850 (vw), 1743 (vs), 1589 (w), 1545 (w), 1519 (s), 1442 (m), 1429 (m), 1394 (m), 1366 (m), 1339 (vs), 1308 (m), 1284 (m), 1229 (br vs), 1145 (m), 1114 (w), 1085 (w), 1044 (vs), 981 (m), 922 (w), 889 (m), 874 (s), 857 (m), 825 (vs), 792 (s), 741 (vs), 728 (m), 699 (m), 667 (m). **HRMS (ED)**: calc. for (C₁₆H₁₁N₃O₄³⁵Cl₄)⁺: 448.9504, found: 448.9497.

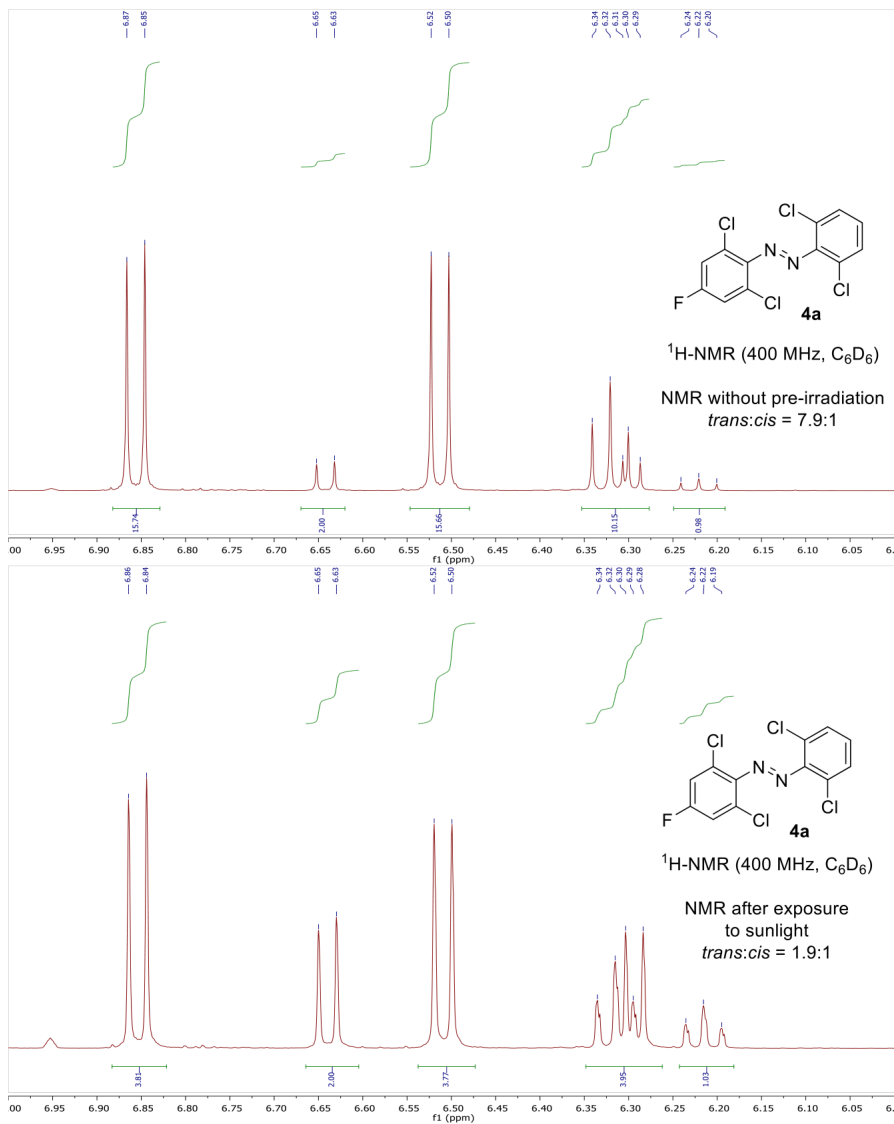
(E)-4-(4-((4-Butyl-2,6-dichlorophenyl)diazenyl)-3,5-dichlorophenyl)-N-(4-hydroxy-3-methoxybenzyl)butanamide (*red-AzCA-4*)

(*E*)-4-(4-((4-Butylphenyl)diazenyl)phenyl)butanoic acid (*red-FAAzo-4*, **4h**, 50.0 mg, 0.108 mmol, 1.0 eq) and TBTU (34.7 mg, 0.108 mmol, 1.0 eq) were dissolved in dry EtOAc (4.3 mL) under a N₂-atmosphere and NEt₃ (45.2 μL, 0.324 mmol, 3.0 eq) was added. The reaction was stirred for 1 hour at room temperature and 4-(aminomethyl)-2-methoxyphenol · HCl (41.0 mg, 0.216 mmol, 2.0 eq) was added. After stirring for additional 2 hours 30 min, the mixture was transferred into a separatory funnel with EtOAc (65 mL) and the organic phase was washed with 3% aq. KHSO₄ (20 mL), sat. aq. NaCl (20 mL) and dried over Na₂SO₄. The solution was concentrated under reduced pressure and purified by flash column chromatography (16.4 g SiO₂, pentane:EtOAc = 1:1) to give (*E*)-4-(4-((4-butyl-2,6-dichlorophenyl)diazenyl)-3,5-dichlorophenyl)-N-(4-hydroxy-3-methoxybenzyl)butanamide (*red-AzCA-4*, 36.7 mg, 0.0613 mmol, 57%) as a dark red gum. ¹H-NMR analysis indicated that the sample contains a 3.0:1.0 mixture of *trans*- to *cis*-isomers.

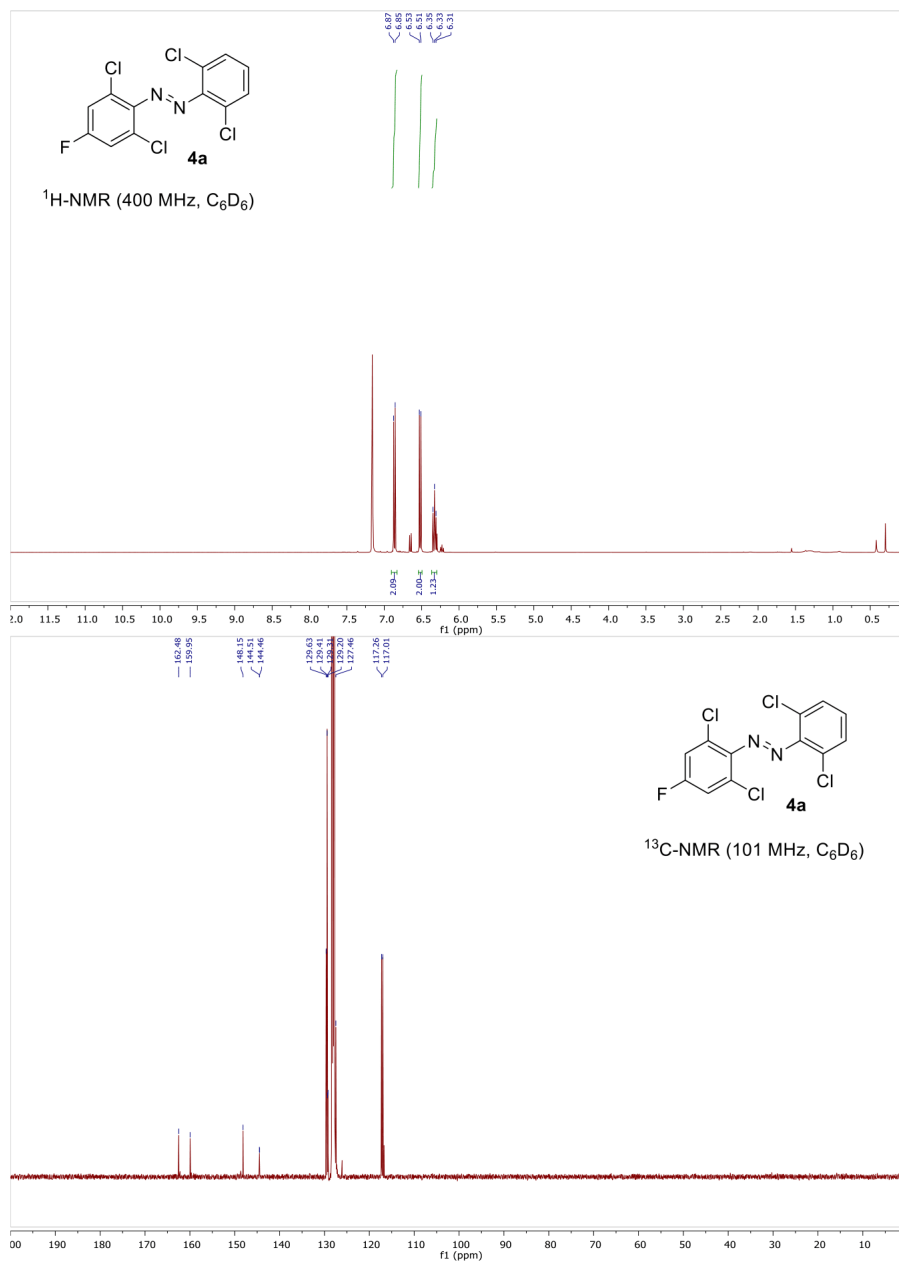
R_f (pentane:EtOAc 1:1) = 0.20. **¹H-NMR (400 MHz, CDCl₃):** δ (ppm) = 7.26 (s, 2H, H6), 7.24 (s, 2H, H11), 6.86 (d, *J* = 8.0 Hz, 1H, H22), 6.81 (d, *J* = 2.0 Hz, 1H, H19), 6.76 (dd, *J* = 8.0, 2.0 Hz, 1H, H23), 5.78 (t, *J* = 5.8 Hz, 1H, NH), 4.35 (d, *J* = 5.6 Hz, 2H, H17), 3.87 (s, 3H, H24), 2.67 (t, *J* = 7.5 Hz, 2H, H13), 2.64 – 2.59 (m, 2H, H4), 2.22 (t, *J* = 7.3 Hz, 2H, H15), 2.01 (p, *J* = 7.6 Hz, 2H, H14), 1.67 – 1.57 (m, 2H, H3), 1.38 (dq, *J* = 14.6, 7.3 Hz, 2H, H2), 0.95 (t, *J* = 7.3 Hz, 3H, H1). **¹³C-NMR (101 MHz, CDCl₃):** δ (ppm) = 171.92 (C16), 146.86 (C20), 145.83 (C5), 145.36 (C8 and C9), 145.34 (C21), 144.20 (C12), 130.28 (C18), 129.51 (C6 and C11), 127.47 (C7 and C10), 121.02 (C23), 114.60 (C22), 110.90 (C19), 56.09 (C24), 43.80 (C17), 35.45 (C15), 35.02 (C4), 34.42 (C13), 33.07 (C3), 26.54 (C14), 22.31 (C2), 13.97 (C1). **IR (Diamond-ATR, neat):** $\tilde{\nu}_{\max}$ (cm⁻¹) = 3285 (w, br), 3062 (vw), 2955 (w), 2930 (w), 2860 (w), 1642 (m), 1590 (s), 1547 (s), 1514 (vs), 1462 (m), 1452 (s), 1429 (s), 1398 (s), 1379 (m), 1273 (s), 1237 (s), 1205 (s), 1154 (s), 1123 (s), 1080 (w), 1034 (s), 910 (w), 855 (m), 799 (vs), 730 (s). **HRMS (ESI):** calc. for (C₂₈H₃₀N₃O₃³⁵Cl₄)⁺: 596.1036, found: 596.1041.

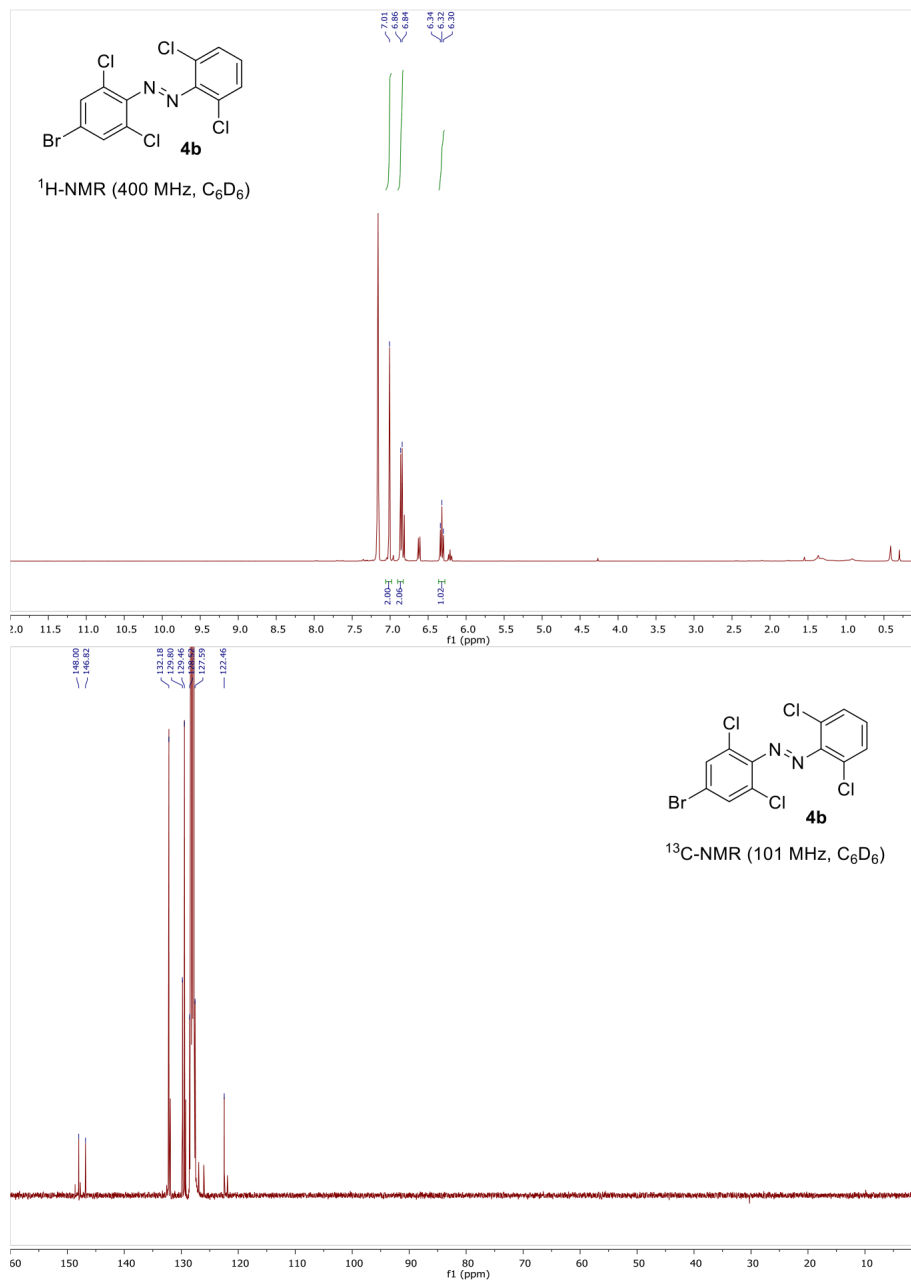
3. NMR Data

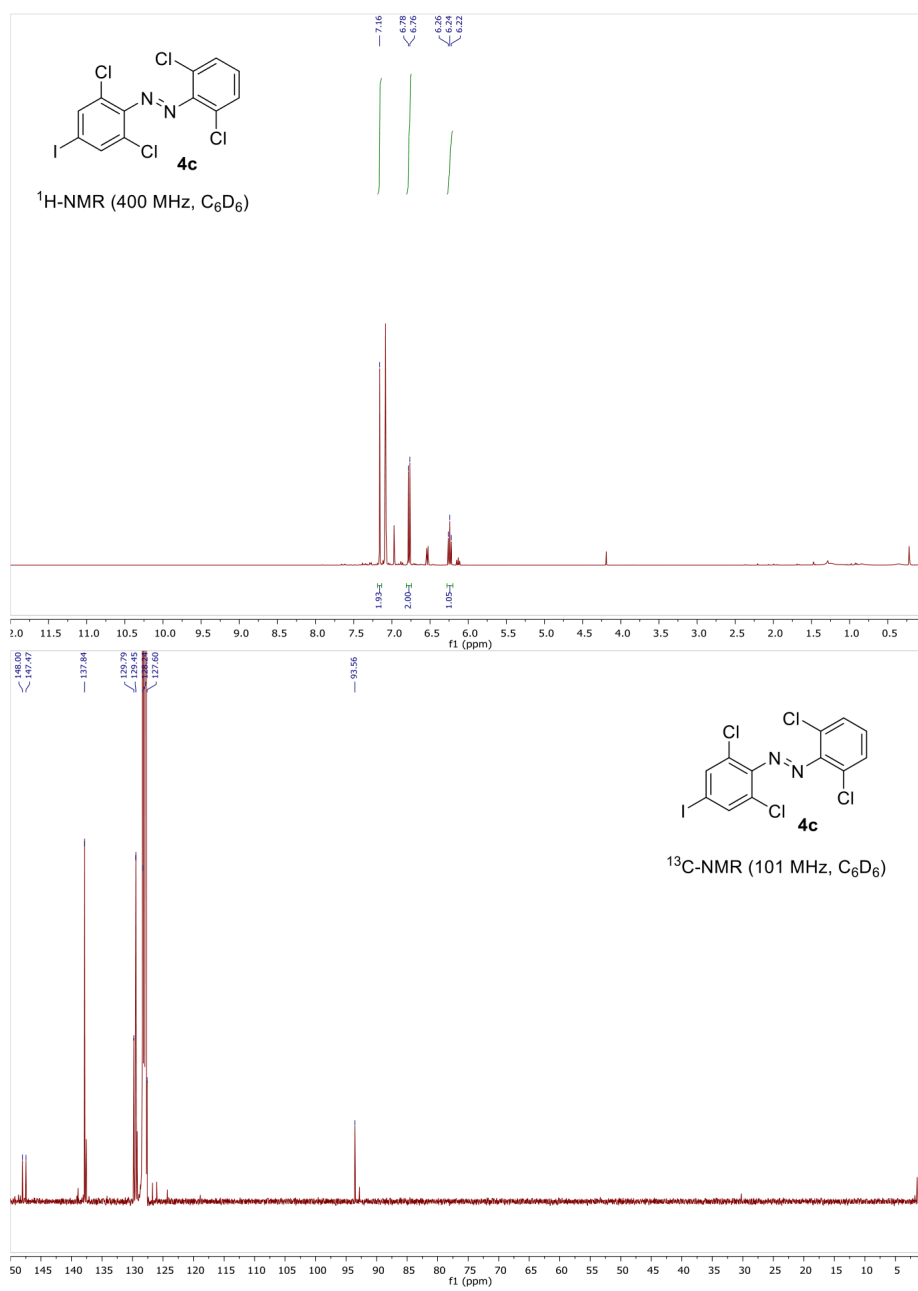
3.1 Photoisomerization Experiments

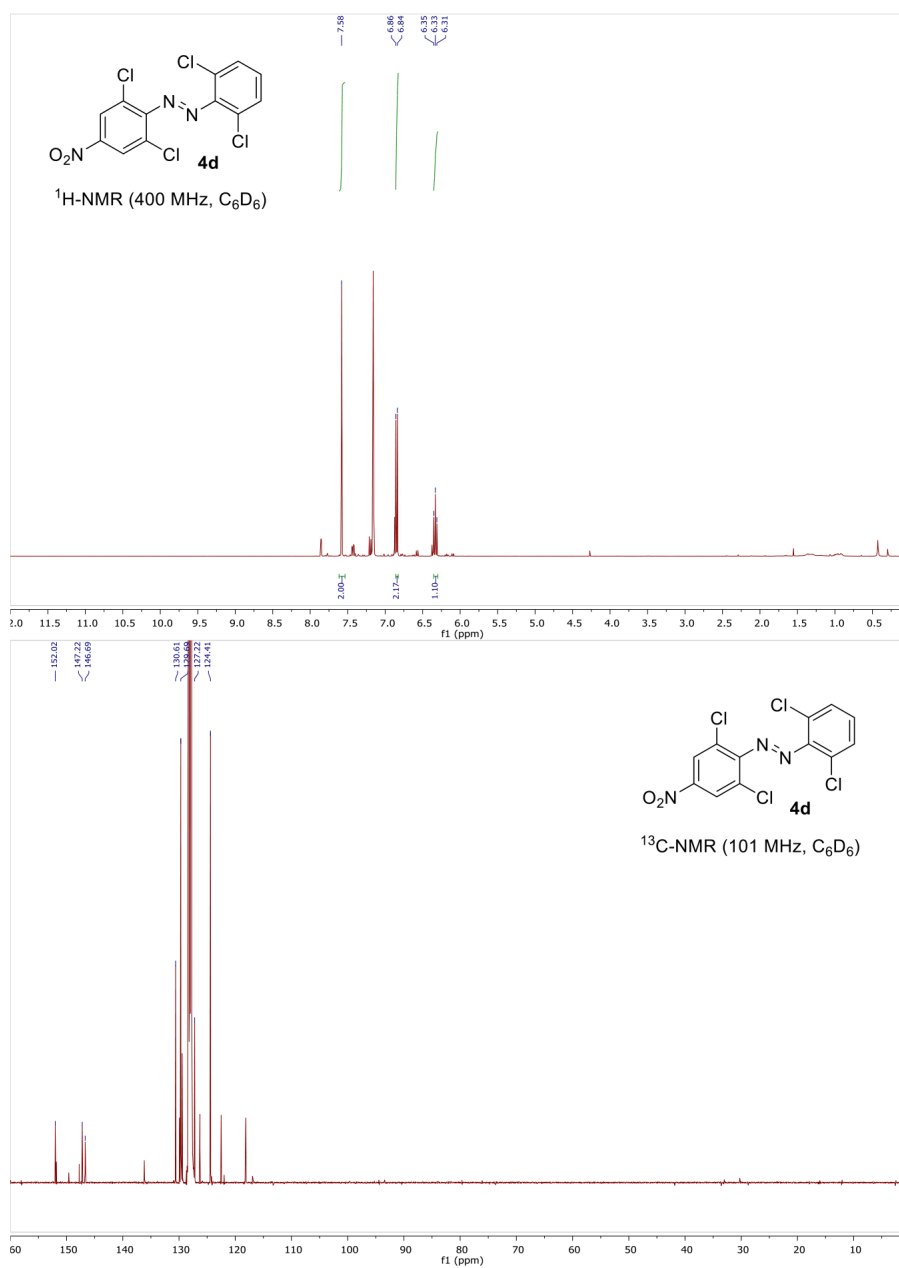


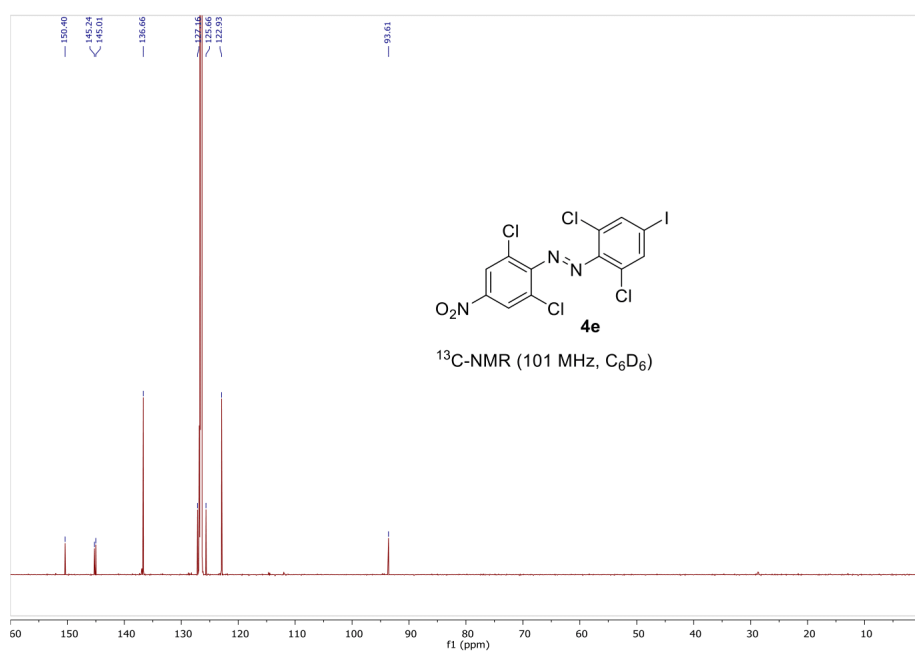
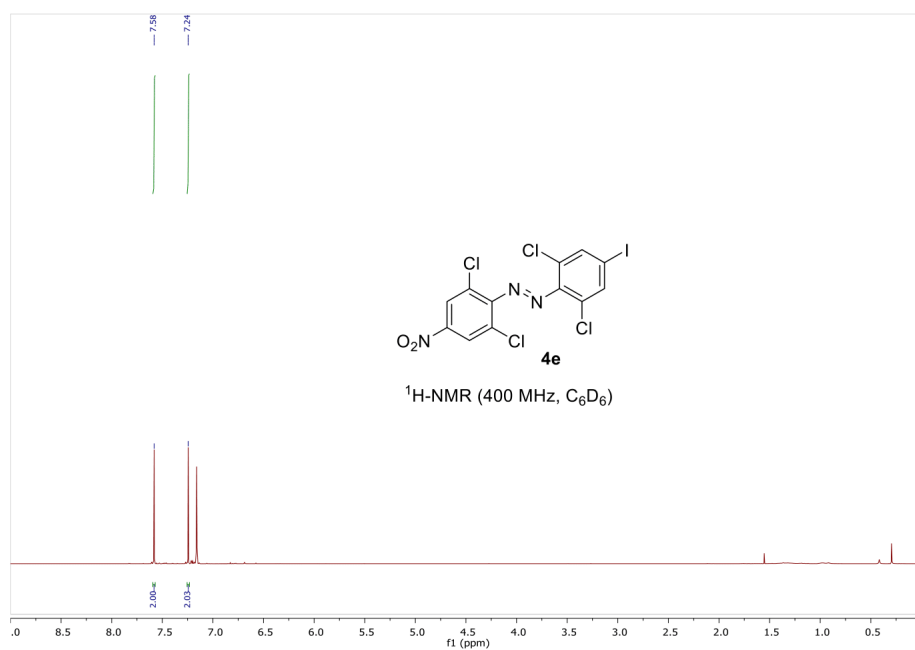
3.2 NMR Spectra

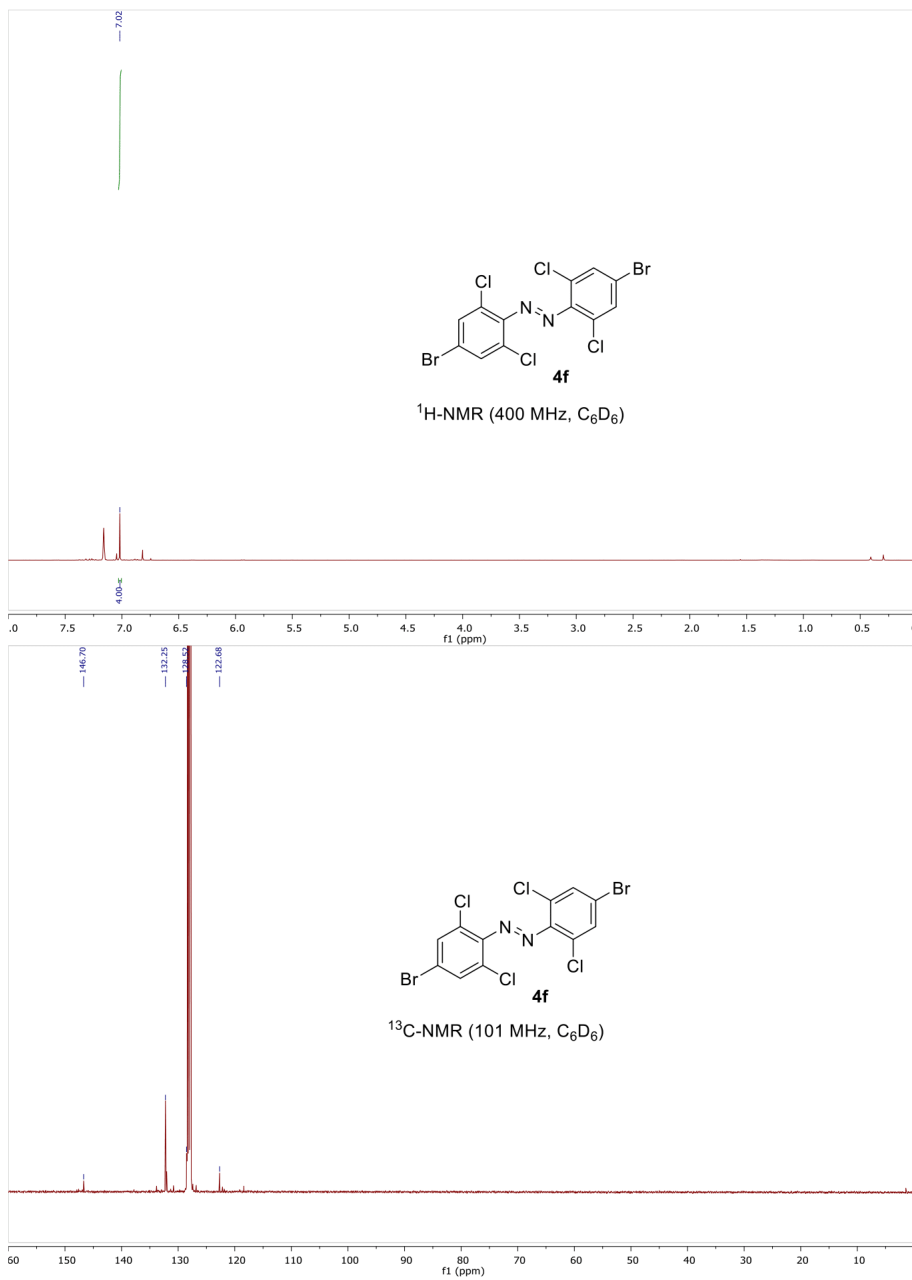


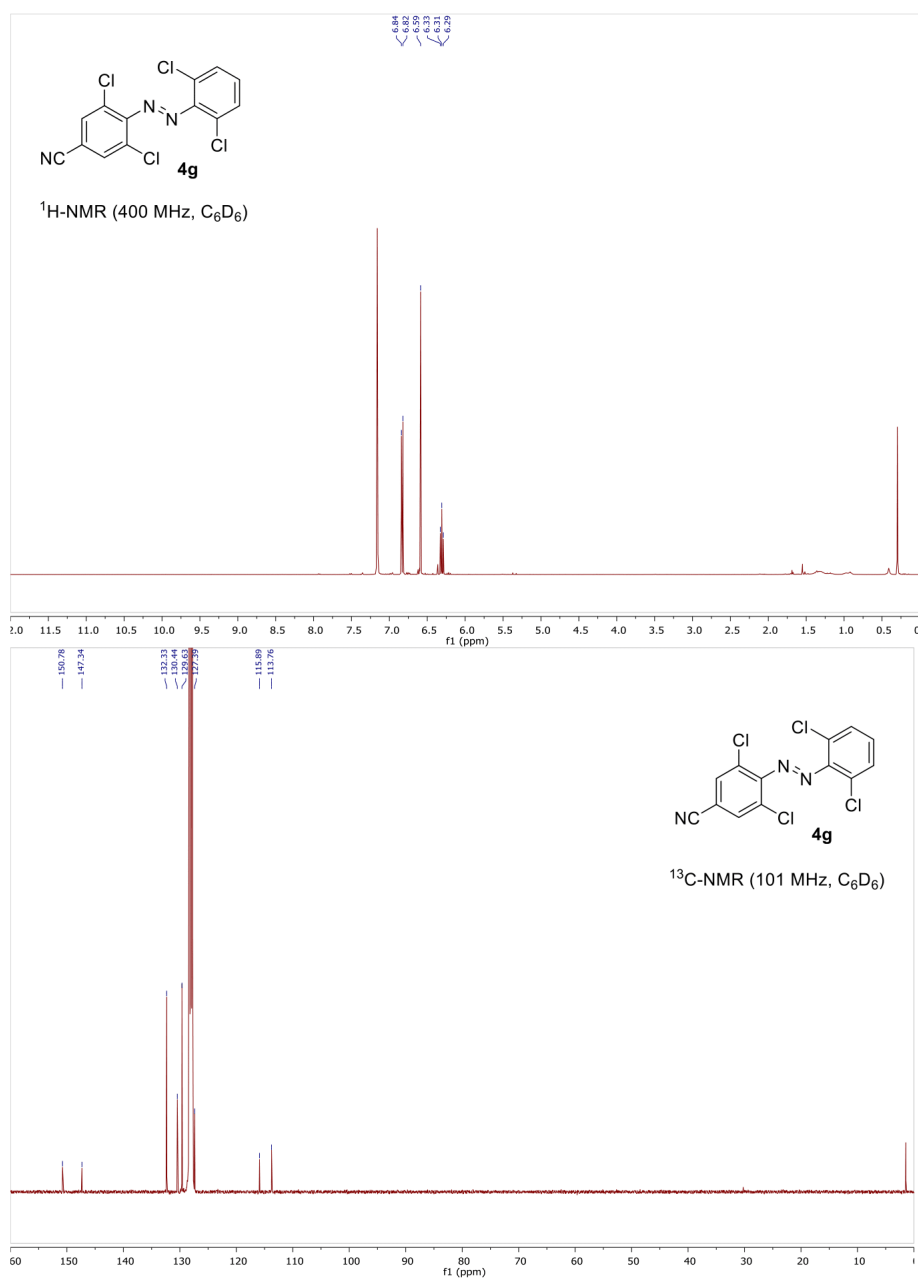


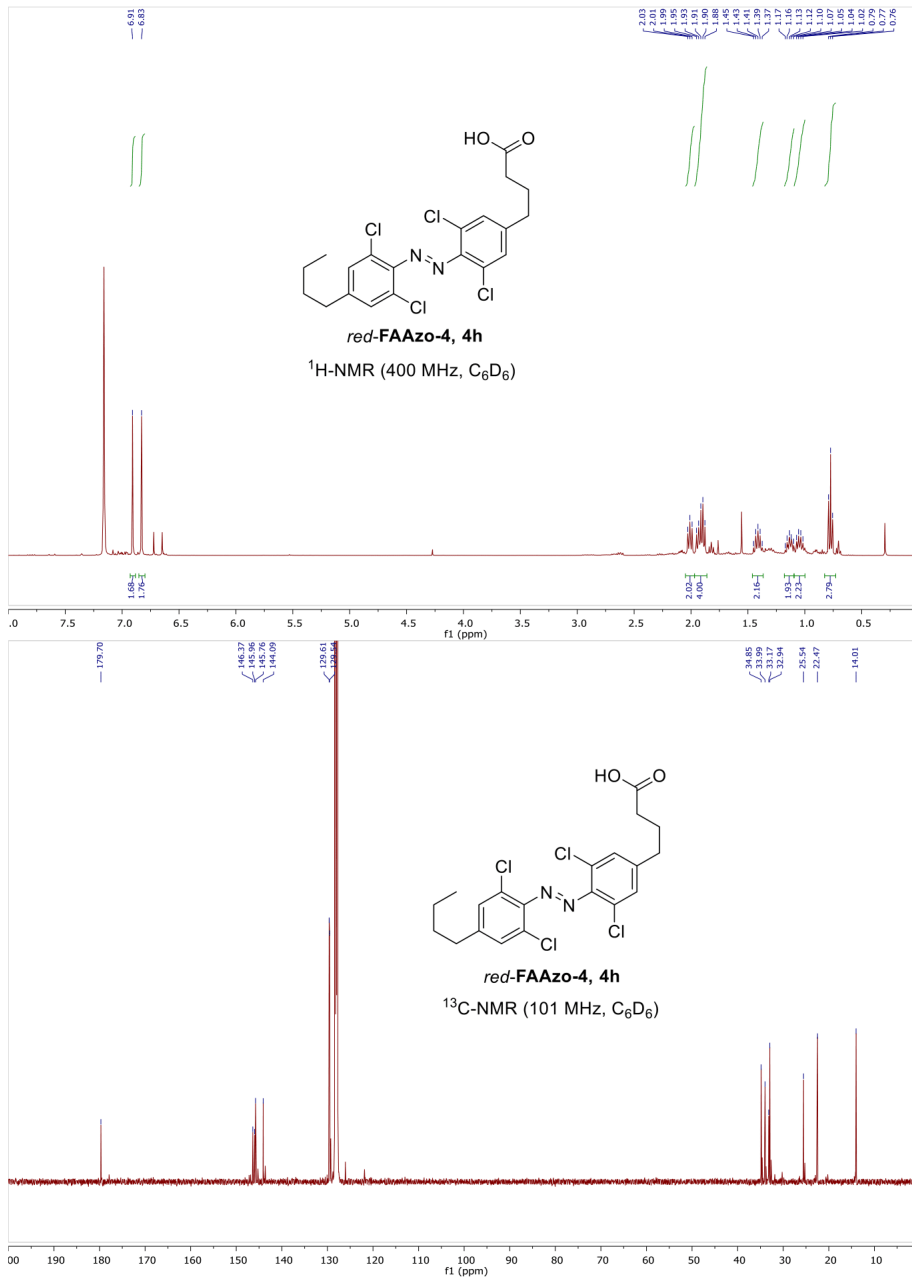


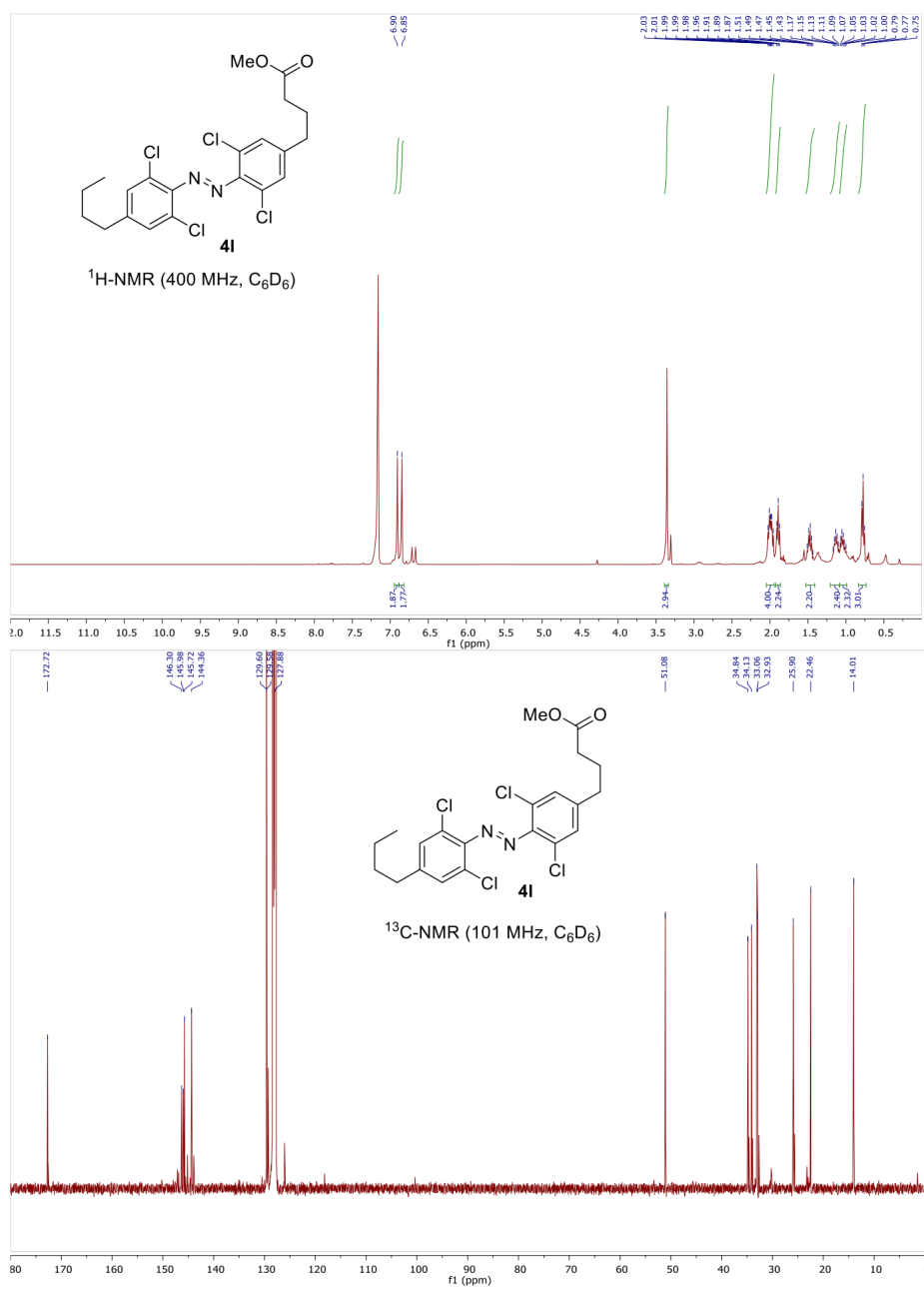


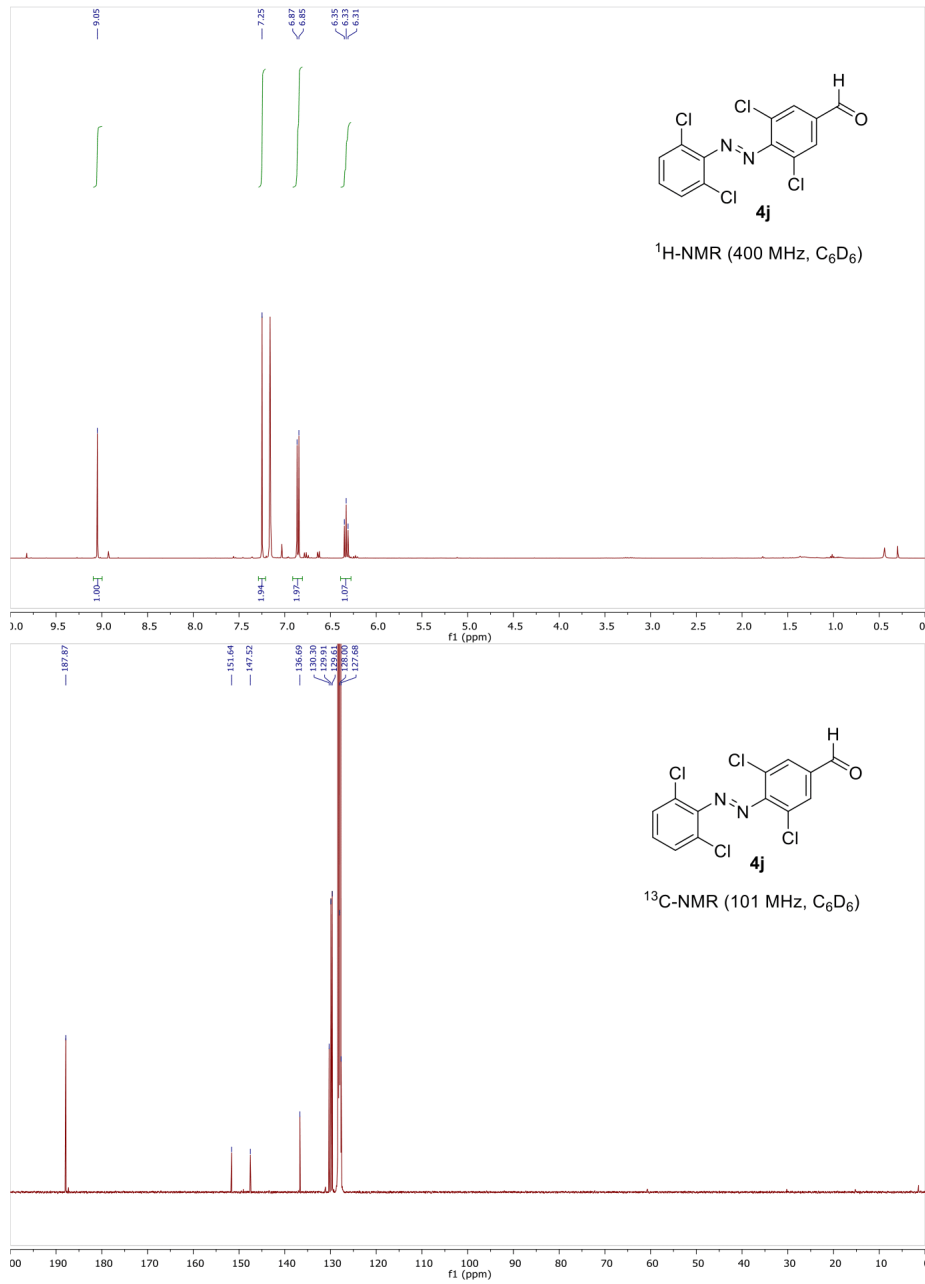


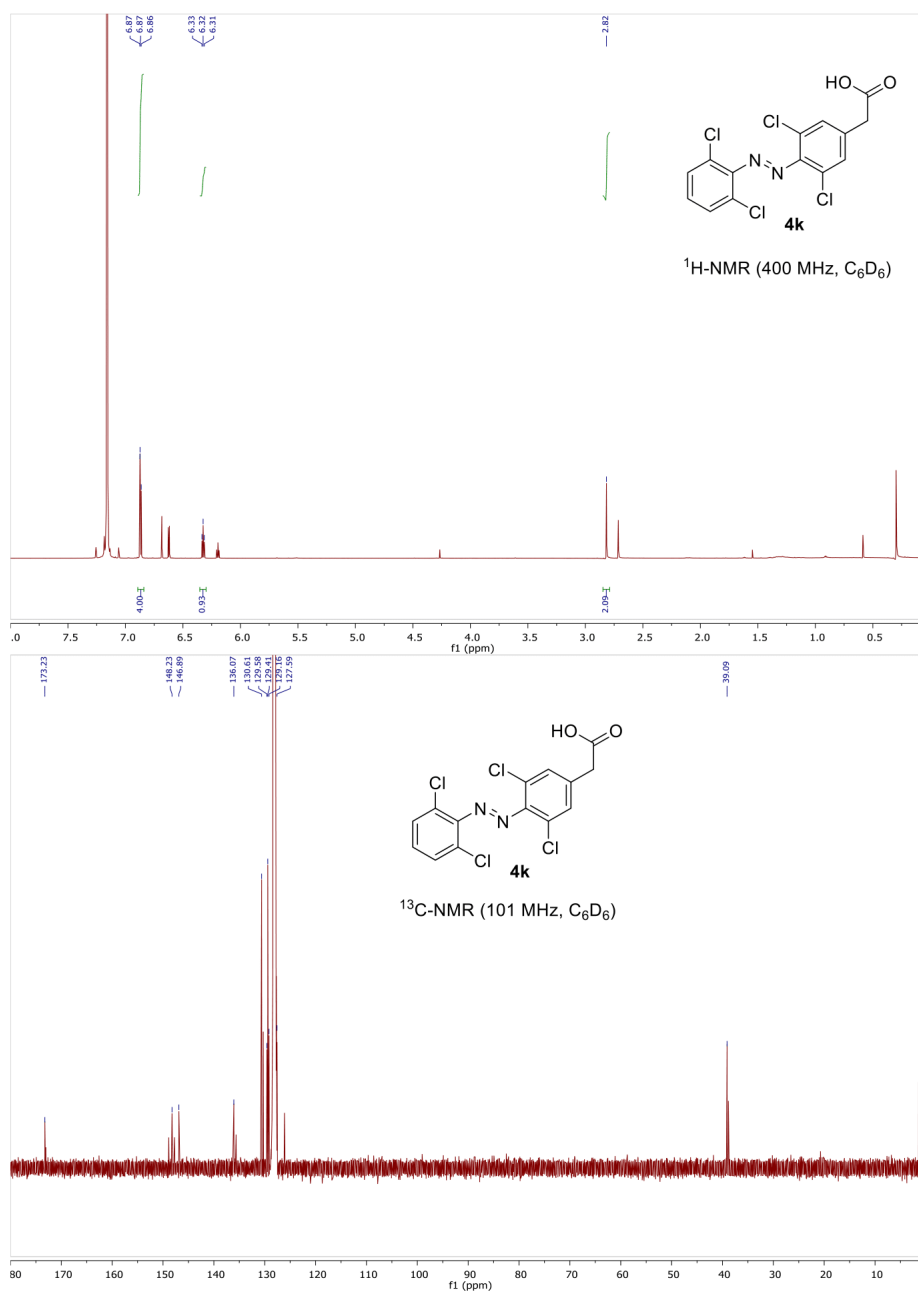


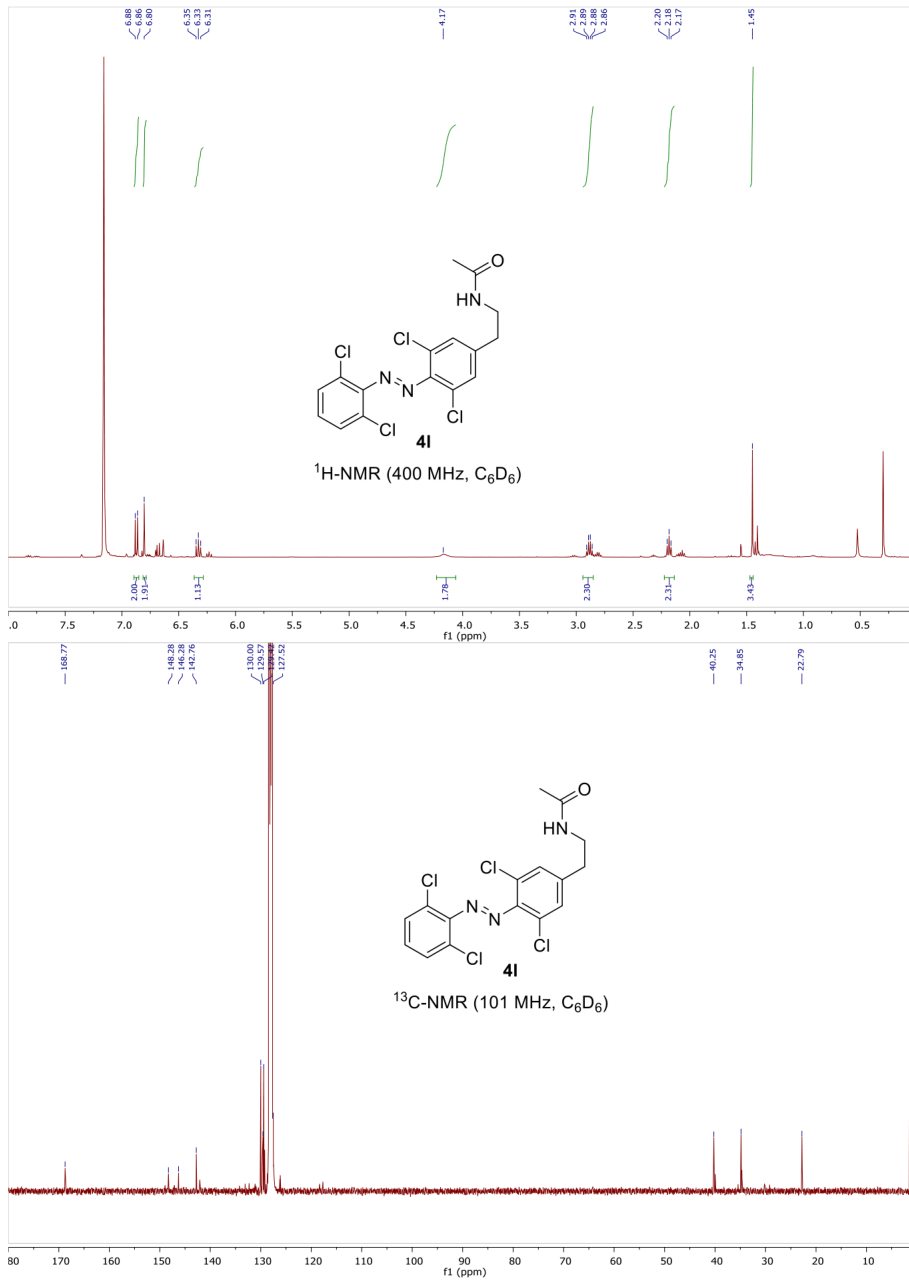


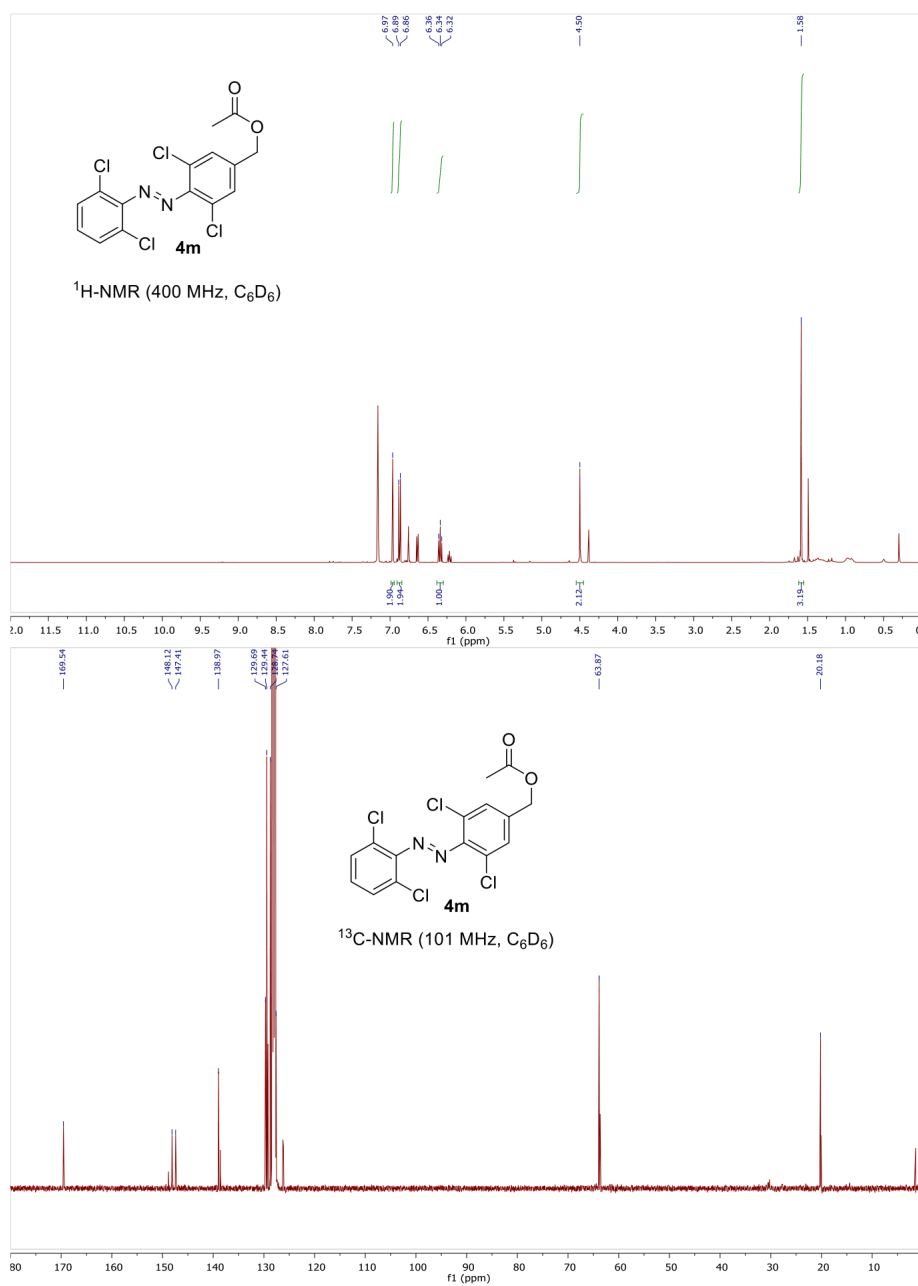


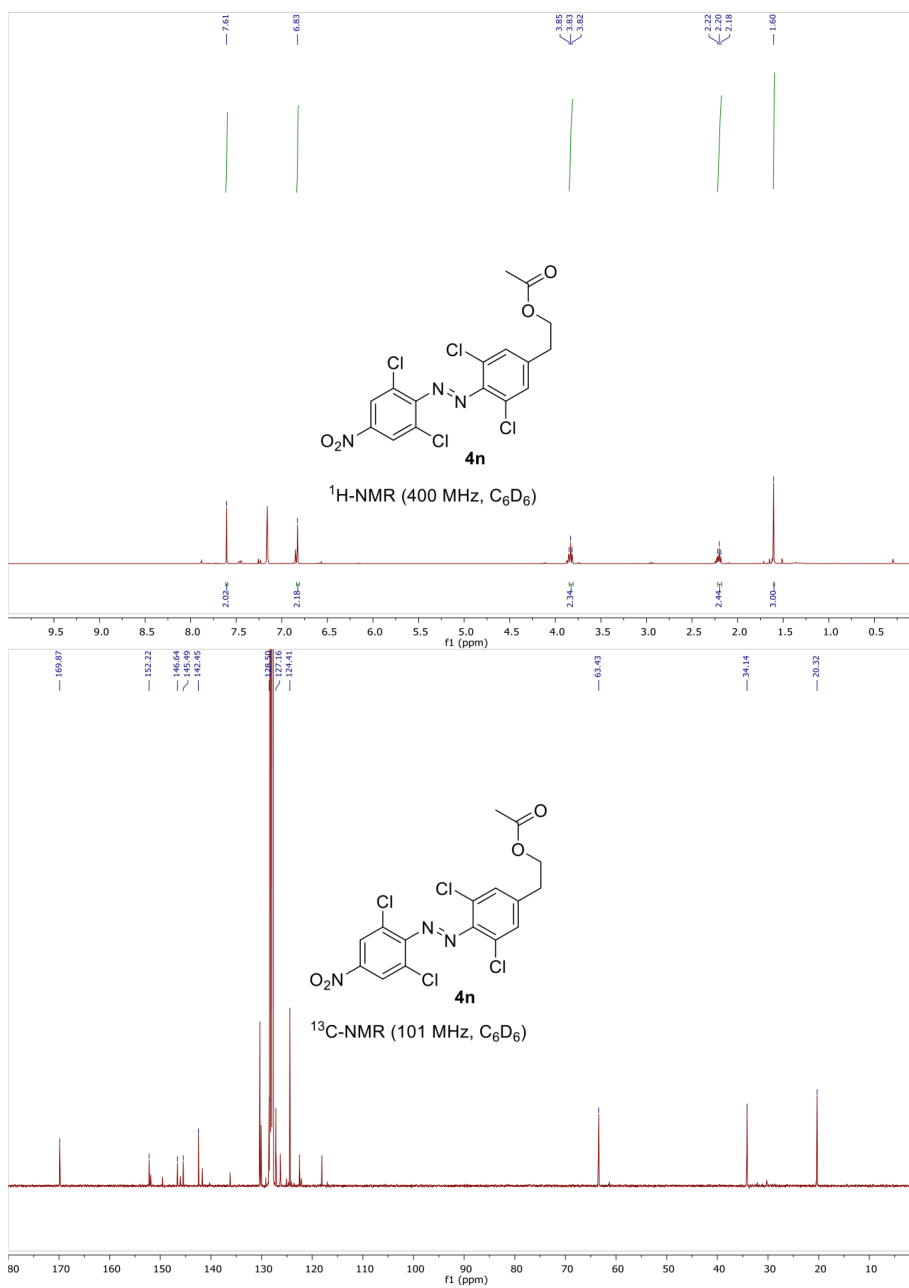


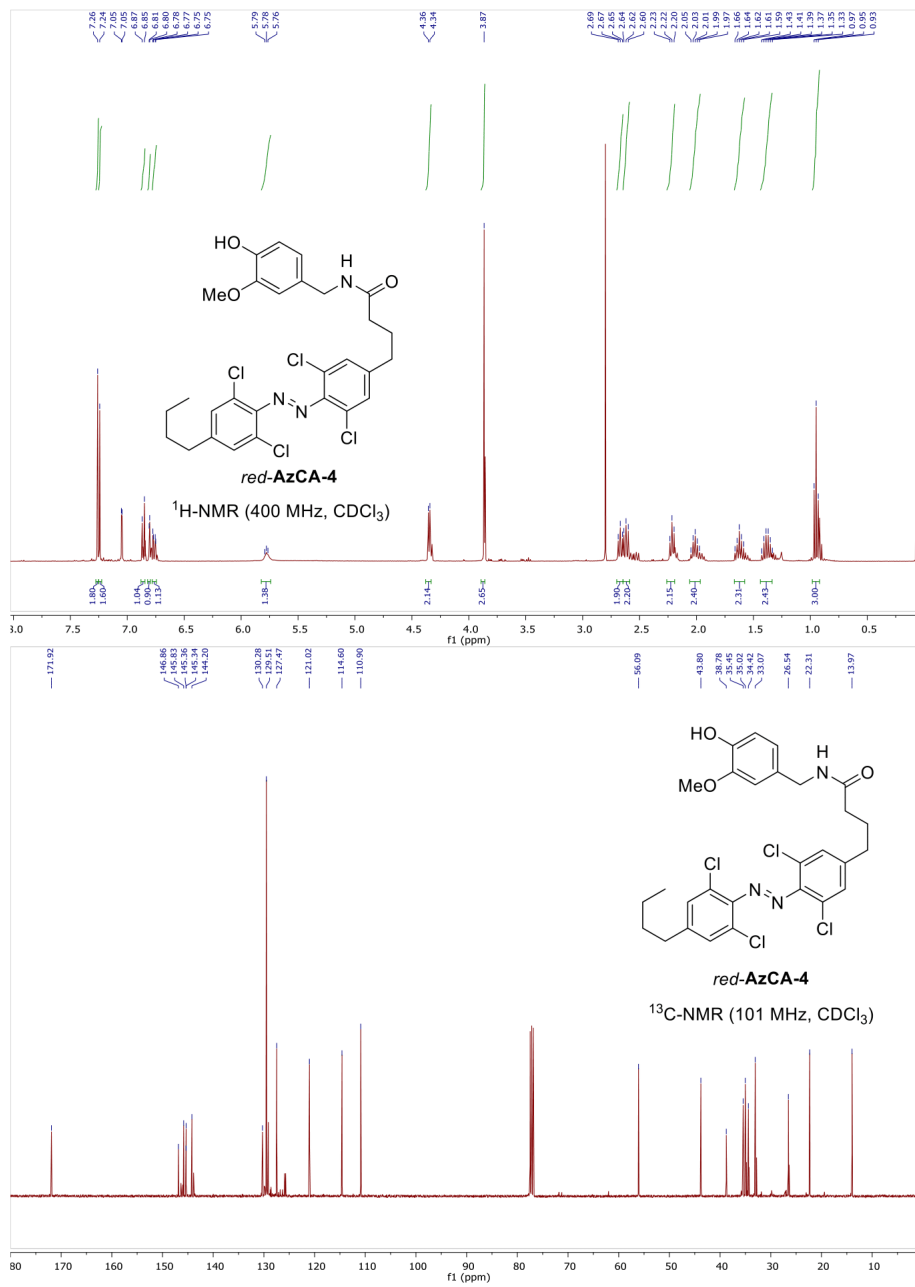




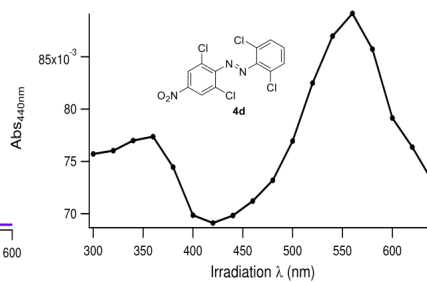
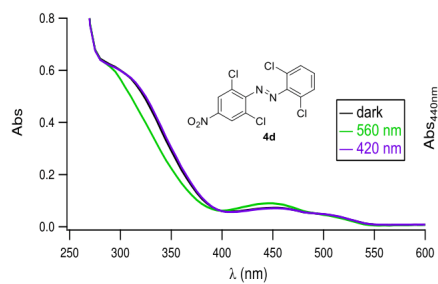
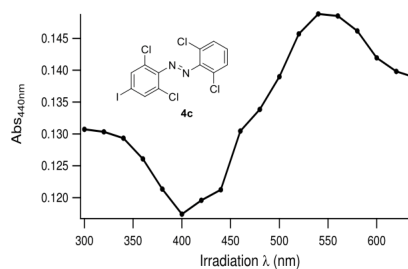
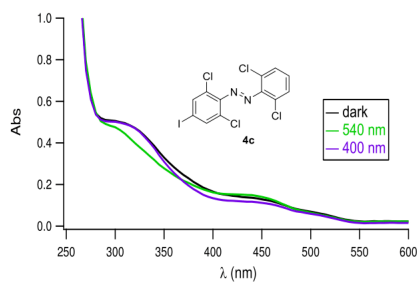
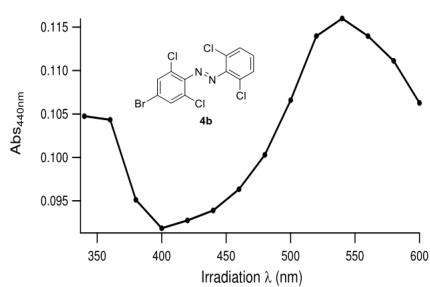
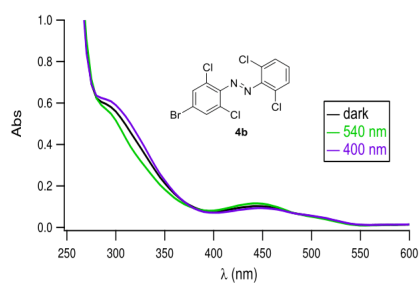
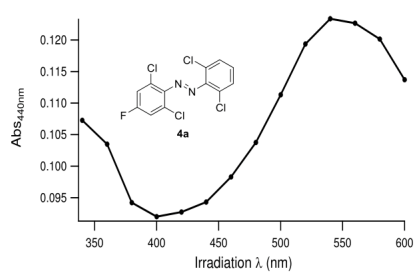
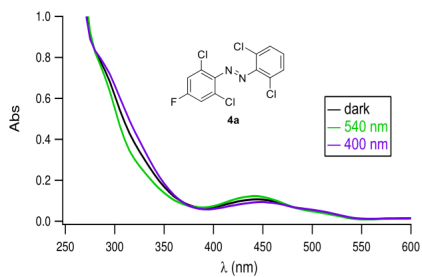


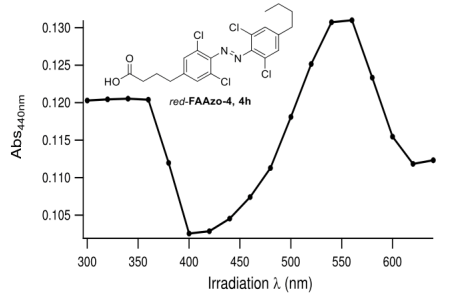
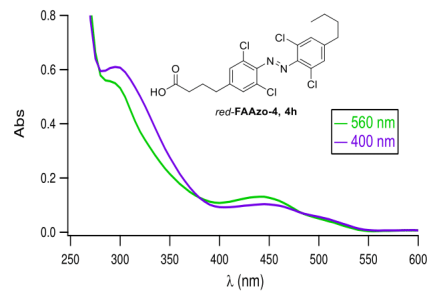
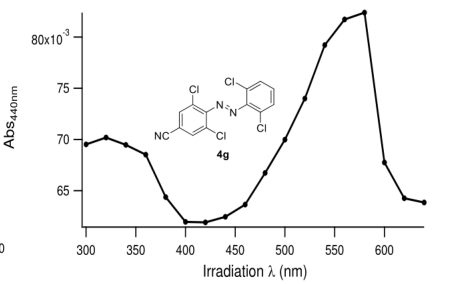
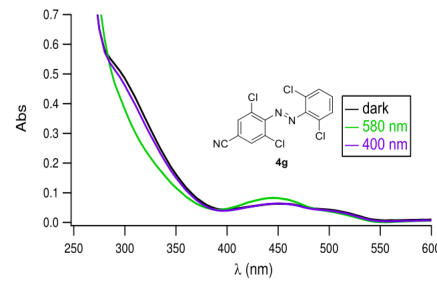
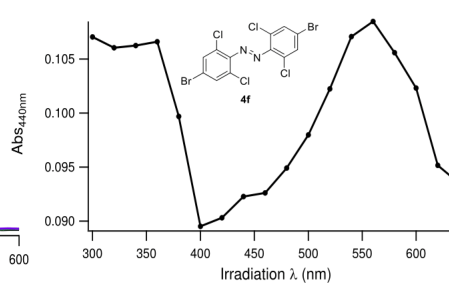
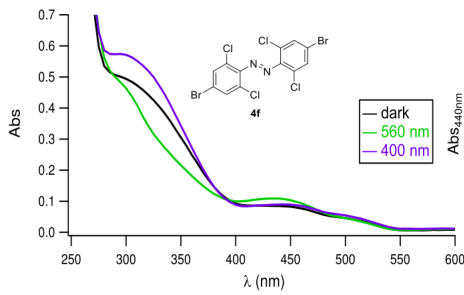
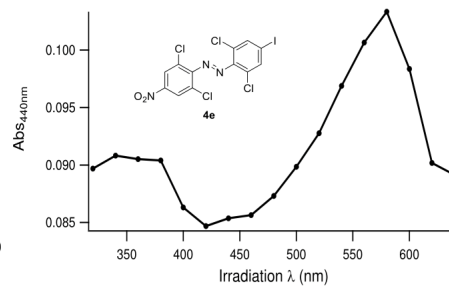
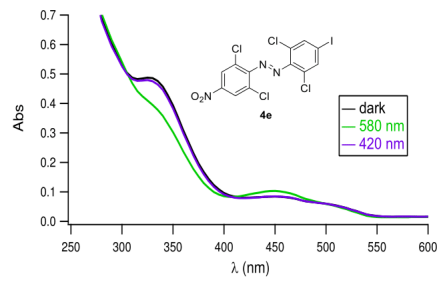


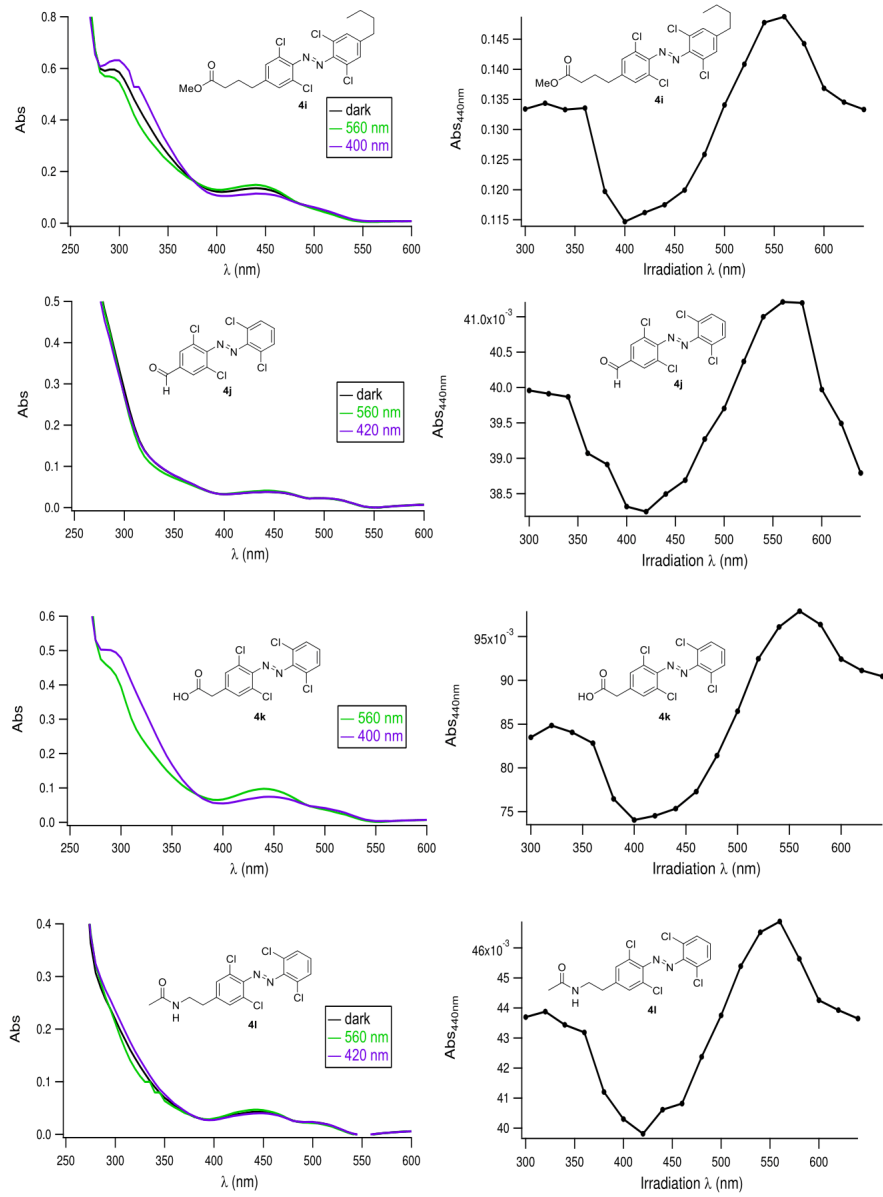


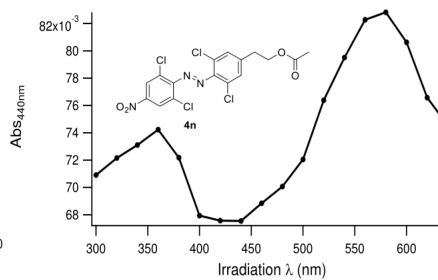
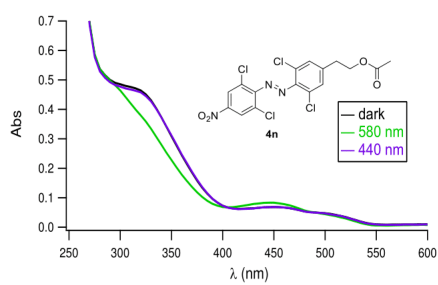
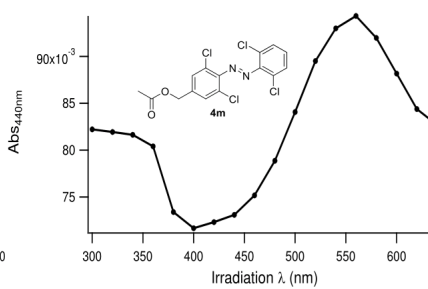
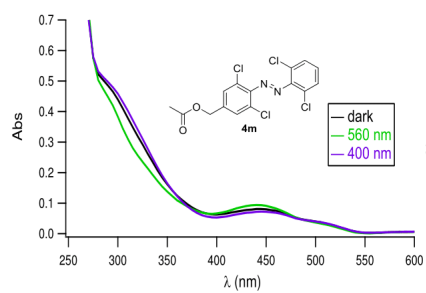


4. UV-Vis Spectra

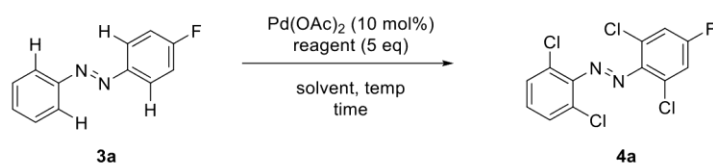








5. Optimization Table



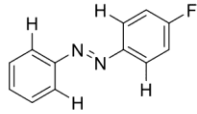
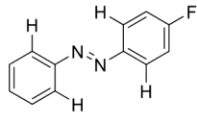
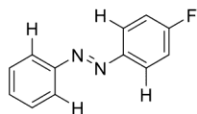
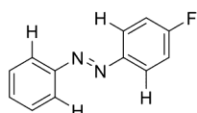
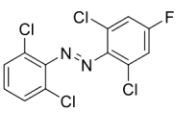
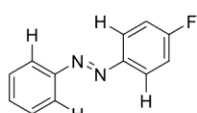
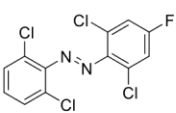
Entry	Precursor	Temp	Electrophile	Solvent	Time	Result
1	 3a	100 °C	NCS	MeCN	26 h	Reisolated starting material
2	 3a	120 °C	NCS	MeCN	22 h	Inseparable mixture of starting material and newly formed compounds
3	 3a	100 °C	NCS	AcOH	13 h	Inseparable mixture of starting material and newly formed compounds
4	 3a	120 °C	NCS	AcOH	13 h	 4a (57%)
5	 3a	140 °C	NCS	AcOH	15 h	 4a (58%)

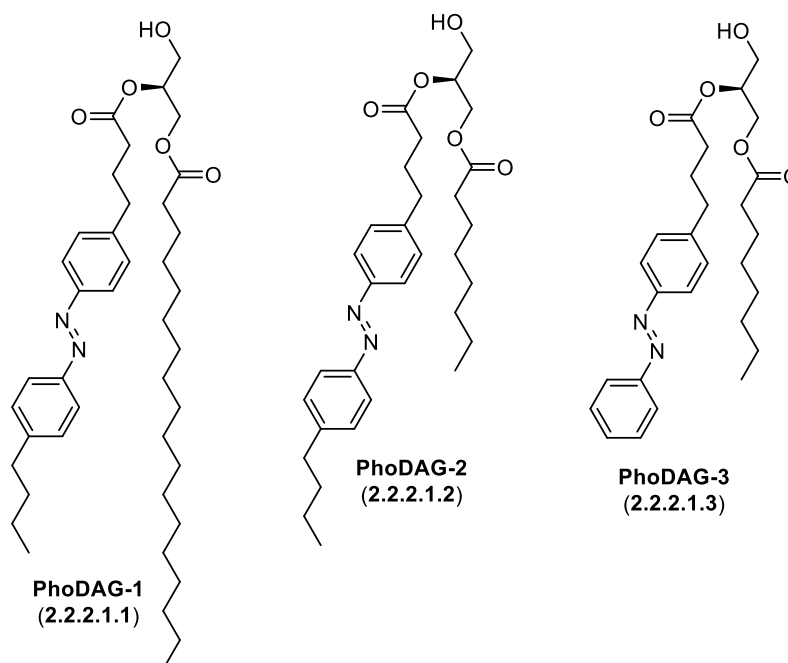
Table 1. Optimization of the tetra-*ortho*-chlorination reaction.

2.2.2 Red-shifting Lipid-based Photopharmaceuticals

We showed that the minimal changes to the structure and size of the lipid-based photopharmaceutical **AzCA-4** through tetra-*ortho*-chloro substitution (*red-AzCA-4*) did not hinder its biological function (Chapter 2.2.1). To demonstrate the generality of this concept and to enable the application of our chemical tools in animals and humans, we applied this method to a variety of pre-existing and new photochromic ligands.

2.2.2.1 Synthesis of *red*-PhoDAG1-3

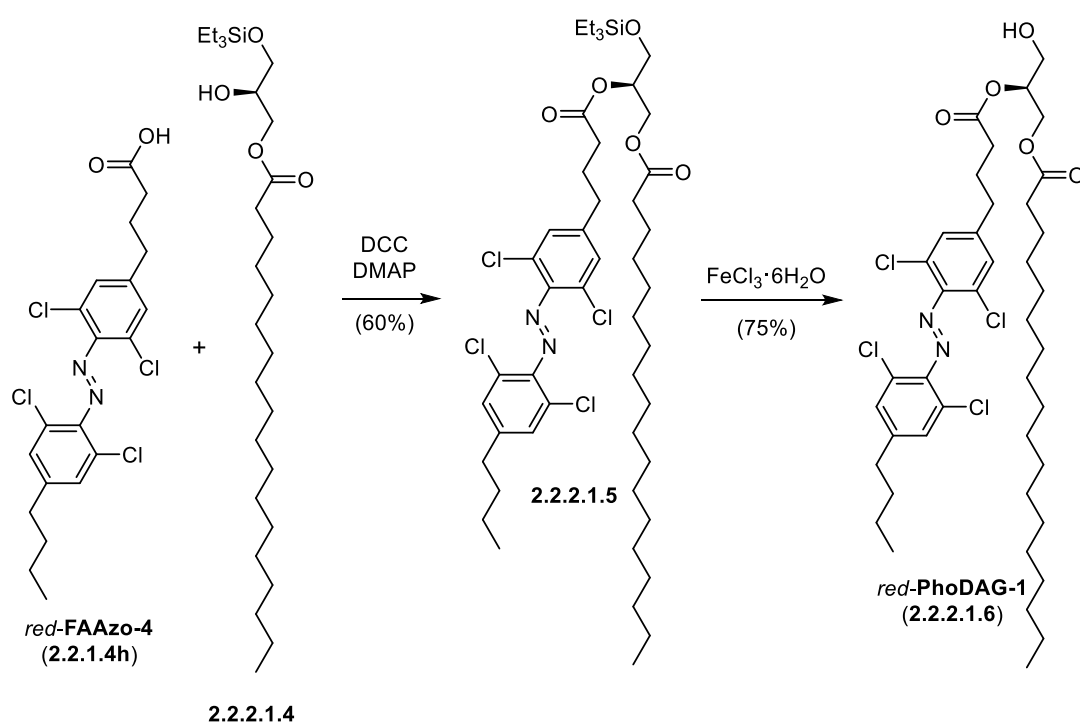
The photoswitchable diacylglycerol-mimics **PhoDAG-1** (2.2.2.1.1), **PhoDAG-2** (2.2.2.1.2) and **PhoDAG-3** (2.2.2.1.3) (Scheme 2.2.2.1.1) have enabled the optical control of protein kinase C as well as TRPC2 and TRPC6 channels.¹⁴⁴⁻¹⁴⁵ In order to prepare the corresponding red-shifted variants *red*-**PhoDAG-1** (2.2.2.1.6), *red*-**PhoDAG-2** (2.2.2.1.9) and *red*-**PhoDAG-3** (2.2.2.1.13), we planned to use the photoswitchable fatty acid building blocks *red*-**FAAzo-4** (2.2.1.4h, Chapter 2.2.1) and *red*-**FAAzo-9** (2.2.2.1.11, Scheme 2.2.2.4) and pursue the ester coupling – TES deprotection sequence that was reported for the synthesis of **PhoDAG-1-3**.¹⁴⁴



Scheme 2.2.2.1.1. Photoswitchable diacylglycerol-mimics.

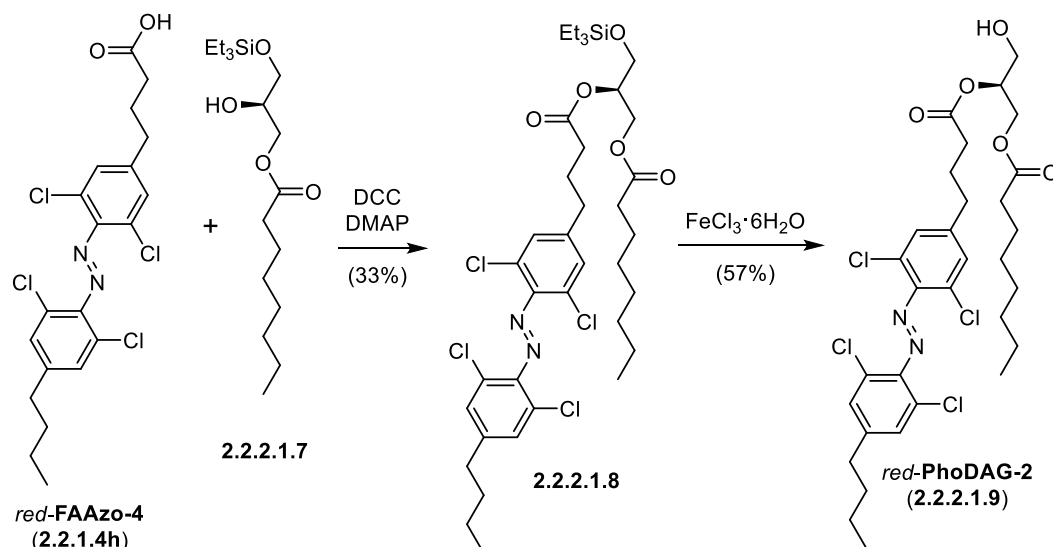
We found that application of the photoswitchable fatty acid *red*-**FAAzo-4** (2.2.1.4h, Chapter 2.2.1) in an EDC-mediated Steglich esterification led to a 1,2-acyl chain migrations to the free

alcohol (2.2.2.1.4) and therefore afforded two differently acylated versions of glycine 2.2.2.1.5. The two regioisomers could not be separated through chromatographic methods which necessitated the optimization of a new ester coupling protocol. We discovered that retaining DMAP as a catalyst and substituting EDC for DCC greatly benefited the reaction outcome. Cooling to 0 °C completely avoided the acyl chain migration and selectively afforded the diester 2.2.2.1.5 in 60% yield. For the TES deprotection using a FeCl₃ catalyst, the temperature also needed to be adjusted to 0 °C to avoid an acyl-chain migration and we reliably obtained *red-PhoDAG-1* (2.2.2.1.6) in good quantities and yields.

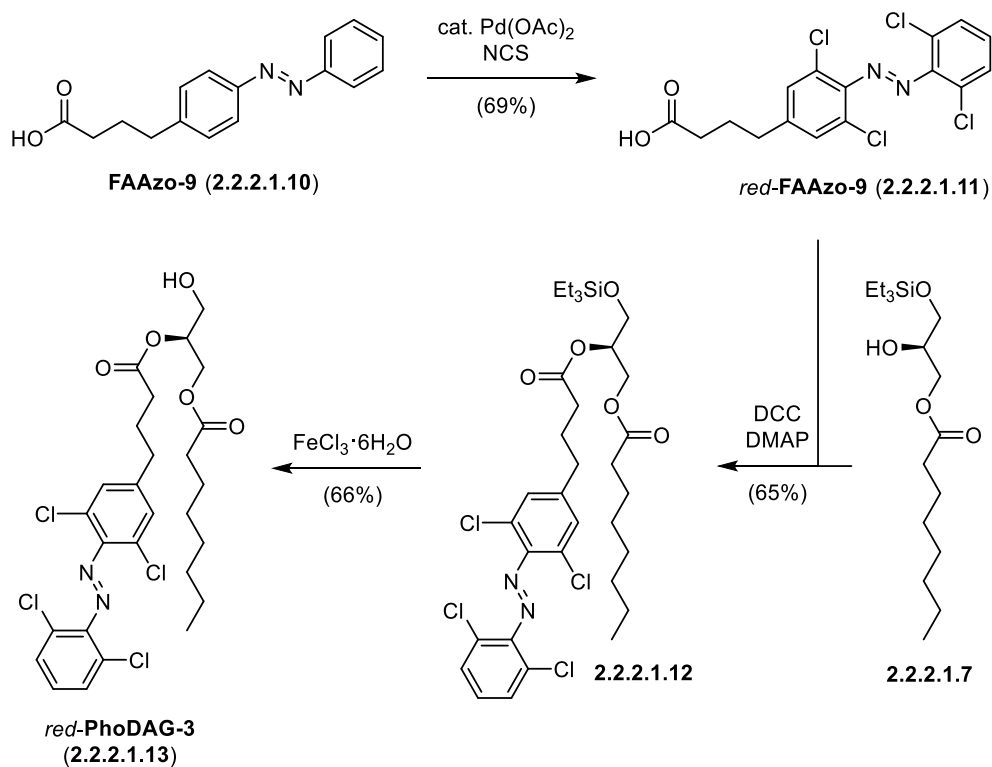


Scheme 2.2.2.1.2. Synthesis of *red-PhoDAG-1* (2.2.2.1.6).

The optimized conditions also allowed the synthesis of *red-PhoDAG-2* (2.2.2.1.9) (Scheme 2.2.2.1.3). Steglich esterification between *red-FAAzo-4* (2.2.1.4h) and alcohol 2.2.2.1.8¹⁴⁴ exclusively afforded the desired regioisomer of diester 2.2.2.1.8. Deprotection using FeCl₃·6H₂O at 0 °C gave the free alcohol 2.2.2.1.9.

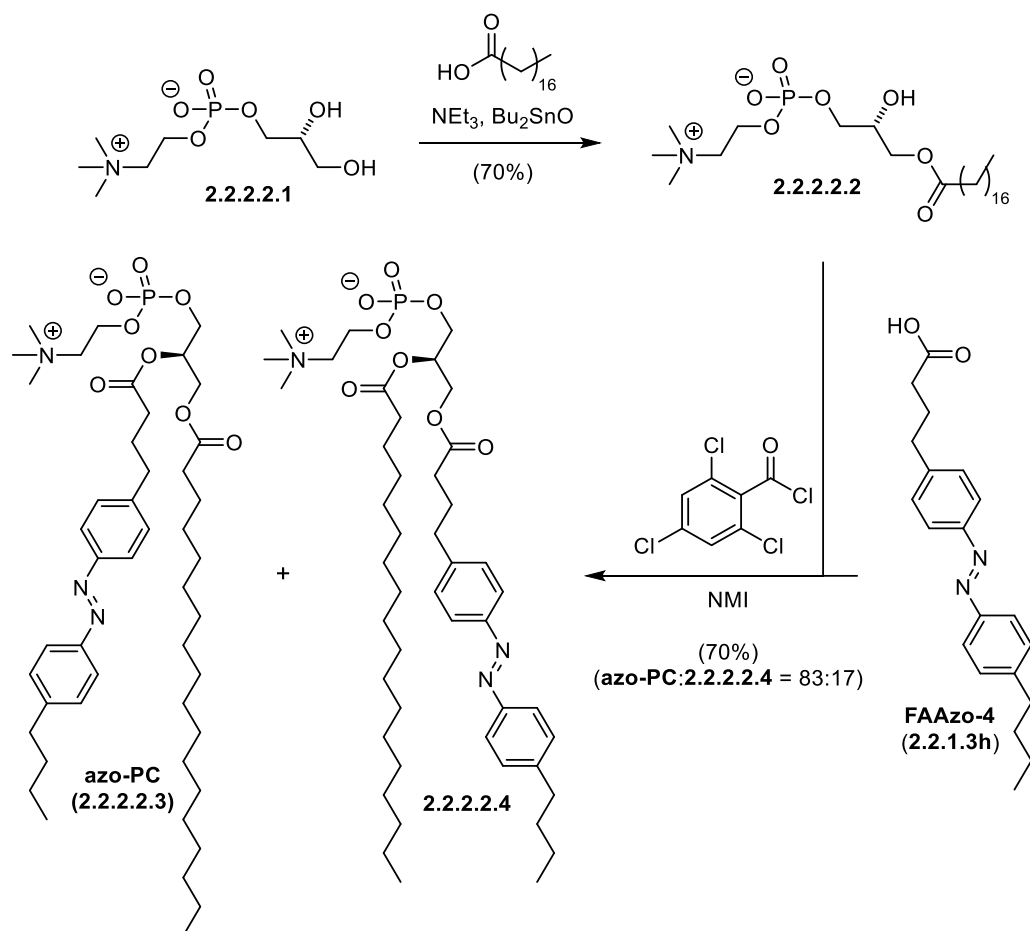
Scheme 2.2.2.1.3. Synthesis of *red-PhoDAG-2* (2.2.2.1.9).

For the synthesis of *red-PhoDAG-3* (2.2.2.1.13), we prepared *red-FAAzo-9* (2.2.2.1.11) in 69% yield by employing our newly developed C–H tetra-chlorination methodology to the known *FAAzo-9* (2.2.2.1.10).¹⁴⁴ Steglich esterification with this fatty acid building block (2.2.2.1.10) proceeded reliably and after deprotection gave *red-PhoDAG-3* (2.2.2.1.13) in good yields.

Scheme 2.2.2.1.4. Synthesis of *red-PhoDAG-3* (2.2.2.1.13).

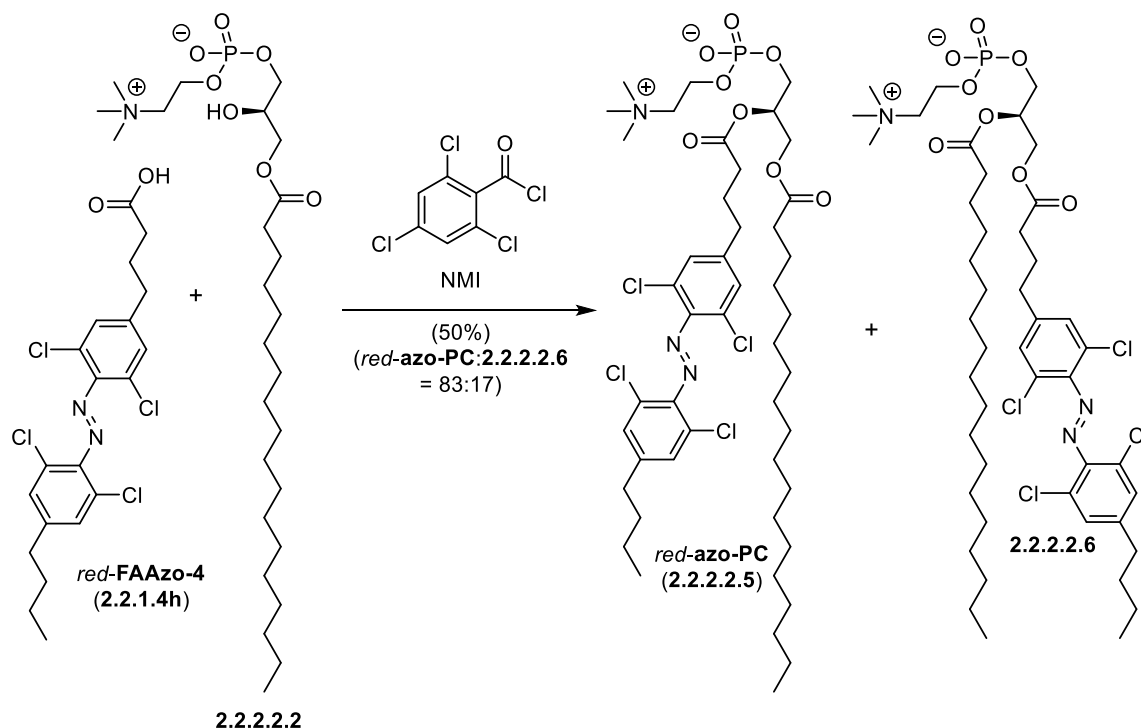
2.2.2.2 Establishing a New Route to azo-PC and *red*-azo-PC

For optically controlling the mechanical properties of lipid vesicles, a photoswitchable phosphatidylcholine (**azo-PC**, **2.2.2.2.3**) was developed by incorporating an azobenzene moiety into the fatty acid substructure.¹⁴⁶ It was found that **azo-PC** (**2.2.2.2.3**)-containing cell-sized lipid vesicles could be stimulated with UV-A and blue light to effect vesicle shape changes. These shape changes included budding transitions, invagination, pearling and the formation of membrane tubes and were controlled by precise applications of light pulses. The synthesis of **azo-PC** (**2.2.2.2.3**) relied on a 4 step procedure from **PhoDAG-1** (**2.2.2.1.1**) which amounts to 8 total steps from commercial starting materials. To allow for a faster access to **azo-PC** (**2.2.2.2.3**) and to prepare its red-shifted variant *red*-**azo-PC** (**2.2.2.2.5**), we devised a new synthetic route. Our approach was planned to utilize two sequential selective mono-acylations of diol **2.2.2.2.1** (Scheme 2.2.2.2.1) to enable the preparation of our target molecules in a 2-step sequence. We optimized a literature procedure for the dibutyltin oxide-mediated selective primary alcohol acylation of 1,2-diols and afforded **2.2.2.2.2** in 70% yield with stearoyl chloride as acylating agent.¹⁴⁷ All evaluated conditions for the esterification reaction of secondary alcohol **2.2.2.2.2** with **FAAzo-4** (**2.2.1.3h**) suffered from acyl chain migrations which led to the formation of **azo-PC** (**2.2.2.2.3**) and its regioisomer **2.2.2.2.4**. Extensive optimization studies revealed that employing a Yamaguchi esterification protocol afforded the highest yields and an acceptable 83:17 regioisomeric mixture. The regioisomers **azo-PC** (**2.2.2.2.3**) and **2.2.2.2.4** could be separated by using flash column chromatography.



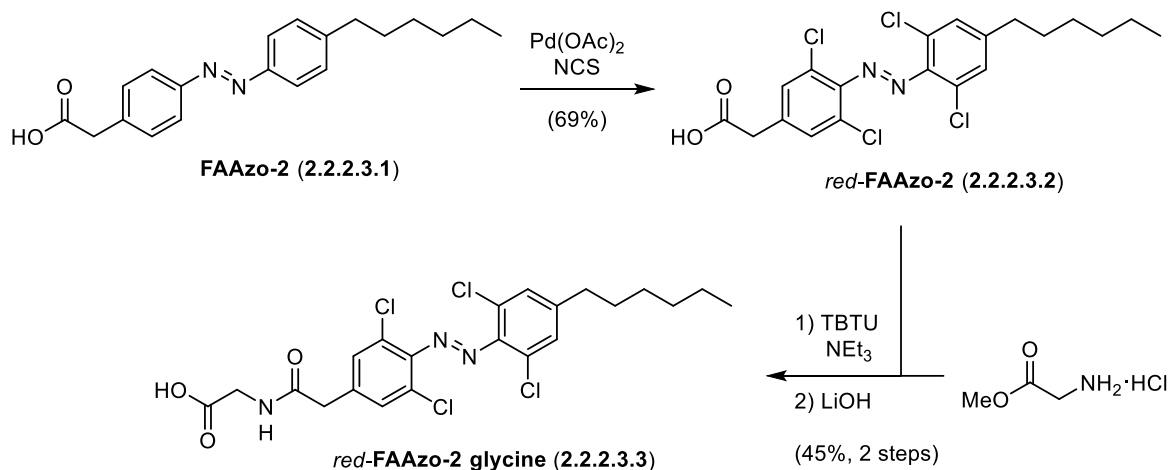
Scheme 2.2.2.1. Optimized 2-step sequence to **azo-PC** (2.2.2.2.3).

We were able to synthesize *red-azo-PC* (2.2.2.2.5) by substituting **FAAzo-4** (2.2.1.3h) for *red-FAAzo-4* (2.2.1.4h) in the Yamaguchi esterification. In accordance with the preparation of **azo-PC** (2.2.2.2.3), this reaction afforded a regioisomeric mixture of 83:17 which was separated by flash column chromatography.

Scheme 2.2.2.2. Synthesis of *red*-azo-PC.

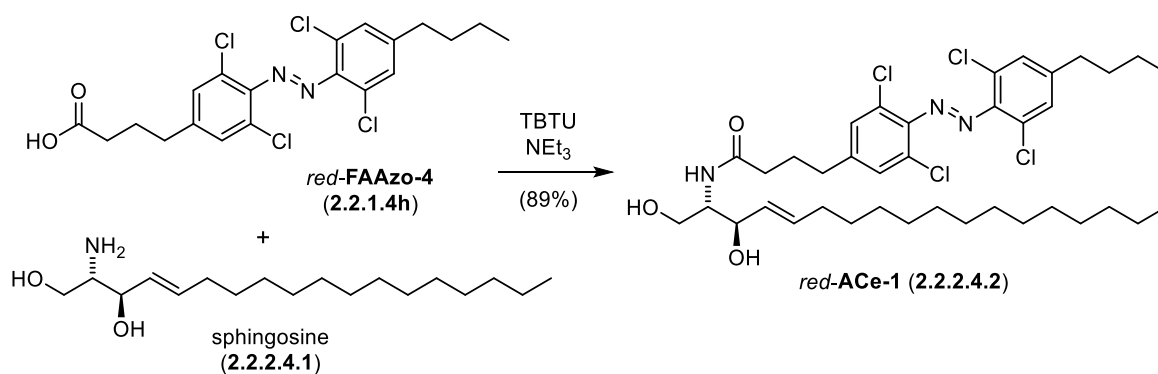
2.2.2.3 Synthesis of *red*-FAAzo-2-glycine

To study lipid functions in the context of the cell membrane, we aimed to establish a diverse library of membrane lipid-based photopharmaceuticals. In this context, the availability of lipids with red-shifted absorption spectra in addition to standard azobenzene-containing variants allows us to use two photochromic ligands in a single system and selectively photoswitch one compound by exploiting their different bathochromic properties. We are planning to combine photoswitchable fatty acids (FAAzos) with varying lengths and azobenzene positions (see *red*-FAAzo-4 (2.2.1.4h) and 2.2.1.4k in chapter 2.1.1 as well as *red*-FAAzo-9 (2.2.2.1.11) in chapter 2.2.2.1) with a number of different head groups to further diversify our library. Therefore, *red*-FAAzo-2 (2.2.2.3.2) was prepared using our tetra-chlorination methodology (Scheme 2.2.2.3.1). This new red-shifted fatty acid derivative (2.2.2.3.2) was coupled with methyl glycine and directly demethylated with LiOH to give the photoswitchable lipid *red*-FAAzo-2-glycine (2.2.2.3.3).



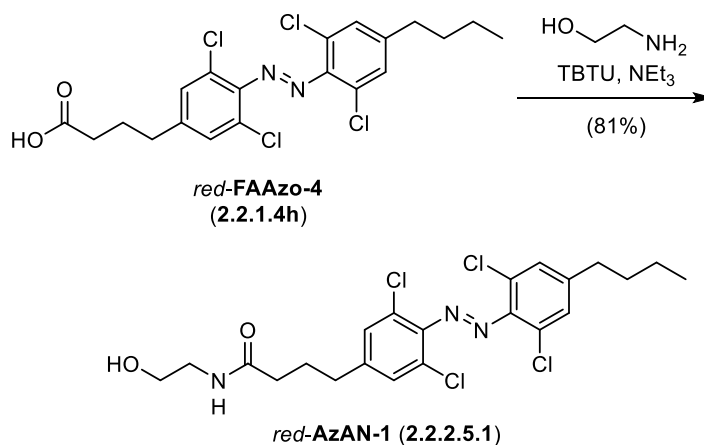
2.2.2.4 Synthesis of red-ACe-1

Previous studies have shown that **ACe-1** has allowed the switching of lipid domains in raft-mimicking supported bilayers.¹⁴⁸ Photoswitching with UV-A light triggered a fluidification of the liquid-ordered phase by formation of liquid-disordered domains in the raft whereas isomerization with blue light effected rigidification in the liquid-disordered phase by formation of liquid-ordered domains. To implement a bathochromic shift and enhance the optical properties by establishing slow-relaxing photostationary states,¹⁴⁹⁻¹⁵⁰ we synthesized the tetra-*ortho*-chloro derivative of **ACe-1**, namely *red-ACe-1* (2.2.2.4.2). This was achieved by an amide coupling reaction between *red-FAAzo-4* (2.2.1.4h) and sphingosine (2.2.2.4.1) which gave the product 2.2.2.4.2 (*red-ACe-1*) in excellent yields.



2.2.2.5 Synthesis of red-AzAN-1

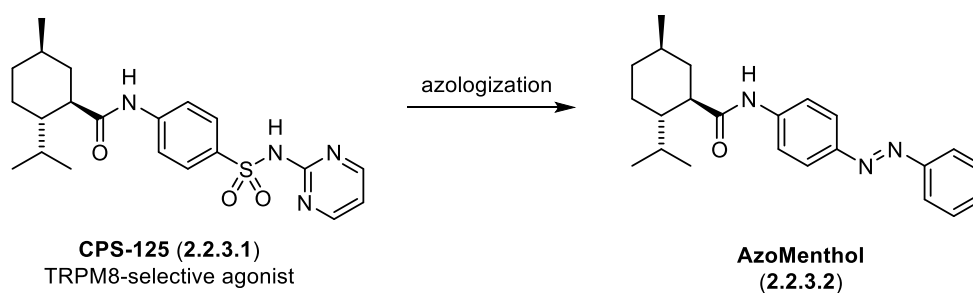
In addition to its potential use as a photoswitchable membrane lipid, the optically controlled anandamide derivative *red-AzAN-1* could enable the control over the endocannabinoid system with light. This hypothesis is based on the fact that the non-photoswitchable parent lipid anandamide is known to act as a CB₁, CB₂ and TRPV1 agonist.¹⁵¹ Our synthesis of *red-AzAN-1* (**2.2.2.5.1**) proceeded by amide coupling of *red-FAAzo-4* (**2.2.1.4h**) with ethanolamine in good yields (Scheme 2.2.2.5.1).



Scheme 2.2.2.5.1. Synthesis of *red-AzAN-1* (**2.2.2.5.1**).

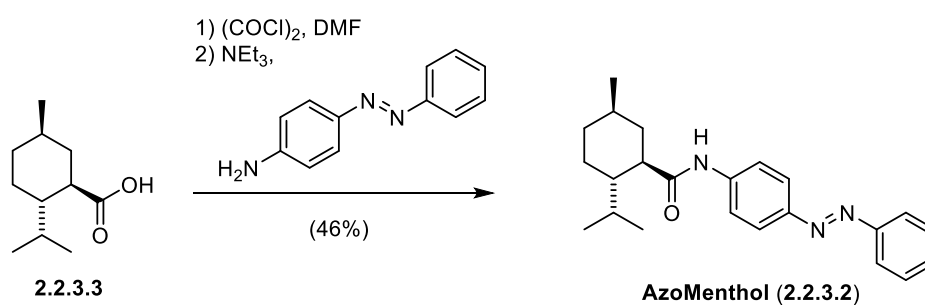
2.2.3 The Designing of a Photoswitchable TRPM8 Agonist

The in-depth study of thermoregulation in animal models requires the availability of biochemical tools that allow for a precise control over key channels such as TRPA1, TRPM8 and TRPV1.¹⁵² We laid the foundation for this research program with the optical control of the heat sensing TRPV1 channel using the photopharmaceuticals **AzCA-4** and *red-AzCA-4* (Chapter 2.2.1).¹⁵³ Our attempts towards the optical control of the cold sensing TRPM8 channel focus on the azologization¹⁴⁰ of CPS-125 (**2.2.3.1**) (Scheme 2.2.3.1) to **AzoMenthol** (**2.2.3.2**). CPS-125 (**2.2.3.1**) is a selective agonist for the TRPM8 channel ($ED_{50} = 32 \pm 6 \mu\text{M}$) and was developed through SAR studies on (-)-menthol ($ED_{50} = 196 \pm 22 \mu\text{M}$). Our azologization strategy is based on the hypothesis that the biaryl sulfonylamide serves as an azoster and could therefore be substituted for an azobenzene moiety without significant loss of bioactivity.



Scheme 2.2.3.1. Azologization of CPS-125 (2.2.3.1).

To synthesize **AzoMenthol (2.2.3.2)**, menthol carboxylic acid (2.2.3.3) was prepared through a literature procedure.¹⁵⁴⁻¹⁵⁵ As part of this 2-step sequence, (-)-menthol was subjected to Lucas reagent to effect an oxygen-chlorine exchange¹⁵⁴ which was followed by magnesium insertion to give the corresponding Grignard reagent¹⁵⁵ and substitution with CO₂. The carboxylic acid 2.2.3.3 was converted to the carboxylic acid chloride with oxalyl chloride and 4-aminoazobenzene was added to give **AzoMenthol (2.2.3.2)**.



Scheme 2.2.3.2. Synthesis of AzoMenthol.

3 Experimental section

3.1 Material and Methods

3.1.1 Equipment and Instruments

Nuclear magnetic resonance (NMR) spectroscopy:

NMR-spectra were acquired with the following spectrometers: Varian INOVA 400 (400 MHz for ^1H and 101 MHz for ^{13}C spectroscopy), Bruker Avance III HD 400 with Cryo-head (400 MHz for ^1H and 101 MHz for ^{13}C spectroscopy), Varian VNMRS 600 (600 MHz for ^1H , 150 MHz for ^{13}C spectroscopy) and Bruker Avance III HD 800 with Cryo-head (800 MHz for ^1H , 201 MHz for ^{13}C spectroscopy). Chemical shifts (δ) are reported in parts per million (ppm) relative to tetramethylsilane (TMS). The deuterated solvents CDCl_3 , $(\text{CD}_3)_2\text{SO}$, $(\text{CD}_3)_2\text{CO}$ MeOD, C_6D_6 and D_2O were used as internal references. Spin multiplicities are described as follows: s (singlet), d (doublet), t (triplet), q (quartet), quint (quintet), six (sxtet), h (heptet), m (multiplet), br (broad) or a combination thereof. Structural analysis was conducted with ^1H - and ^{13}C -NMR spectra with the aid of additional 2D spectra (COSY, HMBC, HSQC, NOESY). Spectra analysis was conducted with the software MestReNova v.10.0.1-14719. The ^{19}F -NMR and ^{31}P -NMR spectra were referenced using the ^1H -NMR spectra of the same compounds as an absolute reference. The atom numbering of the signal assignment does not correspond to IUPAC rules.

Mass spectrometry (MS):

The high resolution MS spectra were recorded either on Thermo Finnigan MAT 95 (EI: electron ionization) or Thermo Finnigan LTQ FT (ESI: electrospray ionization).

Infrared spectroscopy (IR):

IR spectra were recorded on a *PerkinElmer* Spectrum BX II FT-IR device equipped with an attenuated total reflection (ATR) measuring unit. For measurements, the neat substances were directly applied as a thin film on the ATR unit. The measured wavenumbers are reported with their relative intensities which were classified as: vs (very strong), s (strong), m (medium), w (weak), vw (very weak), br (broad) or combinations thereof.

Optical rotation ($[\alpha]_D^T$):

Optical rotation values were measured on an Anton Paar MCP 200 polarimeter. The specific rotation ($[\alpha]_D^T$) values are reported in $\text{deg}\cdot\text{dm}^{-1}\cdot\text{mL}\cdot\text{g}^{-1}$ and calculated by the formula:

$$[\alpha]_D^T = \frac{\alpha \cdot 100}{l \cdot c}$$

T represents the ambient temperature (°C), D represents wavelength (in all cases, D is the sodium line: 589 nm), l represents the length of the cuvette (dm), c represents the concentration of the solution (g/100 mL). α represents the measured rotation in degrees. The appropriate solvent and concentrations are reported in brackets.

High Performance Liquid Chromatography (HPLC):

A Varian Prep Star HPLC System Model SD-1 was used equipped with Varian Dynamax reverse phase columns (semi-preparative: Microsorb 60 C18, 250 x 21.4 mm, particle size 8 μ m; preparative: Microsorb 60 C18, 250 x 41.4 mm, particle size 8 μ m). Prior to injection, samples were filtered through a syringe filter (Chromafil® Xtra GF100/25, pore size 1 μ m).

Melting point (m_p):

Melting points were determined on a B-450 melting point apparatus from BÜCHI Labortechnik AG. The value are uncorrected.

UV-VIS spectroscopy (UV-Vis):

UV-VIS spectra were recorded on a Varian 50 Scan UV-Visible Spectrophotometer. Illumination was provided by a TILL Photonics Polychrome 5000 monochromator. The experiments were conducted using a 50 μ M solution of the compound in DMSO or PBS buffer and the spectra were recorded after irradiation of the sample with the specified wavelength for 3 min. For tetra-*ortho*-chloro azobenzene derivatives, the spectra were recorded after irradiation of the sample with the specified wavelength for 10 min.

3.1.2 Methods

Unless otherwise noted, all reactions were magnetically stirred under inert gas (N₂) atmosphere using standard Schlenk techniques. Glassware was evacuated and dried by heating with a heat-gun (set to 550 °C). Drying over Na₂SO₄ implies stirring with an appropriate amount of anhydrous salt for several minutes followed by filtration through a glass frit and rinsing of the filter cake with additional solvent. Electric heating plates and oil baths were used for reactions at elevated temperature. For reactions below room temperature, the reaction vessel was cooled using a mixture of ice and water (0 °C), acetone and dry ice (-78 °C) or an slurry of acetone and liquid N₂ (-94 °C). Stated reaction temperatures refer to the external bath temperature.

Cannulas and syringes were used for transfer of reagents or solvents which were flooded with inert gas (3×) before use. Purification by column chromatography was performed under elevated pressure (flash column chromatography) on Geduran® Si60 silica gel (40-63 μm) from Merck KGaA. After flash column chromatography, the concentrated fractions were filtered once through a glass frit. Silica gel F₂₅₄ TLC plates from Merck KGaA were used for monitoring reactions, analyzing fractions of column chromatography and measuring R_f values. To visualize the analytes, TLC plates were irradiated with UV light or appropriate staining solutions and subsequent heating. Drying via lyophilization or freeze-drying refers to freezing of the respective sample in liquid nitrogen followed by evacuating the containing flask with high vacuum (< 1 mbar) and slow thawing to rt. Reaction yields refer to spectroscopically pure isolated amounts of compounds.

3.1.3 Chemicals

All chemicals were purchased from *Sigma Aldrich*, *Fisher Scientific*, *TCI Europe*, *Chempur*, *Alfa Aesar* or *Acros Organics*. Solvents purchased in technical grade quality and were distilled under reduced pressure and used for purification procedures. Purchased solvents in HPLC- and analytical-grade quality were used without further purification. The expression “hexanes” refers to a mixture of hexane isomers with a boiling point between 40-80 °C. Oxone® is a mixture of three salts with the chemical formula: 2KHSO₅·KHSO₄·K₂SO₄. Unless otherwise noted, reactions were performed using dry solvents. Dichloromethane (CH₂Cl₂), triethylamine (NEt₃) and diisopropylethylamine (*i*-Pr₂NEt) were dried by distillation from CaH₂. Tetrahydrofuran (THF) and diethyl ether (Et₂O) were dried by distillation from sodium and benzophenone. Other dry solvents were purchased from commercial sources (*Acros Organics*, *Fisher Scientific*) under inert gas atmosphere and over molecular sieves. All other reagents with a purity of >95% were purchased from commercial sources and used without further purification. For running extra dry reactions with synthetic compounds, stock solutions were prepared in PhMe, the respective amounts transferred into dried glassware and the solvent was removed by stirring under high vacuum (<1 mbar). This procedure was followed by freeze-drying the compound to ensure that H₂O was azeotropically removed. Phosphate buffer pH7 (PB pH7) refers to 19.75 g Na₂HPO₄·2H₂O and 9.36 g KH₂PO₄ which were diluted to 1.0 L with H₂O.

Staining solutions were prepared:

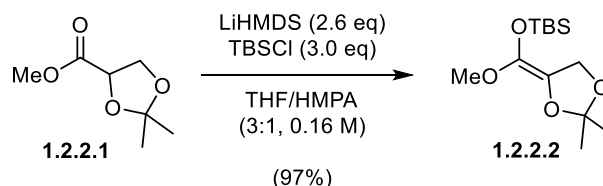
KMnO₄-Stain: KMnO₄ (3.0 g) and K₂CO₃ (20 g) were dissolved in H₂O (300 mL) and aq. NaOH (5%, 5.0 mL) was added.

CAM-Stain: (Ce(NH₄)₂(NO₃)₆ (0.5 g) and (NH₄)₆Mo₇O₂₄ 4H₂O (48 g) were dissolved in H₂O (940 mL) and H₂SO₄ (conc., 60 mL) was added.

3.2 Experimental Procedures

3.2.1 Experimental Procedures – Chapter 1

tert-butyl((2,2-dimethyl-1,3-dioxolan-4-ylidene)(methoxymethoxy)dimethylsilane (1.2.2.2)



TBSCl (28.2 g, 187 mmol, 3.0 eq) was dissolved in THF (135 mL) and HMPA (100 mL) in a 1 L Schlenk flask and cooled to -78°C . LiHMDS (1 M in THF, 162.2 mL, 162.2 mmol, 2.6 eq) was added and the resulting mixture was stirred for 10 min at -78°C before warming to 0°C . The reaction was re-cooled to -78°C after 10 min at 0°C and ester (**1.2.2.1**, 9.17 mL, 62.4 mmol, 1.0 eq) was added dropwise over 5 min and stirring was continued at -78°C for 1h 45min. Sat. aq. NaCl (350 mL) was added at -78°C and the mixture was extracted with pentane (300 mL). The organic layer was concentrated under reduced pressure (30°C , 20 mbar), redissolved in pentane (500 mL) and washed with sat. aq. NaCl (3×100 mL), 10% aq. LiCl (100 mL) and sat. aq. NaCl (100 mL). After drying the organic phase over Na₂SO₄, the solvent was removed *in vacuo* and the remaining orange oil was further freeze-dried (4 cycles) over a period of 14 h. ¹H-NMR analysis indicated that the HMPA was not fully removed. Therefore, the oil was dissolved in pentane (300 mL) and washed with sat. aq. NaCl (100 mL), 10% aq. LiCl (100 mL) and sat. aq. NaCl (100 mL). The organic layer was dried over Na₂SO₄, the solvent was removed under reduced pressure and the residual oil was further freeze-dried (4 cycles) over a period of 14 h. Repeated ¹H-NMR analysis showed that although the amount of HMPA was significantly reduced, traces were still present. The orange oil was redissolved in pentane (300 mL) and washed repeatedly ($3 \times$) with 10% aq. LiCl (150 mL) and sat. aq. NaCl (150 mL). After drying the

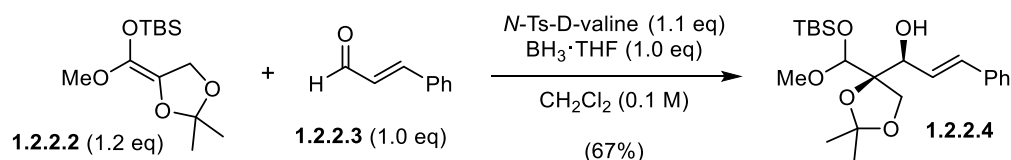
organic layer over Na_2SO_4 , the solvent was removed *in vacuo* and the remaining oil was freeze-dried (3 cycles) over a period of 3 days. *Tert*-butyl((2,2-dimethyl-1,3-dioxolan-4-ylidene)(methoxy)methoxy)dimethylsilane (**1.2.2.2**, 16.6 g, 60.5 mmol, 97%) was obtained as an orange oil.

^1H NMR (400 MHz, C_6D_6) δ (ppm) = 4.55 (s, 2H), 3.56 (s, 3H), 1.36 (s, 6H), 0.91 (s, 9H), 0.10 (s, 6H).

^{13}C NMR (101 MHz, C_6D_6) δ (ppm) = 139.6, 120.6, 110.9, 64.7, 57.9, 25.8, 25.2, 18.0, -4.4.

The analytical data is in accordance with the literature.¹²²

(1*S*,*E*)-1-((4*R*)-4-(((*tert*-butyldimethylsilyl)oxy)(methoxy)methyl)-2,2-dimethyl-1,3-dioxolan-4-yl)-3-phenylprop-2-en-1-ol (**1.2.2.4**)



N-Ts-D-valine¹⁵⁶ (7.82 g, 28.6 mmol, 1.1 eq) was dissolved in CH_2Cl_2 (130 mL), cooled to 0 °C and $\text{BH}_3 \cdot \text{THF}$ (1 M in THF, 26.0 mL, 26.0 mmol, 1.0 eq) was added dropwise over a period of 10 min. The suspension was stirred at 0 °C for 30 min before warming to rt and stirring for 1 h. Continuous bubbling was observed and the white solid slowly dissolved to give a clear solution. After cooling the solution to -78 °C, cinnamaldehyde (**1.2.2.3**, 3.27 mL, 26.0 mmol, 1 eq) in CH_2Cl_2 (70 mL) and TBS ketene acetal (**1.2.2.2**, 8.56 mL, 31.2 mmol, 1.2 eq) in CH_2Cl_2 (70 mL) were successively added via syringe pump (2.5 mL/min). Stirring was continued for 10 min at -78 °C and phosphate buffer (PB pH7, 30 mL) was added before warming to rt. The mixture was diluted with Et_2O (500 mL) and washed with PB pH7/sat. aq. NaCl (4:1, 250 mL), sat. aq. NaHCO_3 (200 mL) and sat. aq. NaCl (200 mL). The organic layer was dried over Na_2SO_4 and concentrated under reduced pressure to give an oil, which was directly dissolved in $\text{EtOH}/\text{H}_2\text{O}$ (9:1, 57.2 mL). After addition of NaHSO_3 (2.70 g, 26.0 mmol, 1.0 eq), the suspension was heated to 37 °C for 3 h followed by filtration through celite and rinsing of the filter cake with Et_2O . The filtrate was concentrated *in vacuo*, redissolved in Et_2O (100 mL) and filtered again through celite. Rotary evaporation gave an oily residue that was purified via flash column chromatography pentane: Et_2O = 185:15) to give an intractable diastereomeric mixture of (1*S*,*E*)-1-

((4*R*)-4-(((*tert*-butyldimethylsilyl)oxy)(methoxy)methyl)-2,2-dimethyl-1,3-dioxolan-4-yl)-3-phenylprop-2-en-1-ol (**1.2.2.4**, 7.08 g, 17.3 mmol, 67%) as a clear oil.

Note: Analytical data for the major diastereomer is reported.

R_f (pentane:Et₂O 9:1) = 0.24. (UV, CAM)

¹H NMR (400 MHz, CDCl₃) δ (ppm) = 7.40 (d, J = 7.3 Hz, 2H), 7.31 (t, J = 7.5 Hz, 2H), 7.22 (t, J = 7.3 Hz, 1H), 6.69 (dd, J = 16.0, 1.6 Hz, 1H), 6.43 (dd, J = 16.0, 5.3 Hz, 1H), 4.81 (s, 1H), 4.50 (t, J = 4.7 Hz, 1H), 4.09 (d, J = 9.2 Hz, 1H), 4.04 (d, J = 9.3 Hz, 1H), 3.46 (s, 3H), 3.18 (d, J = 5.1 Hz, 1H), 1.46 (s, 6H), 0.92 (s, 9H), 0.16 (d, J = 1.8 Hz, 6H).

¹H NMR (400 MHz, CD₂Cl₂) δ (ppm) = 7.42 – 7.38 (m, 2H), 7.34 – 7.28 (m, 2H), 7.25 – 7.19 (m, 1H), 6.65 (dd, J = 16.0, 1.6 Hz, 1H), 6.41 (dd, J = 16.0, 5.4 Hz, 1H), 4.80 (s, 1H), 4.46 (td, J = 6.0, 1.7 Hz, 1H), 4.00 (q, J = 9.3 Hz, 2H), 3.44 (s, 3H), 3.14 (d, J = 6.1 Hz, 1H), 1.43 (s, 6H), 0.92 (s, 9H), 0.17 (s, 3H), 0.17 (s, 3H).

¹³C NMR (101 MHz, CD₂Cl₂) δ (ppm) = 137.8, 130.8, 129.3, 129.0, 127.8, 126.9, 111.3, 102.0, 86.4, 73.7, 67.8, 57.7, 27.1, 26.7, 26.1, 18.5, -4.1, -4.2.

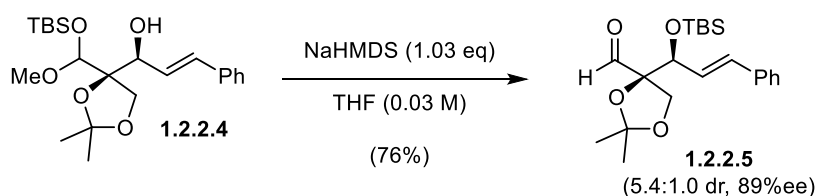
HRMS (EI): calc. for C₂₁H₃₃O₅Si⁺ [M - CH₃]⁺: 393.2092, found: 393.2095.

IR (Diamond-ATR, neat) ν_{\max} (cm⁻¹) = 3504 (vw), 2955 (w), 2931 (w), 2897 (vw), 2858 (vw), 1741 (vw), 1496 (vw), 1472 (w), 1463 (w), 1449 (vw), 1380 (w), 1370 (w), 1252 (m), 1210 (m), 1063 (vs), 1005 (w), 968 (m), 939 (w), 834 (vs), 778 (s), 750 (s), 693 (m), 670 (m).

$[\alpha]_D^{20}$ = -8.00° (c = 1.99, EtOAc).

The analytical data is in accordance with the literature.¹⁵⁷

(*R*)-4-((*S,E*)-1-(((*tert*-butyldimethylsilyl)oxy)-3-phenylallyl)-2,2-dimethyl-1,3-dioxolane-4-carbaldehyde (**1.2.2.5**)



Tert-butyldimethylsilylanol methanol acetal (**1.2.2.4**, 7.08 g, 17.3 mmol, 1.0 eq) was dissolved in THF (577 mL) and the mixture was cooled to -78 °C before NaHMDS (1 M in THF, 17.7 mL,

17.7 mmol, 1.03 eq) was added dropwise over 5 min. The reaction was stirred at $-78\text{ }^{\circ}\text{C}$ for 5 min, warmed to $0\text{ }^{\circ}\text{C}$ and stirred for 1 h 10 min. Sat. aq. NH_4Cl (30 mL) was added and the mixture was diluted with Et_2O (200 mL). The organic layer was washed with sat. aq. NH_4Cl (200 mL) and dried over Na_2SO_4 . After removal of the solvent *in vacuo*, the mixture was purified by flash column chromatography (pentane: Et_2O = 29:1) to give (*R*)-4-((*S,E*)-1-((*tert*-butyldimethylsilyloxy)-3-phenylallyl)-2,2-dimethyl-1,3-dioxolane-4-carbaldehyde (**1.2.2.5**, 4.957 g, 13.16 mmol, 76%) as a slightly yellow clear oil with $\text{dr} = 5.4:1.0$ and 89%ee.

Note: An diastereomerically pure sample was obtained by purification via reverse-phase semi-preparative HPLC ($\text{MeCN}:\text{H}_2\text{O}$ = 60:40 \rightarrow 100:0 over 60 min). The spectral data of a diastereomeric mixture of **ent-7** was reported in the literature.¹⁵⁷

R_f (pentane: Et_2O = 9:1) = 0.36. (UV, CAM)

t_R (reverse-phase semi-preparative HPLC, $\text{MeCN}:\text{H}_2\text{O}$ = 60:40 \rightarrow 100:0 over 60 min) = 41.01 min.

$^1\text{H NMR}$ (400 MHz, C_6D_6) δ (ppm) = 9.91 (d, J = 0.8 Hz, 1H), 7.27 – 7.23 (m, 2H), 7.14 – 7.05 (m, 2H), 7.06 – 7.00 (m, 1H), 6.45 – 6.32 (m, 2H), 4.41 (d, J = 5.8 Hz, 1H), 4.28 (d, J = 8.9 Hz, 1H), 3.76 (dd, J = 8.9, 0.9 Hz, 1H), 1.34 – 1.30 (m, 3H), 1.30 – 1.27 (m, 3H), 0.93 (s, 9H), 0.05 (s, 3H), 0.01 (s, 3H).

$^{13}\text{C NMR}$ (101 MHz, C_6D_6) δ (ppm) = 203.0, 136.6, 133.4, 129.0, 127.4, 127.0, 111.7, 89.9, 76.3, 68.2, 26.8, 26.3, 26.0, 18.3, -3.8 , -4.8 .

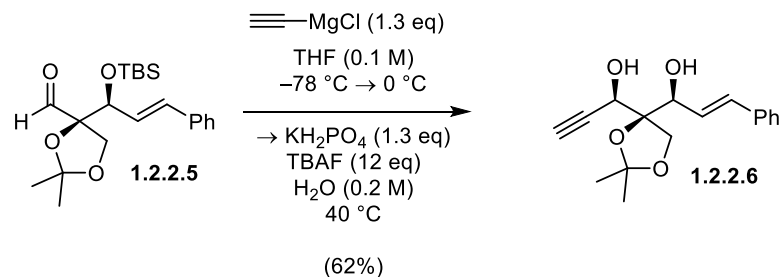
According to the 2D-NMR spectra, one carbon signal is obscured by the NMR solvent.

HRMS (ESI): calc. for $\text{C}_{21}\text{H}_{32}\text{O}_4\text{SiNa}^+$ [$\text{M} + \text{Na}^+$] $^+$: 399.1962, found: 399.1962.

IR (Diamond-ATR, neat) ν_{max} (cm^{-1}) = 2955 (w), 2929 (w), 2886 (vw), 2857 (w), 1734 (m), 1496 (vw), 1472 (w), 1463 (w), 1381 (w), 1372 (w), 1361 (w), 1253 (m), 1217 (w), 1186 (w), 1053 (s), 1004 (w), 972 (m), 939 (w), 887 (m), 865 (m), 829 (vs), 813 (s), 776 (vs), 749 (s), 693 (s).

$[\alpha]_{\text{D}}^{22} = +38^{\circ}$ ($c = 0.48$, CHCl_3).

(*S,E*)-1-((*R*)-4-((*R*)-1-hydroxyprop-2-yn-1-yl)-2,2-dimethyl-1,3-dioxolan-4-yl)-3-phenylprop-2-en-1-ol (**1.2.2.6**)



A solution of aldehyde (**1.2.2.5**, 4.854 g, 12.89 mmol, 1.0 eq) in THF (129 mL) was cooled to $-78\text{ }^{\circ}\text{C}$ and ethynylmagnesium chloride (0.5 M in THF, 33.5 mL, 16.8 mmol, 1.3 eq) was added dropwise over 15 min. The reaction was allowed to warm to $0\text{ }^{\circ}\text{C}$ over a period of 3 h 25 min and KH_2PO_4 (2.28 g, 16.8 mmol, 1.3 eq) in H_2O (64.5 mL) was added followed by dropwise addition of TBAF (1 M in THF, 154.7 mL, 154.7 mmol, 12 eq) over 20 min. The mixture was heated to $40\text{ }^{\circ}\text{C}$ for 1 h 10 min and after cooling to rt, sat. aq. CaCl_2 (75 mL) was added. The THF was removed *in vacuo* and EtOAc (600 mL) was added to the mixture. The organic layer was washed with sat. aq. NaCl (200 mL) and dried over Na_2SO_4 . The solvent was removed under reduced pressure and the thick oil was filtered through a silica plug (\varnothing 5 cm, 15 cm silica) which was rinsed with pentane:EtOAc (1:3, 2.0 L). After removal of the solvent, the residue was purified via flash column chromatography (pentane:EtOAc = 17:3 \rightarrow 4:1) to give the diastereomerically pure (*S,E*)-1-((*R*)-4-((*R*)-1-hydroxyprop-2-yn-1-yl)-2,2-dimethyl-1,3-dioxolan-4-yl)-3-phenylprop-2-en-1-ol (**1.2.2.6**, 2.31 g, 8.00 mmol, 62%) as a clear colorless oil.

Note: Reaction ethynylmagnesium chloride with aldehyde **1.2.2.5** proceeded with a diastereoselectivity of 3.5:1.0. The desired major diastereomer was selectively isolated via flash column chromatography.

R_f (pentane:EtOAc = 4:1) = 0.10. (UV)

$^1\text{H NMR}$ (400 MHz, C_6D_6) δ (ppm) = 7.31 (d, J = 8.0 Hz, 2H), 7.12 (t, J = 7.5 Hz, 2H), 7.04 (t, J = 7.2 Hz, 1H), 6.74 (d, J = 15.9 Hz, 1H), 6.44 (dd, J = 15.9, 5.7 Hz, 1H), 4.75 (s, 1H), 4.65 (d, J = 5.7 Hz, 1H), 4.22 (d, J = 9.2 Hz, 1H), 4.07 (d, J = 9.2 Hz, 1H), 2.83 (s, 1H), 2.64 (s, 1H), 2.03 (s, 1H), 1.41 (s, 3H), 1.33 (s, 3H).

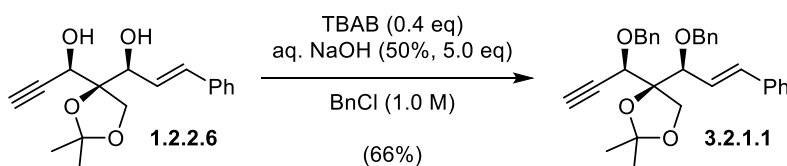
$^{13}\text{C NMR}$ (101 MHz, C_6D_6) δ (ppm) = 137.3, 131.9, 128.9, 127.9, 127.0, 111.5, 87.0, 82.6, 75.0, 73.7, 67.5, 64.1, 26.9, 26.6.

According to the 2D-NMR spectra, one carbon signal is obscured by the NMR solvent.

HRMS (ESI): calc. for $\text{C}_{17}\text{H}_{19}\text{O}_4^-$ [$\text{M} - \text{H}^+$] $^-$: 287.1289, found: 287.1292.

IR (Diamond-ATR, neat) ν_{\max} (cm^{-1}) =, 3410 (w), 3287 (w), 2987 (vw), 1496 (vw), 1449 (w), 1372 (m), 1256 (m), 1214 (s), 1149 (m), 1057 (vs) 969 (vs), 873 (m), 848 (s), 804 (m), 751 (vs), 692 (vs).
 $[\alpha]_{\text{D}}^{22} = -15.8^{\circ}$ ($c = 1.68$, CHCl_3).

(R)-4-((*S,E*)-1-(benzyloxy)-3-phenylallyl)-4-((*R*)-1-(benzyloxy)prop-2-yn-1-yl)-2,2-dimethyl-1,3-dioxolane (**3.2.1.1**)



Diol (**1.2.2.6**, 2.308 g, 8.000 mmol, 1.0 eq) and TBAB (1.032 g, 3.200 mmol, 0.4 eq) were dissolved in BnCl (8.0 mL) and aq. NaOH (50%, 3.20 mL, 40 mmol, 5.0 eq) was added under vigorous stirring at 0 °C. After 5 min, the reaction was allowed to warm to rt and stirred for 2 h 30 min. Sat. aq. NH_4Cl (15 mL) was added followed by pouring the mixture into sat. aq. NaCl (40 mL) and extracting with CH_2Cl_2 (1 × 150 mL, 2 × 80 mL). The combined organic layers were dried over Na_2SO_4 and the solvent was removed *in vacuo*. Purification via column chromatography (pentane:Et₂O = 39:1 → 19:1) gave *(R)*-4-((*S,E*)-1-(benzyloxy)-3-phenylallyl)-4-((*R*)-1-(benzyloxy)prop-2-yn-1-yl)-2,2-dimethyl-1,3-dioxolane (**3.2.1.1**, 2.458 g, 5.244 mmol, 66%) as a white solid.

R_f (pentane:Et₂O = 19:1) = 0.24. (UV, CAM)

$^1\text{H NMR}$ (400 MHz, CD_2Cl_2) δ (ppm) = 7.41 – 7.22 (m, 15H), 6.61 (d, $J = 16.1$ Hz, 1H), 6.26 (dd, $J = 16.1, 8.0$ Hz, 1H), 4.86 (d, $J = 11.5$ Hz, 1H), 4.62 (d, $J = 11.4$ Hz, 1H), 4.58 – 4.51 (m, 2H), 4.42 (d, $J = 11.4$ Hz, 1H), 4.31 (dd, $J = 8.0, 0.9$ Hz, 1H), 4.18 (d, $J = 8.8$ Hz, 1H), 3.95 (d, $J = 8.8$ Hz, 1H), 2.55 (d, $J = 2.1$ Hz, 1H), 1.44 (s, 3H), 1.41 (s, 3H).

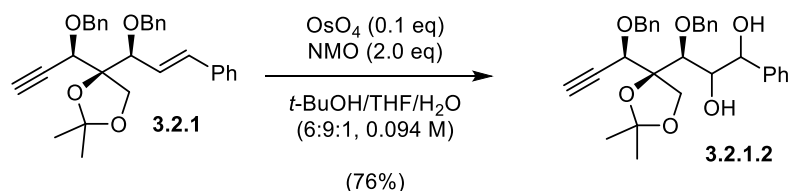
$^{13}\text{C NMR}$ (101 MHz, CD_2Cl_2) δ (ppm) = 138.9, 138.2, 137.0, 134.8, 129.1, 128.8, 128.8, 128.7, 128.5, 128.4, 128.2, 128.0, 127.1, 126.4, 112.1, 87.4, 82.3, 81.0, 76.0, 72.0, 71.7, 71.5, 68.1, 27.03, 26.98.

HRMS (ESI): calc. for $\text{C}_{31}\text{H}_{36}\text{NO}_4^+$ [$\text{M} + \text{NH}_4^+$] $^+$: 486.2639, found: 486.2637.

IR (Diamond-ATR, neat) ν_{\max} (cm^{-1}) = 3267 (w), 3031 (vw), 2897 (vw), 1599 (vw), 1496 (w), 1454 (w), 1392 (w), 1382 (w); 1370 (w), 1311 (vw), 1289 (vw), 1257 (w), 1210 (m), 1188 (w), 1155 (w), 1055 (vs), 1028 (s), 979 (s), 930 (w), 914 (w), 886 (w), 852 (m), 804 (vw), 749 (vs), 695 (vs), 672 (s).
 $[\alpha]_{\text{D}}^{22} = -16.7^{\circ}$ ($c = 1.58$, EtOAc).

mp = 92.5 – 98.9 °C.

(3*S*)-3-(benzyloxy)-3-((*S*)-4-((*R*)-1-(benzyloxy)prop-2-yn-1-yl)-2,2-dimethyl-1,3-dioxolan-4-yl)-1-phenylpropane-1,2-diol (3.2.1.2)



Styrene (3.2.1.1, 2.458 g, 5.244 mmol, 1.0 eq) and NMO (1.23 g, 10.5 mmol, 2.0 eq) were dissolved in *t*-BuOH/THF/H₂O (6:9:1, 55.7 mL) and OsO₄ (4% in H₂O, 3.33 mL, 0.524 mmol, 0.1 eq) was added. After stirring for 3 h 50 min at rt, sat. aq. Na₂S₂O₃ (50 mL) was added followed by pouring the mixture into sat. aq. NaCl (50 mL) and extracting with CH₂Cl₂ (1 × 200 mL, 2 × 100 mL). The combined organic layers were dried over Na₂SO₄ and the solvent was removed *in vacuo*. Purification via flash column chromatography (pentane:Et₂O = 39:1 → 19:1) afforded (3*S*)-3-(benzyloxy)-3-((*S*)-4-((*R*)-1-(benzyloxy)prop-2-yn-1-yl)-2,2-dimethyl-1,3-dioxolan-4-yl)-1-phenylpropane-1,2-diol (3.2.1.2, 1.996 g, 3.971 mmol, 76%) as a clear brown oil.

R_f (pentane:EtOAc = 4:1) = 0.49. (CAM)

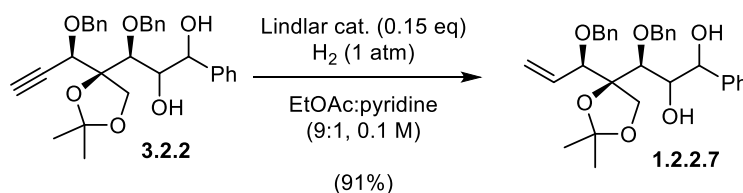
¹H NMR (400 MHz, CD₂Cl₂) δ (ppm) = 7.41 – 7.25 (m, 10H), 7.23 – 7.12 (m, 5H), 4.95 – 4.77 (m, 4H), 4.57 (d, *J* = 11.1 Hz, 1H), 4.46 (d, *J* = 2.2 Hz, 1H), 4.34 – 4.26 (m, 2H), 4.20 (d, *J* = 9.0 Hz, 1H), 4.12 (td, *J* = 5.6, 1.3 Hz, 1H), 3.48 (d, *J* = 5.6 Hz, 1H), 3.21 (d, *J* = 5.5 Hz, 1H), 2.70 (d, *J* = 2.2 Hz, 1H), 1.47 (s, 3H), 1.42 (s, 3H).

¹³C NMR (101 MHz, CD₂Cl₂) δ (ppm) = 142.7, 138.6, 137.0, 129.4, 129.1, 129.0, 128.8, 128.5, 128.4, 128.3, 127.1, 126.4, 111.1, 86.8, 82.9, 79.9, 77.2, 77.0, 74.3, 73.0, 72.5, 71.5, 67.4, 27.6, 26.4.

HRMS (EI): calc. for C₃₀H₃₁O₆⁺ [M – CH₃]⁺: 487.2115, found: 487.2115.

IR (Diamond-ATR, neat) ν_{max} (cm⁻¹) = 3466 (vw), 3282 (vw), 3031 (vw), 2987 (vs), 2933 (vw), 1757 (vw), 1605 (vw), 1496 (vw), 1453 (w), 1381 (w), 1371 (w), 1246 (w), 1213 (m), 1169 (w), 1060 (vs), 1027 (s), 914 (w), 875 (w), 844 (w), 735 (s), 696 (vs).

[α]_D²² = –32.0° (c = 1.50, CHCl₃).

(3*S*)-3-(benzyloxy)-3-((*S*)-4-((*R*)-1-(benzyloxy)allyl)-2,2-dimethyl-1,3-dioxolan-4-yl)-1-phenylpropane-1,2-diol (1.2.2.7)

Alkyne (**3.2.1.2**, 1.089 g, 2.167 mmol, 1.0 eq) was dissolved in EtOAc/pyridine (9:1, 21.6 mL) in a 50 mL round-bottom flask and Lindlar catalyst (5% Pd, 692 mg 0.325 mmol, 0.15 eq) was added under a N_2 -atmosphere. The reaction was purged with H_2 by bubbling the gas through the suspension for 7 min. Thereafter, stirring was continued under a H_2 atmosphere (1 atm) for 10 min 30 sec before purging with N_2 for 2 min. NMR analysis indicated 80% conversion of the starting material. The mixture was purged with H_2 for 85 sec and N_2 for 2 min followed by removal of the solid by filtration through celite and rinsing of the filtercake with EtOAc (250 mL). Rotary evaporation of the solvent gave an oily residue which was purification via flash column chromatography (pentane:EtOAc = 9:1). (3*S*)-3-(benzyloxy)-3-((*S*)-4-((*R*)-1-(benzyloxy)allyl)-2,2-dimethyl-1,3-dioxolan-4-yl)-1-phenylpropane-1,2-diol (**1.2.2.7**, 998.1 mg, 1.979 mmol, 91%) was obtained as a clear oil.

R_f (pentane:EtOAc = 4:1) = 0.43. (CAM)

$^1\text{H NMR}$ (400 MHz, CD_2Cl_2) δ (ppm) = 7.40 – 7.29 (m, 10H), 7.23 – 7.14 (m, 5H), 6.02 (ddd, J = 17.5, 10.5, 7.1 Hz, 1H), 5.48 (dt, J = 10.6, 1.4 Hz, 1H), 5.43 (dt, J = 17.3, 1.5 Hz, 1H), 4.88 (d, J = 11.2 Hz, 1H), 4.81 (d, J = 6.5 Hz, 1H), 4.78 (d, J = 11.2 Hz, 1H), 4.65 (d, J = 10.9 Hz, 1H), 4.41 (d, J = 11.0 Hz, 1H), 4.22 – 4.11 (m, 3H), 4.08 (ddd, J = 6.2, 4.9, 1.2 Hz, 1H), 4.01 (d, J = 6.3 Hz, 1H), 3.47 (d, J = 4.9 Hz, 1H), 3.44 (d, J = 6.3 Hz, 1H), 1.46 (s, 3H), 1.42 (s, 3H).

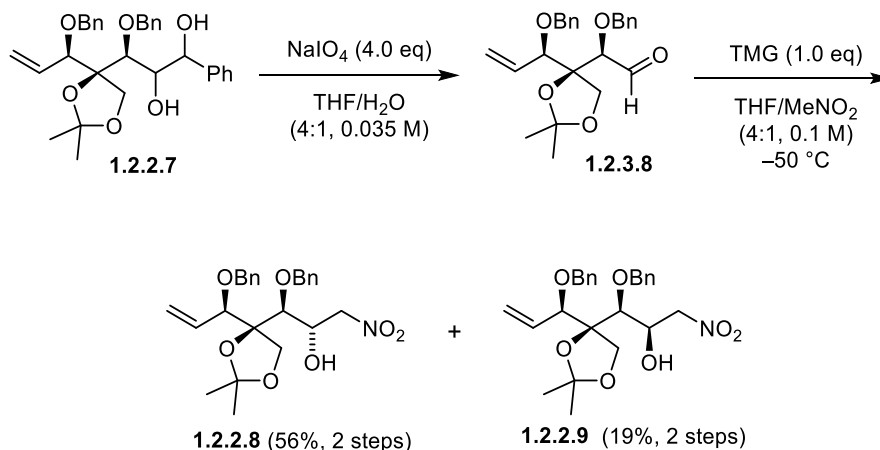
$^{13}\text{C NMR}$ (101 MHz, CD_2Cl_2) δ (ppm) = 143.0, 138.8, 137.9, 134.1, 129.3, 129.0, 129.0, 128.6, 128.5, 128.3, 128.1, 127.3, 126.4, 120.2, 110.7, 87.4, 82.5, 82.2, 77.0, 74.5, 72.9, 72.6, 67.9, 27.6, 26.6.

HRMS (ESI): calc. for $\text{C}_{31}\text{H}_{36}\text{O}_6\text{Na}^+$ [$\text{M} + \text{Na}^+$] $^+$: 527.2400, found: 527.2404.

IR (Diamond-ATR, neat) ν_{max} (cm^{-1}) = 3469 (vw), 3031 (vw), 2986 (vw), 2930 (vw), 1736 (vw), 1605 (vw), 1496 (vw), 1453 (w), 1381 (w), 1370 (w), 1244 (w), 1213, (m), 1158 (w), 1057 (s), 1026 (s), 929 (w), 876 (w), 846 (w), 734 (s), 696 (vs).

$[\alpha]_{\text{D}}^{22} = -25.5^\circ$ ($c = 1.83$, PhMe).

(1*S*,2*S*)-1-(benzyloxy)-1-((*S*)-4-((*R*)-1-(benzyloxy)allyl)-2,2-dimethyl-1,3-dioxolan-4-yl)-3-nitropropan-2-ol (**1.2.2.8**) and (1*S*,2*R*)-1-(benzyloxy)-1-((*S*)-4-((*R*)-1-(benzyloxy)allyl)-2,2-dimethyl-1,3-dioxolan-4-yl)-3-nitropropan-2-ol (**1.2.2.9**)



A solution of the diol (**1.2.2.7**, 2.04 g, 4.04 mmol, 1.0 eq) in THF/H₂O (4:1, 115 mL) was added NaIO_4 (3.46 g, 16.2 mmol, 4.0 eq). The reaction was stirred for 2 h 30 min at rt and diluted with H₂O (40 mL). After extracting the mixture with CH₂Cl₂ (1 × 180 mL, 1 × 90 mL), the combined organic layers were washed with sat. aq. NaCl (40 mL) and dried with Na₂SO₄. The solvent was removed *in vacuo* and the residue was transferred into a 100 mL round-bottom flask with dry PhMe (40 mL). Removal of the solvent was followed by freeze-drying (3 cycles) and stirring under high vacuum (> 1 mbar) for 14 h. The clear colorless oil was dissolved in THF (32.3 mL), cooled to -50 °C and MeNO₂ (8.1 mL) was added. After 10 min, TMG (0.507 mL, 4.04 mmol, 1.0 eq) was added dropwise and stirring was continued at -50 °C for 26 and warmed to rt. CH₂Cl₂ (300 mL) was added and the organic layer was washed with sat. aq. /sat. aq. NaCl (1:1, 80 mL), dried over Na₂SO₄ and concentrated. Purification via reverse-phase semi-preparative HPLC (MeCN:H₂O = 58:41 → 90:10 over 55 min) afforded (1*S*,2*S*)-1-(benzyloxy)-1-((*S*)-4-((*R*)-1-(benzyloxy)allyl)-2,2-dimethyl-1,3-dioxolan-4-yl)-3-nitropropan-2-ol (**1.2.2.8**, 1.037 g, 2.267 mmol, 56%) and (1*S*,2*R*)-1-(benzyloxy)-1-((*S*)-4-((*R*)-1-(benzyloxy)allyl)-2,2-dimethyl-1,3-dioxolan-4-yl)-3-nitropropan-2-ol (**1.2.2.9**, 359.8 mg, 0.7864 mmol, 19%) over two steps as colorless oils.

Analytic data of **1.2.2.8**:

R_f (pentane:EtOAc = 17:3) = 0.27. (CAM)

t_R (reverse-phase semi-preparative HPLC, MeCN:H₂O = 58:42 → 90:10 over 55 min) = 30.39 min.

¹H NMR (800 MHz, C₆D₆) δ (ppm) = 7.18 – 7.13 (m, 8H), 7.10 – 7.06 (m, 2H), 5.88 (ddd, J = 17.5, 10.5, 7.1 Hz, 1H), 5.19 (ddd, J = 10.6, 1.7, 1.1 Hz, 1H), 5.16 (dt, J = 17.4, 1.4 Hz, 1H), 4.69 (td, J = 5.8, 2.7 Hz, 1H), 4.52 (d, J = 11.4 Hz, 1H), 4.44 (d, J = 11.4 Hz, 1H), 4.38 (d, J = 11.5 Hz, 1H), 4.35 (dd, J = 12.8, 3.2 Hz, 1H), 4.28 (dd, J = 12.8, 8.9 Hz, 1H), 4.06 (d, J = 11.5 Hz, 1H), 3.99 (dt, J = 7.1, 1.2 Hz, 1H), 3.95 (d, J = 8.8 Hz, 1H), 3.83 (d, J = 8.8 Hz, 1H), 3.76 (d, J = 5.4 Hz, 1H), 3.66 (d, J = 4.5 Hz, 1H), 1.32 (s, 3H), 1.26 (s, 3H).

The aromatic signals are overlapping with the NMR solvent.

¹³C NMR (201 MHz, C₆D₆) δ (ppm) = 138.3, 137.4, 133.9, 128.8, 128.7, 128.4, 128.3, 127.8, 119.9, 110.6, 86.8, 81.8, 81.6, 78.5, 75.7, 71.9, 69.6, 67.8, 27.4, 26.3.

According to the 2D-NMR spectra, one aromatic carbon signal is obscured by the NMR solvent.

HRMS (ESI): calc. for C₂₅H₃₁NO₇Na⁺ [M + Na⁺]⁺: 480.1993, found: 480.1998.

IR (Diamond-ATR, neat) ν_{\max} (cm⁻¹) = 3434 (br, vw), 3065 (vw), 3031 (vw), 2987 (vw), 2898 (vw), 2360 (vw), 1552 (vs), 1497 (w), 1454 (m), 1420 (w), 1381 (m), 1372 (m), 1246 (m), 1213 (s), 1157 (w), 1089 (vs), 1055 (vs), 1027 (vs), 1001 (s), 932 (m), 881 (m), 852 (m), 734 (vs), 697 (vs), 615 (m).

$[\alpha]_D^{22} = -24.6^\circ$ (c = 0.503, CH₂Cl₂).

Analytic data of 1.2.2.9:

R_f (pentane:EtOAc = 17:3) = 0.24. (CAM)

t_R (reverse-phase semi-preparative HPLC, MeCN:H₂O = 58:42 → 90:10 over 55 min) = 28.53 min.

¹H NMR (800 MHz, C₆D₆) δ (ppm) = 7.19 – 7.11 (m, 8H), 7.10 – 7.04 (m, 2H), 5.94 (ddd, J = 17.2, 10.6, 6.3 Hz, 1H), 5.28 – 5.23 (m, 2H), 4.80 (dddd, J = 8.8, 7.4, 4.0, 2.6 Hz, 1H), 4.67 (d, J = 11.5 Hz, 1H), 4.39 (d, J = 11.3 Hz, 1H), 4.30 – 4.26 (m, 2H), 4.21 (dd, J = 12.8, 8.8 Hz, 1H), 4.08 (d, J = 9.3 Hz, 1H), 4.03 (d, J = 11.4 Hz, 1H), 3.95 (dt, J = 6.4, 1.3 Hz, 1H), 3.83 (dd, J = 12.8, 3.9 Hz, 1H), 3.67 (d, J = 2.7 Hz, 1H), 2.60 (d, J = 7.5 Hz, 1H), 1.37 (s, 3H), 1.27 (s, 3H).

The aromatic signals are overlapping with the NMR solvent.

¹³C NMR (201 MHz, C₆D₆) δ (ppm) = 138.2, 137.6, 133.7, 128.9, 128.8, 128.4, 128.3, 119.2, 109.5, 87.1, 81.9, 79.6, 78.5, 76.2, 72.1, 69.1, 67.8, 27.7, 26.2.

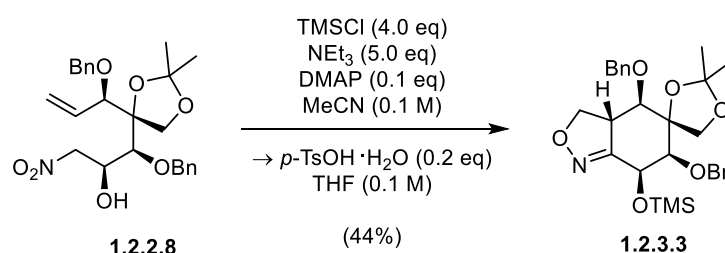
According to the 2D-NMR spectra, two aromatic carbon signals are obscured by the NMR solvent.

HRMS (ESI): calc. for C₂₅H₃₅N₂O₇⁺ [M + NH₄⁺]⁺: 475.2439, found: 475.2442.

IR (Diamond-ATR, neat) ν_{\max} (cm^{-1}) = 3521 (br, vw), 3065 (vw), 3031 (vw), 2987 (vw), 2930 (vw), 2360 (vw), 1552 (vs), 1497 (w), 1454 (m), 1380 (m), 1370 (m), 1245 (m), 1212 (m), 1168 (m), 1087 (vs), 1048 (vs), 1026 (vs), 1001 (s), 928 (m), 887 (m), 854 (m), 735 (vs), 697 (vs), 618 (m), 599 (m), 566 (m).

$[\alpha]_{\text{D}}^{22} = -8.69^{\circ}$ ($c = 0.290$, CH_2Cl_2).

(3*aR*,4*R*,5*S*,6*S*,7*S*)-4,6-bis(benzyloxy)-2',2'-dimethyl-7-((trimethylsilyl)oxy)-3*a*,4,6,7-tetrahydro-3*H*-spiro[benzo[*c*]isoxazole-5,4'-[1,3]dioxolane] (1.2.3.3)



A solution of TMSCl (20.4 μL , 0.160 mmol, 4.0 eq), NEt_3 (27.9 μL , 0.200 mmol, 5.0 eq) and DMAP (0.5 mg, 0.04 mmol, 0.1 eq) in MeCN (0.4 mL) was added to nitro alkene (1.2.2.8, 18.3 mg, 40.0 μmol , 1.0 eq) and the mixture was stirred at 40 $^{\circ}\text{C}$ for 3 h 20 min. PB pH7/sat. aq. NaCl (1:1, 10 mL) was added, the mixture was extracted with CH_2Cl_2 (2 \times 35 mL) and the combined organic layers were dried over Na_2SO_4 . After removal of the solvent *in vacuo*, $p\text{-TsOH}\cdot\text{H}_2\text{O}$ (1.5 mg, 8.0 μmol , 0.2 eq) in THF (0.4 mL) was added to the residue and the solution stirred for 10 min at rt before PB pH7/sat. aq. NaCl (1:1, 10 mL) was added. The mixture was extracted with CH_2Cl_2 (2 \times 35 mL), the combined organic layers were dried over Na_2SO_4 and concentrated. Purification via flash column chromatography (pentane:EtOAc = 92:8) afforded (3*aR*,4*R*,5*S*,6*S*,7*S*)-4,6-bis(benzyloxy)-2',2'-dimethyl-7-((trimethylsilyl)oxy)-3*a*,4,6,7-tetrahydro-3*H*-spiro[benzo[*c*]isoxazole-5,4'-[1,3]dioxolane] (1.2.3.3, 9.0 mg, 18 μmol , 44%) as a colorless oil

R_f (pentane:EtOAc = 9:1) = 0.24. (CAM)

$^1\text{H NMR}$ (400 MHz, C_6D_6) δ (ppm) = 7.35 (d, $J = 7.1$ Hz, 2H), 7.31 (d, $J = 7.0$ Hz, 2H), 7.22 – 7.17 (m, 4H), 7.14 – 7.04 (m, 2H), 4.81 (d, $J = 3.0$ Hz, 1H), 4.78 (d, $J = 8.9$ Hz, 1H), 4.67 (d, $J = 12.0$ Hz, 1H), 4.53 (d, $J = 11.8$ Hz, 1H), 4.42 – 4.34 (m, 2H), 4.29 (d, $J = 12.0$ Hz, 1H), 4.03 (dd, $J = 10.4, 8.5$ Hz, 1H), 3.65 (t, $J = 8.6$ Hz, 1H), 3.35 (d, $J = 3.0$ Hz, 1H), 3.33 – 3.26 (m, 1H), 3.21 (d, $J = 10.4$ Hz, 1H), 1.55 (s, 3H), 1.53 (s, 3H), 0.04 (s, 9H).

The aromatic signals are overlapping with the NMR solvent.

^{13}C NMR (101 MHz, C_6D_6) δ (ppm) = 155.4, 138.8, 138.3, 128.7, 127.6, 109.8, 87.5, 84.1, 80.8, 74.8, 73.44, 73.37, 65.4, 64.8, 50.9, 27.3, 26.9, -0.1.

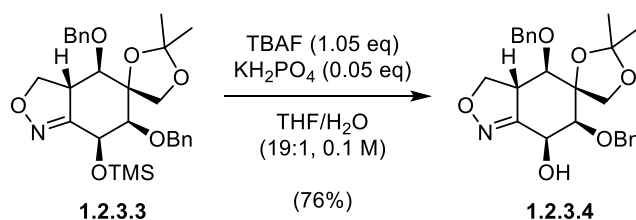
According to the 2D-NMR spectra, four aromatic carbon signals are obscured by the NMR solvent.

HRMS (ESI): calc. for $\text{C}_{28}\text{H}_{51}\text{N}_2\text{O}_6^+$ $[\text{M} + \text{NH}_4^+]^+$: 529.2728, found: 529.2734.

IR (Diamond-ATR, neat) ν_{max} (cm^{-1}) = 2957 (br, vw), 1497 (vw), 1454 (w), 1378 (w), 1366 (w), 1251 (m), 1211 (w), 1159 (w), 1085 (s), 1069 (s), 1028 (m), 986 (w), 920 (w), 842 (vs), 734 (s), 696 (vs).

$[\alpha]_{\text{D}}^{22} = -2.17^\circ$ ($c = 0.341$, CH_2Cl_2).

(3*aR*,4*R*,5*S*,6*S*,7*S*)-4,6-bis(benzyloxy)-2',2'-dimethyl-3*a*,4,6,7-tetrahydro-3H-spiro[benzo[*c*]isoxazole-5,4'-[1,3]dioxolan]-7-ol (1.2.3.4)



TMS alcohol (**1.2.3.3**, 39.3 mg, 76.8 μmol , 1.0 eq) and KH_2PO_4 (0.7 mg, 4 μmol , 0.05 eq) were dissolved in THF/ H_2O (19:1, 0.81 mL) and TBAF (1 M in THF, 0.81 mL, 81 μmol , 1.05 eq) was added at rt. After the solution was stirred for 6 min, PB pH7/sat. aq. NaCl (1:1, 10 mL) was added and the mixture was extracted with CH_2Cl_2 (2 \times 35 mL). The combined organic layers were dried over Na_2SO_4 and concentrated. Purification via flash column chromatography (pentane:EtOAc = 4:1) afforded (3*aR*,4*R*,5*S*,6*S*,7*S*)-4,6-bis(benzyloxy)-2',2'-dimethyl-3*a*,4,6,7-tetrahydro-3H-spiro[benzo[*c*]isoxazole-5,4'-[1,3]dioxolan]-7-ol (**1.2.3.4**, 25.8 mg, 58.7 μmol , 76%) as an off-white foam.

R_f (pentane:EtOAc = 2:1) = 0.48. (CAM)

^1H NMR (800 MHz, C_6D_6) δ (ppm) = 7.25 – 7.21 (m, 4H), 7.18 – 7.14 (m, 4H), 7.11 – 7.06 (m, 2H), 4.69 – 4.64 (m, 2H), 4.52 (d, $J = 8.9$ Hz, 1H), 4.43 (d, $J = 11.7$ Hz, 1H), 4.31 – 4.24 (m, 3H), 3.97 (dd, $J = 10.4, 8.4$ Hz, 1H), 3.66 (t, $J = 8.2$ Hz, 1H), 3.28 (d, $J = 3.5$ Hz, 1H), 3.20 (td, $J = 10.6, 8.0$ Hz, 1H), 3.14 (d, $J = 10.8$ Hz, 1H), 1.51 (s, 3H), 1.47 (s, 3H).

According to the 2D-NMR spectra, the aromatic signals are overlapping with the NMR solvent.

^{13}C NMR (201 MHz, C_6D_6) δ (ppm) = 154.6, 138.6, 138.0, 128.8, 128.7, 128.4, 128.3, 127.7, 109.9, 87.1, 82.9, 80.8, 75.2, 73.4, 73.2, 65.3, 63.8, 50.6, 27.0, 26.8.

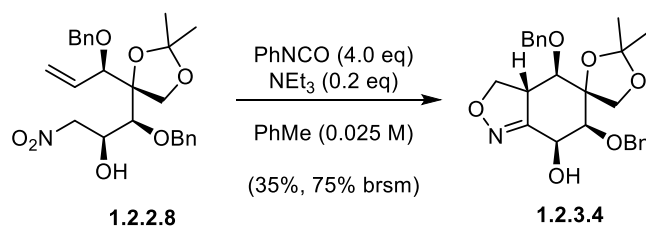
According to the 2D-NMR spectra, one carbon signal is obscured by the NMR solvent.

HRMS (EI): calc. for $\text{C}_{25}\text{H}_{29}\text{NO}_6^+$ $[\text{M}]^+$: 439.1989, found: 439.1970.

IR (Diamond-ATR, neat) ν_{max} (cm^{-1}) = 3392 (vw), 2962 (w), 2918 (w), 2950 (w), 1497 (vw), 1454 (vw), 1378 (vw), 1260 (s), 1212 (vw), 1158 (vw), 1090 (vs), 1019 (vs), 859 (w), 798 (vs), 737 (w), 698 (w).

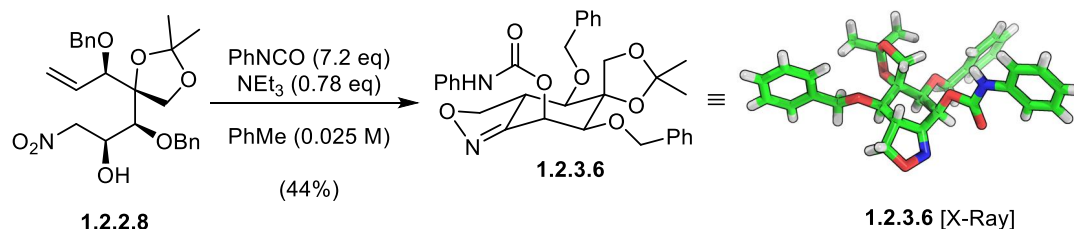
$[\alpha]_{\text{D}}^{22} = -22.7^\circ$ ($c = 0.890$, CH_2Cl_2).

(3*aR*,4*R*,5*S*,6*S*,7*S*)-4,6-bis(benzyloxy)-2',2'-dimethyl-3*a*,4,6,7-tetrahydro-3*H*-spiro[benzo[*c*]isoxazole-5,4'-[1,3]dioxolan]-7-ol (1.2.3.4)



Nitro alkene (**1.2.2.8**, 100 mg, 0.219 mmol, 1.0 eq) was dissolved in PhMe (8.5 mL) and PhNCO (95 μL , 0.87 mmol, 4.0 eq) was added followed by NEt_3 (6.0 μL , 44 μmol , 0.2 eq) in PhMe (0.2 mL). The reaction was stirred for 43 h and the white precipitate was removed by filtration with subsequent rinsing of the filtercake using PhMe (5 mL). After diluting the filtrate with EtOAc (100 mL), the organic layer was extracted with sat. aq. NaHCO_3 /sat. aq. NaCl (1:1, 50 mL) and dried over Na_2SO_4 . The solution was concentrated and purification via flash column chromatography (petane:EtOAc = 9:1 \rightarrow 4:1) afforded (3*aR*,4*R*,5*S*,6*S*,7*S*)-4,6-bis(benzyloxy)-2',2'-dimethyl-3*a*,4,6,7-tetrahydro-3*H*-spiro[benzo[*c*]isoxazole-5,4'-[1,3]dioxolan]-7-ol (**1.2.3.4**, 33.6 mg, 76.4 μmol , 35%) as a slightly yellow foam along with recovered **1.2.2.8** (53.6 mg, 0.117 mmol, 53%).

(3*aR*,4*R*,5*S*,6*S*,7*S*)-4,6-bis(benzyloxy)-2',2'-dimethyl-3*a*,4,6,7-tetrahydro-3*H*-spiro[benzo[*c*]isoxazole-5,4'-[1,3]dioxolan]-7-yl phenylcarbamate (1.2.3.6)



A solution of PhNCO (12.4 μL , 0.114 mmol, 5.2 eq) and NEt₃ (2.37 μL , 17.0 μmol , 0.78 eq) in PhMe (0.26 mL) was added to nitro alkene (**1.2.2.8**, 10.0 mg, 21.9 μmol , 1.0 eq) in PhMe (0.66 mL) at rt. After stirring the reaction for 73 h 30 min, PhNCO (4.7 μL , 44 μmol , 2.0 eq) was added to the white suspension and stirring was continued for 68 h 30 min. The precipitate was removed by filtration with subsequent rinsing of the filtercake using PhMe (5 mL). EtOAc (10 mL) was added to the filtrate and the organic layer was washed NH₄Cl (5.0 mL) and sat. aq. NaHCO₃/sat. aq. NaCl (1:1, 5.0 mL). The solution was and dried over Na₂SO₄ and concentrated. Purification via flash column chromatography (petane:EtOAc = 17:3) afforded (3*aR*,4*R*,5*S*,6*S*,7*S*)-4,6-bis(benzyloxy)-2',2'-dimethyl-3*a*,4,6,7-tetrahydro-3*H*-spiro[benzo[*c*]isoxazole-5,4'-[1,3]dioxolan]-7-yl phenylcarbamate (**1.2.3.6**, 5.4 mg, 9.7 μmol , 44%) as a white solid.

R_f (pentane:EtOAc = 4:1) = 0.26. (UV, CAM)

t_R (reverse-phase semi-preparative HPLC, MeCN:H₂O = 35:65 \rightarrow 100:0 over 70 min) = 50.83 min.

¹H NMR (400 MHz, CDCl₃) δ (ppm) = 7.42 – 7.22 (m, 14H), 7.14 – 7.06 (m, 1H), 6.63 (s, 1H), 6.12 (d, J = 3.8 Hz, 1H), 4.93 (d, J = 12.0 Hz, 1H), 4.83 (d, J = 11.2 Hz, 1H), 4.65 (d, J = 11.2 Hz, 1H), 4.58 (d, J = 12.0 Hz, 1H), 4.52 – 4.38 (m, 1H), 4.33 – 4.17 (m, 2H), 3.68 – 3.56 (m, 2H), 3.47 – 3.35 (m, 2H), 1.50 (s, 3H), 1.44 (s, 3H).

The aromatic signals are overlapping with the NMR solvent.

¹³C NMR (101 MHz, CDCl₃) δ (ppm) = 152.2, 151.5, 137.9, 137.2, 136.9, 129.3, 128.8, 128.6, 128.5, 128.4, 128.2, 128.1, 124.2, 119.1, 110.6, 87.1, 82.2, 78.5, 75.7, 73.5, 73.4, 64.8, 64.6, 51.0, 26.9, 26.5.

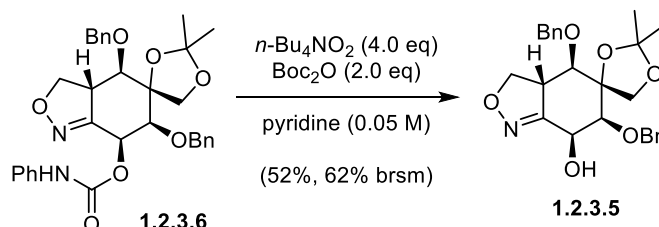
HRMS (ESI): calc. for C₃₂H₃₃N₂O₇ [M – H]⁺: 557.2293, found: 557.2290.

IR (Diamond-ATR, neat) ν_{max} (cm⁻¹) = 3278 (br, vw), 2890 (vw), 1739 (vs), 1602 (m), 1541 (s), 1498 (w), 1443 (m), 1365 (w), 1328 (vw), 1311 (w), 1249 (m), 1215 (s), 1157 (w), 1140 (w), 1091 (vs), 1073 (vs), 1016 (vs), 995 (m), 962 (w), 901 (w), 891 (w), 868 (s), 838 (w), 801 (m), 749 (s), 736 (vs), 695 (s).

$[\alpha]_D^{20} = +34.7^\circ$ (c = 2.54, EtOAc).

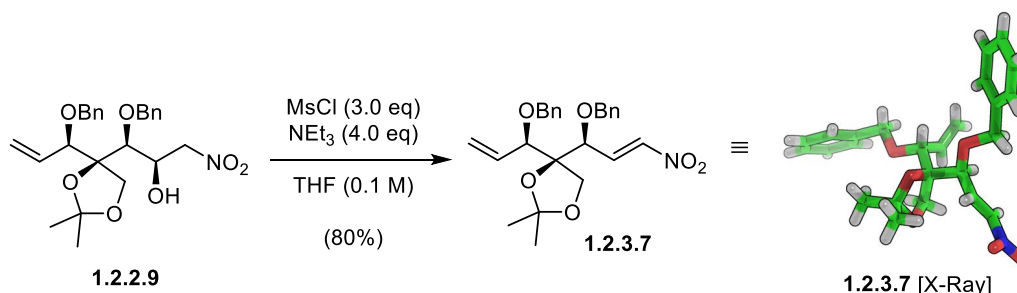
$m_p = 189.8 - 194.1^\circ\text{C}$.

(3*aR*,4*R*,5*S*,6*S*,7*S*)-4,6-bis(benzyloxy)-2',2'-dimethyl-3*a*,4,6,7-tetrahydro-3*H*-spiro[benzo[*c*]isoxazole-5,4'-[1,3]dioxolan]-7-ol (**1.2.3.4**)



Carbamate (**1.2.3.6**, 10.0 mg, 17.9 μmol , 1.0 eq) and $n\text{-Bu}_4\text{NO}_2$ (20.7 mg, 71.6 μmol , 4.0 eq) were dissolved in pyridine (0.96 mL) and Boc_2O (8.2 μL , 36 μmol , 2.0 eq) was added at 0 °C. The reaction was allowed to warm to rt and gradually turned orange while stirring for 5 h 30 min. EtOAc (15 mL) was added and the organic layer was washed with sat. aq. NH_4Cl (5 mL), sat. aq. NaCl (5 mL) and H_2O (5 mL). The solution was dried over Na_2SO_4 and concentrated. Purification via flash column chromatography (pentane:EtOAc = 31:9) afforded (3*aR*,4*R*,5*S*,6*S*,7*S*)-4,6-bis(benzyloxy)-2',2'-dimethyl-3*a*,4,6,7-tetrahydro-3*H*-spiro[benzo[*c*]isoxazole-5,4'-[1,3]dioxolan]-7-ol (**1.2.3.4**, 4.1 mg, 9.3 μmol , 52%) as a slightly yellow foam along with along with recovered **1.2.3.6** (1.6 mg, 2.8 μmol , 16%).

(*S*)-4-((*S*,*E*)-1-(benzyloxy)-3-nitroallyl)-4-((*R*)-1-(benzyloxy)allyl)-2,2-dimethyl-1,3-dioxolane (**1.2.3.7**)



Nitro alcohol (**1.2.2.9**, 359.8 mg, 0.7864 mmol, 1.0 eq) in THF (29 mL) was cooled to 0 °C. NEt_3 (0.438 mL, 3.14 mmol, 4.0 eq) and MeSO_2Cl (0.183 mL, 2.36 mmol, 3.0 eq) were added dropwise

and the reaction was stirred for 30 min at 0 °C before sat. aq. NaHCO₃ (5.0 mL) was added. The suspension was poured into sat. aq. NaHCO₃/sat. aq. NaCl (1:1, 40 mL) and the mixture was extracted with CH₂Cl₂ (2 × 100 mL). The combined organic layers were dried over Na₂SO₄ and concentrated. Purification via flash column chromatography (pentane:Et₂O = 9:1) afforded (*S*)-4-((*S,E*)-1-(benzyloxy)-3-nitroallyl)-4-((*R*)-1-(benzyloxy)allyl)-2,2-dimethyl-1,3-dioxolane (**1.2.3.7**, 839 mg, 1.91 mmol, 80%) as a white solid.

R_f (pentane:EtOAc = 9:1) = 0.62. (CAM)

¹H NMR (400 MHz, C₆D₆) δ (ppm) = 7.47 (dd, J = 13.4, 5.2 Hz, 1H), 7.25 – 7.17 (m, 4H), 7.10 (m, 6H), 6.95 (dd, J = 13.4, 1.7 Hz, 1H), 5.77 (ddd, J = 17.4, 10.5, 7.1 Hz, 1H), 5.10 (ddd, J = 10.5, 1.8, 1.0 Hz, 1H), 5.06 (dt, J = 17.3, 1.4 Hz, 1H), 4.39 (d, J = 11.5 Hz, 1H), 4.15 (d, J = 11.5 Hz, 1H), 4.10 (d, J = 11.5 Hz, 1H), 4.07 (d, J = 11.6 Hz, 1H), 4.03 (dd, J = 5.2, 1.7 Hz, 1H), 3.85 (dt, J = 7.0, 1.1 Hz, 1H), 3.79 (d, J = 9.0 Hz, 1H), 3.75 (d, J = 9.0 Hz, 1H), 1.33 (s, 3H), 1.30 (s, 3H).

¹³C NMR (101 MHz, C₆D₆) δ (ppm) = 140.4, 140.0, 138.01, 137.7, 134.3, 128.7, 128.7, 128.4, 128.3, 128.2, 119.4, 111.3, 86.8, 81.4, 77.5, 73.4, 71.6, 67.8, 26.9, 26.7.

According to the 2D spectra, one aromatic carbon signal is obscured by the NMR solvent.

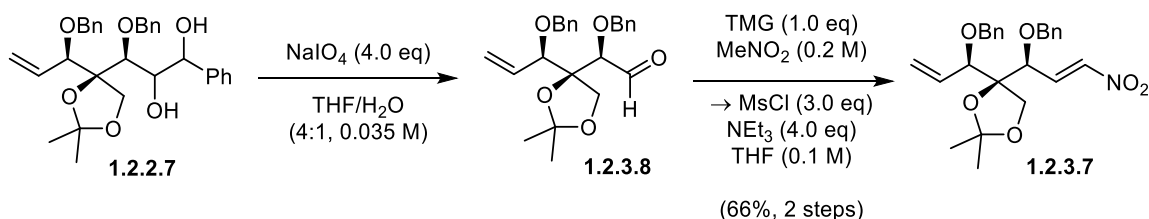
HRMS (ESI): calc. for C₂₅H₃₃N₂O₆⁺ [M + NH₄⁺]⁺: 457.2333, found: 457.2335.

IR (Diamond-ATR, neat) ν_{\max} (cm⁻¹) = 3082 (vw), 2923 (vw), 1651 (vw), 1518 (s), 1454 (w), 1384 (m), 1374 (w), 1364 (s), 1308 (vw), 1293 (vw), 1254 (w), 1215 (m), 1193 (w), 1158 (w), 1070 (vs), 1057 (vs), 1044 (s), 1028 (m), 1011 (s), 983 (s), 955 (s), 918 (w), 886 (vw), 856 (s), 842 (m), 818 (w), 794 (vw), 759 (m), 748 (s), 732 (m), 716 (w), 697 (vs).

$[\alpha]_D^{22} = +13.4^\circ$ (c = 0.0759, CH₂Cl₂).

$m_p = 88.5 - 92.1$ °C.

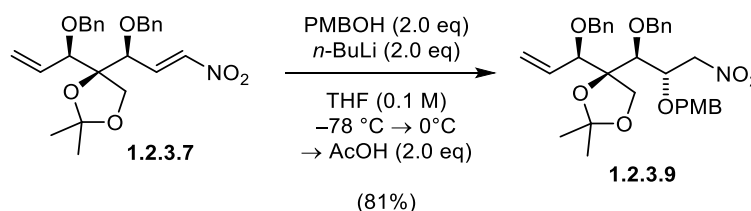
(*S*)-4-((*S,E*)-1-(benzyloxy)-3-nitroallyl)-4-((*R*)-1-(benzyloxy)allyl)-2,2-dimethyl-1,3-dioxolane (**1.2.3.7**)



A solution of the diol (**1.2.2.7**, 1.46 g, 2.90 mmol, 1.0 eq) in THF/H₂O (4:1, 82.9 mL) was added NaIO₄ (2.48 g, 11.6 mmol, 4.0 eq). The reaction was stirred for 2 h at rt and diluted with H₂O (50 mL). After extracting the mixture with CH₂Cl₂ (2 × 100 mL), the combined organic layers were washed with sat. aq. NaCl (50 mL) and dried with Na₂SO₄. The solvent was removed *in vacuo* and the residue was transferred into a 100 mL round-bottom flask with dry PhMe (40 mL). Removal of the solvent was followed by freeze-drying (4 cycles) and stirring under high vacuum (< 1 mbar) for 14 h. Dry PhMe (5 mL) was added and directly removed by stirring under high vacuum (< 1 mbar). The clear colorless oil was freeze-dried (2 cycles) and dissolved in MeNO₂ (14.5 mL). Dropwise addition of TMG (0.346 mL, 2.90 mmol, 1.0 eq) gave a bright yellow solution which was stirred at rt for 15 min. The flask was directly mounted to the rotary evaporator and the solvent was removed (30 °C, 35 – 45 mbar → 10 mbar). The resulting yellow oil was freeze-dried (2 cycles), redissolved in THF (29 mL) and cooled to 0 °C. NEt₃ (1.62 mL, 11.6 mmol, 4.0 eq) and MeSO₂Cl (0.67 mL, 8.7 mmol, 3.0 eq) were added dropwise and the reaction was stirred for 48 min at 0 °C before sat. aq. NaHCO₃ (10 mL) was added. The suspension was poured into sat. aq. NaHCO₃/sat. aq. NaCl (1:1, 40 mL) and the mixture was extracted with CH₂Cl₂ (2 × 100 mL). The combined organic layers were dried over Na₂SO₄ and concentrated. Purification via flash column chromatography (pentane:Et₂O = 19:1 → 9:1) afforded (S)-4-((S,E)-1-(benzyloxy)-3-nitroallyl)-4-((R)-1-(benzyloxy)allyl)-2,2-dimethyl-1,3-dioxolane (**1.2.3.7**, 839 mg, 1.91 mmol, 66%) as a white solid.

Note: The Henry condensation sequence was performed in one pot.

(S)-4-((1S,2S)-1-(benzyloxy)-2-((4-methoxybenzyl)oxy)-3-nitropropyl)-4-((R)-1-(benzyloxy)allyl)-2,2-dimethyl-1,3-dioxolane (**1.2.3.9**)



PMBOH (473 μL, 3.81 mmol, 2.05 eq) was dissolved in THF (9.3 mL), cooled to -78 °C and *n*-BuLi (2.48 M in THF, 1.5 mL, 3.72 mmol, 2.0 eq) was added dropwise. The mixture was stirred at -78 °C for 30 min and added to a solution of nitro alkene (**1.2.3.7**, 819 mg, 1.86 mmol, 1.0 eq)

in THF (3.16 mL) at $-78\text{ }^{\circ}\text{C}$. After stirring for 10 min at $-78\text{ }^{\circ}\text{C}$, the reaction was warmed to $0\text{ }^{\circ}\text{C}$ and stirring was continued for 3 h. AcOH (213 μL , 3.72 mmol, 2.0 eq) was added and the solvent was removed *in vacuo*. Purification via flash column chromatography (pentane:EtOAc = 19:1 \rightarrow 14:1) afforded (S)-4-((1S,2S)-1-(benzyloxy)-2-((4-methoxybenzyl)oxy)-3-nitropropyl)-4-((R)-1-(benzyloxy)allyl)-2,2-dimethyl-1,3-dioxolane (**1.2.3.9**, 865 mg, 1.50 mmol, 81%) as a clear colorless oil.

R_f (pentane:EtOAc = 9:1) = 0.51. (CAM)

$^1\text{H NMR}$ (400 MHz, C_6D_6) δ (ppm) = 7.29 – 7.03 (m, 12H), 6.77 – 6.69 (m, 2H), 5.88 (ddd, J = 17.1, 10.5, 6.3 Hz, 1H), 5.24 (dt, J = 17.4, 1.7 Hz, 1H), 5.16 (dt, J = 10.6, 1.5 Hz, 1H), 4.92 (ddd, J = 9.9, 2.6, 1.6 Hz, 1H), 4.82 (d, J = 10.7 Hz, 1H), 4.69 (d, J = 10.0 Hz, 1H), 4.66 (d, J = 9.9 Hz, 1H), 4.54 (d, J = 10.8 Hz, 1H), 4.49 – 4.43 (m, 3H), 4.37 (dd, J = 13.2, 2.6 Hz, 1H), 4.11 (d, J = 11.6 Hz, 1H), 4.05 – 3.98 (m, 2H), 3.87 (d, J = 8.6 Hz, 1H), 3.70 (d, J = 8.6 Hz, 1H), 3.26 (s, 3H), 1.39 (s, 3H), 1.34 (s, 3H).

The aromatic signals are overlapping with the NMR solvent.

$^{13}\text{C NMR}$ (101 MHz, C_6D_6) δ (ppm) = 160.0, 138.5, 138.0, 134.2, 130.1, 130.0, 128.8, 128.6, 128.2, 128.1, 128.0, 119.0, 114.2, 110.5, 86.3, 82.0, 80.7, 77.4, 77.2, 76.3, 73.1, 72.3, 67.5, 54.8, 27.6, 26.4.

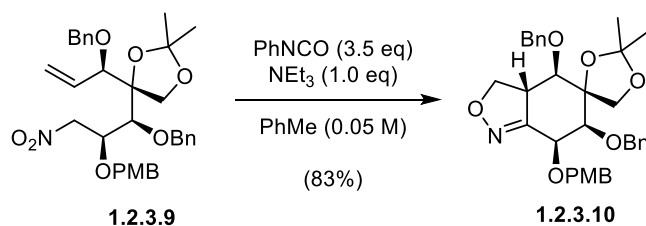
According to the 2D-NMR spectra, one aromatic carbon signal is obscured by the NMR solvent.

HRMS (ESI): calc. for $\text{C}_{33}\text{H}_{43}\text{N}_2\text{O}_8$ $[\text{M} + \text{NH}_4^+]^+$: 595.3014, found: 595.3013.

IR (Diamond-ATR, neat) ν_{max} (cm^{-1}) = 3031 (vw), 2987 (vw), 2935 (vw), 1736 (vw), 1612 (w), 1586 (vw), 1553 (vs), 1513 (m), 1497 (w), 1454 (w), 1420 (vw), 1403 (vw), 1381 (m), 1371 (w), 1302 (w), 1246 (s), 1213 (m), 1173 (m), 1099 (s), 1058 (vs), 1027 (vs), 931 (m), 882 (w), 843 (m), 821 (m), 734 (s), 697 (vs), 657 (w).

$[\alpha]_{\text{D}}^{22} = -14.0^{\circ}$ ($c = 0.759$, CH_2Cl_2).

(3*aR*,4*R*,5*S*,6*S*,7*S*)-4,6-bis(benzyloxy)-7-((4-methoxybenzyl)oxy)-2',2'-dimethyl-3*a*,4,6,7-tetrahydro-3*H*-spiro[benzo[*c*]isoxazole-5,4'-[1,3]dioxolane] (**1.2.3.10**)



Nitro alkene (**1.2.3.9**, 874 mg, 1.51 mmol, 1.0 eq) was dissolved in PhMe (30.2 mL) and PhNCO (576 μ L, 5.30 mmol, 3.5 eq) was added followed by NEt₃ (210 μ L, 1.51 mmol, 1.0 eq). The reaction was stirred for 19 h 30 min and the white precipitate was removed by filtration with subsequent rinsing of the filtercake using PhMe (10 mL). After diluting the filtrate with EtOAc (100 mL), the organic layer was washed with sat. aq. NH₄Cl (40 mL) and sat. aq. NaHCO₃/sat. aq. NaCl (1:1, 40 mL). The solution was dried over Na₂SO₄ and concentrated. Purification via flash column chromatography (petane:EtOAc = 9:1 \rightarrow 4:1) gave (3*aR*,4*R*,5*S*,6*S*,7*S*)-4,6-bis(benzyloxy)-7-((4-methoxybenzyl)oxy)-2',2'-dimethyl-3*a*,4,6,7-tetrahydro-3H-spiro[benzo[*c*]isoxazole-5,4'-[1,3]dioxolane] (**1.2.3.10**, 698 mg, 1.25 mmol, 83%) as a colorless oil.

R_f (pentane:EtOAc = 9:1) = 0.30. (CAM)

¹H NMR (400 MHz, C₆D₆) δ (ppm) = 7.29 (t, *J* = 7.8 Hz, 4H), 7.23 – 7.15 (m, 6H), 7.14 – 7.04 (m, 2H), 6.74 – 6.67 (m, 2H), 4.92 (d, *J* = 8.8 Hz, 1H), 4.68 (d, *J* = 12.0 Hz, 1H), 4.54 (d, *J* = 3.5 Hz, 1H), 4.42 – 4.33 (m, 3H), 4.32 – 4.24 (m, 2H), 4.18 (d, *J* = 11.9 Hz, 1H), 4.04 (dd, *J* = 10.1, 8.5 Hz, 1H), 3.61 (t, *J* = 8.6 Hz, 1H), 3.37 (d, *J* = 3.5 Hz, 1H), 3.27 (s, 3H), 3.23 – 3.07 (m, 2H), 1.58 (s, 3H), 1.51 (s, 3H).

The aromatic signals are overlapping with the NMR solvent.

¹³C NMR (101 MHz, C₆D₆) δ (ppm) = 160.0, 138.5, 138.0, 134.2, 130.1, 130.0, 128.8, 128.6, 128.2, 128.1, 128.0, 119.0, 114.2, 110.5, 86.3, 82.0, 80.7, 77.4, 77.2, 76.3, 73.1, 72.3, 67.5, 54.8, 27.6, 26.4.

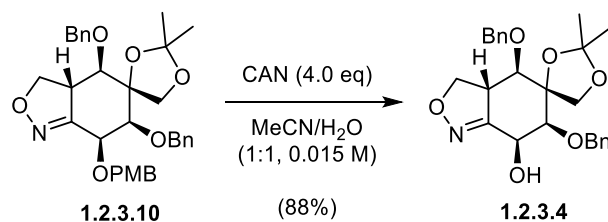
According to the 2D-NMR spectra, two aromatic carbon signals are obscured by the NMR solvent.

HRMS (EI): calc. for C₃₂H₃₄NO₇⁺ [M – CH₃]⁺: 544.2330, found: 544.2331.

IR (Diamond-ATR, neat) ν_{\max} (cm⁻¹) = 2935 (br, vw), 1738 (vw), 1611 (w), 1586 (vw), 1513 (m), 1497 (w), 1454 (w), 1378 (w), 1366 (w), 1302 (w), 1245 (s), 1210 (m), 1174 (m), 1159 (m), 1086 (vs), 1067 (vs), 1027 (vs), 928 (w), 859 (s), 820 (s), 735 (vs), 696 (vs).

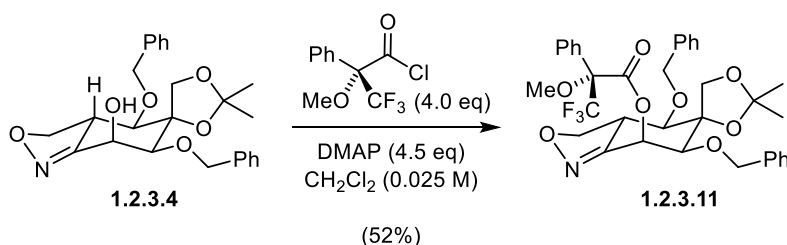
[α]_D²⁰ = +39.6° (c = 1.40, EtOAc).

(3*aR*,4*R*,5*S*,6*S*,7*S*)-4,6-bis(benzyloxy)-2',2'-dimethyl-3*a*,4,6,7-tetrahydro-3H-spiro[benzo[*c*]isoxazole-5,4'-[1,3]dioxolan]-7-ol (**1.2.3.4**)



PMB ether (**1.2.3.10**, 678 mg, 1.13 mmol, 1.0 eq) was dissolved in MeCN/H₂O (4:1, 86.7 mL), cooled to 0 °C and CAN (2.479 g, 4.52 mmol, 4.0 eq) was added in 4 equal portions in 10 min intervals. Thereafter, the reaction was stirred for 3 h 30 min, diluted with CH₂Cl₂ (150 mL) and washed with sat. aq. NaCl (50 mL). The aqueous layer was back-extracted with CH₂Cl₂ (150 mL) and the combined organic layers were dried over Na₂SO₄. Purification via flash column chromatography (pentane:EtOAc = 3:1) afforded (3*aR*,4*R*,5*S*,6*S*,7*S*)-4,6-bis(benzyloxy)-2',2'-dimethyl-3*a*,4,6,7-tetrahydro-3*H*-spiro[benzo[*c*]isoxazole-5,4'-[1,3]dioxolan]-7-ol (**1.2.3.4**, 439 mg, 0.999 mmol, 88%) as a white foam.

(3*aR*,4*R*,5*S*,6*S*,7*S*)-4,6-bis(benzyloxy)-2',2'-dimethyl-3*a*,4,6,7-tetrahydro-3*H*-spiro[benzo[*c*]isoxazole-5,4'-[1,3]dioxolan]-7-yl (*R*)-3,3,3-trifluoro-2-methoxy-2-phenylpropanoate (**1.2.3.11**)



Alcohol (**1.2.3.4**, 7.5 mg, 17 μmol, 1.0 eq) and DMAP (9.1 mg, 75 mmol, 4.5 eq) were dissolved in CH₂Cl₂ (0.66 mL) and (*S*)-α-methoxy-α-(trifluoromethyl)phenylacetyl chloride (15.6 μL, 66.4 mmol, 4.0 eq) was added at rt. The solution stirred for 1 h and concentrated under a stream of N₂. Purification via (3*aR*,4*R*,5*S*,6*S*,7*S*)-4,6-bis(benzyloxy)-2',2'-dimethyl-3*a*,4,6,7-tetrahydro-3*H*-spiro[benzo[*c*]isoxazole-5,4'-[1,3]dioxolan]-7-yl (*R*)-3,3,3-trifluoro-2-methoxy-2-phenylpropanoate (**1.2.3.11**, 5.7 mg, 8.7 μmol, 52%) as a clear colorless oil.

Note: The 16.6:1.0 diastereomeric ratio was determined by ¹⁹F-NMR analysis and corresponds to an 89% enantiopurity of the alcohol **1.2.3.4**.

R_f (pentane:EtOAc = 25:5) = 0.44. (CAM)

$^1\text{H NMR}$ (400 MHz, CD_2Cl_2) δ (ppm) = 7.45 – 7.18 (m, 15H), 6.31 (d, J = 3.6 Hz, 1H), 4.81 (d, J = 11.8 Hz, 1H), 4.73 (d, J = 10.7 Hz, 1H), 4.64 (d, J = 10.7 Hz, 1H), 4.54 (d, J = 11.8 Hz, 1H), 4.42 – 4.35 (m, 1H), 3.79 – 3.73 (m, 1H), 3.70 (d, J = 9.2 Hz, 1H), 3.64 (d, J = 3.6 Hz, 1H), 3.48 (q, J = 1.4 Hz, 3H), 3.40 – 3.31 (m, 3H), 1.37 (s, 3H), 1.24 (s, 3H).

$^{13}\text{C NMR}$ (101 MHz, CD_2Cl_2) δ (ppm) = 165.4, 151.8, 138.5, 137.2, 132.2, 130.2, 129.5, 129.0, 128.9, 128.8, 128.5, 128.4, 127.8, 123.8 (d, J = 288.9 Hz), 110.4, 86.9, 85.0 (q, J = 27.7 Hz), 83.1, 78.9, 75.7, 74.6, 74.5, 66.1, 64.3, 56.2, 51.2, 26.9, 26.5.

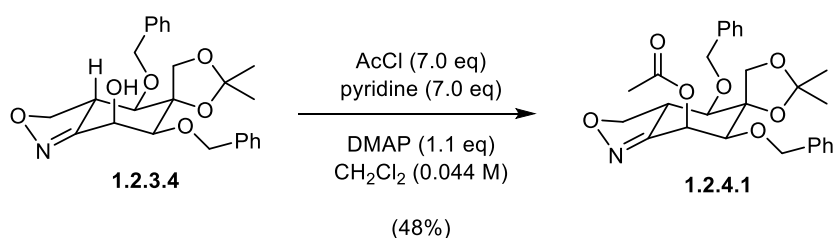
$^{19}\text{F NMR}$ (376 MHz, CD_2Cl_2) δ (ppm) = -71.67, -72.05.

HRMS (ESI): calc. for $\text{C}_{35}\text{H}_{37}\text{F}_3\text{NO}_8^+$ [$\text{M} + \text{H}^+$] $^+$: 656.2466, found: 656.2459.

IR (Diamond-ATR, neat) ν_{max} (cm^{-1}) = 2920 (vw), 2851 (vw), 1758 (m), 1633 (vw), 1498 (vw), 1454 (w), 1380 (w), 1369 (w), 1242 (s), 1216 (m) 1168 (vs), 1072 (vs), 1015 (vs), 989 (s), 918 (w), 864 (vs), 764 (m), 736 (s).

$[\alpha]_{\text{D}}^{20} = +73^\circ$ ($c = 0.71$, EtOAc).

(3*aR*,4*R*,5*S*,6*S*,7*S*)-4,6-bis(benzyloxy)-2',2'-dimethyl-3*a*,4,6,7-tetrahydro-3*H*-spiro[benzo[*c*]isoxazole-5,4'-[1,3]dioxolan]-7-yl acetate (1.2.4.1)



Alcohol (**1.2.3.4**, 25.8 mg, 58.7 μmol , 1.0 eq) and DMAP (7.9 mg, 64.6 μmol , 1.1 eq) were dissolved in CH_2Cl_2 (0.29 mL) and a solution of AcCl (8.4 μL , 0.117 mmol, 2.0 eq) and pyridine (9.5 μL , 0.177 mmol, 2.0 eq) in CH_2Cl_2 (0.30 mL) was added at 0 °C. The solution was allowed to warm to rt and additional portion of AcCl (4.2 μL , 58.7 μmol , 1.0 eq) and pyridine (4.7 μL , 58.7 μmol , 1.0 eq) in CH_2Cl_2 (0.15 mL) was added after stirring for a total of 70 min, 3 h 30 min, 4 h 30 min, 5 h 30 min and 6 h 15 min. After a total reaction time of 6 (3*aR*,4*R*,5*S*,6*S*,7*S*)-4,6-bis(benzyloxy)-2',2'-dimethyl-3*a*,4,6,7-tetrahydro-3*H*-spiro[benzo[*c*]isoxazole-5,4'-[1,3]dioxolan]-7-yl acetate (**1.2.4.1**, 13.6 mg, 28.2 μmol , 48%) as a clear foam.

R_f (pentane:EtOAc = 4:1) = 0.34. (CAM)

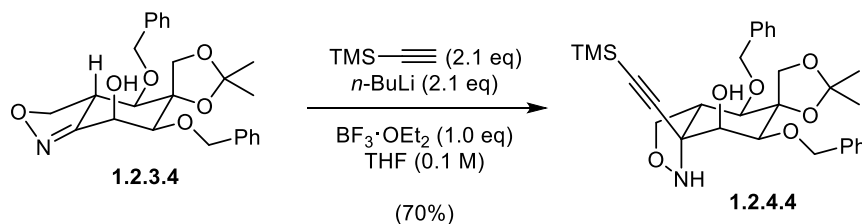
$^1\text{H NMR}$ (800 MHz, C_6D_6) δ (ppm) = 7.37 (d, J = 7.6 Hz, 2H), 7.26 (d, J = 7.5 Hz, 2H), 7.19 (td, J = 7.6, 5.3 Hz, 4H), 7.12 – 7.07 (m, 2H), 6.48 (d, J = 3.6 Hz, 1H), 4.66 (d, J = 11.9 Hz, 1H), 4.57 (d, J = 10.9 Hz, 1H), 4.47 (d, J = 8.6 Hz, 1H), 4.34 (d, J = 10.9 Hz, 1H), 4.28 – 4.21 (m, 2H), 4.00 (dd, J = 10.5, 8.6 Hz, 1H), 3.64 (t, J = 8.5 Hz, 1H), 3.36 (d, J = 3.7 Hz, 1H), 3.12 (d, J = 10.6 Hz, 1H), 3.06 (td, J = 10.5, 8.6 Hz, 1H), 1.50 (s, 3H), 1.50 (s, 3H), 1.48 (s, 3H).

$^{13}\text{C NMR}$ (201 MHz, C_6D_6) δ (ppm) = 168.4, 151.9 138.6, 137.6, 128.8, 128.7, 128.7, 128.2, 127.7, 110.4, 87.2, 83.2, 78.9, 75.1 73.7, 73.2, 64.9, 63.4, 51.1, 27.1, 26.9, 20.1.

According to the 2D spectra, one carbon signal is obscured by the NMR solvent.

HRMS (EI): calc. for $\text{C}_{27}\text{H}_{31}\text{NO}_7^+$ $[M]^+$: 481.2095, found: 481.2091.

(3a*R*,4*R*,5*S*,6*S*,7*S*,7a*S*)-4,6-bis(benzyloxy)-2',2'-dimethyl-7a-((trimethylsilyl)ethynyl)hexahydro-3*H*-spiro[benzo[*c*]isoxazole-5,4'-[1,3]dioxolan]-7-ol
(1.2.4.4)



A stock solution (5×) of lithium TMS-acetylene was prepared by dissolving TMS-acetylene (163 μL , 1.16 mmol, 10.5 eq) in THF (1.16 mL), cooling to $-78\text{ }^\circ\text{C}$ and adding *n*-BuLi (2.48 M in THF, 0.472 mL, 1.16 mmol, 10.5 eq). The mixture was stirred at $-78\text{ }^\circ\text{C}$ for 15 min. In a separate flask, isoxazoline (**1.2.3.4**, 50.4 mg, 0.110 mmol, 1.0 eq) was dissolved in THF (0.55 mL) and cooled to $-78\text{ }^\circ\text{C}$. $\text{BF}_3\cdot\text{OEt}_2$ (46.5% in Et_2O , 29.1 μL , 0.110 mmol, 1.0 eq) in THF (0.55 mL) was added followed by the lithium TMS-acetylene stock solution (0.36 mL). The reaction was stirred for 2 h 20 min and PB pH7 was added followed by sat. aq. NaHCO_3 /sat. aq. NaCl (1:1, 5.0 mL). After warming to rt, the mixture was extracted with EtOAc (2 × 35 mL), the combined organic layers were dried over Na_2SO_4 and concentrated. Purification via flash column chromatography (pentane:EtOAc = 4:1) afforded (3a*R*,4*R*,5*S*,6*S*,7*S*,7a*S*)-4,6-bis(benzyloxy)-2',2'-dimethyl-7a-((trimethylsilyl)ethynyl)hexahydro-3*H*-spiro[benzo[*c*]isoxazole-5,4'-[1,3]dioxolan]-7-ol (**1.2.4.4**, 41.4 mg, 77.0 μmol , 70%) as a white foam.

R_f (pentane:EtOAc = 7:3) = 0.35. (CAM)

$^1\text{H NMR}$ (400 MHz, C_6D_6) δ (ppm) = 7.36 (d, J = 7.2 Hz, 2H), 7.33 (d, J = 7.3 Hz, 2H), 7.25 – 7.06 (m, 6H), 5.47 (br s, 1H), 4.95 (d, J = 11.8 Hz, 1H), 4.68 (d, J = 11.8 Hz, 1H), 4.61 (d, J = 11.6 Hz, 1H), 4.56 (d, J = 9.0 Hz, 1H), 4.42 (d, J = 11.6 Hz, 1H), 4.30 (d, J = 9.0 Hz, 1H), 4.21 (s, 1H), 3.97 (d, J = 3.4 Hz, 1H), 3.93 (dd, J = 7.7, 4.0 Hz, 1H), 3.75 (t, J = 7.7 Hz, 1H), 3.58 (d, J = 7.1 Hz, 1H), 2.90 (s, 1H), 2.77 (td, J = 7.3, 4.2 Hz, 1H), 1.36 (s, 3H), 1.33 (s, 3H), 0.03 (s, 9H).

The aromatic signals are overlapping with the NMR solvent.

$^{13}\text{C NMR}$ (101 MHz, C_6D_6) δ (ppm) = 139.5, 138.9, 128.6, 128.5, 127.7, 127.5, 110.0, 104.3, 91.1, 85.9, 81.7, 78.9, 75.2, 74.5, 73.8, 70.3, 67.6, 65.0, 53.5, 26.8, 26.6, -0.2.

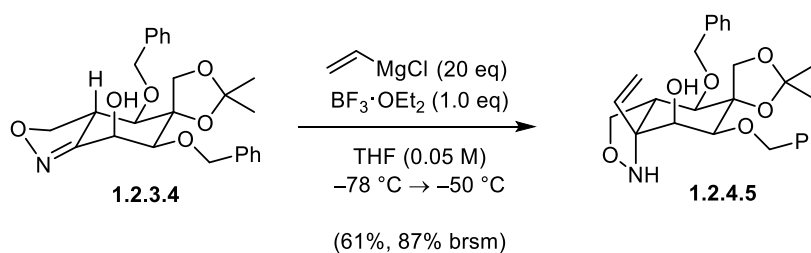
According to the 2D spectra, one carbon signal is obscured by the NMR solvent.

HRMS (EI): calc. for $\text{C}_{30}\text{H}_{39}\text{NO}_6\text{Si}_1^+$ [M] $^+$: 537.2541, found 537.2522.

IR (Diamond-ATR, neat) ν_{max} (cm^{-1}) = 2955 (w), 2924 (w), 2171 (vw), 1602 (vw), 1497 (vw), 1454 (w), 1406 (vw), 1380 (w), 1370 (w), 1249 (m), 1208 (m), 1071 (s), 1050 (s), 1028 (m), 918 (w), 842 (vs), 758 (m), 731 (s), 696 (vs), 677 (m).

$[\alpha]_{\text{D}}^{20}$ = +41.6° (c = 3.37, EtOAc).

(3a*R*,4*R*,5*S*,6*S*,7*S*,7a*R*)-4,6-bis(benzyloxy)-2',2'-dimethyl-7a-vinylhexahydro-3*H*-spiro[benzo[*c*]isoxazole-5,4'-[1,3]dioxolan]-7-ol (1.2.4.5)



Isoxazoline (**1.2.3.4**, 94.5 mg, 0.215 mmol, 1.0 eq) was dissolved in THF (4.3 mL) and cooled to -78 °C. $\text{BF}_3 \cdot \text{OEt}_2$ (46.5% in Et_2O , 56.9 μL , 0.215 mmol, 1.0 eq) and vinylmagnesium chloride (1.6 M in THF, 2.69 mL, 4.30 mmol, 20 eq) were sequentially added dropwise over 8 min. The solution was stirred for 60 min at -78 °C and allowed to warm to -50 °C over a period of 2 h 50 min. Sat. aq. NaHCO_3 (5.0 mL) was added, before warming the reaction to rt and diluting with sat. aq. NaHCO_3 /sat. aq. NaCl (1:1, 20 mL). The mixture was extracted with EtOAc (2 × 70 mL), the combined organic layers were dried over Na_2SO_4 and the solvent was removed *in vacuo*.

Purification via flash column chromatography (pentane:EtOAc = 13:7) afforded (3*aR*,4*R*,5*S*,6*S*,7*S*,7*aR*)-4,6-bis(benzyloxy)-2',2'-dimethyl-7*a*-vinylhexahydro-3*H*-spiro[benzo[*c*]isoxazole-5,4'-[1,3]dioxolan]-7-ol (**1.2.4.5**, 61.2 mg, 0.131 mmol, 61%) as a colorless oil along with recovered **1.2.3.4** (28.4 mg, 64.6 μ mol, 30%).

R_f (pentane:EtOAc = 13:7) = 0.15. (CAM)

$^1\text{H NMR}$ (800 MHz, C_6D_6) δ (ppm) = 7.28 (d, J = 7.1 Hz, 2H), 7.25 (d, J = 7.4 Hz, 2H), 7.18 (t, J = 7.7 Hz, 2H), 7.14 (t, J = 7.6 Hz, 2H), 7.12 – 7.08 (m, 2H), 6.55 – 6.46 (m, 1H), 5.00 (br s, 2H), 4.91 (d, J = 11.3 Hz, 1H), 4.56 (d, J = 11.7 Hz, 1H), 4.42 – 4.37 (m, 2H), 4.36 (d, J = 9.3 Hz, 1H), 4.30 (br s, 1H), 4.20 (d, J = 9.3 Hz, 1H), 4.07 (t, J = 7.0 Hz, 1H), 3.99 (s, 1H), 3.73 (dd, J = 9.5, 7.2 Hz, 1H), 3.55 (d, J = 4.3 Hz, 1H), 2.43 (ddd, J = 10.1, 6.7, 4.3 Hz, 1H), 1.33 (s, 3H), 1.27 (s, 3H).

$^{13}\text{C NMR}$ (201 MHz, C_6D_6) δ (ppm) = 139.5, 138.7, 137.9, 128.6, 128.5, 128.4, 127.7, 127.5, 114.8, 110.4, 85.0, 82.0, 79.5, 75.2, 73.3, 72.2, 70.0, 69.7, 69.3, 50.8, 27.0, 26.7.

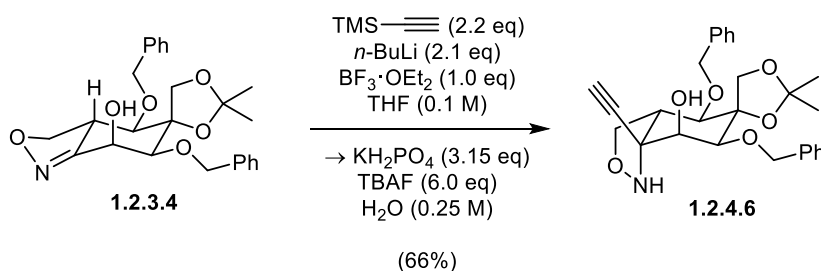
According to the 2D spectra, one aromatic carbon signal is obscured by the NMR solvent.

HRMS (ESI): calc. for $\text{C}_{27}\text{H}_{34}\text{NO}_6^+$ [$\text{M} + \text{H}^+$] $^+$: 468.2381, found: 468.2387.

IR (Diamond-ATR, neat) ν_{max} (cm^{-1}) = 3445 (br, vw), 3063 (vw), 3029 (vw), 2985 (vw), 2877 (vw), 1636 (vw), 1604 (vw), 1496 (w), 1453 (w), 1381 (w), 1370 (w), 1346 (w), 1255 (w), 1212 (m), 1126 (m), 1089 (s), 1054 (vs), 1028 (s), 968 (w), 917 (m), 852 (s), 798 (w), 730 (vs), 695 (vs).

$[\alpha]_{\text{D}}^{20} = -5.80^\circ$ (c = 1.31, EtOAc).

(3*aR*,4*R*,5*S*,6*S*,7*S*,7*aS*)-4,6-bis(benzyloxy)-7*a*-ethynyl-2',2'-dimethylhexahydro-3*H*-spiro[benzo[*c*]isoxazole-5,4'-[1,3]dioxolan]-7-ol (**1.2.4.6**)



A stock solution (2 \times) of lithium TMS-acetylene was prepared by dissolving TMS-acetylene (142 μ L, 1.00 mmol, 4.4 eq) in THF (1.0 mL), cooling to -78°C and adding $n\text{-BuLi}$ (2.42 M in THF, 0.396 mL, 0.958 mmol, 4.2 eq). The mixture was stirred at -78°C for 30 min. In a separate flask, isoxazoline (**1.2.3.4**, 100 mg, 0.228 mmol, 1.0 eq) was dissolved in THF (1.14 mL) and

cooled to $-78\text{ }^{\circ}\text{C}$. $\text{BF}_3\cdot\text{OEt}_2$ (46.5% in Et_2O , 60 μL , 0.228 mmol, 1.0 eq) was added followed by the lithium TMS-acetylene stock solution (0.77 mL). The reaction was stirred for 2 h 25 min before KH_2PO_4 (98.3 mg, 0.718 mmol, 3.15 eq) in H_2O (0.91 mL) and TBAF (1 M in THF, 1.37 mL, 1.37 mmol, 6.0 eq) were sequentially added. After warming to rt, the mixture was stirred for 1 h 15 min and sat. aq. CaCl_2 (1.0 mL) was added. The suspension was poured into sat. aq. NaHCO_3 /sat. aq. NaCl (1:1, 20 mL), extracted with EtOAc ($2 \times 60\text{ mL}$) and the combined organic layers were dried over Na_2SO_4 . Removal of the solution *in vacuo* was then followed by purification via flash column chromatography (pentane: EtOAc = 3:1 \rightarrow 7:3) to give (3a*R*,4*R*,5*S*,6*S*,7*S*,7a*S*)-4,6-bis(benzyloxy)-7a-ethynyl-2',2'-dimethylhexahydro-3H-spiro[benzo[*c*]isoxazole-5,4'-[1,3]dioxolan]-7-ol (**1.2.4.6**, 70.1 mg, 0.151 mmol, 66%) as a colorless gum.

R_f (pentane: EtOAc = 7:3) = 0.11. (CAM)

$^1\text{H NMR}$ (400 MHz, C_6D_6) δ (ppm) = 7.32 (t, J = 7.8 Hz, 4H), 7.20 (d, J = 7.1 Hz, 2H), 7.15 – 7.06 (m, 2H), 5.37 (br s, 1H), 4.86 (d, J = 11.8 Hz, 1H), 4.63 (m, 2H), 4.50 (d, J = 9.1 Hz, 1H), 4.41 (d, J = 11.7 Hz, 1H), 4.28 (d, J = 9.1 Hz, 1H), 4.10 (t, J = 3.7 Hz, 1H), 3.95 (d, J = 3.1 Hz, 1H), 3.90 (dd, J = 7.8, 4.0 Hz, 1H), 3.73 (t, J = 7.5 Hz, 1H), 3.59 (d, J = 7.3 Hz, 1H), 2.66 (td, J = 7.2, 3.9 Hz, 1H), 2.58 (d, J = 4.6 Hz, 1H), 1.86 (s, 1H), 1.36 (s, 3H), 1.33 (s, 3H).

The aromatic signals are overlapping with the NMR solvent.

$^{13}\text{C NMR}$ (101 MHz, C_6D_6) δ (ppm) = 139.3, 138.9, 128.6, 128.5, 127.7, 127.7, 127.6, 109.9, 85.8, 82.6, 81.1, 79.0, 75.1, 74.7, 74.6, 73.3, 70.4, 67.4, 64.2, 53.2, 26.7, 26.6.

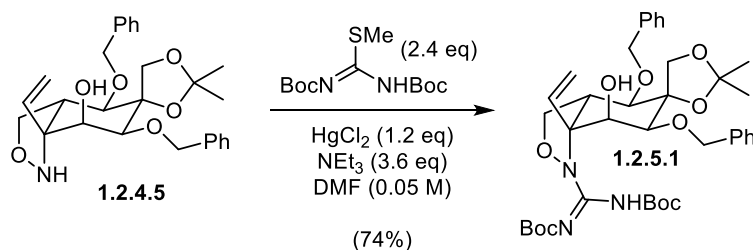
According to the 2D spectra, one carbon signal is obscured by the NMR solvent.

HRMS (ESI): calc. for $\text{C}_{27}\text{H}_{32}\text{NO}_6^+$ [$\text{M} + \text{H}^+$] $^+$: 466.2224, found 466.2224.

IR (Diamond-ATR, neat) ν_{max} (cm^{-1}) = 3440 (br, vw), 3278 (br, vw), 2926 (w), 1603 (vw), 1497 (vw), 1454 (w), 1380 (w), 1369 (w), 1258 (m), 1206 (m), 1156 (m), 1068 (vs), 1045 (vs), 1028 (vs), 917 (w), 853 (m), 819 (m), 732 (vs), 695 (vs).

$[\alpha]_{\text{D}}^{20} = +40.6^{\circ}$ (c = 0.920, EtOAc).

tert-butyl ((*E*)-((3a*R*,4*R*,5*S*,6*S*,7*S*,7a*R*)-4,6-bis(benzyloxy)-7-hydroxy-2',2'-dimethyl-7a-vinyltetrahydro-3H-spiro[benzo[*c*]isoxazole-5,4'-[1,3]dioxolan]-1(4H)-yl))(*tert*-butoxycarbonyl)amino)methylene)carbamate (**1.2.5.1**)



A stock solution (2.5 \times) was prepared by dissolving 1,3-bis(*tert*-butoxycarbonyl)-2-methyl-2-thiopseudourea (182 mg, 626 μmol , 6.0 eq) and HgCl_2 (84.8 mg, 312 μmol , 3.0 eq) in DMF (4.0 mL), adding NEt_3 (130 μL , 933 μmol , 9.0 eq) and stirring the resulting suspension for 20 min at rt. In a separate flask, isoxazolidine (**1.2.4.5**, 48.7 mg, 104 μmol , 1.0 eq) was dissolved in DMF (0.4 mL) and the stock solution (1.65 mL) was added dropwise over 6 min through a syringe filter (Chromafil® Xtra GF45/25 pore size 0.45 μm). The solution was stirred for 40 min rt, diluted with Et_2O (35 mL) and washed with H_2O (10 mL) and sat. aq. NaCl (2 \times 10 mL). The combined aq. layers were extracted with CH_2Cl_2 (40 mL) and the organic layers were combined, dried over Na_2SO_4 and concentrated. Purification via flash column chromatography (pentane:EtOAc = 14:1 \rightarrow 9:1) afforded *tert*-butyl ((*E*)-((3*aR*,4*R*,5*S*,6*S*,7*S*,7*aR*)-4,6-bis(benzyloxy)-7-hydroxy-2',2'-dimethyl-7*a*-vinyltetrahydro-3*H*-spiro[benzo[*c*]isoxazole-5,4'-[1,3]dioxolan]-1(4*H*)-yl)((*tert*-butoxycarbonyl)amino)methylene)carbamate (**1.2.5.1**, 54.7 mg, 77.1 μmol , 74%) as a white foam.

R_f (pentane:EtOAc = 9:1) = 0.56. (CAM)

$^1\text{H NMR}$ (800 MHz, C_6D_6) δ (ppm) = 10.69 (s, 1H), 7.37 (s, 1H), 7.30 (d, J = 8.2 Hz, 4H), 7.19 – 7.16 (m, 2H), 7.13 (t, J = 7.6 Hz, 2H), 7.12 – 7.10 (m, 1H), 7.09 – 7.06 (m, 1H), 6.35 (dd, J = 17.3, 10.8 Hz, 1H), 5.65 (d, J = 17.4 Hz, 1H), 5.14 (d, J = 10.9 Hz, 1H), 5.11 (d, J = 11.3 Hz, 1H), 5.06 (d, J = 10.8 Hz, 1H), 4.82 (d, J = 11.3 Hz, 1H), 4.61 (t, J = 2.0 Hz, 1H), 4.59 (d, J = 9.2 Hz, 1H), 4.36 (d, J = 10.8 Hz, 1H), 4.25 (d, J = 9.2 Hz, 1H), 4.13 (d, J = 1.5 Hz, 1H), 4.03 (d, J = 8.2 Hz, 1H), 3.93 – 3.90 (m, 2H), 2.53 (dd, J = 12.3, 4.3 Hz, 1H), 1.40 (s, 9H), 1.39 (s, 3H), 1.29 (s, 9H), 1.08 (s, 3H).

$^{13}\text{C NMR}$ (201 MHz, C_6D_6) δ (ppm) = 162.1, 150.5, 149.9, 138.8, 138.3, 135.9, 129.2, 128.7, 128.6, 128.4, 128.3, 116.1, 109.4, 85.6, 84.9, 81.8, 79.4, 79.1, 76.1, 75.8, 75.4, 72.5, 68.2, 66.4, 51.8, 28.2, 27.9, 27.0, 24.9.

According to the 2D spectra, one aromatic carbon signal is obscured by the NMR solvent.

HRMS (ESI): calc. for $\text{C}_{38}\text{H}_{50}\text{N}_3\text{O}_{10}^-$ [$\text{M} - \text{H}^+$]: 708.3502, found: 708.3510.

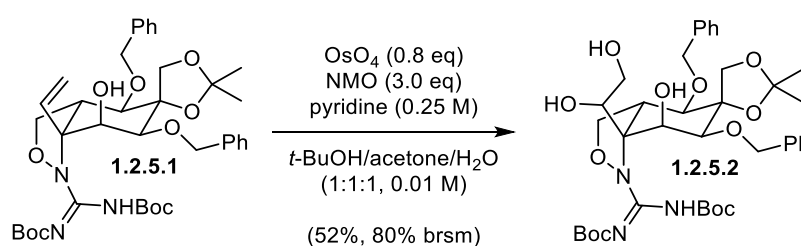
IR (Diamond-ATR, neat) ν_{max} (cm^{-1}) = 3214 (br, vw), 2979 (vw), 2930 (vw), 1752 (m), 1645 (m), 1599 (m), 1498 (w), 1454 (w), 1392 (w), 1368 (m), 1352 (w), 1292 (m), 1252 (m), 1229 (m), 1208

(m), 1134 (vs), 1042 (s), 1012 (s), 965 (m), 928 (m), 884 (vw), 850 (m), 823 (w), 791 (w), 769 (w), 736 (m), 698 (s).

$[\alpha]_{\text{D}}^{20} = +59.4^{\circ}$ ($c = 1.25$, EtOAc).

$m_p = 61.2 - 66.5^{\circ}\text{C}$.

tert-butyl ((*E*)-((3*aR*,4*R*,5*S*,6*S*,7*S*,7*aS*)-4,6-bis(benzyloxy)-7*a*-(1,2-dihydroxyethyl)-7-hydroxy-2',2'-dimethyltetrahydro-3*H*-spiro[benzo[*c*]isoxazole-5,4'-[1,3]dioxolan]-1(4*H*)-yl)((*tert*-butoxycarbonyl)amino)methylene)carbamate (1.2.5.2)



Alkene (**1.2.5.1**, 15.0 mg, 21.1 μmol , 1.0 eq.) and NMO (7.4 g, 63 μmol , 3.0 eq.) were dissolved in *t*-BuOH/acetone/ H_2O (1:1:1, 2.1 mL) and pyridine (85 μL) was added followed by OsO_4 (4% in H_2O , 107 μL , 16.9 μmol , 0.8 eq.) at rt. After stirring for 23 h, sat. aq. NaHSO_3 (4.0 mL) was added followed by pouring the mixture into sat. aq. NaCl (5.0 mL) and extracting with EtOAc (2 \times 35 mL). The combined organic layers were dried over Na_2SO_4 and the solvent was removed *in vacuo*. Purification via flash column chromatography (pentane:EtOAc = 9:1 \rightarrow 13:7 \rightarrow 6:4 \rightarrow 1:1) afforded a single diastereomer of *tert*-butyl ((*E*)-((3*aR*,4*R*,5*S*,6*S*,7*S*,7*aS*)-4,6-bis(benzyloxy)-7*a*-(1,2-dihydroxyethyl)-7-hydroxy-2',2'-dimethyltetrahydro-3*H*-spiro[benzo[*c*]isoxazole-5,4'-[1,3]dioxolan]-1(4*H*)-yl)((*tert*-butoxycarbonyl)amino)methylene)carbamate (**1.2.5.2**, 7.9 mg, 11 μmol , 52%) as a yellow oil along with recovered **1.2.5.1** (5.3 mg, 7.5 μmol , 35%).

R_f (pentane:EtOAc = 1:1) = 0.22. (CAM)

t_R (reverse-phase semi-preparative HPLC, MeCN: H_2O = 41:59 \rightarrow 95:5 over 54 min) = 40.03 min.

$^1\text{H NMR}$ (800 MHz, CD_2Cl_2) δ (ppm) = 7.40 – 7.26 (m, 10H), 6.22 (s, 1H), 5.01 (d, $J = 11.6$ Hz, 1H), 4.80 (d, $J = 11.4$ Hz, 1H), 4.68 (d, $J = 11.5$ Hz, 1H), 4.63 (d, $J = 11.7$ Hz, 1H), 4.41 (br s, 1H), 4.25 (d, $J = 9.4$ Hz, 1H), 4.12 (br s, 1H), 4.07 (d, $J = 9.3$ Hz, 1H), 3.86 – 3.81 (m, 2H), 3.76 (dd, $J = 11.7$, 5.8 Hz, 1H), 3.73 (d, $J = 8.0$ Hz, 1H), 3.68 (dd, $J = 11.4$, 5.4 Hz, 1H), 3.62 (d, $J = 9.4$ Hz, 1H), 2.68 (br s, 1H), 1.43 (s, 18H), 1.42 (s, 3H), 1.41 (s, 3H).

^{13}C NMR (201 MHz, C_6D_6) δ (ppm) = 153.5, 153.1, 139.0, 138.4, 129.0, 128.9, 128.7, 128.6, 128.2, 128.1, 109.6, 109.1, 85.9, 81.3, 81.1, 81.0, 80.9, 79.6, 76.8, 75.1, 74.6, 74.0, 73.3, 65.6, 60.5, 49.0, 28.5, 26.9, 26.4.

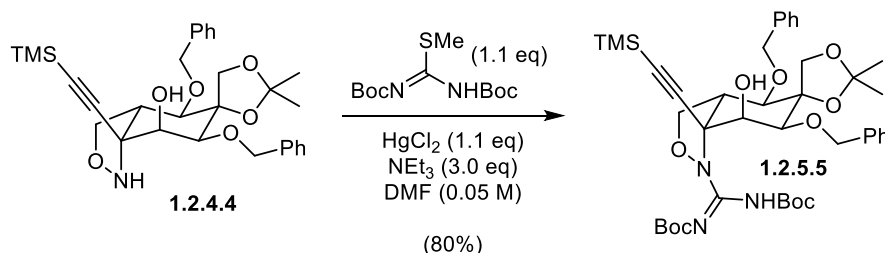
HRMS (ESI): calc. for $\text{C}_{38}\text{H}_{52}\text{N}_3\text{O}_{12}^-$ [$\text{M} - \text{H}^+$]: 742.3556, found: 742.3553.

IR (Diamond-ATR, neat) ν_{max} (cm^{-1}) = 3428 (br, vw), 2977 (vw), 2928 (vw), 1718 (m), 1455 (m), 1392 (w), 1367 (m), 1243 (m), 1205 (w), 1151 (s), 1049 (vs), 1027 (vs), 928 (w), 862 (m), 799 (m), 735 (s), 697 (s).

$[\alpha]_{\text{D}}^{20} = +60.5^\circ$ ($c = 0.800$, EtOAc).

$m_p = 98.7 - 102.5^\circ\text{C}$.

tert-butyl ((*E*)-((3*aR*,4*R*,5*S*,6*S*,7*S*,7*aS*)-4,6-bis(benzyloxy)-7-hydroxy-2',2'-dimethyl-7*a*-((trimethylsilyl)ethynyl)tetrahydro-3*H*-spiro[benzo[*c*]isoxazole-5,4'-[1,3]dioxolan]-1(4*H*)-yl)((*tert*-butoxycarbonyl)amino)methylene)carbamate (1.2.5.5)



Isioxazolidine (**1.2.4.4**, 20.0 mg, 37.2 μmol , 1.0 eq) and 1,3-bis(*tert*-butoxycarbonyl)-2-methyl-2-thiopseudourea (11.9 mg, 40.9 μmol , 1.1 eq) were dissolved in DMF (0.2 mL) and NEt_3 (15.6 μL , 112 μmol , 3.0 eq) in DMF (0.54 mL) was added followed by HgCl_2 (11.1 mg, 40.9 μmol , 1.1 eq). After stirring the resulting suspension for 40 min at rt, the solid was removed by filtration through celite and rinsing of the filtercake with CH_2Cl_2 (10 mL). The solvent was removed *in vacuo* and the residue was purified via flash column chromatography (pentane:EtOAc = 14:1 \rightarrow 9:1) to give *tert*-butyl ((*E*)-((3*aR*,4*R*,5*S*,6*S*,7*S*,7*aS*)-4,6-bis(benzyloxy)-7-hydroxy-2',2'-dimethyl-7*a*-((trimethylsilyl)ethynyl)tetrahydro-3*H*-spiro[benzo[*c*]isoxazole-5,4'-[1,3]dioxolan]-1(4*H*)-yl)((*tert*-butoxycarbonyl)amino)methylene)carbamate (**1.2.5.5**, 23.1 mg, 29.6 μmol , 80%) as a white solid.

R_f (pentane:EtOAc = 9:1) = 0.46. (UV, CAM)

$^1\text{H NMR}$ (400 MHz, CD_2Cl_2) δ (ppm) = 8.89 (s, 1H), 7.46 – 7.23 (m, 10H), 6.58 (s, 1H), 5.17 (d, J = 12.0 Hz, 1H), 4.99 (d, J = 10.8 Hz, 1H), 4.75 (d, J = 12.0 Hz, 1H), 4.48 (d, J = 10.9 Hz, 1H), 4.38 (d, J = 9.4 Hz, 1H), 4.28 (dd, J = 8.2, 5.0 Hz, 1H), 4.18 (s, 1H), 4.12 (dd, J = 8.2, 1.3 Hz, 1H), 4.11 – 4.06 (m, 1H), 3.82 (d, J = 1.1 Hz, 1H), 3.72 (d, J = 12.2 Hz, 1H), 3.26 (ddd, J = 12.3, 5.0, 1.3 Hz, 1H), 1.49 (s, 9H), 1.48 (s, 9H), 1.45 (s, 3H), 1.18 (s, 3H), 0.03 (s, 9H).

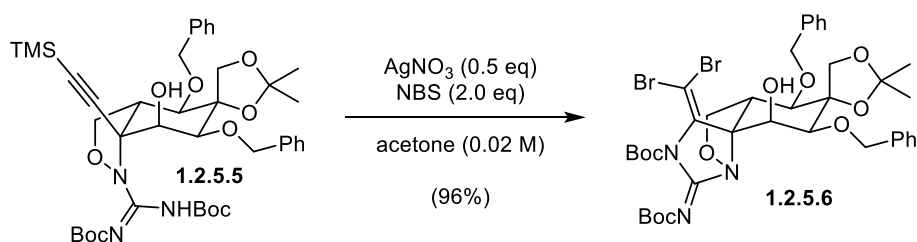
$^{13}\text{C NMR}$ (101 MHz, CD_2Cl_2) δ (ppm) = 159.8, 150.7, 149.7, 139.1, 138.7, 128.9, 128.5, 128.5, 128.4, 127.9, 109.9, 101.5, 92.0, 85.4, 83.7, 82.9, 80.0, 79.6, 76.2, 75.3, 73.1, 70.7, 68.0, 66.6, 54.1, 28.4, 28.2, 27.1, 25.0, -0.1.

HRMS (ESI): calc. for $\text{C}_{41}\text{H}_{58}\text{N}_3\text{O}_{10}\text{Si}_1^+$ $[\text{M} + \text{H}]^+$: 780.3886, found 780.3890.

IR (Diamond-ATR, neat) ν_{max} (cm^{-1}) = 3260 (br, vw), 2981 (vw), 1761 (w), 1697 (vw), 1651 (w) 1597 (m), 1498 (w), 1454 (w), 1393 (w), 1368 (m), 1293 (m), 1250 (m), 1228 (m), 1209 (m), 1134 (vs), 1091 (s), 1063 (s), 1013 (s), 967 (w), 927 (w), 844 (vs), 798 (w), 760 (m), 732 (s), 698 (s), 667 (w).

$[\alpha]_{\text{D}}^{20} = +57.8^\circ$ ($c = 1.60$, EtOAc).

tert-butyl (6*aR*,7*R*,8*S*,9*S*,10*S*,10*aS*,*Z*)-7,9-bis(benzyloxy)-3-((*tert*-butoxycarbonyl)imino)-1-(dibromomethylene)-10-hydroxy-2',2'-dimethyltetrahydro-1*H*,6*H*-spiro[benzo[*c*]imidazo[1,5-*b*]isoxazole-8,4'-[1,3]dioxolane]-2(3*H*)-carboxylate (1.2.5.6)



Guanidine (**1.2.5.5**, 5.0 mg, 6.4 μmol , 1.0 eq), NBS (2.3 mg, 13 mmol, 1.2 eq) and AgNO_3 (0.4 mg, 3 μmol , 0.5 eq) were dissolved in acetone (0.32 mL) and stirred at rt for 75 min. Sat. aq. NaHCO_3 /sat. aq. NaCl (1:1, 5.0 mL) was added and the mixture was extracted with CH_2Cl_2 (2×15 mL). The organic layer was dried over Na_2SO_4 and concentrated. Purification via flash column chromatography (pentane:EtOAc = 17:3 \rightarrow 4:1) afforded *tert*-butyl (6*aR*,7*R*,8*S*,9*S*,10*S*,10*aS*,*Z*)-7,9-bis(benzyloxy)-3-((*tert*-butoxycarbonyl)imino)-1-(dibromomethylene)-10-hydroxy-2',2'-dimethyltetrahydro-1*H*,6*H*-spiro[benzo[*c*]imidazo[1,5-

b]isoxazole-8,4'-[1,3]dioxolane]-2(3H)-carboxylate (**1.2.5.6**, 5.3 mg, 6.1 μmol , 96%) as a white solid.

R_f (pentane:EtOAc 4:1) = 0.32. (UV, CAM)

$^1\text{H NMR}$ (400 MHz, CD_2Cl_2) δ (ppm) = 7.39 – 7.28 (m, 10H), 5.03 (d, J = 11.8 Hz, 1H), 4.86 (d, J = 11.4 Hz, 1H), 4.67 (d, J = 11.9 Hz, 1H), 4.62 (d, J = 11.4 Hz, 1H), 4.42 (d, J = 9.3 Hz, 1H), 4.19 (d, J = 9.2 Hz, 1H), 4.01 (t, J = 2.9 Hz, 1H), 3.73 (d, J = 3.3 Hz, 1H), 3.68 – 3.63 (m, 2H), 3.60 (dd, J = 9.4, 2.2 Hz, 1H), 3.49 (d, J = 9.0 Hz, 1H), 2.66 (d, J = 2.6 Hz, 1H), 1.55 (s, 3H), 1.50 (s, 9H), 1.49 (s, 3H), 1.46 (s, 9H).

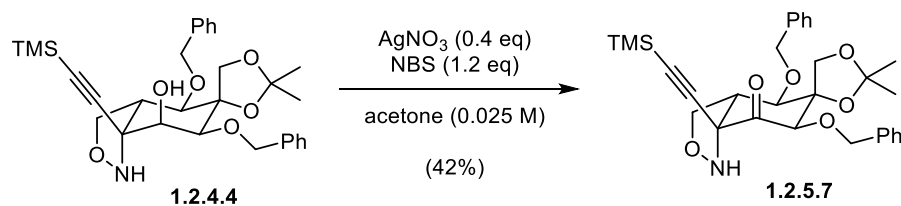
$^{13}\text{C NMR}$ (101 MHz, CD_2Cl_2) δ (ppm) = 157.6, 150.9, 147.1, 138.7, 138.2, 136.9, 129.1, 128.6, 128.6, 128.5, 128.5, 109.8, 86.1, 85.6, 81.8, 80.1, 78.2, 77.0, 75.1, 74.8, 74.3, 72.6, 65.3, 47.8, 28.3, 28.1, 26.9, 26.3.

HRMS (ESI): calc. for $\text{C}_{38}\text{H}_{48}\text{Br}_2\text{N}_3\text{O}_{10}^+$ $[\text{M} + \text{H}]^+$: 864.1701, found 864.1713.

IR (Diamond-ATR, neat) ν_{max} (cm^{-1}) = 3415 (br, vw), 2963 (vw), 2928 (vw), 1759 (w), 1705 (m), 1497 (vw), 1455 (w), 1394 (vw), 1368 (m), 1257 (s), 1206 (w), 1135 (vs), 1101 (vs), 1064 (vs), 1028 (s), 916 (m), 853 (m), 799 (s), 736 (s), 698 (s).

$[\alpha]_{\text{D}}^{20} = +32^\circ$ ($c = 0.66$, EtOAc).

(3*aR*,4*R*,5*S*,6*R*,7*aS*)-4,6-bis(benzyloxy)-2',2'-dimethyl-7a-((trimethylsilyl)ethynyl)tetrahydro-3H-spiro[benzo[*c*]isoxazole-5,4'-[1,3]dioxolan]-7(6H)-one (**1.2.5.7**)



Alcohol (**1.2.4.4**, 5.0 mg, 9.3 μmol , 1.0 eq), NBS (1.9 mg, 11 mmol, 1.2 eq) and AgNO_3 (0.6 mg, 4 μmol , 0.4 eq) were dissolved in acetone (0.37 mL) and stirred for 15 min at rt. Sat. aq. NaCl (5.0 mL) was added and the mixture was extracted with EtOAc (15 mL). The organic layer was dried over Na_2SO_4 and concentrated. Purification via flash column chromatography (pentane:EtOAc = 92:8) afforded (3*aR*,4*R*,5*S*,6*R*,7*aS*)-4,6-bis(benzyloxy)-2',2'-dimethyl-7a-

((trimethylsilyl)ethynyl)tetrahydro-3H-spiro[benzo[c]isoxazole-5,4'-[1,3]dioxolan]-7(6H)-one (**1.2.5.7**, 2.1 mg, 3.9 μmol , 42%) as a colorless oil.

R_f (pentane:EtOAc = 9:1) = 0.31. (CAM)

$^1\text{H NMR}$ (800 MHz, C_6D_6) δ (ppm) = 9.69 (s, 1H), 7.49 (d, $J = 7.0$ Hz, 2H), 7.21 – 7.18 (m, 2H), 7.15 – 7.12 (m, 3H), 7.10 (t, $J = 7.3$ Hz, 1H), 7.03 (t, $J = 7.4$ Hz, 1H), 4.83 (t, $J = 8.4$ Hz, 1H), 4.80 (d, $J = 11.3$ Hz, 1H), 4.74 (d, $J = 10.0$ Hz, 1H), 4.72 (d, $J = 10.0$ Hz, 1H), 4.29 (s, 25H), 4.26 (dd, $J = 12.0$, 8.5 Hz, 1H), 4.16 (d, $J = 11.3$ Hz, 1H), 3.85 (d, $J = 9.5$ Hz, 1H), 3.55 (d, $J = 9.5$ Hz, 1H), 3.54 (s, 1H), 3.39 (dd, $J = 11.7$, 8.7 Hz, 1H), 1.13 (s, 3H), 1.05 (s, 3H), 0.08 (s, 9H).

The aromatic signals are overlapping with the NMR solvent.

$^{13}\text{C NMR}$ (201 MHz, C_6D_6) δ (ppm) = 197.6, 144.9, 137.8, 137.3, 129.5, 128.7, 128.7, 111.6, 105.4, 94.9, 87.3, 84.2, 76.8, 74.7, 73.9, 71.8, 69.9, 51.2, 26.8, 26.7, -0.6.

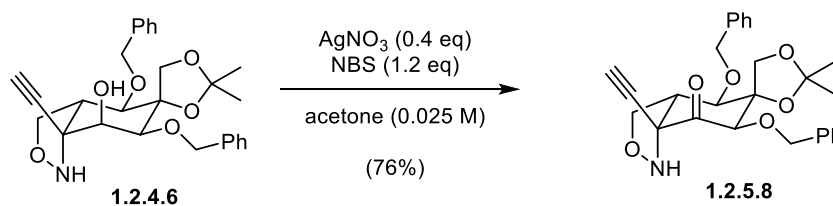
According to the 2D spectra, three carbon signals are obscured by the NMR solvent.

HRMS (ESI): calc. for $\text{C}_{30}\text{H}_{38}\text{NO}_6\text{Si}^+$ [$\text{M} + \text{H}^+$] $^+$: 536.2463, found 536.2467.

IR (Diamond-ATR, neat) ν_{max} (cm^{-1}) = 2952 (m), 2921 (vs), 2850 (m), 1724 (w), 1497 (vw), 1454 (m), 1374 (m), 1329 (w), 1285 (w), 1253 (m), 1232 (w), 1213 (m), 1129 (m), 1090 (s), 1080 (s), 1050 (s), 1025 (s), 984 (w), 925 (s), 890(w), 840 (vs), 803 (m), 759 (s), 738 (m), 696 (vs).

$[\alpha]_{\text{D}}^{20} = -8.8^\circ$ ($c = 0.39$, EtOAc).

(3*aR*,4*R*,5*S*,6*R*,7*aS*)-4,6-bis(benzyloxy)-7*a*-ethynyl-2',2'-dimethyltetrahydro-3H-spiro[benzo[c]isoxazole-5,4'-[1,3]dioxolan]-7(6H)-one (**1.2.5.8**)



Alcohol (**1.2.4.6**, 6.2 mg, 13 μmol , 1.0 eq), NBS (2.7 mg, 15 mmol, 1.2 eq) and AgNO_3 (0.9 mg, 5 μmol , 0.4 eq) were dissolved in acetone (0.53 mL) and stirred for 10 min at rt. The solvent was removed *in vacuo* and directly purified via flash column chromatography (pentane:EtOAc = 87.5:12.5) to give (3*aR*,4*R*,5*S*,6*R*,7*aS*)-4,6-bis(benzyloxy)-7*a*-ethynyl-2',2'-dimethyltetrahydro-3H-spiro[benzo[c]isoxazole-5,4'-[1,3]dioxolan]-7(6H)-one (**1.2.5.8**, 4.7 mg, 10 μmol , 77%) as a colorless oil.

R_f (pentane:EtOAc 7:3) = 0.83. (CAM)

$^1\text{H NMR}$ (800 MHz, C_6D_6) δ (ppm) = 9.69 (s, 1H), 7.52 (d, $J = 7.1$ Hz, 2H), 7.23 – 7.00 (m, 8H), 4.85 – 4.73 (m, 3H), 4.61 (d, $J = 9.8$ Hz, 1H), 4.27 – 4.16 (m, 2H), 4.14 (s, 1H), 3.81 (d, $J = 9.5$ Hz, 1H), 3.53 (s, 1H), 3.45 (d, $J = 9.5$ Hz, 1H), 3.21 (dd, $J = 12.1, 8.1$ Hz, 1H), 2.54 (s, 1H), 1.08 (s, 3H), 0.97 (s, 3H).

The aromatic signals are overlapping with the NMR solvent.

$^{13}\text{C NMR}$ (201 MHz, C_6D_6) δ (ppm) = 197.5, 143.7, 137.5, 137.2, 129.6, 128.8, 128.8, 128.7, 111.6, 87.5, 86.3, 83.8, 76.6, 74.9, 74.0, 73.7, 72.0, 69.9, 51.2, 26.8, 26.5.

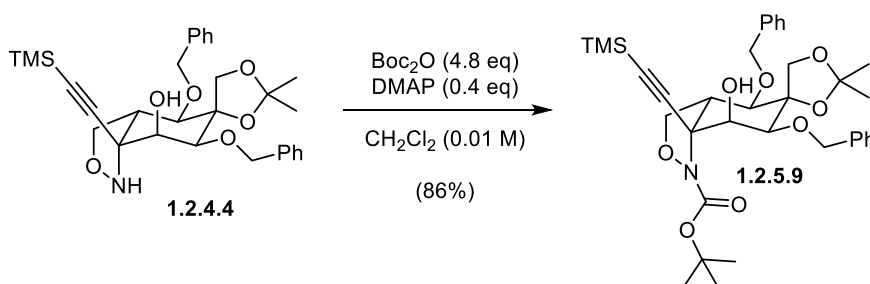
According to the 2D spectra, two carbon signals are obscured by the NMR solvent.

HRMS (ESI): calc. for $\text{C}_{27}\text{H}_{30}\text{NO}_6^+$ [$\text{M} + \text{H}^+$] $^+$: 464.2068, found 464.2073.

IR (Diamond-ATR, neat) ν_{max} (cm^{-1}) = 3229 (br, w), 2961 (vw), 2921 (w), 2852 (vw), 1727 (w), 1633 (vw), 1454 (w), 1374 (w), 1260 (m), 1214 (m), 1092 (vs), 1052 (vs), 1025 (vs), 919 (m), 840 (m), 800 (s), 735 (s), 697 (vs).

$[\alpha]_{\text{D}}^{20} = -13^\circ$ ($c = 0.79$, EtOAc).

tert-butyl (3*aR*,4*R*,5*S*,6*S*,7*S*,7*aS*)-4,6-bis(benzyloxy)-7-hydroxy-2',2'-dimethyl-7*a*-((trimethylsilyl)ethynyl)tetrahydro-3*H*-spiro[benzo[*c*]isoxazole-5,4'-[1,3]dioxolane]-1(4*H*)-carboxylate (1.2.5.9)



Isoxazolidine (**1.2.4.4**, 5.0 mg, 9.3 μmol , 1.0 eq) was dissolved in CH_2Cl_2 (0.17 mL) and a solution of Boc_2O (2.6 μL , 11 μmol , 1.2 eq) and DMAP (0.1 mg, 0.9 μmol , 0.1 eq) in CH_2Cl_2 (0.2 mL) was added at rt. After stirring for 2 h 20 min, a solution of Boc_2O (7.7 μL , 34 μmol , 3.6 eq) and DMAP (0.3 mg, 3 μmol , 0.3 eq) in CH_2Cl_2 (0.6 mL) was added and stirring was continued for 75 min.

The mixture was diluted with EtOAc (15 mL), washed with sat. aq. NH_4Cl (5.0 mL) and sat. aq. NaCl (5.0 mL). The organic layer was dried over Na_2SO_4 and concentrated. Purification via flash

column chromatography (pentane:EtOAc = 9:1) afforded *tert*-butyl (3*aR*,4*R*,5*S*,6*S*,7*S*,7*aS*)-4,6-bis(benzyloxy)-7-hydroxy-2',2'-dimethyl-7*a*-((trimethylsilyl)ethynyl)tetrahydro-3*H*-spiro[benzo[*c*]isoxazole-5,4'-[1,3]dioxolane]-1(4*H*)-carboxylate (**1.2.5.9**, 5.1 mg, 8.0 μ mol, 86%) as a colorless oil.

R_f (pentane:EtOAc 4:1) = 0.67. (CAM)

$^1\text{H NMR}$ (400 MHz, C_6D_6) δ (ppm) = 7.45 (d, J = 7.6 Hz, 2H), 7.31 (d, J = 7.5 Hz, 2H), 7.26 – 7.17 (m, 4H), 7.14 – 7.05 (m, 2H), 5.73 (s, 1H), 5.57 (d, J = 2.9 Hz, 1H), 4.88 (d, J = 11.9 Hz, 1H), 4.84 (d, J = 11.1 Hz, 1H), 4.67 (d, J = 9.0 Hz, 1H), 4.54 (d, J = 11.1 Hz, 1H), 4.48 – 4.38 (m, 2H), 4.14 (d, J = 2.9 Hz, 1H), 4.03 (dd, J = 8.0, 4.9 Hz, 1H), 3.85 (d, J = 7.7 Hz, 1H), 3.77 (d, J = 9.0 Hz, 1H), 2.72 (dd, J = 9.3, 4.6 Hz, 1H), 1.44 (s, 3H), 1.39 (s, 3H), 1.35 (s, 9H), 0.13 (s, 9H).

$^{13}\text{C NMR}$ (101 MHz, C_6D_6) δ (ppm) = 153.4, 139.2, 138.7, 128.5, 128.5, 127.6, 127.6, 109.7, 105.8, 90.1, 86.5, 81.9, 80.2, 77.5, 75.0, 74.0, 73.3, 72.5, 65.8, 62.9, 54.3, 27.8, 26.9, 26.6, -0.1.

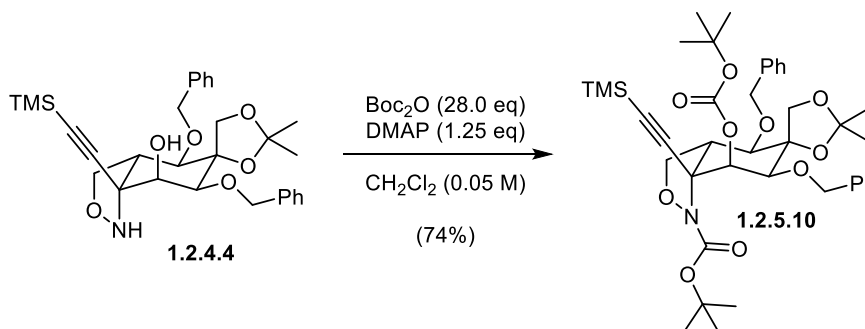
According to the 2D spectra, two carbon signals are obscured by the NMR solvent.

HRMS (ESI): calc. for $\text{C}_{35}\text{H}_{48}\text{NO}_8\text{Si}^+$ [$\text{M} + \text{H}^+$] $^+$: 638.3144, found 638.3148.

IR (Diamond-ATR, neat) ν_{max} (cm^{-1}) = 3250 (vw), 2960 (w), 2922 (w), 2851 (vw), 2166 (vw), 1814 (vw), 1748 (m), 1498 (vw), 1455 (w), 1369 (m), 1344 (w), 1275 (s), 1250 (s), 1207 (w), 1158 (s), 1110 (s), 1088 (vs), 1068 (vs), 1029 (m), 1015 (m), 922 (w), 842 (vs), 785 (m), 758 (s), 734 (s), 697 (vs), 678 (m).

$[\alpha]_{\text{D}}^{20} = +56.3^\circ$ ($c = 0.625$, EtOAc).

tert-butyl (3*aR*,4*R*,5*S*,6*S*,7*S*,7*aS*)-4,6-bis(benzyloxy)-7-((*tert*-butoxycarbonyl)oxy)-2',2'-dimethyl-7*a*-((trimethylsilyl)ethynyl)tetrahydro-3*H*-spiro[benzo[*c*]isoxazole-5,4'-[1,3]dioxolane]-1(4*H*)-carboxylate (**1.2.5.10**)



Isoxazolidine (**1.2.4.4**, 20.0 mg, 37.2 μmol , 1.0 eq) and DMAP (2.3 mg, 19 μmol , 0.5 eq) were dissolved in CH_2Cl_2 (0.75 mL) and Boc_2O (34.2 μL , 149 μmol , 4.0 eq) was added at rt. Another portion of Boc_2O (17.1 μL , 74.4 μmol , 2.0 eq) was added after stirring for a total of 2 h 30 min, 4 h 50 min and 5 h 30 min. After stirring the reaction for a total of 5 h 50 min, Boc_2O (34.2 μL , 149 μmol , 4.0 eq) and DMAP (2.3 mg, 19 μmol , 0.5 eq) were added and stirring was continued for 16 h 50 min. Boc_2O (34.2 μL , 149 μmol , 4.0 eq) and DMAP (1.1 mg, 9.3 μmol , 0.25 eq) were added and after 1 h, a final portion of Boc_2O (34.2 μL , 149 μmol , 4.0 eq) was added to the mixture. Stirring was continued for 2 h 20 min and after a total of 26 h reaction time, the solution was diluted with EtOAc (35 mL) and washed with sat. aq. NH_4Cl (10 mL) and sat. aq. NaHCO_3 /sat. aq. NaCl (1:1, 10 mL). The organic layer was dried over Na_2SO_4 and concentrated. Purification via flash column chromatography (pentane:EtOAc = 9:1 \rightarrow 4:1) afforded *tert*-butyl (3*aR*,4*R*,5*S*,6*S*,7*S*,7*aS*)-4,6-bis(benzyloxy)-7-((*tert*-butoxycarbonyl)oxy)-2',2'-dimethyl-7a-((trimethylsilyl)ethynyl)tetrahydro-3H-spiro[benzo[*c*]isoxazole-5,4'-[1,3]dioxolane]-1(4H)-carboxylate (**1.2.5.10**, 20.3 mg, 27.5 μmol , 74%) as a colorless oil.

R_f (pentane:EtOAc = 9:1) = 0.41. (CAM)

$^1\text{H NMR}$ (400 MHz, C_6D_6) δ (ppm) = 7.47 (d, J = 7.5 Hz, 2H), 7.31 (d, J = 7.5 Hz, 2H), 7.25 – 7.04 (m, 6H), 6.48 (br s, 1H), 5.07 (d, J = 12.0 Hz, 1H), 4.81 (d, J = 10.6 Hz, 1H), 4.71 (d, J = 9.0 Hz, 1H), 4.52 (d, J = 10.6 Hz, 1H), 4.48 (d, J = 9.1 Hz, 1H), 4.44 (d, J = 12.0 Hz, 1H), 4.27 (dd, J = 7.9, 3.3 Hz, 1H), 4.09 – 4.05 (d, J = 1.4 Hz, 1H), 3.83 (d, J = 10.2 Hz, 1H), 3.73 (d, J = 7.9 Hz, 1H), 2.69 (dd, J = 10.2, 3.2 Hz, 1H), 1.55 (s, 9H), 1.49 (s, 3H), 1.45 (s, 3H), 1.34 (s, 9H), 0.16 (s, 9H).

The aromatic signals are overlapping with the NMR solvent.

$^{13}\text{C NMR}$ (101 MHz, C_6D_6) δ (ppm) = 153.4, 139.5, 138.5, 129.3, 128.8, 127.9, 127.7, 109.7, 102.8, 90.7, 87.4, 83.0, 82.3, 80.3, 77.1, 76.1, 73.7, 73.4, 70.5, 65.3, 65.0, 54.8, 28.8, 28.1, 27.4, 26.9, 0.2.

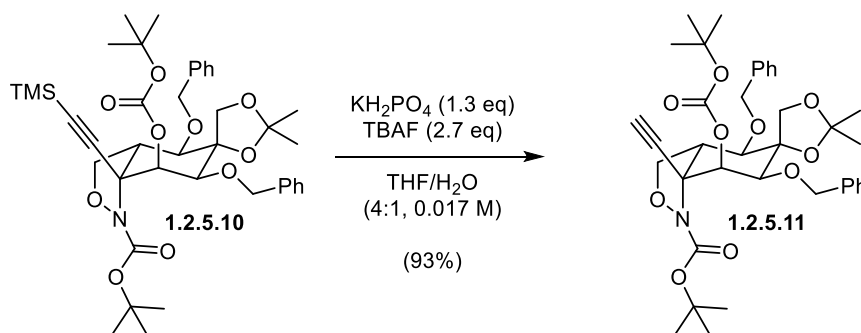
According to the 2D spectra, two carbon signals are obscured by the NMR solvent.

HRMS (ESI): calc. for $\text{C}_{40}\text{H}_{59}\text{N}_2\text{O}_{10}\text{Si}^+$ [$\text{M} + \text{NH}_4^+$] $^+$: 755.3933, found 755.3947.

IR (Diamond-ATR, neat) ν_{max} (cm^{-1}) = 2962 (br, vw), 1750 (s), 1455 (w), 1369 (m), 1318 (w), 1275 (s), 1251 (vs), 1206 (w), 1159 (s), 1068 (vs), 927 (w), 843 (vs), 787 (m), 757 (s), 735 (s), 698 (s).

$[\alpha]_{\text{D}}^{20} = +44.4^\circ$ (c = 0.500, EtOAc).

tert-butyl (3*aR*,4*R*,5*S*,6*S*,7*S*,7*aS*)-4,6-bis(benzyloxy)-7-((*tert*-butoxycarbonyl)oxy)-7a-ethynyl-2',2'-dimethyltetrahydro-3H-spiro[benzo[*c*]isoxazole-5,4'-[1,3]dioxolane]-1(4H)-carboxylate (**1.2.5.11**)



TMS-alkyne (**1.2.5.10**, 5.4 mg, 7.3 μmol , 1.0 eq) and KH_2PO_4 (1.3 mg, 10 μmol , 1.4 eq) were dissolved in THF/H₂O (4:1, 0.43 mL) and TBAF (1 M in THF, 0.20 mL, 20 μmol , 2.7 eq) was added. The clear solution was stirred for 26 h and sat. aq. CaCl_2 (0.2 mL) was added followed by sat. aq. NHCO_3 /sat. aq. NaCl (1:1, 5.0 mL). After extraction with CH_2Cl_2 (2 \times 15 mL), the combined organic layers were dried over Na_2SO_4 and concentrated. Purification via flash column chromatography (pentane:EtOAc = 9:1 \rightarrow 17:1) afforded *tert*-butyl (3*aR*,4*R*,5*S*,6*S*,7*S*,7*aS*)-4,6-bis(benzyloxy)-7-((*tert*-butoxycarbonyl)oxy)-7*a*-ethynyl-2',2'-dimethyltetrahydro-3H-spiro[benzo[*c*]isoxazole-5,4'-[1,3]dioxolane]-1(4H)-carboxylate (**1.2.5.11**, 4.5 mg, 6.8 μmol , 93%) as a beige gum.

R_f (pentane:EtOAc = 17:3) = 0.34. (CAM)

$^1\text{H NMR}$ (400 MHz, C_6D_6) δ (ppm) = 7.47 (d, J = 7.5 Hz, 2H), 7.31 (d, J = 7.6 Hz, 2H), 7.24 – 7.18 (m, 3H), 7.15 – 7.05 (m, 3H), 6.49 (s, 1H), 5.06 (d, J = 12.0 Hz, 1H), 4.80 (d, J = 10.8 Hz, 1H), 4.73 (d, J = 9.1 Hz, 1H), 4.55 (d, J = 10.8 Hz, 1H), 4.49 (d, J = 9.1 Hz, 1H), 4.42 (d, J = 12.1 Hz, 1H), 4.13 (dd, J = 8.0, 3.4 Hz, 1H), 4.08 – 4.04 (d, J = 2.0 Hz, 1H), 3.80 (d, J = 10.2 Hz, 1H), 3.70 (d, J = 8.0 Hz, 1H), 2.58 (dd, J = 10.2, 3.2 Hz, 1H), 1.91 (s, 1H), 1.52 (s, 9H), 1.49 (s, 3H), 1.45 (s, 3H), 1.32 (s, 9H).

The aromatic signals are overlapping with the NMR solvent.

$^{13}\text{C NMR}$ (101 MHz, C_6D_6) δ (ppm) = 153.1, 139.1, 138.1, 129.0, 128.5, 128.5, 127.6, 127.4, 109.5, 87.0, 82.8, 82.0, 80.8, 79.9, 76.7, 75.5, 74.0, 73.3, 73.0, 70.0, 64.9, 64.2, 54.3, 28.4, 27.6, 27.1, 26.5.

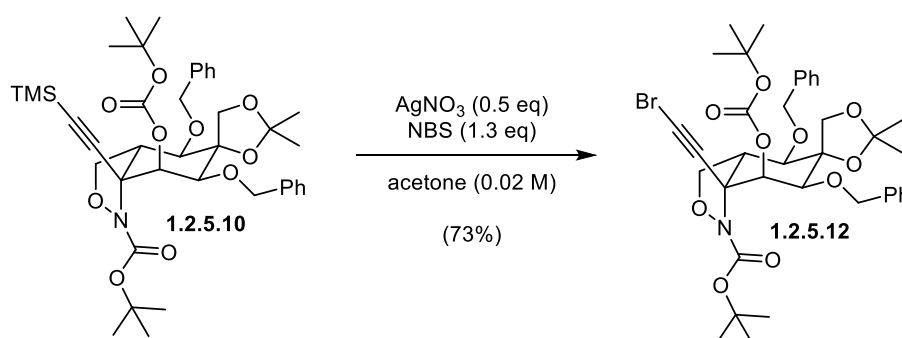
According to the 2D spectra, one carbon signal is obscured by the NMR solvent.

HRMS (ESI): calc. for $\text{C}_{37}\text{H}_{51}\text{N}_2\text{O}_{10}^+$ [$\text{M} + \text{NH}_4^+$] $^+$: 683.3538, found 683.3541.

IR (Diamond-ATR, neat) ν_{max} (cm^{-1}) = 3260 (br, vw), 2958 (w), 2924 (m), 2853 (w), 1749 (s), 1498 (vw), 1456 (w), 1369 (m), 1318 (w), 1275 (s), 1257 (s), 1205 (m), 1159 (s), 1101 (vs), 1068 (vs), 1020 (s), 968 (w), 924 (w), 850 (s), 795 (s), 736 (s), 697 (s), 661 (w).

$[\alpha]_{\text{D}}^{20} = +41.6^\circ$ (c = 0.563, EtOAc).

tert-butyl (3*aR*,4*R*,5*S*,6*S*,7*S*,7*aS*)-4,6-bis(benzyloxy)-7*a*-(bromoethynyl)-7-((*tert*-butoxycarbonyl)oxy)-2',2'-dimethyltetrahydro-3*H*-spiro[benzo[*c*]isoxazole-5,4'-[1,3]dioxolane]-1(4*H*)-carboxylate (1.2.5.12)



TMS-alkyne (**1.2.5.10**, 11.0 mg, 14.9 μmol , 1.0 eq), NBS (3.6 mg, 20 mmol, 1.3 eq) and AgNO_3 (1.1 mg, 6.5 μmol , 0.5 eq) were dissolved in acetone (0.80 mL) and heated to 40 °C for 2 h 30 min. Sat. aq. $\text{Na}_2\text{S}_2\text{O}_3$ (1.0 mL) was added and the mixture was diluted with EtOAc (35 mL). After washing with sat. aq. NaHCO_3 /sat. aq. NaCl (1:1, 10 mL), the organic layer was dried over Na_2SO_4 and the solvent was removed *in vacuo*. Purification via flash column chromatography (pentane:EtOAc = 9:1) afforded *tert*-butyl (3*aR*,4*R*,5*S*,6*S*,7*S*,7*aS*)-4,6-bis(benzyloxy)-7*a*-(bromoethynyl)-7-((*tert*-butoxycarbonyl)oxy)-2',2'-dimethyltetrahydro-3*H*-spiro[benzo[*c*]isoxazole-5,4'-[1,3]dioxolane]-1(4*H*)-carboxylate (**1.2.5.12**, 8.1 mg, 11 mmol, 73%) as an off-white solid.

R_f (pentane:EtOAc = 9:1) = 0.28. (CAM)

$^1\text{H NMR}$ (400 MHz, C_6D_6) δ (ppm) = 7.45 (d, J = 7.5 Hz, 2H), 7.31 (d, J = 7.5 Hz, 2H), 7.20 (dd, J = 13.7, 6.2 Hz, 4H), 7.10 (q, J = 7.8 Hz, 2H), 6.42 (br s, 1H), 5.04 (d, J = 12.0 Hz, 1H), 4.80 – 4.69 (m, 2H), 4.53 (d, J = 10.8 Hz, 1H), 4.47 (d, J = 9.0 Hz, 1H), 4.39 (d, J = 12.1 Hz, 1H), 4.01 (d, J = 2.8 Hz, 1H), 3.95 (dd, J = 8.2, 3.3 Hz, 1H), 3.74 (d, J = 10.2 Hz, 1H), 3.60 (d, J = 8.2 Hz, 1H), 2.41 (dd, J = 10.2, 3.1 Hz, 1H), 1.52 (s, 9H), 1.47 (s, 3H), 1.44 (s, 3H), 1.35 (s, 9H).

The aromatic signals are overlapping with the NMR solvent.

$^{13}\text{C NMR}$ (101 MHz, C_6D_6) δ (ppm) = 155.5, 153.1, 139.1, 138.1, 128.9, 128.6, 128.5, 127.6, 127.4, 109.5, 86.9, 82.9, 82.2, 79.8, 77.6, 76.7, 75.3, 73.4, 73.0, 70.1, 65.4, 64.9, 54.2, 46.6, 28.3, 27.6, 27.1, 26.4.

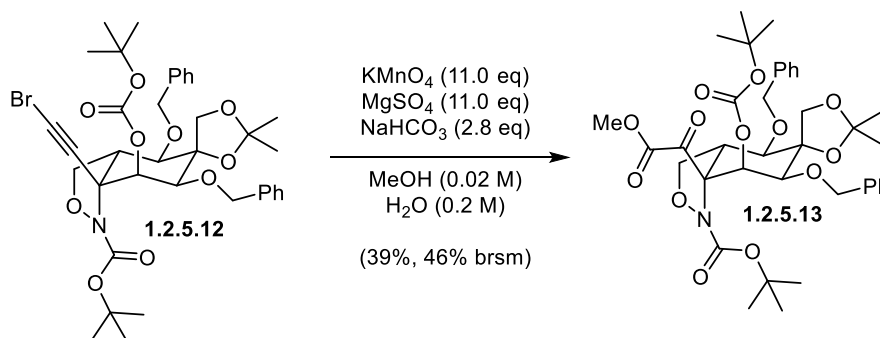
According to the 2D spectra, one carbon signal is obscured by the NMR solvent.

HRMS (ESI): calc. for $C_{37}H_{50}N_2O_{10}Br^+$ $[M + NH_4^+]^+$: 761.2643, found 761.2663.

IR (Diamond-ATR, neat) ν_{max} (cm^{-1}) = 3208 (br, vw), 2925 (w), 1748 (s), 1497 (vw), 1454 (w), 1368 (m), 1318 (w), 1274 (s), 1255 (vs), 1205 (m), 1158 (s), 1087 (vs), 1067 (vs), 1028 (s), 968 (w), 928 (w), 847(s), 794 (s), 734 (s), 697 (s).

$[\alpha]_D^{20} = +47^\circ$ (c = 0.30, EtOAc).

tert-butyl (3*aR*,4*R*,5*S*,6*S*,7*S*,7*aR*)-4,6-bis(benzyloxy)-7-((*tert*-butoxycarbonyl)oxy)-7*a*-(2-methoxy-2-oxoacetyl)-2',2'-dimethyltetrahydro-3*H*-spiro[benzo[*c*]isoxazole-5,4'-[1,3]dioxolane]-1(4*H*)-carboxylate (1.2.5.13)



Bromoalkyne (**1.2.5.12**, 5.0 mg, 6.7 μ mol, 1.0 eq), $MgSO_4$ (1.6 mg, 13 μ mol, 2.0 eq), $KMnO_4$ (2.1 mg, 13 μ mol, 2.0 eq) and $NaHCO_3$ (0.3 mg, 3 μ mol, 0.5 eq) were dissolved in $MeOH/H_2O$ (10:1, 3.74 mL). After stirring for 1 h at rt, the dark purple/brown suspension was filtered through celite and concentrated. The residue was redissolved in $MeOH/H_2O$ (10:1, 3.74 mL) and $MgSO_4$ (4.0 mg, 27 μ mol, 4.0 eq), $KMnO_4$ (4.2 mg, 27 μ mol, 4.0 eq) and $NaHCO_3$ (0.6 mg, 7 μ mol, 1.0 eq) were added. After stirring for 95 min, the dark purple/brown suspension was filtered through celite and concentrated. The residue was redissolved in $MeOH/H_2O$ (10:1, 3.74 mL) and $MgSO_4$ (3.2 mg, 34 μ mol, 5.0 eq), $KMnO_4$ (5.3 mg, 34 μ mol, 5.0 eq) and $NaHCO_3$ (0.8 mg, 8 μ mol, 1.3 eq) were added. After stirring for 80 min, the dark purple/brown suspension was filtered through celite and concentrated. Purification via flash column chromatography (pentane:EtOAc = 9:1 \rightarrow 17:3) afforded an intractable 3:1 mixture of *tert*-butyl (3*aR*,4*R*,5*S*,6*S*,7*S*,7*aR*)-4,6-bis(benzyloxy)-7-((*tert*-butoxycarbonyl)oxy)-7*a*-(2-methoxy-2-oxoacetyl)-2',2'-dimethyltetrahydro-3*H*-spiro[benzo[*c*]isoxazole-5,4'-[1,3]dioxolane]-1(4*H*)-carboxylate (**1.2.5.13**, 1.9 mg, 2.6 μ mol, 39%) with a minor impurity as an off-white gum along with recovered **1.2.5.12** (0.8 mg, 1 μ mol, 16%).

R_f (pentane:EtOAc = 4:1) = 0.34. (CAM)

$^1\text{H NMR}$ (400 MHz, C_6D_6) δ (ppm) = 7.47 (d, J = 7.1 Hz, 2H), 7.30 (d, J = 7.8 Hz, 2H), 7.23 – 7.05 (m, 6H), 6.83 (s, 1H), 5.04 (d, J = 12.4 Hz, 1H), 4.90 (d, J = 10.6 Hz, 1H), 4.66 (d, J = 9.0 Hz, 1H), 4.57 (d, J = 6.0 Hz, 1H), 4.55 (d, J = 4.7 Hz, 1H), 4.39 (d, J = 13.0 Hz, 1H), 4.09 (d, J = 2.8 Hz, 1H), 3.78 (d, J = 10.1 Hz, 1H), 3.71 (dd, J = 8.6, 4.0 Hz, 2H), 3.65 (d, J = 8.4 Hz, 1H), 3.56 (dd, J = 9.9, 3.7 Hz, 1H), 3.30 (s, 3H), 1.51 (s, 9H), 1.50 (s, 3H), 1.45 (s, 3H), 1.23 (s, 9H).

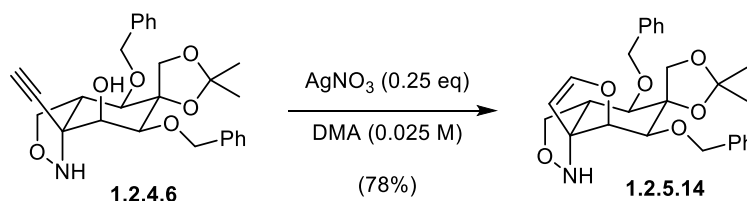
The aromatic signals are overlapping with the NMR solvent.

$^{13}\text{C NMR}$ (101 MHz, C_6D_6) δ (ppm) = 191.4, 164.0, 163.7, 151.8, 138.8, 137.9, 129.1, 127.5, 109.7, 86.6, 82.99, 82.95, 81.1, 76.92, 76.90, 75.1, 73.5, 71.1, 68.8, 64.8, 52.5, 49.7, 28.3, 27.6, 27.0, 26.6.

According to the 2D spectra, four carbon signals are obscured by the NMR solvent.

HRMS (ESI): calc. for $\text{C}_{38}\text{H}_{53}\text{N}_2\text{O}_{13}^+$ [$\text{M} + \text{NH}_4^+$] $^+$: 745.3542, found 745.3545.

(3*aR*,4*R*,5*S*,6*S*,6*aS*,9*aR*)-4,6-bis(benzyloxy)-2',2'-dimethyl-3*a*,4,6,6*a*-tetrahydro-1*H*,3*H*-spiro[benzofuro[3*a*,4-*c*]isoxazole-5,4'-[1,3]dioxolane] (1.2.5.14)



Alkyne (**1.2.4.6**, 127.2 mg, 0.273 mmol, 1.0 eq) and AgNO_3 (11.6 mg, 68.3 μmol , 0.25 eq) were dissolved in DMA (10.9 mL) and stirred at 65 °C for 6 h 10 min. After cooling to rt, the mixture was diluted with sat. aq. NaHCO_3 /sat. aq. NaCl (1:1, 20 mL) and extracted with CH_2Cl_2 (2 \times 100 mL). The combined organic layers were dried over Na_2SO_4 , concentrated and the residual solvent was removed by stirring under high vacuum (< 1 mbar) overnight. Purification via flash column chromatography (pentane:EtOAc: NEt_3 = 3:1:1%) provided (3*aR*,4*R*,5*S*,6*S*,6*aS*,9*aR*)-4,6-bis(benzyloxy)-2',2'-dimethyl-3*a*,4,6,6*a*-tetrahydro-1*H*,3*H*-spiro[benzofuro[3*a*,4-*c*]isoxazole-5,4'-[1,3]dioxolane] (**1.2.5.14**, 99.4 mg, 0.214 mmol, 78%) as a colorless oil.

R_f (pentane:EtOAc = 7:3) = 0.15. (CAM)

$^1\text{H NMR}$ (400 MHz, C_6D_6) δ (ppm) = 7.33 (d, J = 7.6 Hz, 2H), 7.29 (d, J = 7.6 Hz, 2H), 7.21 – 7.06 (m, 6H), 5.99 (d, J = 2.6 Hz, 1H), 5.04 (s, 1H), 4.94 – 4.80 (m, 2H), 4.67 (d, J = 11.7 Hz, 1H), 4.52 –

4.39 (m, 3H), 4.36 (s, 2H), 3.82 (d, $J = 4.3$ Hz, 1H), 3.74 (d, $J = 8.6$ Hz, 1H), 3.66 (d, $J = 8.9$ Hz, 1H), 3.45 (br s, 1H), 2.35 (dd, $J = 10.2, 5.3$ Hz, 1H), 1.42 (d, 6H).

The aromatic signals are overlapping with the NMR solvent.

^{13}C NMR (101 MHz, C_6D_6) δ (ppm) = 147.2, 139.0, 138.8, 128.6, 128.6, 127.9, 110.2, 107.0, 85.1, 84.1, 82.2, 79.9, 75.4, 74.9, 74.2, 73.8, 66.3, 54.3, 26.9, 26.5.

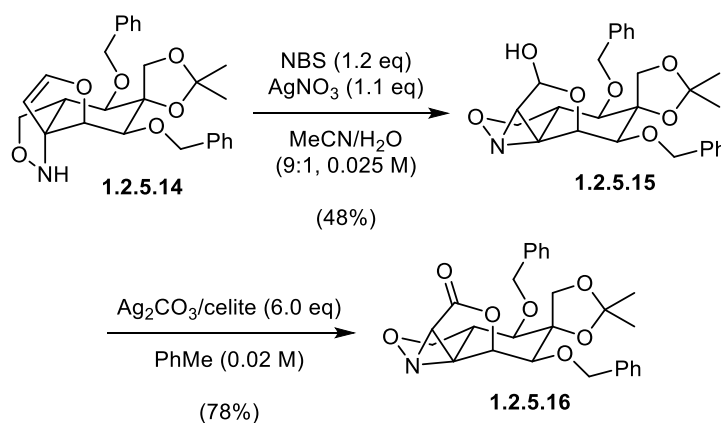
According to the 2D spectra, three carbon signals are obscured by the NMR solvent.

HRMS (ESI): calc. for $\text{C}_{27}\text{H}_{32}\text{NO}_6^+$ $[\text{M} + \text{H}]^+$: 466.2224, found 466.2231.

IR (Diamond-ATR, neat) ν_{max} (cm^{-1}) = 3227 (br, vw), 3089 (vw), 3063 (vw), 3030 (vw), 2984 (vw), 2933 (vw), 2873 (vw), 1614 (w), 1497 (vw), 1454 (w), 1379 (w), 1368 (w), 1330 (vw), 1244 (m), 1207 (m), 1158 (w), 1139 (m), 1125 (m), 1068 (vs), 1027 (s), 971 (w), 928 (w), 912 (w), 852 (s), 814 (w), 733 (vs), 696 (vs), 672 (m).

$[\alpha]_{\text{D}}^{20} = +40^\circ$ ($c = 0.80$, EtOAc).

(4a*R*,5*R*,6*S*,7*S*,8*S*,8a*S*)-5,7-bis(benzyloxy)-2',2'-dimethyltetrahydro-1*H*,4*H*-spiro[[8,1](epoxymethano)azirino[1,2-*b*]benzo[*c*]isoxazole-6,4'-[1,3]dioxolan]-10-one (1.2.5.16)



Dihydrofuran (1.2.5.14, 27.3 mg, 58.6 μmol , 1.0 eq), NBS (8.3 mg, 70 μmol , 1.2 eq) and AgNO_3 (11.0 mg, 64.5 μmol , 1.1 eq) were dissolved in H_2O (0.23 mL) and MeCN (2.11 mL) at 0 $^\circ\text{C}$. The reaction was warmed to rt and stirred for 65 min. Sat. aq. $\text{Na}_2\text{S}_2\text{O}_3$ (1.0 mL) was added followed sat. aq. NaHCO_3 / sat. aq. NaCl (1:1, 5 mL) and the mixture was extracted with EtOAc (2 \times 15 mL). The combined organic layers were dried over Na_2SO_4 and concentrated. Purification via flash column chromatography (pentane:EtOAc = 7:3) afforded (4a*R*,5*R*,6*S*,7*S*,8*S*,8a*S*)-5,7-bis(benzyloxy)-2',2'-dimethyltetrahydro-1*H*,4*H*-spiro[[8,1](epoxymethano)azirino[1,2-

b]benzo[c]isoxazole-6,4'-[1,3]dioxolan]-10-ol (**1.2.5.15**, 13.6 mg, 28.2 μmol , 48%) as a colorless oil with R_f (pentane:EtOAc = 7:3) = 0.23 (CAM). The lactol (**1.2.5.15**, 13.6 mg, 28.2 μmol , 1.0 eq) and $\text{Ag}_2\text{CO}_3/\text{celite}$ (50% Ag_2CO_3 , 46.0 mg, 85.1 μmol , 3.0 eq) were dissolved in PhMe (1.42 mL) and heated to 115 °C for 3 h. $\text{Ag}_2\text{CO}_3/\text{celite}$ (50% Ag_2CO_3 , 46.0 mg, 85.1 μmol , 3.0 eq) was added and stirring was continued for 3 h 15 min at 115 °C. The suspension was cooled to rt, the solid removed by filtration and the filtrate was concentrated. Purification via flash column chromatography (pentane:EtOAc = 17:3) afforded (4*aR*,5*R*,6*S*,7*S*,8*S*,8*aS*)-5,7-bis(benzyloxy)-2',2'-dimethyltetrahydro-1*H*,4*H*-spiro[[8,1](epoxymethano)azirino[1,2-*b*]benzo[c]isoxazole-6,4'-[1,3]dioxolan]-10-one (**1.2.5.16**, 10.6 mg, 22.1 μmol , 78%) as a colorless oil.

R_f (pentane:EtOAc = 9:1) = 0.21. (CAM)

$^1\text{H NMR}$ (400 MHz, C_6D_6) δ (ppm) = 7.23 – 7.02 (m, 10H), 4.71 (s, 1H), 4.61 (d, J = 11.3 Hz, 1H), 4.54 (d, J = 10.5 Hz, 1H), 4.48 (d, J = 9.4 Hz, 1H), 4.31 (d, J = 10.5 Hz, 1H), 4.11 (t, J = 10.8 Hz, 2H), 3.85 (t, J = 7.8 Hz, 1H), 3.78 (d, J = 1.9 Hz, 1H), 3.63 (t, J = 8.3 Hz, 1H), 3.53 (d, J = 11.4 Hz, 1H), 2.69 (s, 1H), 2.55 (dt, J = 11.4, 7.7 Hz, 1H), 1.33 (s, 3H), 1.11 (s, 3H).

The aromatic signals are overlapping with the NMR solvent.

$^{13}\text{C NMR}$ (101 MHz, C_6D_6) δ (ppm) = 168.0, 138.3, 137.1, 129.1, 128.9, 128.7, 128.7, 127.4, 110.2, 86.7, 83.9, 82.2, 80.8, 76.6, 76.6, 75.0, 66.5, 63.1, 54.4, 43.3, 26.7, 25.7.

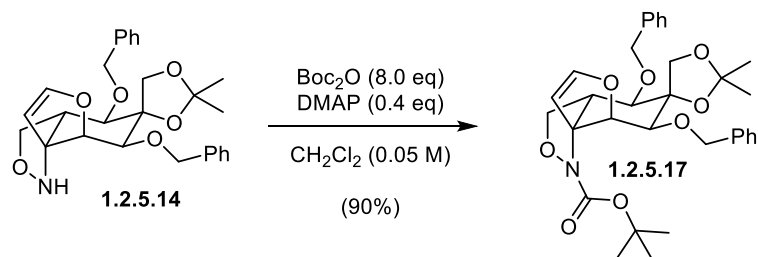
According to the 2D-NMR spectra, two carbon signals are obscured by the NMR solvent.

HRMS (ESI): calc. for $\text{C}_{27}\text{H}_{33}\text{N}_2\text{O}_7^+$ [$\text{M} + \text{NH}_4^+$] $^+$: 497.2282, found: 497.2290.

IR (Diamond-ATR, neat) ν_{max} (cm^{-1}) = 3310 (vw), 2962 (w), 2920 (w), 2852 (vw), 1788 (vw), 1632 (vw), 1537 (vw), 1468 (vw), 1412 (vw), 1378 (vw), 1260 (s), 1088 (s), 1019 (vs), 865 (vw), 797 (vs), 700 (vw).

$[\alpha]_{\text{D}}^{20} = +81^\circ$ ($c = 0.16$, EtOAc).

tert-butyl (3*aR*,4*R*,5*S*,6*S*,6*aS*,9*aR*)-4,6-bis(benzyloxy)-2',2'-dimethyl-3*a*,4,6,6*a*-tetrahydro-1*H*,3*H*-spiro[benzofuro[3*a*,4-*c*]isoxazole-5,4'-[1,3]dioxolane]-1-carboxylate (**1.2.5.17**)



Isoxazolidine (**1.2.5.14**, 65.7 mg, 0.141 mmol, 1.0 eq) and DMAP (6.9 mg, 56 μmol , 0.4 eq) were dissolved in CH_2Cl_2 (2.8 mL) and Boc_2O (0.130 mL, 0.564 mmol, 4.0 eq) was added. The mixture was stirred at rt for 1 h 30 min and the second portion of Boc_2O (65 μL , 0.28 mmol, 2.0 eq) was added. Stirring was continued for 1 h before the last portion of Boc_2O (65 μL , 0.28 mmol, 2.0 eq) was added. After 1 h 10 min, the mixture was poured into sat. aq. NaHCO_3 /sat. aq. NaCl (1:1, 20 mL) and extracted with CH_2Cl_2 (2 \times 70 mL). The combined organic layers were dried over Na_2SO_4 and concentrated. Purification via flash column chromatography (pentane:EtOAc:NEt₃ = 17:3:1%) afforded *tert*-butyl (3a*R*,4*R*,5*S*,6*S*,6a*S*,9a*R*)-4,6-bis(benzyloxy)-2',2'-dimethyl-3a,4,6,6a-tetrahydro-1*H*,3*H*-spiro[benzofuro[3a,4-c]isoxazole-5,4'-[1,3]dioxolane]-1-carboxylate (**1.2.5.17**, 71.5 mg, 0.126 mmol, 90%) as an off-white foam.

R_f (pentane:EtOAc = 17:3) = 0.22. (CAM)

$^1\text{H NMR}$ (400 MHz, CD_2Cl_2) δ (ppm) = 7.38 – 7.26 (m, 10H), 6.56 (d, J = 2.7 Hz, 1H), 5.04 (d, J = 2.7 Hz, 1H), 5.01 – 4.92 (m, 2H), 4.82 (d, J = 11.4 Hz, 1H), 4.67 (d, J = 11.5 Hz, 1H), 4.55 (d, J = 11.1 Hz, 1H), 4.37 (d, J = 9.2 Hz, 1H), 4.09 (d, J = 9.2 Hz, 1H), 3.99 (dd, J = 8.4, 4.6 Hz, 1H), 3.94 – 3.87 (m, 2H), 3.71 (d, J = 11.1 Hz, 1H), 2.71 (ddd, J = 11.0, 4.6, 1.2 Hz, 1H), 1.50 (s, 3H), 1.44 (s, 9H), 1.43 (s, 3H).

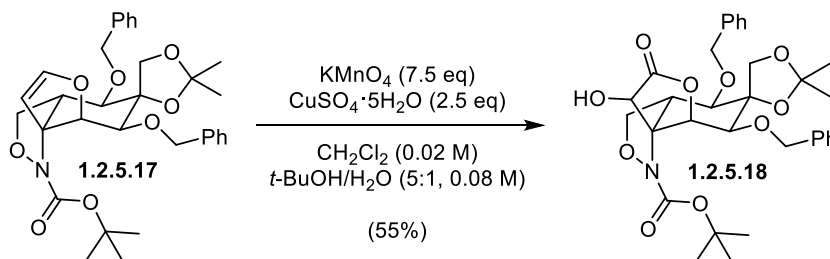
$^{13}\text{C NMR}$ (101 MHz, CD_2Cl_2) δ (ppm) = 154.7, 149.0, 138.6, 129.0, 128.9, 128.8, 128.6, 128.4, 128.4, 128.3, 110.7, 104.6, 84.9, 82.3, 82.2, 81.5, 81.1, 76.3, 76.0, 75.4, 69.9, 67.2, 52.8, 28.6, 27.2, 26.2.

HRMS (ESI): calc. for $\text{C}_{32}\text{H}_{43}\text{N}_2\text{O}_8^+$ [$\text{M} + \text{NH}_4^+$] $^+$: 583.3014, found 583.3022.

IR (Diamond-ATR, neat) ν_{max} (cm^{-1}) = 3032 (vw), 2980 (vw), 2927 (w), 1727 (m), 1618 (vw), 1498 (vw), 1454 (w), 1368 (s), 1329 (w), 1255 (m), 1209 (m), 1147 (s), 1070 (vs), 1042 (vs), 1028 (vs), 983 (m), 930 (w), 851 (s), 797 (w), 733 (vs), 697 (vs), 678 (m).

$[\alpha]_{\text{D}}^{20}$ = +263° (c = 0.225, EtOAc).

tert-butyl (3*aR*,4*R*,5*S*,6*S*,6*aS*,9*R*,9*aS*)-4,6-bis(benzyloxy)-9-hydroxy-2',2'-dimethyl-8-oxohexahydro-1*H*,3*H*-spiro[benzofuro[3*a*,4-*c*]isoxazole-5,4'-[1,3]dioxolane]-1-carboxylate (**1.2.5.18**)



KMnO₄ (45.1 mg, 0.285 mmol, 7.5 eq) and CuSO₄·5H₂O (23.7 mg, 95.0 μmol, 2.5 eq) were dissolved in *t*-BuOH/H₂O (5:1, 0.48 mL) and dihydrofuran (**1.2.5.17**, 21.5 mg, 38.8 μmol, 1.0 eq) in CH₂Cl₂ (1.9 mL) was added in one portion. The suspension turned from purple to purple/brown while stirring for 45 min at rt. Sat. aq. NaHSO₃/sat. aq. NaCl (1:1, 10 mL) was added and the brown suspension turned colorless. The mixture was extracted with CH₂Cl₂ (2 × 35 mL) and the combined organic layers were dried over Na₂SO₄. After removal of the solvent *in vacuo*, the residue was purified via flash column chromatography (pentane:EtOAc = 7:2 → 3:1) to give *tert*-butyl (3*aR*,4*R*,5*S*,6*S*,6*aS*,9*R*,9*aS*)-4,6-bis(benzyloxy)-9-hydroxy-2',2'-dimethyl-8-oxohexahydro-1*H*,3*H*-spiro[benzofuro[3*a*,4-*c*]isoxazole-5,4'-[1,3]dioxolane]-1-carboxylate (**1.2.5.18**, 12.6 mg, 21.1 μmol, 55%) as an off-white foam.

R_f (pentane:EtOAc = 3:1) = 0.26. (CAM)

¹H NMR (400 MHz, C₆D₆) δ (ppm) = 7.28 – 7.19 (m, 4H), 7.17 – 7.03 (m, 6H), 5.31 (d, *J* = 3.1 Hz, 1H), 5.17 (d, *J* = 5.4 Hz, 1H), 4.86 (d, *J* = 11.6 Hz, 1H), 4.51 – 4.39 (m, 3H), 4.35 (d, *J* = 11.6 Hz, 1H), 4.20 (d, *J* = 9.1 Hz, 1H), 3.94 (dd, *J* = 8.0, 4.7 Hz, 1H), 3.76 (d, *J* = 3.2 Hz, 1H), 3.63 (dd, *J* = 8.1, 1.4 Hz, 1H), 3.59 (d, *J* = 9.8 Hz, 1H), 3.07 (d, *J* = 6.2 Hz, 1H), 2.70 (ddd, *J* = 9.8, 4.8, 1.5 Hz, 1H), 1.39 (s, 9H), 1.37 (s, 3H), 1.36 (s, 3H).

The aromatic signals are overlapping with the NMR solvent.

¹³C NMR (101 MHz, C₆D₆) δ (ppm) = 173.2, 153.7, 138.5, 137.5, 128.8, 128.6, 128.5, 127.6, 110.1, 85.0, 82.7, 79.8, 77.3, 76.9, 76.2, 74.7, 70.5, 70.0, 69.2, 65.4, 47.4, 28.2, 26.8, 26.2.

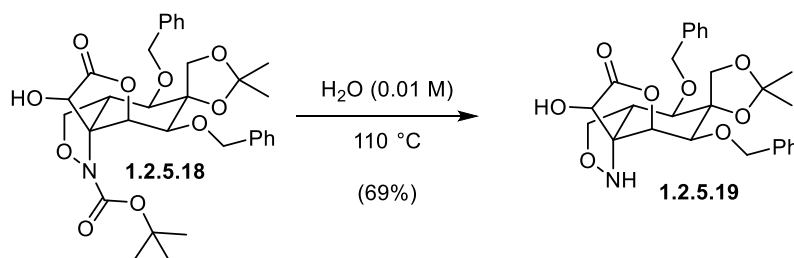
According to the 2D spectra, two carbon signals are obscured by the NMR solvent.

HRMS (ESI): calc. for C₃₂H₄₃N₂O₁₀⁺ [M + NH₄⁺]⁺: 615.2912, found 615.2915.

IR (Diamond-ATR, neat) ν_{\max} (cm^{-1}) = 3285 (br, vw), 2921 (vw), 1782 (vw), 1740 (w), 1651 (vw), 1496 (vw), 1453 (w), 1368 (m), 1248 (m), 1207 (m) 1152 (m), 1065 (vs), 1026 (vs), 911 (w), 847 (m), 800 (m), 735 (s), 696 (vs).

$[\alpha]_{\text{D}}^{20} = +9.0^{\circ}$ ($c = 0.80$, EtOAc).

(3a*R*,4*R*,5*S*,6*S*,6a*S*,9*R*,9a*S*)-4,6-bis(benzyloxy)-9-hydroxy-2',2'-dimethyltetrahydro-1*H*,3*H*-spiro[benzofuro[3a,4-*c*]isoxazole-5,4'-[1,3]dioxolan]-8(9*H*)-one (1.2.5.19)



Carbamate (**1.2.5.18**, 7.0 mg, 12.2 μmol , 1.0 eq) was suspended in H_2O (1.22 mL) and heated to $110\text{ }^{\circ}\text{C}$ for 5 h 20 min. The slightly grey mixture was cooled to rt, transferred with MeCN (5 mL) and EtOAc (5 mL) the solvent was removed *in vacuo*. Purification via flash column chromatography (pentane:EtOAc = 7:3 \rightarrow 45:55) afforded (3a*R*,4*R*,5*S*,6*S*,6a*S*,9*R*,9a*S*)-4,6-bis(benzyloxy)-9-hydroxy-2',2'-dimethyltetrahydro-1*H*,3*H*-spiro[benzofuro[3a,4-*c*]isoxazole-5,4'-[1,3]dioxolan]-8(9*H*)-one (**1.2.5.19**, 4.2 mg, 8.4 μmol , 69%) as an off-white foam.

R_f (pentane:EtOAc = 1:1) = 0.22. (CAM)

^1H NMR (400 MHz, C_6D_6) δ (ppm) = 7.16 – 6.99 (m, 10H), 4.90 (br s, 1H), 4.64 (d, $J = 10.8$ Hz, 1H), 4.61 (br s, 1H), 4.35 (d, $J = 10.9$ Hz, 1H), 4.05 (d, $J = 10.7$ Hz, 1H), 4.03 – 3.89 (m, 3H), 3.86 (m, 2H), 3.68 – 3.59 (m, 2H), 3.46 (br s, 1H), 3.29 (br s, 1H), 2.71 (t, $J = 10.3$ Hz, 1H).

The aromatic signals are overlapping with the NMR solvent.

^{13}C NMR (101 MHz, C_6D_6) δ (ppm) = 174.7, 137.5, 136.7, 128.85, 128.79, 128.78, 111.1, 81.9, 80.0, 79.3, 78.9, 76.6, 75.5, 72.6, 70.7, 70.2, 44.5, 26.9, 26.2.

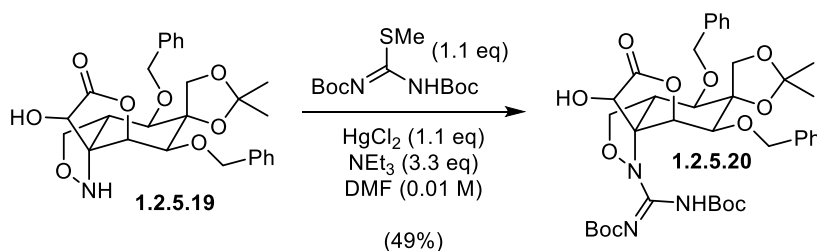
According to the 2D spectra, three carbon signals are obscured by the NMR solvent.

HRMS (ESI): calc. for $\text{C}_{27}\text{H}_{32}\text{NO}_8^+$ [$\text{M} + \text{H}^+$] $^+$: 498.2122, found: 498.2121.

IR (Diamond-ATR, neat) ν_{\max} (cm^{-1}) = 3437 (vw), 2962 (vw), 2925 (vw), 1784 (m), 1498 (vw), 1454 (w), 1372 (w), 1345 (w), 1259 (s), 1208 (m) 1067 (vs), 1014 (vs), 968 (m), 846 (m), 800 (s), 736 (s), 697 (vs), 660 (w).

$[\alpha]_{\text{D}}^{20} = +0.82^{\circ}$ ($c = 0.49$, EtOAc).

tert-butyl ((*E*)-((3*aR*,4*R*,5*S*,6*S*,6*aS*,9*R*,9*aS*)-4,6-bis(benzyloxy)-9-hydroxy-2',2'-dimethyl-8-oxohexahydro-1*H*,3*H*-spiro[benzofuro[3*a*,4-*c*]isoxazole-5,4'-[1,3]dioxolan]-1-yl))(*tert*-butoxycarbonyl)amino)methylene)carbamate (1.2.5.20)



Isioxazolidine (**1.2.5.19**, 3.9 mg, 7.8 μmol , 1.0 eq), HgCl_2 (2.3 mg, 8.6 μmol , 1.1 eq) and 1,3-bis(*tert*-butoxycarbonyl)-2-methyl-2-thiopseudourea (2.5 mg, 8.62 μmol , 1.1 eq) were dissolved in DMF (0.38 mL) and NEt_3 (3.5 μL , 25.9 μmol , 3.3 eq) in DMF (0.4 mL) was added at rt. After stirring the reaction for 40 min, it was diluted with sat. aq. NaCl (5 mL) and extracted with Et_2O (15 mL). The organic layer was dried over Na_2SO_4 and concentrated. Purification via flash column chromatography (pentane: EtOAc = 7:3 \rightarrow 2:1) afforded *tert*-butyl ((*E*)-((3*aR*,4*R*,5*S*,6*S*,6*aS*,9*R*,9*aS*)-4,6-bis(benzyloxy)-9-hydroxy-2',2'-dimethyl-8-oxohexahydro-1*H*,3*H*-spiro[benzofuro[3*a*,4-*c*]isoxazole-5,4'-[1,3]dioxolan]-1-yl))(*tert*-butoxycarbonyl)amino)methylene)carbamate (**1.2.5.20**, 2.8 mg, 3.8 μmol , 49%) as a colorless gum.

R_f (pentane:EtOAc = 7:3) = 0.20. (UV, CAM)

$^1\text{H NMR}$ (400 MHz, C_6D_6) δ (ppm) = 9.20 (br s, 1H), 7.35 (d, $J = 6.8$ Hz, 2H), 7.26 (d, $J = 6.8$ Hz, 2H), 7.24 – 7.06 (m, 6H), 5.79 (d, $J = 3.0$ Hz, 1H), 5.50 (br s, 1H), 4.96 (d, $J = 11.8$ Hz, 1H), 4.60 (d, $J = 11.5$ Hz, 1H), 4.53 – 4.46 (m, 2H), 4.40 (d, $J = 11.9$ Hz, 1H), 4.16 (d, $J = 9.1$ Hz, 1H), 3.88 (dd, $J = 7.9, 4.5$ Hz, 1H), 3.81 (d, $J = 3.0$ Hz, 1H), 3.59 (d, $J = 10.3$ Hz, 1H), 3.54 (d, $J = 8.4$ Hz, 1H), 3.12 (br s, 1H), 2.72 (dd, $J = 10.4, 4.2$ Hz, 1H), 1.51 (s, 9H), 1.38 (s, 3H), 1.37 (s, 3H), 1.31 (s, 9H).

The aromatic signals are overlapping with the NMR solvent.

$^{13}\text{C NMR}$ (101 MHz, C_6D_6) δ (ppm) = 171.6, 161.0, 149.8, 149.7, 138.6, 137.5, 128.77, 128.75, 128.6, 127.7, 109.9, 85.1, 82.1, 79.9, 79.8, 76.5, 76.4, 74.6, 73.9, 71.3, 71.0, 69.1, 65.0, 47.7, 28.3, 27.9, 26.8, 26.2.

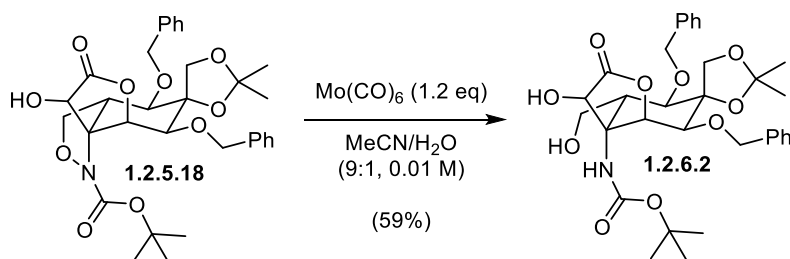
According to the 2D spectra, two carbon signals are obscured by the NMR solvent.

HRMS (ESI): calc. for $C_{38}H_{50}N_3O_{12}^+$ $[M + H]^+$: 740.3389, found: 740.3385.

IR (Diamond-ATR, neat) ν_{\max} (cm^{-1}) = 2963 (w), 2926 (vw), 1797 (w), 1760 (w), 1598 (w), 1497 (m), 1455 (w), 1394 (w), 1368 (m), 1286 (m), 1258 (s), 1207 (m) 1131 (vs), 1069 (vs), 1018 (vs), 970 (m), 930 (w), 861 (m), 799 (s), 734 (m), 697 (s).

$[\alpha]_D^{20} = +91^\circ$ (c = 0.51, EtOAc).

tert-butyl ((3*R*,3*aS*,4*R*,5*R*,6*S*,7*S*,7*aS*)-5,7-bis(benzyloxy)-3-hydroxy-4-(hydroxymethyl)-2',2'-dimethyl-2-oxohexahydro-3*aH*-spiro[benzofuran-6,4'-[1,3]dioxolan]-3*a*-yl)carbamate (**1.2.6.2**)



Boc-isoxazolidine (**1.2.5.18**, 6.8 mg, 11 μmol , 1.0 eq) and $\text{Mo}(\text{CO})_6$ (3.6 mg, 14 μmol , 1.2 eq) were dissolved in $\text{MeCN}/\text{H}_2\text{O}$ (9:1, 1.14 mL) and heated to 82.5 $^\circ\text{C}$ for 2 h. After cooling to rt, the mixture was diluted with sat. aq. NaHCO_3 /sat. aq. NaCl (1:1, 5 mL) and extracted with CH_2Cl_2 (2 \times 15 mL). The combined organic layers were dried over Na_2SO_4 and concentrated. Purification via flash column chromatography (pentane:EtOAc = 2:1 \rightarrow 6:4) afforded *tert*-butyl ((3*R*,3*aS*,4*R*,5*R*,6*S*,7*S*,7*aS*)-5,7-bis(benzyloxy)-3-hydroxy-4-(hydroxymethyl)-2',2'-dimethyl-2-oxohexahydro-3*aH*-spiro[benzofuran-6,4'-[1,3]dioxolan]-3*a*-yl)carbamate (**1.2.6.2**, 3.9 mg, 6.5 μmol , 59%) as an off-white gum.

R_f (pentane:EtOAc = 6:4) = 0.34. (CAM)

$^1\text{H NMR}$ (400 MHz, C_6D_6) δ (ppm) = 7.34 (d, J = 7.3 Hz, 2H), 7.29 (d, J = 7.4 Hz, 2H), 7.24 – 7.03 (m, 6H), 5.73 – 5.69 (d, J = 1.8 Hz, 1H), 5.60 (br s, 1H), 4.95 (d, J = 12.1 Hz, 1H), 4.68 (d, J = 8.7 Hz, 1H), 4.64 – 4.54 (m, 2H), 4.52 (d, J = 12.1 Hz, 1H), 4.15 (d, J = 8.7 Hz, 1H), 4.13 – 4.05 (dd, J = 10.2, 1.6 Hz, 1H), 3.84 (d, J = 3.1 Hz, 1H), 3.72 (d, J = 11.8 Hz, 1H), 3.52 (d, J = 10.0 Hz, 1H), 2.43 (s, 1H), 1.61 (dd, J = 11.8, 3.6 Hz, 1H), 1.52 (s, 3H), 1.41 (s, 3H), 1.38 (s, 9H).

The aromatic signals are overlapping with the NMR solvent.

^{13}C NMR (101 MHz, C_6D_6) δ (ppm) = 173.9, 154.9, 139.4, 137.9, 128.7, 128.5, 127.5, 126.8, 109.8, 86.8, 80.0, 76.6, 75.1, 74.9, 74.5, 73.0, 71.9, 64.6, 63.3, 59.8, 41.6, 28.4, 27.0, 26.6.

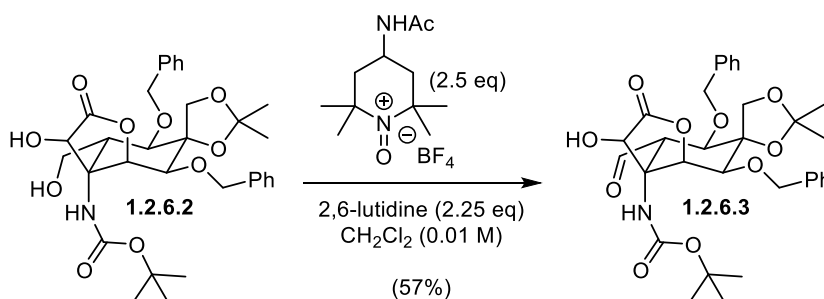
According to the 2D spectra, two carbon signals are obscured by the NMR solvent.

HRMS (ESI): calc. for $\text{C}_{32}\text{H}_{45}\text{N}_2\text{O}_{10}^+$ [$\text{M} + \text{NH}_4^+$] $^+$: 617.3069, found: 617.3069.

IR (Diamond-ATR, neat) ν_{max} (cm^{-1}) = 3311 (br, vw), 2924 (w), 2854 (vw), 1786 (w), 1706 (m), 1522 (w), 1498 (w), 1455 (w), 1368 (m), 1284 (m), 1258 (m), 1206 (m), 1159 (s), 1084 (vs), 1063 (vs), 1030 (vs), 972 (m), 912 (w), 865 (m), 801 (m), 734 (s), 697 (s).

$[\alpha]_{\text{D}}^{20} = +13^\circ$ ($c = 0.48$, EtOAc).

tert-butyl ((3*R*,3*aS*,4*S*,5*R*,6*S*,7*S*,7*aS*)-5,7-bis(benzyloxy)-4-formyl-3-hydroxy-2',2'-dimethyl-2-oxohexahydro-3*aH*-spiro[benzofuran-6,4'-[1,3]dioxolan]-3*a*-yl)carbamate (1.2.6.3)



Primary alcohol (**1.2.6.2**, 4.7 mg, 7.8 μmol , 1.0 eq) and Bobbit's salt¹³⁵ (5.9 mg, 20 μmol , 2.6 eq) were dissolved in CH_2Cl_2 (0.58 mL) and 2,6-lutidine (2.0 μL , 18 μmol , 2.3 eq) in CH_2Cl_2 (0.2 mL) was added at rt. The reaction was stirred for 12 min before it was diluted with sat. aq. $\text{Na}_2\text{S}_2\text{O}_3$ (0.5 mL). After addition of sat. aq. NaHCO_3 /sat. aq. NaCl (1:1, 5 mL), the was extracted with CH_2Cl_2 (2×15 mL). The combined organic layers were dried over Na_2SO_4 and concentrated. Purification via flash column chromatography (pentane:EtOAc = 4:1) afforded *tert*-butyl ((3*R*,3*aS*,4*S*,5*R*,6*S*,7*S*,7*aS*)-5,7-bis(benzyloxy)-4-formyl-3-hydroxy-2',2'-dimethyl-2-oxohexahydro-3*aH*-spiro[benzofuran-6,4'-[1,3]dioxolan]-3*a*-yl)carbamate (**1.2.6.3**, 2.6 mg, 4.4 μmol , 56%) as an off-white gum.

R_f (pentane:EtOAc = 11:4) = 0.28. (CAM)

^1H NMR (400 MHz, C_6D_6) δ (ppm) = 9.44 (d, $J = 2.3$ Hz, 1H), 7.33 (d, $J = 7.2$ Hz, 2H), 7.24 (d, $J = 7.1$ Hz, 2H), 7.19 (m, 3H), 7.09 (m, 3H), 6.35 (s, 1H), 5.44 (d, $J = 2.9$ Hz, 1H), 5.00 (s, 1H), 4.70 (d, J

= 11.2 Hz, 1H), 4.59 – 4.51 (m, 2H), 4.48 (d, $J = 12.1$ Hz, 1H), 4.16 (d, $J = 11.2$ Hz, 1H), 4.08 (d, $J = 8.7$ Hz, 1H), 3.78 – 3.68 (m, 2H), 2.82 – 2.74 (dd, $J = 12.1, 2.0$ Hz, 1H), 2.71 (s, 1H), 1.47 (s, 3H), 1.35 (d, 12H).

The aromatic signals are overlapping with the NMR solvent.

^{13}C NMR (101 MHz, C_6D_6) δ (ppm) = 203.1, 172.4, 154.6, 138.2, 137.7, 128.7, 128.5, 127.3, 110.2, 86.2, 80.9, 79.5, 75.9, 75.3, 73.6, 73.0, 71.4, 65.2, 64.6, 49.8, 28.2, 26.8, 26.6.

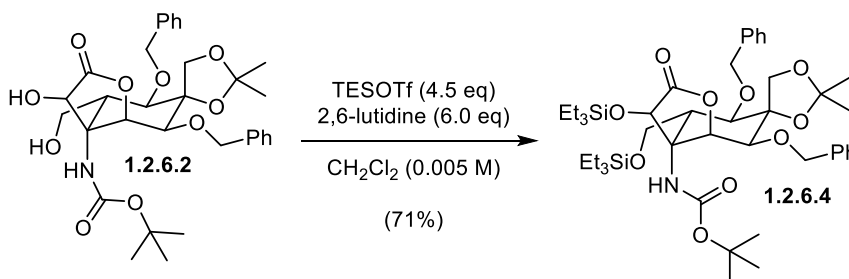
According to the 2D spectra, three carbon signals are obscured by the NMR solvent.

HRMS (ESI): calc. for $\text{C}_{32}\text{H}_{43}\text{N}_2\text{O}_{10}^+$ $[\text{M} + \text{NH}_4^+]^+$: 615.2912, found: 615.2914.

IR (Diamond-ATR, neat) ν_{max} (cm^{-1}) = 3365 (br, vw), 2927 (w), 2366 (vw), 1795 (w), 1710 (m), 1498 (w), 1454 (w), 1368 (m), 1259 (m), 1205 (m), 1160 (m), 1069 (vs), 1027 (vs), 864 (m), 799 (s), 735 (s), 697 (s).

$[\alpha]_{\text{D}}^{20} = +22^\circ$ ($c = 0.26$, EtOAc).

tert-butyl ((3*R*,3*aR*,4*R*,5*R*,6*S*,7*S*,7*aS*)-5,7-bis(benzyloxy)-2',2'-dimethyl-2-oxo-3-((triethylsilyl)oxy)-4-(((triethylsilyl)oxy)methyl)hexahydro-3*aH*-spiro[benzofuran-6,4'-[1,3]dioxolan]-3*a*-yl)carbamate (1.2.6.4)



Diol (**1.2.6.3**, 1.0 mg, 1.7 μmol , 1.0 eq) was dissolved in CH_2Cl_2 (0.23 mL) and a solution of 2,6-lutidine (1.16 μL , 10.0 μmol , 6.0 eq) and TESOTf (1.70 μL , 7.50 μmol , 4.5 eq) in CH_2Cl_2 (0.1 mL) was added. The reaction was stirred for 25 min at rt and after addition of sat. aq. NH_4Cl (0.5 mL), the mixture was diluted with sat. aq. NaHCO_3 /sat. aq. NaCl (1:1, 5 mL) and extracted with CH_2Cl_2 (2×15 mL). The combined organic layers were dried over Na_2SO_4 and concentrated. Purification via flash column chromatography (pentane:Et₂O = 19:1 \rightarrow 9:1 \rightarrow pentane:EtOAc = 9:1) provided *tert*-butyl ((3*R*,3*aR*,4*R*,5*R*,6*S*,7*S*,7*aS*)-5,7-bis(benzyloxy)-2',2'-dimethyl-2-oxo-3-((triethylsilyl)oxy)-4-(((triethylsilyl)oxy)methyl)hexahydro-3*aH*-spiro[benzofuran-6,4'-[1,3]dioxolan]-3*a*-yl)carbamate (**1.2.6.4**, 1.0 mg, 1.2 mmol, 71%) as a colorless oil.

R_f (pentane:EtOAc = 9:1) = 0.73. (CAM)

$^1\text{H NMR}$ (400 MHz, C_6D_6) δ (ppm) = 7.42 (d, J = 7.6 Hz, 2H), 7.38 – 7.28 (m, 4H), 7.23 (m, 3H), 7.13 – 7.02 (m, 3H), 6.00 (s, 1H), 5.67 (d, J = 3.0 Hz, 1H), 5.26 (d, J = 12.1 Hz, 1H), 4.84 (d, J = 12.1 Hz, 1H), 4.76 (d, J = 8.8 Hz, 1H), 4.61 (d, J = 10.0 Hz, 1H), 4.57 (s, 2H), 4.25 (d, J = 8.8 Hz, 1H), 4.11 (dd, J = 10.0, 3.7 Hz, 1H), 3.99 (d, J = 11.7 Hz, 1H), 3.88 (d, J = 3.1 Hz, 1H), 1.96 (dd, J = 11.7, 3.4 Hz, 1H), 1.52 (s, 3H), 1.41 (d, 12H), 1.06 (t, J = 7.9 Hz, 9H), 0.93 (t, J = 7.9 Hz, 9H), 0.87 – 0.74 (m, 6H), 0.57 (dq, J = 10.5, 7.9 Hz, 6H).

The aromatic signals are overlapping with the NMR solvent.

$^{13}\text{C NMR}$ (101 MHz, C_6D_6) δ (ppm) = 172.2, 159.1, 139.0, 137.7, 128.5, 128.3, 127.0, 126.9, 125.9, 109.3, 86.7, 79.4, 76.4, 75.0, 74.3, 73.5, 72.9, 72.5, 64.4, 63.0, 60.1, 41.9, 28.0, 26.5, 26.2, 6.8, 6.7, 4.8, 4.2.

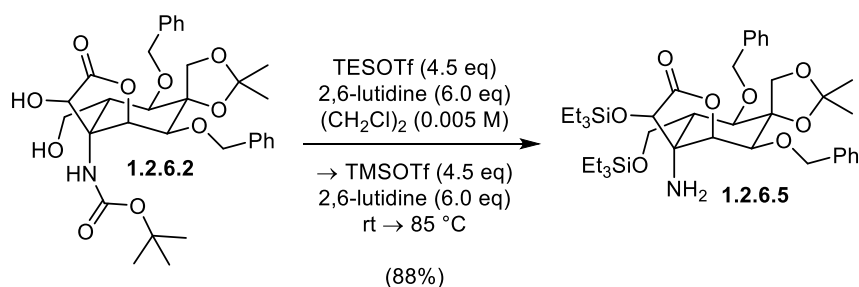
According to the 2D spectra, two carbon signals are obscured by the NMR solvent.

HRMS (ESI): calc. for $\text{C}_{44}\text{H}_{73}\text{N}_2\text{O}_{10}\text{Si}_2^+$ [$\text{M} + \text{NH}_4^+$] $^{+}$: 845.4898, found: 845.4891.

IR (Diamond-ATR, neat) ν_{max} (cm^{-1}) = 3347 (br, vw), 2956 (m), 2918 (s), 2878 (w), 2851 (m), 1944 (vw), 1801 (m), 1710 (m), 1579 (w), 1519 (m), 1456 (m), 1413 (w), 1368 (m), 1284 (m), 1259 (s), 1205 (m), 1148 (vs), 1067 (vs), 1018 (s), 972 (m), 945 (w), 916 (w), 868 (m), 798 (s), 733 (vs), 696 (s).

$[\alpha]_{\text{D}}^{20} = +4.6^\circ$ ($c = 0.13$, EtOAc).

(3*R*,3*aR*,4*R*,5*R*,6*S*,7*S*,7*aS*)-3*a*-amino-5,7-bis(benzyloxy)-2',2'-dimethyl-3-((triethylsilyl)oxy)-4-(((triethylsilyl)oxy)methyl)hexahydro-2*H*-spiro[benzofuran-6,4'-[1,3]dioxolan]-2-one (1.2.6.5)



Diol (**1.2.6.2**, 1.5 mg, 2.5 μmol , 1.0 eq) was dissolved (CH_2Cl_2) (0.5 mL) and a solution of 2,6-lutidine (1.73 μL , 15.0 μmol , 6.0 eq) and TESOTf (2.55 μL , 11.3 μmol , 4.5 eq) in (CH_2Cl_2) (0.05 mL) was added. The reaction was stirred for 1 h before a solution of 2,6-lutidine (1.73 μL ,

15.0 μmol , 6.0 eq) and TMSOTf (2.04 μL , 11.3 μmol , 4.5 eq) in $(\text{CH}_2\text{Cl})_2$ (0.05 mL) was added and the reaction was heated to 85 $^\circ\text{C}$. After 1 h 20 min at 85 $^\circ\text{C}$, MeOH (2 drops) was added. The mixture was diluted with sat. aq. NaHCO_3 /sat. aq. NaCl (1:1, 5 mL) and extracted with CH_2Cl_2 (2 \times 15 mL). The combined organic layers were dried over Na_2SO_4 and concentrated. Purification via flash column chromatography (pentane:Et₂O = 4:1) gave (3*R*,3*aR*,4*R*,5*R*,6*S*,7*S*,7*aS*)-3*a*-amino-5,7-bis(benzyloxy)-2',2'-dimethyl-3-(((triethylsilyl)oxy)-4-(((triethylsilyl)oxy)methyl)hexahydro-2*H*-spiro[benzofuran-6,4'-[1,3]dioxolan]-2-one (1.2.6.5, 1.6 mg, 2.2 mmol, 88%) as a colorless gum.

R_f (pentane:EtOAc = 9:1) = 0.18. (CAM)

$^1\text{H NMR}$ (400 MHz, $(\text{CD}_3)_2\text{CO}$) δ (ppm) = 7.46 – 7.18 (m, 10H), 5.05 (d, J = 12.1 Hz, 1H), 4.93 (d, J = 12.1 Hz, 1H), 4.77 (s, 2H), 4.65 (s, 1H), 4.59 (d, J = 10.0 Hz, 1H), 4.48 (d, J = 3.1 Hz, 1H), 4.28 (d, J = 8.3 Hz, 1H), 4.14 (dd, J = 10.0, 3.9 Hz, 1H), 4.09 – 4.02 (m, 2H), 4.00 (d, J = 8.3 Hz, 1H), 1.62 (dd, J = 11.5, 3.6 Hz, 1H), 1.36 (s, 3H), 1.26 (s, 3H), 1.02 (t, J = 7.9 Hz, 9H), 0.94 (t, J = 7.9 Hz, 9H), 0.76 (qd, J = 8.4, 7.9, 3.4 Hz, 6H), 0.68 – 0.57 (m, 6H).

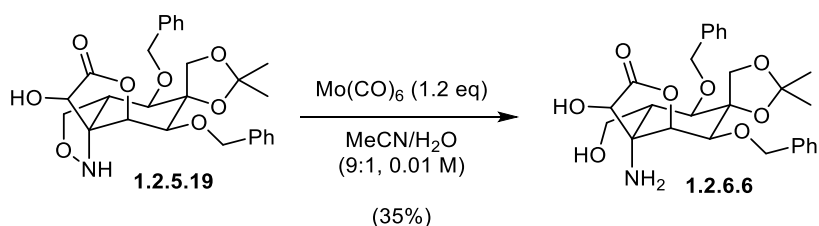
$^{13}\text{C NMR}$ (101 MHz, $(\text{CD}_3)_2\text{CO}$) δ (ppm) = 174.2, 140.3, 139.3, 129.1, 128.8, 128.5, 128.4, 127.5, 126.8, 109.8, 88.2, 82.5, 81.1, 77.5, 76.5, 74.8, 73.6, 64.7, 62.4, 60.6, 43.5, 27.0, 26.8, 7.3, 7.1, 5.4, 5.0.

HRMS (ESI): calc. for $\text{C}_{39}\text{H}_{62}\text{NO}_{10}\text{Si}_2^+$ [$\text{M} + \text{H}^+$] $^+$: 728.4008, found: 728.4005.

IR (Diamond-ATR, neat) ν_{max} (cm^{-1}) = 2954 (m), 2923 (s), 2877 (m), 2854 (m), 2361 (vw), 1797 (m), 1735 (br, vw), 1498 (vw), 1456 (m), 1413 (vw), 1378 (w), 1243 (m), 1205 (m), 1148 (s), 1095 (vs), 1070 (vs), 1016 (s), 974 (m), 948 (m), 870 (w), 812 (m), 731 (vs), 696 (m).

$[\alpha]_{\text{D}}^{20} = +11^\circ$ (c = 0.20, EtOAc).

(3*R*,3*aS*,4*R*,5*R*,6*S*,7*S*,7*aS*)-3*a*-amino-5,7-bis(benzyloxy)-3-hydroxy-4-(hydroxymethyl)-2',2'-dimethylhexahydro-2*H*-spiro[benzofuran-6,4'-[1,3]dioxolan]-2-one (1.2.6.6)



Isoxazolidine (**1.2.5.19**, 2.0 mg, 4.0 μmol , 1.0 eq) and $\text{Mo}(\text{CO})_6$ (1.3 mg, 4.8 μmol , 1.2 eq) were dissolved in MeCN/ H_2O (9:1, 0.8 mL) and heated to 85 $^\circ\text{C}$ for 47 min. After cooling to rt, the mixture was diluted with sat. aq. NaHCO_3 /sat. aq. NaCl (1:1, 5 mL) and extracted with EtOAc (2×15 mL). The combined organic layers were dried over Na_2SO_4 and concentrated. Purification via flash column chromatography (EtOAc \rightarrow CH_2Cl_2 :MeOH = 29:1 \rightarrow 14:1) afforded (3*R*,3*aS*,4*R*,5*R*,6*S*,7*S*,7*aS*)-3*a*-amino-5,7-bis(benzyloxy)-3-hydroxy-4-(hydroxymethyl)-2',2'-dimethylhexahydro-2*H*-spiro[benzofuran-6,4'-[1,3]dioxolan]-2-one (**1.2.6.6**, 0.70 mg, 1.4 μmol , 35%) as an clear colorless gum.

R_f (EtOAc) = 0.12. (CAM)

^1H NMR (400 MHz, $(\text{CD}_3)_2\text{CO}$) δ (ppm) = 7.47 – 7.20 (m, 10H), 4.96 (d, J = 11.5 Hz, 1H), 4.86 (d, J = 11.5 Hz, 1H), 4.83 – 4.73 (m, 2H), 4.49 (m, 2H), 4.41 (dd, J = 10.8, 2.2 Hz, 1H), 4.28 (d, J = 8.3 Hz, 1H), 4.07 (d, J = 3.3 Hz, 1H), 4.00 – 3.96 (m, 2H), 3.94 (d, J = 11.9 Hz, 1H), 1.65 (ddd, J = 11.7, 4.9, 2.1 Hz, 1H), 1.37 (s, 3H), 1.33 (s, 3H).

^{13}C NMR (101 MHz, $(\text{CD}_3)_2\text{CO}$) δ (ppm) = 174.7, 140.1, 139.3, 129.1, 128.9, 128.5, 128.3, 127.8, 127.7, 109.9, 87.9, 81.2, 80.8, 78.6, 76.8, 75.5, 73.5, 64.7, 62.3, 59.6, 44.3, 27.1, 26.9.

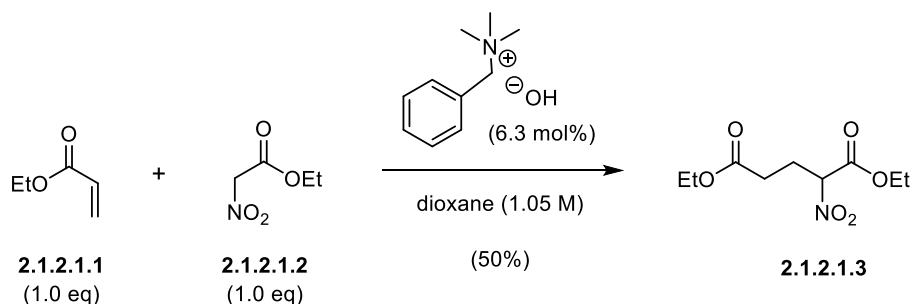
HRMS (ESI): calc. for $\text{C}_{27}\text{H}_{34}\text{NO}_8$ $[\text{M} + \text{H}]^+$: 500.2279, found: 500.2278.

IR (Diamond-ATR, neat) ν_{max} (cm^{-1}) = 3311 (br, vw), 2921 (s), 2852 (m), 1782 (w), 1713 (w), 1660 (vw), 1624 (vw), 1606 (vw), 1498 (vw), 1455 (m), 1413 (w), 1378 (w), 1369 (w), 1245 (m), 1206 (m), 1142 (s), 1067 (vs), 1028 (s), 969 (m), 931 (w), 890 (w), 866 (m), 832 (w), 801 (w), 734 (s).

$[\alpha]_{\text{D}}^{20} = +46^\circ$ (c = 0.13, EtOAc).

3.2.2 Experimental Procedures – Chapter 2

diethyl 2-nitropentanedioate (2.1.2.1.3)



Benzyltrimethylammonium hydroxide (40% in dioxane, 1.90 mL, 2.38 mmol, 0.063 eq) and ethyl 2-nitroacetate (**2.1.2.1.2**, 4.17 mL, 37.6 mmol, 1.0 eq) were dissolved in dioxane (35.8 mL), heated to 65 °C and ethyl acrylate (**2.1.2.1.1**, 4.10 mL, 37.6 mmol, 1.0 eq) was added dropwise. The orange solution was stirred for 15 h and after cooling to rt, CH₂Cl₂ (45 mL) and 2 M aq. HCl (65 mL) were added followed by vigorous stirring for 15 minutes. The mixture was diluted with CH₂Cl₂ (150 mL), the layers were separated and the organic phase was washed with H₂O (2 × 100 mL) and dried over Na₂SO₄. Removal of the solvent *in vacuo* and purification via flash column chromatography (pentane:EtOAc = 19:1) afforded diethyl 2-nitropentanedioate (**2.1.2.1.3**, 4.41 g, 18.9 mmol, 50%) as a clear colorless oil.

R_f (pentane:EtOAc = 9:1) = 0.23. (KMnO₄)

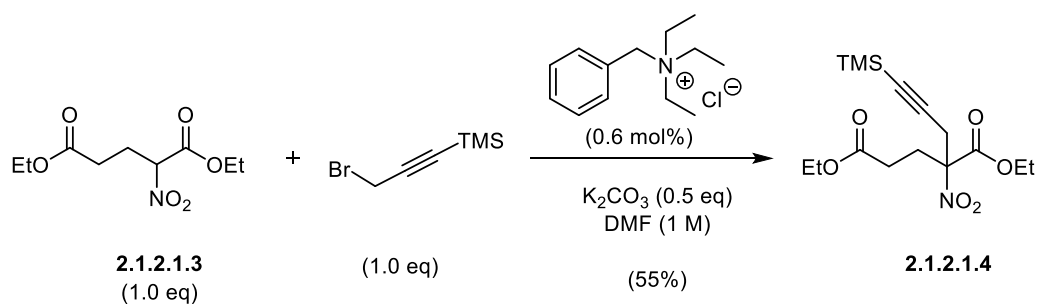
¹H NMR (400 MHz, CDCl₃) δ (ppm) = 5.34 – 5.27 (m, 1H), 4.30 (q, *J* = 7.2 Hz, 2H), 4.16 (q, *J* = 7.1 Hz, 2H), 2.62 – 2.36 (m, 4H), 1.31 (t, *J* = 7.2 Hz, 3H), 1.27 (t, *J* = 7.1 Hz, 3H).

¹³C NMR (101 MHz, CDCl₃) δ (ppm) = 171.6, 164.3, 86.9, 63.3, 61.2, 29.8, 25.5, 14.3, 14.0.

HRMS (EI): calc. for C₉H₁₆NO₆⁺ [M + H]⁺: 234.0972, found: 234.0955.

IR (Diamond-ATR, neat) ν_{max} (cm⁻¹) = 2985 (vw), 2361 (vw), 1730 (vs), 1559 (vs), 1466 (vw), 1444 (w), 1373 (m), 1297 (m), 1259 (s), 1193 (s), 1096 (m), 1019 (s), 890 (vw), 857 (w), 795 (w), 736 (w), 688 (w).

diethyl 2-nitro-2-(3-(trimethylsilyl)prop-2-yn-1-yl)pentanedioate (**2.1.2.1.4**)



Benzyltriethylammonium chloride (17.6 mg, 77.4 μmol, 0.006 eq), K₂CO₃ (891 mg, 6.45 mmol, 0.5 eq) and diethyl 2-nitropentanedioate (**2.1.2.1.3**, 3.00 g, 12.9 mmol, 1.0 eq) were dissolved in DMF (12.9 mL) and 3-bromo-1-(trimethylsilyl)propyne (2.11 mL, 12.9 mmol, 1.0 eq) was added. The pink solution gradually darkened to purple and brown while stirring for 15 hours at 60 °C. Thereafter, the mixture was cooled to rt and the solvent was removed *in vacuo*. The

residue was dissolved in Et₂O (150 mL), washed with 10% aq. LiCl (2 × 100 mL) and the organic layer was dried over Na₂SO₄ and concentrated. Purification via column chromatography (pentane:Et₂O = 39:1) afforded diethyl 2-nitro-2-(3-(trimethylsilyl)prop-2-yn-1-yl)pentanedioate (**2.1.2.1.4**, 2.44 g, 7.10 mmol, 55%) as a colorless oil.

R_f (pentane:Et₂O = 9:1) = 0.29. (KMnO₄)

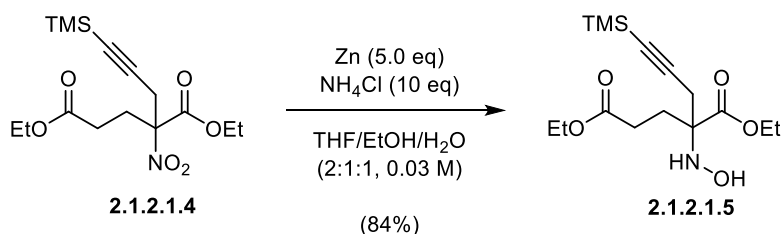
¹H NMR (400 MHz, CDCl₃) δ (ppm) = 4.31 – 4.21 (m, 2H), 4.13 (q, *J* = 7.1 Hz, 2H), 3.21 (d, *J* = 17.4 Hz, 1H), 3.10 (d, *J* = 17.5 Hz, 1H), 2.71 – 2.59 (m, 2H), 2.44 – 2.35 (m, 2H), 1.26 (dt, *J* = 14.0, 7.1 Hz, 6H), 0.11 (s, 9H).

¹³C NMR (101 MHz, CDCl₃) δ (ppm) = 171.6, 165.3, 97.2, 93.2, 91.0, 63.4, 61.0, 28.9, 26.8, 14.2, 13.9, –0.2.

HRMS (EI): calc. for C₁₄H₂₂NO₆Si⁺ [M – CH₃]⁺: 328.1211, found: 328.1212.

IR (Diamond-ATR, neat) ν_{max} (cm⁻¹) = 2960 (w), 2900 (vw), 2361 (vw), 2339 (vw), 2183 (w), 1737 (s), 1556 (s), 1465 (vw), 1444 (vw), 1422 (vw), 1370 (w), 1349 (w), 1299 (w), 1250 (s), 1185 (s), 1092 (w), 1029 (m), 840 (vs), 760 (m), 701 (w), 681 (vw), 667 (m).

diethyl 2-(hydroxyamino)-2-(3-(trimethylsilyl)prop-2-yn-1-yl)pentanedioate (**2.1.2.1.5**)



Nitroalkane (**2.1.2.1.4**, 438 mg, 1.28 mmol, 1.0 eq) was dissolved in THF/EtOH/H₂O (2:1:1, 42.5 mL) and NH₄Cl (682 mg, 12.8 mmol, 10.0 eq) and zinc powder (417 mg, 6.38 mmol, 5.0 eq) were sequentially added under vigorous stirring at 0 °C. After stirring for 50 min at 0 °C, the mixture was filtered through celite and the filtercake was rinsed with EtOAc (50 mL). The layers were separated and the organic phase was washed with sat. aq. NaCl (50 mL), dried over Na₂SO₄ and was concentrated. Purification by flash column chromatography (pentane:EtOAc = 17:3) afforded diethyl 2-(hydroxyamino)-2-(3-(trimethylsilyl)prop-2-yn-1-yl)pentanedioate (**2.1.2.1.5**, 353 mg, 1.07 mmol, 84%) as a clear colorless oil.

R_f (pentane:EtOAc = 4:1) = 0.33. (KMnO₄)

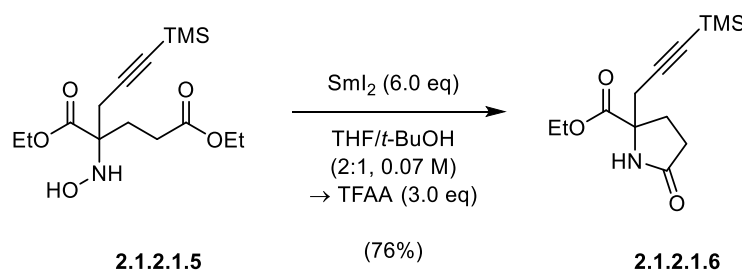
¹H NMR (400 MHz, CDCl₃) δ (ppm) = 5.69 (s, 2H), 4.20 (qd, J = 7.1, 2.0 Hz, 2H), 4.11 (q, J = 7.1 Hz, 2H), 2.68 (d, J = 16.9 Hz, 1H), 2.62 (d, J = 17.0 Hz, 1H), 2.33 (td, J = 7.1, 2.5 Hz, 2H), 2.11 (td, J = 7.1, 4.9 Hz, 2H), 1.27 (t, J = 7.1 Hz, 3H), 1.23 (t, J = 7.2 Hz, 3H), 0.11 (s, 9H).

¹³C NMR (101 MHz, CDCl₃) δ (ppm) = 174.4, 172.3, 100.7, 88.6, 67.9, 61.5, 60.9, 29.2, 27.2, 25.0, 14.3, 14.2, 0.0.

HRMS (EI): calc. for C₁₅H₂₈NO₅²⁹Si⁺ [M]⁺: 330.1687, found: 330.1716.

IR (Diamond-ATR, neat) ν_{\max} (cm⁻¹) = 3451 (br, vw), 2959 (vw), 2361 (vw), 2175 (vw), 1730 (s), 1446 (vw), 1377 (w), 1311 (w), 1249 (m), 1184 (br, m), 1094 (w), 1030 (m), 911 (w), 840 (vs), 759 (m), 730 (vs), 699 (w).

ethyl 5-oxo-2-(3-(trimethylsilyl)prop-2-yn-1-yl)pyrrolidine-2-carboxylate (2.1.2.1.6)



Hydroxylamine (**2.1.2.1.5**, 353 mg, 1.07 mmol, 1.0 eq) was dissolved in THF/*t*-BuOH (15.3 mL) and SmI₂ (0.1 M in THF, 64.3 mL, 6.43 mmol, 6.0 eq) was added dropwise over a period of 17 minutes. After stirring the dark blue reaction for 25 min, trifluoroacetic anhydride (0.446 mL, 3.21 mmol, 3.0 eq) was added and the resulting yellow solution was stirred for additional 30 min at rt. The mixture was diluted with Et₂O (25 mL), washed with sat. aq. NaCl (25 mL), dried over Na₂SO₄ and concentrated. Purification via flash column chromatography (pentane:EtOAc = 4:1 → 2:1) afforded ethyl 5-oxo-2-(3-(trimethylsilyl)prop-2-yn-1-yl)pyrrolidine-2-carboxylate (**2.1.2.1.6**, 218 mg, 0.815 mmol, 76%) as a slightly yellow oil.

R_f (pentane:EtOAc = 1:1) = 0.36. (KMnO₄)

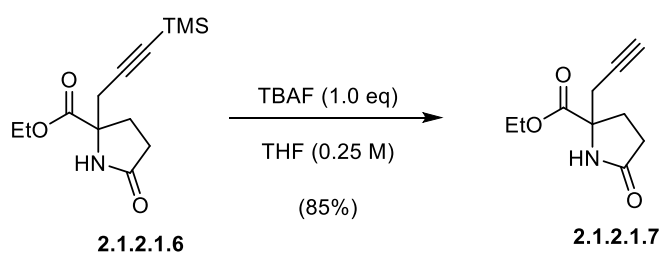
¹H NMR (400 MHz, CDCl₃) δ (ppm) = 6.01 (s, 1H), 4.24 (qd, J = 7.2, 1.3 Hz, 2H), 2.84 (d, J = 16.7 Hz, 1H), 2.59 (d, J = 16.7 Hz, 1H), 2.51 – 2.33 (m, 3H), 2.24 – 2.08 (m, 1H), 1.30 (t, J = 7.1 Hz, 3H), 0.14 (s, 9H).

^{13}C NMR (101 MHz, CDCl_3) δ (ppm) = 176.6, 172.4, 100.0, 89.2, 64.8, 62.3, 31.1, 30.3, 29.9, 14.3, 0.0.

HRMS (ESI): calc. for $\text{C}_{13}\text{H}_{22}\text{NO}_3\text{Si}^+$ $[\text{M} + \text{H}]^+$: 268.1363, found: 268.1362.

IR (Diamond-ATR, neat) ν_{max} (cm^{-1}) = 3199 (br, vw), 2963 (vw), 2358 (vw), 2176 (w), 1740 (s), 1697 (vs), 1455 (vw), 1419 (w), 1357 (w), 1315 (w), 1284 (w), 1241 (vs), 1178 (m), 1132 (w), 1084 (m), 1065 (s), 1031 (s), 1014 (m), 956 (w), 837 (vs), 753 (s), 700 (m), 641 (s).

ethyl 5-oxo-2-(prop-2-yn-1-yl)pyrrolidine-2-carboxylate (2.1.2.1.7)



TMS-alkyne (**2.1.2.1.6**, 711 mg, 2.66 mmol, 1.0 eq) as dissolved in THF (10.6 mL) and TBAF (1 M in THF, 2.66 mL, 2.66 mmol, 1.0 eq) was added dropwise over a period of 3 minutes at 0 °C. The yellow solution was allowed to warm to rt and stirred for 30 min before sat. aq. NH_4Cl (2.6 mL) was added. The mixture was diluted with EtOAc (150 mL), washed with sat. aq. NH_4Cl (20 mL), sat. aq. NaCl (100 mL), dried over Na_2SO_4 and concentrated. Purification by flash column chromatography (pentane:EtOAc = 1:1) afforded ethyl 5-oxo-2-(prop-2-yn-1-yl)pyrrolidine-2-carboxylate (**2.1.2.1.7**, 441 mg, 2.26 mmol, 85%) as a beige wax.

R_f (pentane:EtOAc = 1:1) = 0.19. (KMnO_4)

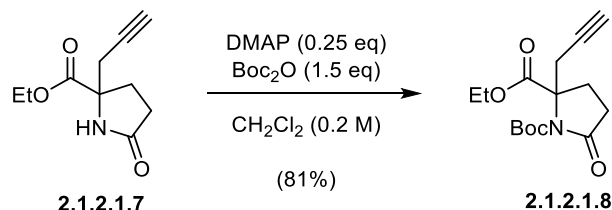
^1H NMR (400 MHz, CDCl_3) δ (ppm) = 6.02 (s, 1H), 4.25 (q, J = 7.1 Hz, 2H), 2.82 (dd, J = 16.6, 2.6 Hz, 1H), 2.60 (dd, J = 16.6, 2.7 Hz, 1H), 2.52 – 2.36 (m, 3H), 2.24 – 2.12 (m, 1H), 2.08 (t, J = 2.6 Hz, 1H), 1.30 (t, J = 7.1 Hz, 3H).

^{13}C NMR (101 MHz, CDCl_3) δ (ppm) = 176.7, 172.2, 78.0, 72.1, 64.5, 62.1, 30.1, 29.8, 29.4, 14.1.

HRMS (ESI): calc. for $\text{C}_{10}\text{H}_{14}\text{NO}_3^+$ $[\text{M} + \text{H}]^+$: 196.0968, found: 196.0967.

IR (Diamond-ATR, neat) ν_{max} (cm^{-1}) = 3249 (w), 3916 (w), 3082 (vw), 2984 (vw), 2928 (vw), 1736 (s), 1688 (vs), 1481 (vw), 1462 (vw), 1433 (w), 1366 (m), 1327 (m), 1296 (m), 1242 (m), 1211 (vs), 1137 (s), 1071 (s), 1016 (m), 941 (vw), 894 (vw), 866 (w), 840 (vw), 740 (s), 709 (s), 674 (vs).

m_p = 34.2 – 36.0 °C.

1-(*tert*-butyl) 2-ethyl 5-oxo-2-(prop-2-yn-1-yl)pyrrolidine-1,2-dicarboxylate (2.1.2.1.8)

Amide (**2.1.2.1.7**, 200 mg, 1.02 mmol, 1.0 eq) was dissolved in CH_2Cl_2 (5.10 mL), cooled to 0 °C and DMAP (31.3 mg, 0.256 mmol, 0.25 eq) was added followed by and Boc_2O (0.351 mL, 1.53 mmol, 1.5 eq). The reaction mixture was allowed to warm to rt and stirred for 8 h before it was diluted with CH_2Cl_2 (10 mL) and washed with 3% aq. KHSO_4 (20 mL) and sat. aq. NaCl (20 mL). The organic layer was dried over Na_2SO_4 and concentrated. Purification via flash column chromatography (pentane:EtOAc = 19:1) yielded 1-(*tert*-butyl) 2-ethyl 5-oxo-2-(prop-2-yn-1-yl)pyrrolidine-1,2-dicarboxylate (**2.1.2.1.8**, 243 mg, 0.822 mmol, 81%) as a white solid.

R_f (pentane:EtOAc = 1:1) = 0.76. (KMnO_4)

$^1\text{H NMR}$ (400 MHz, CDCl_3) δ (ppm) = 4.20(q, $J = 7.1$ Hz, 2H), 3.27 (dd, $J = 17.5, 2.7$ Hz, 1H), 2.90 (dd, $J = 17.5, 2.7$ Hz, 1H), 2.74 (ddd, $J = 17.7, 10.2, 6.3$ Hz, 1H), 2.60 (ddd, $J = 17.6, 10.5, 7.0$ Hz, 1H), 2.31 (ddd, $J = 13.4, 10.2, 7.0$ Hz, 1H), 2.15 (ddd, $J = 13.4, 10.5, 6.2$ Hz, 1H), 2.03 (t, $J = 2.7$ Hz, 1H), 1.51 (s, 9H), 1.27 (t, $J = 7.1$ Hz, 3H).

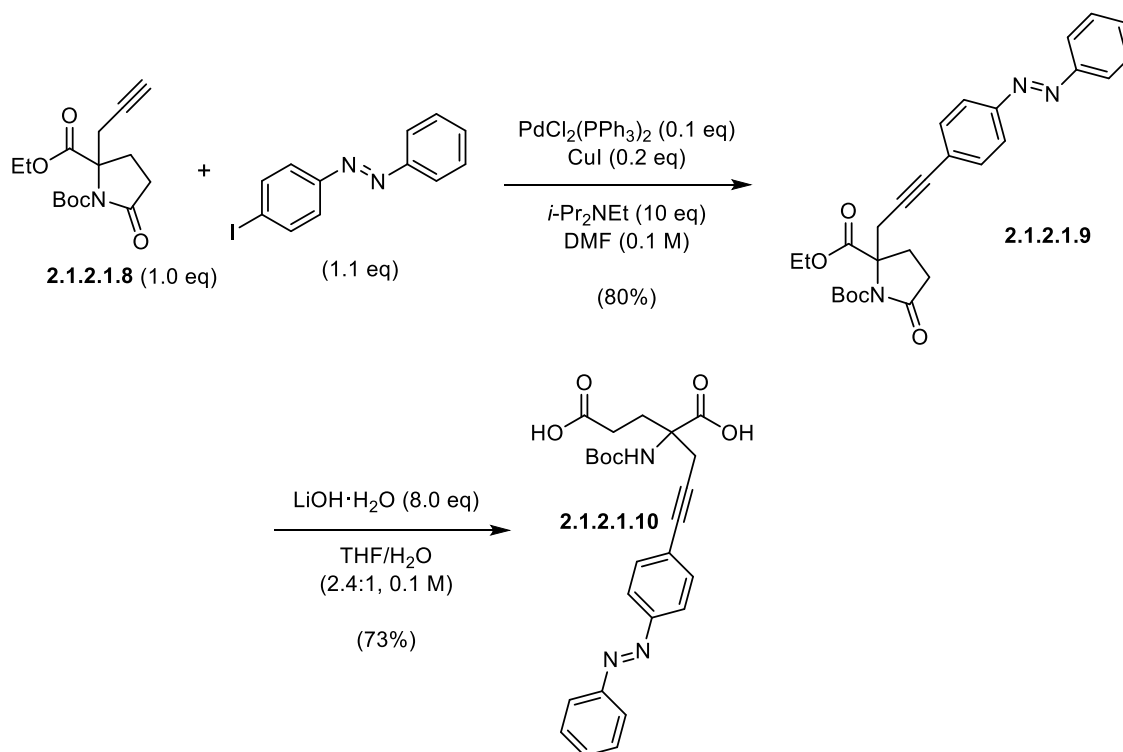
$^{13}\text{C NMR}$ (101 MHz, CDCl_3) δ (ppm) = 174.1, 171.8, 149.3, 84.1, 78.5, 72.3, 67.0, 62.2, 31.2, 28.0, 27.8, 26.4, 14.2.

HRMS (EI): calc. for $\text{C}_{15}\text{H}_{21}\text{NO}_5^+$ $[M]^+$: 295.1414, found: 295.1410.

IR (Diamond-ATR, neat) ν_{max} (cm^{-1}) = 3269 (w), 2984 (vw), 2936 (vw), 1794 (vw), 1738 (vs), 1713 (s), 1460 (w), 1423 (vw), 1396 (vw), 1370 (m), 1305 (vs), 1248 (vs), 1145 (vs), 1090 (s), 1073 (s), 1010 (s), 932 (w), 842 (m), 783 (m), 736 (m), 688 (m).

$m_p = 49.0 - 51.3$ °C.

2-((*tert*-butoxycarbonyl)amino)-2-(3-(4-(phenyldiazenyl)phenyl)prop-2-yn-1-yl)pentanedioic acid (2.1.2.1.10)



Alkyne (**2.1.2.1.8**, 100 mg, 0.339 mmol, 1.0 eq), 1-(4-iodophenyl)-2-phenyldiazene (125 mg, 0.406 mmol, 1.1 eq) and CuI (12.1 mg, 67.8 μmol , 0.2 eq) were dissolved in DMF (3.39 mL) and $i\text{-Pr}_2\text{NEt}$ (0.59 mL, 3.4 mmol, 10 eq) was added. The mixture was degassed via freeze-pump-thaw (2 cycles), $\text{PdCl}_2(\text{PPh}_3)_2$ (23.8 mg, 33.9 μmol , 0.1 eq) was added and the reaction was stirred for 2 h at rt. Thereafter, the solvent was removed *in vacuo* and purified via flash column chromatography (pentane:EtOAc = 17:3) to give 1-(*tert*-butyl) 2-ethyl (*E*)-5-oxo-2-(3-(4-(phenyldiazenyl)phenyl)prop-2-yn-1-yl)pyrrolidine-1,2-dicarboxylate (**2.1.2.1.9**, 130 mg, 0.273 mmol, 80%) as an orange solid with R_f (pentane:EtOAc = 4:1) = 0.33 (visible). The product was dissolved in $\text{THF}/\text{H}_2\text{O}$ (2.4:1, 2.66 mL) and $\text{LiOH}\cdot\text{H}_2\text{O}$ (90.0 mg, 2.18 mmol, 8.0 eq) was added and heated to 60 °C for 12 h. Thereafter, the solution was acidified to pH2 by careful addition of 1 M aq. HCl (1.85 mL) at 0 °C. The aqueous phase was extracted with EtOAc (3 \times 30 mL) and the combined organic layers were dried over Na_2SO_4 and concentrated. Purification via flash column chromatography (CH_2Cl_2 :MeOH:AcOH = 95:4:1) afforded 2-((*tert*-butoxycarbonyl)amino)-2-(3-(4-(phenyldiazenyl)phenyl)prop-2-yn-1-yl)pentanedioic acid (**2.1.2.1.10**, 97.9 mg, 0.198 mmol, 73%) as an orange solid.

Note: Due to the photoswitching properties of the **2.1.2.1.10** azobenzene moiety, the NMR spectra show a mixture of *cis*- and *trans*-isomers. The ^1H - and ^{13}C -NMRs are reported for the thermodynamically more stable *trans*-isomer.

R_f (CH₂Cl₂:MeOH:AcOH = 94:4:2) = 0.23. (visible)

¹H NMR (400 MHz, (CD₃)SO) δ (ppm) = 12.68 (br s, 1H), 12.33 (br s, 1H), 7.97 – 7.84 (m, 4H), 7.65 – 7.54 (m, 5H), 3.17 (d, J = 17.3 Hz, 1H), 2.97 (d, J = 17.2 Hz, 1H), 2.26 – 2.16 (m, 2H), 2.16 – 2.06 (m, 1H), 1.39 (s, 9H).

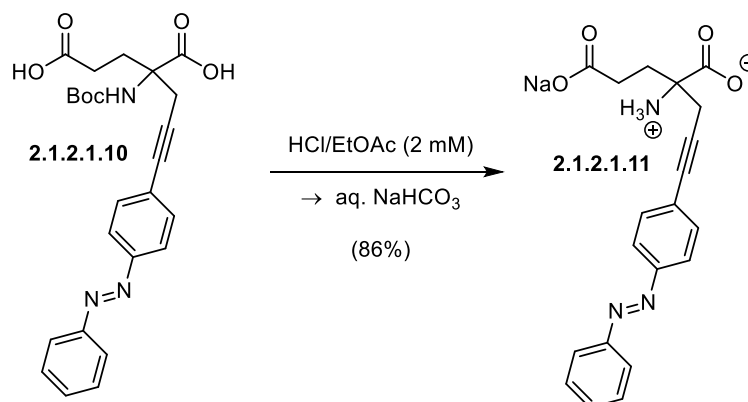
¹³C NMR (101 MHz, (CD₃)SO) δ (ppm) = 173.9, 173.3, 154.3, 151.9, 150.9, 132.5, 131.8, 129.6, 126.2, 122.8, 122.7, 89.9, 78.3, 60.2, 30.0, 28.8, 28.2, 25.4.

HRMS (ESI): calc. for C₂₅H₂₇N₃O₆Na⁺ [M + Na⁺]⁺: 488.1792, found: 488.1791.

IR (Diamond-ATR, neat) ν_{\max} (cm⁻¹) = 2928 (w), 1705 (vs), 1597 (w), 1495 (m), 1394 (m), 1368 (m), 1282 (m), 1236 (s), 1156 (vs), 1055 (s), 923 (m), 845 (s), 768 (s), 726 (m), 687 (s).

m_p = 140.8 – 143.1 °C.

sodium 2-ammonio-2-(3-(4-(phenyldiazenyl)phenyl)prop-2-yn-1-yl)pentanedioate (2.1.2.1.11)



A concentrated solution of HCl/EtOAc was prepared by bubbling HCl gas through EtOAc for 30 min. The HCl gas was generated by dropwise addition of H₂SO₄ onto solid NaCl. Boc amide (**2.1.2.1.10**, 7.1 mg, 15.3 μ mol, 1.0 eq) was dissolved in HCl/EtOAc (7.15 mL) and the reaction was stirred for 4 h 20 min at rt. The precipitate was collected by centrifugation and decanting the solvent. This procedure was repeated after suspending the pellet in Et₂O (7.0 mL). The solid residue was dissolved in sat. aq. NaHCO₃ (0.5 mL) and the solution subjected to reverse-phase flash column chromatography (H₂O:MeCN = 100:0 \rightarrow 95:5 \rightarrow 90:10) to give sodium 2-ammonio-2-(3-(4-(phenyldiazenyl)phenyl)prop-2-yn-1-yl)pentanedioate (**2.1.2.1.11**, 5.1 mg, 13 μ mol, 86%).

Note: Due to the photoswitching properties of the **2.1.2.1.11** azobenzene moiety, the NMR spectra show a mixture of *cis*- and *trans*-isomers. The ^1H - and ^{13}C -NMRs are reported for the thermodynamically more stable *trans*-isomer.

tr (reverse-phase semi-preparative HPLC, MeCN:H₂O:HCOOH = 80:20:0.1% → 20:80:0.1% over 60 min) = 20.39 min.

^1H NMR (800 MHz, D₂O) δ (ppm) = 7.91 – 7.88 (m, 2H), 7.87 – 7.84 (m, 2H), 7.71 – 7.68 (m, 2H), 7.67 – 7.62 (m, 3H), 2.93 (d, J = 16.8 Hz, 1H), 2.71 (d, J = 16.8 Hz, 1H), 2.28 (ddd, J = 14.4, 12.7, 4.9 Hz, 1H), 2.13 (ddd, J = 14.4, 12.6, 4.7 Hz, 1H), 2.04 (td, J = 13.1, 4.7 Hz, 1H), 1.89 (td, J = 13.0, 4.9 Hz, 1H).

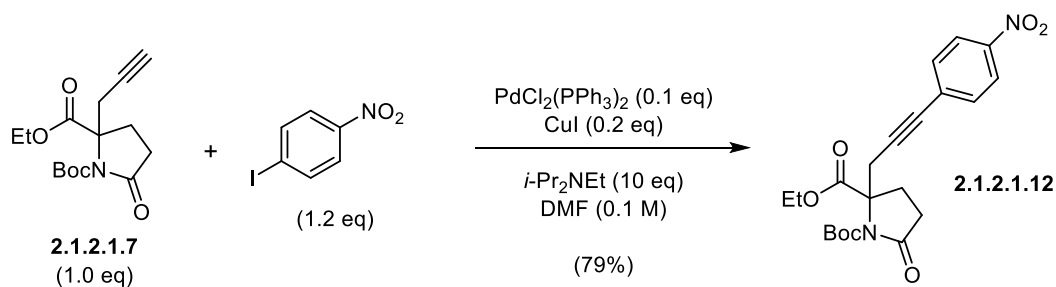
^{13}C NMR (201 MHz, D₂O) δ (ppm) = 182.6, 181.7, 152.3, 151.3, 132.9, 131.9, 129.6, 126.4, 122.5, 122.5, 89.9, 82.5, 61.4, 36.0, 32.9, 30.4

HRMS (ESI): calc. for C₂₀H₁₈N₃O₄⁻ [M – H]⁺: 364.1303, found: 364.1303.

IR (Diamond-ATR, neat) ν_{max} (cm⁻¹) = 2923 (m), 2853 (w), 1713 (m), 1596 (vs), 1536 (w), 1495 (w), 1481 (w), 1462 (w), 1451 (w), 1411 (s), 1392 (s), 1322 (w), 1285 (m), 1232 (s), 1156 (s), 1106 (s), 1071 (m), 1038 (m), 923 (m), 869 (m), 847 (vs), 802 (m), 765 (vs), 724 (m), 685 (vs).

m_p = 158.5 – 161.3 °C.

1-(*tert*-butyl) 2-ethyl 2-(3-(4-nitrophenyl)prop-2-yn-1-yl)-5-oxopyrrolidine-1,2-dicarboxylate (**2.1.2.12**)



Alkyne (**2.1.2.1.7**, 400 mg, 1.35 mmol, 1.0 eq), 1-iodo-4-nitrobenzene (405 mg, 1.63 mmol, 1.2 eq) and CuI (51.4 mg, 270 μmol , 0.2 eq) were dissolved in DMF (13.5 mL) and *i*-Pr₂NEt (2.35 mL, 13.5 mmol, 10 eq) was added. The mixture was degassed via freeze-pump-thaw (2 cycles), PdCl₂(PPh₃)₂ (94.8 mg, 135 μmol , 0.1 eq) was added and the reaction was stirred for 2 h at rt. Thereafter, the solvent was removed *in vacuo* and purified via flash column

chromatography (pentane:EtOAc = 4:1) gave 1-(*tert*-butyl) 2-ethyl 2-(3-(4-nitrophenyl)prop-2-yn-1-yl)-5-oxopyrrolidine-1,2-dicarboxylate (**2.1.2.1.12**, 445 mg, 1.07 mmol, 79%) as an orange oil.

R_f (pentane:EtOAc = 2:1) = 0.48. (UV)

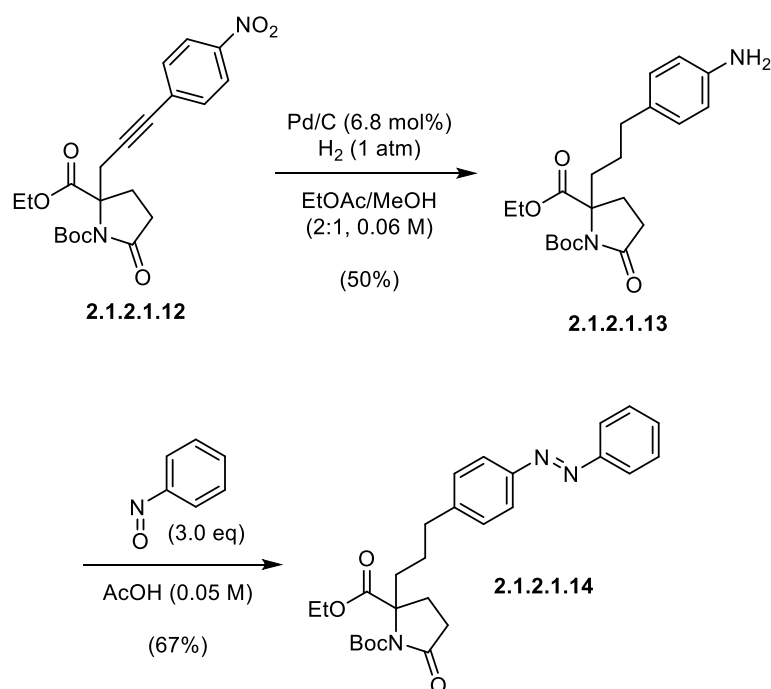
$^1\text{H NMR}$ (400 MHz, CDCl_3) δ (ppm) = 8.15 (d, J = 8.2 Hz, 2H), 7.53 – 7.47 (m, 2H), 4.25 (q, J = 7.1 Hz, 2H), 3.55 (d, J = 17.7 Hz, 1H), 3.16 (d, J = 17.7 Hz, 1H), 2.70 (qdd, J = 17.7, 10.1, 6.8 Hz, 2H), 2.28 (dddd, J = 30.6, 13.5, 10.0, 6.9 Hz, 2H), 1.52 (s, 9H), 1.30 (td, J = 7.1, 1.2 Hz, 3H).

$^{13}\text{C NMR}$ (101 MHz, CDCl_3) δ (ppm) = 173.9, 171.6, 149.3, 147.2, 132.6, 129.7, 123.8, 89.7, 84.4, 82.7, 67.1, 62.4, 31.2, 28.3, 28.1, 27.8, 14.2.

HRMS (ESI): calc. for $\text{C}_{21}\text{H}_{24}\text{N}_2\text{O}_7\text{Na}^+$ [$\text{M} + \text{Na}^+$] $^+$: 439.1476, found: 439.1478.

IR (Diamond-ATR, neat) ν_{max} (cm^{-1}) = 2980 (vw), 2936 (vw), 2227 (vw), 1790 (m), 1740 (s), 1714 (s), 1593 (m), 1492 (vw), 1477 (vw), 1457 (w), 1423 (vw), 1394 (vw), 1369 (w), 1342 (vs), 1305 (vs), 1250 (vs), 1216 (m), 1151 (vs), 1091 (s), 1068 (s), 1045 (w), 1023 (m), 1010 (m), 946 (w), 852 (vs), 777 (m), 749 (s), 688 (m).

1-(*tert*-butyl) 2-ethyl-5-oxo-2-(3-(4-(phenyldiazenyl)phenyl)propyl)pyrrolidine-1,2-dicarboxylate (**2.1.2.1.14**)



Alkyne (**2.1.2.1.12**, 24.0 mg, 57.6 μmol , 1.0 eq) was dissolved in degassed EtOAc/MeOH (2:1, 1.5 mL) and Pd/C (10% Pd, 4.2 mg, 3.9 μmol , 6.8 mol%) was added. The suspension was stirred under a H_2 atmosphere (1 atm) for 2 h 30 min followed by filtration through celite and removal of the solvent *in vacuo*. The residue was redissolved in degassed EtOAc/MeOH (2:1, 1.5 mL) and Pd/C (10% Pd, 4.2 mg, 3.9 μmol , 6.8 mol%) was added. After stirring under a H_2 atmosphere (1 atm) for 4 h 40 min, the solid was removed by filtering through celite. The solution was concentrated *in vacuo* and the residue was purified via flash column chromatography (pentane:EtOAc = 2:1 \rightarrow 1:1 \rightarrow 1:2) to give 1-(*tert*-butyl) 2-ethyl 2-(3-(4-aminophenyl)propyl)-5-oxopyrrolidine-1,2-dicarboxylate (**2.1.2.1.13**, 11.3 mg, 28.9 μL , 50%) as a slightly orange clear oil with R_f (pentane:EtOAc = 2:1) = 0.27 (UV). The aniline (**2.1.2.1.13**) was directly dissolved in AcOH (0.6 mL) and nitrosobenzene (9.3 mg, 86.7 μmol , 3.0 eq) was added. After stirring for 40 h at rt the solvent was removed *in vacuo* and the residue was purified via flash column chromatography (pentane:EtOAc = 4:1) to give 1-(*tert*-butyl) 2-ethyl 5-oxo-2-(3-(4-(phenyldiazenyl)phenyl)propyl)pyrrolidine-1,2-dicarboxylate (**2.1.2.1.14**, 9.3 mg, 19 μmol , 67%) as a red/orange oil.

Note: Due to the photoswitching properties of the **2.1.2.1.14** azobenzene moiety, the NMR spectra show a mixture of *cis*- and *trans*-isomers. The ^1H - and ^{13}C -NMRs are reported for the thermodynamically more stable *trans*-isomer.

R_f (pentane:EtOAc = 2:1) = 0.65. (visible)

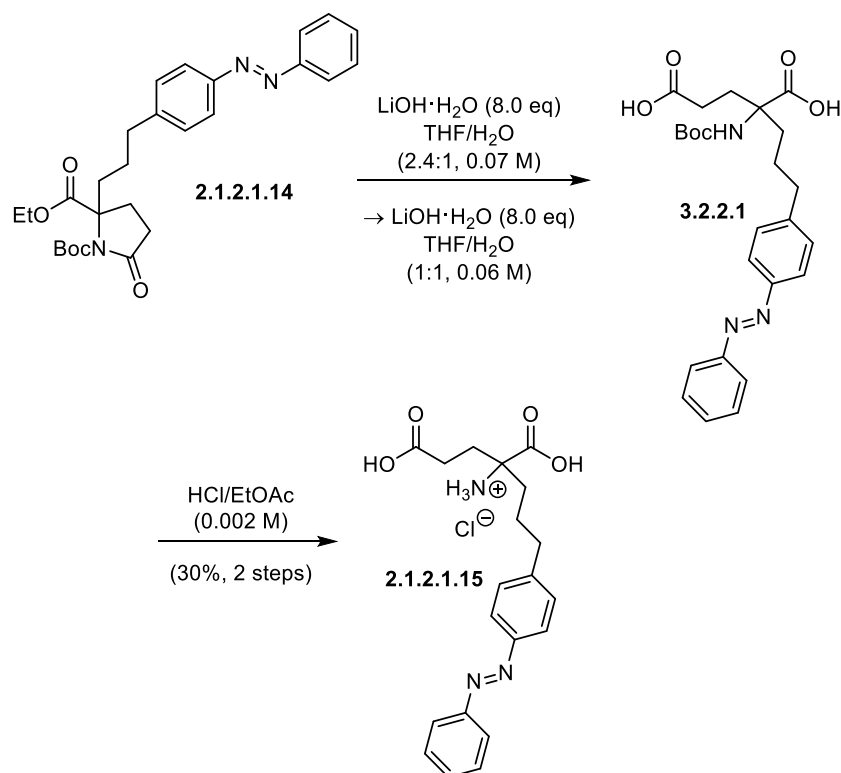
^1H NMR (400 MHz, CDCl_3) δ (ppm) = 7.90 (d, J = 7.4 Hz, 2H), 7.85 (d, J = 8.3 Hz, 2H), 7.56 – 7.42 (m, 3H), 7.31 (d, J = 8.3 Hz, 2H), 4.19 (q, J = 7.1 Hz, 2H), 2.74 (hept, J = 7.0 Hz, 2H), 2.68 – 2.43 (m, 2H), 2.34 (td, J = 13.5, 4.6 Hz, 1H), 2.13 – 1.89 (m, 3H), 1.71 (dddd, J = 19.8, 12.4, 7.1, 4.1 Hz, 1H), 1.55 (dddd, J = 20.0, 12.4, 7.4, 4.7 Hz, 1H), 1.42 (s, 9H), 1.26 (t, J = 7.1 Hz, 3H).

^{13}C NMR (101 MHz, CDCl_3) δ (ppm) = 174.5, 173.1, 152.8, 151.3, 149.4, 145.1, 131.0, 129.3, 129.2, 123.2, 122.9, 83.8, 67.9, 61.8, 35.7, 34.5, 30.9, 28.0, 27.3, 25.0, 14.3.

HRMS (ESI): calc. for $\text{C}_{27}\text{H}_{33}\text{N}_3\text{O}_5\text{Na}^+$ $[\text{M} + \text{Na}^+]^+$: 502.2312, found: 502.2315.

IR (Diamond-ATR, neat) ν_{max} (cm^{-1}) = 2978 (vw), 2918 (w), 2849 (vw), 1786 (s), 1739 (vs), 1717 (s), 1602 (vw), 1499 (vw), 1463 (w), 1446 (w), 1416 (vw), 1393, (vw), 1368 (m), 1292 (s), 1252 (s), 1222 (m), 1151 (vs), 1109 (m), 1094 (m), 1073 (m), 1048 (m), 1020 (m), 967 (vw), 913 (w), 884 (w), 845 (m), 768 (m), 729 (s), 688 (s).

1,3-dicarboxy-6-(4-(phenyldiazenyl)phenyl)hexan-3-aminium chloride (2.1.2.1.15)

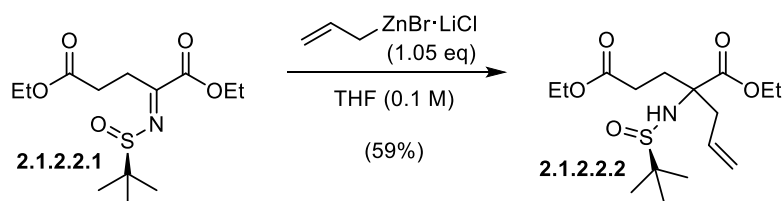


Lactam **2.1.2.1.14** (16.9 mg, 35.2 μmol , 1.0 eq) was dissolved in THF/H₂O (2.4:1, 0.474 mL), LiOH·H₂O (12.1 mg, 0.282 mmol, 8.0 eq) was added and the reaction was heated to 60 °C for 8 h. After cooling to rt, the solvent was removed *in vacuo*. Due to incomplete conversion of the lactam (**2.1.2.1.14**), as determined by LCMS analysis, the residue was redissolved in THF/H₂O (1:1, 0.6 mL) and LiOH·H₂O (12.1 mg, 0.282 mmol, 8.0 eq) was added. The mixture was heated to 60 °C for 5 h. After cooling to rt, HCOOH (10 drops) was added and solvent was removed *in vacuo*. The residue was dissolved in HCl/EtOAc (20 mL), which was prepared by bubbling HCl gas through EtOAc for 30 min, and the reaction was stirred for 19 h at rt. After concentration of the resulting suspension, the remaining gum was purified by reverse-phase semi-preparative HPLC (MeCN:H₂O = 20:80 → 70:30 over 70 min) to give 1,3-dicarboxy-6-(4-(phenyldiazenyl)phenyl)hexan-3-aminium chloride (**2.1.2.1.15**, 4.3 mg, 11 μmol , 30%).

¹H NMR (400 MHz, (CD₃)SO) δ (ppm) = 12.58 (br s, 1H), 12.16 (br s, 1H), 7.87 (d, J = 7.4 Hz, 2H), 7.82 (d, J = 7.9 Hz, 2H), 7.65 – 7.52 (m, 3H), 7.38 (d, J = 8.0 Hz, 2H), 2.64 (t, J = 7.7 Hz, 2H), 2.18 – 1.90 (m, 4H), 1.92 – 1.63 (m, 2H), 1.57 – 1.42 (m, 2H).

^{13}C NMR (101 MHz, $(\text{CD}_3)_2\text{SO}$) δ (ppm) = 174.9, 174.7, 152.4, 150.7, 146.7, 131.8, 129.9, 129.8, 123.1, 122.9, 61.3, 35.4, 33.8, 29.5, 29.2, 25.6.

diethyl 2-allyl-2-(((*R*)-*tert*-butylsulfinyl)amino)pentanedioate (2.1.2.2.2)



Allyl bromide (0.438 mL, 5.19 mmol, 3.16 eq) was added dropwise to a suspension of flame-dried LiCl (241 mg, 5.69 mmol, 3.47 eq), zinc (675.9 mg, 10.33 mmol, 6.30 eq) and 1,2-dibromoethane (3 drops) in THF (7.8 mL). As soon as bubbling of the mixture was observed, the reaction was cooled to 0 °C and stirred for 1 h. Thereafter, the grey suspension was allowed to warm to rt and stirring was continued for 30 min. The solid residue was removed by filtration through a syringe filter (Chromafil® Xtra GF100/25, pore size 1 μm) to give a clear solution. The concentration of the reactive allyl zinc species was determined to be 0.594 M by titration.¹⁵⁸ In a separate flask, diethyl (*R,E*)-2-((*tert*-butylsulfinyl)imino)pentanedioate¹³⁸ (2.1.2.2.1, 500.0 mg, 1.637 mmol, 1.0 eq) was dissolved in THF (16.4 mL), cooled to -78 °C and allyl zinc bromide lithium chloride (0.594 M in THF, 2.90 mL, 1.72 mmol, 1.05 eq) was added dropwise. The clear solution was stirred for 30 min and sat. aq. NH_4Cl (7.0 mL) was added. After diluting the mixture with EtOAc (400 mL), the organic layer was washed with sat. aq. NH_4Cl /sat. aq. NaCl (1:1, 100 mL), dried over Na_2SO_4 and concentrated. Purification via flash column chromatography (pentane:EtOAc = 7:3) afforded a single diastereomer of diethyl 2-allyl-2-(((*R*)-*tert*-butylsulfinyl)amino)pentanedioate (2.1.2.2.2, 335.2 mg, 0.9647 mmol, 59%) as a pale yellow oil.

R_f (pentane:EtOAc = 7:3) = 0.25. (KMnO_4)

^1H NMR (400 MHz, CDCl_3) δ (ppm) = 5.82 – 5.67 (m, 1H), 5.00 (d, J = 4.0 Hz, 1H), 4.97 (s, 1H), 4.57 (s, 1H), 4.00 – 3.76 (m, 4H), 3.05 (ddd, J = 15.7, 10.4, 5.4 Hz, 1H), 2.68 – 2.50 (m, 3H), 2.45 – 2.31 (m, 1H), 1.03 (s, 9H), 0.90 (dt, J = 14.2, 7.1 Hz, 6H).

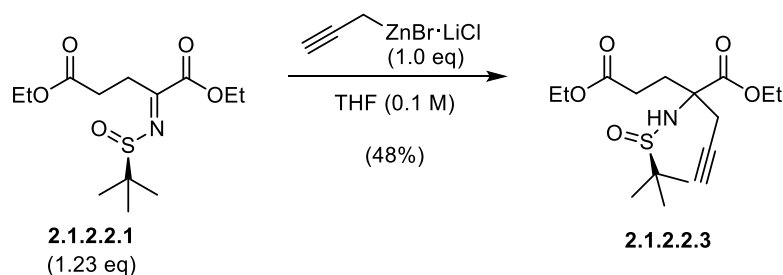
^{13}C NMR (101 MHz, CDCl_3) δ (ppm) = 172.9, 172.5, 133.0, 118.8, 64.9, 61.9, 60.4, 56.0, 42.5, 34.6, 29.2, 22.7, 14.2, 14.0.

HRMS (ESI): calc. for $C_{16}H_{28}NO_5S^- [M - H]^+$: 346.1694, found: 346.1695.

IR (Diamond-ATR, neat) ν_{\max} (cm^{-1}) = 3321 (br, vw), 2980 (w), 2358 (vw), 1728 (vs), 1641 (vw), 1446 (w), 1366 (m), 1295 (w), 1221 (s), 1180 (vs), 1070, (vs), 1018 (s), 972 (w), 920 (m), 852 (m), 794 (w), 668 (w).

$[\alpha]_D^{20} = -24.2^\circ$ ($c = 5.58$, EtOAc).

diethyl 2-(((*R*)-*tert*-butylsulfinyl)amino)-2-(prop-2-yn-1-yl)pentanedioate (2.1.2.2.3)



Propargyl bromide (80% in PhMe, 0.383 mL, 3.45 mmol, 2.6 eq) was added dropwise to a suspension of flame-dried LiCl (161 mg, 3.79 mmol, 2.85 eq), Mg (168 mg, 6.89 mmol, 5.2 eq), ZnCl₂ (776 mg, 3.45 mmol, 2.6 eq) and 1,2-dibromoethane (3 drops) in THF (7.0 mL). The grey suspension was stirred for 3 h at rt. Thereafter, the solid residue was removed by filtration through a syringe filter (Chromafil® Xtra GF100/25, pore size 1 μm) to give a clear solution. The concentration of the reactive propargyl zinc species was determined to be 0.324 M by titration.¹⁵⁸ In a separate flask, diethyl (*R,E*)-2-((*tert*-butylsulfinyl)imino)pentanedioate¹³⁸ (**2.1.2.2.1**, 500.0 mg, 1.637 mmol, 1.23 eq) was dissolved in THF (16.4 mL), cooled to -78°C and propargyl zinc bromide lithium chloride (0.324 M in THF, 4.10 mL, 1.33 mmol, 1.00 eq) was added dropwise over a period of 10 min. The clear solution was stirred for 75 min and sat. aq. NH₄Cl (7.0 mL) was added. After diluting the mixture with EtOAc (400 mL), the organic layer was washed with sat. aq. NH₄Cl/sat. aq. NaCl (1:1, 100 mL), dried over Na₂SO₄ and concentrated. Purification via flash column chromatography (pentane:EtOAc = 13:7) afforded a single diastereomer of diethyl 2-(((*R*)-*tert*-butylsulfinyl)amino)-2-(prop-2-yn-1-yl)pentanedioate (**2.1.2.2.3**, 219.4 mg, 0.6351 mmol, 48%) as a colorless solid.

R_f (pentane:EtOAc = 7:3) = 0.18. (KMnO₄)

$^1\text{H NMR}$ (400 MHz, C_6D_6) δ (ppm) = 4.43 (s, 1H), 4.00 – 3.84 (m, 4H), 2.99 (dd, J = 16.9, 2.6 Hz, 1H), 2.73 (dd, J = 16.9, 2.6 Hz, 1H), 2.57 – 2.41 (m, 3H), 2.41 – 2.27 (m, 1H), 1.78 (t, J = 2.6 Hz, 1H), 1.03 (s, 9H), 0.98 – 0.89 (m, 6H).

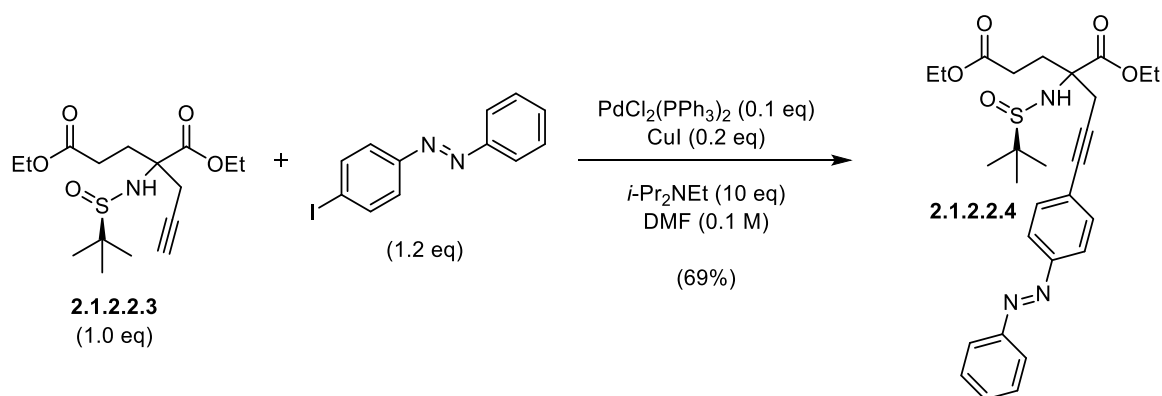
$^{13}\text{C NMR}$ (101 MHz, C_6D_6) δ (ppm) = 172.1, 171.7, 79.1, 72.6, 63.8, 62.0, 60.5, 56.1, 31.3, 29.4, 22.5, 14.2, 14.0.

HRMS (ESI): calc. for $\text{C}_{16}\text{H}_{26}\text{NO}_5\text{S}^-$ [$\text{M} - \text{H}^+$] $^-$: 344.1537, found: 344.1538.

IR (Diamond-ATR, neat) ν_{max} (cm^{-1}) = 3293 (vw), 3138 (vw), 2985 (w), 2906 (vw), 2870 (vw), 1733 (vs), 1445 (w), 1410 (w), 1386 (w), 1365 (w), 1310 (w), 1257 (s), 1205 (s), 1179 (vs), 1149 (m), 1111 (w), 1072 (s), 1055 (s), 1041 (vs), 1019 (vs), 969 (m), 942 (w), 870 (m), 859 (m), 795 (w), 763 (m).

$[\alpha]_{\text{D}}^{20} = -31.5^\circ$ (c = 3.65, EtOAc).

diethyl 2-(((*R*)-*tert*-butylsulfinyl)amino)-2-(3-(4-((*E*)-phenyldiazenyl)phenyl)prop-2-yn-1-yl)pentanedioate (2.1.2.2.4)



Alkyne (**2.1.2.2.3**, 168 mg, 0.486 mmol, 1.0 eq.) was dissolved in DMF (4.86 mL), and CuI (18.5 mg, 97.2 μmol , 0.2 eq), $i\text{-Pr}_2\text{NEt}$ (0.845 mL, 4.86 mmol, 10.0 eq.) and 4-iodoazobenzene (179.6 mg, 0.5813 mmol, 1.2 eq.) were added. The orange solution was degassed by freeze-pump-thaw (2 cycles) and $\text{Pd}(\text{PPh}_3)_2\text{Cl}_2$ (34.1 mg, 48.6 μmol , 0.1 eq.) was added. After stirring the mixture for 2 h at rt, the solvent was removed *in vacuo*. The residue was purified via flash column chromatography (pentane:EtOAc = 7:3) to give diethyl 2-(((*R*)-*tert*-butylsulfinyl)amino)-2-(3-(4-((*E*)-phenyldiazenyl)phenyl)prop-2-yn-1-yl)pentanedioate (**2.1.2.2.4**, 176.2 mg, 0.3352 mmol, 69%) as a red/orange oil.

Note: Due to the photoswitching properties of the **2.1.2.2.4** azobenzene moiety, the NMR spectra show a mixture of *cis*- and *trans*-isomers. The ^1H - and ^{13}C -NMRs are reported for the thermodynamically more stable *trans*.

R_f (pentane:EtOAc = 7:3) = 0.18. (visible)

^1H NMR (400 MHz, C_6D_6) δ (ppm) = 8.00 – 7.94 (m, 2H), 7.86 (d, J = 8.5 Hz, 2H), 7.51 (d, J = 8.5 Hz, 2H), 7.20 – 7.12 (m, 2H), 7.08 (t, J = 7.3 Hz, 1H), 4.55 (s, 1H), 4.04 – 3.82 (m, 4H), 3.29 (d, J = 17.0 Hz, 1H), 3.06 (d, J = 17.0 Hz, 1H), 2.62 – 2.47 (m, 3H), 2.47 – 2.32 (m, 1H), 1.05 (s, 9H), 1.00 – 0.87 (m, 6H).

One aromatic signal is overlapping with the NMR solvent.

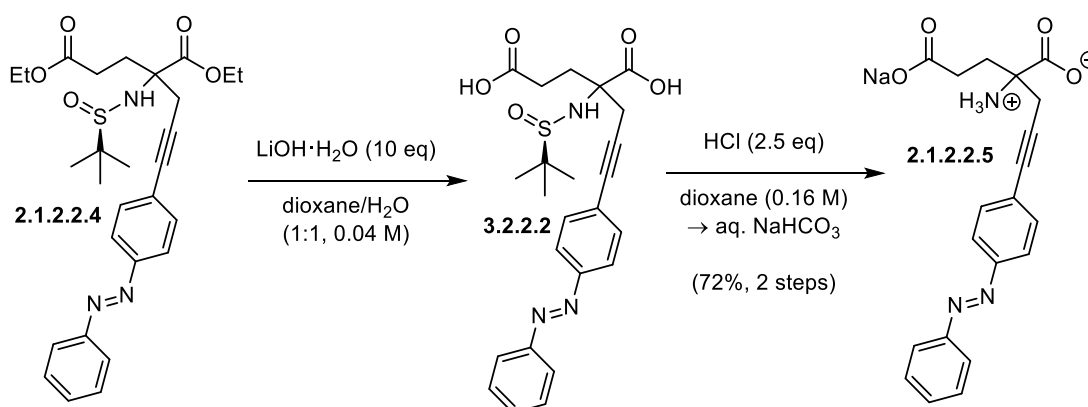
^{13}C NMR (101 MHz, C_6D_6) δ (ppm) = 172.1, 171.9, 153.2, 152.2, 132.9, 131.3, 129.3, 126.6, 123.4, 87.9, 84.7, 64.3, 62.1, 60.6, 56.1, 31.5, 30.6, 29.5, 22.5, 14.2, 14.1.

HRMS (ESI): calc. for $\text{C}_{28}\text{H}_{36}\text{N}_3\text{O}_5\text{S}^+$ $[\text{M} + \text{H}]^+$: 526.2370, found: 526.2372.

IR (Diamond-ATR, neat) ν_{max} (cm^{-1}) = 3247 (br, vw), 2959 (w), 2854 (vw), 1731 (vs), 1597 (vw), 1496 (w), 1464 (w), 1444 (w), 1366 (m), 1288 (w), 1253 (s), 1182 (s), 1153 (m), 1120 (s), 1072 (vs), 1018 (s), 929 (w), 887 (m), 873 (vs), 846 (vs), 792 (w), 768 (s), 726 (m), 687 (vs).

$[\alpha]_{\text{D}}^{20} = -17.2^\circ$ ($c = 2.43$, EtOAc).

sodium 2-ammonio-2-(3-(4-(phenyldiazenyl)phenyl)prop-2-yn-1-yl)pentanedioate (**2.1.2.2.5**)



Sulfynilamide diester **2.1.2.2.4** (15.0 mg, 28.5 μmol , 1.0 eq.) was dissolved in a dioxane/ H_2O (1:1, 1.86 mL), cooled to 0 $^\circ\text{C}$ and $\text{LiOH}\cdot\text{H}_2\text{O}$ (12.0 mg, 1.64 mmol, 10 eq) was added. The orange solution was stirred at 0 $^\circ\text{C}$ for 3 h 15 min before it was diluted with EtOAc (30 mL) and washed

with 3% aq. KHSO_4 (10 mL) and sat. aq. NaCl (10 mL). Thereafter, the organic layer was dried over Na_2SO_4 , concentrated and redissolved in dioxane (0.158 mL). HCl (4 M in dioxane, 17.8 μL , 71.3 μL , 2.5 eq) was added at rt and the solution was stirred for 2 h. After removal of the solvent *in vacuo*, the residue was purified via reverse-phase semi-preparative HPLC ($\text{MeCN}:\text{H}_2\text{O}:\text{HCOOH} = 80:20:1\% \rightarrow 20:80:1\%$ over 60 min). The organic solvent was removed under reduced pressure followed by freeze-drying. The residue was dissolved in sat. aq. NaHCO_3 (1.0 mL) and purification via reversed phase flash column chromatography ($\text{H}_2\text{O}:\text{MeCN} = 100:0 \rightarrow 95:5 \rightarrow 90:10 \rightarrow 85:15$) afforded give sodium 2-ammonio-2-(3-(4-(phenyldiazenyl)phenyl)prop-2-yn-1-yl)pentanedioate (**2.1.2.2.5**, 7.9 mg, 20 μmol , 70%) as a yellow/orange solid

Note: Due to the photoswitching properties of the **2.1.2.2.5** azobenzene moiety, the NMR spectra show a mixture of *cis*- and *trans*-isomers. The ^1H - and ^{13}C -NMRs are reported for the thermodynamically more stable *trans*.

t_{R} (reverse-phase semi-preparative HPLC, $\text{MeCN}:\text{H}_2\text{O}:\text{HCOOH} = 80:20:0.1\% \rightarrow 20:80:0.1\%$ over 60 min) = 20.39 min.

^1H NMR (800 MHz, D_2O) δ (ppm) = 7.91 – 7.88 (m, 2H), 7.87 – 7.84 (m, 2H), 7.71 – 7.68 (m, 2H), 7.67 – 7.62 (m, 3H), 2.93 (d, $J = 16.8$ Hz, 1H), 2.71 (d, $J = 16.8$ Hz, 1H), 2.28 (ddd, $J = 14.4, 12.7, 4.9$ Hz, 1H), 2.13 (ddd, $J = 14.4, 12.6, 4.7$ Hz, 1H), 2.04 (td, $J = 13.1, 4.7$ Hz, 1H), 1.89 (td, $J = 13.0, 4.9$ Hz, 1H).

^{13}C NMR (201 MHz, D_2O) δ (ppm) = 182.6, 181.7, 152.3, 151.3, 132.9, 131.9, 129.6, 126.4, 122.5, 122.5, 89.9, 82.5, 61.4, 36.0, 32.9, 30.4

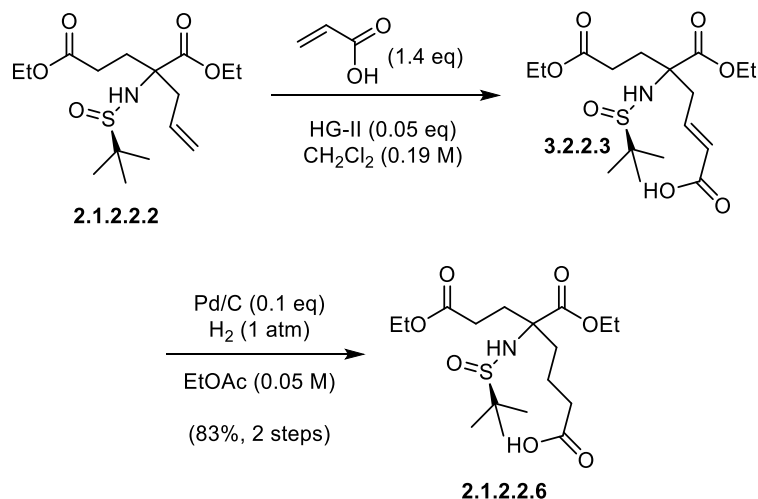
HRMS (ESI): calc. for $\text{C}_{20}\text{H}_{18}\text{N}_3\text{O}_4^-$ [$\text{M} - \text{H}^+$] $^-$: 364.1303, found: 364.1303.

IR (Diamond-ATR, neat) ν_{max} (cm^{-1}) = 2923 (m), 2853 (w), 1713 (m), 1596 (vs), 1536 (w), 1495 (w), 1481 (w), 1462 (w), 1451 (w), 1411 (s), 1392 (s), 1322 (w), 1285 (m), 1232 (s), 1156 (s), 1106 (s), 1071 (m), 1038 (m), 923 (m), 869 (m), 847 (vs), 802 (m), 765 (vs), 724 (m), 685 (vs).

$[\alpha]_{\text{D}}^{20} = -207^\circ$ ($c = 0.474$, H_2O).

$m_{\text{p}} = 158.5 - 161.3$ $^\circ\text{C}$.

5-(((*R*)-*tert*-butylsulfinyl)amino)-8-ethoxy-5-(ethoxycarbonyl)-8-oxooctanoic acid
(2.1.2.2.6)



Alkene (**2.1.2.2.2**, 50.0 mg, 0.144 mmol, 1.0 eq) was dissolved in CH_2Cl_2 (0.86 mL) and freshly distilled acrylic acid (16.6 μL , 0.230 mmol, 1.4 eq) was added. The mixture was degassed by freeze-pump-thaw (2 cycles) and Hoveyda-Grubbs II (5.1 mg, 8.2 μmol , 0.05 eq) was added. After heating the mixture to 40 °C for 4 h, it was filtered through celite and the filtercake was rinsed with EtOAc (50 mL). The organic solvent was removed *in vacuo* and the residue was redissolved in degassed EtOAc (3.0 mL) and Pd/C (10% Pd, 15.3 mg, 14.4 μmol , 0.1 eq) was added. H_2 gas was bubbled through the black suspension for 15 min followed by stirring under a H_2 atmosphere (1 atm) for 23 h. The suspension was purged with N_2 , and the solid was removed by filtration through celite and rinsing of the filtercake with EtOAc (50 mL). Thereafter, the solvent was removed *in vacuo* and the residue was purified via flash column chromatography ($\text{CH}_2\text{Cl}_2:\text{MeOH}:\text{AcOH} = 39:1:1\%$) to give 5-(((*R*)-*tert*-butylsulfinyl)amino)-8-ethoxy-5-(ethoxycarbonyl)-8-oxooctanoic acid (**2.1.2.2.6**, 47.3 mg, 0.120 mmol, 83%) as a colorless oil.

R_f ($\text{CH}_2\text{Cl}_2:\text{MeOH}:\text{AcOH} = 39:1:1\%$) = 0.25. (CAM)

$^1\text{H NMR}$ (400 MHz, C_6D_6) δ (ppm) = 5.18 (s, 1H), 3.99 – 3.91 (m, 4H), 2.81 (ddd, $J = 14.7, 10.2, 5.3$ Hz, 1H), 2.58 – 2.51 (m, 1H), 2.39 – 2.32 (m, 2H), 2.16 (dt, $J = 15.9, 7.0$ Hz, 1H), 2.10 (dt, $J = 16.3, 7.0$ Hz, 1H), 1.96 – 1.87 (m, 2H), 1.69 (tq, $J = 12.9, 6.8$ Hz, 1H), 1.53 (qq, $J = 12.9, 7.0, 6.0$ Hz, 1H), 1.09 (s, 12H), 0.98 (t, $J = 7.1$ Hz, 3H), 0.96 (td, $J = 7.1, 1.0$ Hz, 4H).

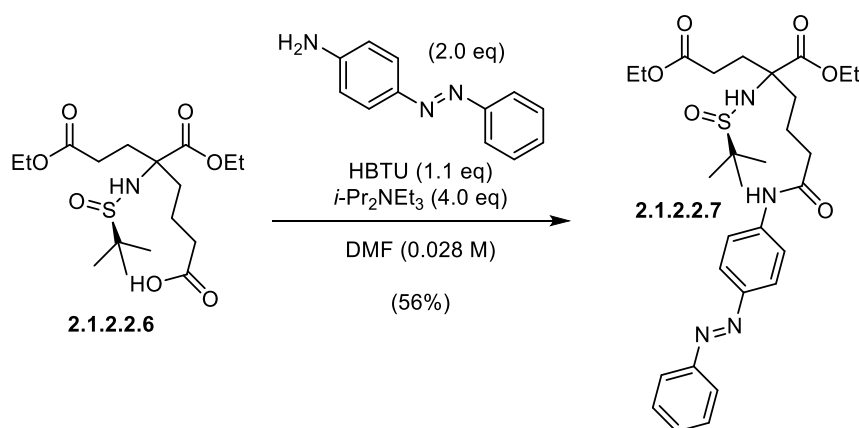
$^{13}\text{C NMR}$ (101 MHz, C_6D_6) δ (ppm) = 177.6, 173.0, 172.6, 65.0, 61.9, 60.5, 56.7, 36.7, 33.9, 33.6, 29.2, 22.7, 19.3, 14.2, 14.0.

HRMS (ESI): calc. for $\text{C}_{17}\text{H}_{30}\text{NO}_7$ [$\text{M} - \text{H}^+$]: 392.1748, found: 392.1746.

IR (Diamond-ATR, neat) ν_{\max} (cm^{-1}) = 2980 (br, w), 1726 (vs) 1451 (w), 1367 (m), 1181 (vs), 1095 (s), 1014 (vs), 957 (m), 896 (m), 853 (m), 794 (m).

$[\alpha]_{\text{D}}^{20} = -17.4^{\circ}$ ($c = 1.84$, EtOAc).

diethyl 2-(((*R*)-*tert*-butylsulfinyl)amino)-2-(4-oxo-4-((4-((phenyldiazenyl)phenyl)amino)butyl)pentanedioate (2.1.2.2.7)



Carboxylic acid (**2.1.2.2.6**, 50.0 mg, 0.125 mmol, 1.0 eq), was dissolved in DMF (4.46 mL) and HBTU (53.1 mg, 0.140 mmol, 1.1 eq), 4-((phenyldiazenyl)aniline (49.3 mg, 0.250 mmol, 2.0 eq) and *i*-Pr₂NEt (87 μ L, 0.50 mmol, 4.0 eq) were added. The mixture was stirred at rt for 2 h followed by heating to 40 $^{\circ}$ C for 3 h. EtOAc (150 mL) was added and the mixture was washed with sat. aq. NaHCO₃ (100 mL), H₂O (100 mL) and sat. aq. NaCl (50 mL). The organic layer was dried over Na₂SO₄ and concentrated. Purification via flash column chromatography (pentane:EtOAc = 1:1 \rightarrow 1:2) afforded diethyl 2-(((*R*)-*tert*-butylsulfinyl)amino)-2-(4-oxo-4-((4-((phenyldiazenyl)phenyl)amino)butyl)pentanedioate (**2.1.2.2.7**, 38.3 mg, 67.0 μ mol, 54%) as a red solid.

Note: Due to the photoswitching properties of the **2.1.2.2.7** azobenzene moiety, the NMR spectra show a mixture of *cis*- and *trans*-isomers. The ¹H- and ¹³C-NMRs are reported for the thermodynamically more stable *trans*.

R_f (pentane:EtOAc:AcOH = 1:1:1%) = 0.27. (visible)

$^1\text{H NMR}$ (400 MHz, C_6D_6) δ (ppm) = 8.26 (s, 1H), 8.15 – 8.10 (m, 2H), 8.06 – 7.98 (m, 4H), 7.21 – 7.17 (m, 2H), 7.12 – 7.05 (m, 1H), 4.53 (s, 1H), 4.04 – 3.81 (m, 4H), 2.84 – 2.70 (m, 1H), 2.45 – 1.96 (m, 7H), 1.85 – 1.71 (m, 2H), 1.09 (s, 9H), 0.93 (q, $J = 7.2$ Hz, 6H).

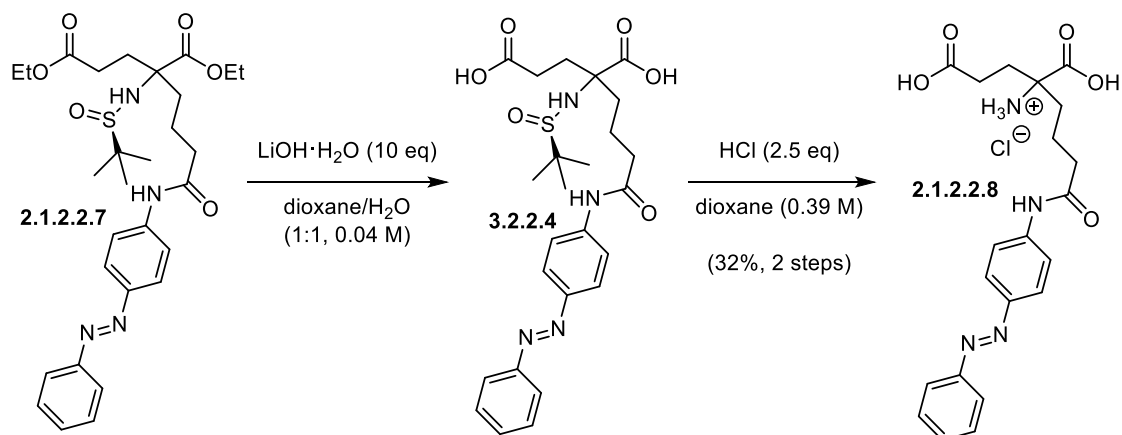
$^{13}\text{C NMR}$ (101 MHz, C_6D_6) δ (ppm) = 173.1, 173.0, 170.7, 153.4, 149.2, 142.4, 130.7, 129.3, 124.5, 123.2, 119.0, 65.4, 62.0, 60.7, 56.6, 37.6, 37.5, 34.4, 29.2, 22.7, 19.7, 14.2 14.1.

HRMS (ESI): calc. for $\text{C}_{29}\text{H}_{39}\text{N}_4\text{O}_6^-$ [$\text{M} - \text{H}^+$] $^-$: 571.2596, found: 571.2591.

IR (Diamond-ATR, neat) ν_{max} (cm^{-1}) = 3640 (vw), 3399 (vw), 2962 (vw), 2929 (vw), 1724 (w), 1672 (w), 1628 (vw), 1594 (w), 1531 (w), 1501 (w), 1462 (w), 1443 (w), 1407 (w), 1370 (w), 1300 (w), 1252 (m), 1184 (w), 1153 (m), 1095 (w), 1019 (br, m), 963 (vw), 928 (vw), 838 (br, vs), 768 (m), 739 (w), 723 (w), 689 (m), 663 (w).

$[\alpha]_{\text{D}}^{20} = -8.54^\circ$ ($c = 4.80$, EtOAc).

1,3-dicarboxy-7-oxo-7-((4-(phenyldiazenyl)phenyl)amino)heptan-3-aminium chloride (2.1.2.2.8)



Sulfanyl amide (**2.1.2.2.7**, 38.4 mg, 66.9 μmol , 1.0 eq) was dissolved in dioxane/ H_2O (1:1, 1.68 mL), cooled to 0 $^\circ\text{C}$ and $\text{LiOH}\cdot\text{H}_2\text{O}$ (31.5 mg, 0.670 mmol, 10 eq) was added. The orange solution was stirred at 0 $^\circ\text{C}$ for 7 h 30 min, diluted with EtOAc (150 mL) and washed with 3% aq. KHSO_4 (100 mL) as well as sat. aq. NaCl (50 mL). After drying the organic layer over Na_2SO_4 , the solvent was removed under reduced pressure and the residue was redissolved in dioxane (0.170 mL). HCl (4 M in dioxane, 41 μL , 0.17 mmol, 2.5 eq) was added and the orange solution was stirred at rt for 15 min while gradually turning red. The solvent was removed under high vacuum (< 1 mbar) and the residue was purified via semi-preparative HPLC ($\text{MeCN}:\text{H}_2\text{O}:\text{HCOOH} = 80:20:1\% \rightarrow 20:80:1$ over 60 min) to give 1,3-dicarboxy-7-oxo-7-((4-(phenyldiazenyl)phenyl)amino)heptan-3-aminium chloride (**2.1.2.2.8**).

(phenyldiazenyl)phenyl)amino)heptan-3-aminium chloride (**2.1.2.2.8**, 9.6 mg, 21 μmol , 32%) as a yellow solid.

Note: Due to the photoswitching properties of the **2.1.2.2.8** azobenzene moiety, the NMR spectra show a mixture of *cis*- and *trans*-isomers. The ^1H - and ^{13}C -NMRs are reported for the thermodynamically more stable *trans*.

t_{R} (reverse-phase semi-preparative HPLC, MeCN:H₂O:HCOOH = 80:20:0.1% \rightarrow 20:80:0.1% over 60 min) = 17.87 min.

^1H NMR (800 MHz, (CD₃)₂SO) δ (ppm) = 10.42 (s, 1H), 7.89 – 7.83 (m, 6H), 7.58 (dd, J = 8.4, 6.9 Hz, 2H), 7.54 – 7.52 (m, 1H), 2.38 – 2.27 (m, 3H), 2.16 (ddd, J = 16.4, 8.0, 5.9 Hz, 1H), 1.87 – 1.82 (m, 1H), 1.79 – 1.74 (m, 1H), 1.74 – 1.68 (m, 2H), 1.60 (dd, J = 11.8, 9.2 Hz, 1H), 1.55 (p, J = 8.1, 7.5 Hz, 1H).

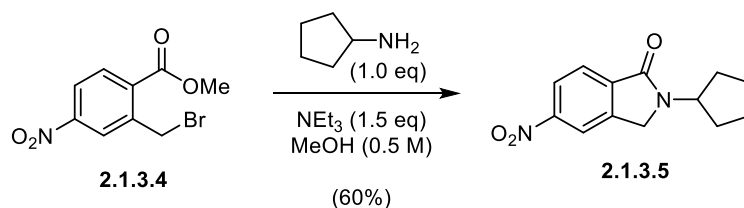
^{13}C NMR (201 MHz, (CD₃)₂SO) δ (ppm) = 175.1, 171.6, 152.0, 147.3, 142.5, 131.0, 129.4, 123.7, 122.3, 119.2, 62.3, 36.8, 36.5, 32.1, 31.1, 19.9.

HRMS (ESI): calc. for C₂₁H₂₃N₄O₅⁻ [M – 2H⁺]⁻: 411.1674, found: 411.1671.

IR (Diamond-ATR, neat) ν_{max} (cm⁻¹) = 2926 (br, m), 1594 (vs), 1533 (vs), 1505 (vs), 1440 (m), 1406 (s), 1301 (s), 1248 (s), 1153 (s), 1105 (s), 1035 (m), 845 (s), 764 (vs), 722 (s), 686 (vs).

$[\alpha]_{\text{D}}^{20}$ = -57° (c = 0.13, DMSO).

2-cyclopentyl-5-nitroisindolin-1-one (2.1.3.5)



Methyl 2-(bromomethyl)-4-nitrobenzoate¹⁵⁹ (**2.1.3.4**, 450 mg, 1.64 mmol, 1.0 eq) was dissolved in MeOH (3.28 mL) followed by addition of NEt₃ (0.343 mL, 2.46 mmol, 1.5 eq) and cyclopentylamine (0.162 mL, 1.64 mmol, 1.0 eq). The mixture was stirred in a pressure tube at 100 °C for 4 h. After cooling to rt, the solvent was removed *in vacuo*. Purification via flash column chromatography (pentane:EtOAc = 4:1) afforded 2-cyclopentyl-5-nitroisindolin-1-one (**2.1.3.5**, 251.6 mg, 1.022 mmol, 62%) as a yellow powder.

R_f (pentane:EtOAc = 1:1) = 0.54. (UV)

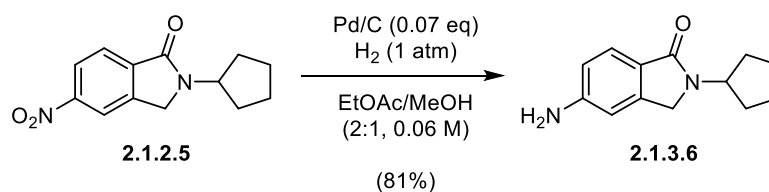
$^1\text{H NMR}$ (400 MHz, CDCl_3) δ (ppm) = 8.38 – 8.31 (m, 2H), 7.98 (d, J = 8.2 Hz, 1H), 4.78 (p, J = 8.0 Hz, 1H), 4.48 (s, 2H), 2.15 – 1.98 (m, 2H), 1.91 – 1.60 (m, 6H).

$^{13}\text{C NMR}$ (101 MHz, CDCl_3) δ (ppm) = 166.3, 150.0, 142.0, 138.8, 124.7, 124.0, 118.6, 53.3, 46.3, 30.3, 24.2.

HRMS (ESI): calc. for $\text{C}_{13}\text{H}_{15}\text{N}_2\text{O}_3^+$ [$\text{M} + \text{H}^+$] $^+$: 247.1077, found: 247.1077.

IR (Diamond-ATR, neat) ν_{max} (cm^{-1}) = 3107 (vw), 3039 (vw), 2961 (vw), 2872 (vw), 1669 (vs), 1625 (vw), 1600 (vw), 1525 (s), 1470 (w), 1454 (m), 1416 (w), 1339 (vs), 1312 (w), 1274 (w), 1240 (w), 1215 (w), 1183 (vw), 1140 (vw), 1117 (vw), 1091 (vw), 1068 (vw), 944 (vw), 918 (vw), 895 (w), 859 (w), 818 (w), 784 (vw), 730 (vs), 673 (w), 665 (m).

5-amino-2-cyclopentylisoindolin-1-one (2.1.3.6)



Nitroaryl (**2.1.3.5**, 125 mg, 0.508 mmol, 1.0 eq) was dissolved in degassed EtOAc/MeOH (2:1, 21 mL) and Pd/C (10% Pd, 37.8 mg, 35.6 μmol , 0.07 eq) was added. The solution was stirred under H_2 atmosphere (1 atm) for 13 h, filtered through celite and concentrated. Purification via flash column chromatography (hexanes:EtOAc = 1:1) afforded 5-amino-2-cyclopentylisoindolin-1-one (**2.1.3.6**, 89.4 mg, 0.413 mmol, 81%) as a white foam.

R_f (pentane:EtOAc = 1:1) = 0.11. (UV)

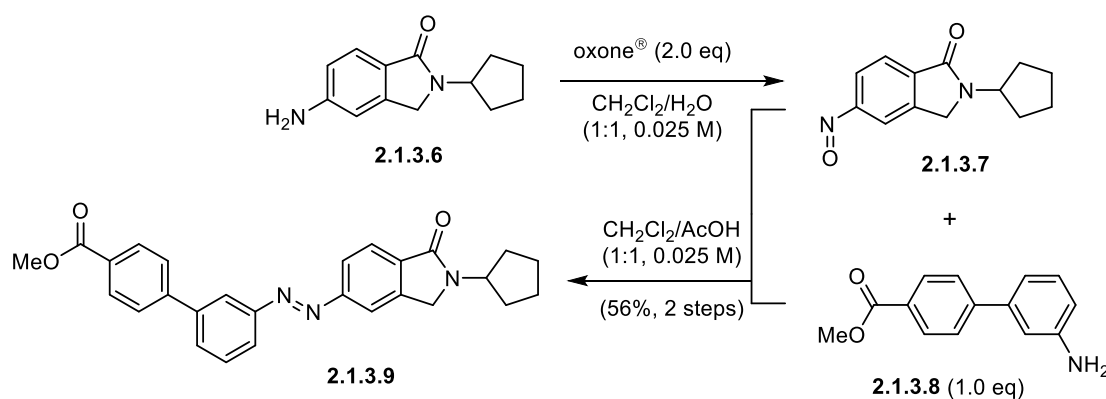
$^1\text{H NMR}$ (400 MHz, CDCl_3) δ (ppm) 7.61 (d, J = 8.2 Hz, 1H), 6.70 (d, J = 8.2 Hz, 1H), 6.67 (s, 1H), 4.73 (p, J = 8.0 Hz, 1H), 4.24 (s, 2H), 3.98 (br s, 2H), 2.05 – 1.89 (m, 2H), 1.83 – 1.49 (m, 6H).

$^{13}\text{C NMR}$ (101 MHz, CDCl_3) δ (ppm) = 168.9, 149.7, 143.7, 125.0, 123.9, 114.9, 108.0, 52.4, 45.9, 30.1, 24.2.

HRMS (ESI): calc. for $\text{C}_{13}\text{H}_{17}\text{N}_2\text{O}^+$ [$\text{M} + \text{H}^+$] $^+$: 217.1335, found: 217.1335.

IR (Diamond-ATR, neat) ν_{\max} (cm⁻¹) = 3324 (vw), 3210 (vw), 2963 (vw), 1662 (s), 1648 (s), 1633 (m), 1609 (vs), 1495 (w), 1453 (s), 1414 (m), 1373 (w), 1326 (w), 1282 (m), 1238 (w), 1135 (w), 859 (w), 832 (m), 790 (w), 772 (s), 693 (s), 632 (m), 573 (m), 560 (m).

methyl 3'-((2-cyclopentyl-1-oxoisindolin-5-yl)diazenyl)-[1,1'-biphenyl]-4-carboxylate (2.1.3.9)



Aniline (**2.1.3.6**, 62.7 mg, 0.290 mmol, 1.0 eq) and oxone[®] (365 mg, 0.580 mmol, 2.0 eq) were dissolved in CH₂Cl₂/H₂O (1:1, 11.6 mL) and stirred at rt for 14 h 45 min. After diluting the green solution with CH₂Cl₂ (70 mL), it was washed with H₂O (20 mL), 3% aq. KHSO₄ (20 mL), sat. aq. NaHCO₃ (20 mL) and H₂O (20 mL). The organic layer was dried over Na₂SO₄ and concentrated. Methyl 3'-amino-[1,1'-biphenyl]-4-carboxylate¹⁶⁰ (**2.1.3.8**, 65.9 mg, 0.290 mmol, 1.0 eq) was added to the residue and the mixture was dissolved in CH₂Cl₂/AcOH (1:1, 11.6 mL). The green solution was stirred for 6 h 30 min and gradually turned orange/red. After diluting with CH₂Cl₂ (70 mL), the organic layer was washed with 1 M aq. HCl (2 × 20 mL), sat. aq. NaHCO₃ (20 mL) and sat. aq. NaCl (20 mL) followed by drying over Na₂SO₄. The solution was concentrated and purified via flash column chromatography (pentane:EtOAc = 4:1) to give methyl 3'-((2-cyclopentyl-1-oxoisindolin-5-yl)diazenyl)-[1,1'-biphenyl]-4-carboxylate (**2.1.3.9**, 71.5 mg, 0.163 mmol, 56%) as an orange powder.

Note: Due to the photoswitching properties of the **2.1.3.9** azobenzene moiety, the NMR spectra show a mixture of *cis*- and *trans*-isomers. The ¹H- and ¹³C-NMRs are reported for the thermodynamically more stable *trans*-isomer.

R_f (pentane:EtOAc = 2:1) = 0.59. (visible)

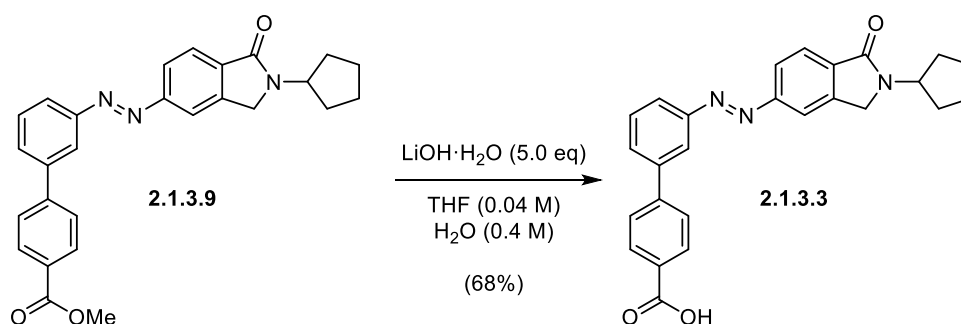
$^1\text{H NMR}$ (400 MHz, CDCl_3) δ (ppm) = 8.24 – 8.12 (m, 3H), 8.06 (d, J = 8.1 Hz, 1H), 8.02 – 7.94 (m, 2H), 7.77 (t, J = 7.2 Hz, 3H), 7.64 (t, J = 7.8 Hz, 1H), 4.81 (p, J = 8.0 Hz, 1H), 4.47 (s, 2H), 3.96 (s, 3H), 2.13 – 1.98 (m, 2H), 1.90 – 1.61 (m, 6H).

$^{13}\text{C NMR}$ (101 MHz, CDCl_3) δ (ppm) = 167.8, 167.0, 154.6, 153.1, 144.7, 142.1, 141.3, 135.5, 130.4, 129.9, 129.5, 127.3, 124.5, 124.1, 122.9, 122.0, 116.6, 53.0, 52.4, 46.3, 30.3, 24.3.

HRMS (EI): calc. for $\text{C}_{27}\text{H}_{25}\text{N}_3\text{O}_3^+$ $[\text{M}]^+$: 439.1890, found: 439.1890.

IR (Diamond-ATR, neat) ν_{max} (cm^{-1}) = 2921 (vw), 1718 (m), 1671 (vs), 1606 (w), 1440 (w), 1399 (w), 1267 (m), 1195 (m), 1109 (m), 1016 (w), 893 (vw), 858 (w), 798 (w), 778 (w), 769 (s), 701 (m), 686 (m).

3'-((2-cyclopentyl-1-oxoisindolin-5-yl)diazenyl)-[1,1'-biphenyl]-4-carboxylic acid (2.1.3.3)



Methyl ester (**2.1.3.9**, 20.0 mg, 45.5 μmol , 1.0 eq) was dissolved in THF/H₂O (10:1, 1.25 mL) and LiOH·H₂O (9.5 mg, 0.23 mmol, 5.0 eq) was added. After stirring the reaction at rt for 6 h, it was diluted with EtOAc (35 mL) and washed with 1 M aq. HCl (10 mL) as well as sat. aq. NaCl (10 mL). The organic layer was dried over Na₂SO₄ and concentrated. Purification via flash column chromatography (CH₂Cl₂:AcOH = 99:1) afforded 3'-((2-cyclopentyl-1-oxoisindolin-5-yl)diazenyl)-[1,1'-biphenyl]-4-carboxylic acid (**2.1.3.3**, 13.2 mg, 31.0 μmol , 68%) as an orange powder.

Note: Due to the photoswitching properties of the **2.1.3.3** azobenzene moiety, the NMR spectra show a mixture of *cis*- and *trans*-isomers. The ^1H - and ^{13}C -NMRs are reported for the thermodynamically more stable *trans*-isomer.

R_f (pentane:EtOAc:AcOH = 9:1:1%) = 0.29. (visible)

$^1\text{H NMR}$ (800 MHz, $(\text{CD}_3)_2\text{SO}$) δ (ppm) 8.25 (t, J = 1.9 Hz, 1H), 8.10 (d, J = 0.7 Hz, 1H), 8.07 – 8.03 (m, 3H), 8.00 – 7.95 (m, 2H), 7.87 (dd, J = 8.1, 6.1 Hz, 3H), 7.75 (t, J = 7.8 Hz, 1H), 4.68 – 4.57 (m, 3H), 1.94 – 1.88 (m, 2H), 1.80 – 1.75 (m, 2H), 1.75 – 1.69 (m, 2H), 1.67 – 1.61 (m, 2H).

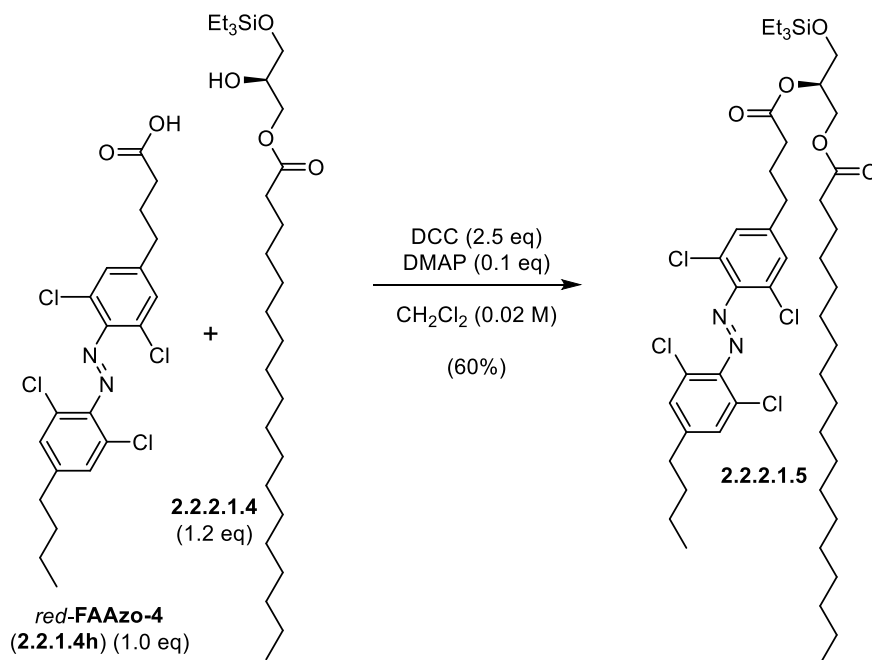
$^{13}\text{C NMR}$ (201 MHz, $(\text{CD}_3)_2\text{SO}$) δ (ppm) = 168.2, 166.7, 154.2, 152.9, 143.6, 142.4, 141.3, 135.5, 130.8, 130.5, 127.1, 124.1, 123.7, 122.4, 121.7, 117.6, 52.9, 46.6, 30.2, 24.3.

According to the 2D-NMR spectra, one carbon signal was not observed due to line broadening.

HRMS (ESI): calc. for $\text{C}_{26}\text{H}_{22}\text{N}_3\text{O}_3^-$ $[\text{M} - \text{H}^+]^-$: 424.1667, found: 424.1669.

IR (Diamond-ATR, neat) ν_{max} (cm^{-1}) = 3556 (vw), 2922 (w), 2855 (vw), 1671 (vs), 1606 (m), 1455 (w), 1428 (m), 1407 (m), 1354 (w), 1291 (m), 1246 (w), 1205 (w), 1182 (w), 1152 (w), 1120 (w), 1017 (w), 937 (w), 917 (w), 883 (w), 856 (m), 803 (m), 771 (s), 723 (w), 702 (m), 690 (s), 675 (w).

(*R*)-2-((4-(4-((4-butyl-2,6-dichlorophenyl)diazenyl)-3,5-dichlorophenyl)butanoyl)oxy)-3-((triethylsilyl)oxy)propyl stearate (2.2.2.1.5)

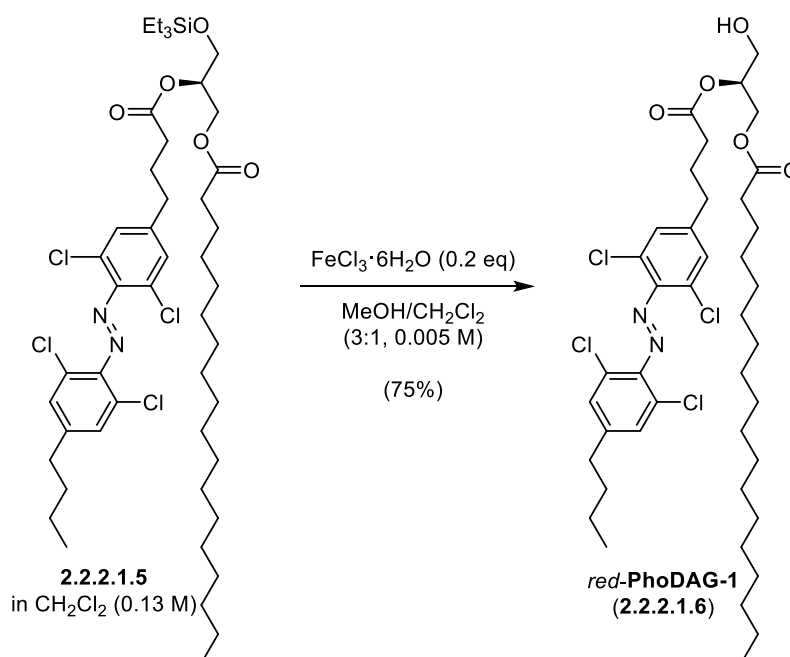


Red-FAAzo-4 (**2.2.1.4h**, 100 mg, 217 μmol , 1.0 eq), DCC (112 mg, 542 μmol , 2.5 eq) and DMAP (2.7 mg, 22 μmol , 0.1 eq) were dissolved in CH_2Cl_2 (12.0 mL) and stirred at rt for 50 min. The red solution was cooled to 0 $^\circ\text{C}$ and alcohol¹⁴⁴ (**2.2.2.1.4**, 120 mg, 254 μmol , 1.2 eq) was added. After

stirring for 22 h 20 min at 0 °C, the solution was diluted with EtOAc (35 mL) and washed with H₂O (20 mL) as well as sat. aq. NaCl (20 mL). The organic layer was dried over Na₂SO₄ and concentrated. Purification via flash column chromatography (pentane:Et₂O = 19:1) afforded (*R*)-2-((4-(4-((4-butyl-2,6-dichlorophenyl)diazenyl)-3,5-dichlorophenyl)butanoyl)oxy)-3-((triethylsilyl)oxy)propyl stearate (**2.2.2.1.5**, 119 mg, 130 μmol, 60%) as a red oil which was directly used in the next step.

R_f (pentane:Et₂O = 9:1) = 0.39. (visible)

(*S*)-2-((4-(4-((4-butyl-2,6-dichlorophenyl)diazenyl)-3,5-dichlorophenyl)butanoyl)oxy)-3-hydroxypropyl stearate (*red-PhoDAG-1*, **2.2.2.1.6**)



TES-alcohol (**2.2.2.1.5**, 39.4 mg, 43.0 μmol, 1.0 eq) was dissolved in CH₂Cl₂ (0.33 mL), cooled to 0 °C and FeCl₃·6H₂O (2.3 mg, 8.6 μmol, 0.2 eq) in MeOH/CH₂Cl₂ (3:1, 1.72 mL) was added dropwise. After stirring the red solution for 70 min at 0 °C, it was diluted with H₂O/sat. aq. NaCl (1:1, 10 mL) and extracted with EtOAc (35 mL). The organic layer was washed with sat. aq. NaCl (10 mL), dried over Na₂SO₄ and concentrated. Purification via flash column chromatography (pentane:EtOAc = 3:1) afforded (*S*)-2-((4-(4-((4-butyl-2,6-dichlorophenyl)diazenyl)-3,5-dichlorophenyl)butanoyl)oxy)-3-hydroxypropyl stearate (*red-PhoDAG-1*, **2.2.2.1.6**, 25.9 mg, 32.3 μmol, 75%) as a red oil.

Note: Due to the photoswitching properties of the *red*-PhoDAG-1 (2.2.2.1.6) azobenzene moiety, the NMR spectra show a mixture of *cis*- and *trans*-isomers. The $^1\text{H-NMR}$ is reported for the thermodynamically more stable *trans*-isomer whereas a selection of diagnostic signals is reported for the $^{13}\text{C-NMR}$.

R_f (pentane:EtOAc = 4:1) = 0.12. (visible, CAM)

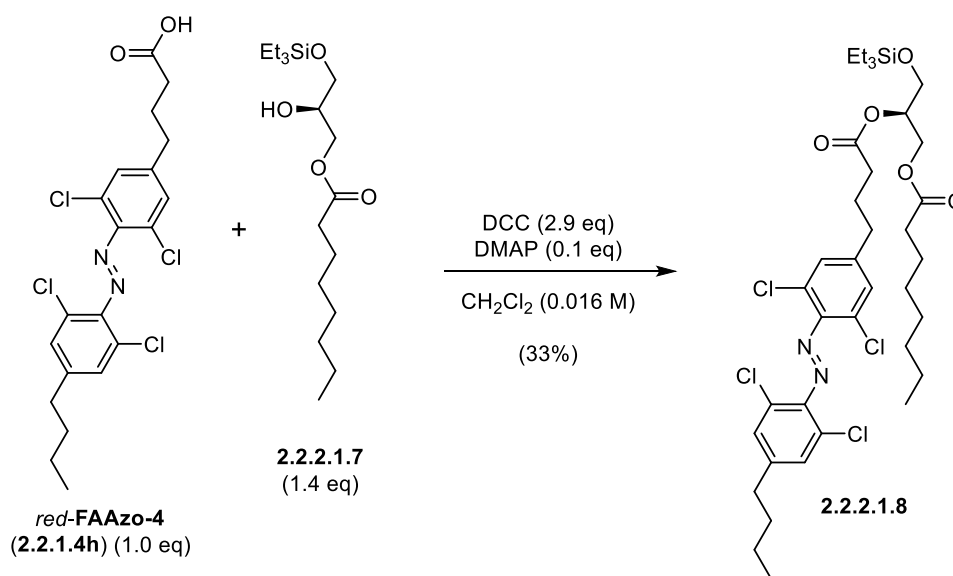
$^1\text{H-NMR}$ (400 MHz, C_6D_6) δ (ppm) = 6.93 (s, 2H), 6.92 (s, 2H), 5.13 (qd, $J = 5.6, 3.6$ Hz, 1H), 4.36 (dd, $J = 12.0, 3.7$ Hz, 1H), 4.14 (dd, $J = 12.0, 5.9$ Hz, 1H), 3.49 – 3.42 (m, 2H), 2.17 (td, $J = 7.4, 2.4$ Hz, 2H), 2.08 (ddd, $J = 8.7, 7.2, 2.2$ Hz, 2H), 2.04 – 1.98 (m, 4H), 1.61 – 1.52 (m, 4H), 1.37 – 1.18 (m, 28H), 1.17 – 1.11 (m, 2H), 1.09 – 1.03 (m, 2H), 0.92 (t, $J = 7.1$ Hz, 3H), 0.78 (t, $J = 7.3$ Hz, 3H).

$^{13}\text{C-NMR}$ (101 MHz, C_6D_6) δ (ppm) = 173.2, 172.3, 146.4, 146.0, 145.7, 144.3, 72.8, 62.5, 61.5, 34.8, 34.2, 34.1, 32.9, 32.4, 30.23, 30.18, 30.16, 30.1, 30.0, 29.9, 29.7, 29.5, 26.0, 25.3, 23.1, 22.5, 14.4, 14.0.

HRMS (ESI): calc. for $\text{C}_{41}\text{H}_{61}\text{Cl}_4\text{N}_2\text{O}_5^+$ $[\text{M} + \text{H}]^+$: 803.3300, found: 803.3334.

IR (Diamond-ATR, neat) ν_{max} (cm^{-1}) = 3499 (br, vw), 2920 (vs), 2850 (s), 1736 (vs), 1708 (m), 1589 (w), 1548 (w), 1465 (m), 1396 (m), 1378 (m), 1338 (w), 1260 (m), 1160 (vs), 1100 (s), 1079 (s), 968 (w), 855 (s), 801 (vs), 721 (m).

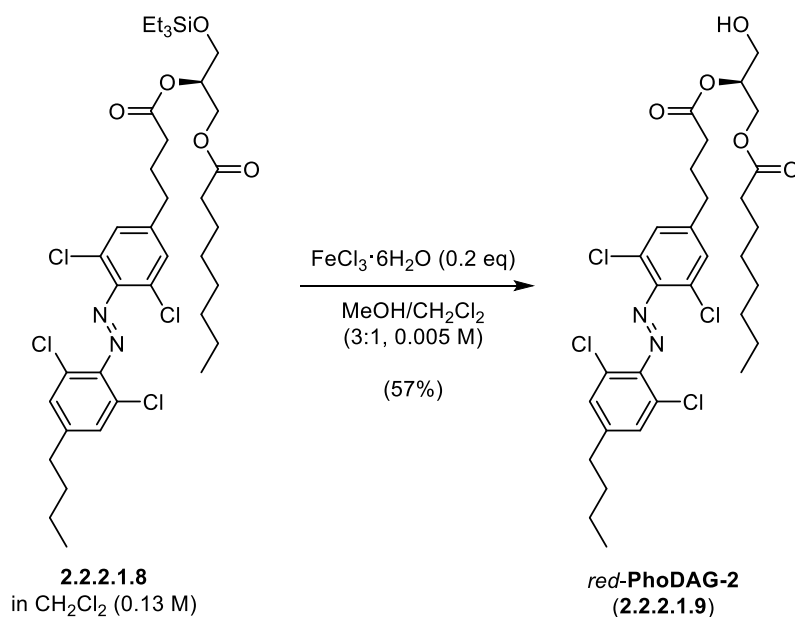
(*R*)-2-((4-(4-((4-butyl-2,6-dichlorophenyl)diazenyl)-3,5-dichlorophenyl)butanoyl)oxy)-3-((triethylsilyl)oxy)propyl octanoate (2.2.2.1.8)



Red-FAAzo-4 (**2.2.1.4h**, 25.0 mg, 52.9 μmol , 1.0 eq), DCC (31.8 mg, 154 μmol , 2.9 eq) and DMAP (0.8mg, 6 μmol , 0.1 eq) were dissolved in CH_2Cl_2 (3.21 mL) and stirred at rt for 45 min. The red solution was cooled to 0 °C and alcohol¹⁴⁴ (**2.2.2.1.7**, 24.5 mg, 73.7 μmol , 1.4 eq) was added. After stirring for 8 h at 0 °C, the solution was diluted with EtOAc (35 mL) and washed with sat. aq. $\text{NH}_4\text{Cl}/\text{H}_2\text{O}$ (1:1, 10 mL) as well as sat. aq. NaCl (10 mL). The organic layer was dried over Na_2SO_4 and concentrated. Purification via flash column chromatography (pentane:Et₂O = 19:1 \rightarrow 9:1) afforded (*R*)-2-((4-(4-((4-butyl-2,6-dichlorophenyl)diazenyl)-3,5-dichlorophenyl)butanoyl)oxy)-3-((triethylsilyl)oxy)propyl octanol (**2.2.2.1.8**, 13.6 mg, 17.5 μmol , 33%) as a red oil which was directly subjected to the next reaction.

R_f (pentane:Et₂O = 9:1) = 0.36. (visible)

(*S*)-2-((4-(4-((4-butyl-2,6-dichlorophenyl)diazenyl)-3,5-dichlorophenyl)butanoyl)oxy)-3-hydroxypropyl octanoate (*red-PhoDAG-2*, **2.2.2.1.9**)



TES-alcohol (**2.2.2.1.8**, 13.6 mg, 17.5 μmol , 1.0 eq) was dissolved in CH_2Cl_2 (0.135 mL), cooled to 0 °C and $\text{FeCl}_3 \cdot 6\text{H}_2\text{O}$ (1.0 mg, 3.7 μmol , 0.2 eq) in $\text{MeOH}/\text{CH}_2\text{Cl}_2$ (3:1, 0.7 mL) was added dropwise. After stirring the red solution for 60 min at 0 °C, it was diluted with $\text{H}_2\text{O}/\text{sat. aq. NaCl}$ (1:1, 5.0 mL) and extracted with EtOAc (15 mL). The organic layer was washed with sat. aq. NaCl (10 mL), dried over Na_2SO_4 and concentrated. Purification via flash column

chromatography (pentane:EtOAc = 3:1) afforded (*S*)-2-((4-(4-((4-butyl-2,6-dichlorophenyl)diazenyl)-3,5-dichlorophenyl)butanoyl)oxy)-3-hydroxypropyl octanoate (*red-PhoDAG-2*, **2.2.2.1.9**, 6.9 mg, 10 μ mol, 57%) as a red gum.

Note: Due to the photoswitching properties of the *red-PhoDAG-2* (**2.2.2.1.9**) azobenzene moiety, the NMR spectra show a mixture of *cis*- and *trans*-isomers. The $^1\text{H-NMR}$ is reported for the thermodynamically more stable *trans*-isomer whereas a selection of diagnostic signals is reported for the $^{13}\text{C-NMR}$.

R_f (pentane:EtOAc = 4:1) = 0.10. (visible, CAM)

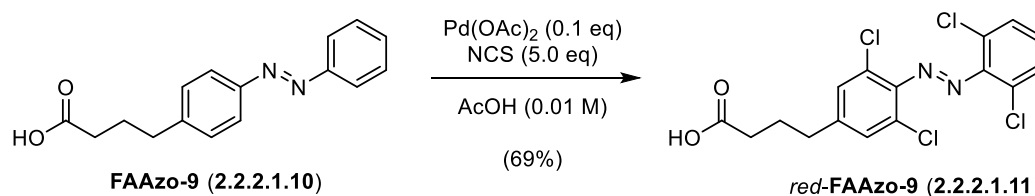
$^1\text{H-NMR}$ (400 MHz, C_6D_6) δ (ppm) = 6.92 (s, 2H), 6.91 (s, 2H), 5.13 (qd, $J = 5.6, 3.7$ Hz, 1H), 4.35 (dd, $J = 12.0, 3.7$ Hz, 1H), 4.13 (dd, $J = 12.0, 5.9$ Hz, 1H), 3.48 – 3.40 (m, 2H), 2.15 (td, $J = 7.4, 2.3$ Hz, 2H), 2.07 (td, $J = 7.5, 1.9$ Hz, 2H), 2.03 – 1.97 (m, 4H), 1.58 – 1.52 (m, 4H), 1.31 (t, $J = 6.1$ Hz, 1H), 1.24 (q, $J = 6.9$ Hz, 2H), 1.16 (br s, 6H), 1.16 – 1.11 (m, 2H), 1.08 – 1.02 (m, 2H), 0.88 (t, $J = 7.3$ Hz, 3H), 0.77 (t, $J = 7.3$ Hz, 3H).

$^{13}\text{C-NMR}$ (101 MHz, C_6D_6) δ (ppm) = 173.2, 172.3, 146.4, 146.0, 145.7, 144.3, 129.7, 129.6, 72.8, 62.5, 61.5, 34.8, 34.2, 34.0, 32.9, 32.0, 29.4, 29.3, 26.0, 25.2, 23.0, 22.4, 14.3, 14.0.

HRMS (ESI): calc. for $\text{C}_{31}\text{H}_{41}\text{Cl}_4\text{N}_2\text{O}_5^+$ [$\text{M} + \text{H}^+$] $^+$: 661.1764, found: 661.1776.

IR (Diamond-ATR, neat) ν_{max} (cm^{-1}) = 3461 (br, vw), 2956 (w), 2928 (m), 2857 (w), 1736 (vs), 1589 (m), 1550 (w), 1456 (w), 1399 (m), 1378 (w), 1260 (m), 1161 (s), 1100 (s), 1050 (s), 857 (m), 801 (vs), 726 (w), 660 (w).

4-(3,5-dichloro-4-((2,6-dichlorophenyl)diazenyl)phenyl)butanoic acid (*red-FAAzo-9*, **2.2.2.1.11**)



FAAzo-9 (**2.2.2.1.10.**, 0.500 g, 1.86 mmol, 1.0 eq), NCS (1.24 g, 9.32 mmol, 5.0 eq) and Pd(OAc)_2 (41.8 mg, 0.186 mmol, 0.1 eq) were dissolved in AcOH (18.6 mL) and heated to 120 $^\circ\text{C}$ for 14 h. The dark red solution was cooled to rt and the solvent was removed *in vacuo*. Purification via

flash column chromatography (CH₂Cl₂:AcOH = 199:1) afforded 4-(3,5-dichloro-4-((2,6-dichlorophenyl)diazenyl)phenyl)butanoic acid (*red-FAAzo-9*, **2.2.2.1.11**, 520.5 mg, 1.28 mmol, 69%) as an orange/red oily gum.

R_f (CH₂Cl₂:AcOH = 99:1) = 0.20. (visible)

¹H NMR (400 MHz, C₆D₆) δ (ppm) = 6.89 (d, J = 8.1 Hz, 1H), 6.81 (s, 1H), 6.35 (t, J = 8.1 Hz, 1H), 1.91 (m, 4H), 1.41 (p, J = 7.5 Hz, 2H).

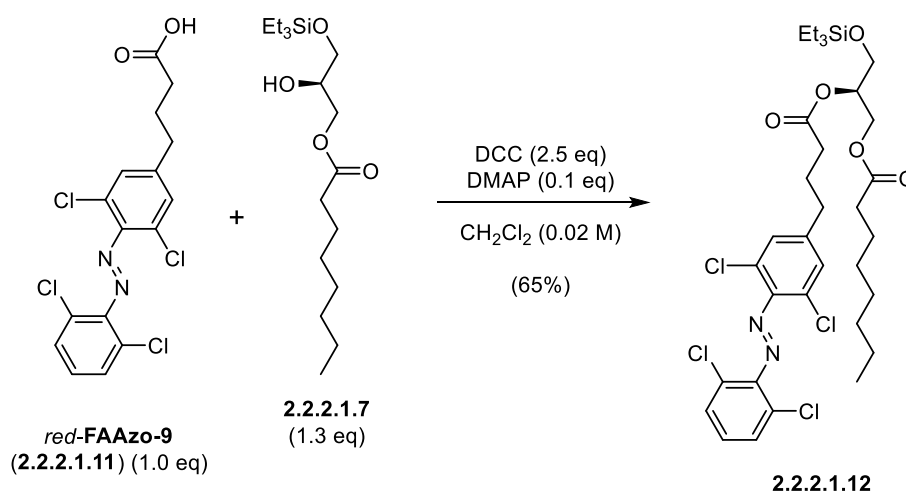
¹³C NMR (101 MHz, C₆D₆) δ [ppm] = 179.4, 148.4, 146.1, 144.4, 129.6, 129.5, 129.4, 127.5, 34.0, 33.1, 25.5.

According to the 2D-NMR spectra, one aromatic carbon signal of the *red-FAAzo-9* (**2.2.2.1.11**) *trans*-isomer is obscured by the solvent.

HRMS (ESI): calc. for C₁₆H₁₁Cl₄N₂O₂⁻ [M - H]⁻: 402.9580, found: 402.9581.

IR (Diamond-ATR, neat) ν_{\max} (cm⁻¹) = 2926 (br, w), 2631 (vw), 1703 (vs), 1590 (w), 1573 (w), 1560 (w), 1544 (w), 1457 (w), 1433 (s), 1398 (m), 1364 (w), 1340 (w), 1288 (m), 1204 (s), 1191 (s), 1155 (m), 1097 (w), 1081 (w), 1045 (m), 915 (m), 881 (m), 829 (m), 805 (vs), 778 (vs), 736 (s), 679 (m).

(*R*)-2-((4-(3,5-dichloro-4-((2,6-dichlorophenyl)diazenyl)phenyl)butanoyl)oxy)-3-((triethylsilyl)oxy)propyl octanoate (**2.2.2.1.12**)

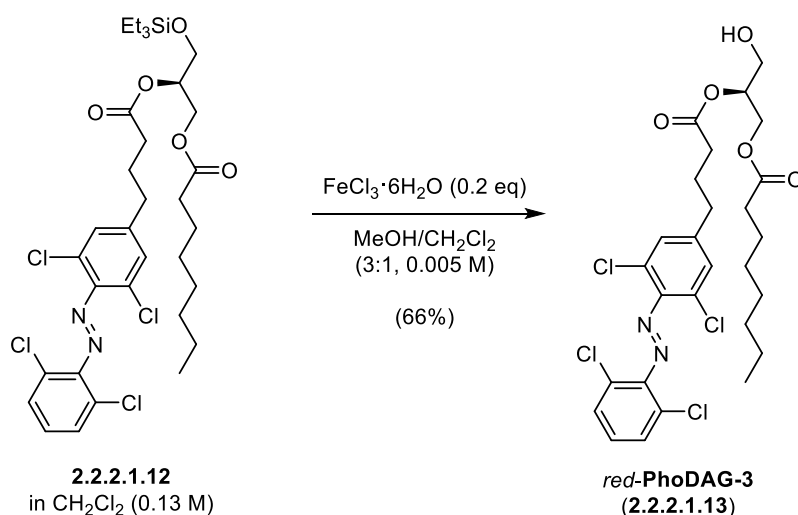


Red-FAAzo-9 (**2.2.2.1.11**, 38.0 mg, 93.6 μ mol, 1.0 eq), DCC (48.3 mg, 234 μ mol, 2.5 eq) and DMAP (1.3 mg, 10 μ mol, 0.1 eq) were dissolved in CH₂Cl₂ (4.7 mL) and stirred at rt for 40 min. The red solution was cooled to 0 °C, stirred for 40 min and alcohol¹⁴⁴ (**2.2.2.1.7**, 40.0 mg, 120 μ mol, 1.3 eq)

was added. After stirring for 7 h at 0 °C, the solution was diluted with EtOAc (35 mL) and washed with H₂O (10 mL) as well as sat. aq. NaCl (10 mL). The organic layer was dried over Na₂SO₄ and concentrated. Purification via flash column chromatography (pentane:Et₂O = 19:1 → 9:1) afforded (*R*)-2-((4-(3,5-dichloro-4-((2,6-dichlorophenyl)diazenyl)phenyl)butanoyl)oxy)-3-((triethylsilyl)oxy)propyl octanoate (**2.2.2.1.12**, 43.8 mg, 60.7 μmol, 59%) as a red oil which was directly used in the next step.

R_f (pentane:EtOAc = 9:1) = 0.53. (visible)

(*S*)-2-((4-(3,5-dichloro-4-((2,6-dichlorophenyl)diazenyl)phenyl)butanoyl)oxy)-3-hydroxypropyl octanoate (*red-PhoDAG-3*, **2.2.2.1.13**)



TES-alcohol (**2.2.2.1.12**, 19.7 mg, 27.3 μmol, 1.0 eq) was dissolved in CH₂Cl₂ (0.21 mL), cooled to 0 °C and FeCl₃·6H₂O (1.5 mg, 5.5 μmol, 0.2 eq) in MeOH/CH₂Cl₂ (3:1, 1.1 mL) was added dropwise. After stirring the red solution for 75 min at 0 °C, it was diluted with H₂O/sat. aq. NaCl (1:1, 5.0 mL) and extracted with EtOAc (15 mL). The organic layer was washed with sat. aq. NaCl (5.0 mL), dried over Na₂SO₄ and concentrated. Purification via flash column chromatography (pentane:EtOAc = 7:3) afforded (*S*)-2-((4-(3,5-dichloro-4-((2,6-dichlorophenyl)diazenyl)phenyl)butanoyl)oxy)-3-hydroxypropyl octanoate (*red-PhoDAG-3*, **2.2.2.1.13**, 11.0 mg, 18.1 μmol, 66%) as a red gum.

Note: Due to the photoswitching properties of the *red-PhoDAG-3* (**2.2.2.1.13**) azobenzene moiety, the NMR spectra show a mixture of *cis*- and *trans*-isomers. The $^1\text{H-NMR}$ is reported for the thermodynamically more stable *trans*-isomer whereas a selection of diagnostic signals is reported for the $^{13}\text{C-NMR}$.

R_f (pentane:EtOAc = 7:3) = 0.23. (visible, CAM)

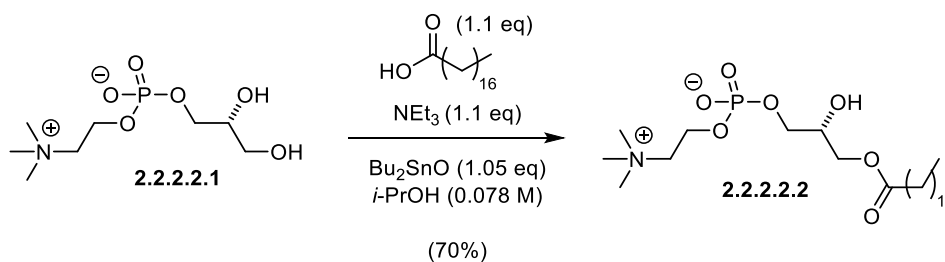
$^1\text{H-NMR}$ (400 MHz, C_6D_6) δ (ppm) = 6.89 (s, 2H), 6.87 (d, $J = 8.1$ Hz, 2H), 6.32 (t, $J = 8.1$ Hz, 1H), 5.12 (qd, $J = 5.6, 3.7$ Hz, 1H), 4.35 (dd, $J = 12.1, 3.7$ Hz, 1H), 4.12 (dd, $J = 12.0, 5.9$ Hz, 1H), 3.45 – 3.41 (m, 2H), 2.13 (t, $J = 7.4$ Hz, 2H), 2.08 – 2.00 (m, 2H), 2.00 – 1.94 (m, 2H), 1.59 – 1.47 (m, 4H), 1.31 (t, $J = 6.2$ Hz, 1H), 1.28 – 1.17 (m, 2H), 1.15 (br s, 6H), 0.87 (t, $J = 7.0$ Hz, 2H).

$^{13}\text{C-NMR}$ (101 MHz, C_6D_6) δ (ppm) = 173.2, 172.3, 148.4, 146.0, 144.6, 129.7, 129.5, 129.4, 127.5, 72.8, 62.5, 61.4, 34.2, 34.0, 33.3, 32.0, 29.4, 29.3, 25.9, 25.2, 23.0, 14.3.

HRMS (ESI): calc. for $\text{C}_{27}\text{H}_{31}\text{Cl}_4\text{N}_2\text{O}_5^-$ $[\text{M} - \text{H}^+]$: 603.0993, found: 603.0989.

IR (Diamond-ATR, neat) ν_{max} (cm^{-1}) = 3366 (br, vw), 2954 (w), 2927 (w), 2856 (w), 1733 (vs), 1591 (w), 1562 (w), 1548 (w), 1455 (w), 1434 (m), 1416 (w), 1397 (m), 1378 (m), 1259 (m), 1162 (vs), 1098 (s), 1046 (s), 1025 (s), 950 (w), 855 (m), 803 (vs), 777 (vs), 734 (m), 665 (m)

(*R*)-2-hydroxy-3-(stearoyloxy)propyl (2-(trimethylammonio)ethyl) phosphate
(**2.2.2.2.2**)



(*R*)-2,3-dihydroxypropyl (2-(trimethylammonio)ethyl) phosphate (**2.2.2.2.1**, 2.00 g, 7.78 mmol, 1.0 eq) and dibutyltin oxide (2.03 g, 8.16 mmol, 1.05 eq) were dissolved in *i*-PrOH (99.7 mL) and heated to 100 °C for 6 h 30 min. After cooling to 0 °C, NEt₃ (1.19 mL, 8.56 mmol, 1.1 eq) and stearoyl chloride (2.89 mL, 8.56 mmol, 1.1 eq) were added. The reaction was allowed to warm to rt and stirred for 16 h 30 min. Thereafter, the solvent was removed *in vacuo* and the residue directly purified by flash column chromatography ($\text{CH}_2\text{Cl}_2:\text{MeOH}:\text{H}_2\text{O} = 9:1:0 \rightarrow 10:4:0.5 \rightarrow$

10:8:2) to give (*R*)-2-hydroxy-3-(stearoyloxy)propyl (2-(trimethylammonio)ethyl) phosphate (2.2.2.2.2, 2.851 g, 5.444 mmol, 70%) as a white gum.

R_f (CH₂Cl₂:MeOH:H₂O = 10:4:0.5) = 0.19. (CAM)

¹H-NMR (400 MHz, CD₃OD) δ (ppm) = 4.33 – 4.25 (m, 2H), 4.18 (dd, *J* = 11.3, 4.5 Hz, 1H), 4.11 (dd, *J* = 11.4, 6.1 Hz, 1H), 4.03 – 3.93 (m, 1H), 3.93 – 3.85 (m, 2H), 3.68 – 3.62 (m, 2H), 3.23 (s, 9H), 2.36 (t, *J* = 7.5 Hz, 2H), 1.62 (quint, *J* = 7.1 Hz, 2H), 1.29 (s, 28H), 0.90 (t, *J* = 6.7 Hz, 3H).

¹³C-NMR (101 MHz, CD₃OD) δ (ppm) = 175.4, 69.8 (d, *J* = 7.8 Hz), 67.4 (dt, *J* = 6.7, 3.1 Hz), 66.2, 60.4 (d, *J* = 5.0 Hz), 54.6 (t, *J* = 3.5 Hz), 34.9, 33.1, 30.8, 30.6, 30.5, 30.5, 30.2, 26.0, 23.8, 14.5.

HRMS (ESI): calc. for C₂₆H₅₅NO₇P⁺ [M + H]⁺: 524.3711, found: 524.3704.

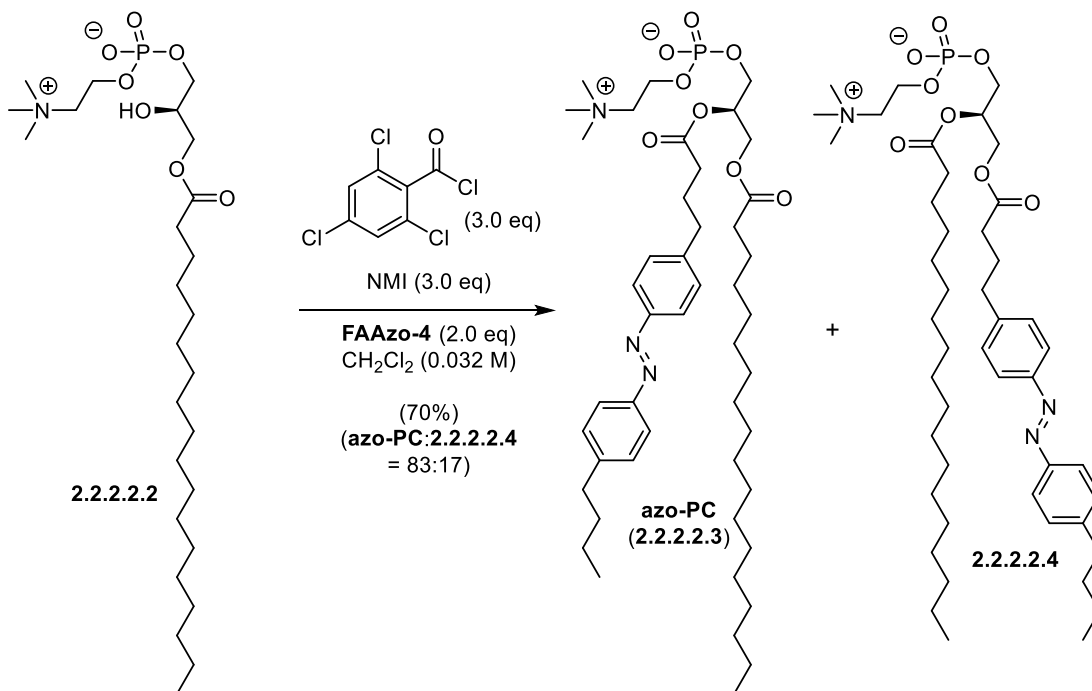
IR (Diamond-ATR, neat) ν_{\max} (cm⁻¹) = 3272 (br, w), 2916 (vs), 2850 (s), 1733 (m), 1467 (m), 1418 (vw), 1388 (vw), 1330 (vw), 1312 (vw), 1293 (w), 1273 (w), 1233, (s), 1215 (s), 1195 (m), 1176 (m), 1136 (m), 1985 (vs), 1053 (vs), 968 (s), 926 (m), 875 (w), 825 (m), 760 (m), 720 (s).

$[\alpha]_D^{20} = +1.22^\circ$ (c = 1.15, MeOH).

$m_p = 118.2 - 124.8^\circ\text{C}$.

The analytical data is in accordance with the literature.¹⁶¹

(*R*)-2-((4-(4-((4-butylphenyl)diazenyl)phenyl)butanoyl)oxy)-3-(stearoyloxy)propyl (2-(trimethylammonio)ethyl) phosphate (azo-PC, 2.2.2.2.3) and (*R*)-3-((4-(4-((4-butylphenyl)diazenyl)phenyl)butanoyl)oxy)-2-(stearoyloxy)propyl (2-(trimethylammonio)ethyl) phosphate (2.2.2.2.4)



FAAzo-4 (2.2.1.3h), 613.5 mg, 1.91 mmol, 2.0 eq) was dissolved in CH₂Cl₂ (20 mL) and NMI (228 μL, 2.87 mmol, 3.0 eq) was added. The mixture was transferred to alcohol (**2.2.2.2.2**, 500 mg, 0.955 mmol, 1.0 eq) in CH₂Cl₂ (10 mL) and 2,4,6-trichlorobenzoyl chloride (410 μL, 2.87 mmol, 3.0 eq) was added dropwise. After stirring for 21 h at rt, the solution was directly subjected to purification via flash column chromatography (CH₂Cl₂:MeOH:H₂O = 1:0:0 → 99:1:0 → 95:5:0 → 8:2:0.1 → 7.5:2.5:0.1 → 7:3:0.2) to give a 83:17 mixture of (*R*)-2-((4-(4-((4-butylphenyl)diazenyl)phenyl)butanoyl)oxy)-3-(stearoyloxy)propyl (2-(trimethylammonio)ethyl) phosphate (**azo-PC**, **2.2.2.2.3**) and (*R*)-3-((4-(4-((4-butylphenyl)diazenyl)phenyl)butanoyl)oxy)-2-(stearoyloxy)propyl (2-(trimethylammonio)ethyl) phosphate (**2.2.2.2.4**) (555.3 mg, 0.6690 mmol, 70%) as an orange gum. The regioisomers could be separated using flash column chromatography (CH₂Cl₂:MeOH:conc. aq. NH₃ = 8:2:2%).

Note: Due to the photoswitching properties of the **azo-PC (2.2.2.2.3)** and **2.2.2.2.4** azobenzene moiety, the NMR spectra show a mixture of *cis*- and *trans*-isomers. The ¹H-NMR is reported for the thermodynamically more stable *trans*-isomer whereas a selection of diagnostic signals is reported for the ¹³C-NMR.

Analytic data of **azo-PC (2.2.2.2.3)**:

R_f (CH₂Cl₂:MeOH:H₂O = 10:4:0.5) = 0.41. (visible, CAM)

¹H NMR (400 MHz, CDCl₃) δ (ppm) = 7.80 (dd, *J* = 8.2, 2.2 Hz, 4H), 7.31 – 7.26 (m, 4H), 5.32 – 5.03 (m, 1H), 4.44 – 4.34 (m, 1H), 4.27 (s, 2H), 4.12 (dd, *J* = 12.2, 7.2 Hz, 1H), 3.98 – 3.86 (m, 2H), 3.75 (s, 2H), 3.31 (s, 9H), 2.76 – 2.59 (m, 4H), 2.39 – 2.29 (m, 2H), 2.29 – 2.17 (m, 2H), 2.01 – 1.88 (m, 2H), 1.62 (quint, *J* = 7.6 Hz, 2H), 1.56 – 1.46 (m, 2H), 1.35 (dt, *J* = 14.5, 7.3 Hz, 2H), 1.30 – 1.11 (m, 28H), 0.92 (t, *J* = 7.4 Hz, 3H), 0.85 (t, *J* = 6.7 Hz, 3H).

¹³C NMR (101 MHz, CDCl₃) δ (ppm) = 173.7, 172.8, 151.3, 151.0, 146.4, 144.6, 129.2, 129.1, 122.9, 122.8, 70.8 (d, *J* = 7.5 Hz), 66.3 (d, *J* = 6.6 Hz), 63.5 (d, *J* = 4.4 Hz), 63.0, 59.4 (d, *J* = 4.5 Hz), 54.4, 35.7 34.9, 34.2, 33.6, 33.5, 32.0, 29.8, 29.8, 29.6, 29.5, 29.4, 29.3, 26.5, 25.0, 22.8, 22.4, 14.2, 14.0.

³¹P NMR (162 MHz, CDCl₃) δ (ppm) = -1.08.

HRMS (ESI): calc. for C₄₆H₇₇N₃O₈P⁺ [M + H]⁺: 830.5443, found: 830.5440.

The analytical data is in accordance with the literature.¹⁴⁶

Analytic data of 2.2.2.2.4:

R_f (CH₂Cl₂:MeOH:H₂O = 10:4:0.5) = 0.41. (visible, CAM)

¹H NMR (400 MHz, CDCl₃) δ (ppm) = 7.81 (d, *J* = 7.5 Hz, 4H), 7.30 (d, *J* = 7.9 Hz, 4H), 4.53 (s, 1H), 4.44 – 4.13 (m, 6H), 3.80 (s, 2H), 3.31 (s, 9H), 2.75 – 2.63 (m, 4H), 2.36 (t, *J* = 7.3 Hz, 2H), 2.28 (t, *J* = 7.5 Hz, 2H), 1.96 (quint, *J* = 7.5 Hz, 2H), 1.63 (quint, *J* = 7.7 Hz, 2H), 1.59 – 1.49 (m, 2H), 1.37 (dq, *J* = 14.6, 7.4 Hz, 2H), 1.23 (d, *J* = 5.0 Hz, 28H), 0.93 (t, *J* = 7.3 Hz, 3H), 0.87 (t, *J* = 6.7 Hz, 3H).

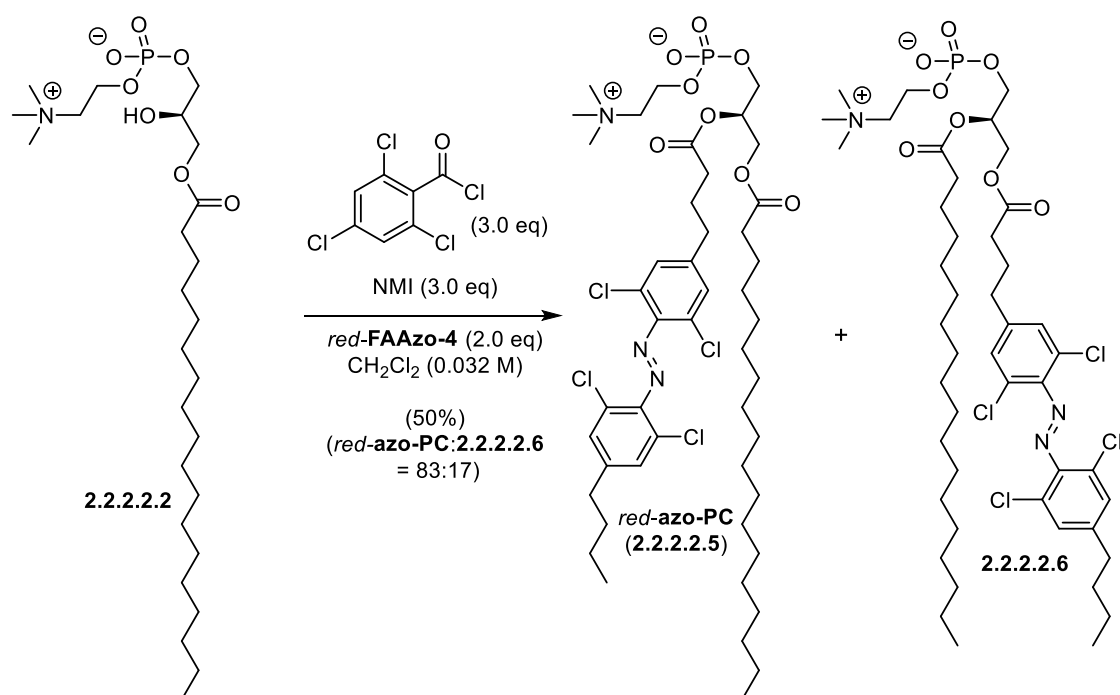
¹³C NMR (101 MHz, CDCl₃) δ (ppm) = 173.5, 173.1, 151.2, 150.9, 146.4, 144.5, 129.2, 129.1, 122.9, 122.8, 70.9, 66.4, 66.3, 63.1, 62.7, 59.6, 54.5, 35.6, 34.9, 34.1, 33.5, 33.4, 31.9, 29.7, 29.7, 29.7, 29.6, 29.4, 29.2, 26.2, 24.9, 22.7, 22.4, 14.2, 14.0.

³¹P NMR (162 MHz, CDCl₃) δ (ppm) = -2.17.

HRMS (ESI): calc. for C₄₆H₇₇N₃O₈P⁺ [M + H]⁺: 830.5443, found: 830.5439.

IR (Diamond-ATR, neat) ν_{max} (cm⁻¹) = 3250 (br, vw), 3028 (vw), 2957 (w), 2920 (vs), 2851 (s), 1734 (s), 1602 (w), 1580 (vw), 1495 (w), 1468 (m), 1416 (w), 1397, (w), 1378 (w), 1216 (s), 1180 (s), 1155 (s), 1085 (vs), 1057 (vs), 1012 (s), 968 (s), 928 (s), 874 (m), 838 (s), 799 (s), 722 (s).

(*R*)-2-((4-(4-((4-butyl-2,6-dichlorophenyl)diazenyl)-3,5-dichlorophenyl)butanoyl)oxy)-3-(stearoyloxy)propyl (2-(trimethylammonio)ethyl) phosphate (*red-azo-PC*, 2.2.2.2.5) and
 (*R*)-3-((4-(4-((4-butyl-2,6-dichlorophenyl)diazenyl)-3,5-dichlorophenyl)butanoyl)oxy)-2-(stearoyloxy)propyl (2-(trimethylammonio)ethyl) phosphate (2.2.2.2.6)



Red-FAAzo-4 (**2.2.1.4h**, 458.7 mg, 0.970 mmol, 2.0 eq) was dissolved in CH_2Cl_2 (5.0 mL) and NMI (116 μL , 1.46 mmol, 3.0 eq) was added. The mixture was transferred to alcohol (**2.2.2.2.2**, 254.0 mg, 0.485 mmol, 1.0 eq) in CH_2Cl_2 (10.2 mL) and 2,4,6-trichlorobenzoyl chloride (208 μL , 1.46 mmol, 3.0 eq) was added dropwise. After stirring for 25 h at rt, the solution was directly subjected to purification via flash column chromatography ($\text{CH}_2\text{Cl}_2:\text{MeOH}:\text{H}_2\text{O} = 1:0:0 \rightarrow 99:1:0 \rightarrow 95:5:0 \rightarrow 8:2:0.1 \rightarrow 7.5:2.5:0.1 \rightarrow 7:3:0.2$) to give a 85:15 mixture of (*R*)-2-((4-(4-((4-butyl-2,6-dichlorophenyl)diazanyl)-3,5-dichlorophenyl)butanoyl)oxy)-3-(stearoyloxy)propyl (2-(trimethylammonio)ethyl) phosphate (*red-azo-PC*, **2.2.2.2.5**) and (*R*)-3-((4-(4-((4-butyl-2,6-dichlorophenyl)diazanyl)-3,5-dichlorophenyl)butanoyl)oxy)-2-(stearoyloxy)propyl (2-(trimethylammonio)ethyl) phosphate (**2.2.2.2.6**) (236.3 mg, 0.2441 mmol, 50%) as a red gum. The regioisomers could be separated using flash column chromatography ($\text{CH}_2\text{Cl}_2:\text{MeOH}:\text{conc. aq. NH}_3 = 8:2:2\%$).

Note: Due to the photoswitching properties of the *red-azo-PC* (**2.2.2.2.5**) and **2.2.2.2.6** azobenzene moiety, the NMR spectra show a mixture of *cis*- and *trans*-isomers. The $^1\text{H-NMR}$ is reported for the thermodynamically more stable *trans*-isomer whereas a selection of diagnostic signals is reported for the $^{13}\text{C-NMR}$.

R_f ($\text{CH}_2\text{Cl}_2:\text{MeOH}:\text{H}_2\text{O} = 10:4:0.5$) = 0.46. (visible, CAM)

$^1\text{H NMR}$ (400 MHz, CDCl_3) δ (ppm) = 7.27 (d, J = 10.4 Hz, 4H), 5.23 (br s, 1H), 4.48 – 4.37 (m, 1H), 4.31 (s, 2H), 4.13 (dt, J = 12.2, 6.1 Hz, 1H), 3.97 (q, J = 6.6 Hz, 2H), 3.81 (s, 2H), 3.37 (s, 9H), 2.72 – 2.49 (m, 4H), 2.43 – 2.32 (m, 2H), 2.28 (p, J = 7.4 Hz, 2H), 2.01 – 1.84 (m, 2H), 1.68 – 1.49 (m, 4H), 1.39 (p, J = 7.4 Hz, 2H), 1.24 (br s, 28H), 0.95 (t, J = 7.3 Hz, 3H), 0.87 (t, J = 6.7 Hz, 3H).

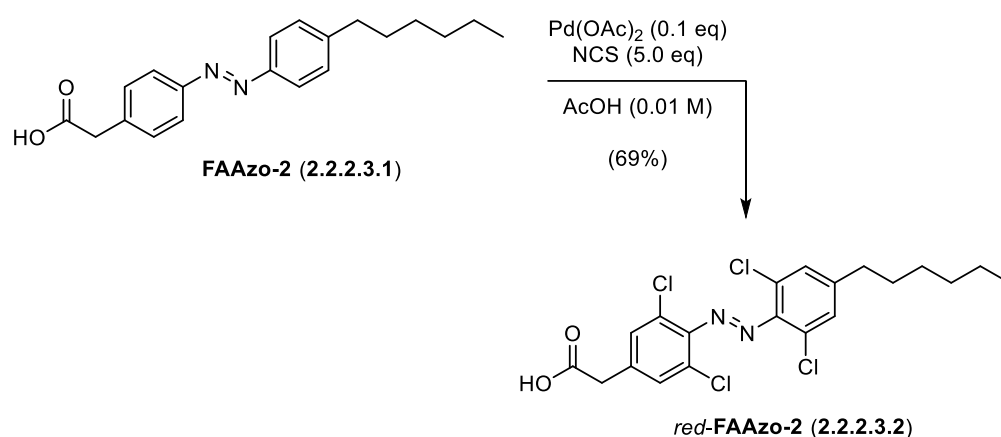
$^{13}\text{C NMR}$ (101 MHz, CDCl_3) δ (ppm) = 173.7, 172.5, 145.9, 145.8, 145.3, 144.1, 129.5, 127.4, 127.4, 71.1 (d, J = 7.0 Hz), 66.4 (d, J = 5.9 Hz), 63.5, 63.0, 59.4 (d, J = 4.0 Hz), 54.5, 35.0, 34.2, 33.4, 33.0, 32.0, 29.8, 29.8, 29.6, 29.5, 29.4, 29.3, 26.1, 25.0, 22.8, 22.3, 14.2, 13.9.

$^{31}\text{P NMR}$ (162 MHz, CDCl_3) δ (ppm) = -0.80.

HRMS (ESI): calc. for $\text{C}_{46}\text{H}_{73}\text{Cl}_4\text{N}_3\text{O}_8\text{P}^+$ [$\text{M} + \text{H}^+$] $^+$: 968.3854, found: 968.3854.

IR (Diamond-ATR, neat) ν_{max} (cm^{-1}) = 3366 (br, w), 2956 (w), 2923 (s), 2852 (m), 1732 (s), 1590 (w), 1550 (w), 1466 (m), 1400 (m), 1378 (w), 1339 (w), 1235, (s), 1177 (m), 1145 (m), 1088 (vs), 1063 (vs), 969 (s), 925 (m), 809 (vs), 721 (s).

2-(3,5-dichloro-4-((2,6-dichloro-4-hexylphenyl)diazenyl)phenyl)acetic acid (*red*-FAAzo-2, 2.2.2.3.2)



FAAzo-2 (2.2.2.3.1, 20.0 g, 61.6 μmol , 1.0 eq), **NCS** (41.1 mg, 0.308 mmol, 5.0 eq) and **Pd(OAc)₂** (1.4 mg, 6.2 μmol , 0.1 eq) were dissolved in **AcOH** (0.62 mL) and heated to 140 °C for 14 h. The dark red solution was cooled to rt and the solvent was removed *in vacuo*. Purification via flash column chromatography (pentane:EtOAc:AcOH = 19:1:1%) afforded 2-(3,5-dichloro-4-((2,6-dichloro-4-hexylphenyl)diazenyl)phenyl)acetic acid (*red*-FAAzo-2, 2.2.2.3.2, 13.3 mg, 28.7 μmol , 47%) as an orange/brown gum.

Note: Due to the photoswitching properties of the *red*-FAAzo-2 (2.2.2.3.2) azobenzene moiety, the NMR spectra show a mixture of *cis*- and *trans*-isomers. The ^1H - and ^{13}C -NMRs are reported for the thermodynamically more stable *trans*.

R_f (pentane:EtOAc:AcOH = 9:1:1%) = 0.24. (visible)

^1H NMR (400 MHz, C_6D_6) δ (ppm) = 6.92 (s, 2H), 6.90 (s, 2H), 2.85 (s, 2H), 2.07 – 1.98 (m, 2H), 1.33 – 1.01 (m, 8H), 0.90 (t, J = 7.2 Hz, 3H).

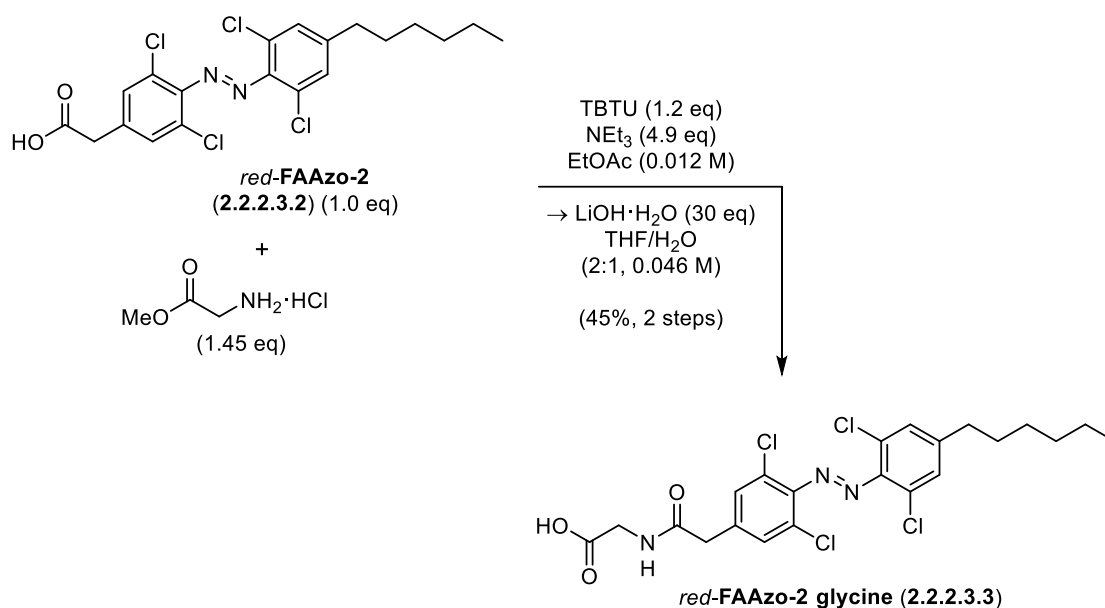
^{13}C NMR (101 MHz, C_6D_6) δ (ppm) = 175.7, 147.3, 146.0, 145.8, 135.6, 130.6, 129.6, 127.6, 39.3, 35.2, 31.9, 30.9, 29.1, 22.9, 14.3.

According to the 2D-NMR spectra, one aromatic carbon signal of the *red*-FAAzo-2 (2.2.2.3.2) *trans*-isomer is obscured by the solvent.

HRMS (ESI): calc. for $\text{C}_{20}\text{H}_{21}\text{Cl}_4\text{N}_2\text{O}_2^+$ [$\text{M} + \text{H}^+$] $^+$: 461.0352, found: 461.0356.

IR (Diamond-ATR, neat) ν_{max} (cm^{-1}) = 2924 (s), 2853 (m), 1700 (vs), 1592 (m), 1542 (w), 1489 (w) 1455 (m), 1404 (vs), 1224 (vs), 1166 (vs), 1068 (w), 1053 (m), 963 (m), 931 (m), 878 (m), 797 (s), 756 (s), 737 (m), 718 (m), 665 (m).

2-(3,5-dichloro-4-((2,6-dichloro-4-hexylphenyl)diazenyl)phenyl)acetyl)glycine (*red*-FAAzo-2 glycine, 2.2.2.3.3)



Red-FAAzo-2 (2.2.2.3.2, 8.5 mg, 26 μmol , 1.0 eq) and TBTU (8.4 mg, 26 μmol , 1.2 eq) were dissolved in EtOAc (1.75 mL) and NEt_3 (14.6 μL , 0.105 mmol, 4.9 eq) was added. The reaction

was stirred at rt for 1 h before glycine hydrochloride (4.0 mg, 31 μmol , 1.45 eq) was added to the red solution and stirring was continued for 2 h. Thereafter, the mixture was diluted with EtOAc (15 mL) and washed with H₂O (5.0 mL) as well as sat. aq. NaCl (5.0 mL). The organic layer was dried over Na₂SO₄ and concentrated. The residue was dissolved in THF/H₂O (2:1, 0.47 mL) and LiOH·H₂O (15.7 mg, 0.655 mmol, 30 eq) was added at 0 °C. After warming the solution to rt, the reaction was stirred for 1 h before formic acid (24.7 μL , 0.655 mmol, 30 eq) was added. The mixture was diluted with EtOAc (15 mL) and the organic layer was washed with 3% aq. KHSO₄ (5.0 mL) as well as sat. aq. NaCl (5.0 mL). Thereafter, the organic fraction was dried over Na₂SO₄ and concentrated. Purification via flash column chromatography (CH₂Cl₂:MeOH:AcOH = 98:1:1 → 97:2:1) afforded 2-(3,5-dichloro-4-((2,6-dichloro-4-hexylphenyl)diazenyl)phenyl)acetyl)glycine (*red-FAAzo-2 glycine*, **2.2.2.3.3**, 5.1 mg, 9.8 μmol , 38%) as an orange solid.

Note: Due to the photoswitching properties of the *red-FAAzo-2 glycine*, (**2.2.2.3.3**) azobenzene moiety, the NMR spectra show a mixture of *cis*- and *trans*-isomers. The ¹H- and ¹³C-NMRs are reported for the major isomer.

R_f (CH₂Cl₂:MeOH:AcOH = 19:1:1%) = 0.28. (visible)

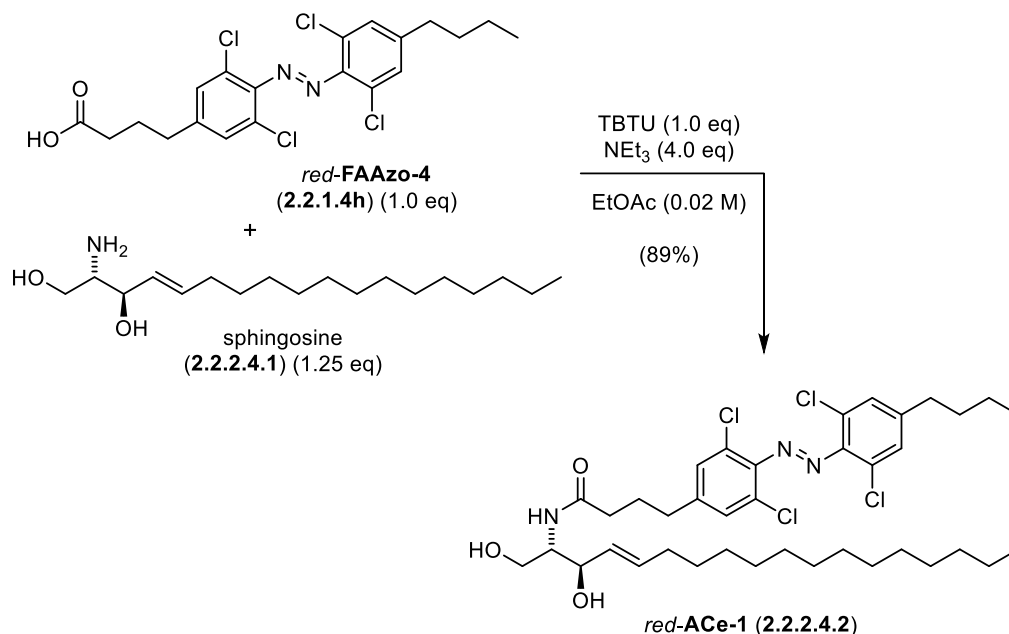
¹H NMR (400 MHz, CD₃OD) δ (ppm) = 7.36 (s, 2H), 7.20 (s, 2H), 3.92 (s, 2H), 3.57 (s, 2H), 2.58 (dd, *J* = 9.0, 6.5 Hz, 2H), 1.59 (p, *J* = 7.1 Hz, 2H), 1.30 (d, *J* = 8.3 Hz, 6H), 0.95 – 0.85 (m, 3H).

¹³C NMR (101 MHz, CD₃OD) δ (ppm) = 172.9, 172.5, 147.9, 147.6, 147.1, 139.8, 131.2, 130.4, 126.7, 126.6, 42.1, 41.9, 35.8, 32.7, 31.9, 29.8, 23.6, 14.4.

HRMS (ESI): calc. for C₂₂H₂₂ Cl₄N₃O₃⁻ [M – H]⁺: 516.0422, found: 516.0421.

IR (Diamond-ATR, neat) ν_{max} (cm⁻¹) = 3297 (w), 2955 (w), 2921 (m), 2849 (w), 1717 (s), 1643 (vs), 1590 (m), 1547 (s), 1446 (m), 1428 (m), 1455 (m), 1409 (m), 1400 (s), 1348 (w), 1256 (s), 1238 (s), 1203 (m), 1080 (m), 1014 (s), 930 (m), 863 (s), 814 (vs), 740 (m), 723 (m), 659 (s).

4-(4-((4-butyl-2,6-dichlorophenyl)diazenyl)-3,5-dichlorophenyl)-*N*-(2-hydroxyethyl)butanamide (*red-ACe-1*, **2.2.2.4.2**)



Red-FAAzo-4 (2.2.1.4h), 29.5 mg, 64.0 μmol , 1.0 eq) and TBTU (20.6 mg, 64.0 μmol , 1.0 eq) were dissolved in EtOAc (3.2 mL) and NEt₃ (35.6 μL , 0.256 mmol, 4.0 eq) was added. The reaction was stirred at rt for 1 h and sphingosine (**2.2.2.4.1**, 25.0 mg, 79.5 μmol , 1.0 eq) was added to the red solution before stirring was continued to for 2 h 20 min. Thereafter, the mixture was diluted with EtOAc (35 mL) and washed with sat. aq. NaHCO₃ (10 mL), 3% aq. KHSO₄ (10 mL) and sat. aq. NaCl (10 mL). The organic layer was dried over Na₂SO₄ and concentrated. Purification via flash column chromatography (pentane:EtOAc= 9:1) afforded 4-(4-((4-butyl-2,6-dichlorophenyl)diazenyl)-3,5-dichlorophenyl)-N-(2-hydroxyethyl)butanamide (**red-ACe-1, 2.2.2.4.1**, 42.4 mg, 57.0 mg, 89%) as a red gum.

Note: Due to the photoswitching properties of the **red-ACe-1 (2.2.2.4.2)** azobenzene moiety, the NMR spectra show a mixture of *cis*- and *trans*-isomers. The ¹H-NMR is reported for the thermodynamically more stable *trans*-isomer whereas a selection of diagnostic signals is reported for the ¹³C-NMR.

R_f (pentane:EtOAc:AcOH = 4:6:1%) = 0.13. (visible)

¹H NMR (400 MHz, C₆D₆) δ (ppm) = 7.07 (s, 2H), 6.92 (s, 2H), 6.18 (t, *J* = 8.9 Hz, 1H), 5.80 (td, *J* = 13.4, 12.1, 6.5 Hz, 1H), 5.61 – 5.53 (m, 1H), 4.38 (d, *J* = 5.2 Hz, 1H), 4.12 (dt, *J* = 7.9, 4.2 Hz, 1H), 3.94 (dd, *J* = 11.3, 4.5 Hz, 1H), 3.75 (dd, *J* = 11.4, 4.0 Hz, 1H), 3.58 (br s, 2H), 2.25 (t, *J* = 7.4 Hz, 2H), 2.08 – 1.98 (m, 4H), 1.87 – 1.79 (m, 2H), 1.78 – 1.68 (m, 2H), 1.40 – 1.25 (m, 20H), 1.21 – 1.07 (m, 2H), 1.10 – 0.99 (m, 2H), 0.93 (t, *J* = 6.7 Hz, 3H), 0.78 (t, *J* = 7.2 Hz, 3H).

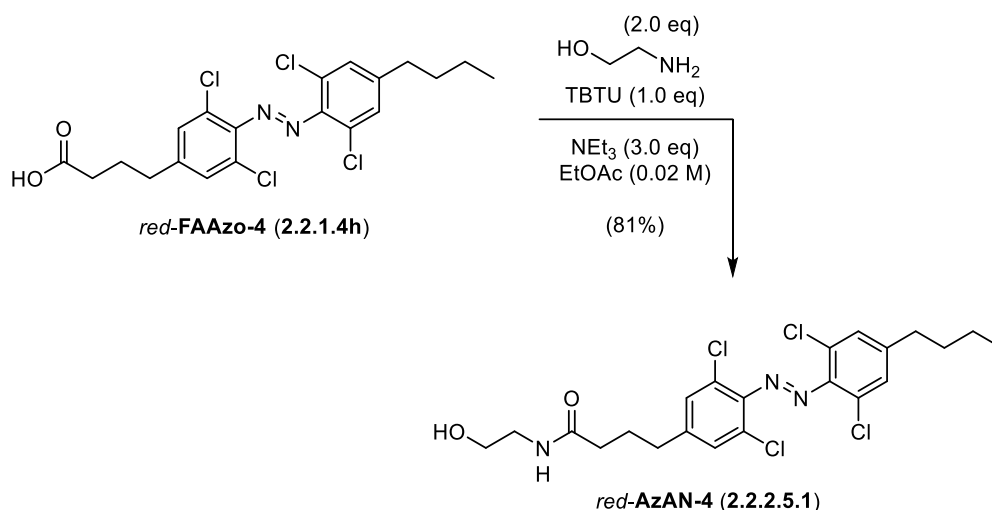
^{13}C NMR (101 MHz, C_6D_6) δ (ppm) = 173.0, 146.3, 145.9, 145.8, 144.7, 133.6, 129.9, 129.8, 129.6, 74.2, 62.5, 55.6, 35.2, 34.9, 34.3, 32.9, 32.9, 32.4, 30.3, 30.2, 30.2, 30.1, 29.9, 29.9, 29.8, 26.5, 23.2, 22.5, 14.4, 14.0.

According to the 2D-NMR spectra, three aromatic carbon signals of the *red-ACe-1* (2.2.2.4.2) *trans*-isomer are obscured by the solvent.

HRMS (ESI): calc. for $\text{C}_{38}\text{H}_{56}\text{Cl}_4\text{N}_3\text{O}_3^+$ $[\text{M} + \text{H}]^+$: 742.3070, found: 742.3070.

IR (Diamond-ATR, neat) ν_{max} (cm^{-1}) = 3292 (br, w), 2921 (vs), 2852 (s), 1645 (s), 1590 (m), 1547 (vs), 1458 (m), 1401 (m), 1379 (m), 1344 (w), 1262 (w), 1205 (w), 1054 (m), 1027 (m), 964 (m), 858 (m), 809 (s), 740 (m), 721 (s).

4-(4-((4-butyl-2,6-dichlorophenyl)diazenyl)-3,5-dichlorophenyl)-*N*-(2-hydroxyethyl)butanamide (*red-AzAN-4*, 2.2.2.5.1)



Red-FAAzo-4 (2.2.1.4h, 25.0 mg, 54.1 μmol , 1.0 eq) and TBTU (17.4 mg, 54.1 μmol , 1.0 eq) were dissolved in EtOAc (2.2 mL) and NEt_3 (22.6 μL , 0.162 mmol, 3.0 eq) was added before stirring at rt for 30 min. 2-Aminoethanol (6.5 μL , 0.108 mmol, 2.0 eq) in EtOAc (0.5 mL) was added to the red suspension and stirring was continued for 2 h 30 min. Thereafter, the mixture was diluted with EtOAc (35 mL) and washed with sat. aq. NaHCO_3 (10 mL), 3% aq. KHSO_4 (10 mL) and sat. aq. NaCl (10 mL). The organic layer was dried over Na_2SO_4 and concentrated. Purification via flash column chromatography (pentane:EtOAc = 1:1) afforded 4-(4-((4-butyl-2,6-dichlorophenyl)diazenyl)-3,5-dichlorophenyl)-*N*-(2-hydroxyethyl)butanamide (*red-AzAN-4*, 2.2.2.5.1, 22.2 mg, 43.9 μmol , 81%) as a orange/red solid.

Note: Due to the photoswitching properties of the *red-AzAN-4* (2.2.2.5.1) azobenzene moiety, the NMR spectra show a mixture of *cis*- and *trans*-isomers. The ^1H - and ^{13}C -NMRs are reported for the thermodynamically more stable *trans*.

R_f (pentane:EtOAc:AcOH = 4:6:1%) = 0.25. (visible)

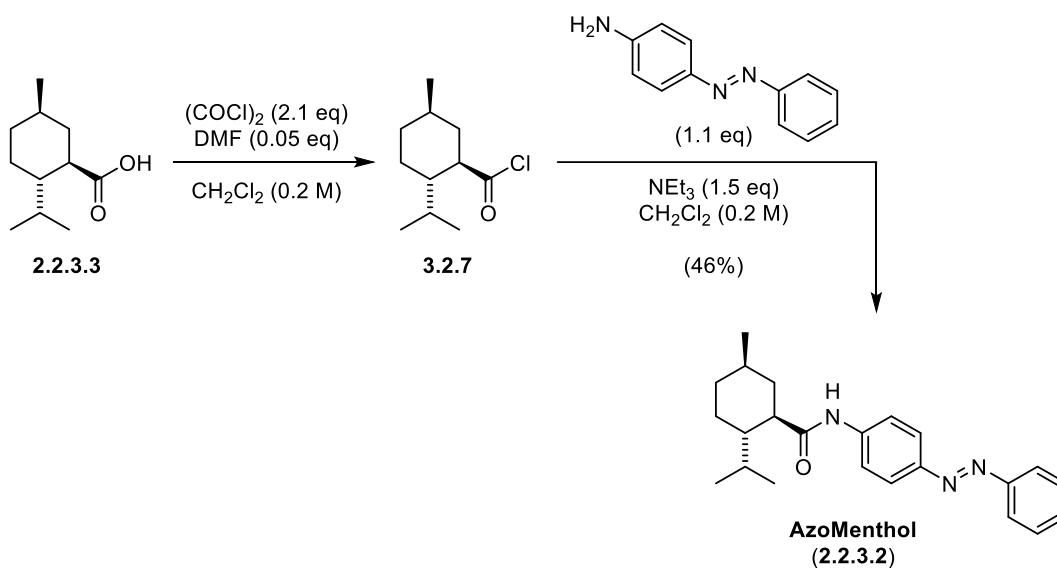
^1H NMR (400 MHz, CDCl_3) δ (ppm) = 7.28 (s, 2H), 7.26 (s, 2H), 6.05 (s, 1H), 3.73 (t, J = 4.9 Hz, 2H), 3.43 (q, J = 4.7 Hz, 2H), 2.74 (br s, 1H), 2.69 (t, J = 7.4 Hz, 2H), 2.66 – 2.58 (m, 2H), 2.24 (t, J = 7.3 Hz, 2H), 2.02 (q, J = 7.2 Hz, 2H), 1.69 – 1.57 (m, 2H), 1.38 (dq, J = 14.6, 7.3 Hz, 2H), 0.95 (t, J = 7.3 Hz, 3H).

^{13}C NMR (101 MHz, CDCl_3) δ (ppm) = 173.5, 145.9, 145.9, 145.3, 144.1, 129.6, 129.5, 127.5, 127.5, 62.6, 42.5, 35.3, 35.0, 34.4, 33.1, 26.4, 22.3, 14.0.

HRMS (ESI): calc. for $\text{C}_{22}\text{H}_{26}\text{Cl}_4\text{N}_3\text{O}_2^+$ [$\text{M} + \text{H}^+$] $^+$: 504.0774, found: 504.0777.

IR (Diamond-ATR, neat) ν_{max} (cm^{-1}) = 3284 (br, m), 3087 (vw), 2952 (m), 2924 (m), 2870 (w), 2856 (w), 2361 (vw), 1737 (vw), 1648 (vs), 1590 (m), 1548 (vs), 1457 (m), 1439 (m), 1415 (m), 1401 (vs), 1341 (w), 1274 (m), 1203 (m), 1103 (w), 1055 (s), 1028 (s), 925 (w), 861 (s), 815 (vs), 739 (s), 668 (s).

(1*R*,2*S*,5*R*)-2-isopropyl-5-methyl-*N*-(4-(phenyldiazenyl)phenyl)cyclohexane-1-carboxamide (AzoMenthol, 2.2.3.2)



(1*R*,2*S*,5*R*)-2-Isopropyl-5-methylcyclohexane-1-carboxylic acid¹⁵⁴⁻¹⁵⁵ (**2.2.3.3**, 100 mg, 0.543 mmol, 1.0 eq) was dissolved in CH₂Cl₂ (2.7 mL) and oxalyl chloride (2 M in CH₂Cl₂, 0.570 mL, 1.14 mmol, 2.1 eq) was added at 0 °C followed DMF (2.1 μL, 27 μmol, 0.05 eq). After the solution was allowed to warm to rt, it was stirred for 2 h and concentrated over a stream of N₂. The residue was dissolved in CH₂Cl₂ (2.7 mL) and added to a mixture of 4-(phenyldiazenyl)aniline (113mg, 0.597 mmol, 1.1 eq) and NEt₃ (114 μL, 0.815 mmol, 1.5 eq) at 0 °C. After warming the orange solution to rt and stirring for 1 h, it was diluted with CH₂Cl₂ (70 mL) and washed with 0.1 M aq. HCl (20 mL), H₂O (20 mL), 0.1 M aq. NaOH (20 mL) and sat. aq. NaCl (20 mL). The organic layer was dried over Na₂SO₄ and concentrated. Purification via flash column chromatography (pentane:EtOAc = 14:1) afforded (1*R*,2*S*,5*R*)-2-isopropyl-5-methyl-*N*-(4-(phenyldiazenyl)phenyl)cyclohexane-1-carboxamide (**AzoMenthol**, **2.2.3.2**, 90.6 mg, 0.249 mmol, 46%) as an orange powder.

R_f (pentane:Et₂O = 9:1) = 0.53. (visible)

¹H NMR (400 MHz, CDCl₃) δ (ppm) = 7.91 (t, *J* = 9.1 Hz, 4H), 7.72 (d, *J* = 8.5 Hz, 2H), 7.57 – 7.42 (m, 4H), 2.21 (td, *J* = 11.5, 3.1 Hz, 1H), 1.92 (d, *J* = 10.9 Hz, 1H), 1.89 – 1.79 (m, 1H), 1.75 (t, *J* = 13.4 Hz, 2H), 1.66 (t, *J* = 11.2 Hz, 1H), 1.46 – 1.27 (m, 2H), 1.12 – 0.97 (m, 2H), 0.93 (dd, *J* = 8.6, 6.8 Hz, 6H), 0.84 (d, *J* = 6.9 Hz, 3H).

¹³C NMR (101 MHz, CDCl₃) δ (ppm) = 174.7, 152.8, 149.0, 140.7, 130.9, 129.2, 124.2, 122.9, 119.9, 51.1, 44.7, 39.6, 34.6, 32.4, 29.0, 24.0, 22.4, 21.6, 16.5.

HRMS (ESI): calc. for C₂₃H₃₀N₃O⁺ [*M* + H]⁺: 364.2383, found: 364.2381.

IR (Diamond-ATR, neat) ν_{max} (cm⁻¹) = 3298 (br, w), 3066 (vw), 2953 (w), 2915 (w), 2870 (w), 1658 (s), 1594 (s), 1519 (vs), 1455(w), 1442 (m), 1406 (s), 1386 (m), 1370 (m), 1341 (w), 1300 (m), 1247 (m), 1180 (m), 1144 (m), 1104 (w), 1070 (vw), 1010 (w), 921 (w), 883 (vw), 866 (vw), 840 (s), 764 (s), 716 (m), 685 (vs).

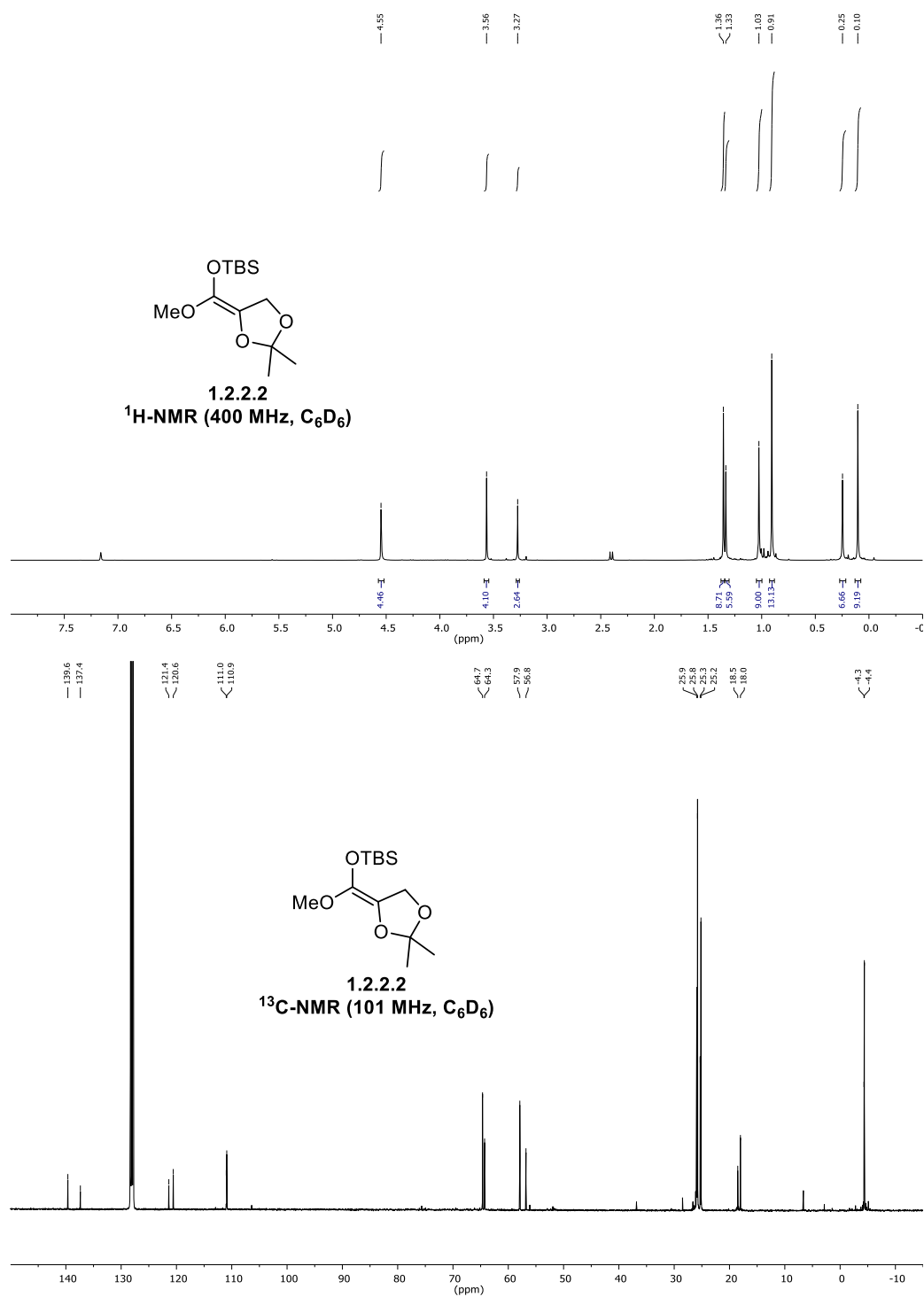
4 Appendix

4.1 NMR-Spectra

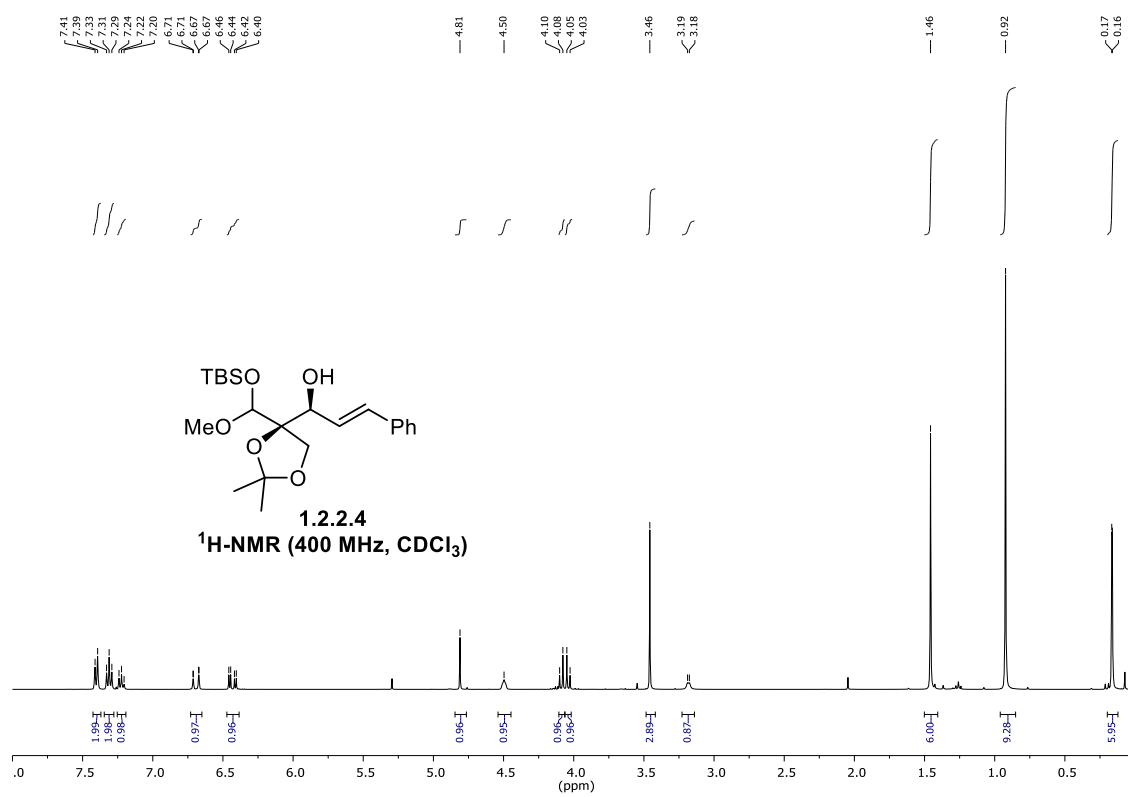
4.1.1 NMR-Spectra – Chapter 1

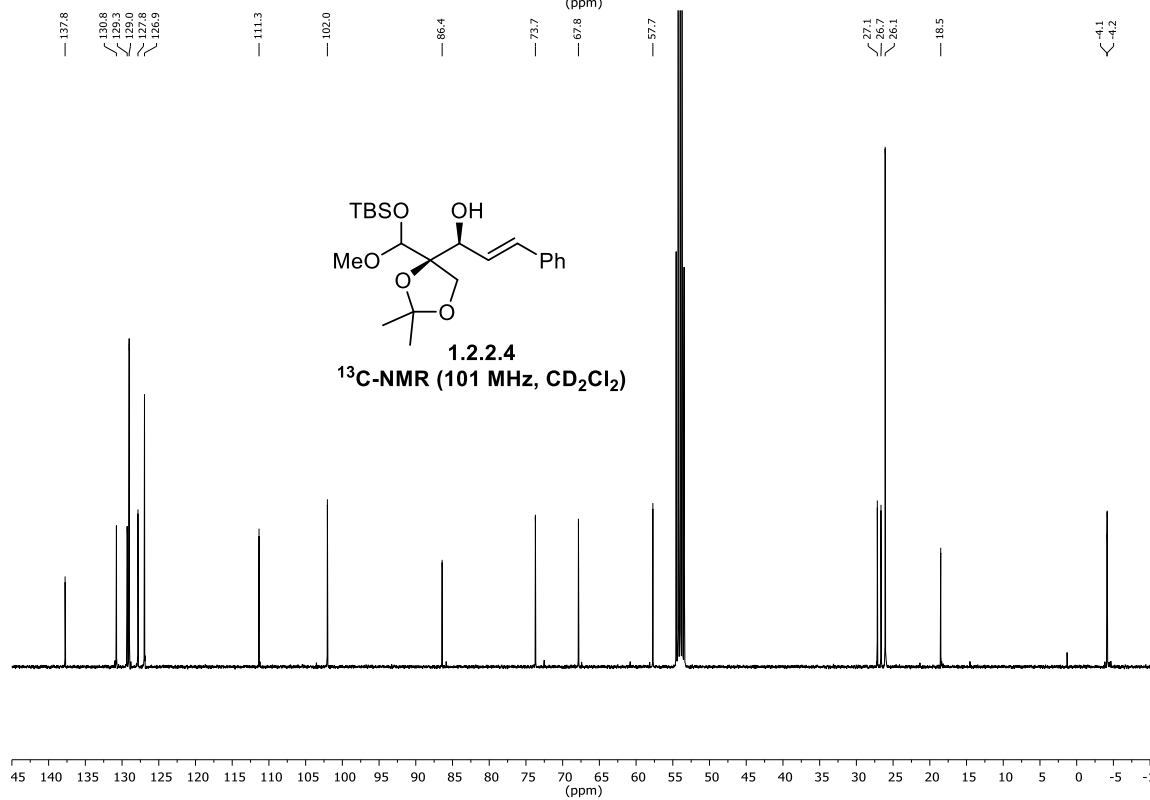
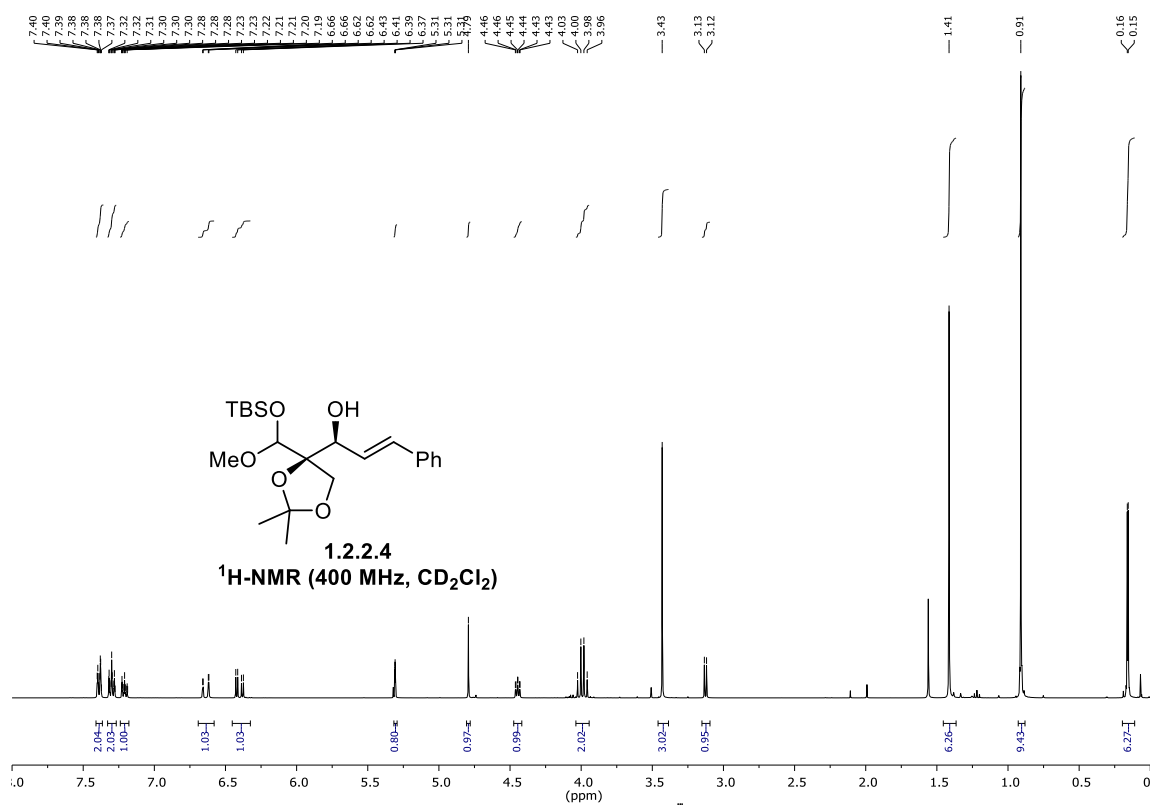
Tert-butyl((2,2-dimethyl-1,3-dioxolan-4-ylidene)(methoxy)methoxy)dimethylsilane

(1.2.2.2)

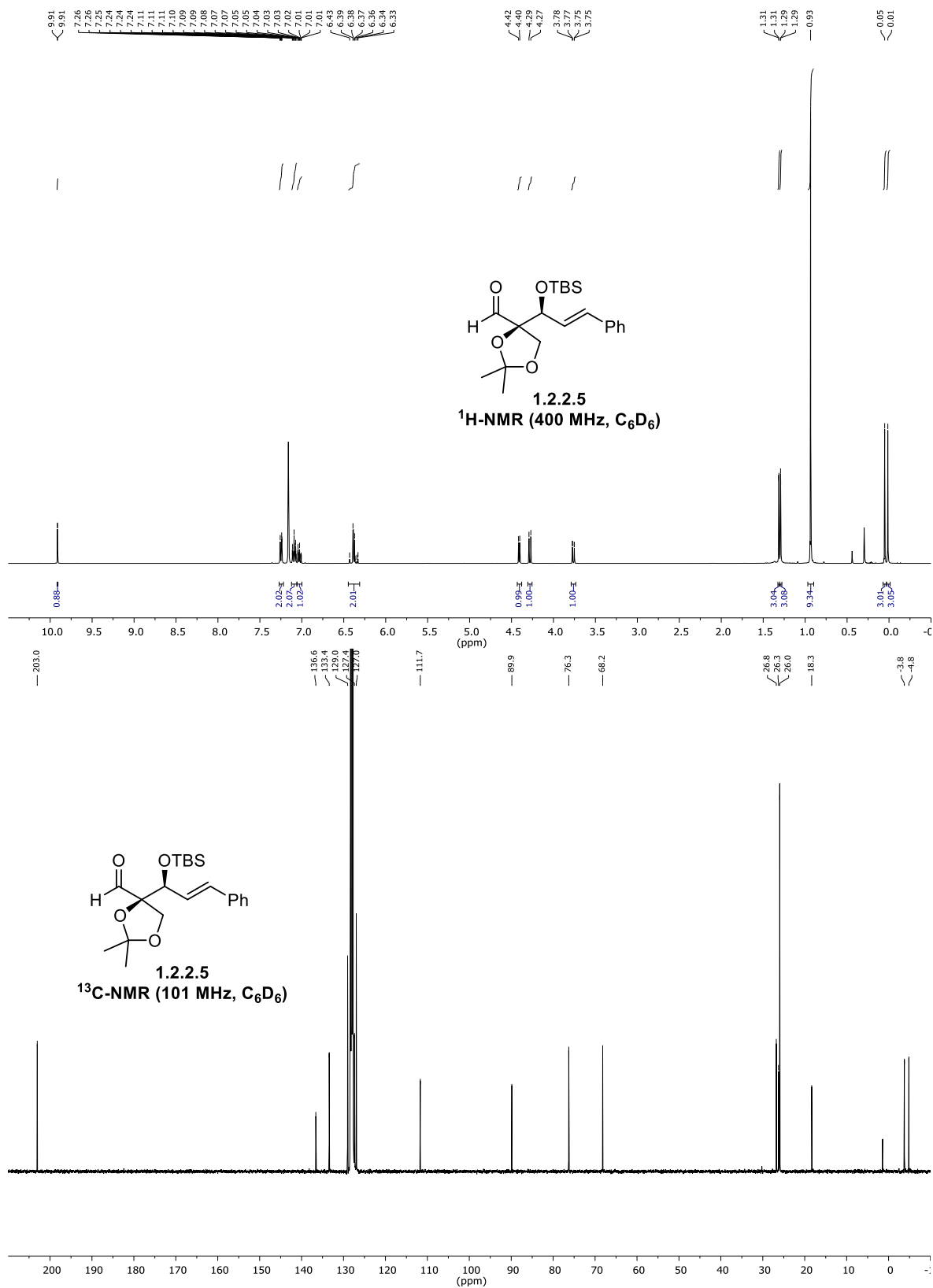


(1*S*,*E*)-1-((4*R*)-4-(((*tert*-butyldimethylsilyl)oxy)(methoxy)methyl)-2,2-dimethyl-1,3-dioxolan-4-yl)-3-phenylprop-2-en-1-ol (1.2.2.4)

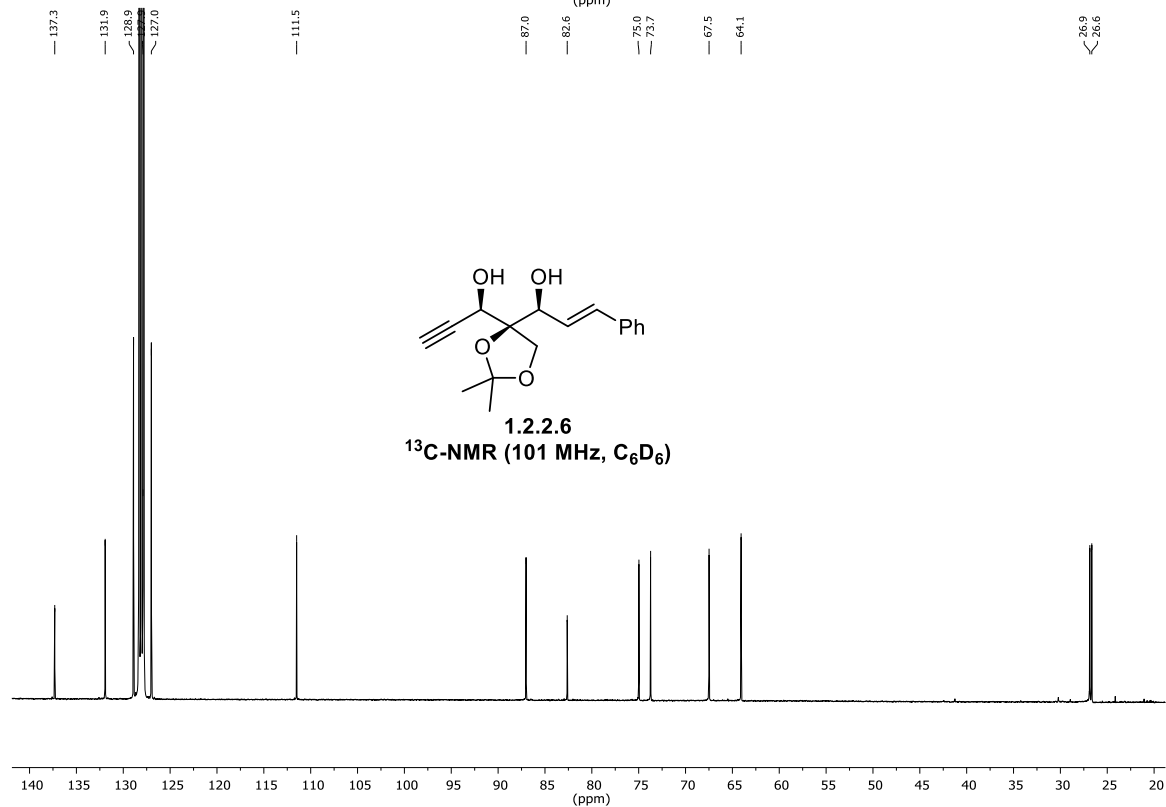
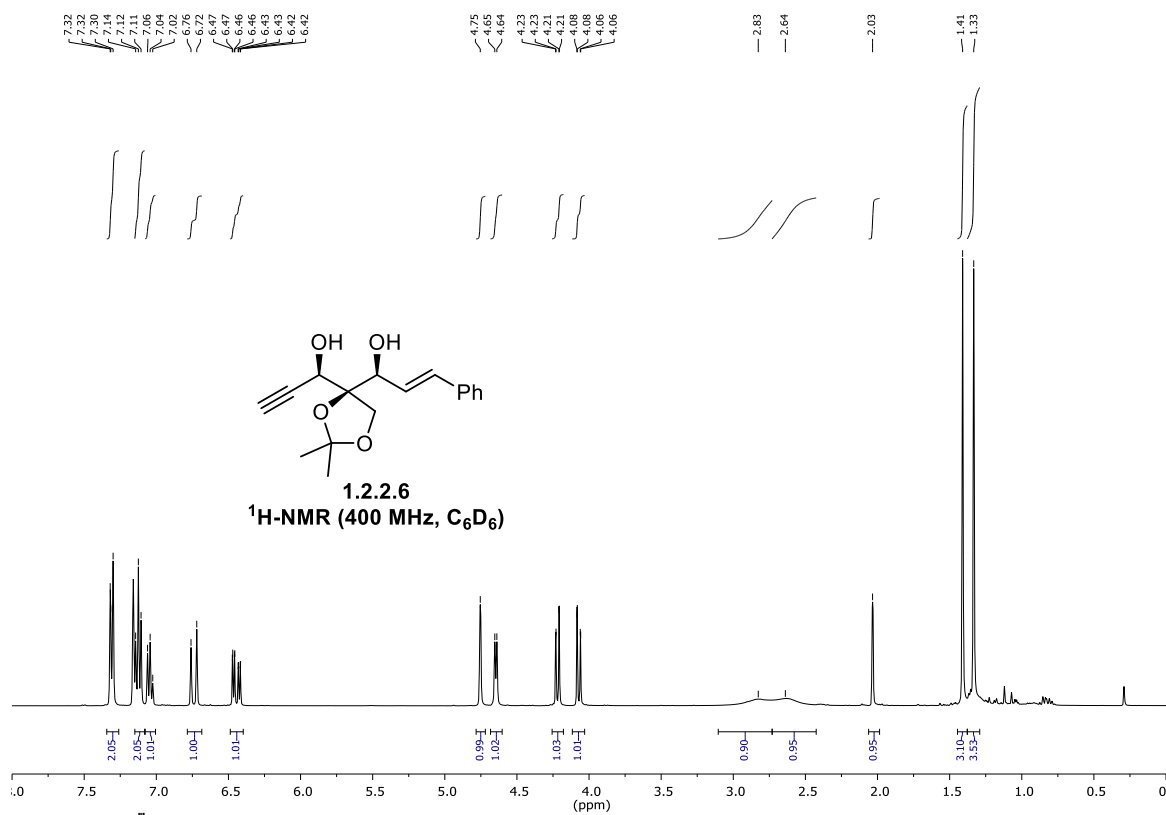




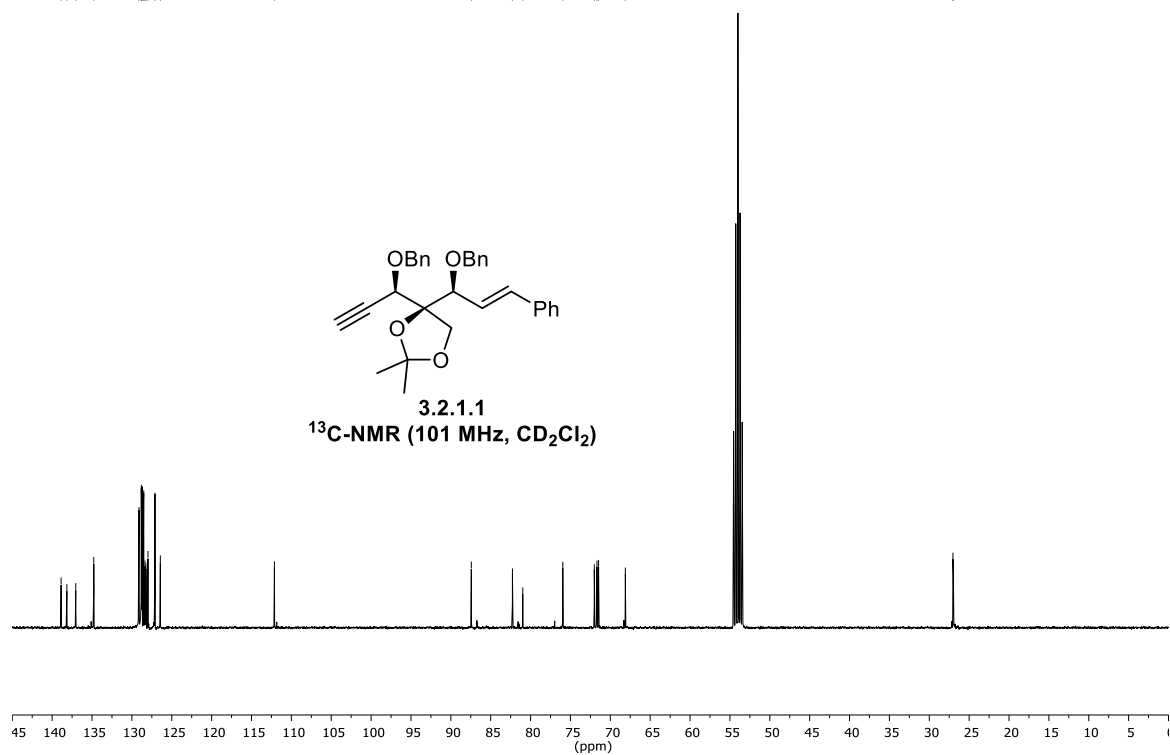
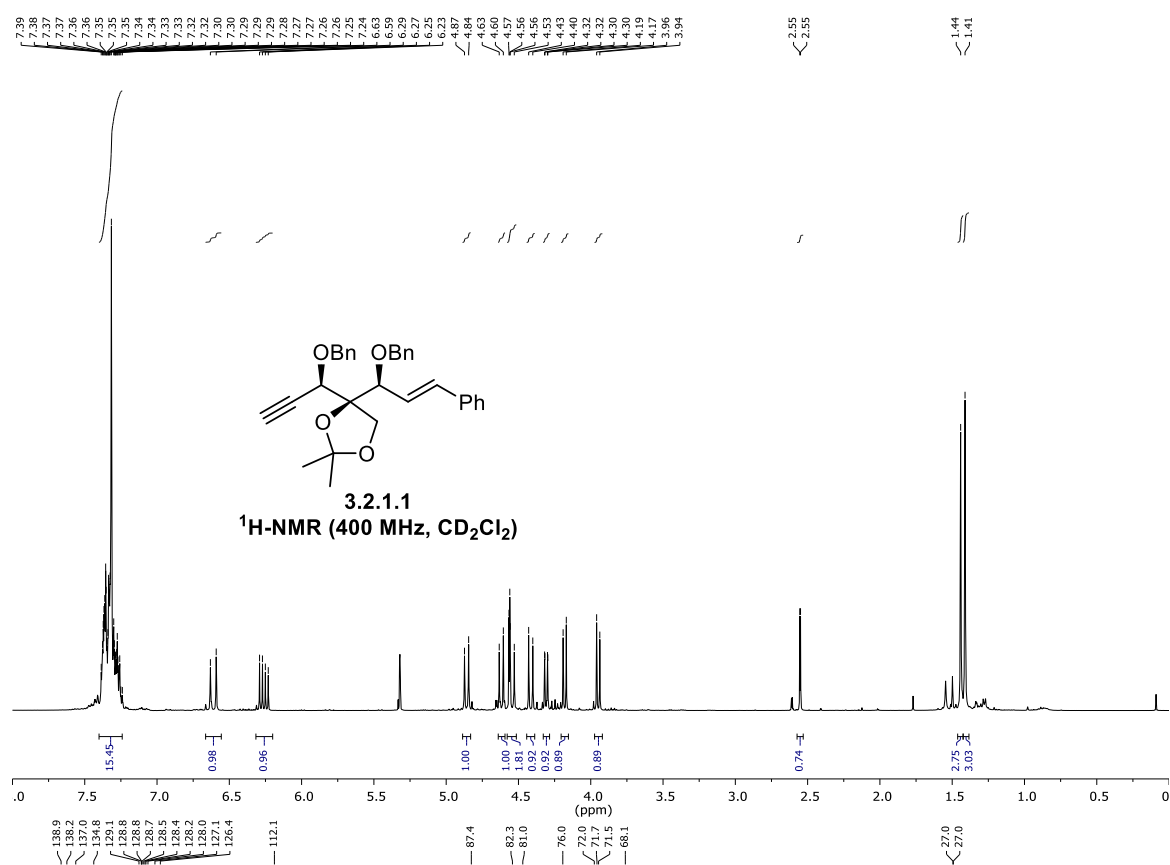
(R)-4-((*S,E*)-1-((*tert*-butyldimethylsilyloxy)-3-phenylallyl)-2,2-dimethyl-1,3-dioxolane-4-carbaldehyde (1.2.2.5)



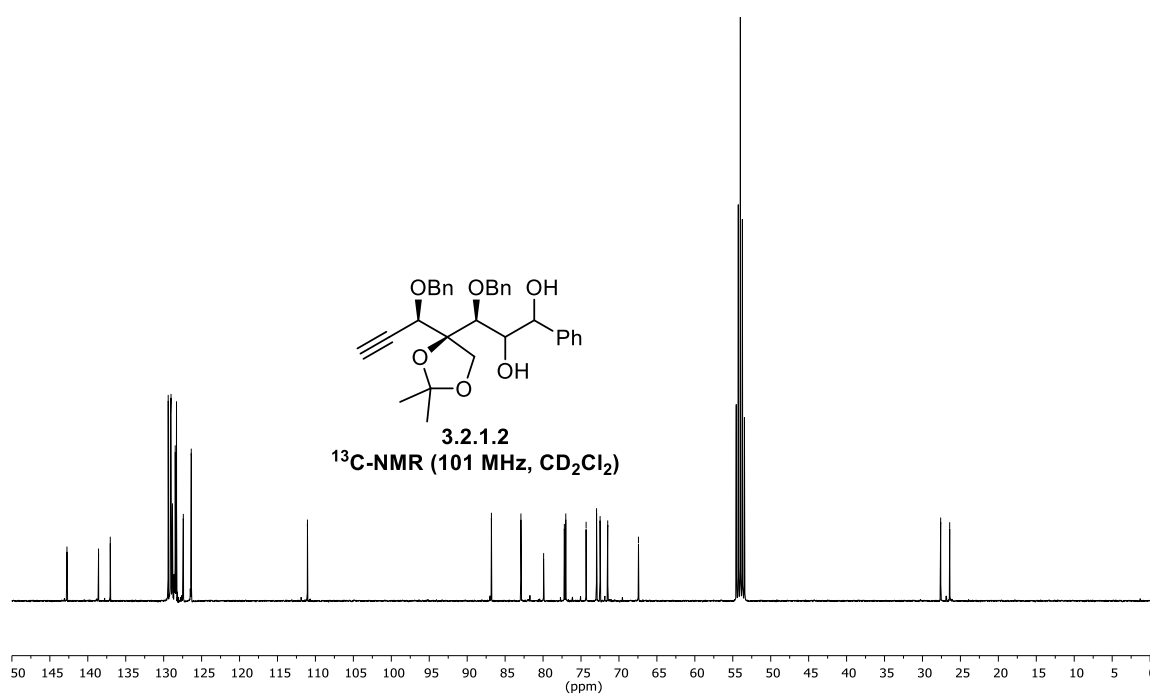
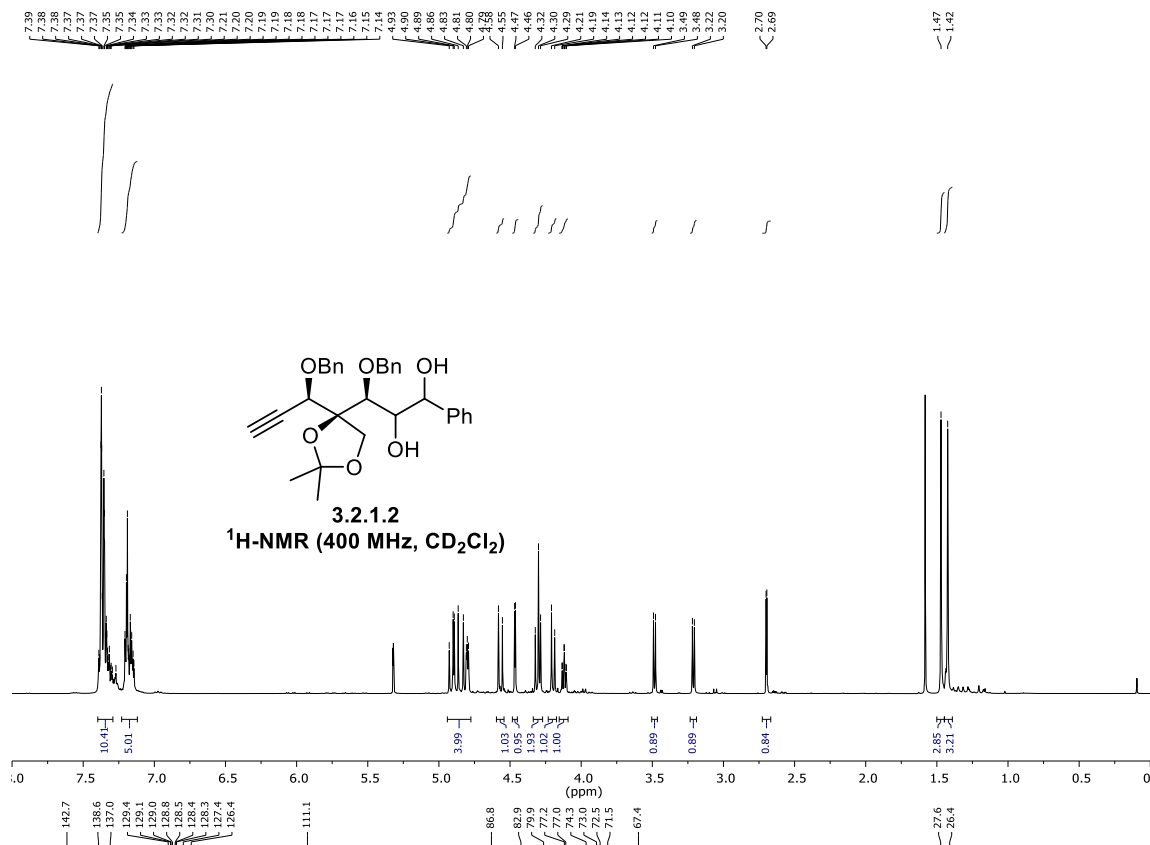
(*S,E*)-1-((*R*)-4-((*R*)-1-hydroxyprop-2-yn-1-yl)-2,2-dimethyl-1,3-dioxolan-4-yl)-3-phenylprop-2-en-1-ol (1.2.2.6)



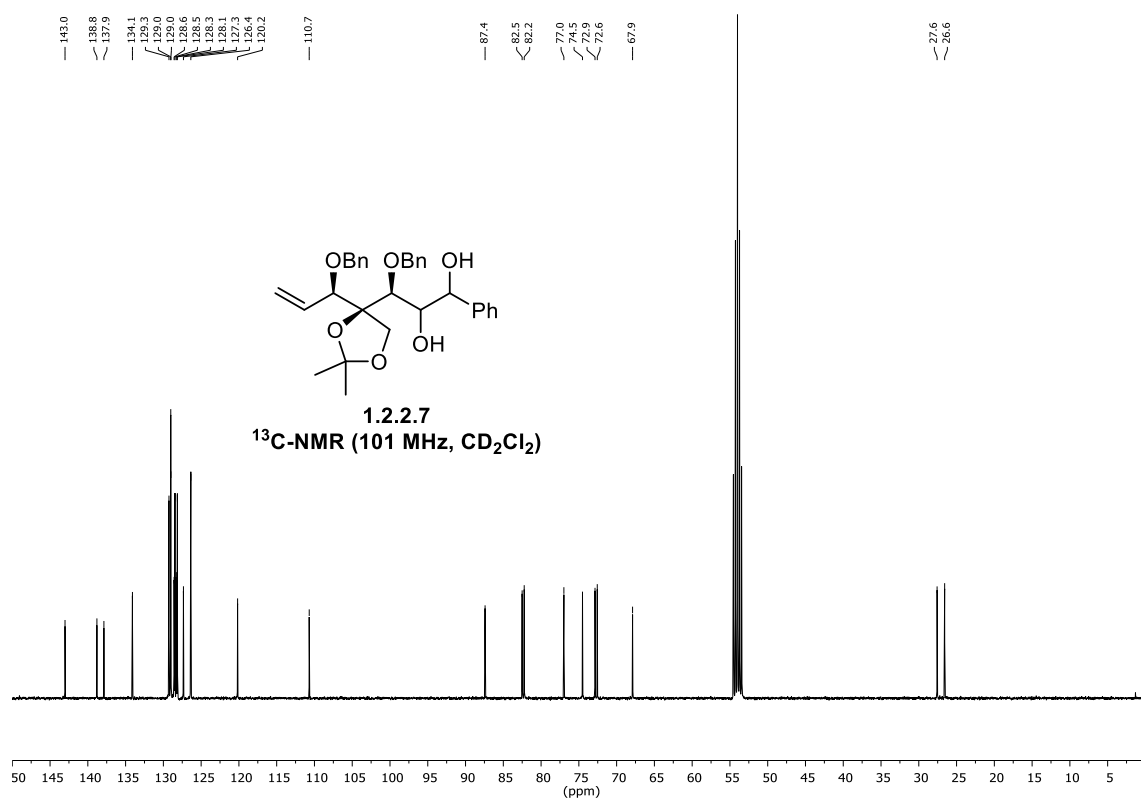
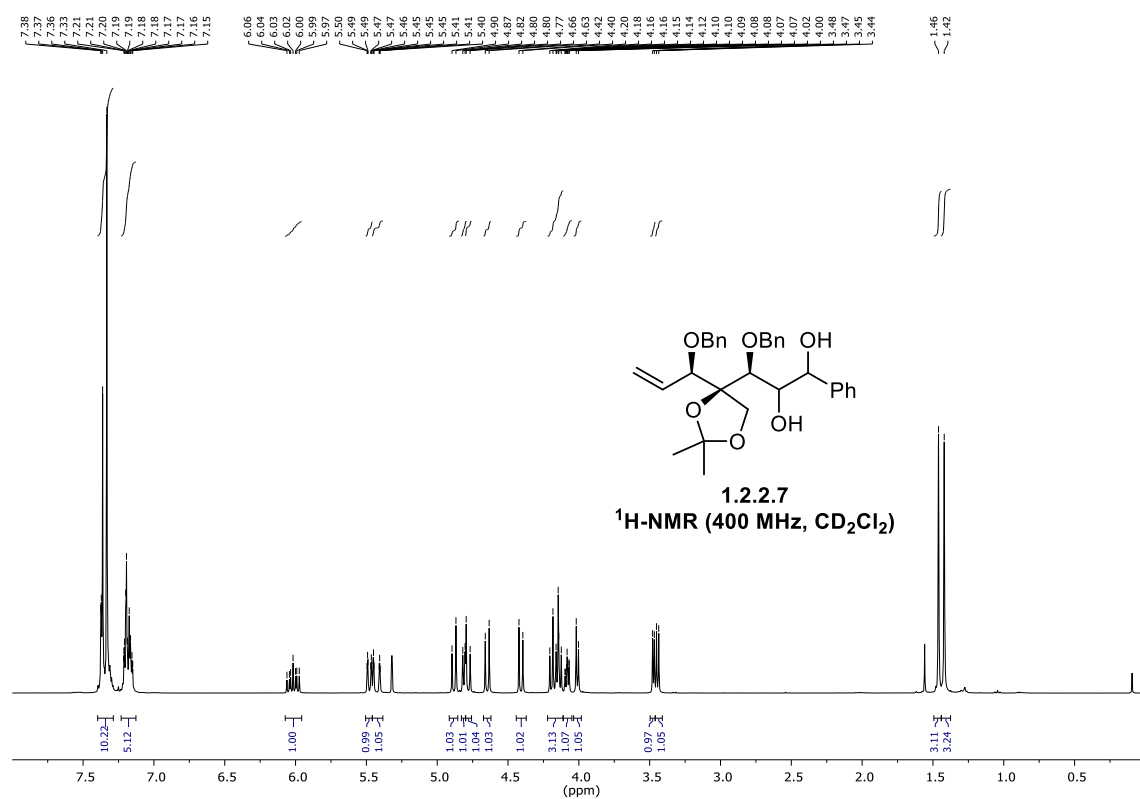
(R)-4-((*S,E*)-1-(benzyloxy)-3-phenylallyl)-4-((*R*)-1-(benzyloxy)prop-2-yn-1-yl)-2,2-dimethyl-1,3-dioxolane (3.2.1.1)



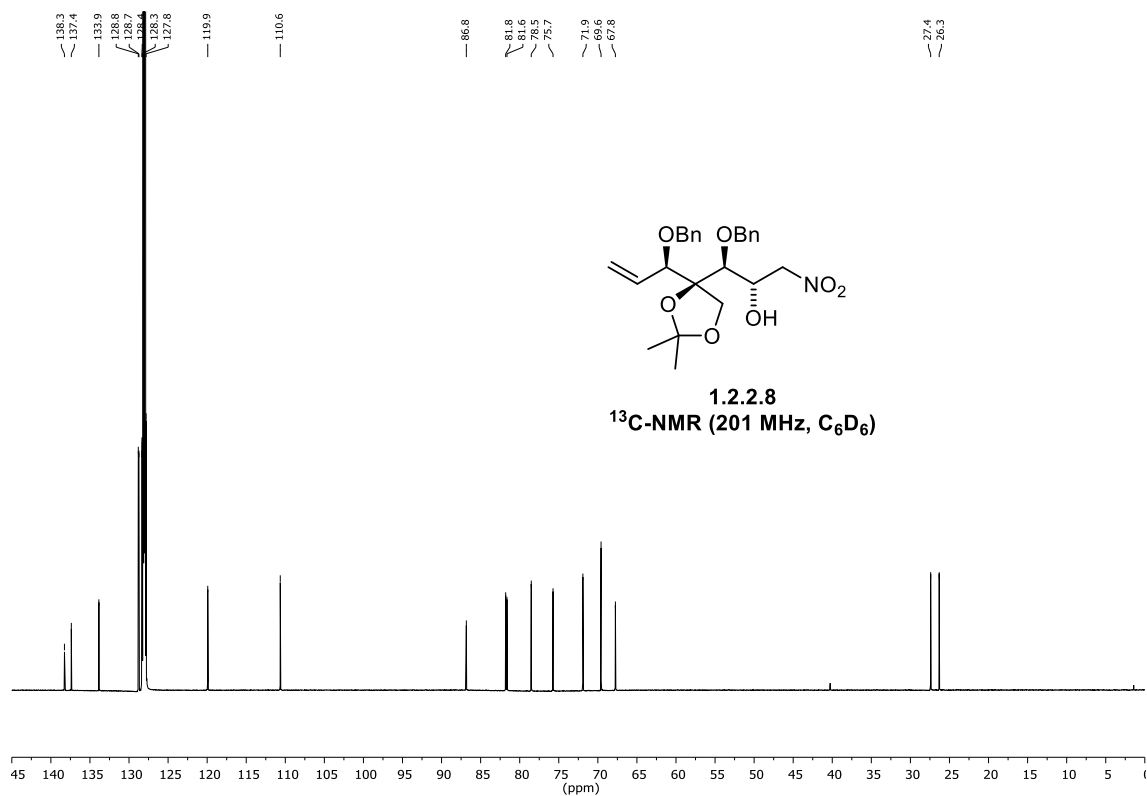
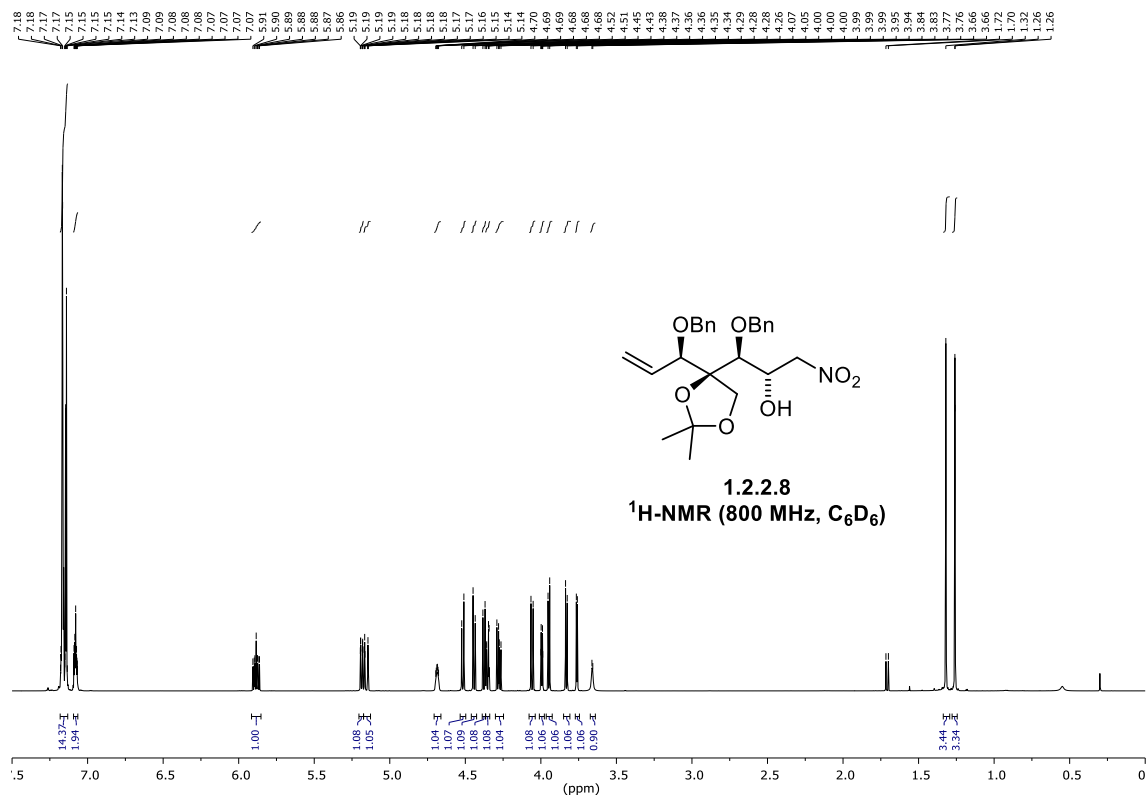
(3S)-3-(benzyloxy)-3-((S)-4-((R)-1-(benzyloxy)prop-2-yn-1-yl)-2,2-dimethyl-1,3-dioxolan-4-yl)-1-phenylpropane-1,2-diol (3.2.1.2)



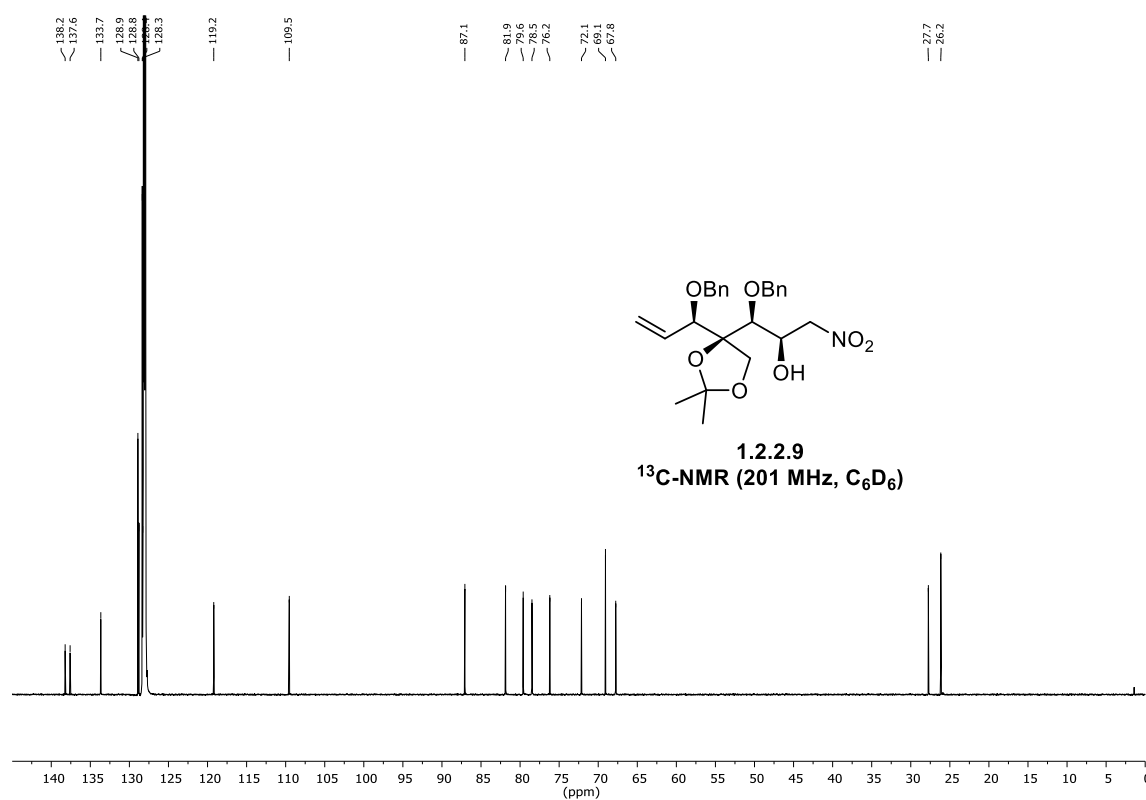
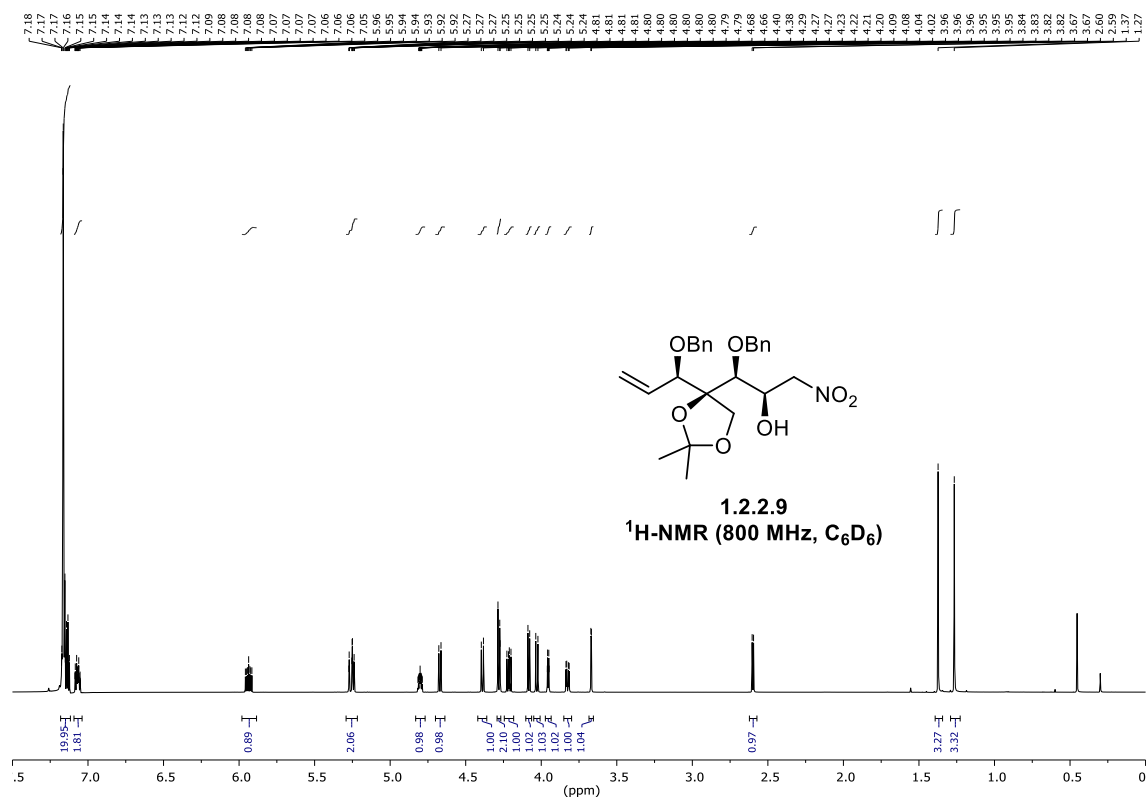
(3*S*)-3-(benzyloxy)-3-((*S*)-4-((*R*)-1-(benzyloxy)allyl)-2,2-dimethyl-1,3-dioxolan-4-yl)-1-phenylpropane-1,2-diol (1.2.2.7)



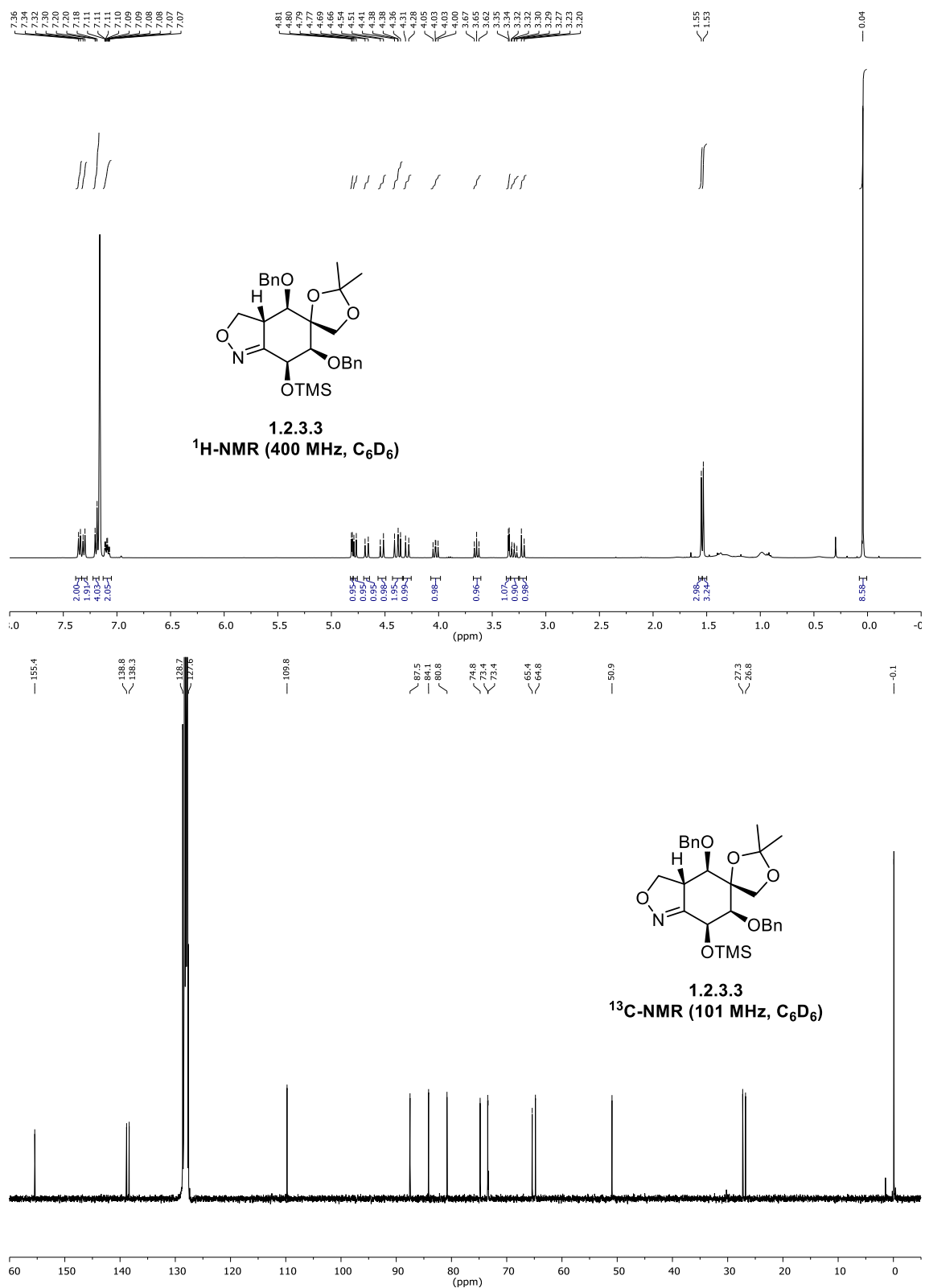
(1*S*,2*S*)-1-(benzyloxy)-1-((*S*)-4-((*R*)-1-(benzyloxy)allyl)-2,2-dimethyl-1,3-dioxolan-4-yl)-3-nitropropan-2-ol (1.2.2.8)



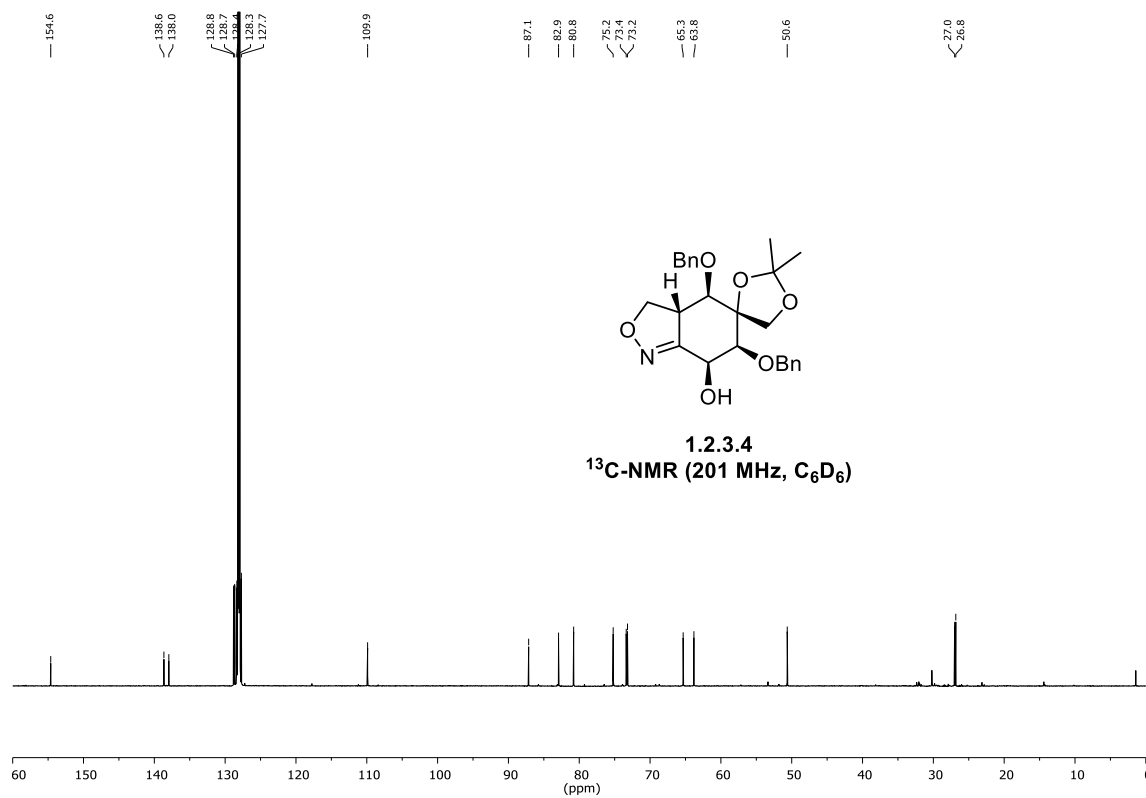
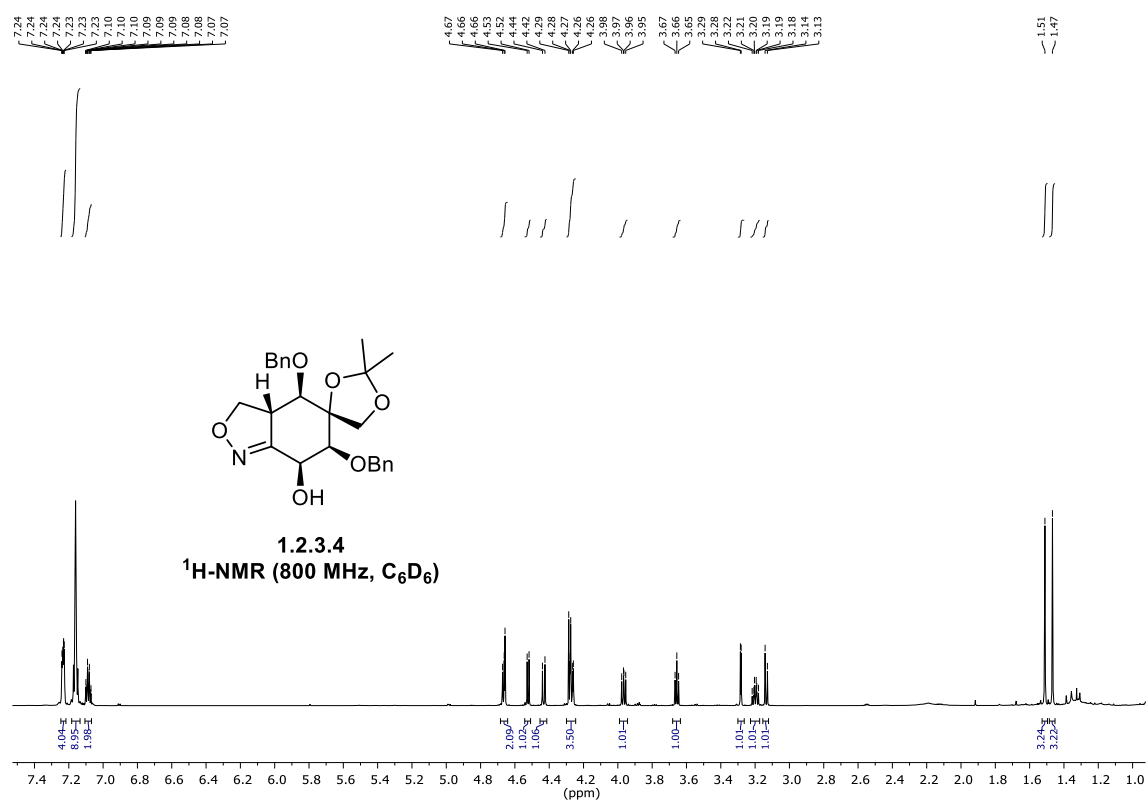
(1*S*,2*R*)-1-(benzyloxy)-1-((*S*)-4-((*R*)-1-(benzyloxy)allyl)-2,2-dimethyl-1,3-dioxolan-4-yl)-3-nitropropan-2-ol (1.2.2.9)



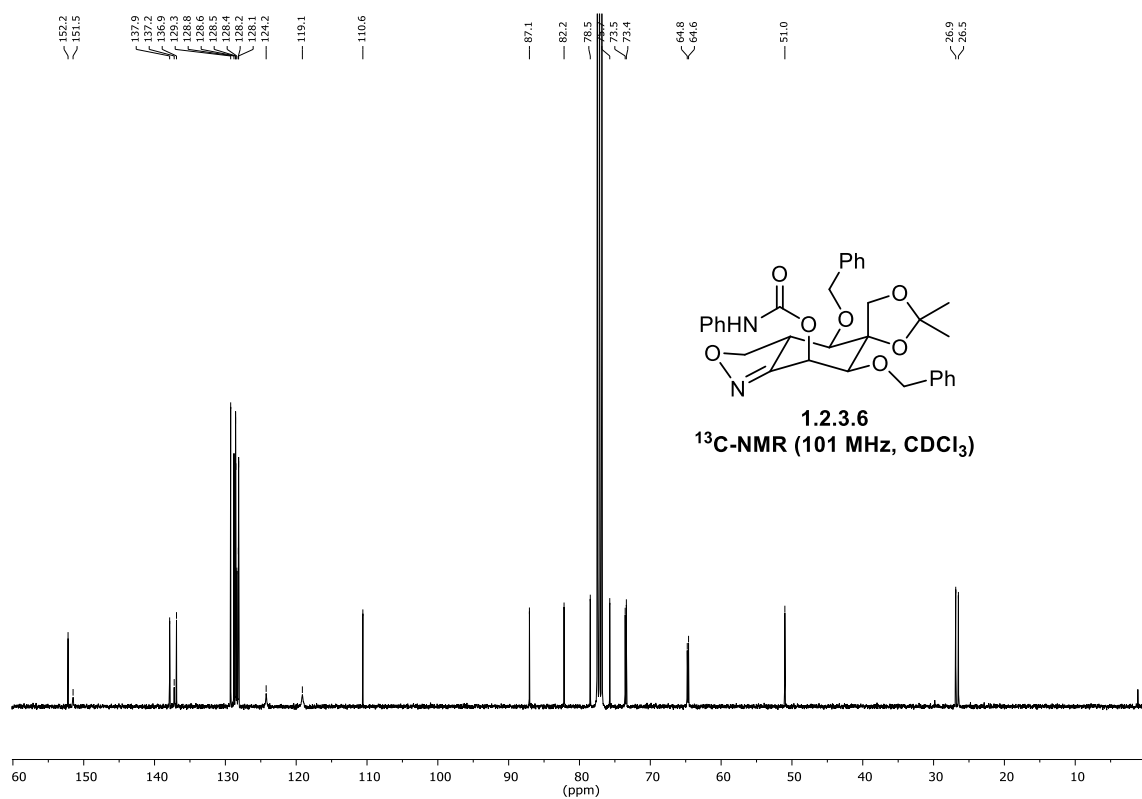
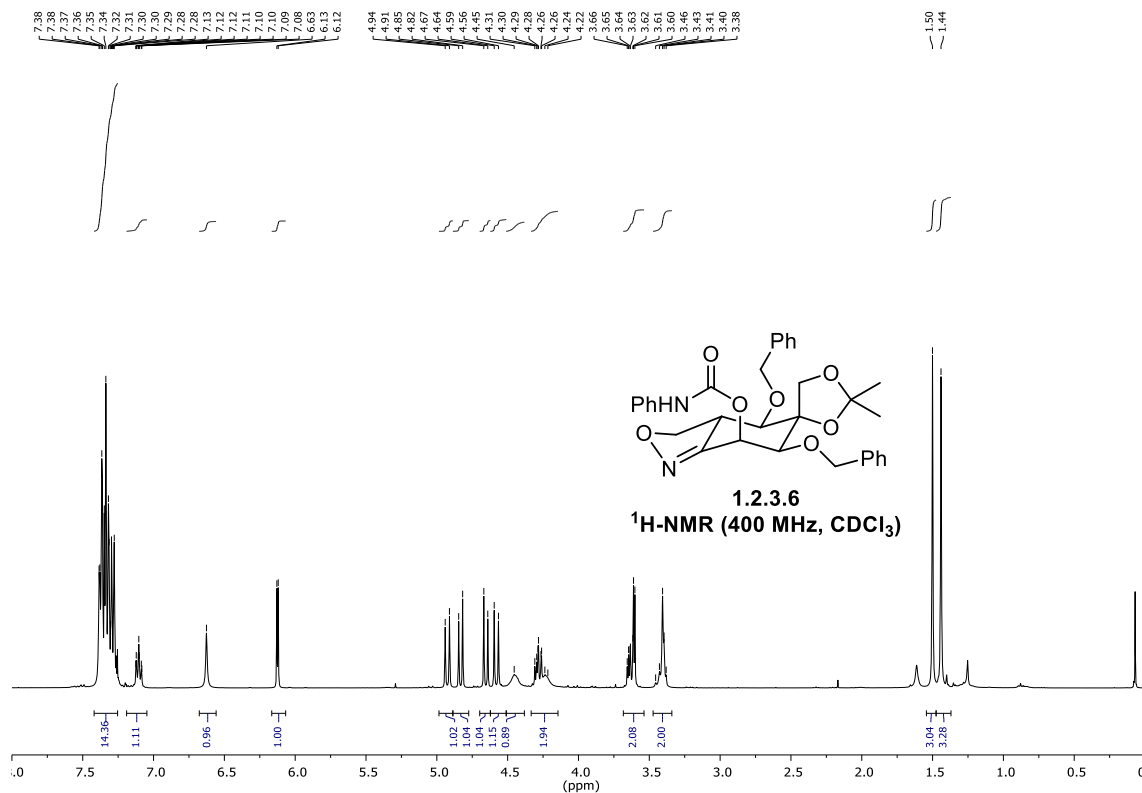
(3a*R*,4*R*,5*S*,6*S*,7*S*)-4,6-bis(benzyloxy)-2',2'-dimethyl-7-((trimethylsilyl)oxy)-3a,4,6,7-tetrahydro-3H-spiro[benzo[*c*]isoxazole-5,4'-[1,3]dioxolane] (1.2.3.3)



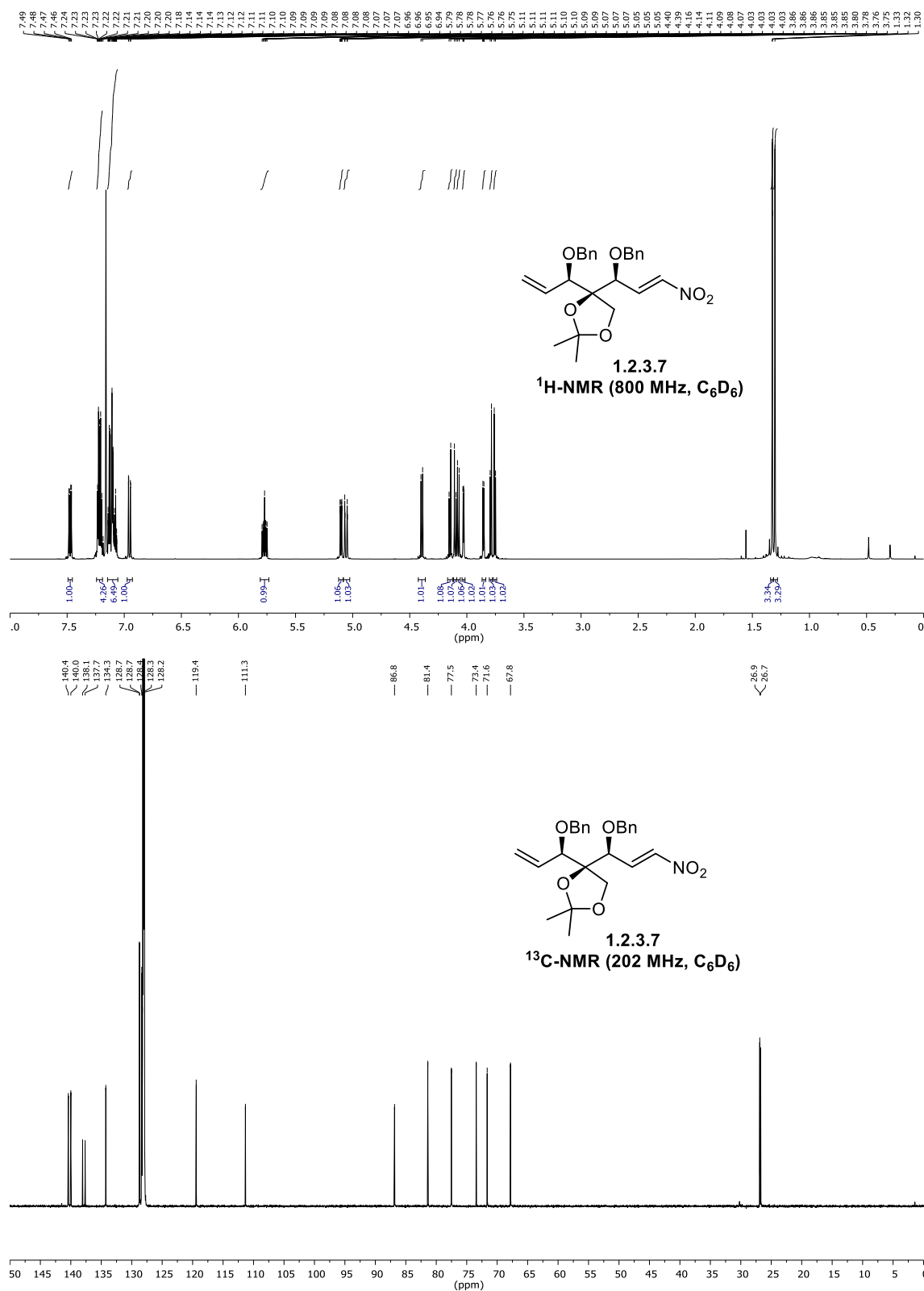
(3*aR*,4*R*,5*S*,6*S*,7*S*)-4,6-bis(benzyloxy)-2',2'-dimethyl-3*a*,4,6,7-tetrahydro-3*H*-spiro[benzo[*c*]isoxazole-5,4'-[1,3]dioxolan]-7-ol (1.2.3.4)



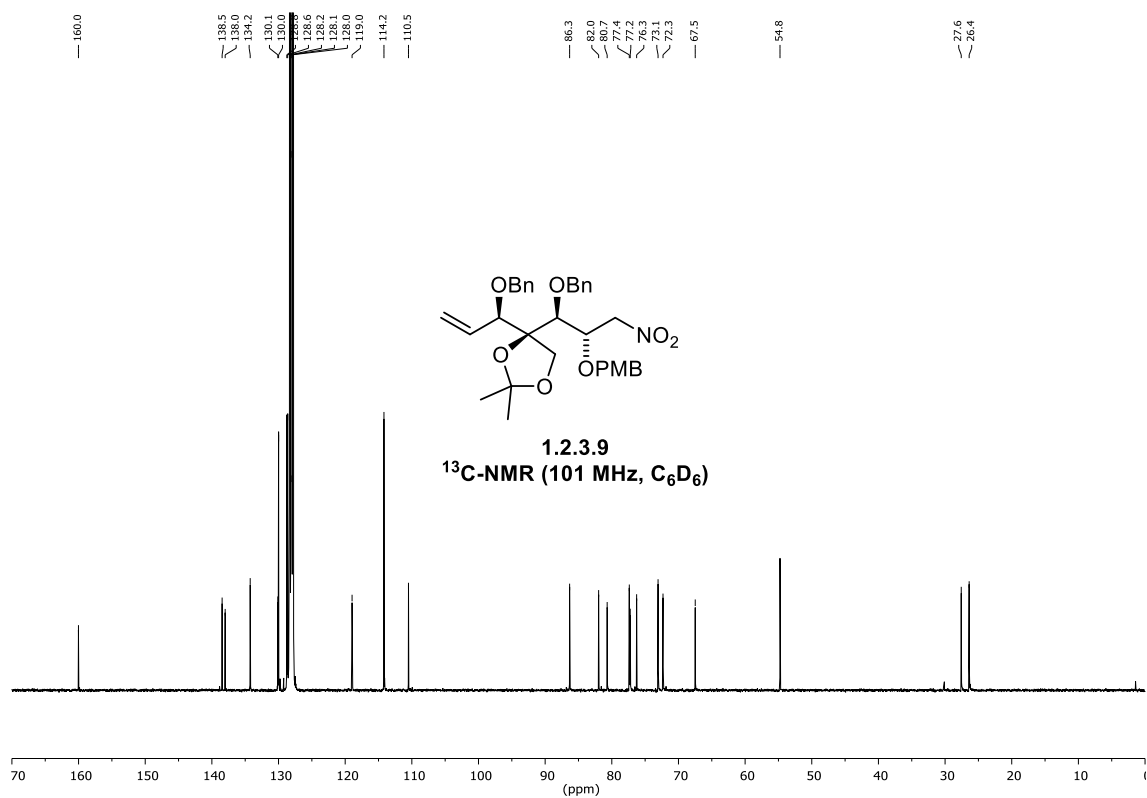
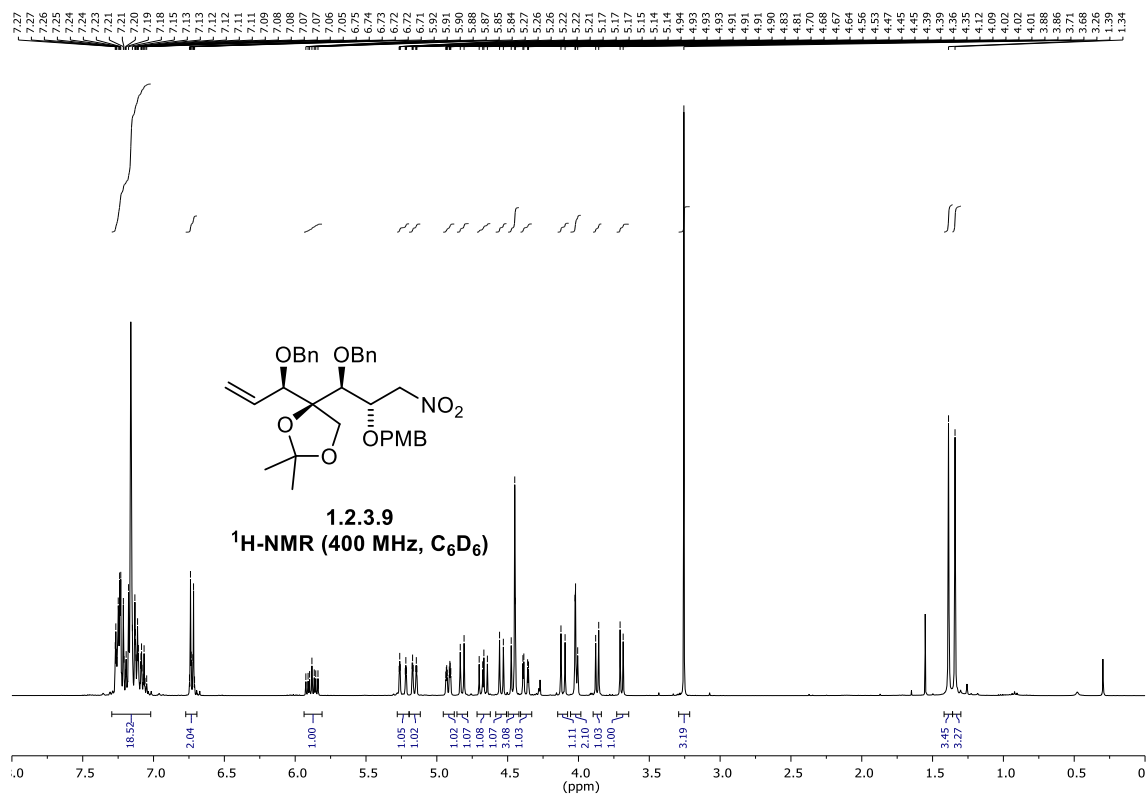
(3a*R*,4*R*,5*S*,6*S*,7*S*)-4,6-bis(benzyloxy)-2',2'-dimethyl-3a,4,6,7-tetrahydro-3*H*-spiro[benzo[*c*]isoxazole-5,4'-[1,3]dioxolan]-7-yl phenylcarbamate (1.2.3.6)



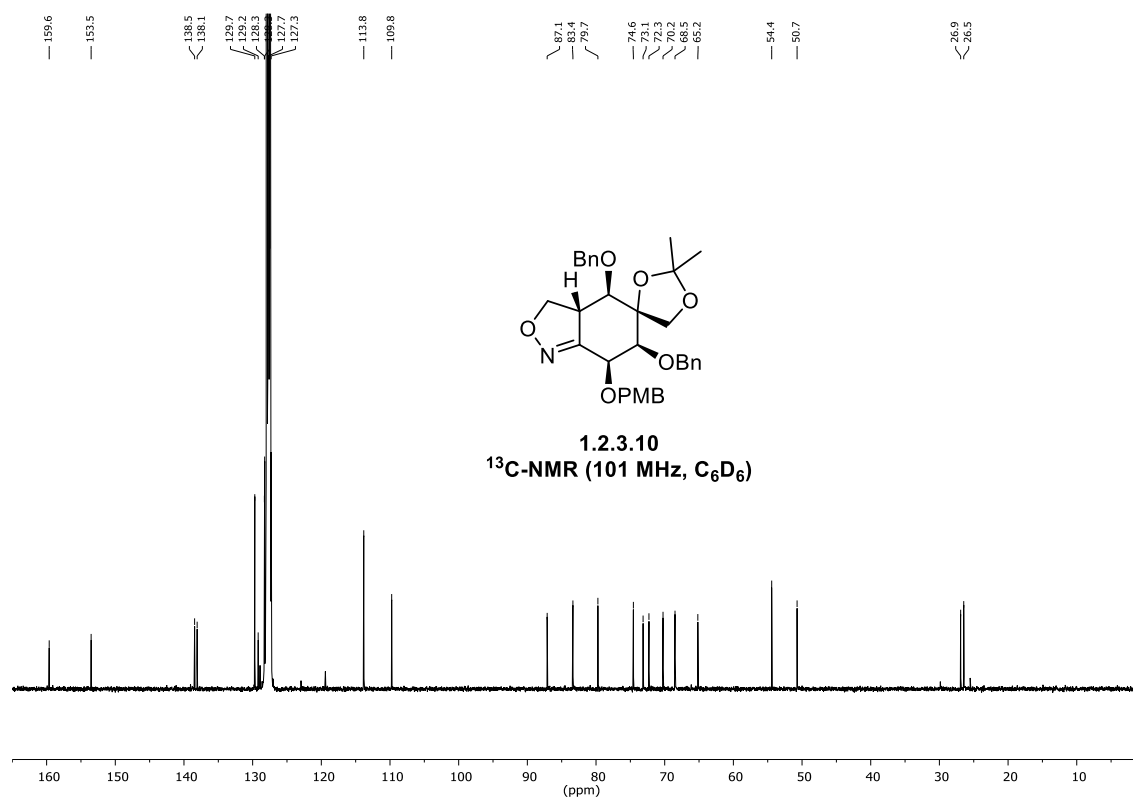
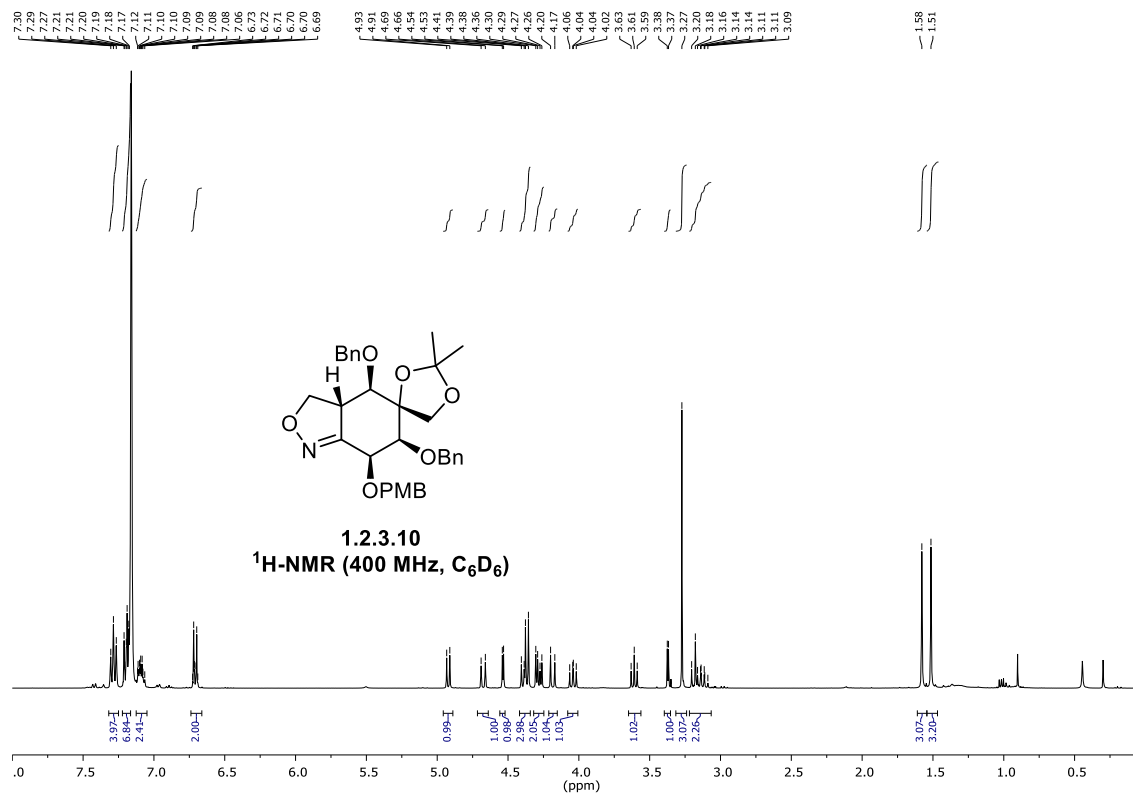
(S)-4-((S,E)-1-(benzyloxy)-3-nitroallyl)-4-((R)-1-(benzyloxy)allyl)-2,2-dimethyl-1,3-dioxolane (1.2.3.7)



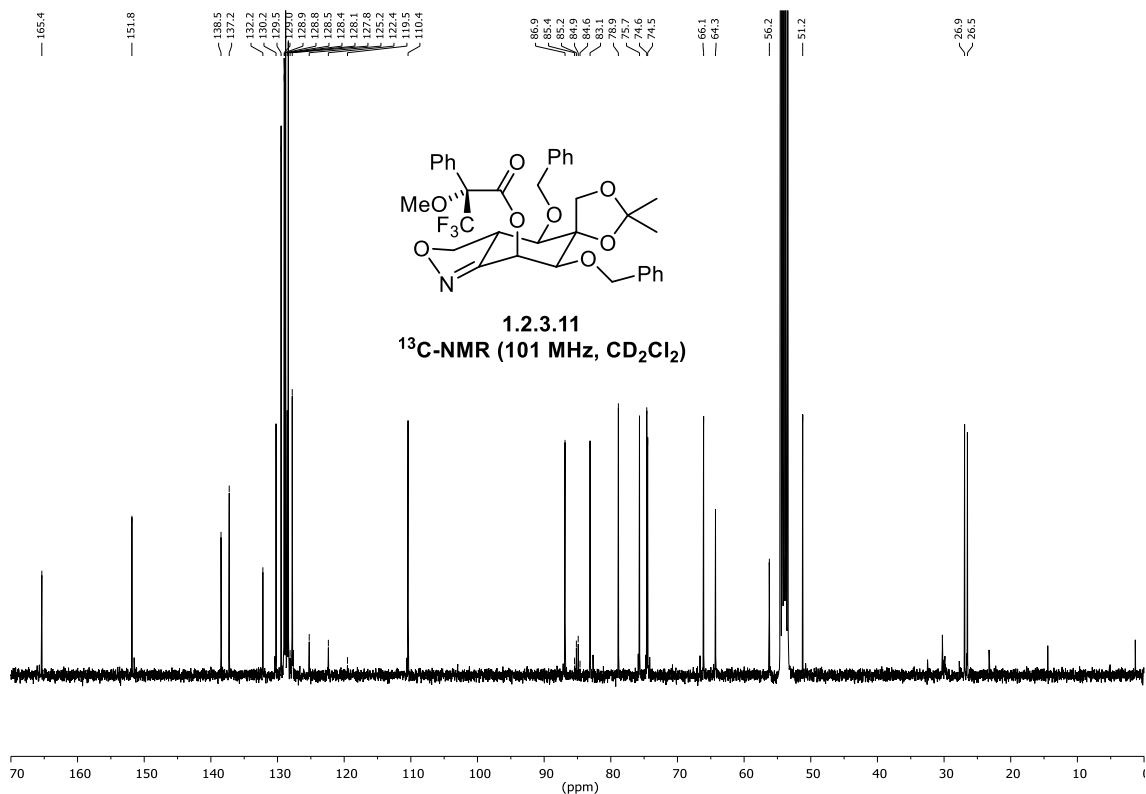
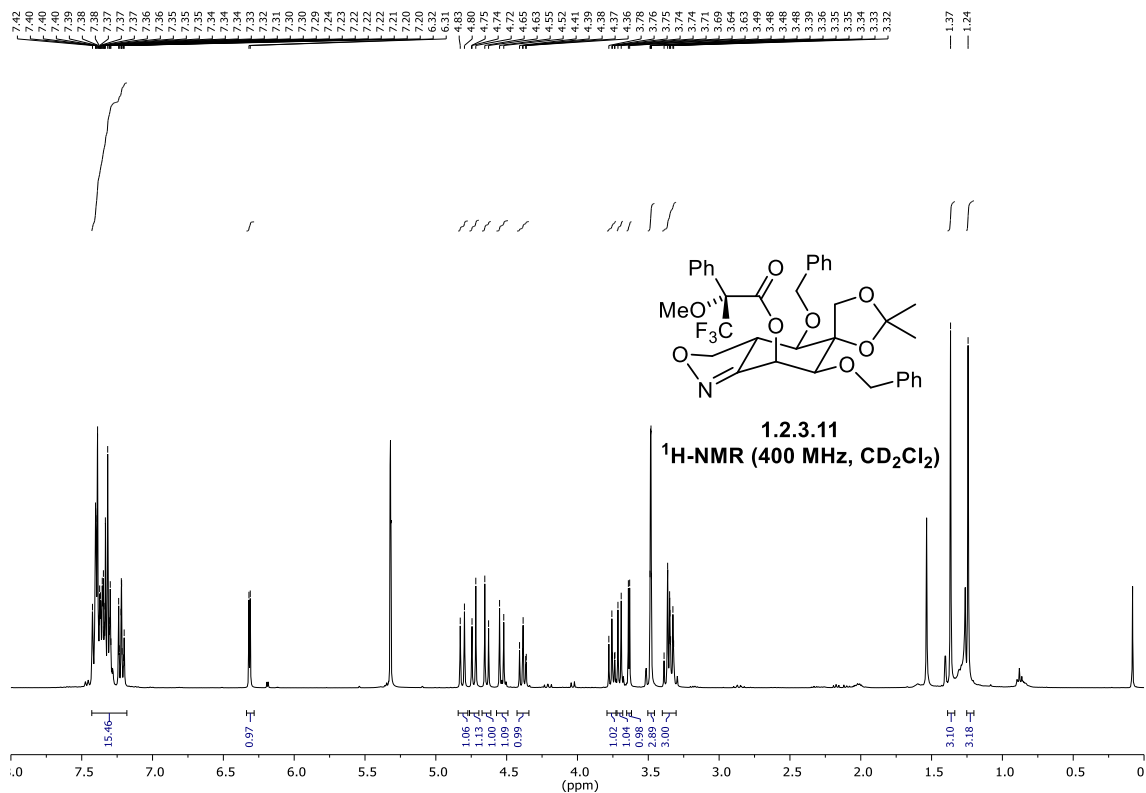
(S)-4-((1S,2S)-1-(benzyloxy)-2-((4-methoxybenzyl)oxy)-3-nitropropyl)-4-((R)-1-(benzyloxy)allyl)-2,2-dimethyl-1,3-dioxolane (1.2.3.9)

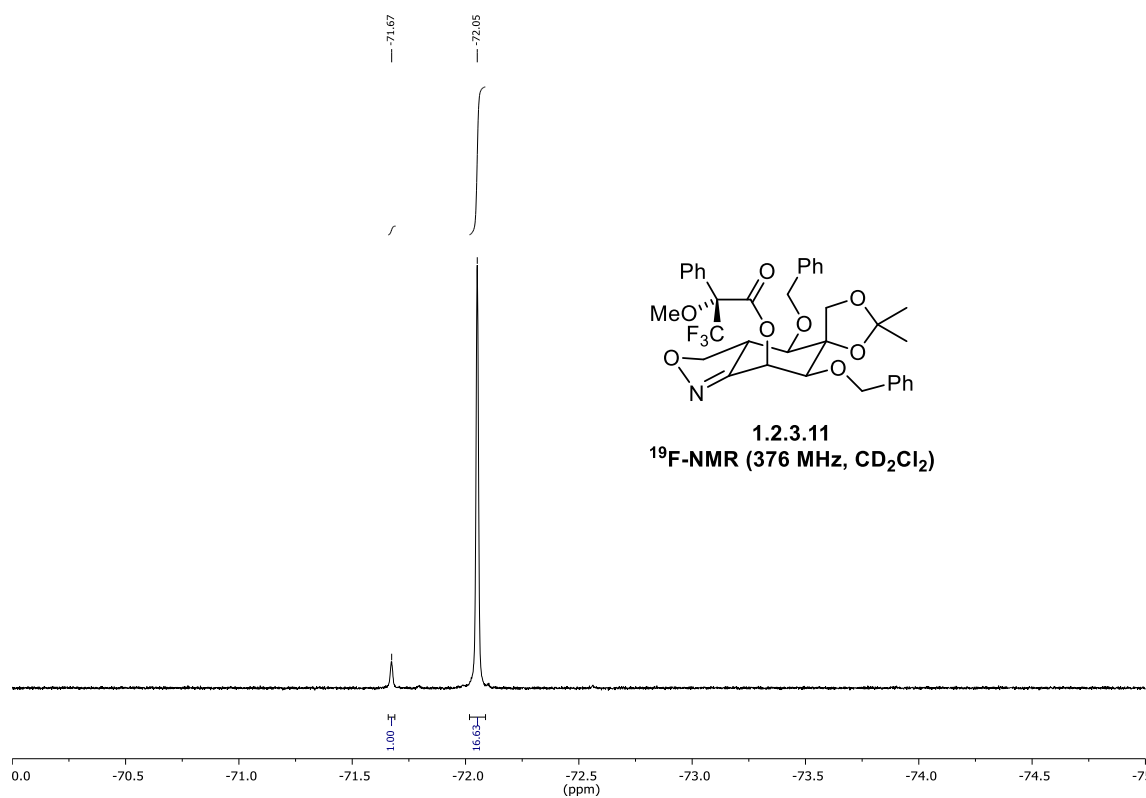


(3*aR*,4*R*,5*S*,6*S*,7*S*)-4,6-bis(benzyloxy)-7-((4-methoxybenzyl)oxy)-2',2'-dimethyl-3*a*,4,6,7-tetrahydro-3H-spiro[benzo[*c*]isoxazole-5,4'-[1,3]dioxolane] (1.2.3.10)

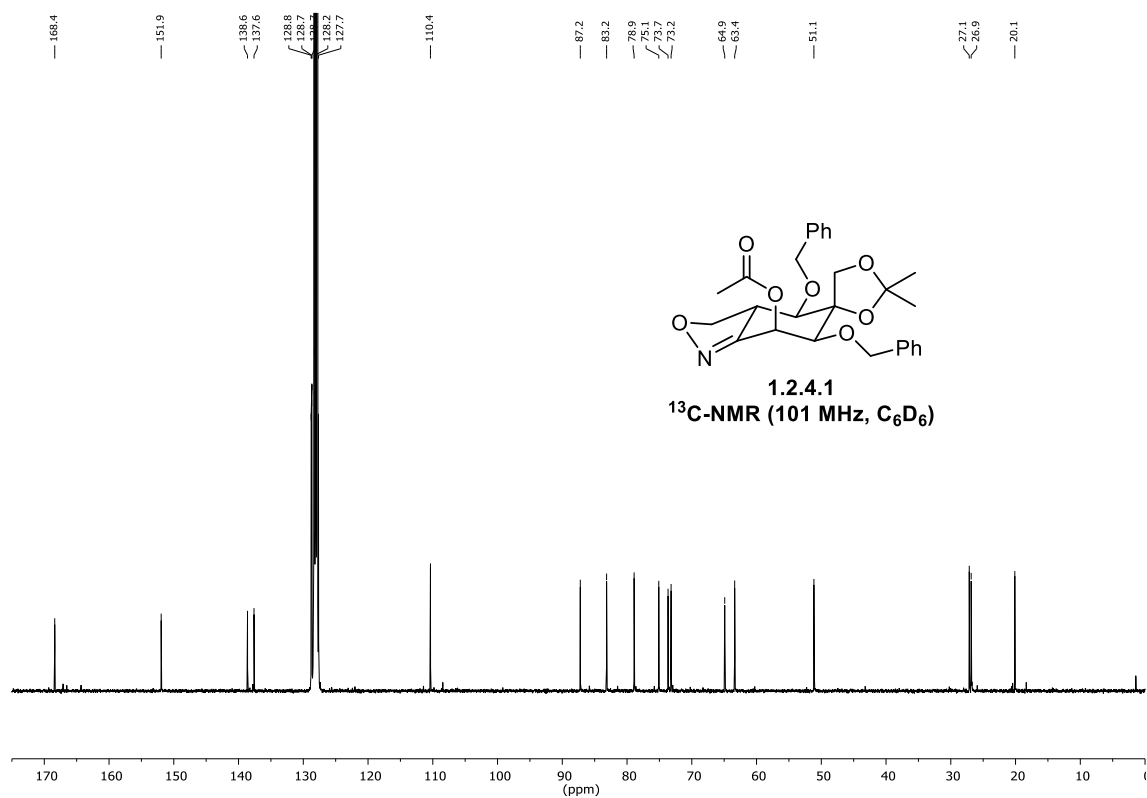
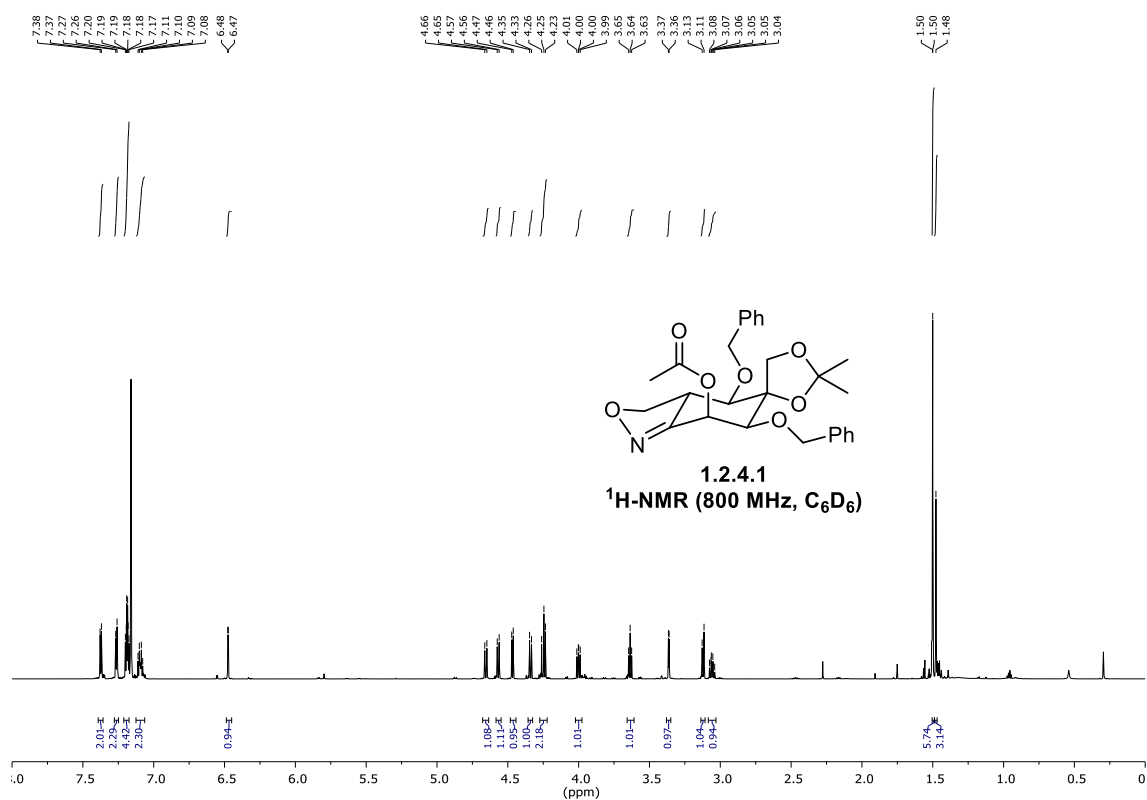


(3*aR*,4*R*,5*S*,6*S*,7*S*)-4,6-bis(benzyloxy)-2',2'-dimethyl-3*a*,4,6,7-tetrahydro-3*H*-
 spiro[benzo[*c*]isoxazole-5,4'-[1,3]dioxolan]-7-yl (R)-3,3,3-trifluoro-2-methoxy-2-
 phenylpropanoate (1.2.3.11)

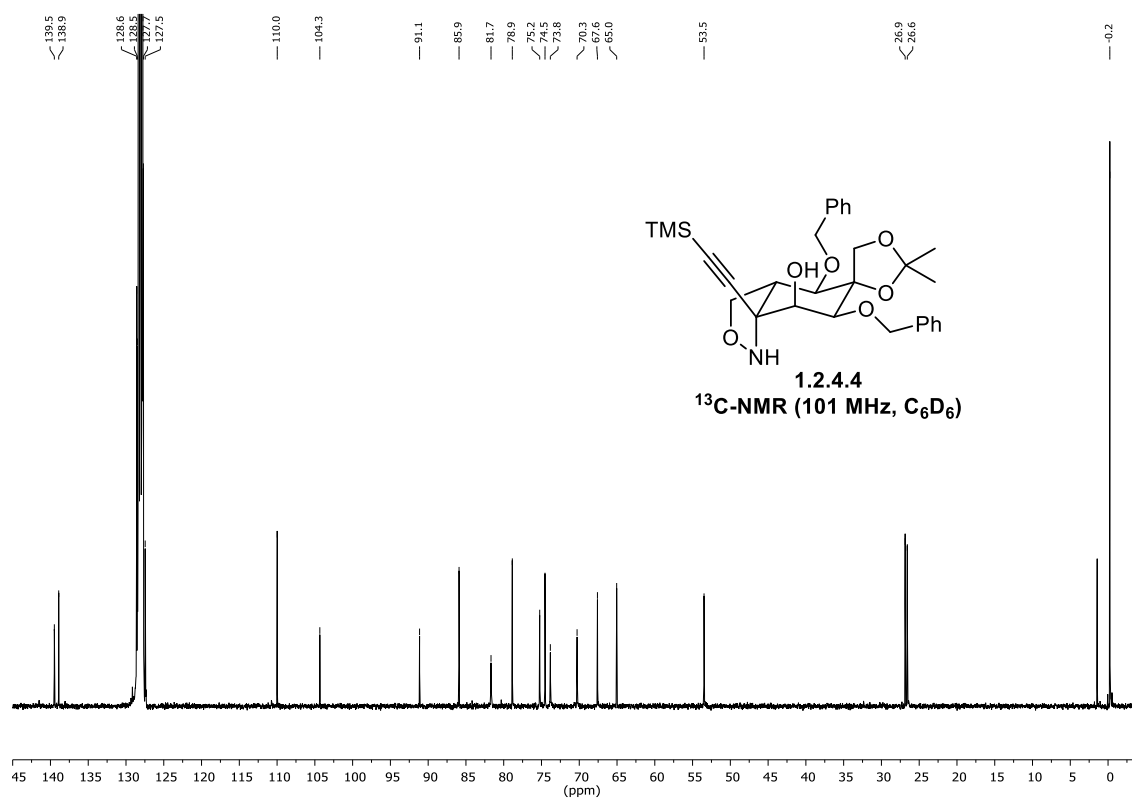
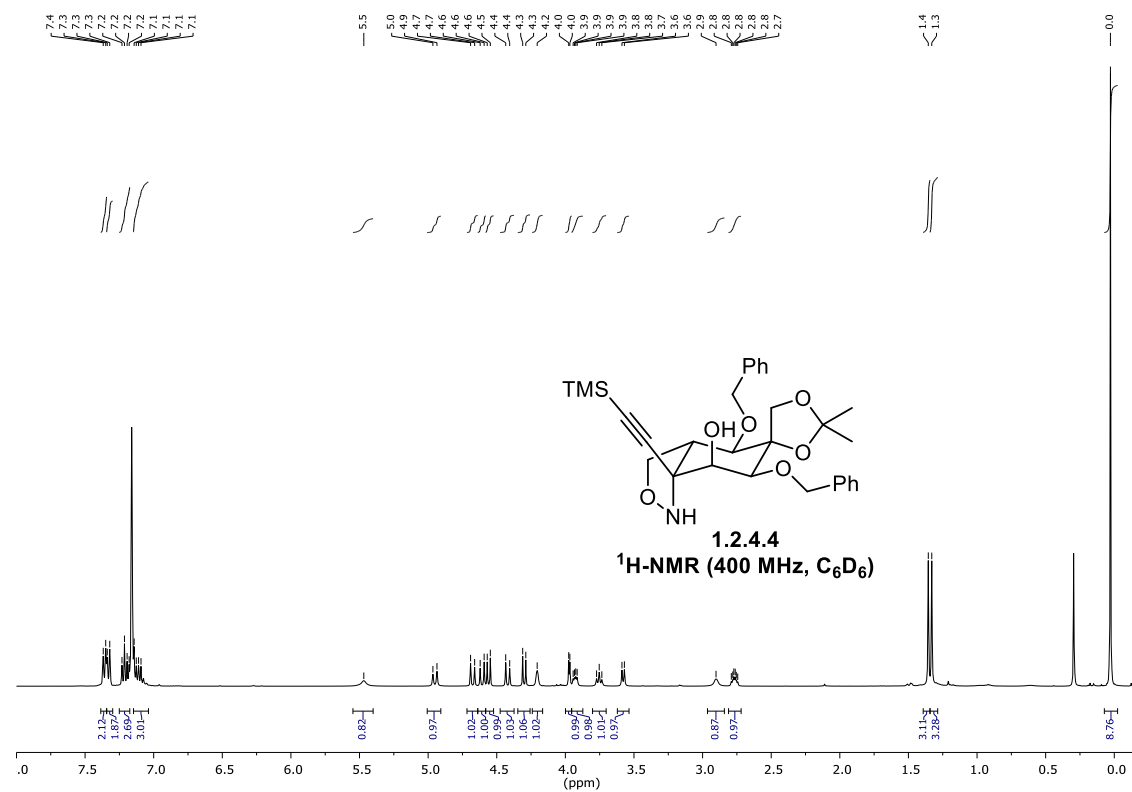




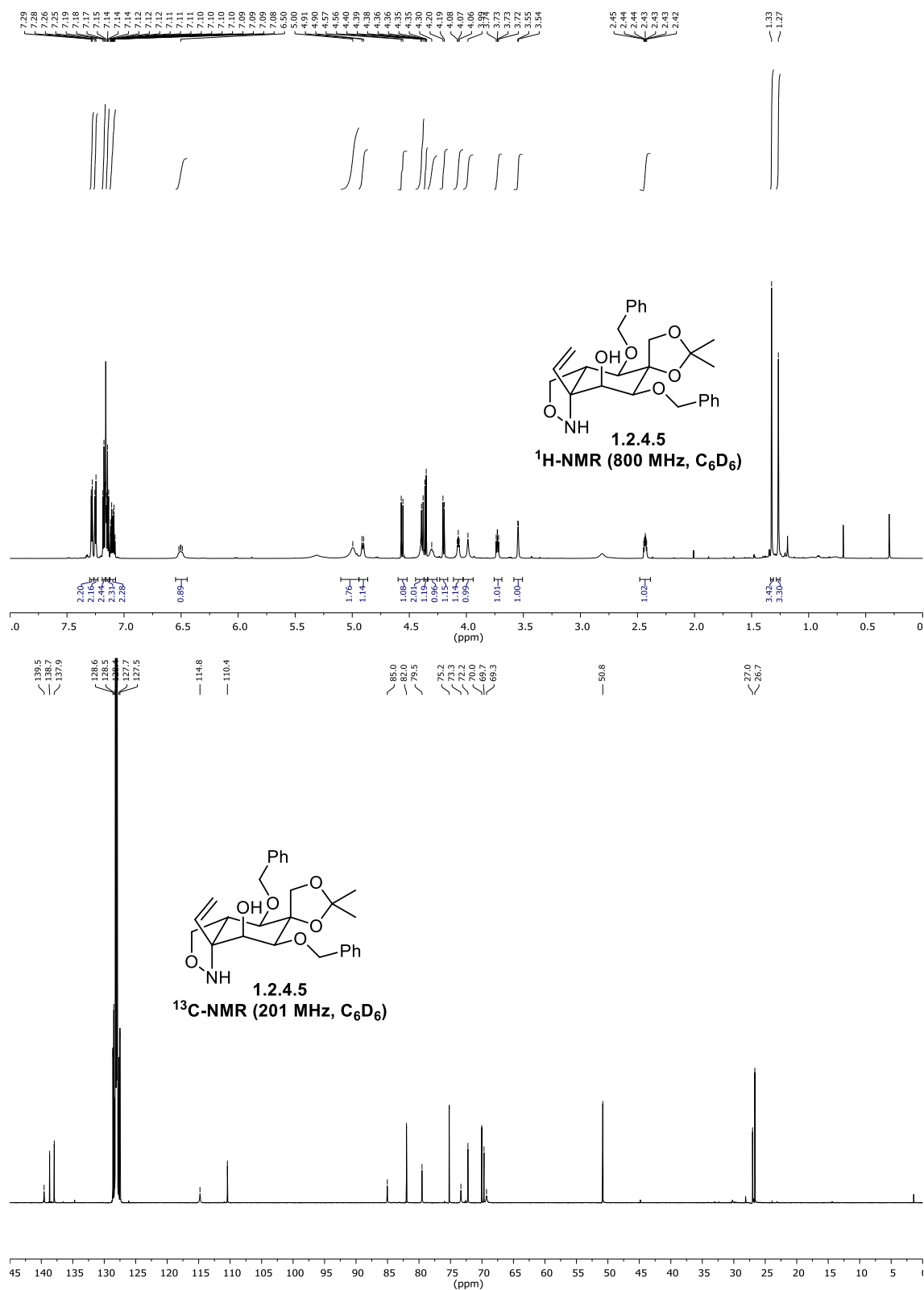
(3a*R*,4*R*,5*S*,6*S*,7*S*)-4,6-bis(benzyloxy)-2',2'-dimethyl-3a,4,6,7-tetrahydro-3H-spiro[benzo[*c*]isoxazole-5,4'-[1,3]dioxolan]-7-yl acetate (1.2.4.1)



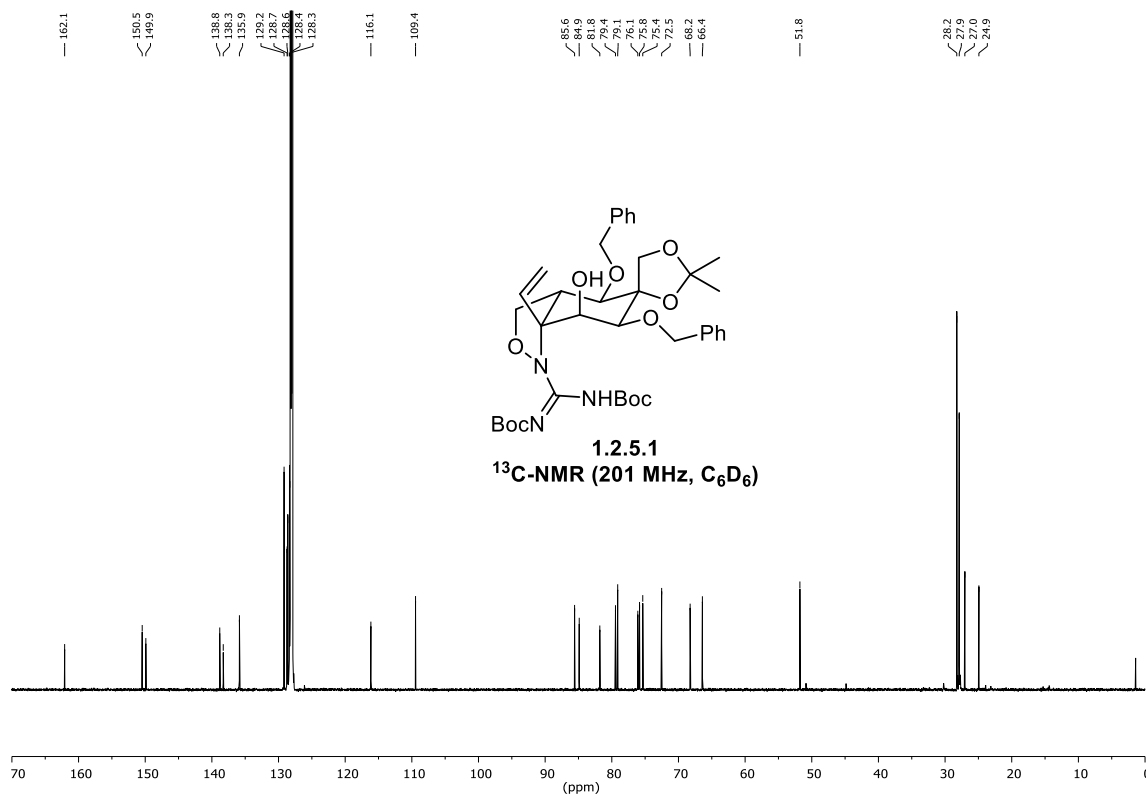
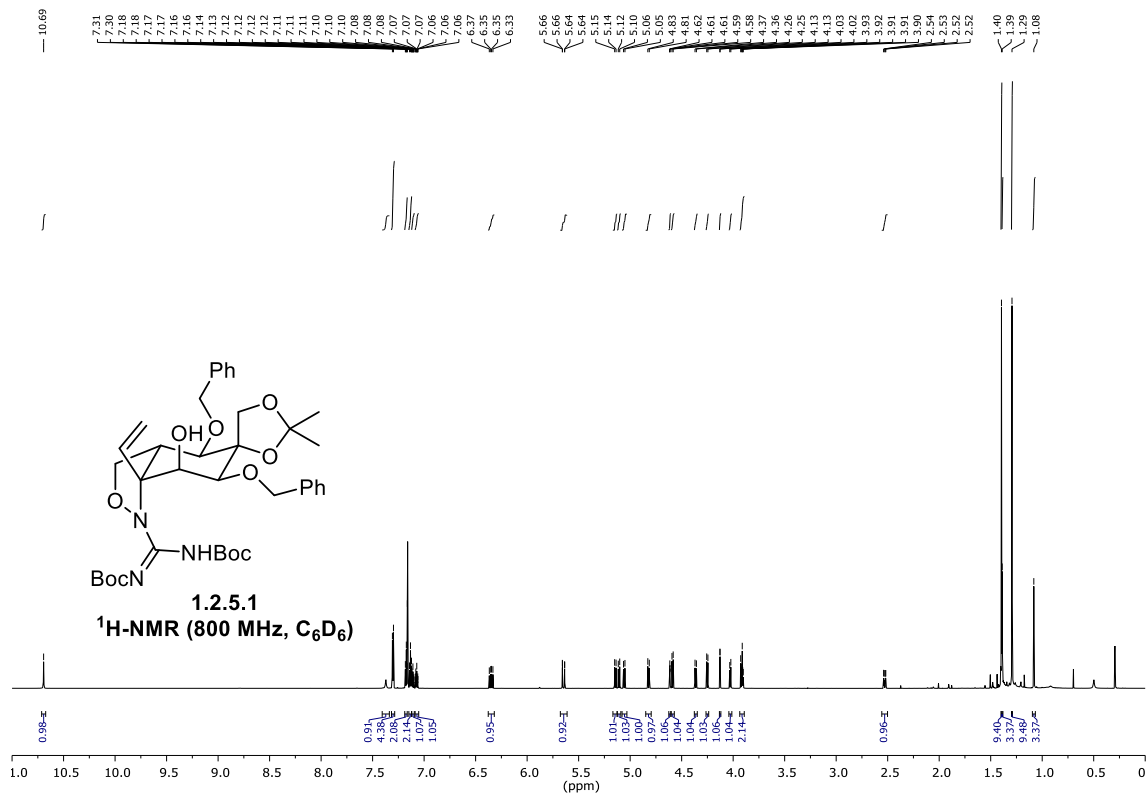
(3*aR*,4*R*,5*S*,6*S*,7*S*,7*aS*)-4,6-bis(benzyloxy)-2',2'-dimethyl-7a-
 ((trimethylsilyl)ethynyl)hexahydro-3H-spiro[benzo[*c*]isoxazole-5,4'-[1,3]dioxolan]-7-ol
 (1.2.4.4)



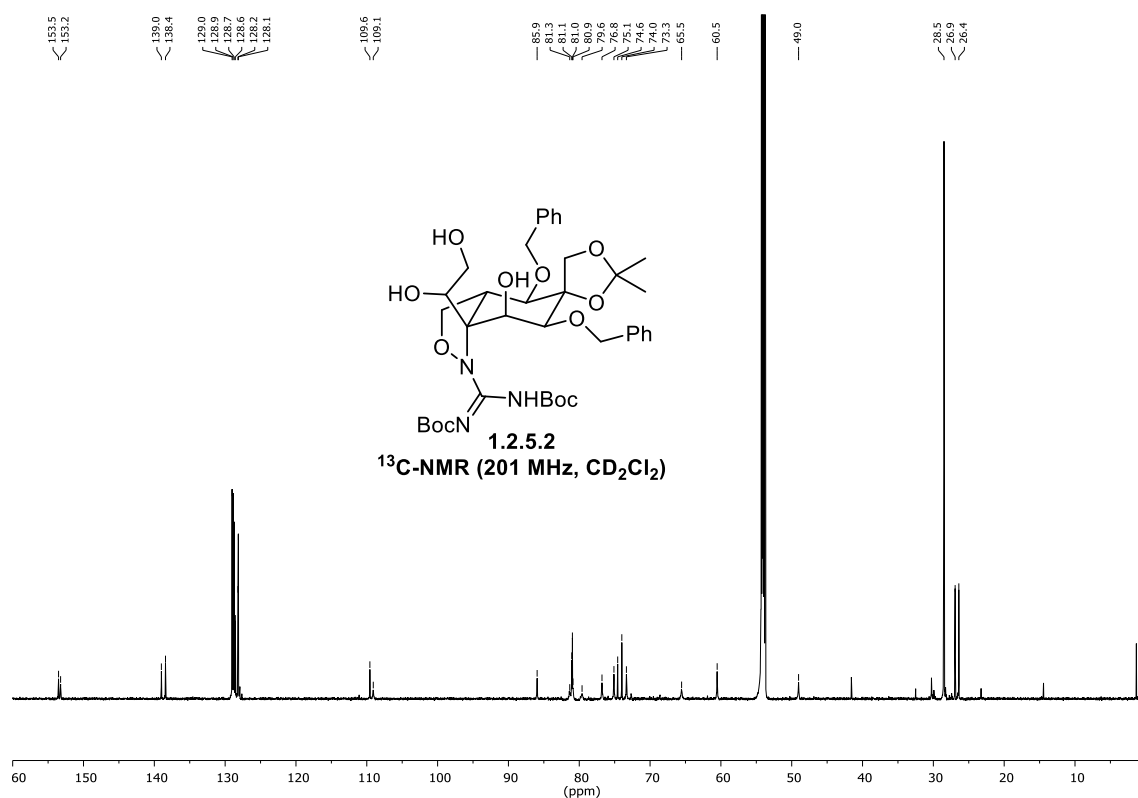
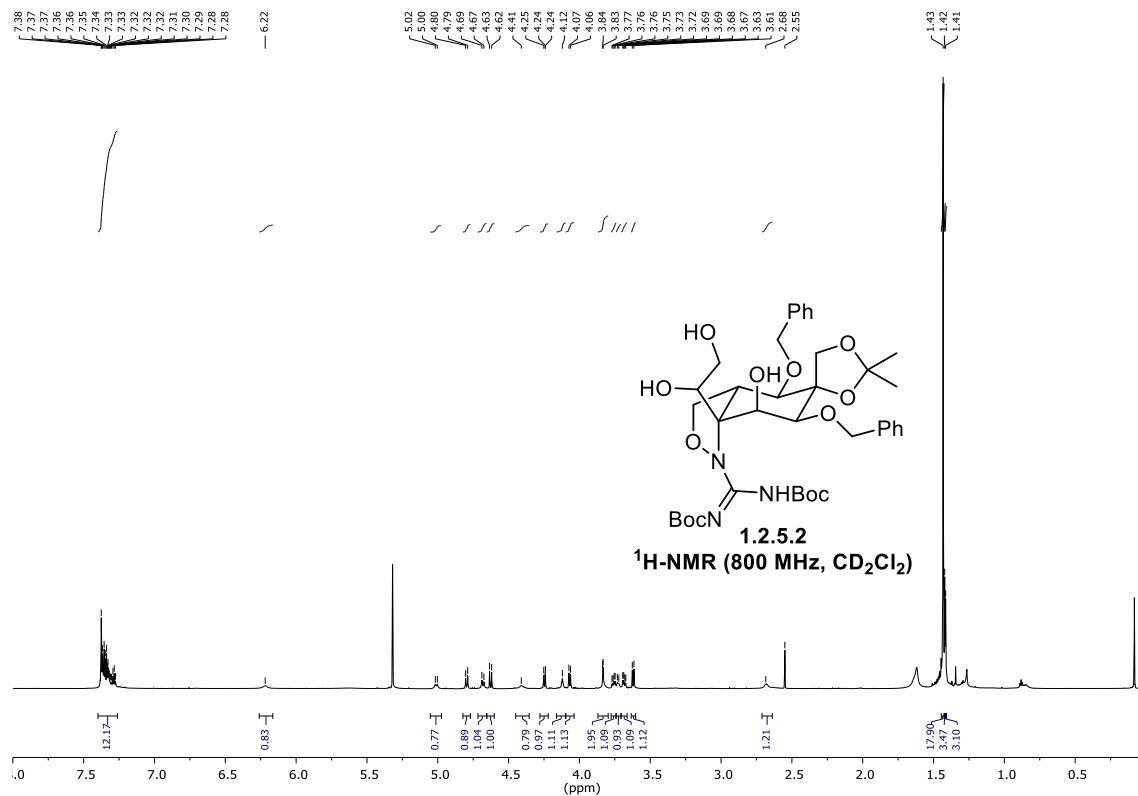
(3a*R*,4*R*,5*S*,6*S*,7*S*,7a*R*)-4,6-bis(benzyloxy)-2',2'-dimethyl-7a-vinylhexahydro-3*H*-spiro[benzo[*c*]isoxazole-5,4'-[1,3]dioxolan]-7-ol (1.2.4.5)



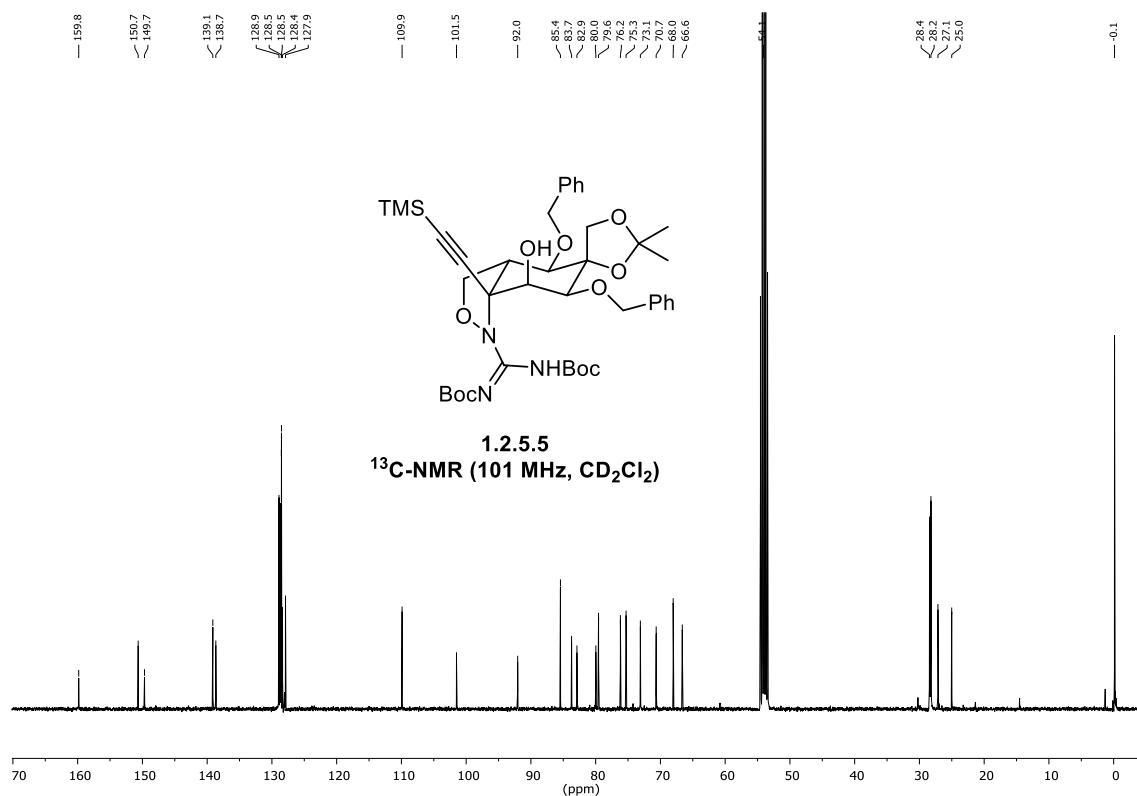
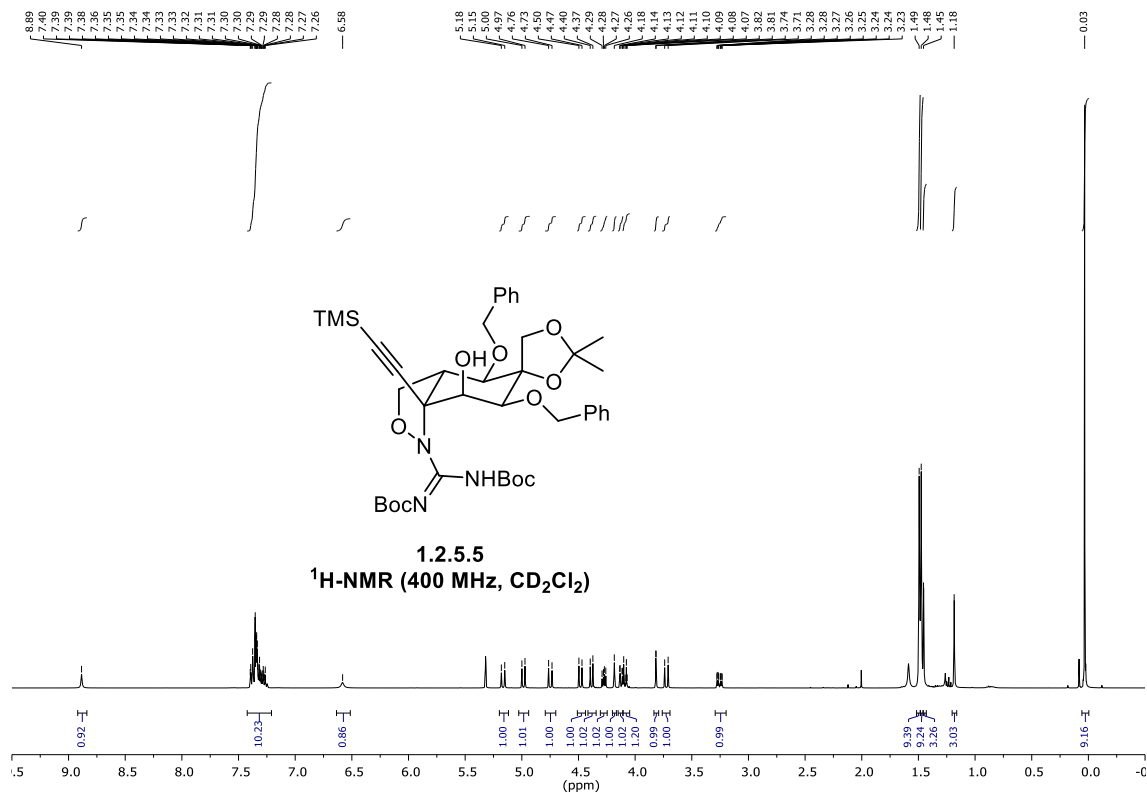
tert-butyl ((*E*)-((3*aR*,4*R*,5*S*,6*S*,7*S*,7*aR*)-4,6-bis(benzyloxy)-7-hydroxy-2',2'-dimethyl-7*a*-vinyltetrahydro-3*H*-spiro[benzo[*c*]isoxazole-5,4'-[1,3]dioxolan]-1(4*H*)-yl)((*tert*-butoxycarbonyl)amino)methylene)carbamate (1.2.5.1)



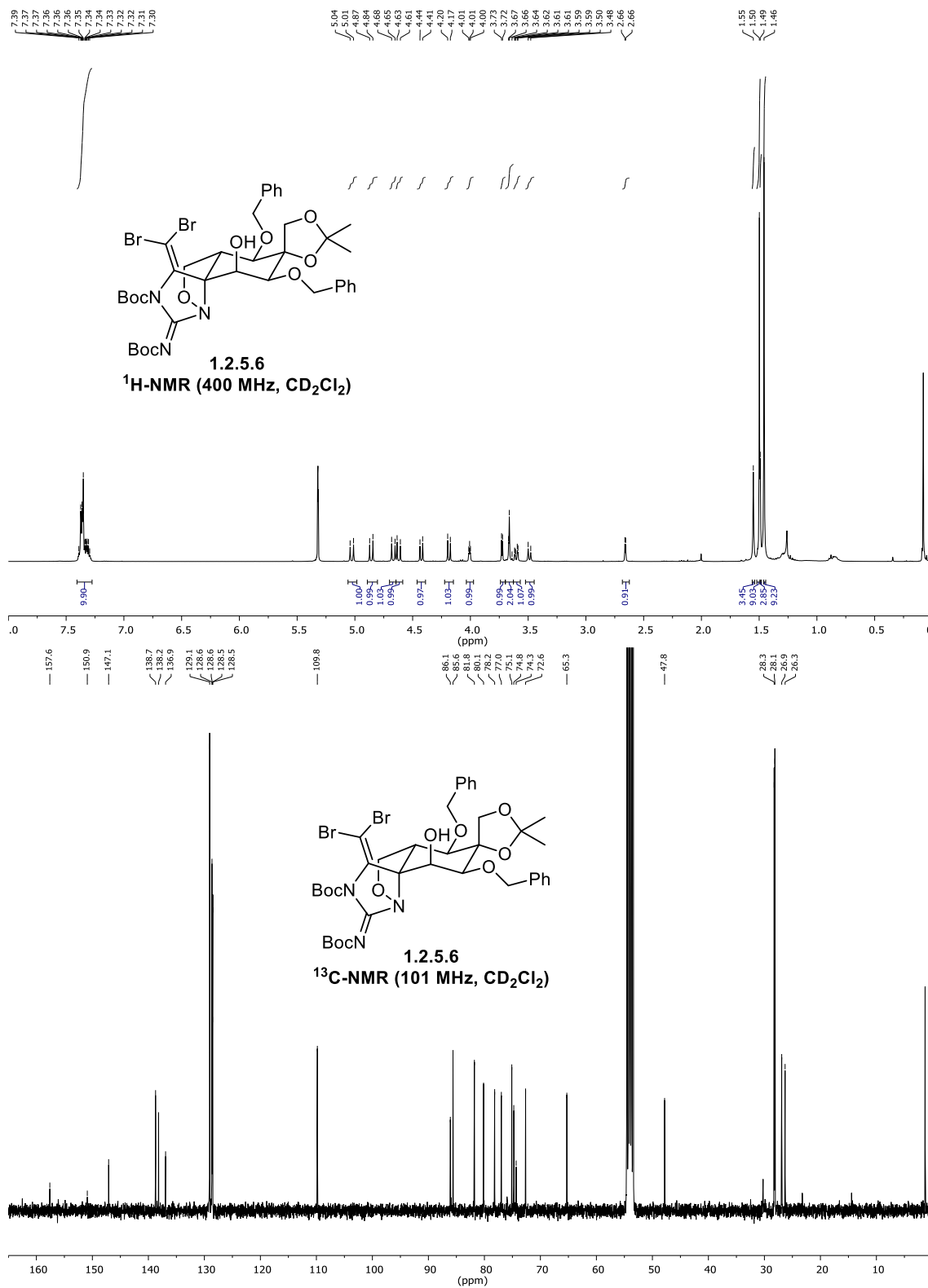
tert-butyl ((*E*)-((3*aR*,4*R*,5*S*,6*S*,7*S*,7*aS*)-4,6-bis(benzyloxy)-7*a*-(1,2-dihydroxyethyl)-7-hydroxy-2',2'-dimethyltetrahydro-3*H*-spiro[benzo[*c*]isoxazole-5,4'-[1,3]dioxolan]-1(4*H*)-yl)((*tert*-butoxycarbonyl)amino)methylene)carbamate (1.2.5.2)



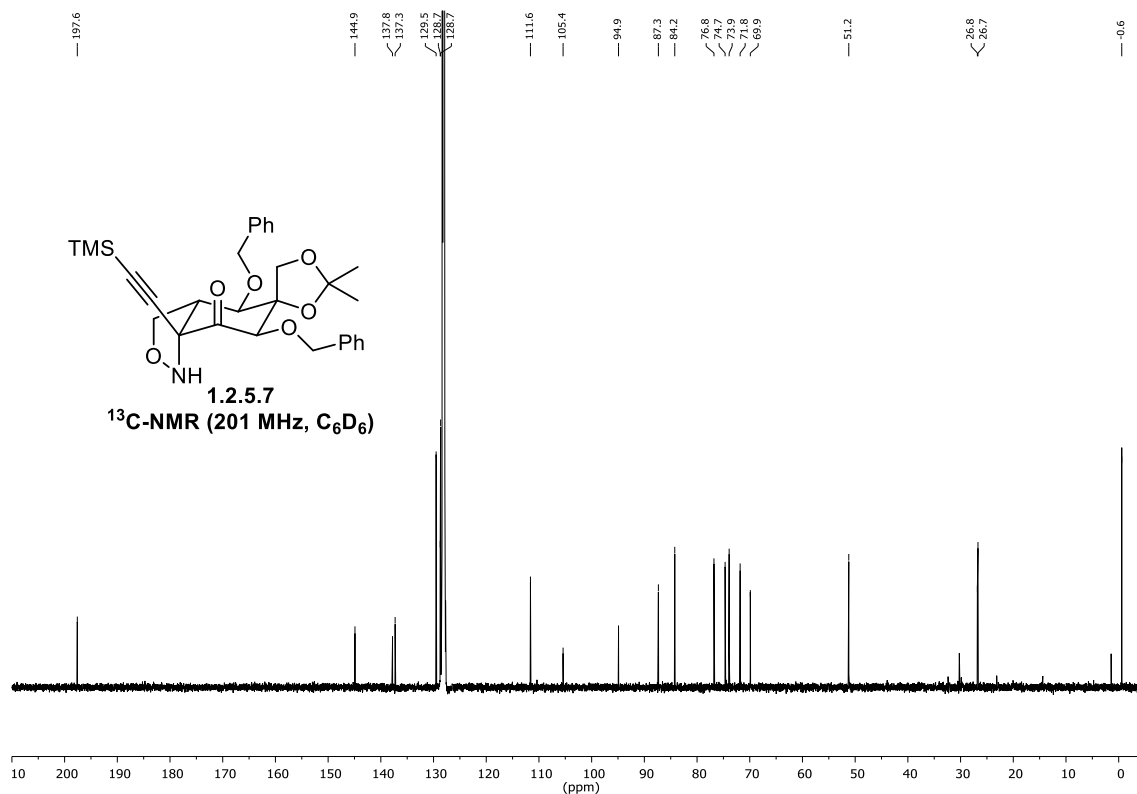
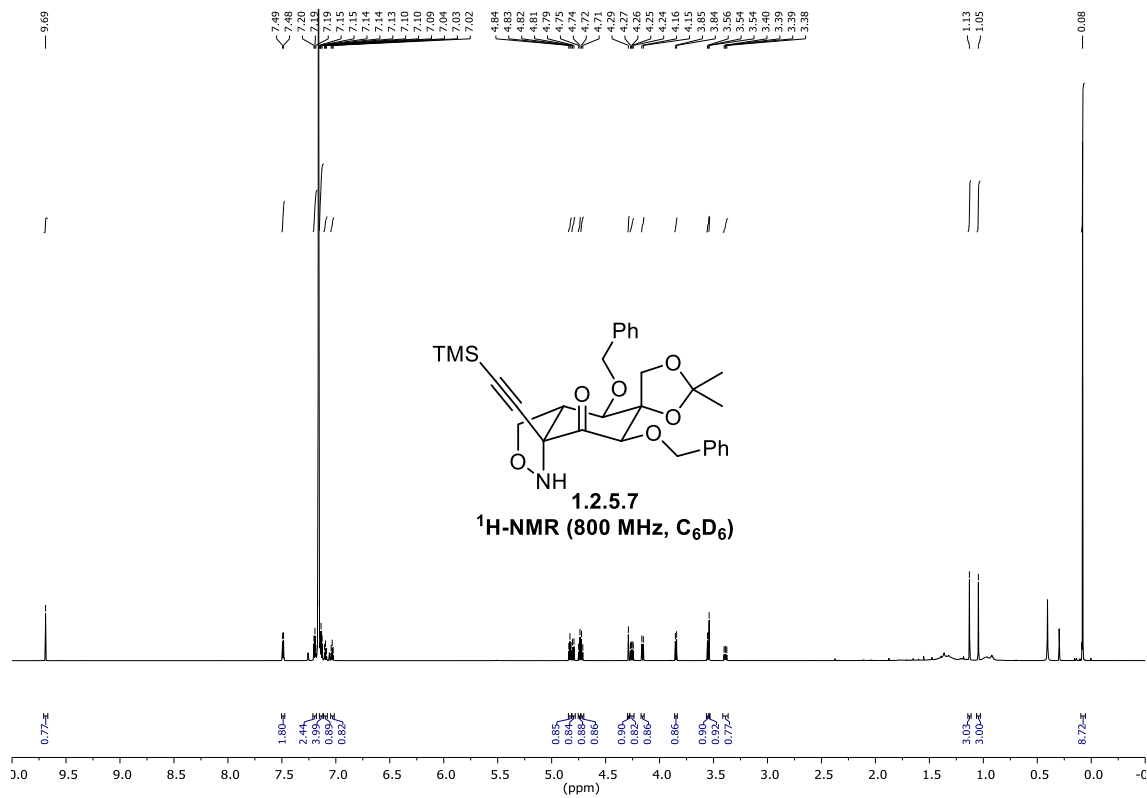
tert-butyl ((*E*)-((3*aR*,4*R*,5*S*,6*S*,7*S*,7*aS*)-4,6-bis(benzyloxy)-7-hydroxy-2',2'-dimethyl-7*a*-((trimethylsilyl)ethynyl)tetrahydro-3*H*-spiro[benzo[*c*]isoxazole-5,4'-[1,3]dioxolan]-1(4*H*)-yl)((*tert*-butoxycarbonyl)amino)methylene)carbamate (1.2.5.5)



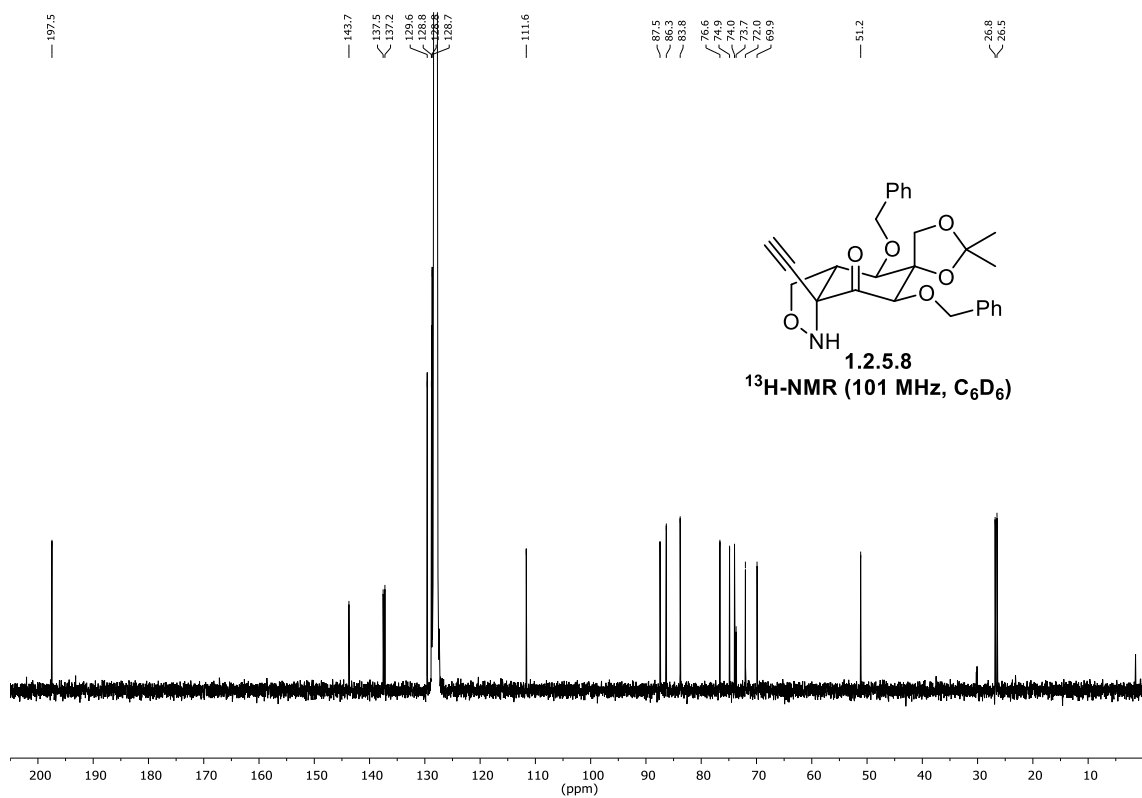
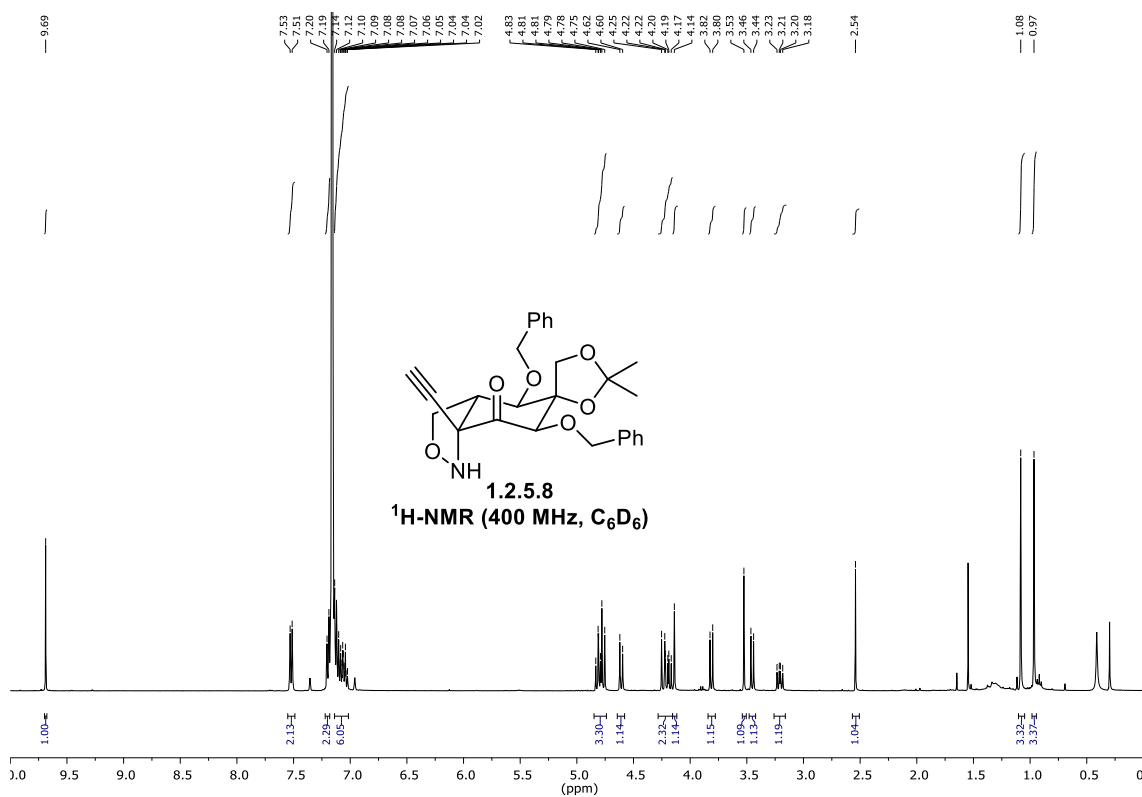
tert-butyl (6*R*,7*R*,8*S*,9*S*,10*S*,10*aS*,*Z*)-7,9-bis(benzyloxy)-3-((*tert*-butoxycarbonyl)imino)-1-(dibromomethylene)-10-hydroxy-2',2'-dimethyltetrahydro-1*H*,6*H*-spiro[benzo[*c*]imidazo[1,5-*b*]isoxazole-8,4'-[1,3]dioxolane]-2(3*H*)-carboxylate (1.2.5.6)



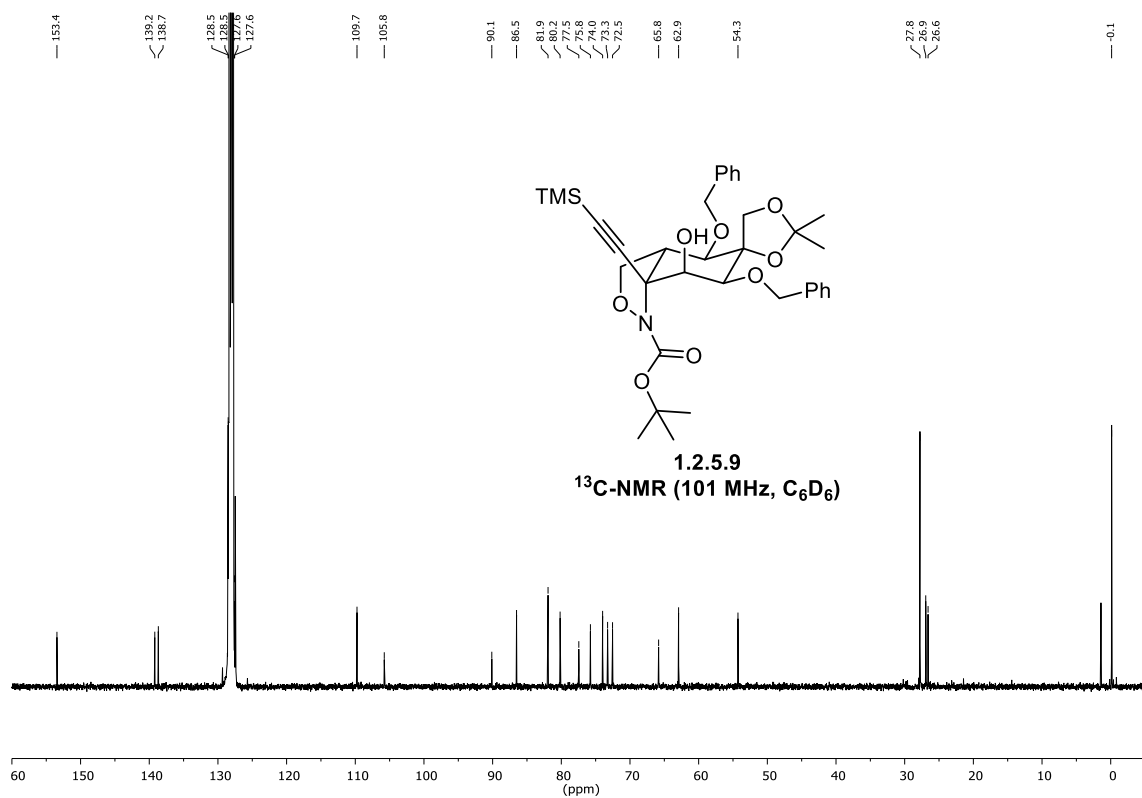
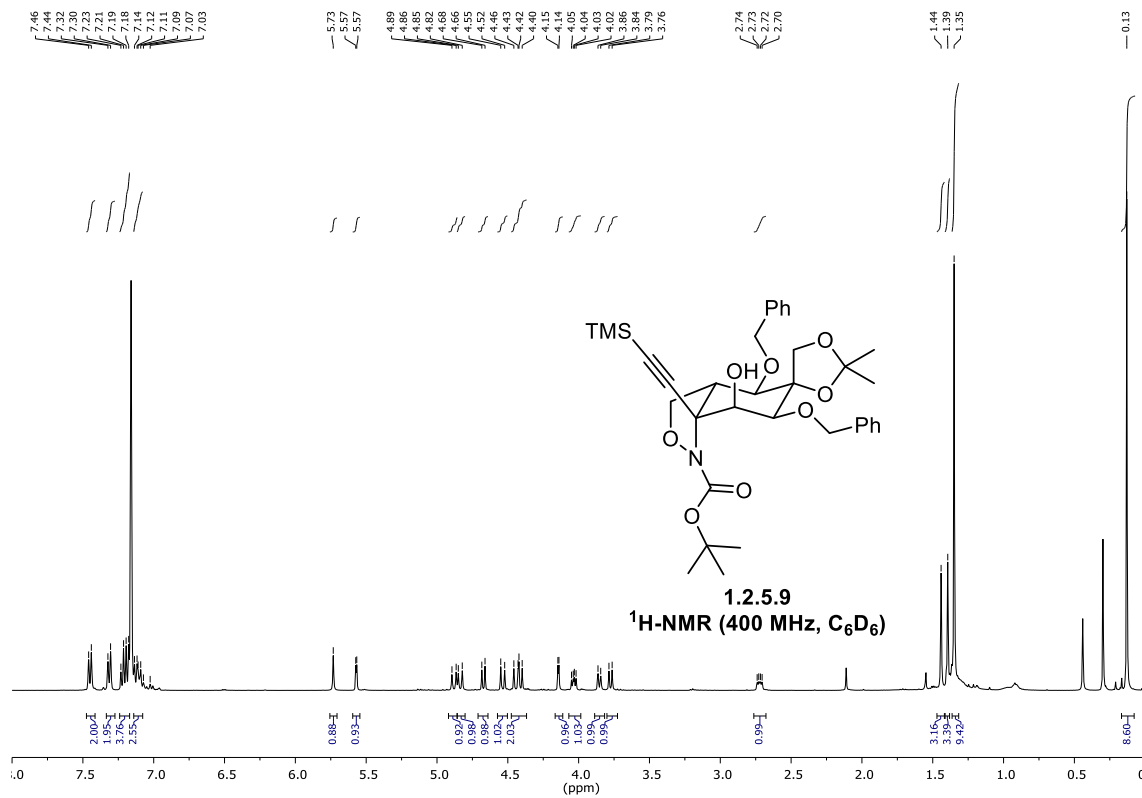
(3a*R*,4*R*,5*S*,6*R*,7*aS*)-4,6-bis(benzyloxy)-2',2'-dimethyl-7a-
((trimethylsilyl)ethynyl)tetrahydro-3H-spiro[benzo[*c*]isoxazole-5,4'-[1,3]dioxolan]-
7(6*H*)-one (1.2.5.7)



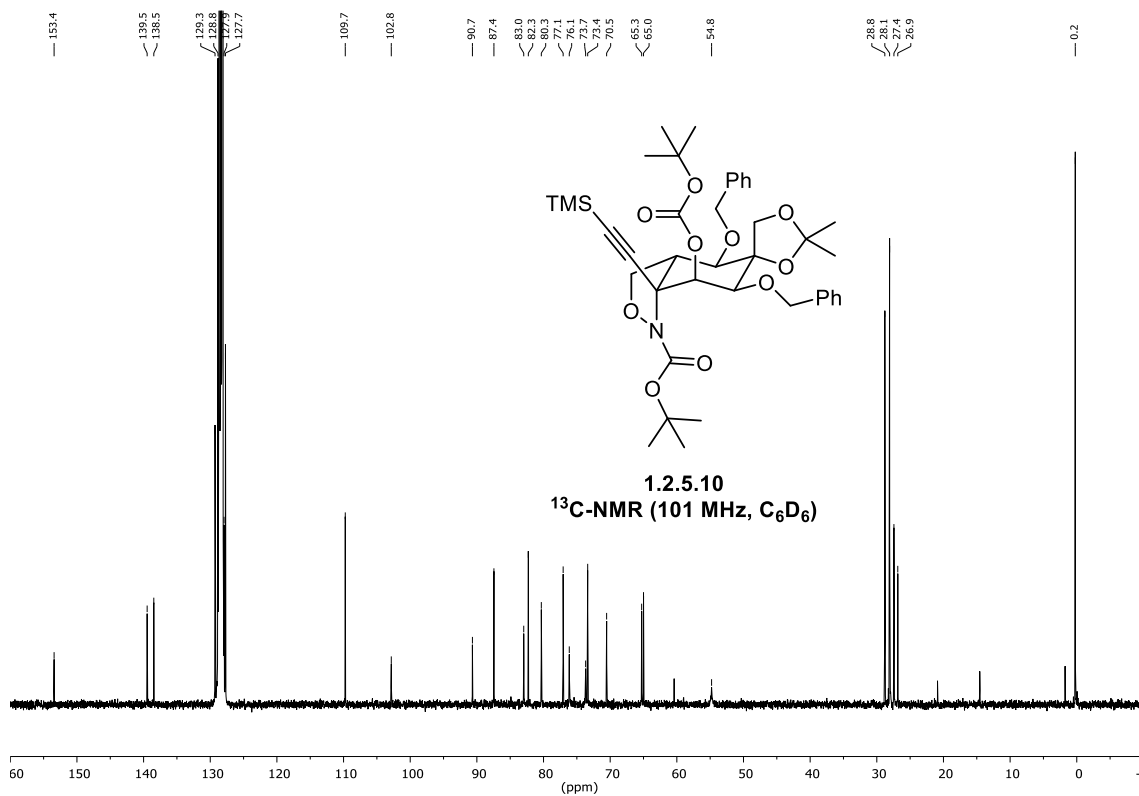
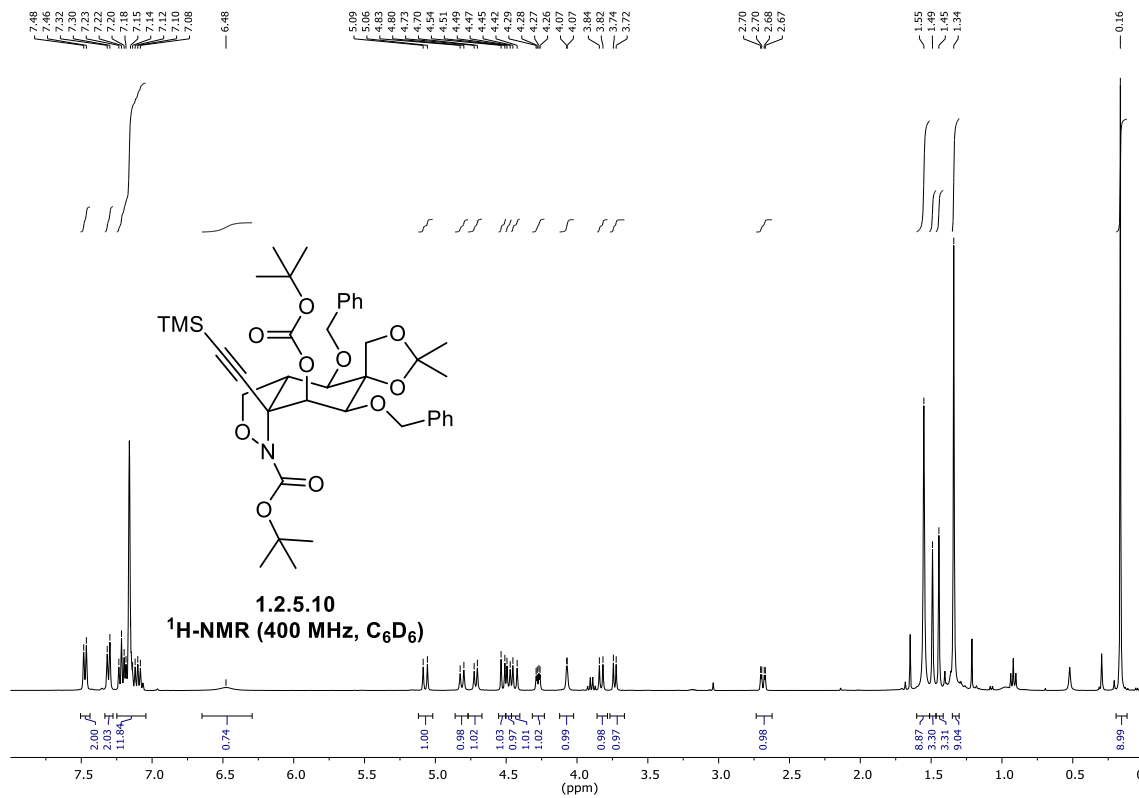
(3*aR*,4*R*,5*S*,6*R*,7*aS*)-4,6-bis(benzyloxy)-7*a*-ethynyl-2',2'-dimethyltetrahydro-3*H*-spiro[benzo[*c*]isoxazole-5,4'-[1,3]dioxolan]-7(6*H*)-one (1.2.5.8)



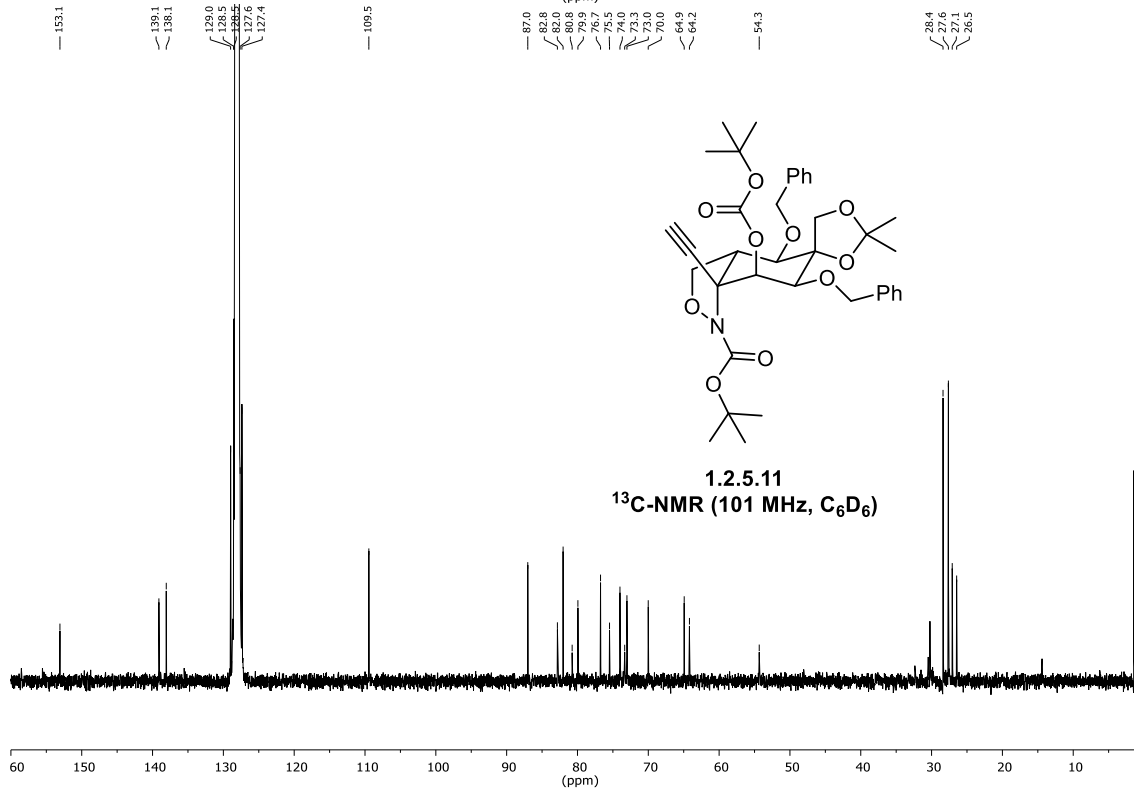
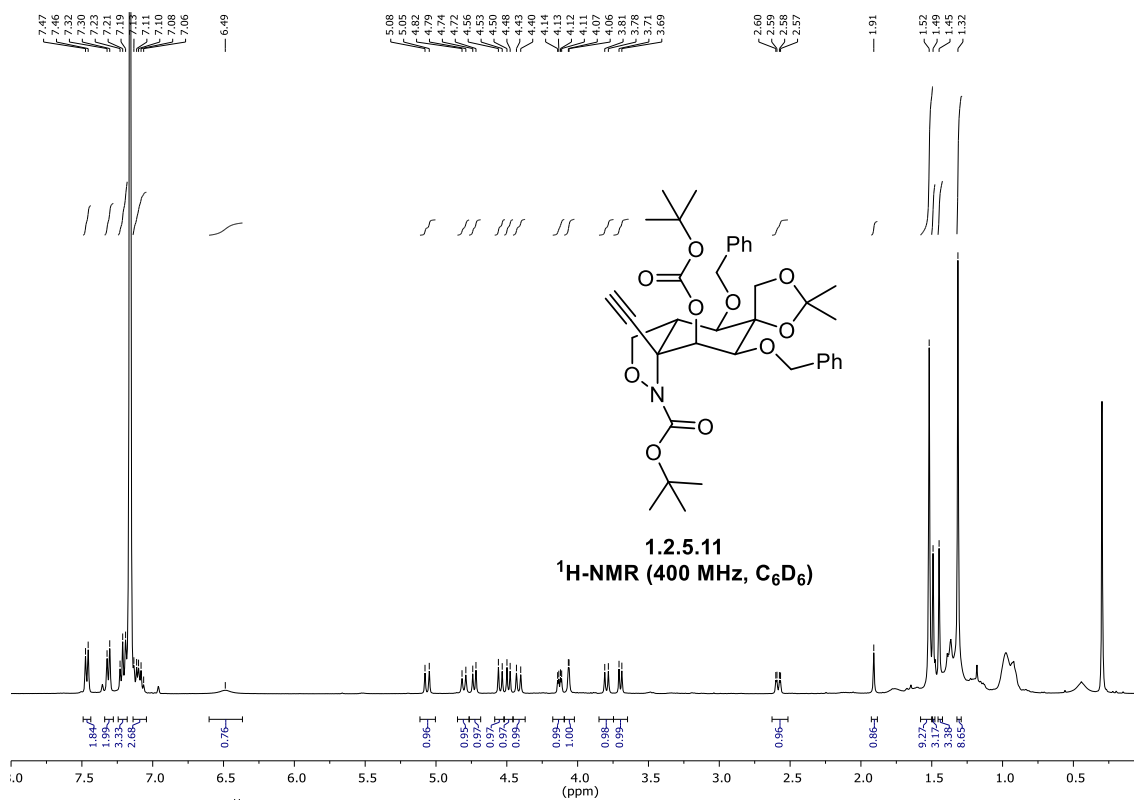
tert-butyl (3*aR*,4*R*,5*S*,6*S*,7*S*,7*aS*)-4,6-bis(benzyloxy)-7-hydroxy-2',2'-dimethyl-7a-((trimethylsilyl)ethynyl)tetrahydro-3H-spiro[benzo[*c*]isoxazole-5,4'-[1,3]dioxolane]-1(4*H*)-carboxylate (1.2.5.9)



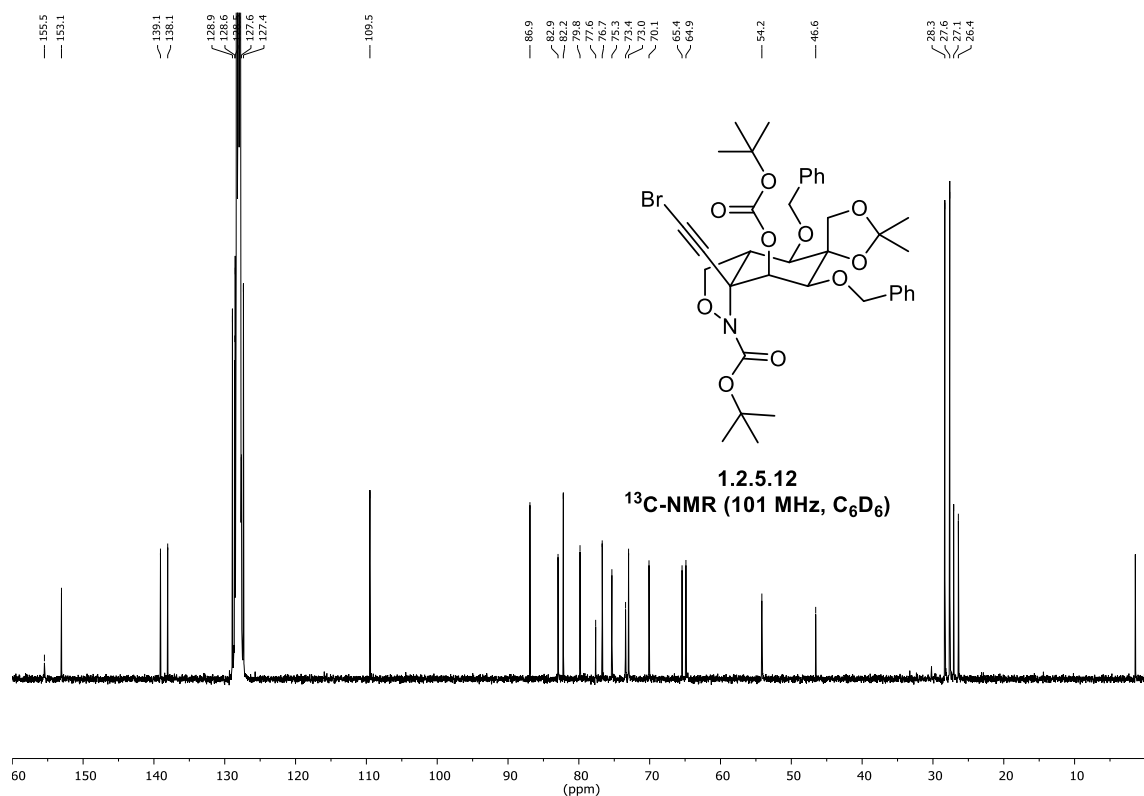
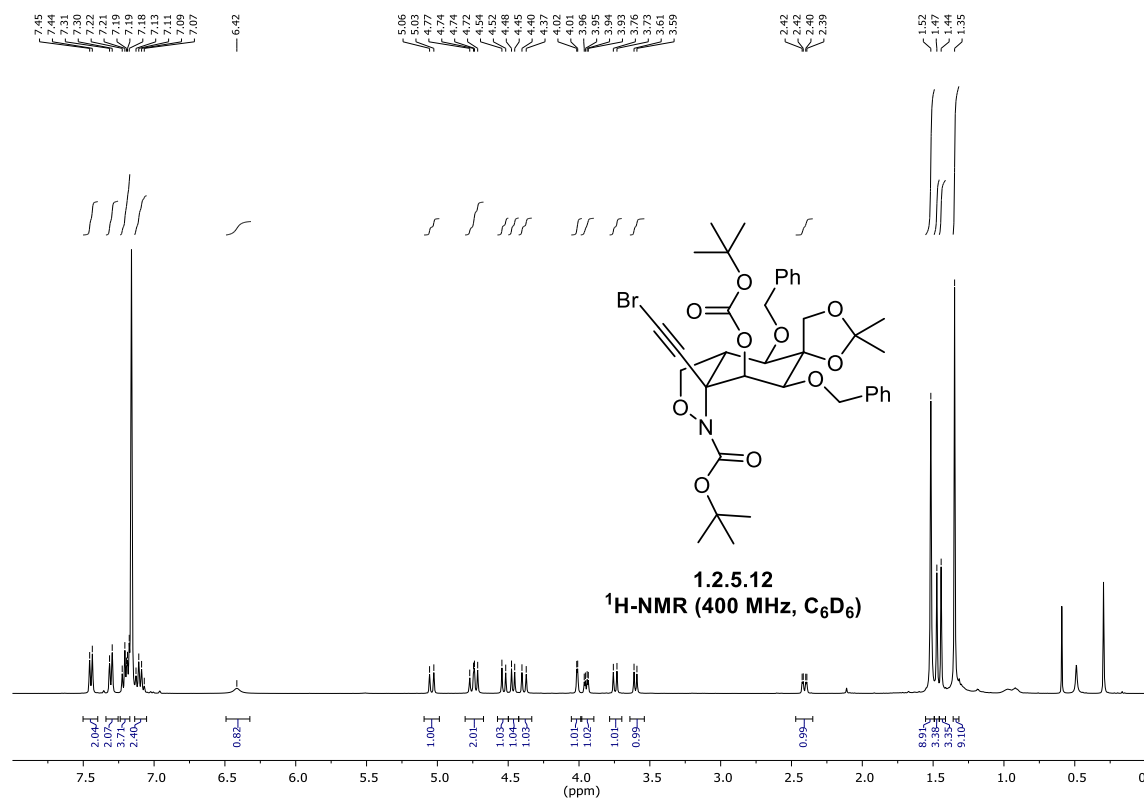
tert-butyl (3*aR*,4*R*,5*S*,6*S*,7*S*,7*aS*)-4,6-bis(benzyloxy)-7-((*tert*-butoxycarbonyl)oxy)-2',2'-dimethyl-7*a*-((trimethylsilyl)ethynyl)tetrahydro-3*H*-spiro[benzo[*c*]isoxazole-5,4'-[1,3]dioxolane]-1(4*H*)-carboxylate (1.2.5.10)



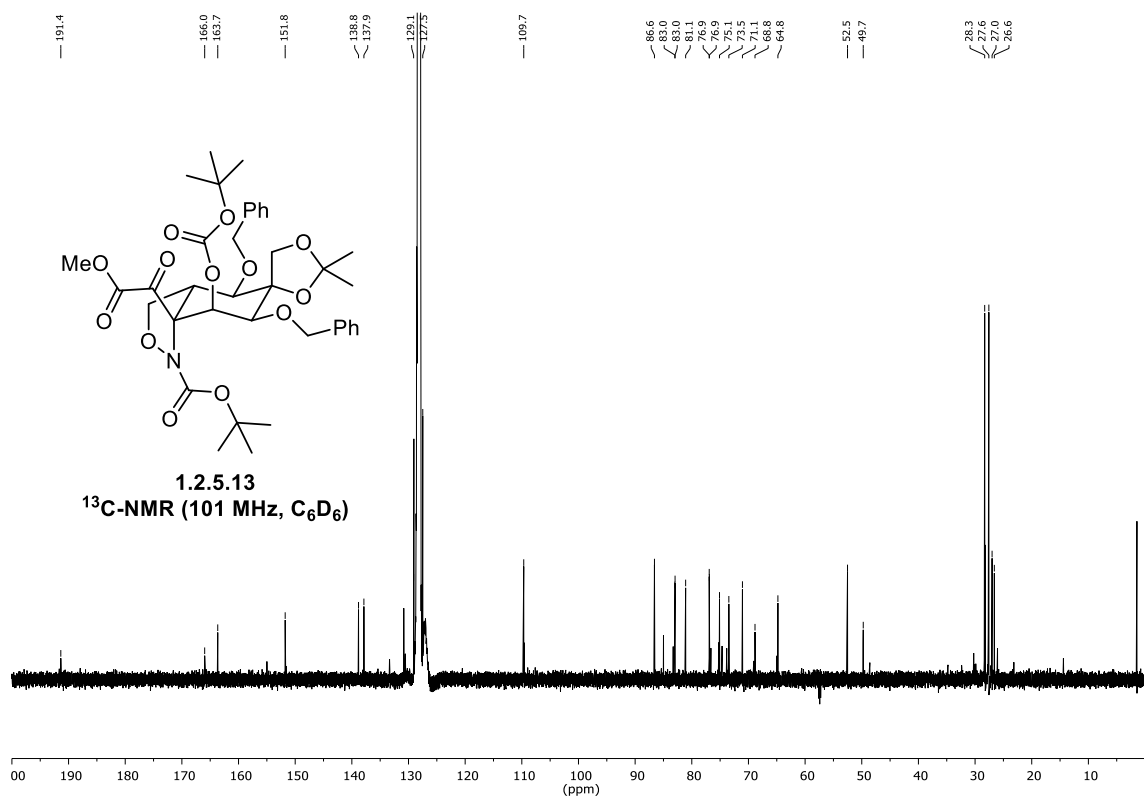
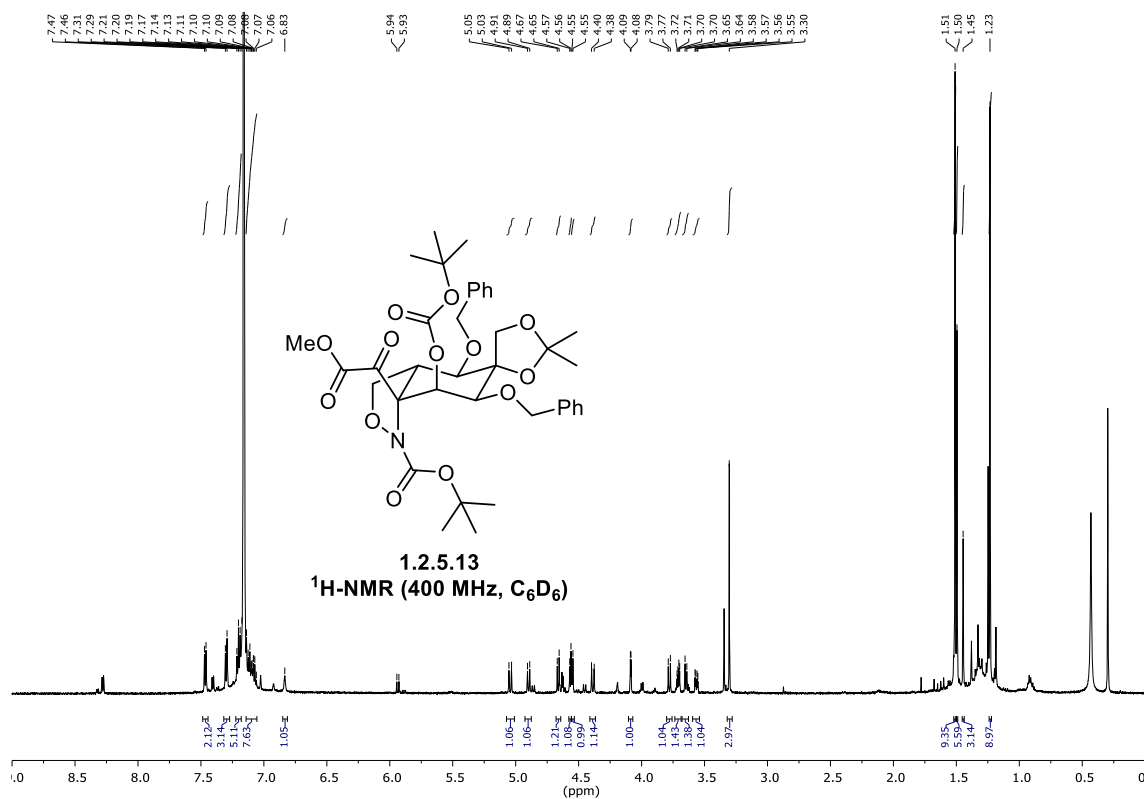
tert-butyl (3*aR*,4*R*,5*S*,6*S*,7*S*,7*aS*)-4,6-bis(benzyloxy)-7-((*tert*-butoxycarbonyl)oxy)-7*a*-ethynyl-2',2'-dimethyltetrahydro-3*H*-spiro[benzo[*c*]isoxazole-5,4'-[1,3]dioxolane]-1(4*H*)-carboxylate (1.2.5.11)



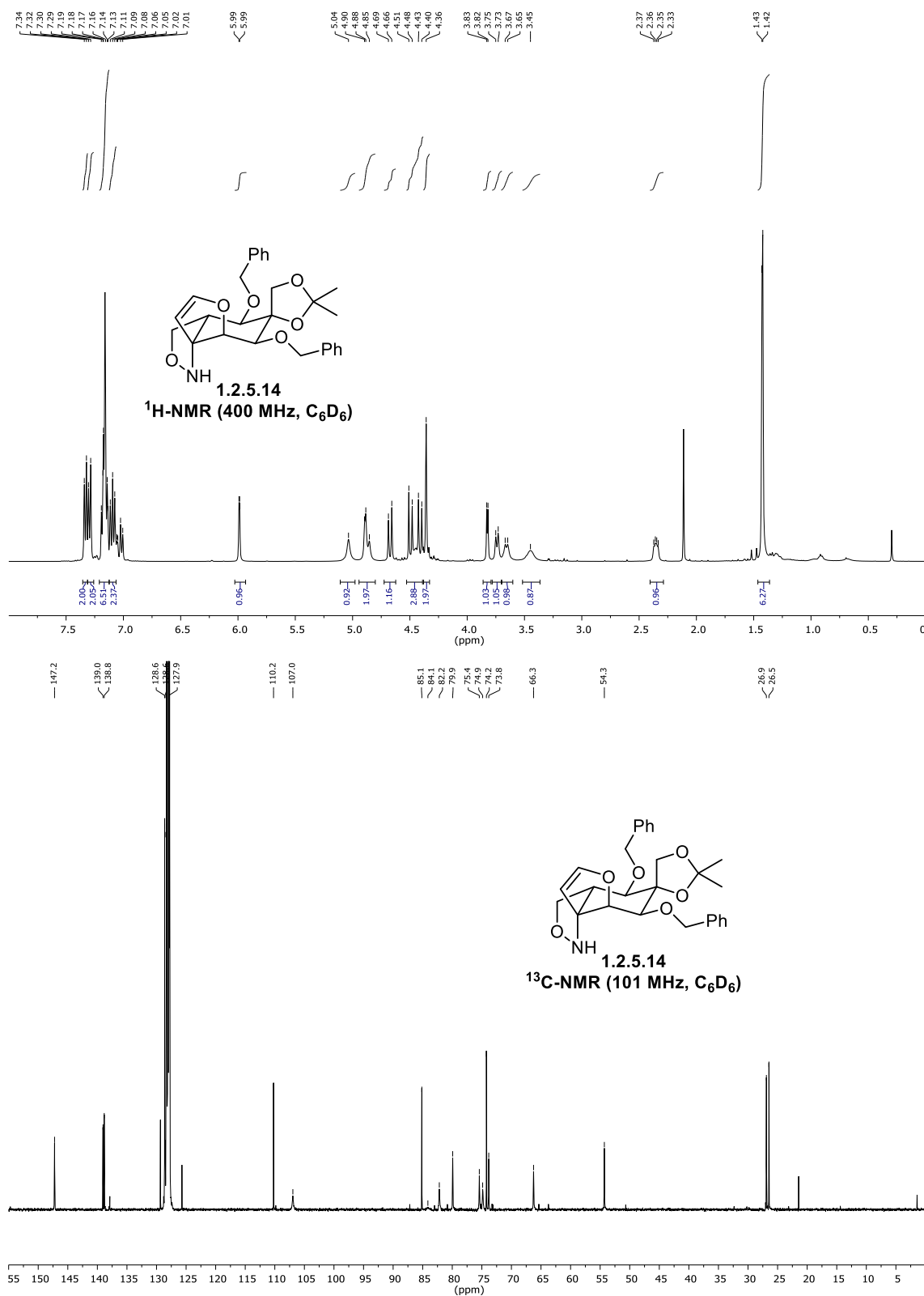
tert-butyl (3*aR*,4*R*,5*S*,6*S*,7*S*,7*aS*)-4,6-bis(benzyloxy)-7*a*-(bromoethynyl)-7-((*tert*-butoxycarbonyl)oxy)-2',2'-dimethyltetrahydro-3*H*-spiro[benzo[*c*]isoxazole-5,4'-[1,3]dioxolane]-1(4*H*)-carboxylate (1.2.5.12)



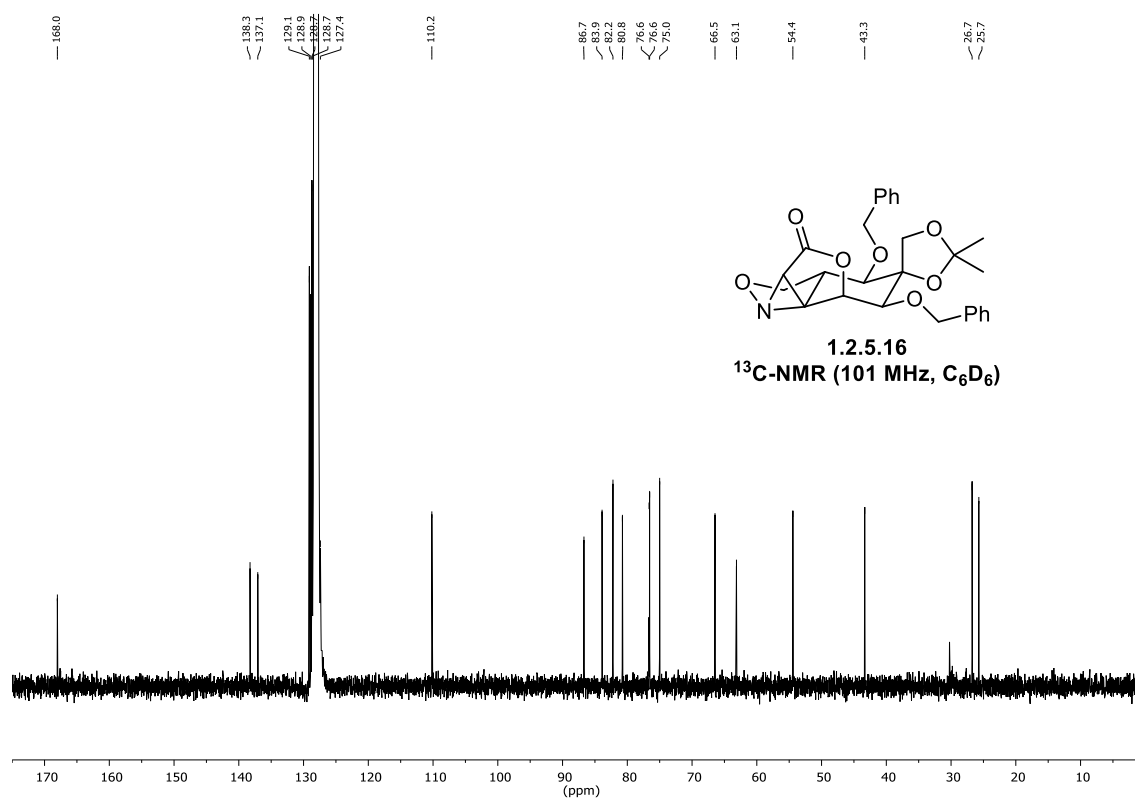
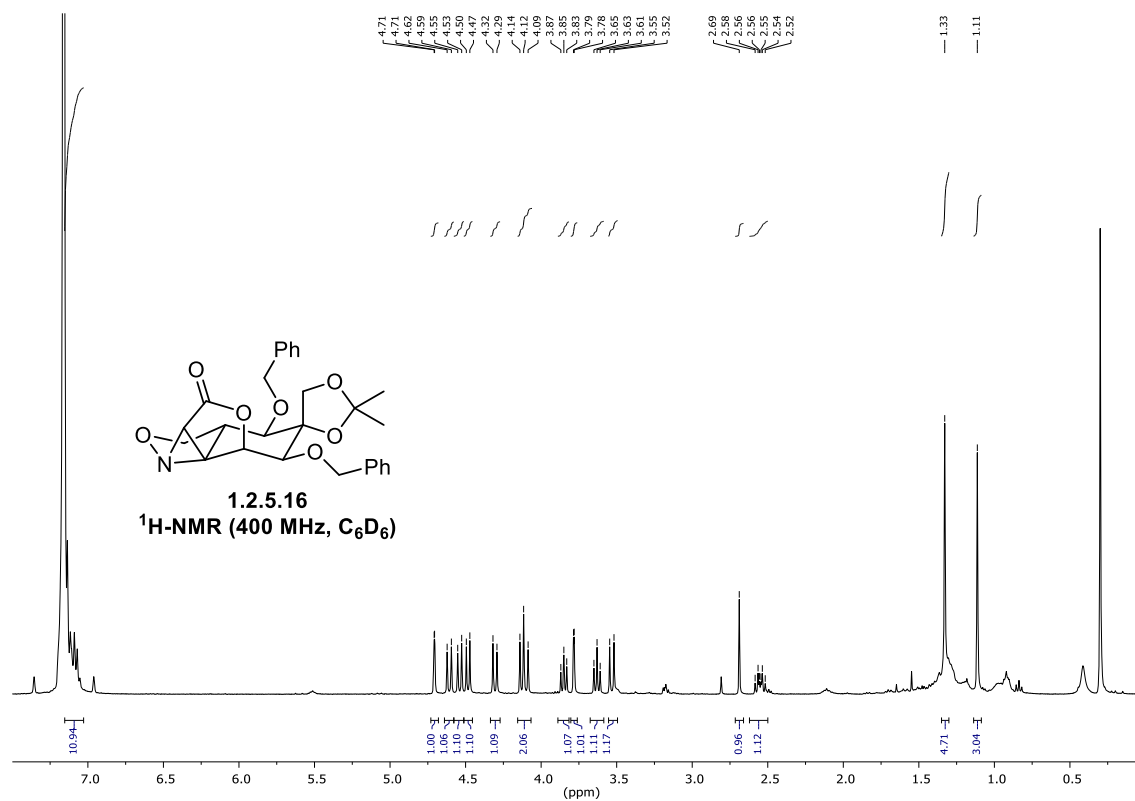
tert-butyl (3*aR*,4*R*,5*S*,6*S*,7*S*,7*aR*)-4,6-bis(benzyloxy)-7-((*tert*-butoxycarbonyl)oxy)-7*a*-(2-methoxy-2-oxoacetyl)-2',2'-dimethyltetrahydro-3*H*-spiro[benzo[*c*]isoxazole-5,4'-[1,3]dioxolane]-1(4*H*)-carboxylate (1.2.5.13)



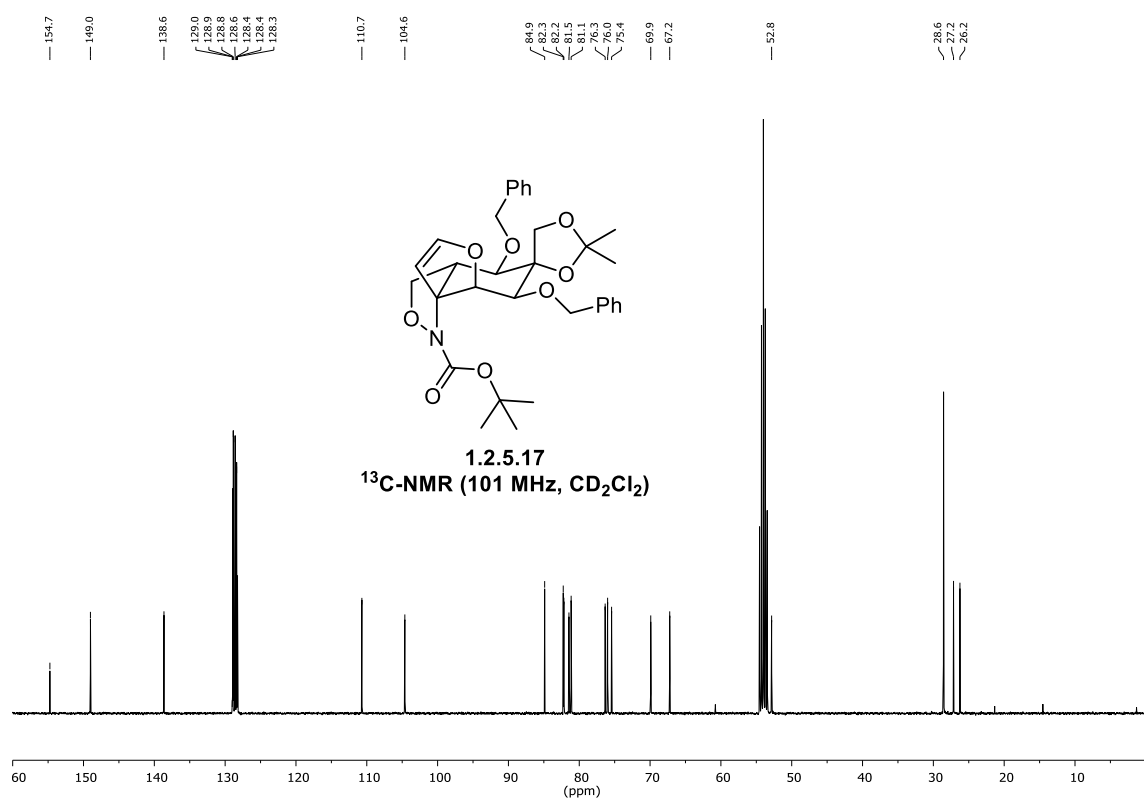
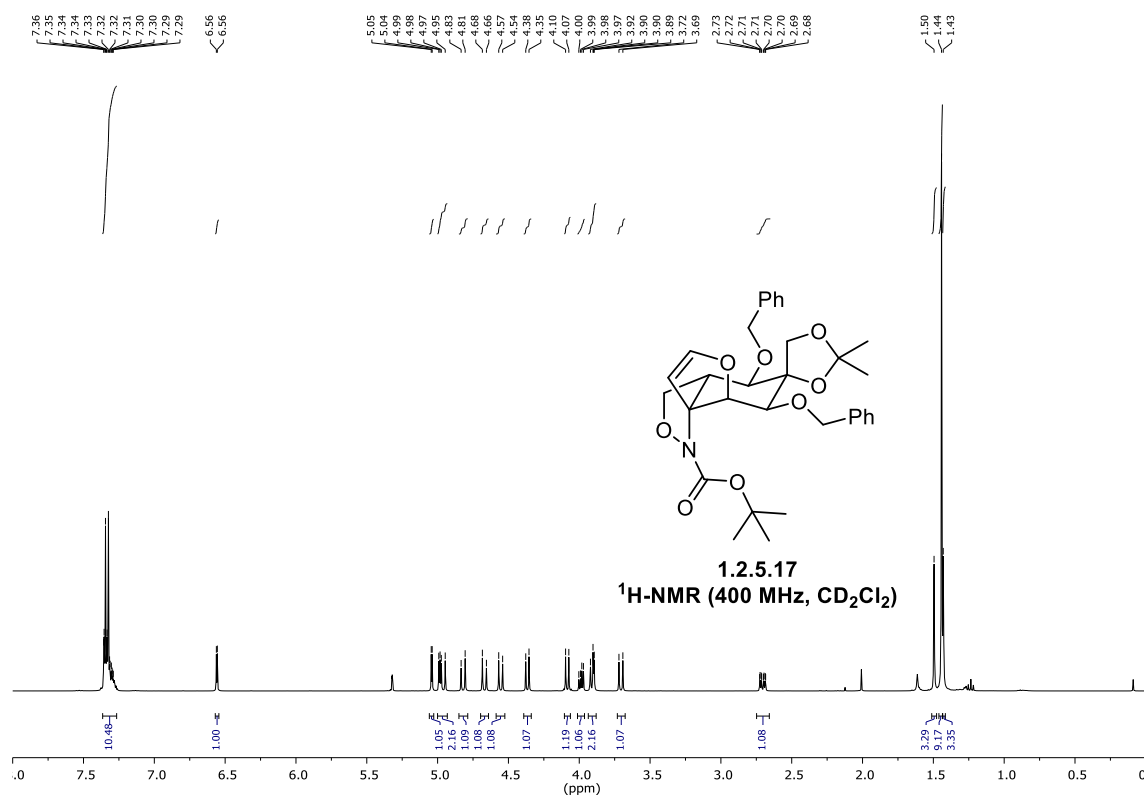
(3*aR*,4*R*,5*S*,6*S*,6*aS*,9*aR*)-4,6-bis(benzyloxy)-2',2'-dimethyl-3*a*,4,6,6*a*-tetrahydro-1*H*,3*H*-spiro[benzofuro[3*a*,4-*c*]isoxazole-5,4'-[1,3]dioxolane] (1.2.5.14)



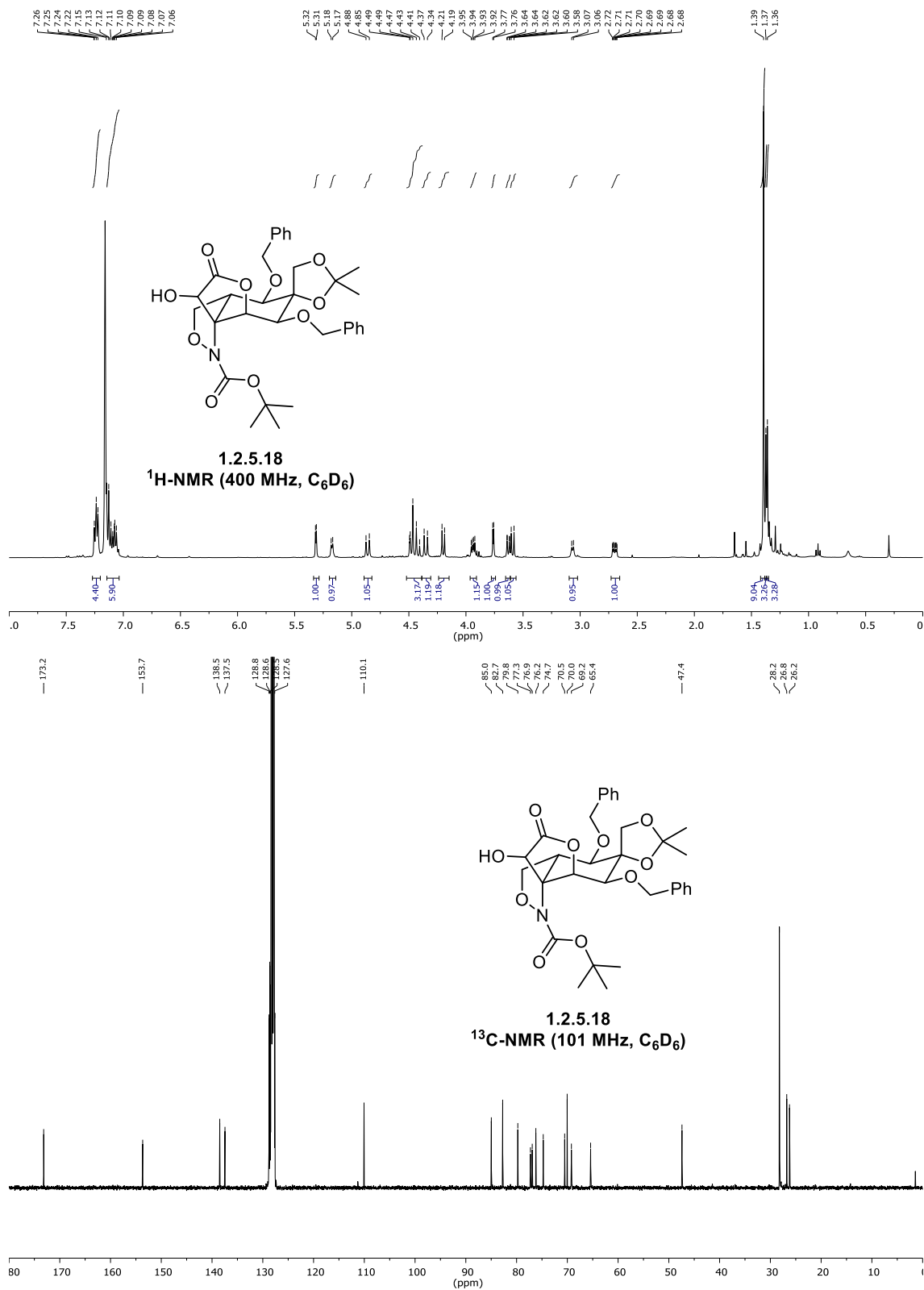
(4*aR*,5*R*,6*S*,7*S*,8*S*,8*aS*)-5,7-bis(benzyloxy)-2',2'-dimethyltetrahydro-1*H*,4*H*-spiro[[8,1](epoxymethano)azirino[1,2-*b*]benzo[*c*]isoxazole-6,4'-[1,3]dioxolan]-10-one (1.2.5.16)



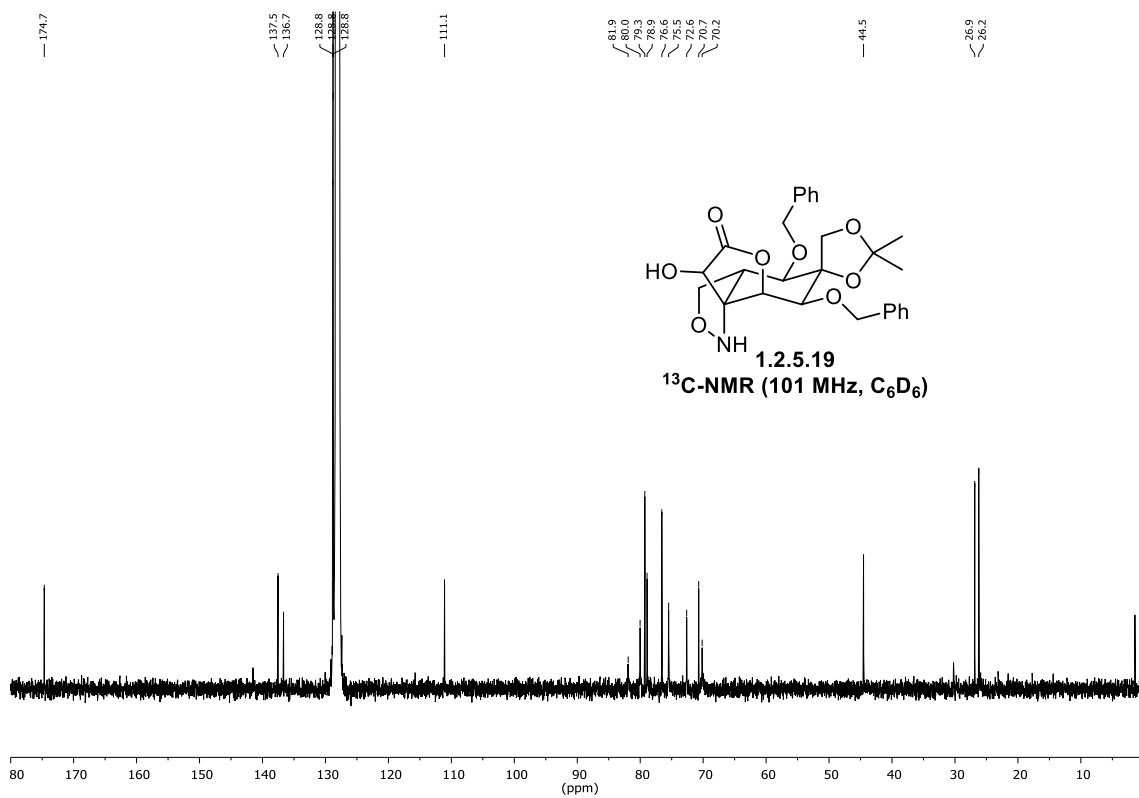
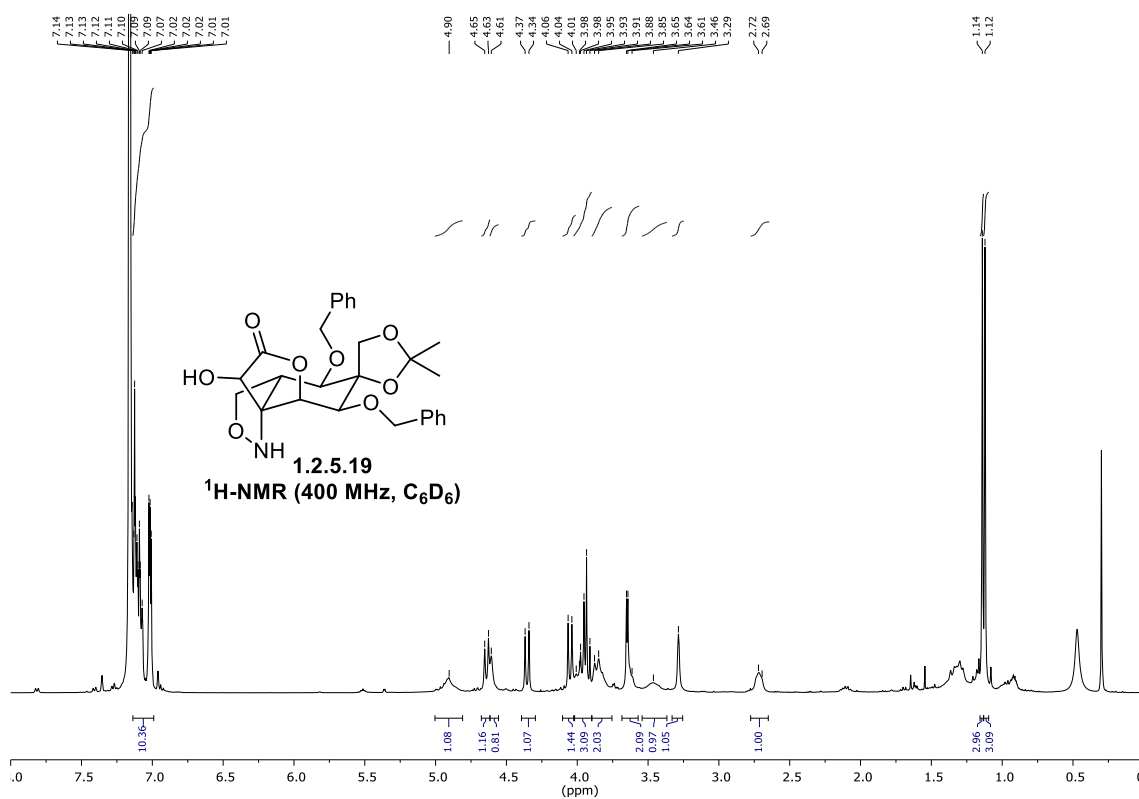
tert-butyl (3*aR*,4*R*,5*S*,6*S*,6*aS*,9*aR*)-4,6-bis(benzyloxy)-2',2'-dimethyl-3*a*,4,6,6*a*-tetrahydro-1*H*,3*H*-spiro[benzofuro[3*a*,4-*c*]isoxazole-5,4'-[1,3]dioxolane]-1-carboxylate (1.2.5.17)



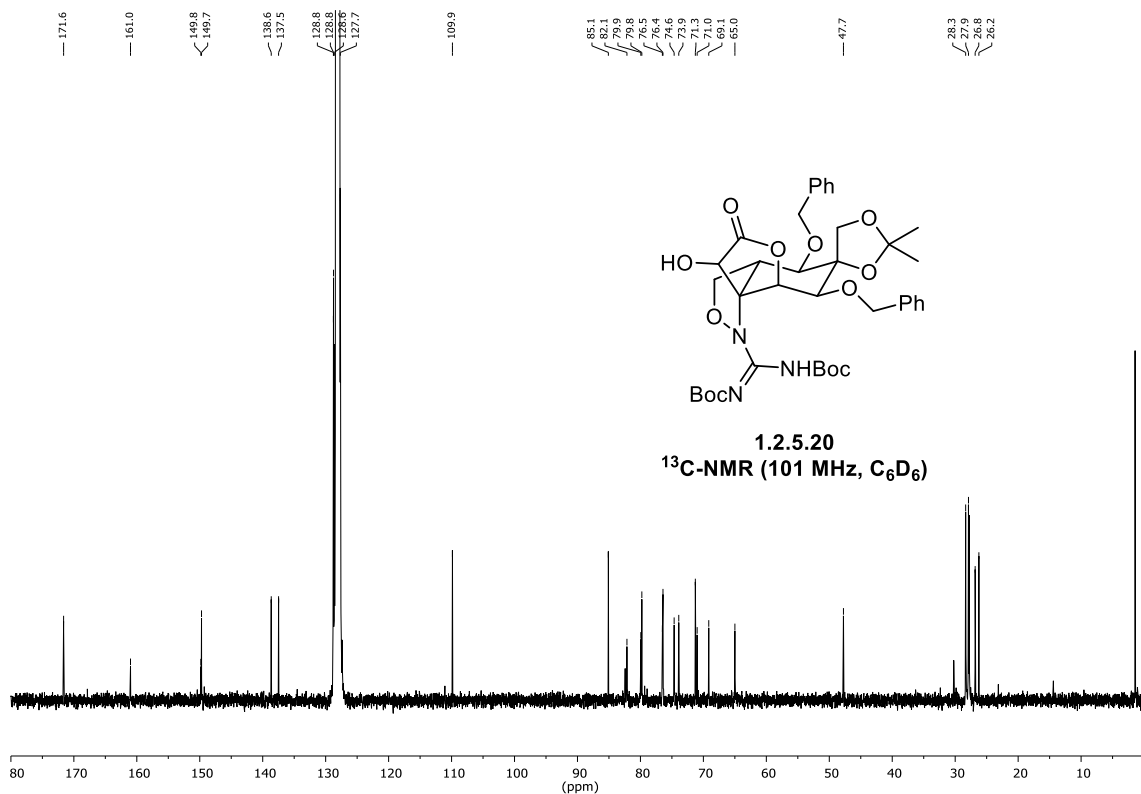
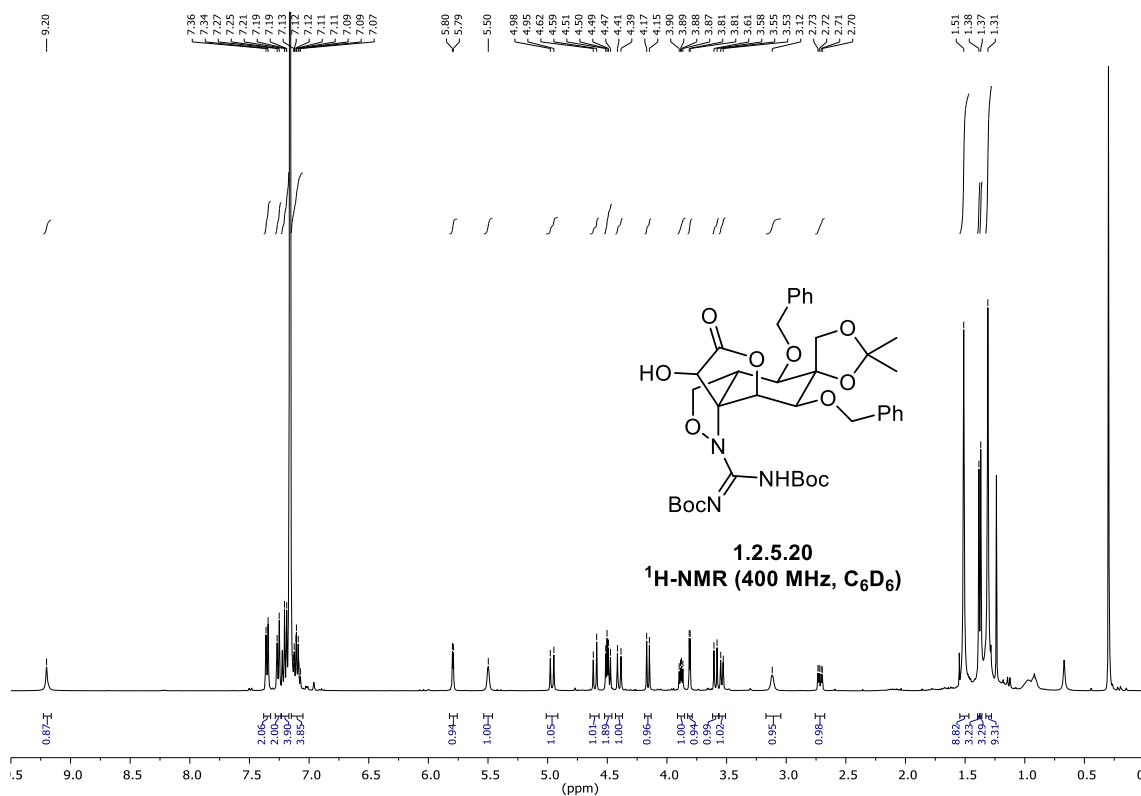
tert-butyl (3*aR*,4*R*,5*S*,6*S*,6*aS*,9*R*,9*aS*)-4,6-bis(benzyloxy)-9-hydroxy-2',2'-dimethyl-8-oxohexahydro-1*H*,3*H*-spiro[benzofuro[3*a*,4-*c*]isoxazole-5,4'-[1,3]dioxolane]-1-carboxylate (1.2.5.18)



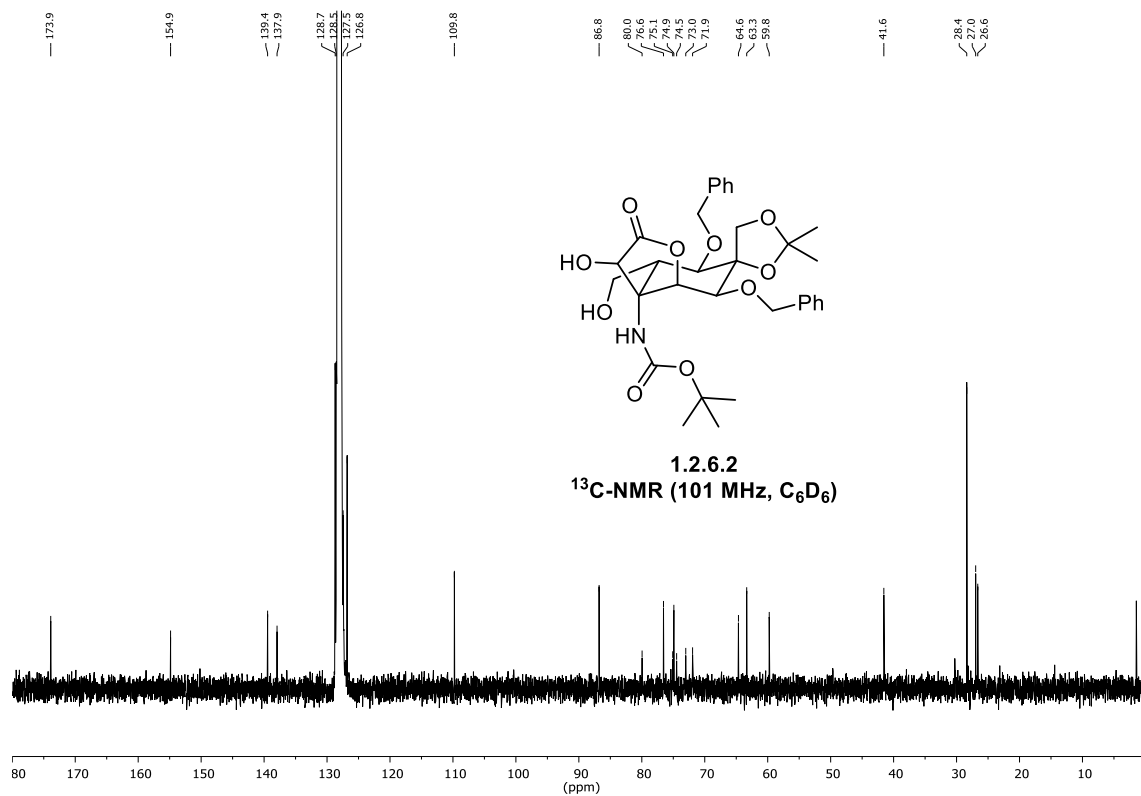
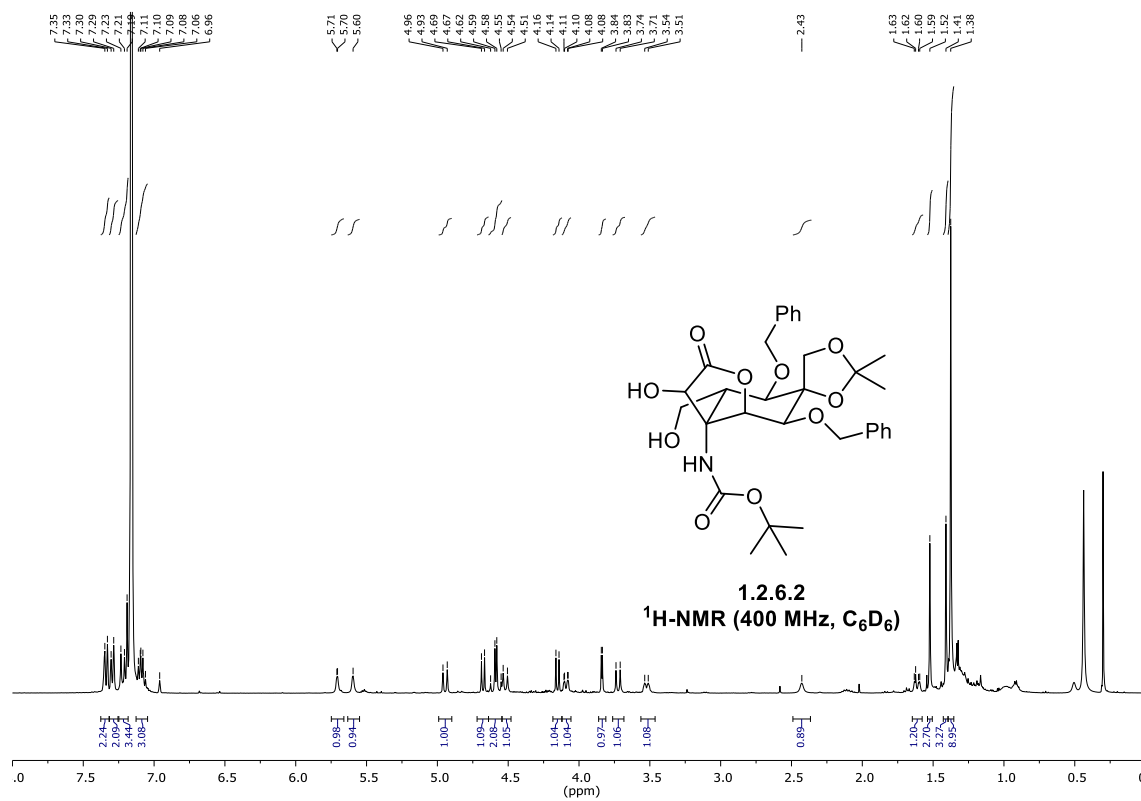
(3a*R*,4*R*,5*S*,6*S*,6a*S*,9*R*,9a*S*)-4,6-bis(benzyloxy)-9-hydroxy-2',2'-dimethyltetrahydro-1*H*,3*H*-spiro[benzofuro[3a,4-c]isoxazole-5,4'-[1,3]dioxolan]-8(9*H*)-one (1.2.5.19)



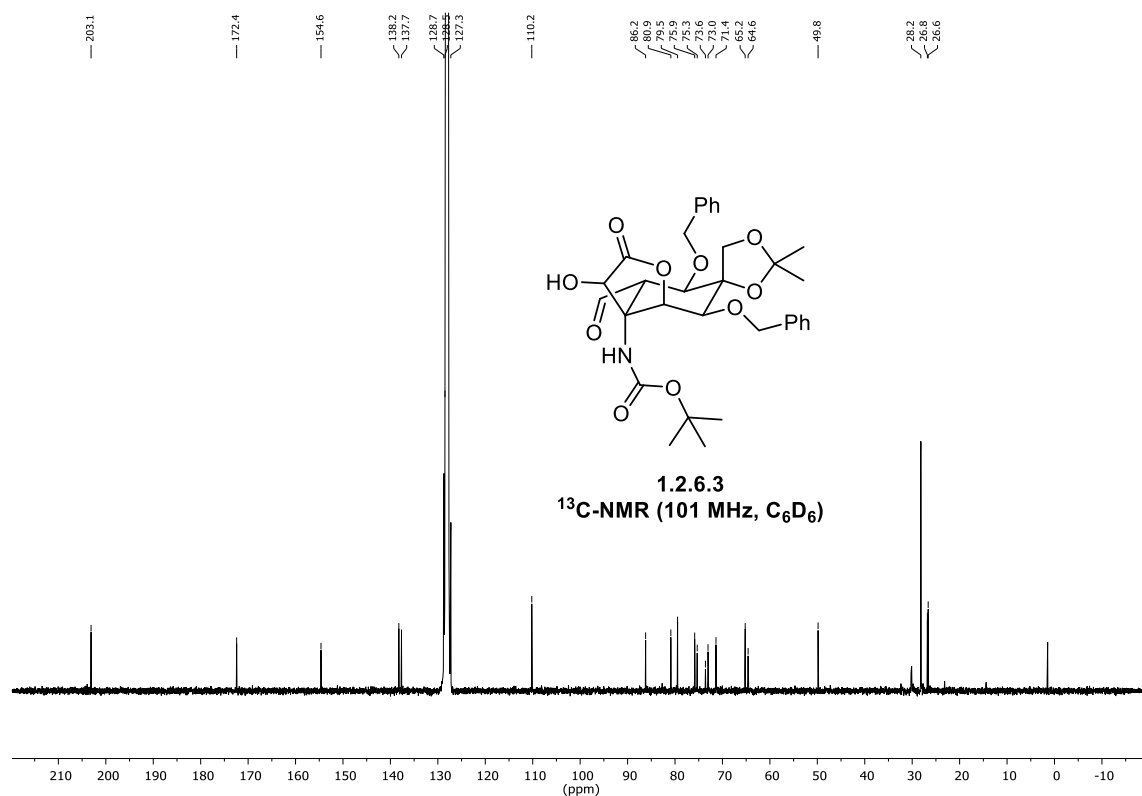
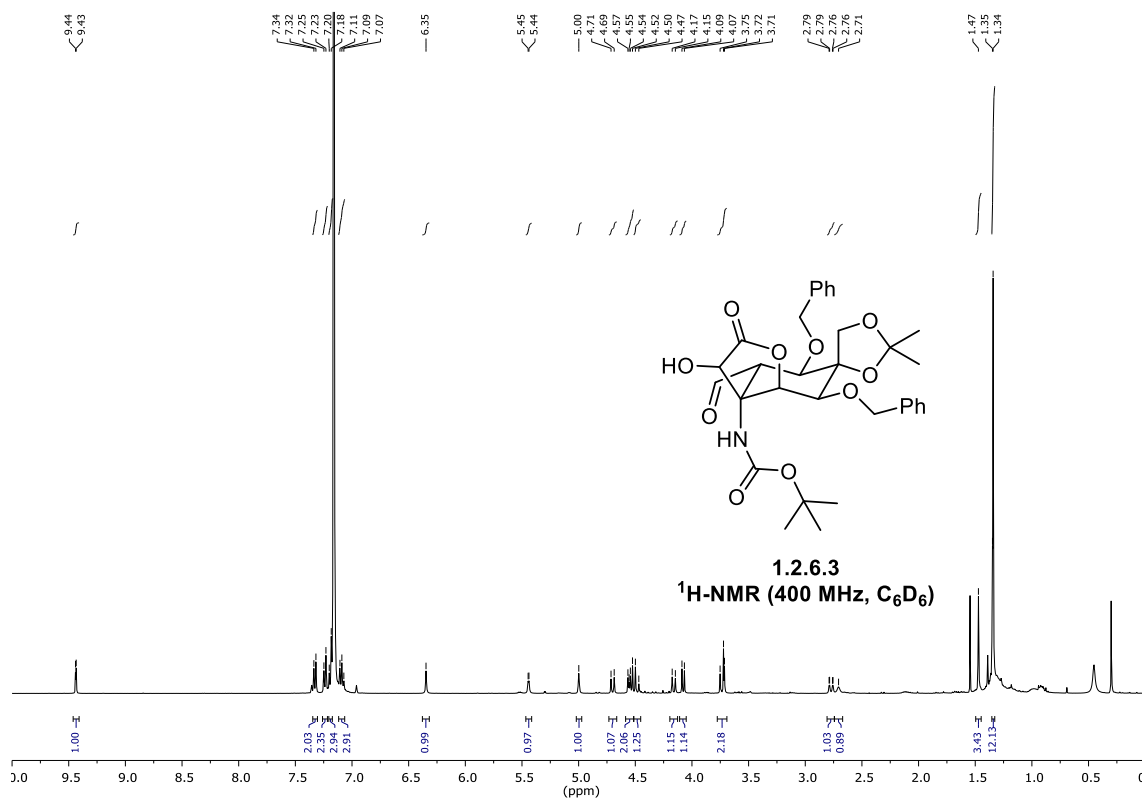
tert-butyl ((*E*)-((3*aR*,4*R*,5*S*,6*S*,6*aS*,9*R*,9*aS*)-4,6-bis(benzyloxy)-9-hydroxy-2',2'-dimethyl-8-oxohexahydro-1*H*,3*H*-spiro[benzofuro[3*a*,4-*c*]isoxazole-5,4'-[1,3]dioxolan]-1-yl)((*tert*-butoxycarbonyl)amino)methylene)carbamate (1.2.5.20)



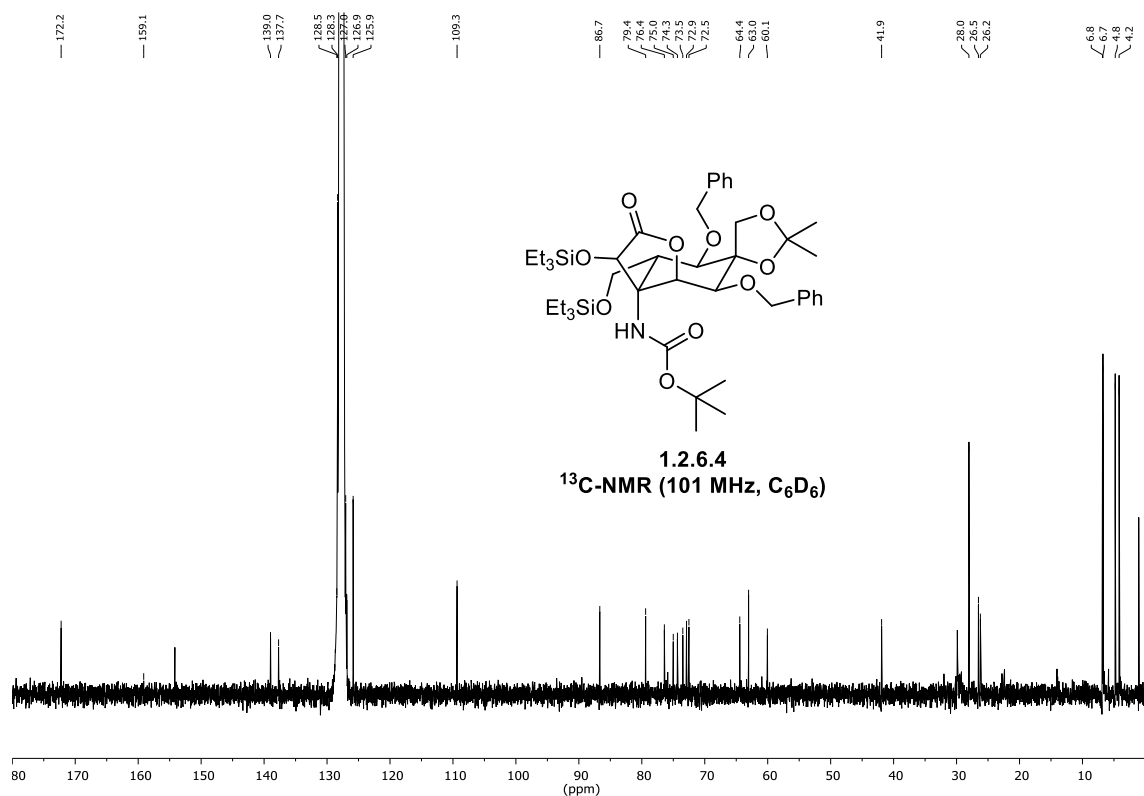
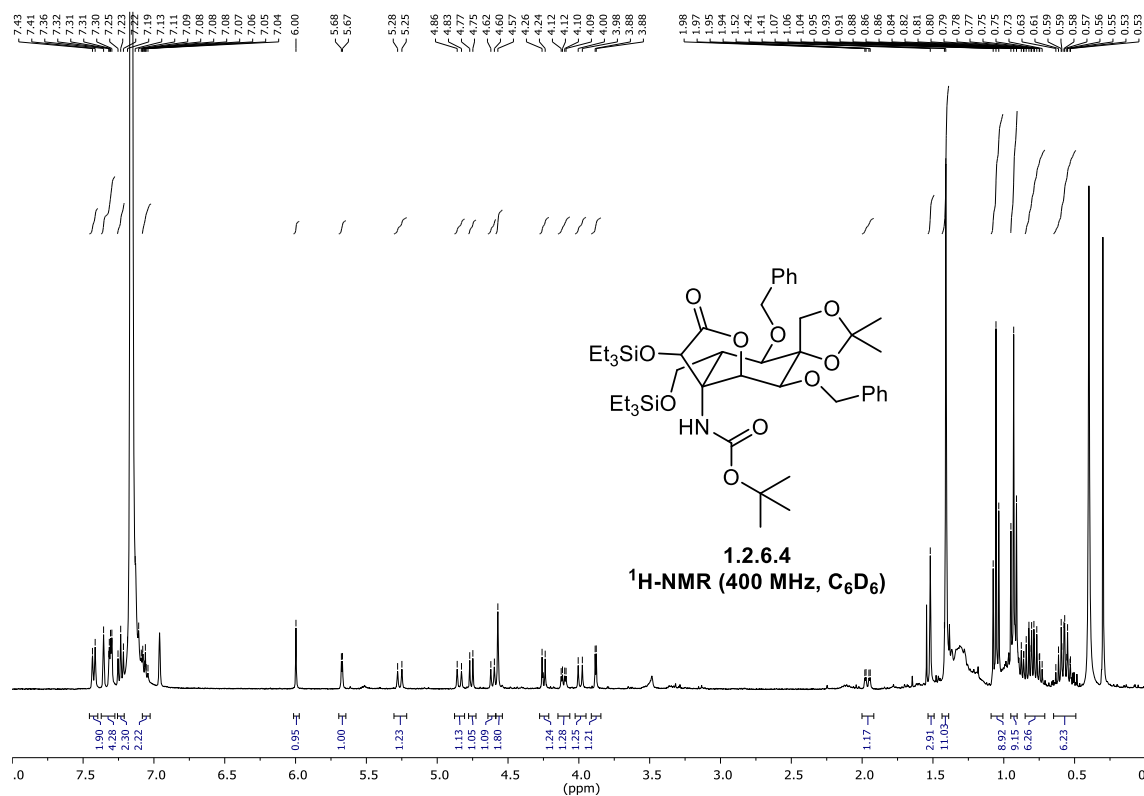
tert-butyl ((3*R*,3*aS*,4*R*,5*R*,6*S*,7*S*,7*aS*)-5,7-bis(benzyloxy)-3-hydroxy-4-(hydroxymethyl)-2',2'-dimethyl-2-oxohexahydro-3*aH*-spiro[benzofuran-6,4'-[1,3]dioxolan]-3*a*-yl)carbamate (1.2.6.2)



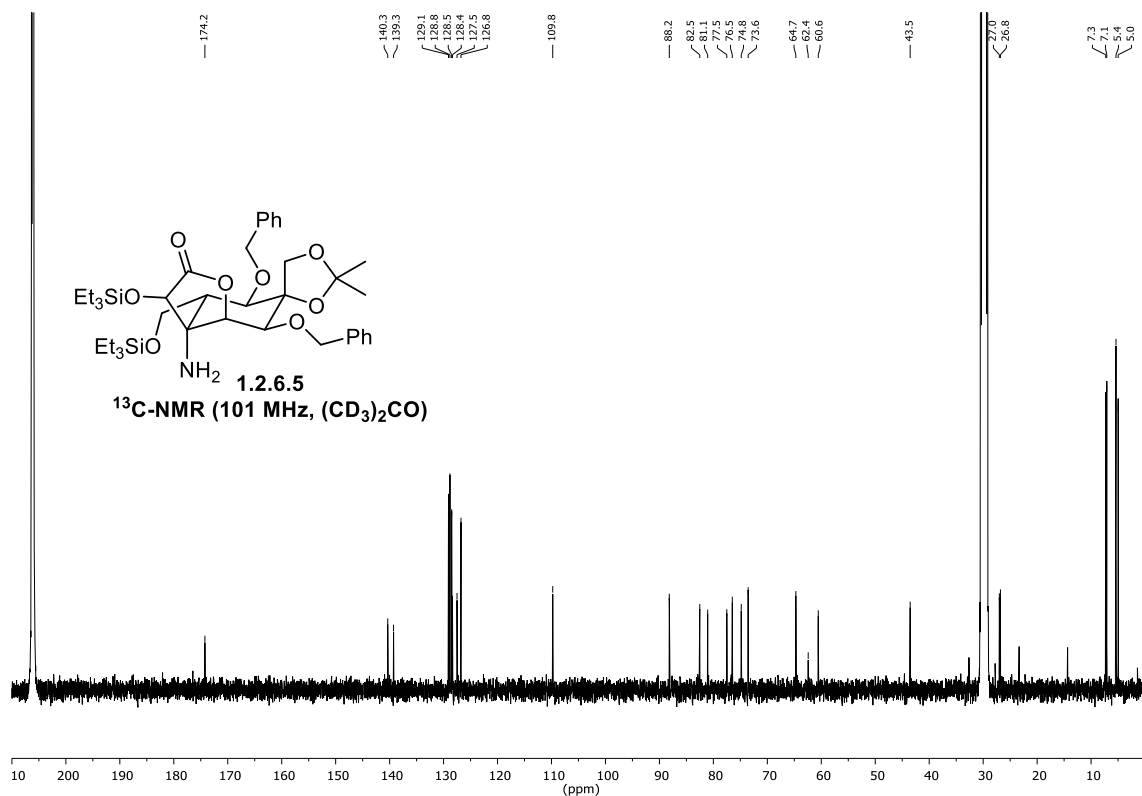
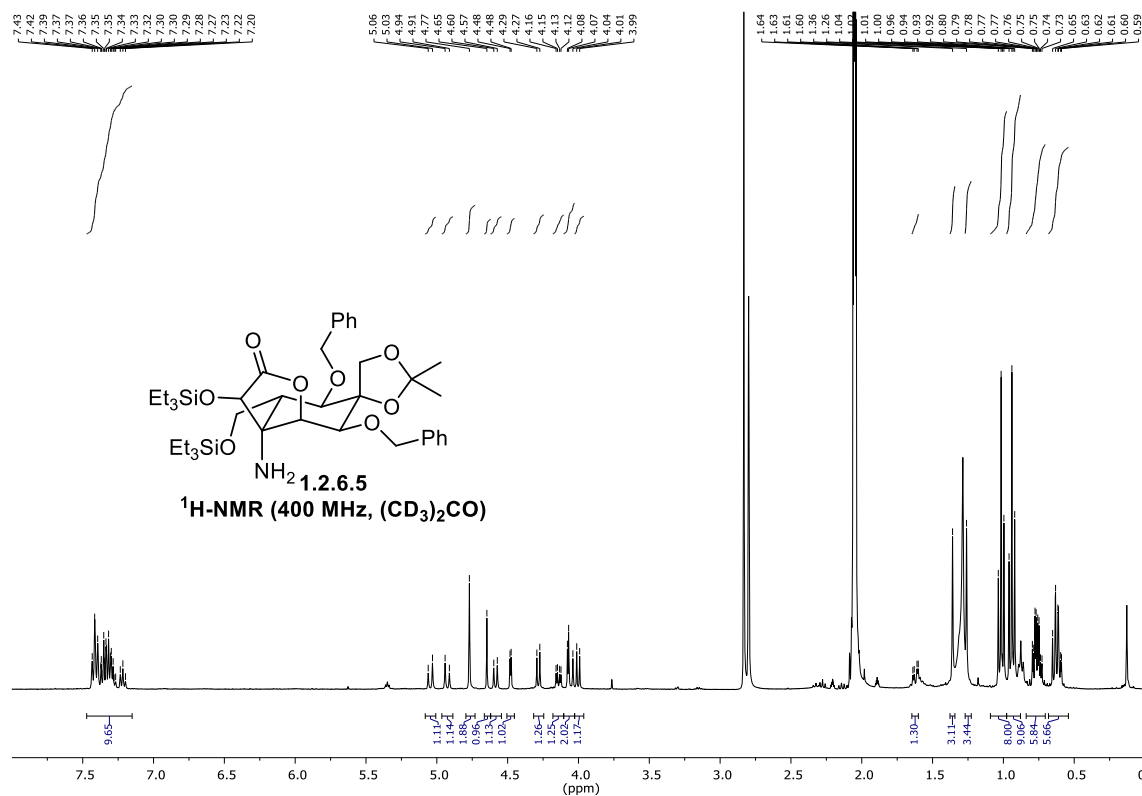
tert-butyl ((3*R*,3*aS*,4*S*,5*R*,6*S*,7*S*,7*aS*)-5,7-bis(benzyloxy)-4-formyl-3-hydroxy-2',2'-dimethyl-2-oxohexahydro-3*aH*-spiro[benzofuran-6,4'-[1,3]dioxolan]-3*a*-yl)carbamate (1.2.6.3)



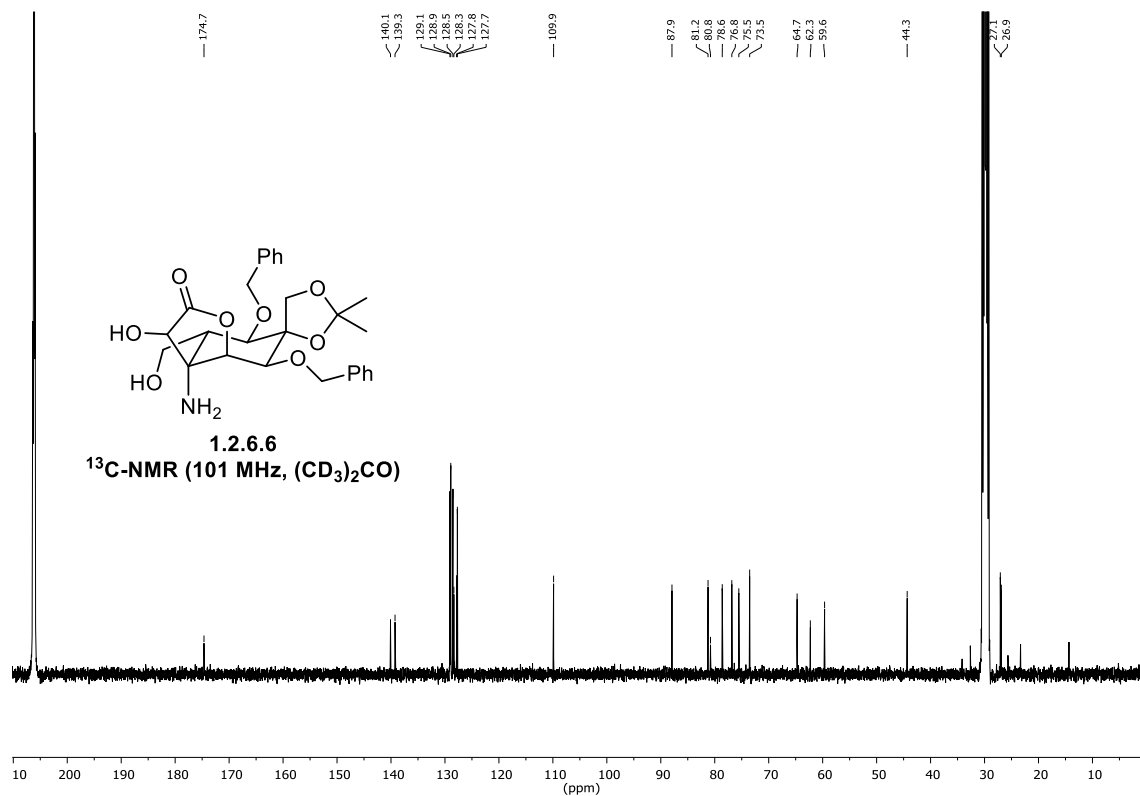
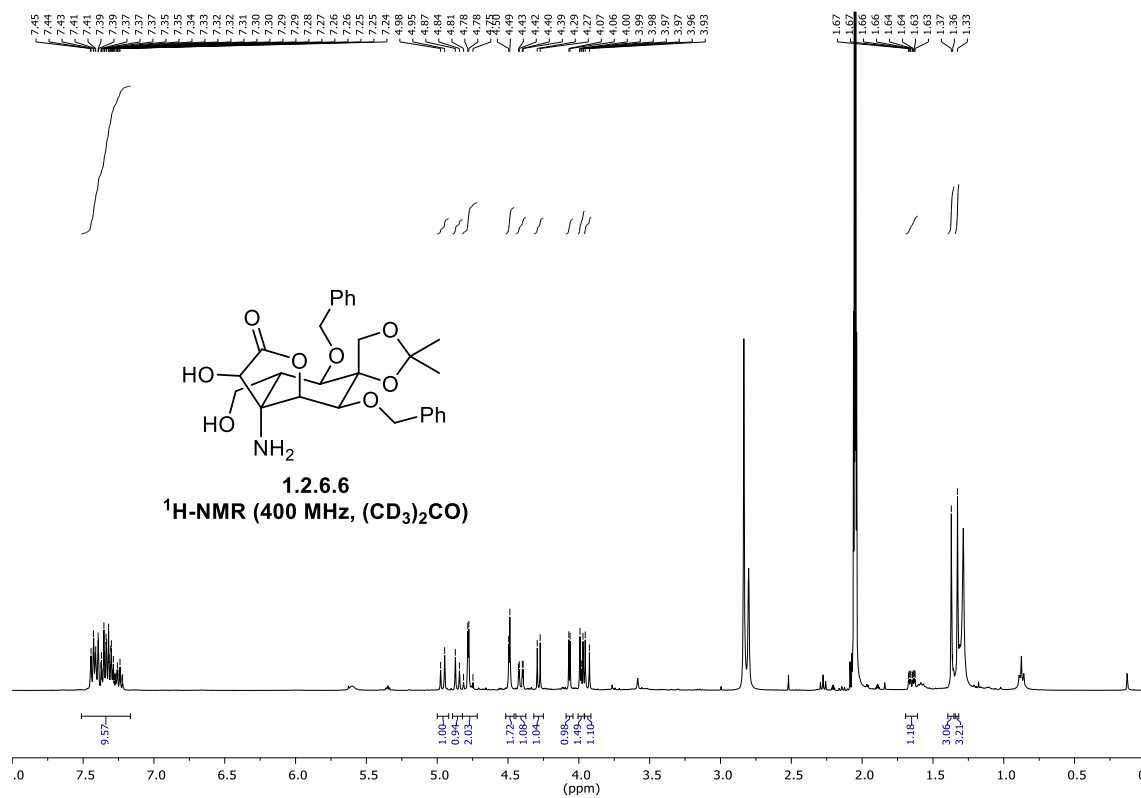
tert-butyl ((3*R*,3*aR*,4*R*,5*R*,6*S*,7*S*,7*aS*)-5,7-bis(benzyloxy)-2',2'-dimethyl-2-oxo-3-((triethylsilyl)oxy)-4-(((triethylsilyl)oxy)methyl)hexahydro-3*aH*-spiro[benzofuran-6,4'-[1,3]dioxolan]-3*a*-yl)carbamate (1.2.6.4)



(3*R*,3*aR*,4*R*,5*R*,6*S*,7*S*,7*aS*)-3*a*-amino-5,7-bis(benzyloxy)-2',2'-dimethyl-3-((triethylsilyl)oxy)-4-(((triethylsilyl)oxy)methyl)hexahydro-2*H*-spiro[benzofuran-6,4'-[1,3]dioxolan]-2-one (1.2.6.5)

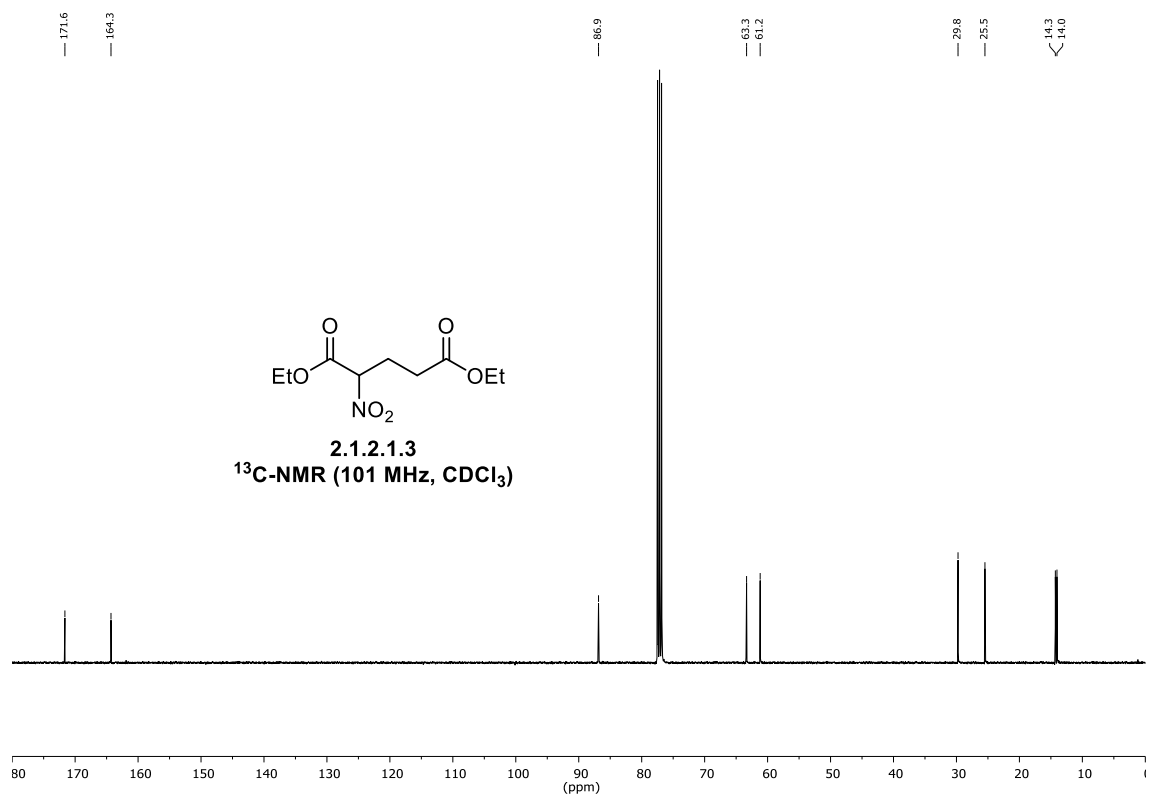
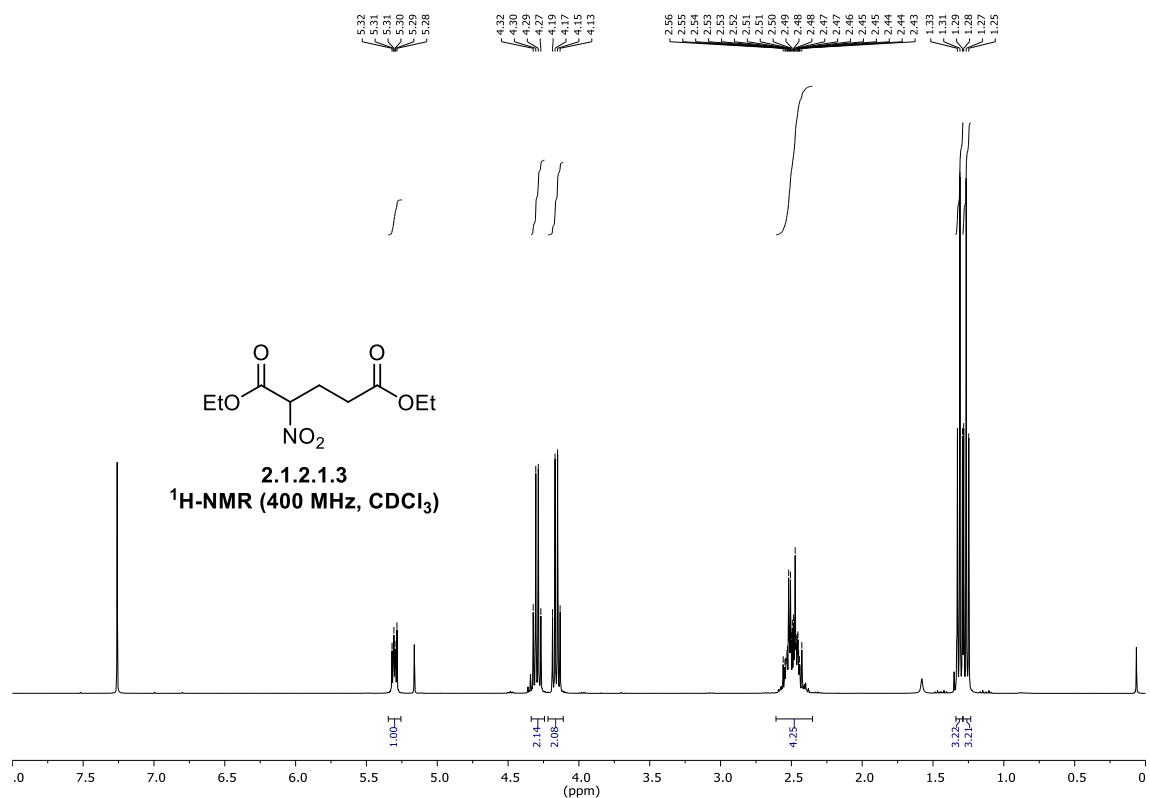


(3*R*,3*aS*,4*R*,5*R*,6*S*,7*S*,7*aS*)-3*a*-amino-5,7-bis(benzyloxy)-3-hydroxy-4-(hydroxymethyl)-2',2'-dimethylhexahydro-2*H*-spiro[benzofuran-6,4'-[1,3]dioxolan]-2-one (1.2.6.6)

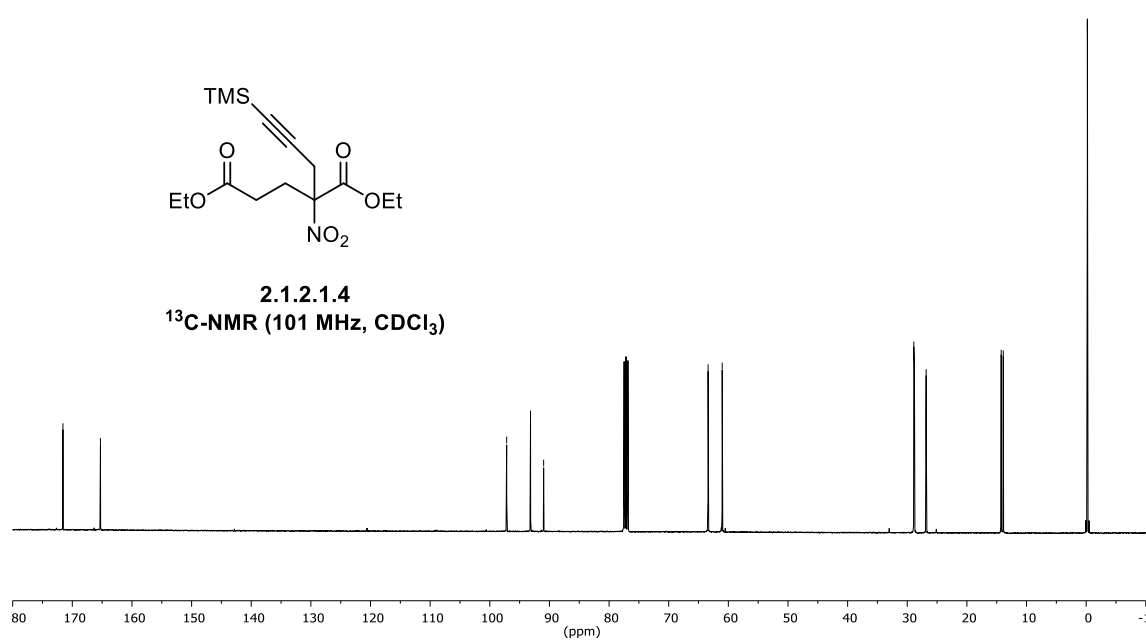
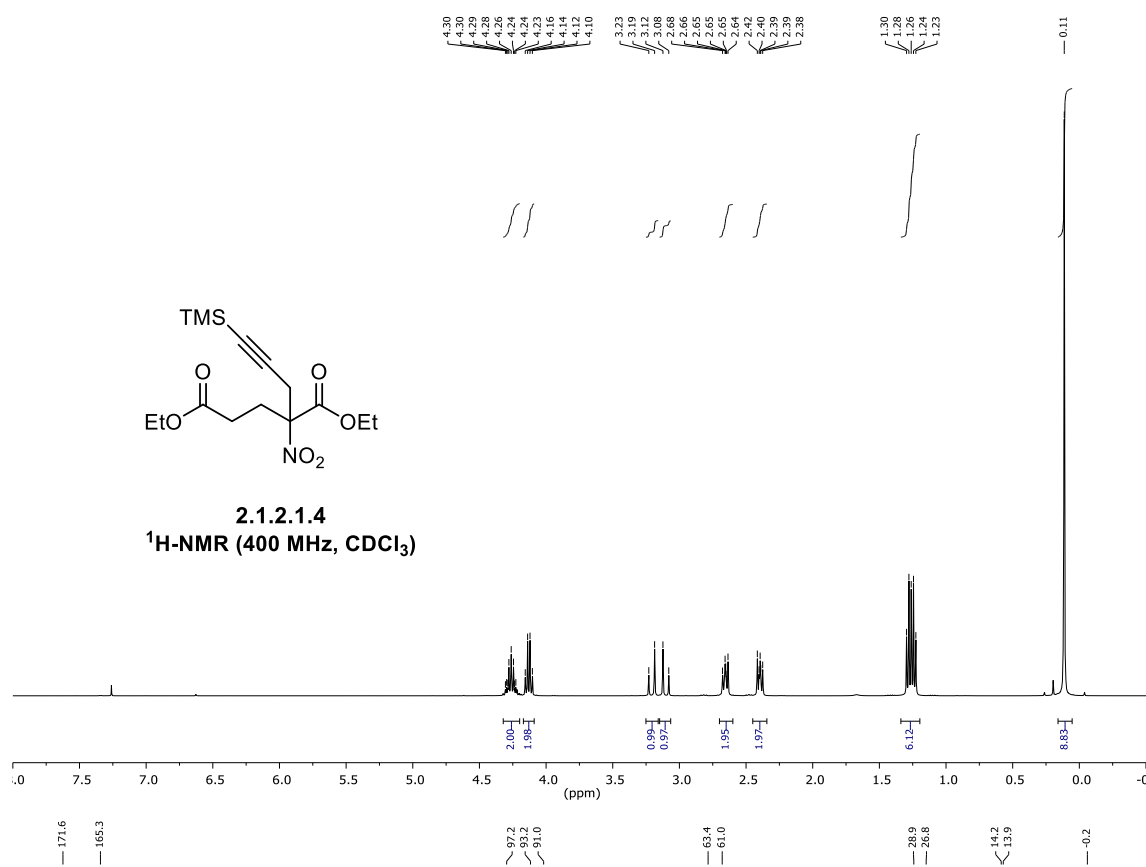


4.1.2 NMR-Spectra – Chapter 2

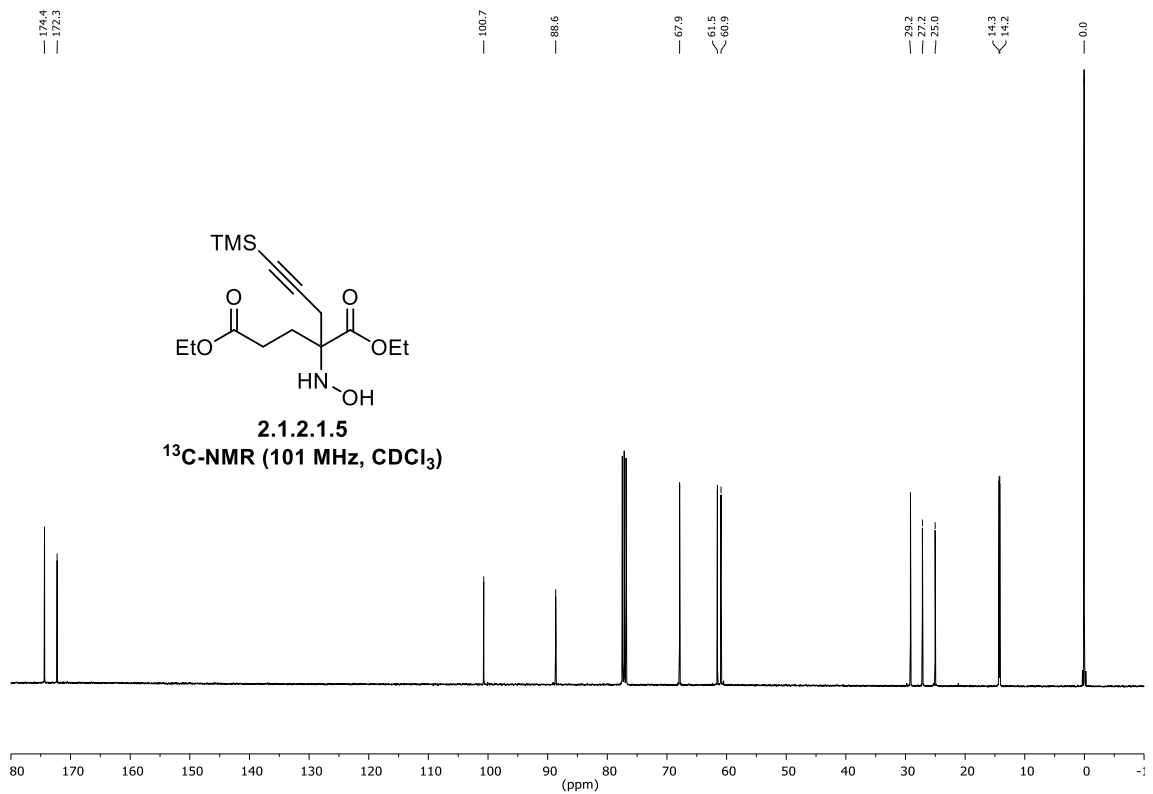
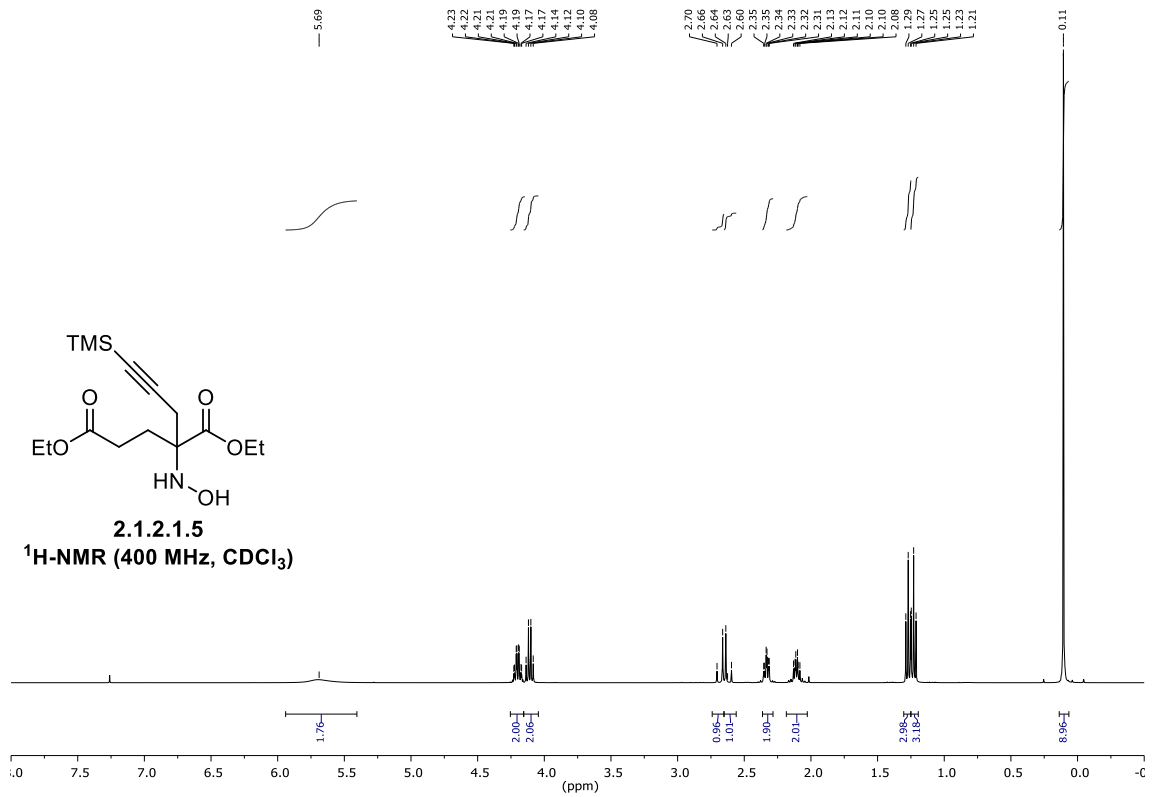
diethyl 2-nitropentanedioate (2.1.2.1.3)



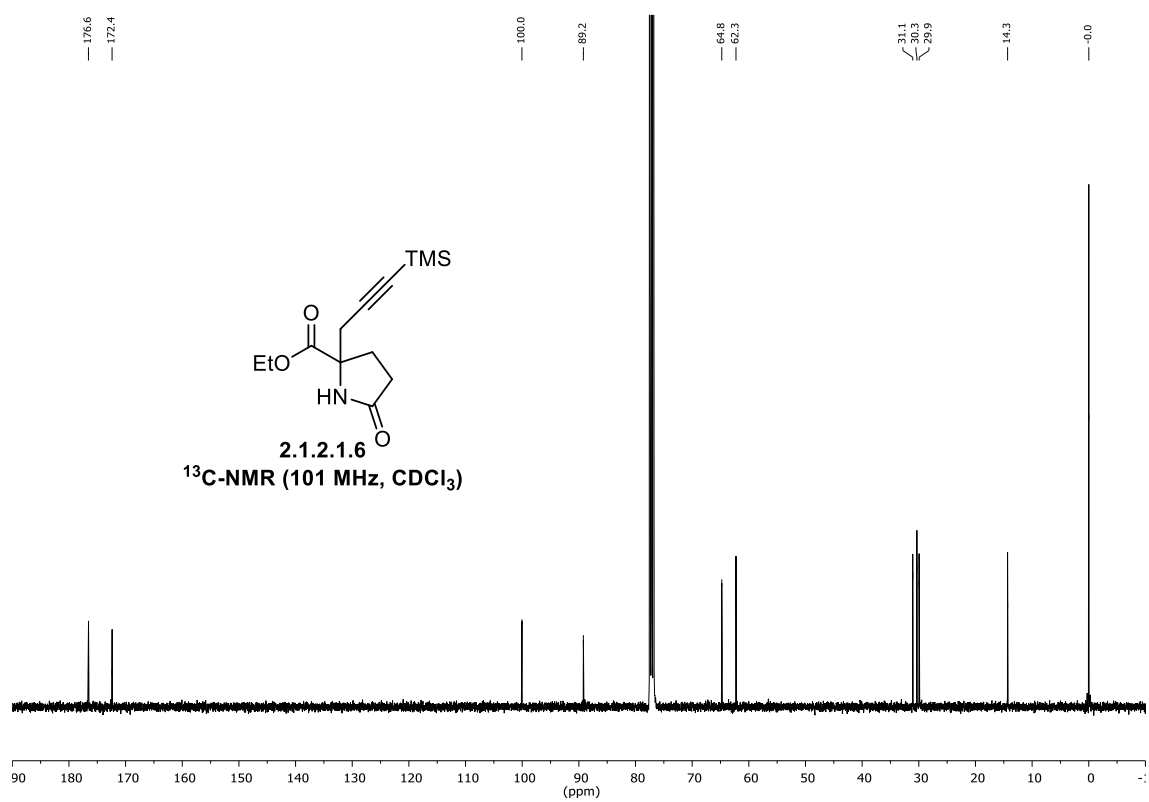
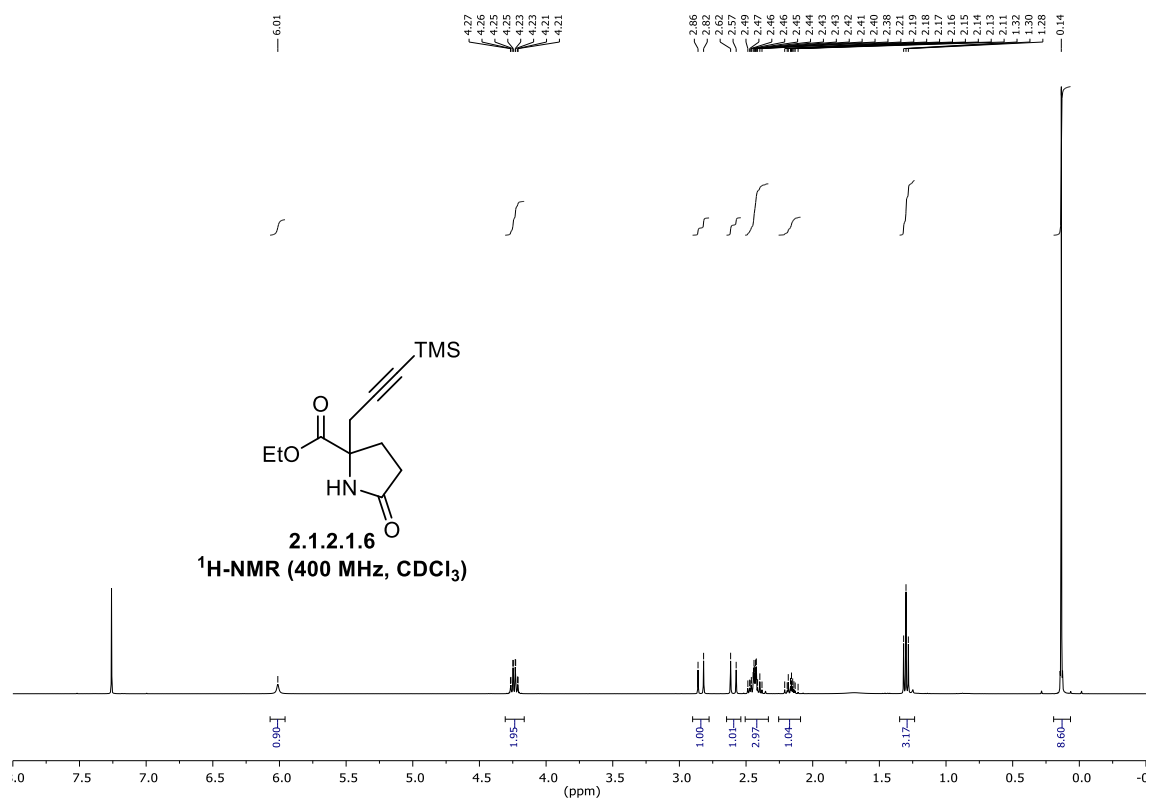
diethyl 2-nitro-2-(3-(trimethylsilyl)prop-2-yn-1-yl)pentanedioate (2.1.2.1.4)



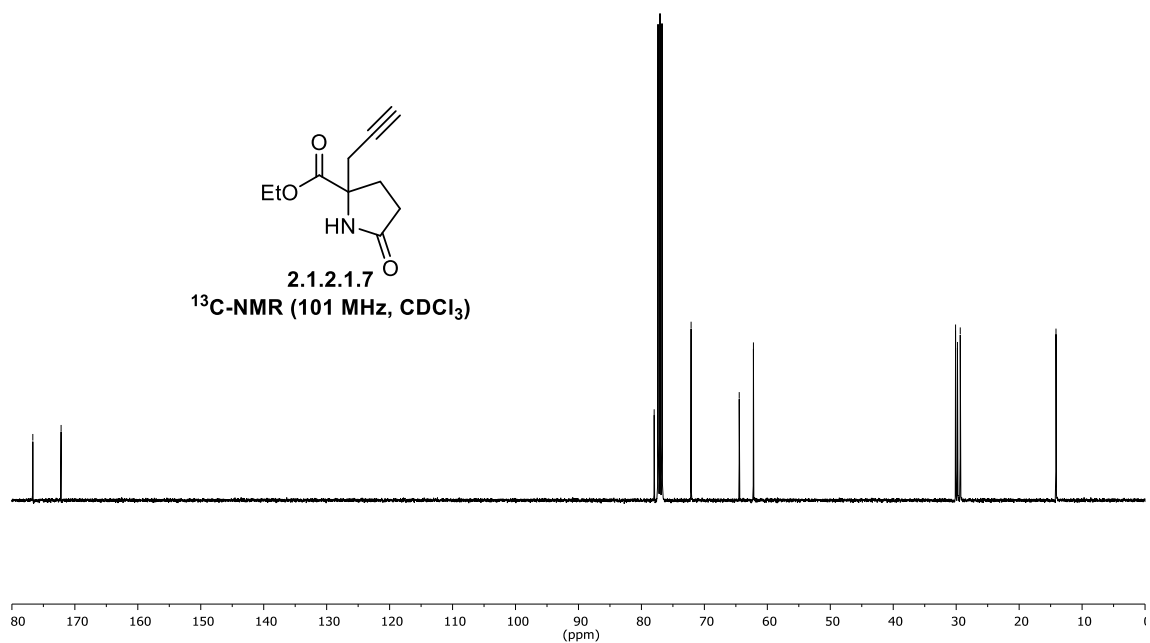
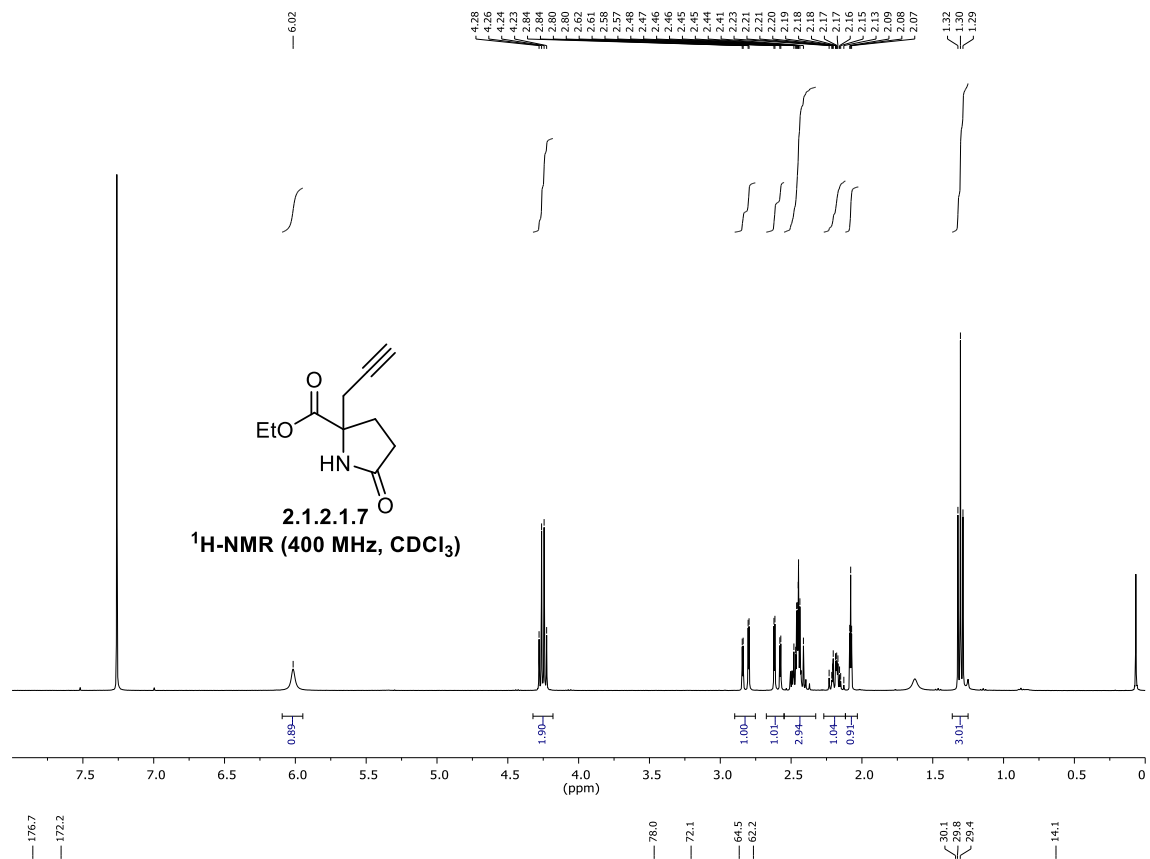
diethyl 2-(hydroxyamino)-2-(3-(trimethylsilyl)prop-2-yn-1-yl)pentanedioate (2.1.2.1.5)

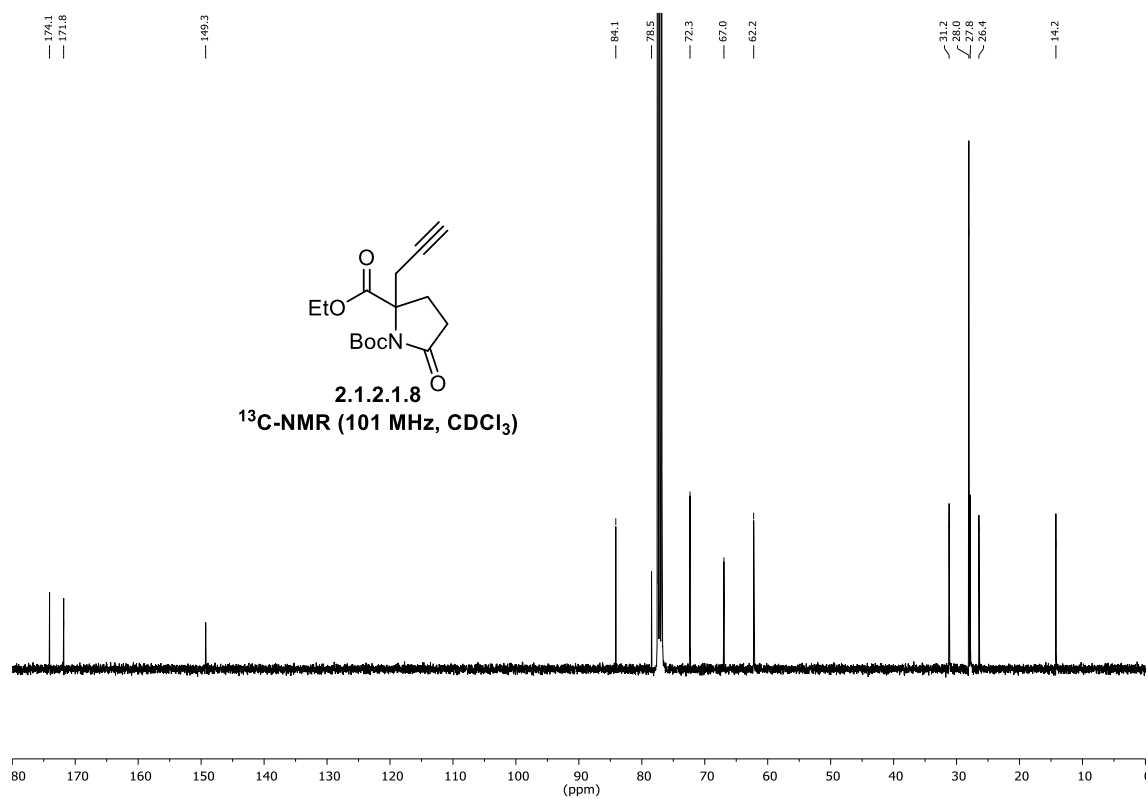
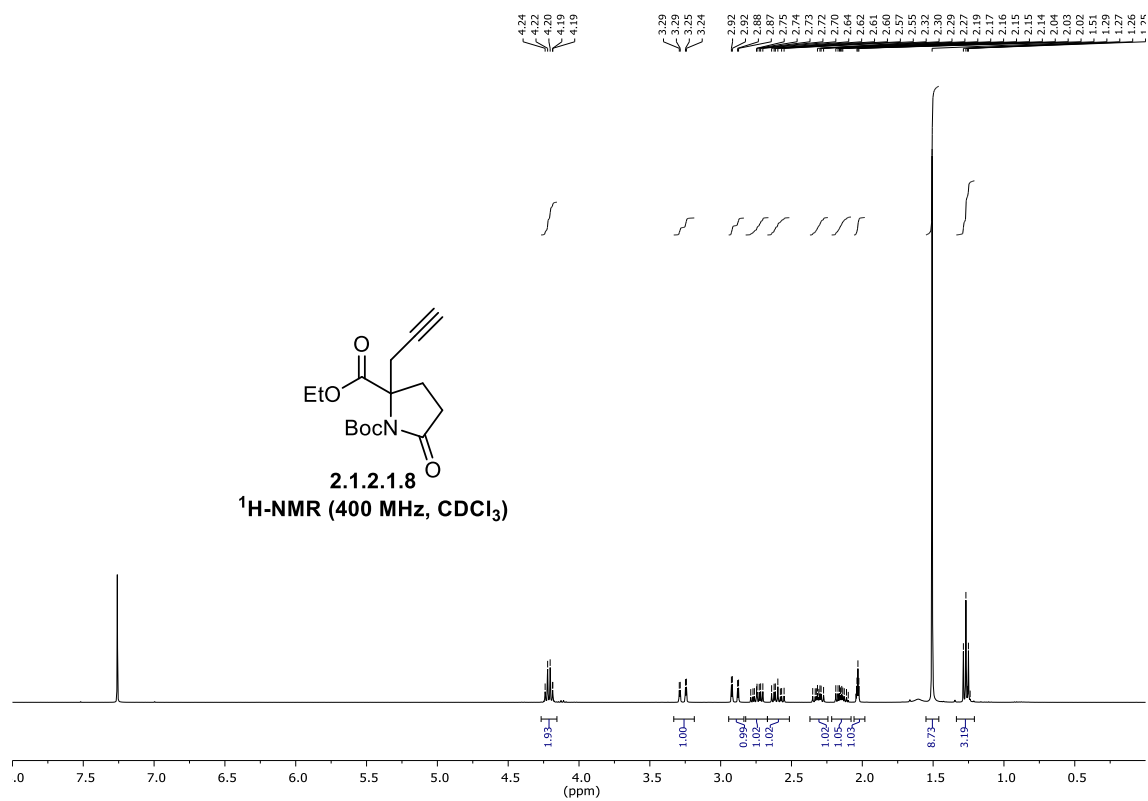


ethyl 5-oxo-2-(3-(trimethylsilyl)prop-2-yn-1-yl)pyrrolidine-2-carboxylate (2.1.2.1.6)

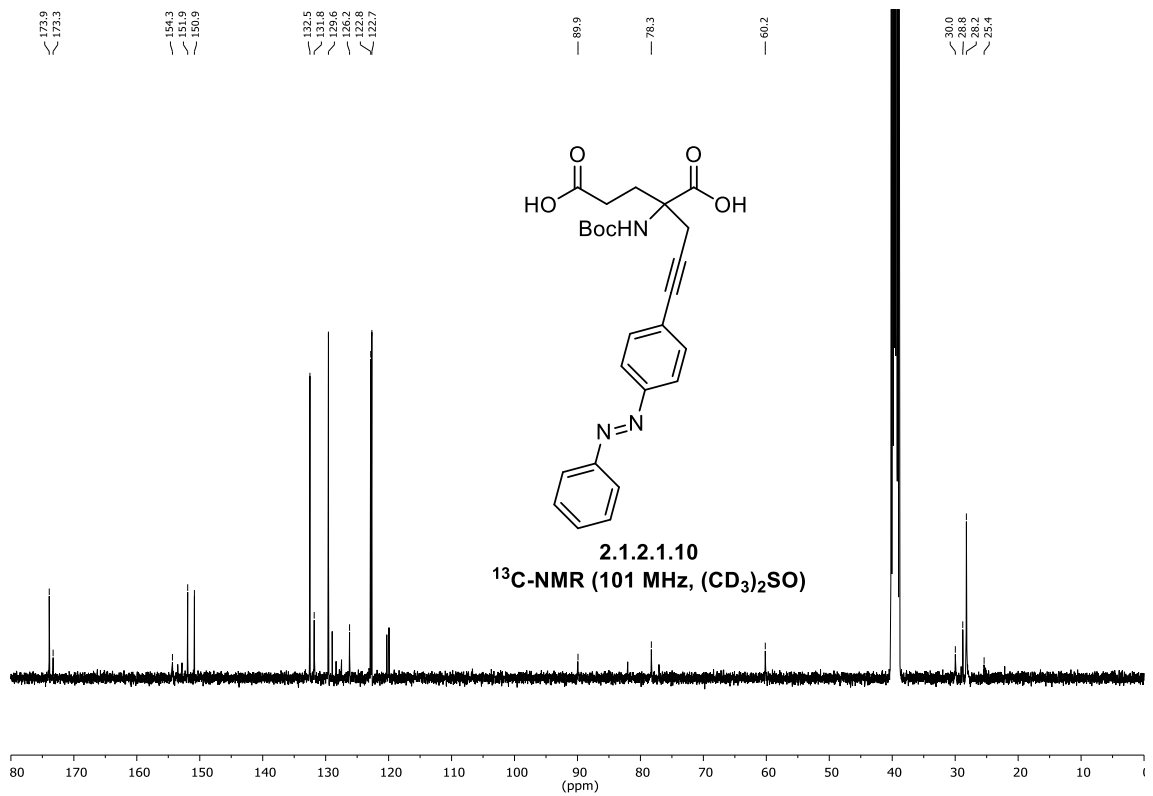
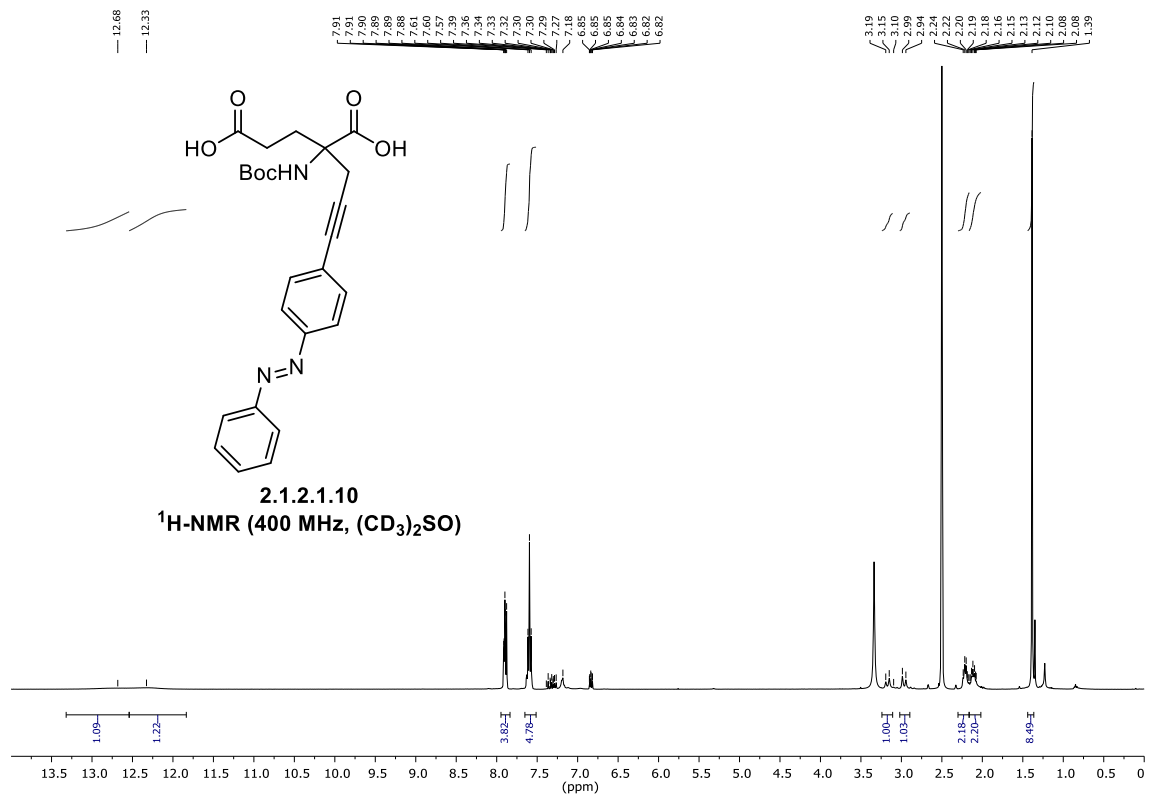


ethyl 5-oxo-2-(prop-2-yn-1-yl)pyrrolidine-2-carboxylate (2.1.2.1.7)

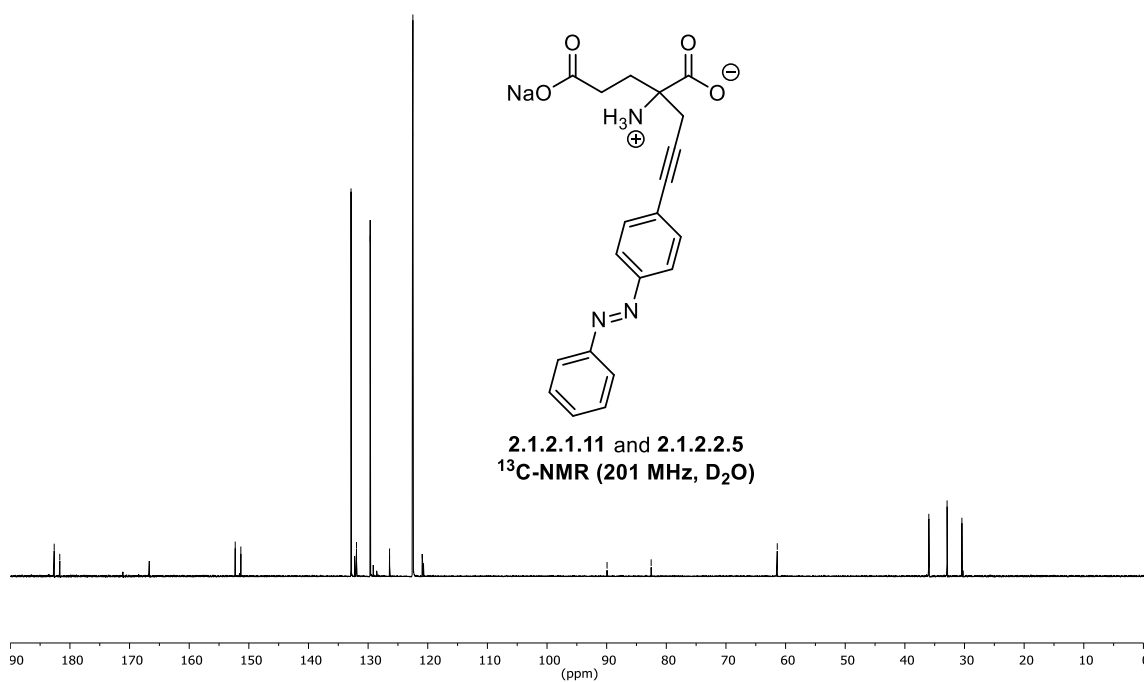
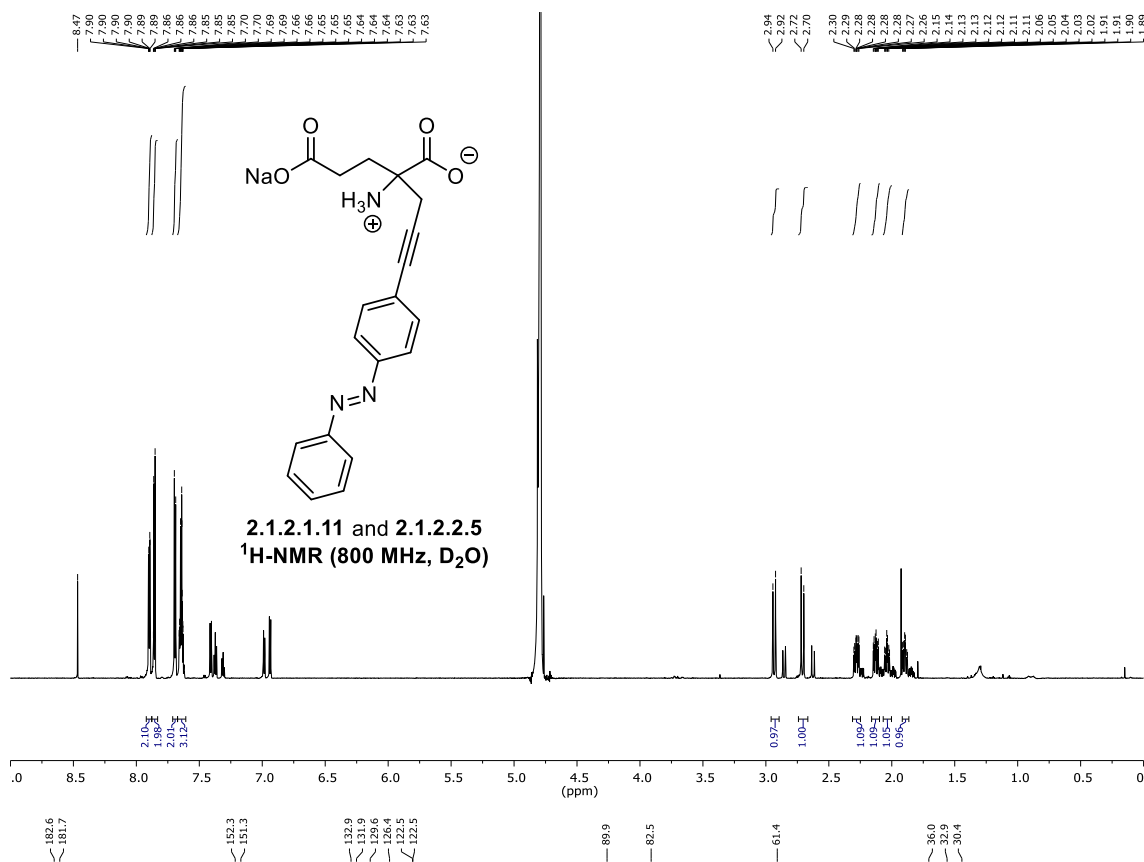


1-(*tert*-butyl) 2-ethyl 5-oxo-2-(prop-2-yn-1-yl)pyrrolidine-1,2-dicarboxylate (2.1.2.1.8)

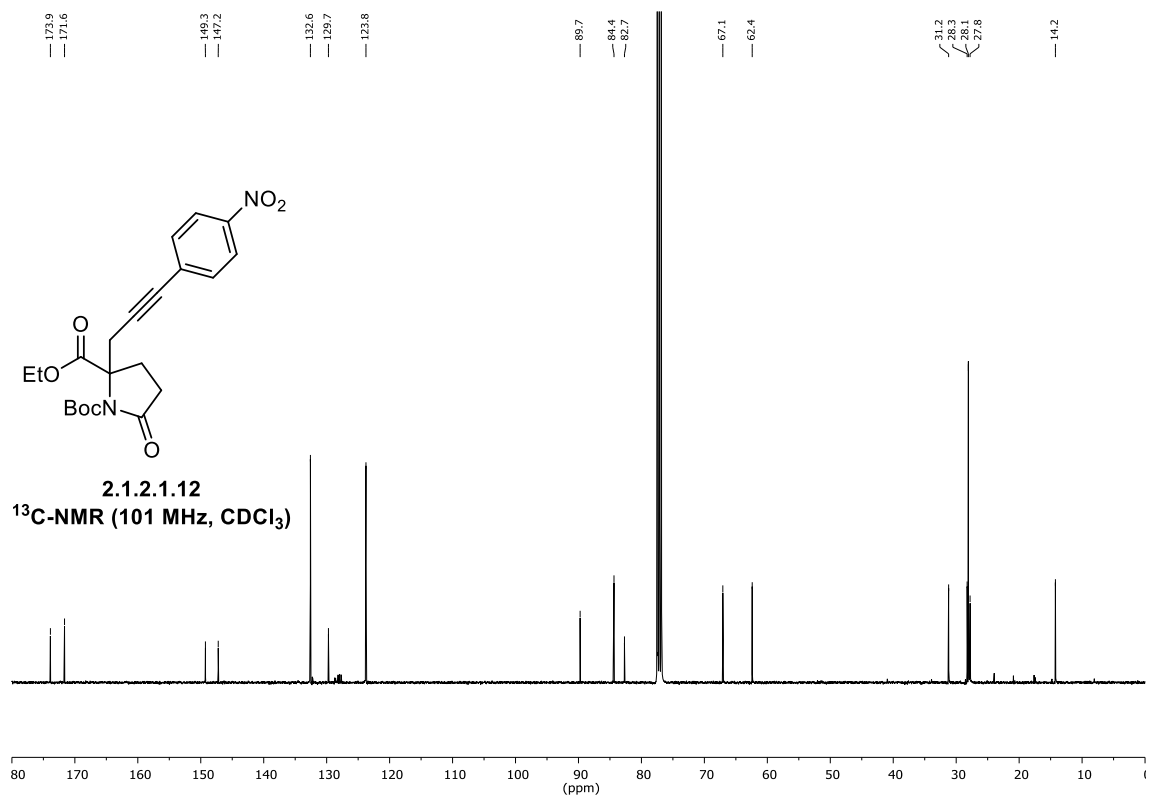
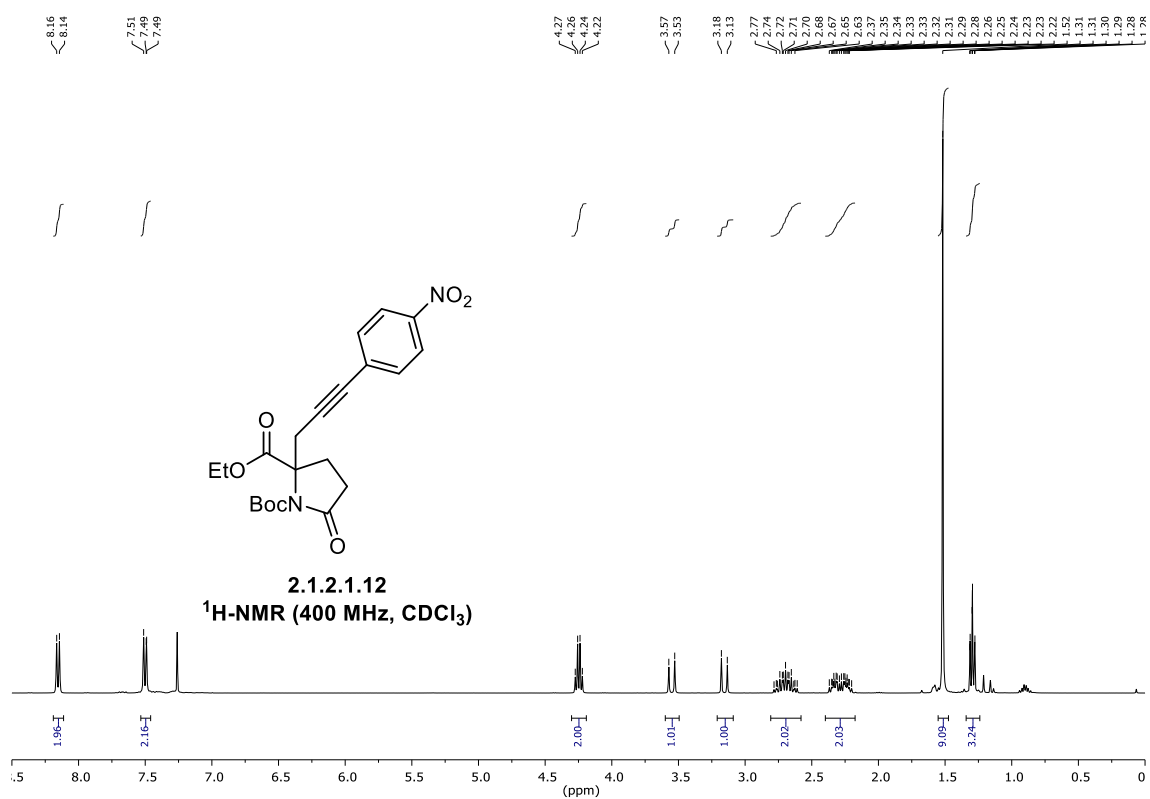
2-((*tert*-butoxycarbonyl)amino)-2-(3-(4-(phenyldiazenyl)phenyl)prop-2-yn-1-yl)pentanedioic acid (2.1.2.1.10)



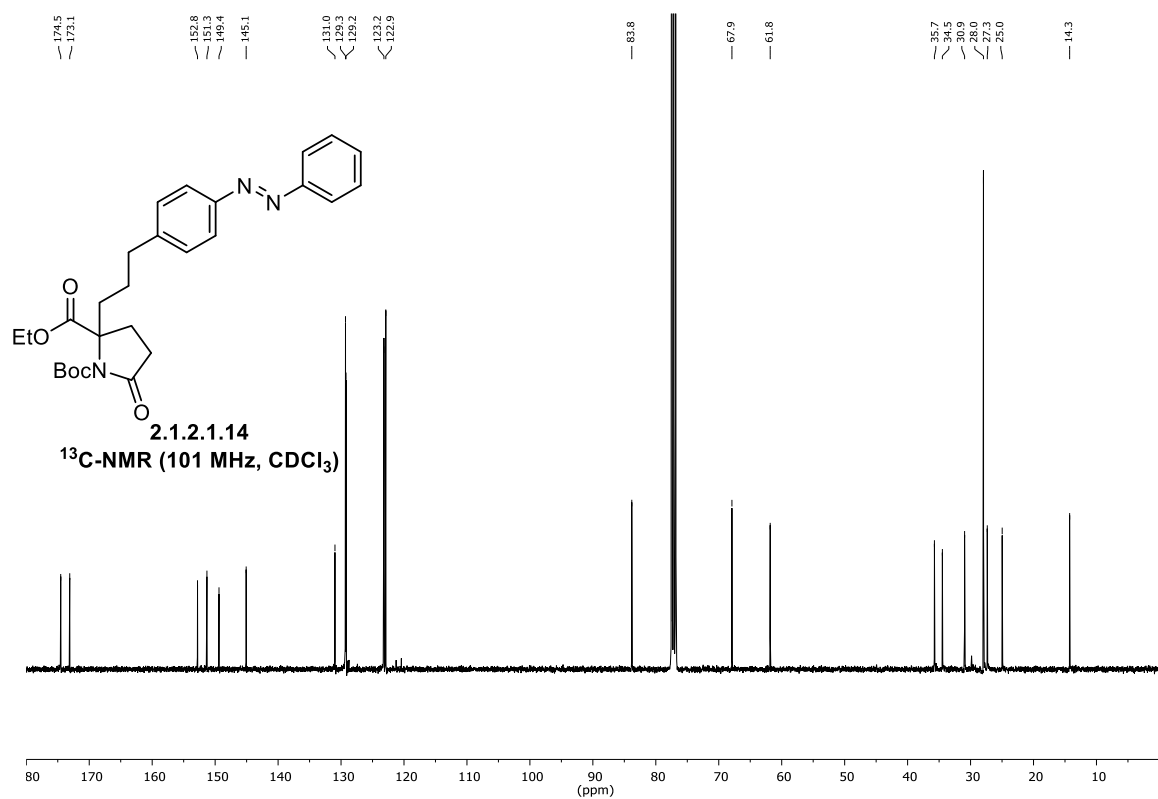
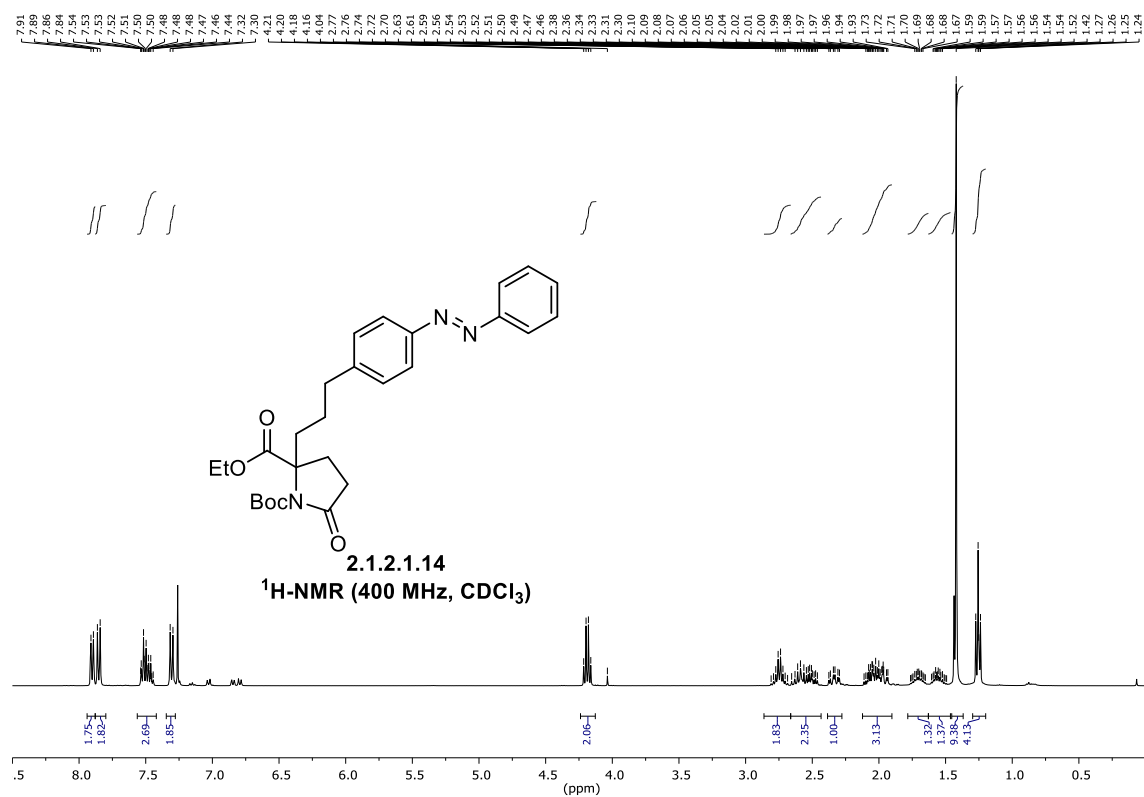
sodium 2-ammonio-2-(3-(4-(phenyldiazenyl)phenyl)prop-2-yn-1-yl)pentanedioate
(2.1.2.1.11 and 2.1.2.2.5)



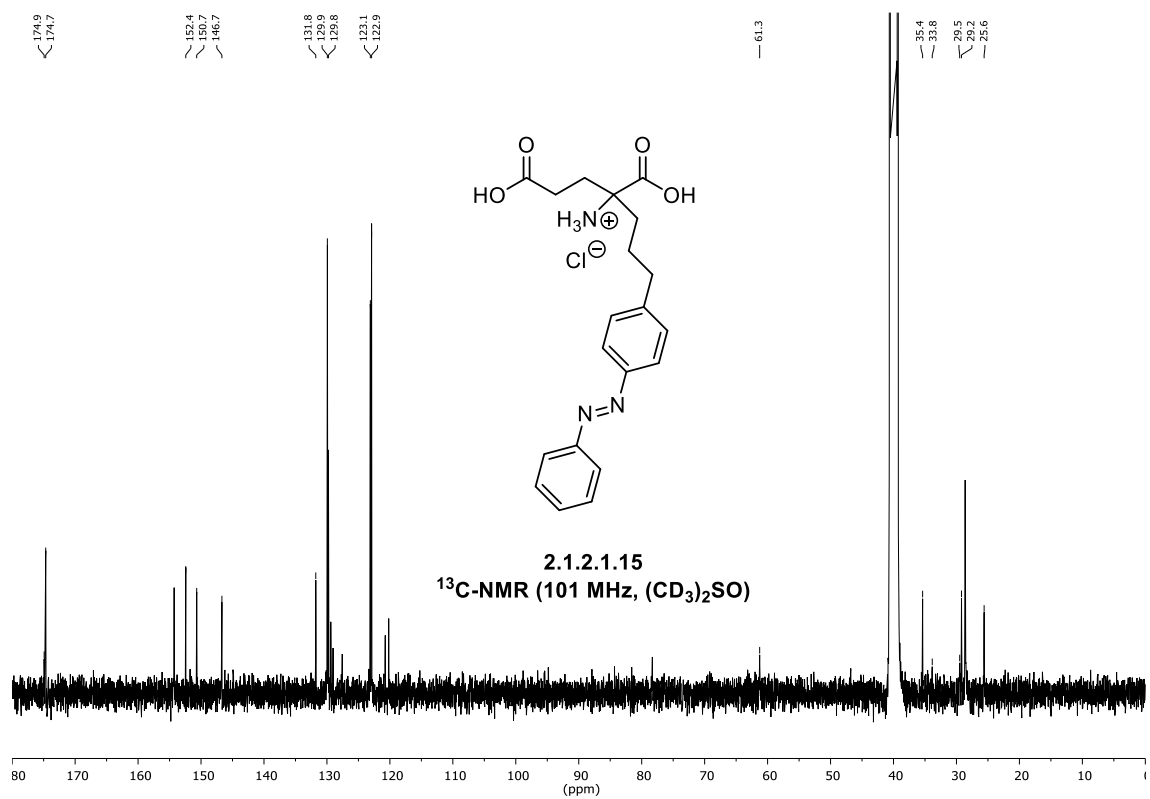
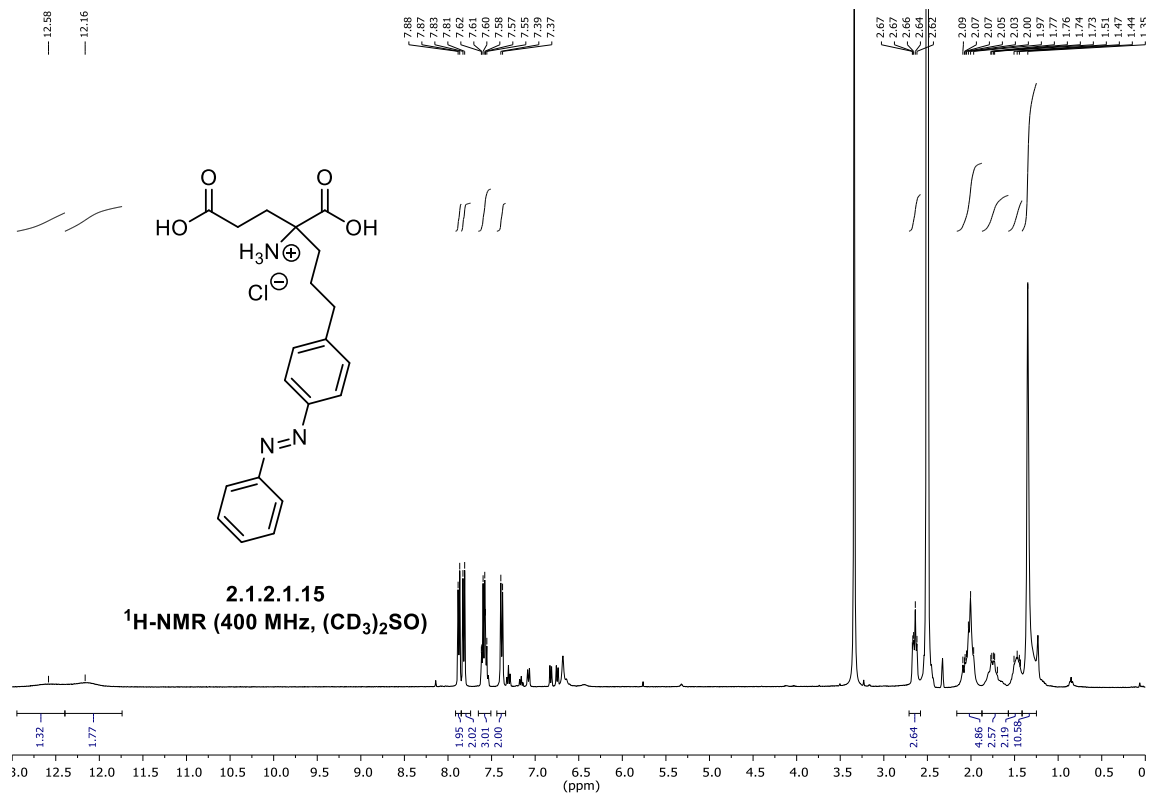
1-(*tert*-butyl) 2-ethyl 2-(3-(4-nitrophenyl)prop-2-yn-1-yl)-5-oxopyrrolidine-1,2-dicarboxylate (2.1.2.1.12)

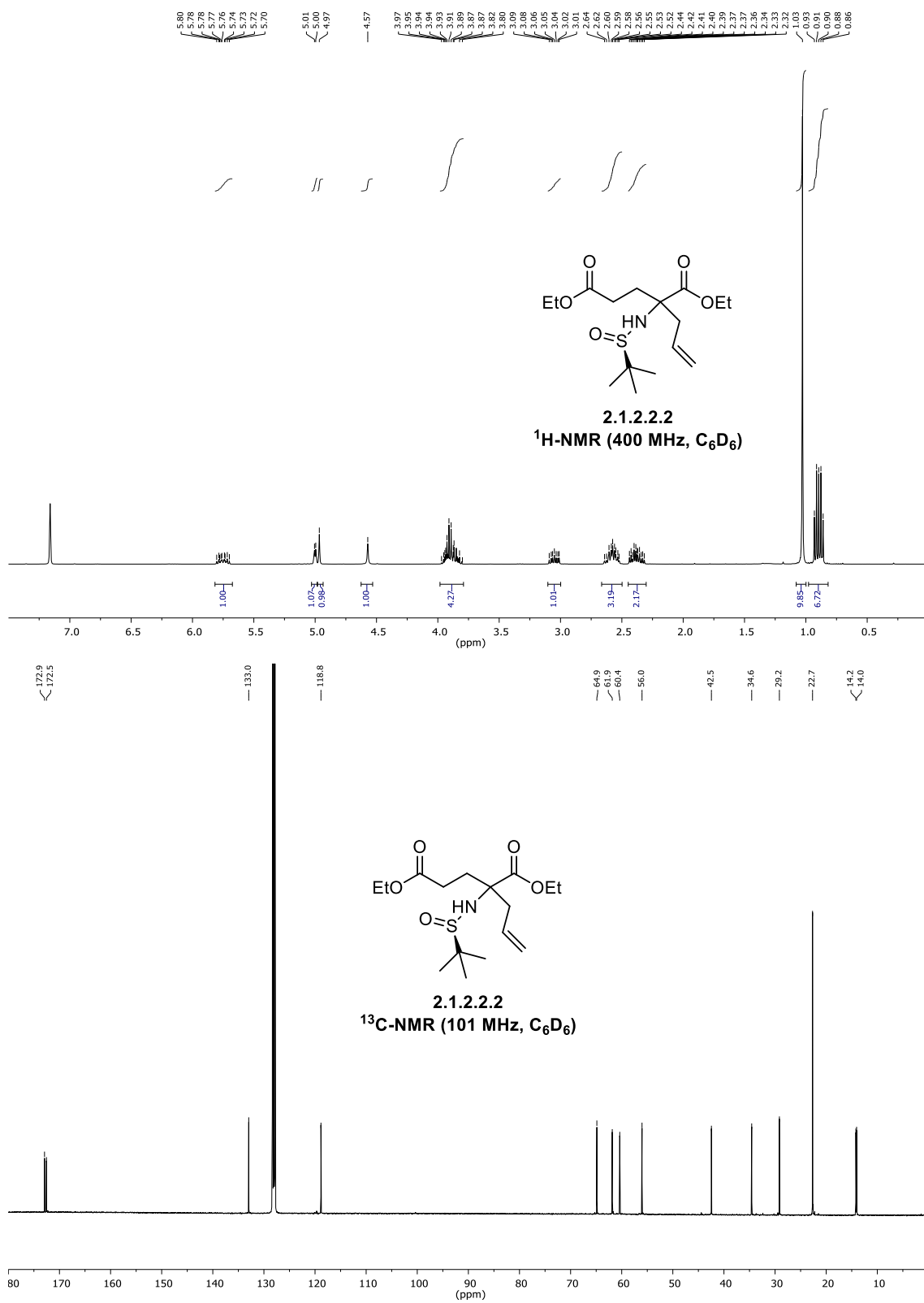


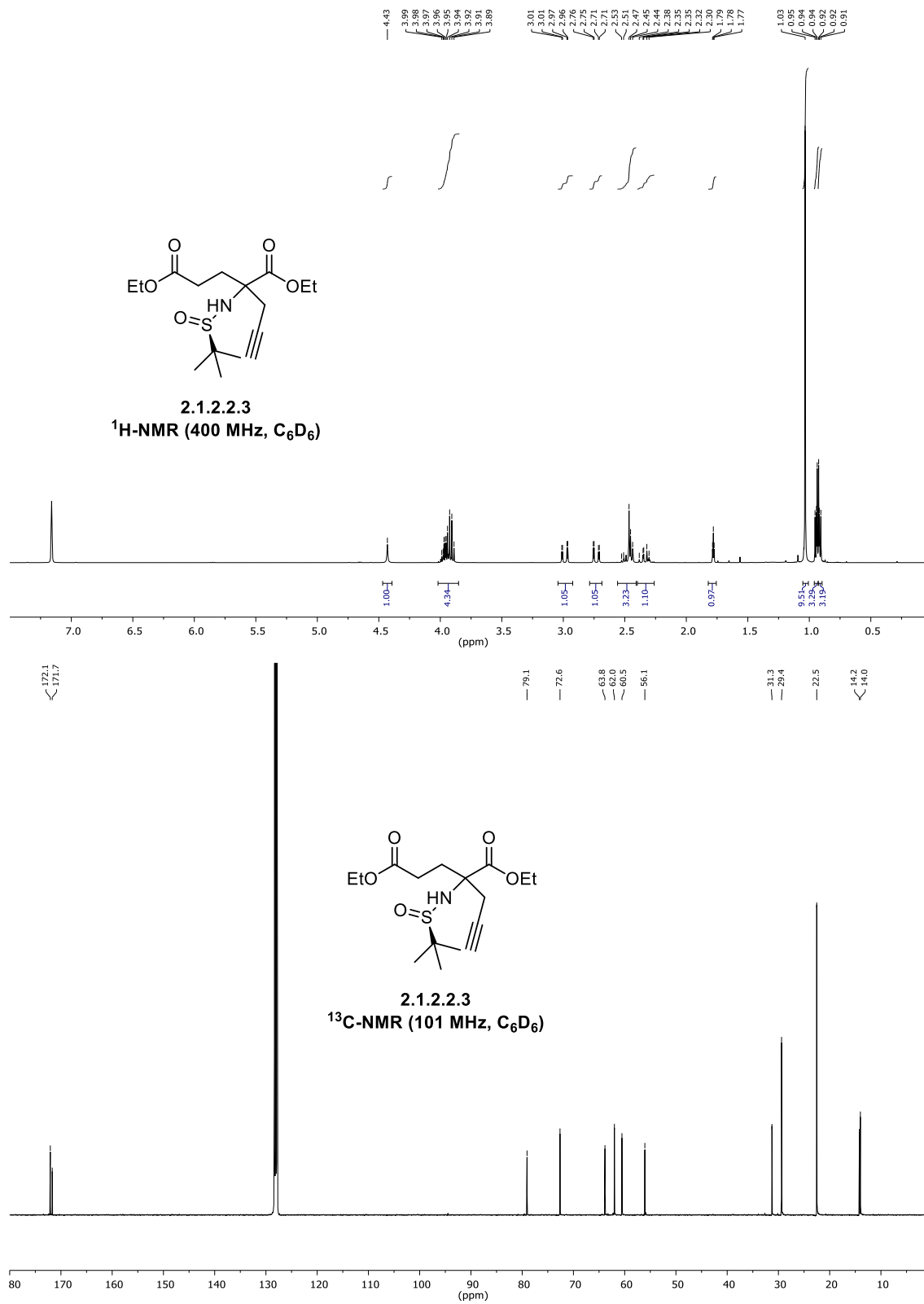
1-(*tert*-butyl) 2-ethyl-5-oxo-2-(3-(4-(phenyldiazenyl)phenyl)propyl)pyrrolidine-1,2-dicarboxylate (2.1.2.1.14)



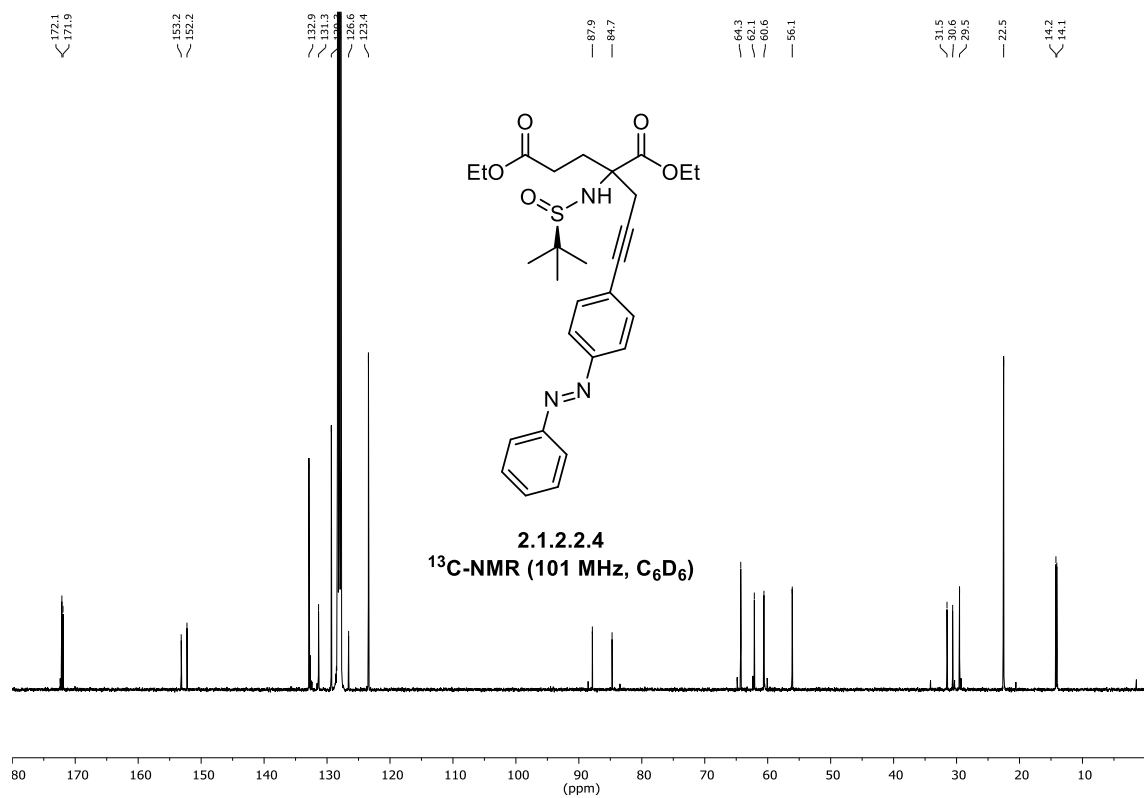
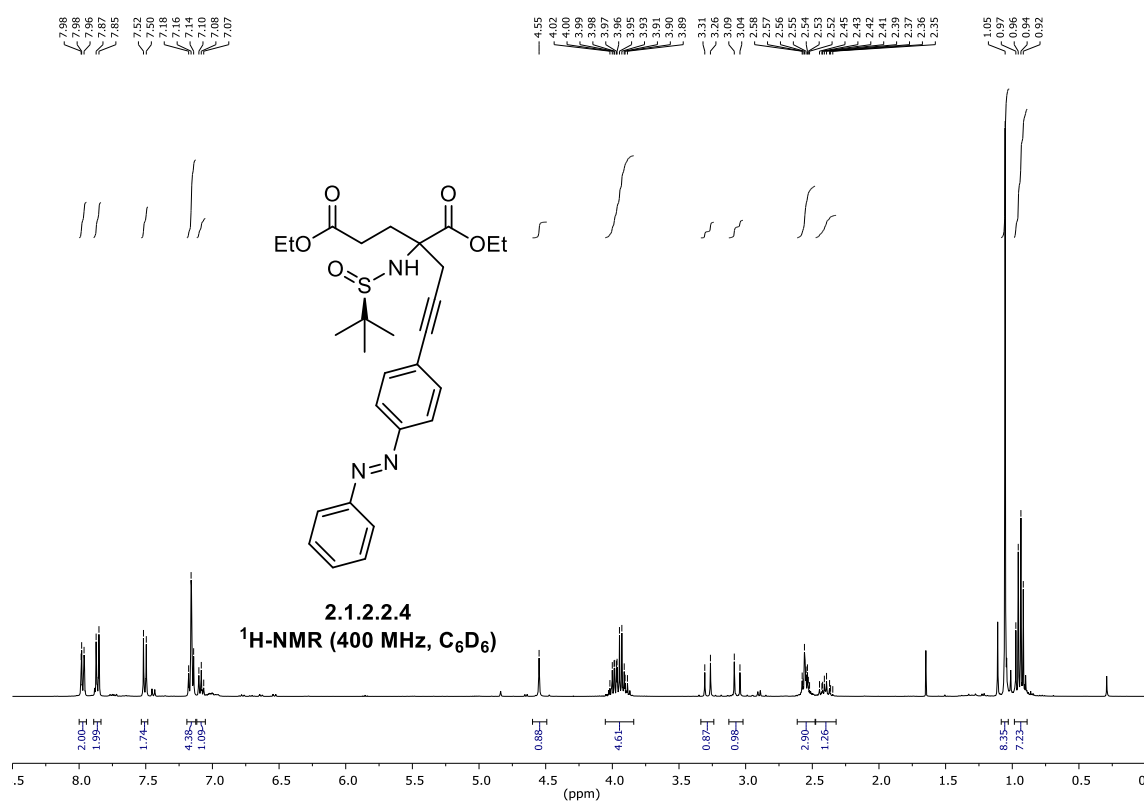
1,3-dicarboxy-6-(4-(phenyldiazenyl)phenyl)hexan-3-aminium chloride (2.1.2.1.15)



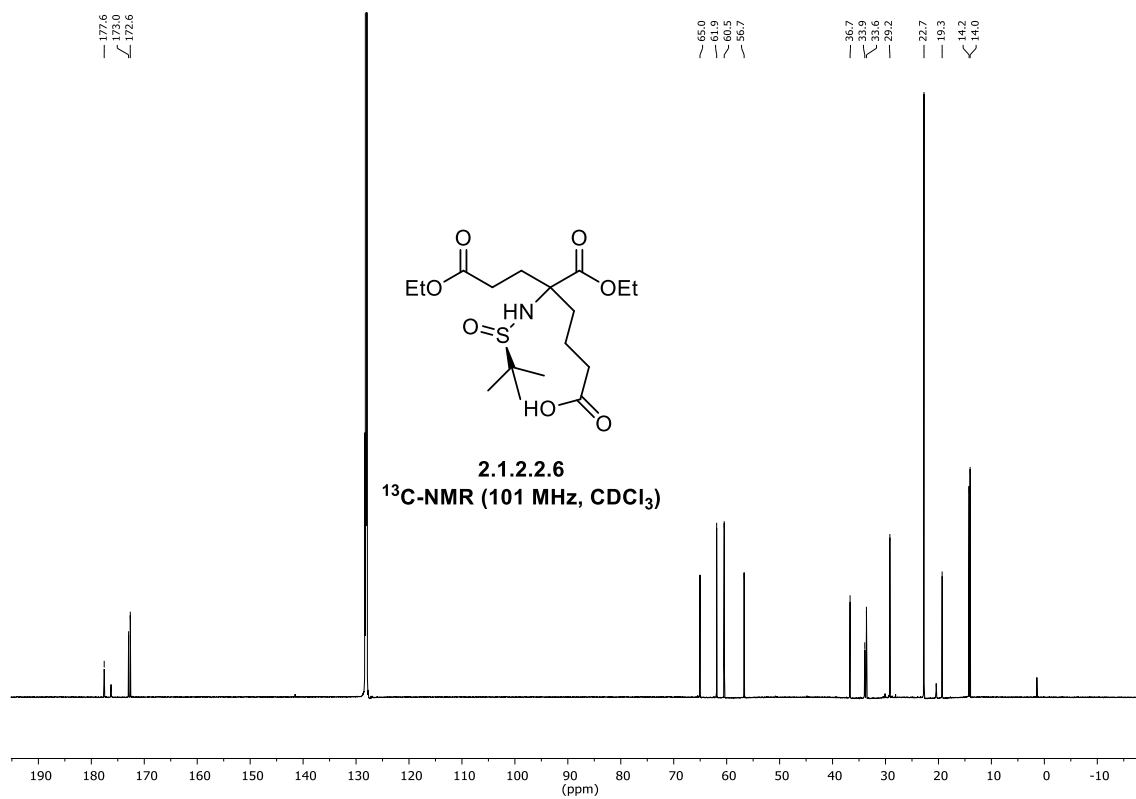
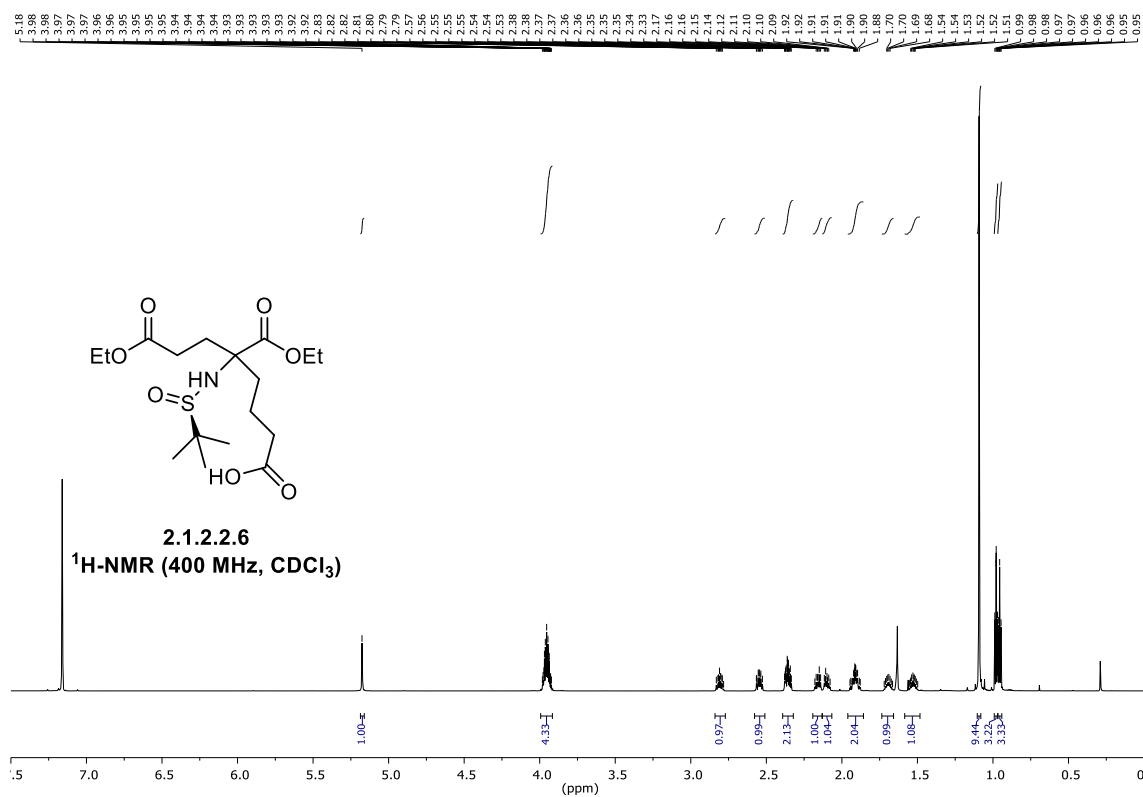
diethyl 2-allyl-2-(((*R*)-*tert*-butylsulfinyl)amino)pentanedioate (2.1.2.2.2)

diethyl 2-(((*R*)-*tert*-butylsulfinyl)amino)-2-(prop-2-yn-1-yl)pentanedioate (2.1.2.2.3)

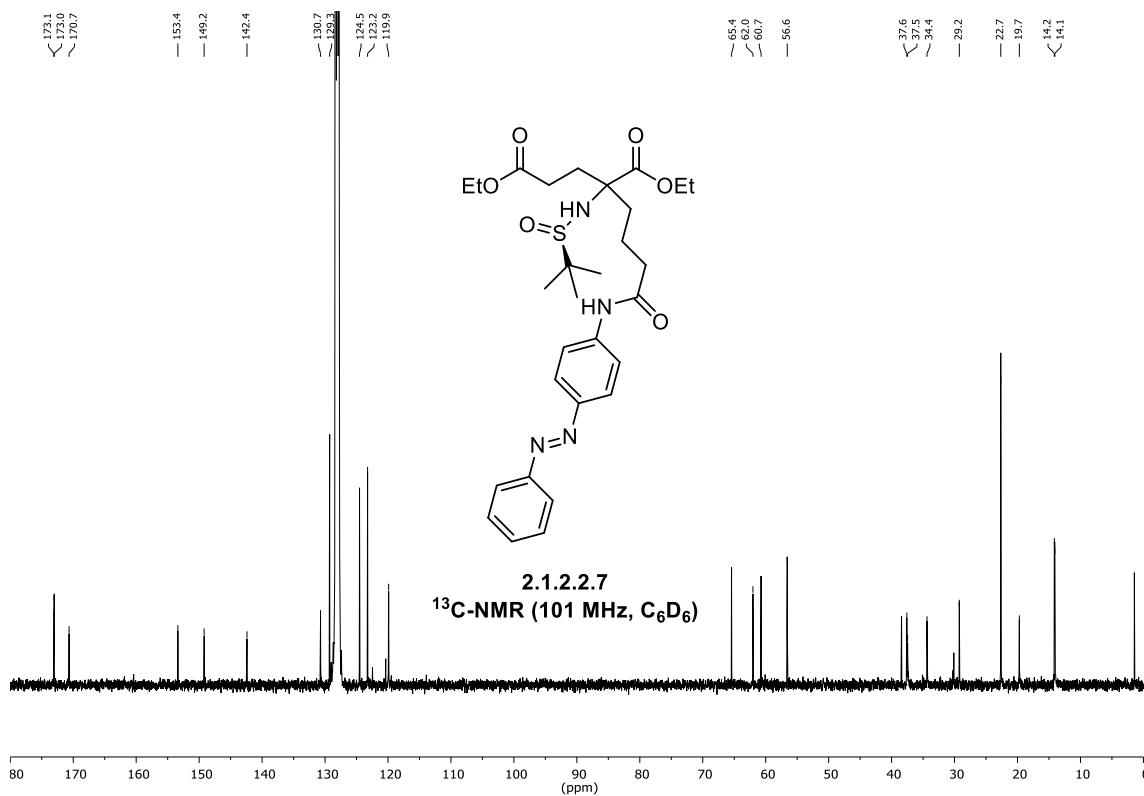
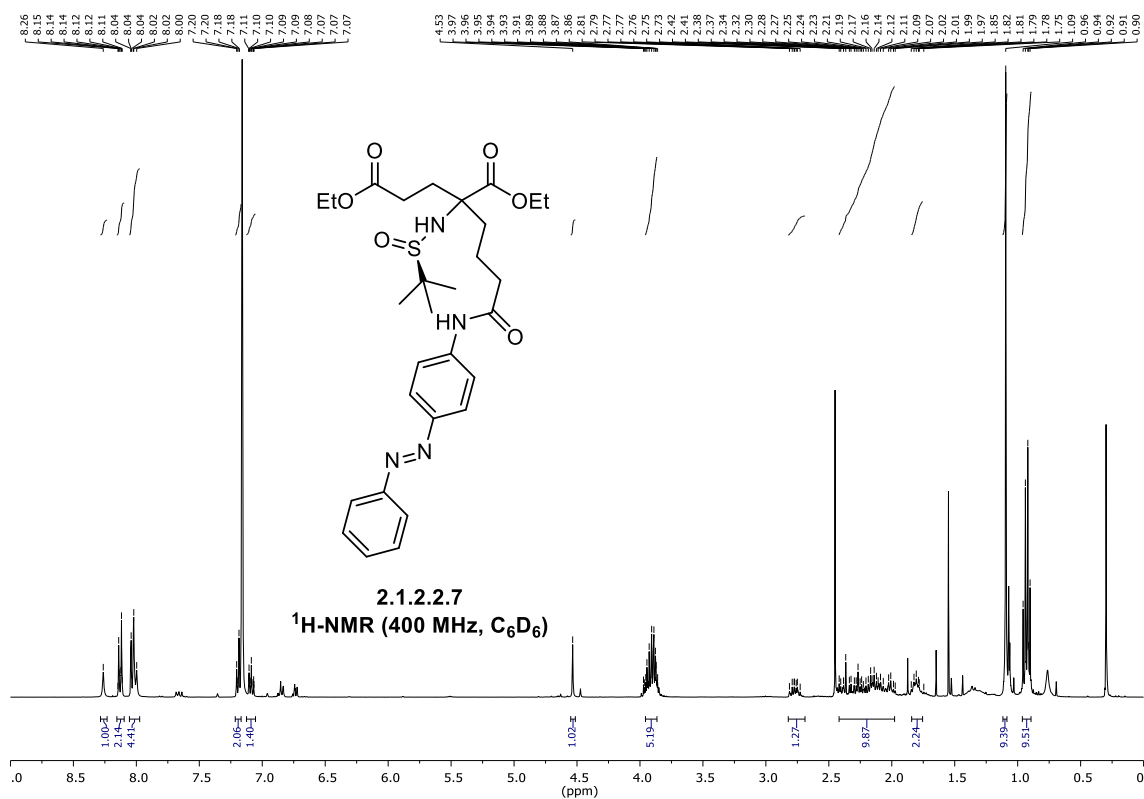
diethyl 2-(((*R*)-*tert*-butylsulfinyl)amino)-2-(3-(4-phenyldiazenyl)phenyl)prop-2-yn-1-yl)pentanedioate (2.1.2.2.4)



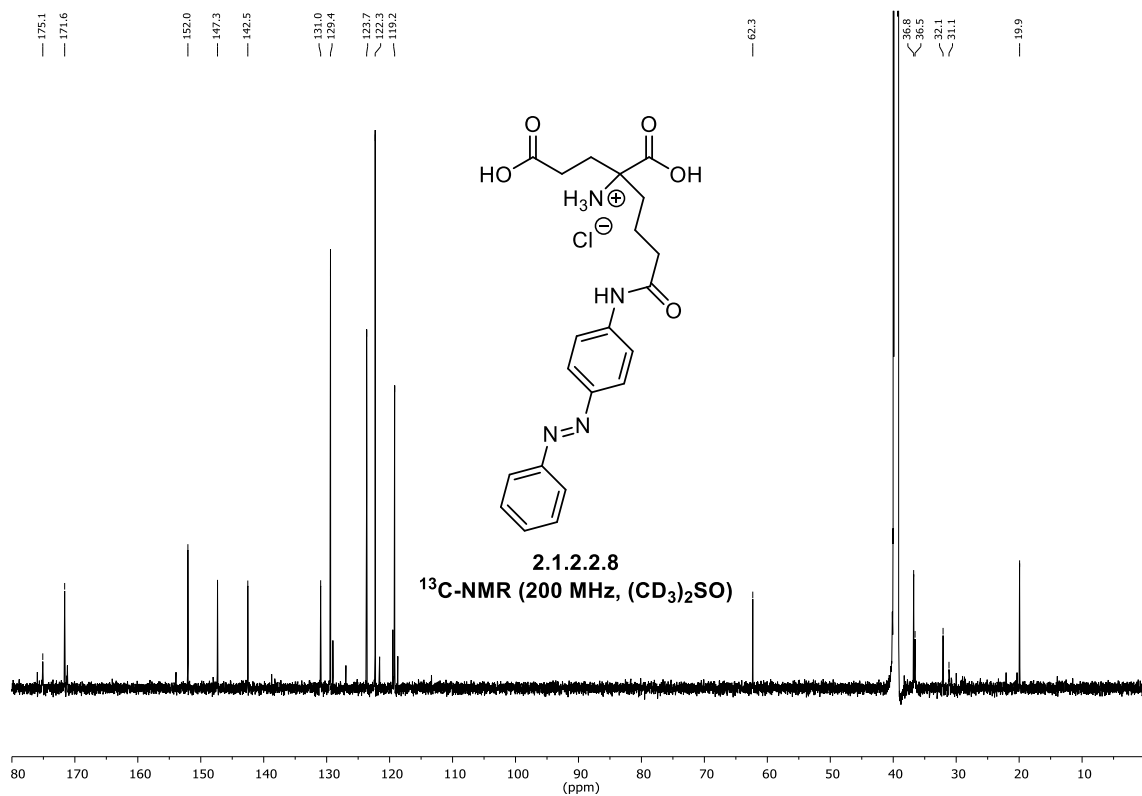
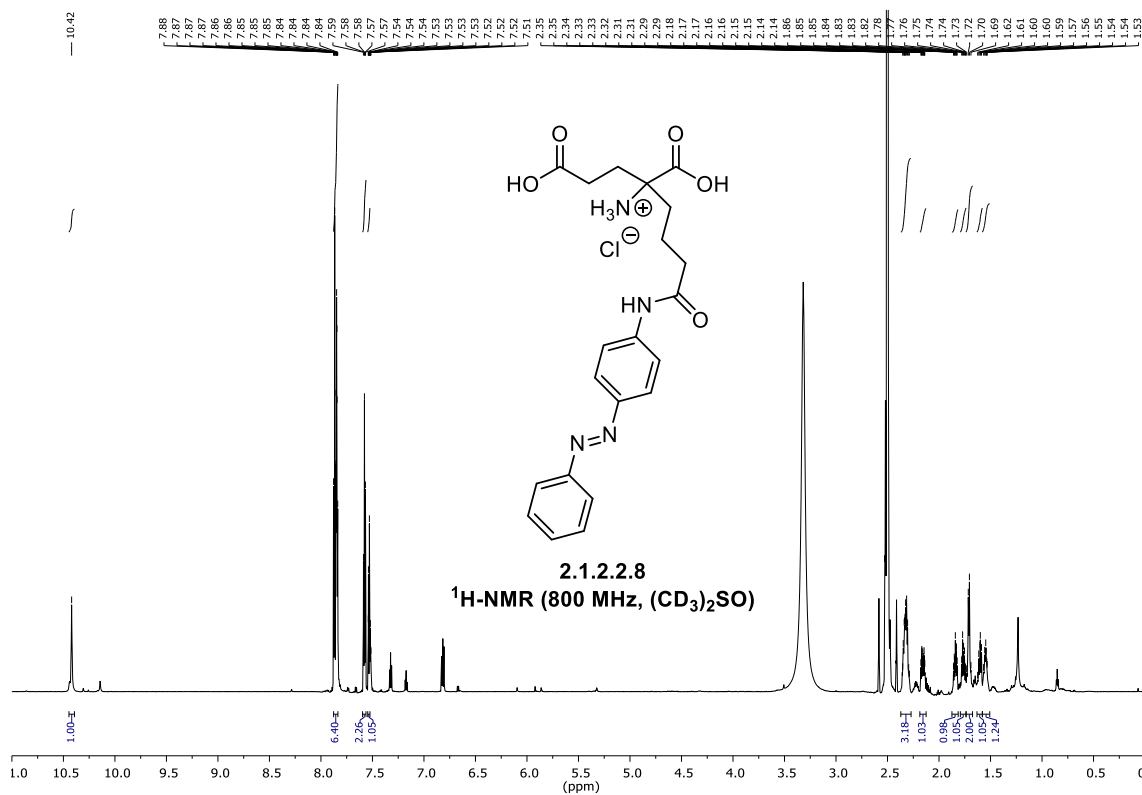
5-(((*R*)-*tert*-butylsulfinyl)amino)-8-ethoxy-5-(ethoxycarbonyl)-8-oxooctanoic acid
(2.1.2.2.6)



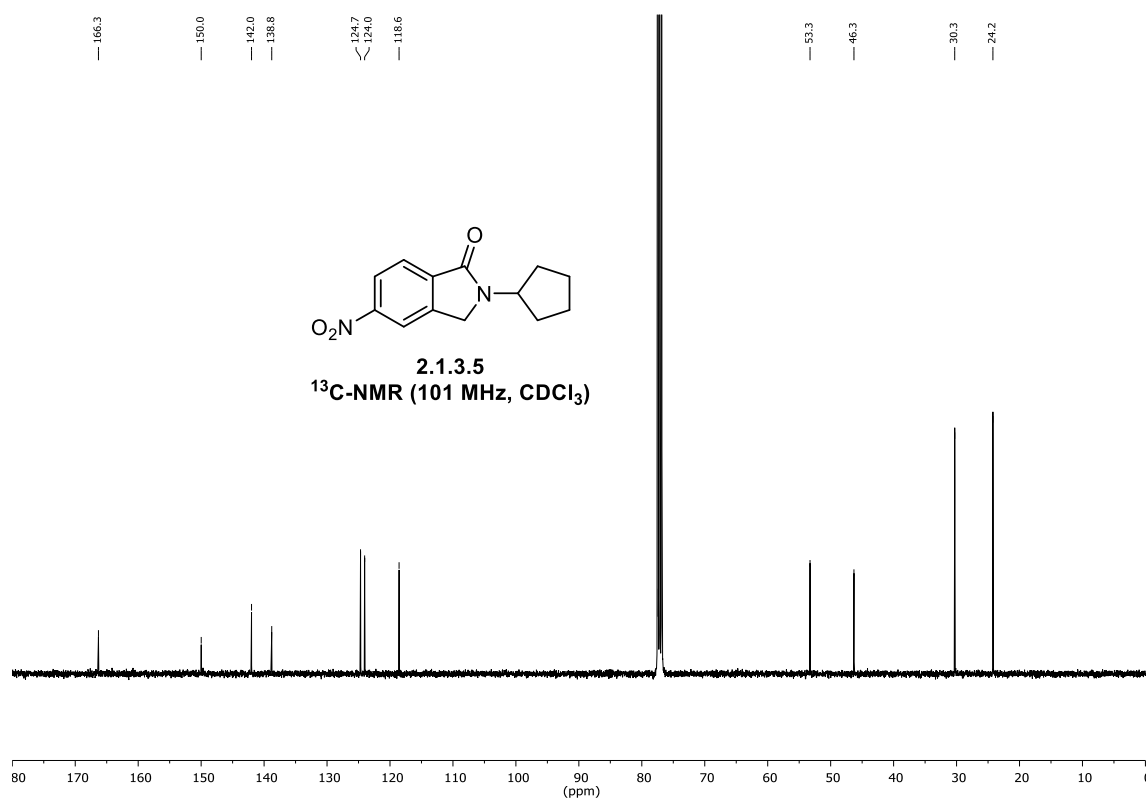
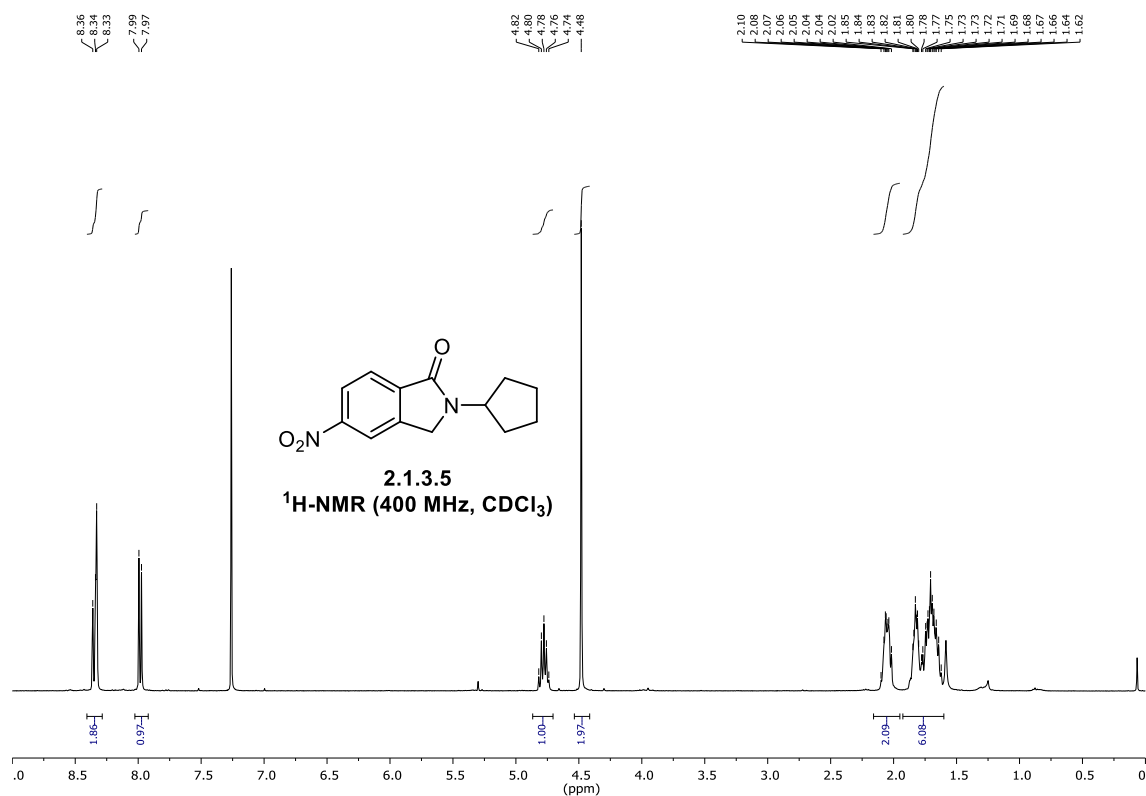
diethyl 2-(((*R*)-*tert*-butylsulfinyl)amino)-2-(4-oxo-4-((4-
 ((phenyldiazenyl)phenyl)amino)butyl)pentanedioate (2.1.2.2.7)



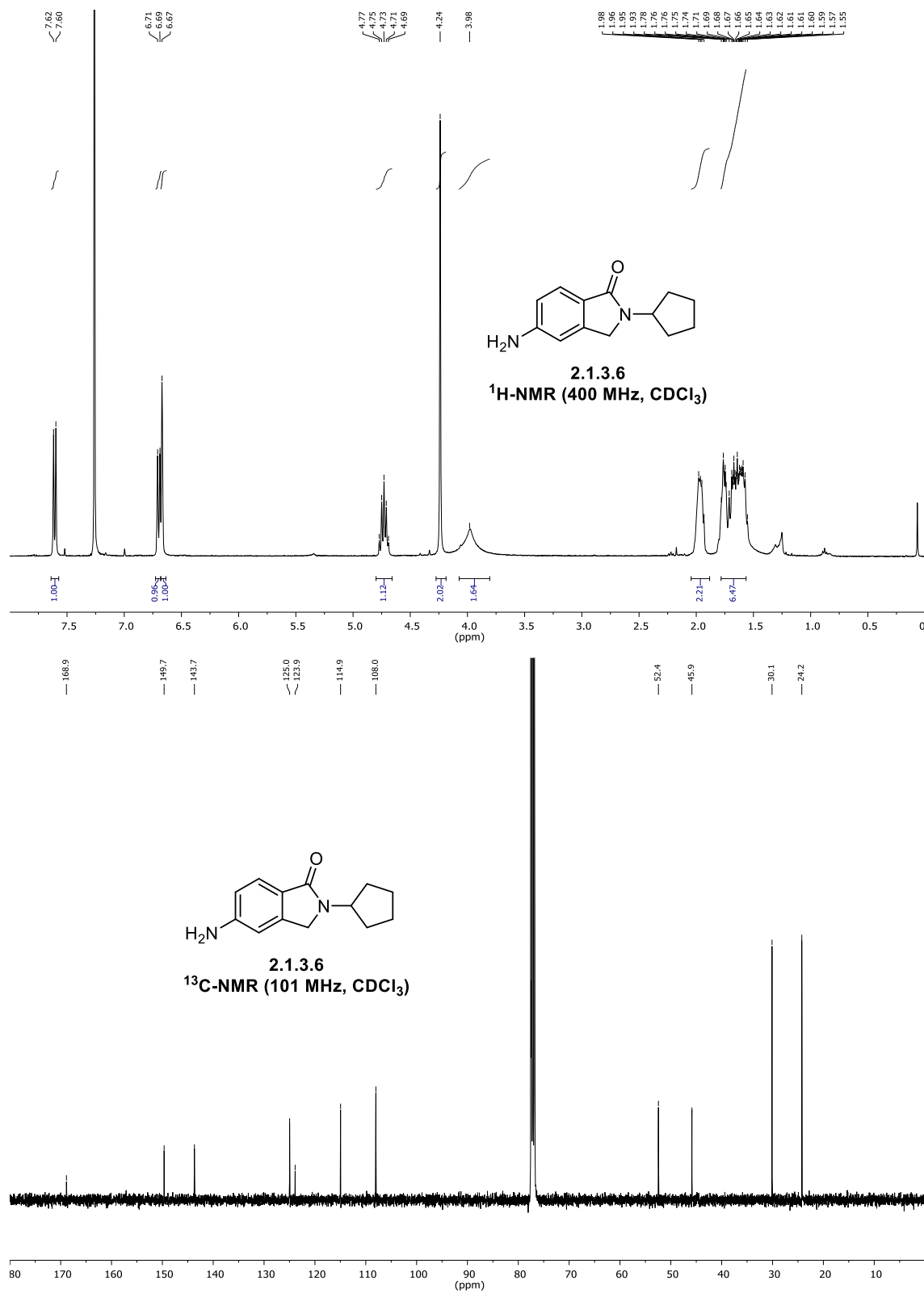
1,3-dicarboxy-7-oxo-7-((4-(phenyldiazenyl)phenyl)amino)heptan-3-aminium chloride
(2.1.2.2.8)



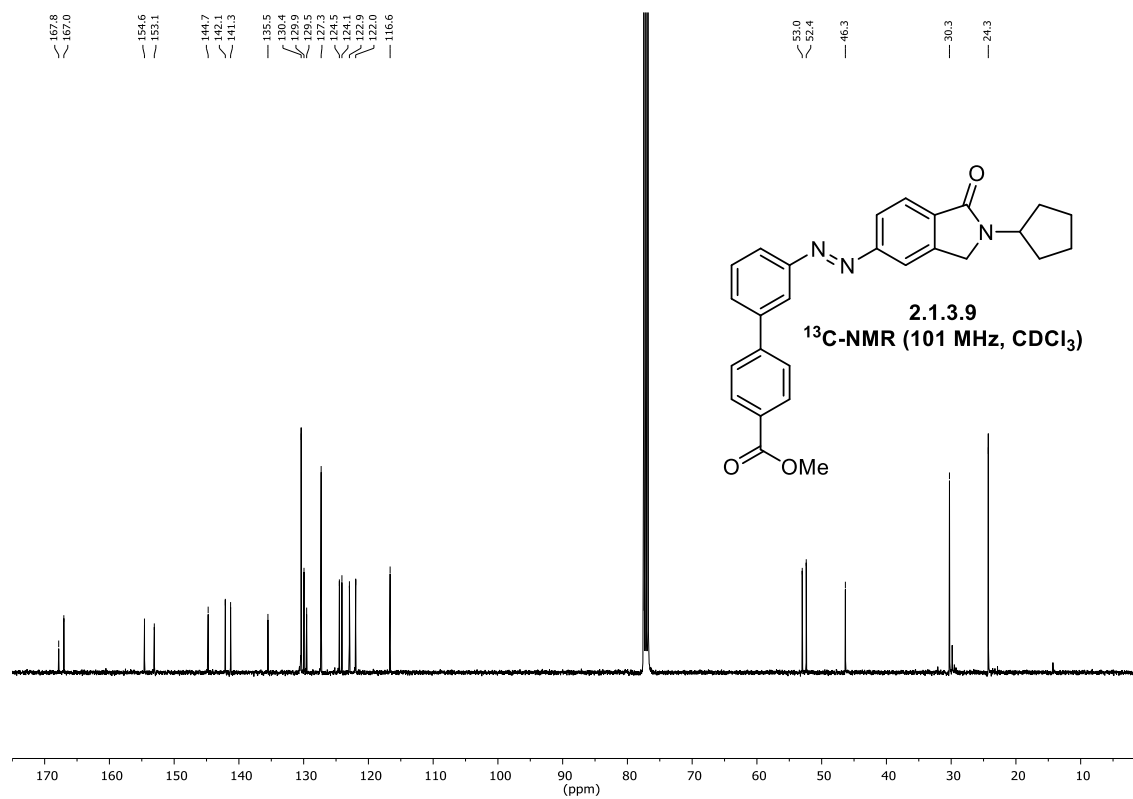
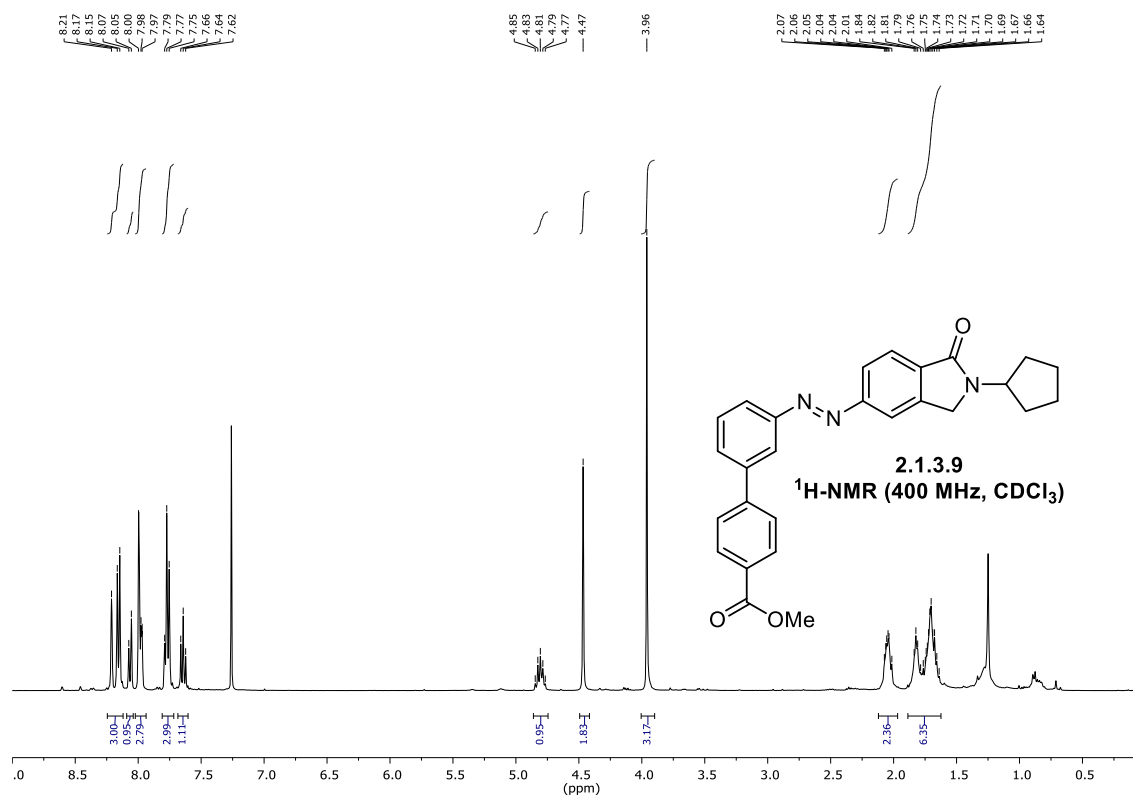
2-cyclopentyl-5-nitroisindolin-1-one (2.1.3.5)

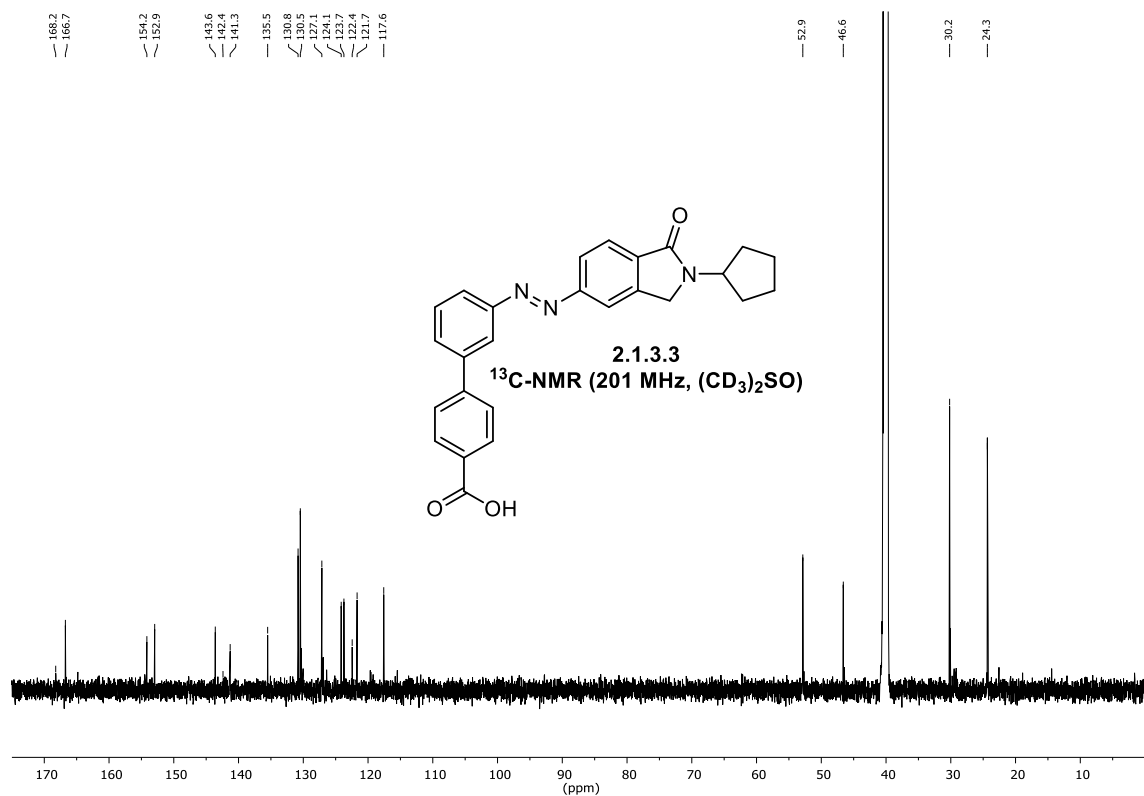
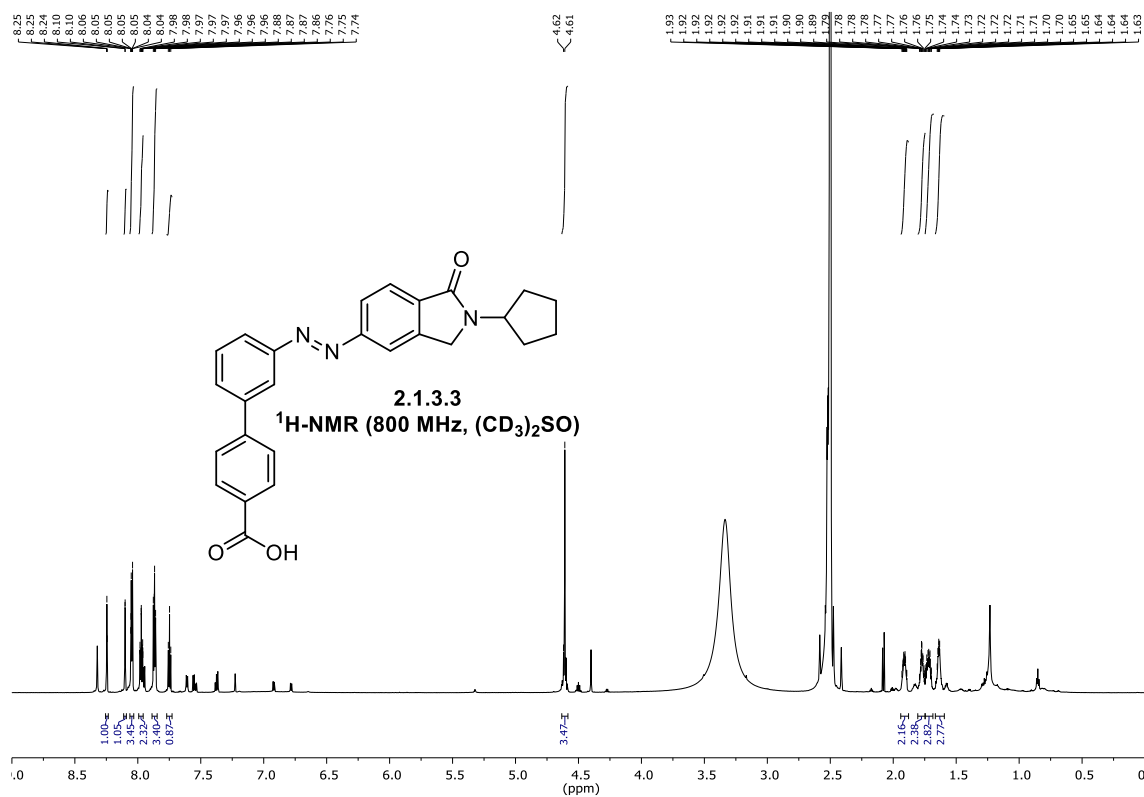


5-amino-2-cyclopentylisoindolin-1-one (2.1.3.6)

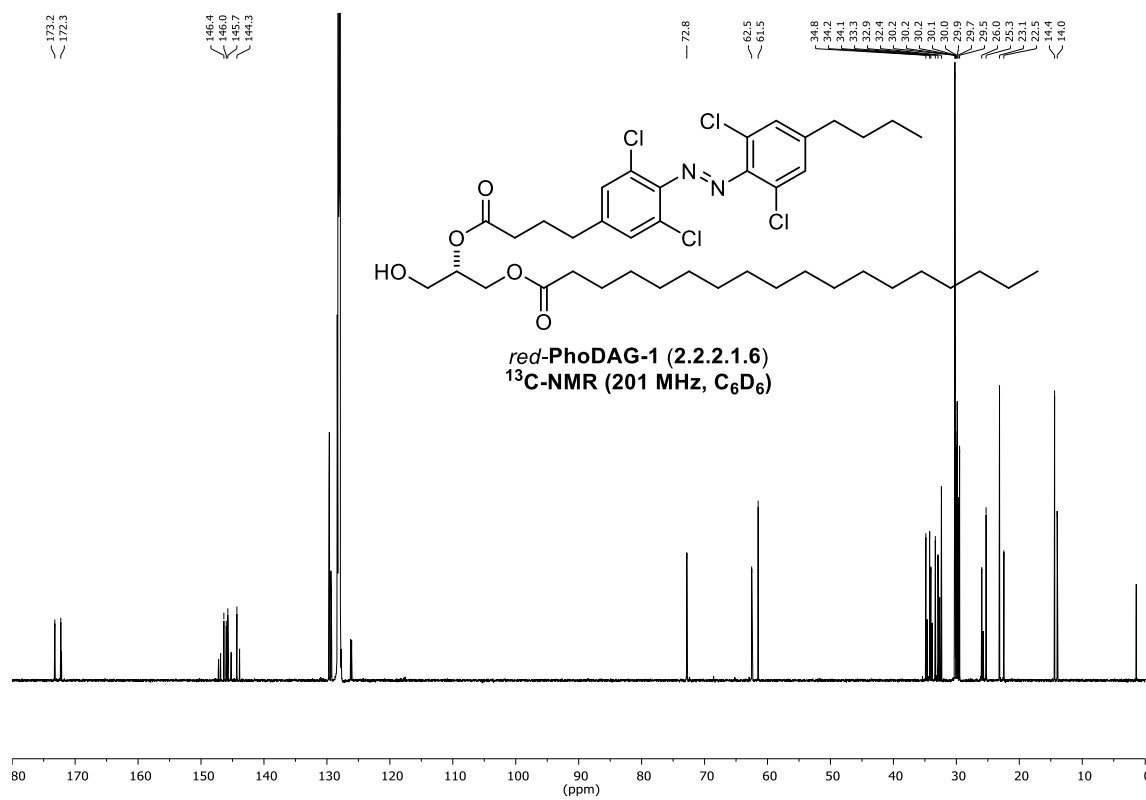
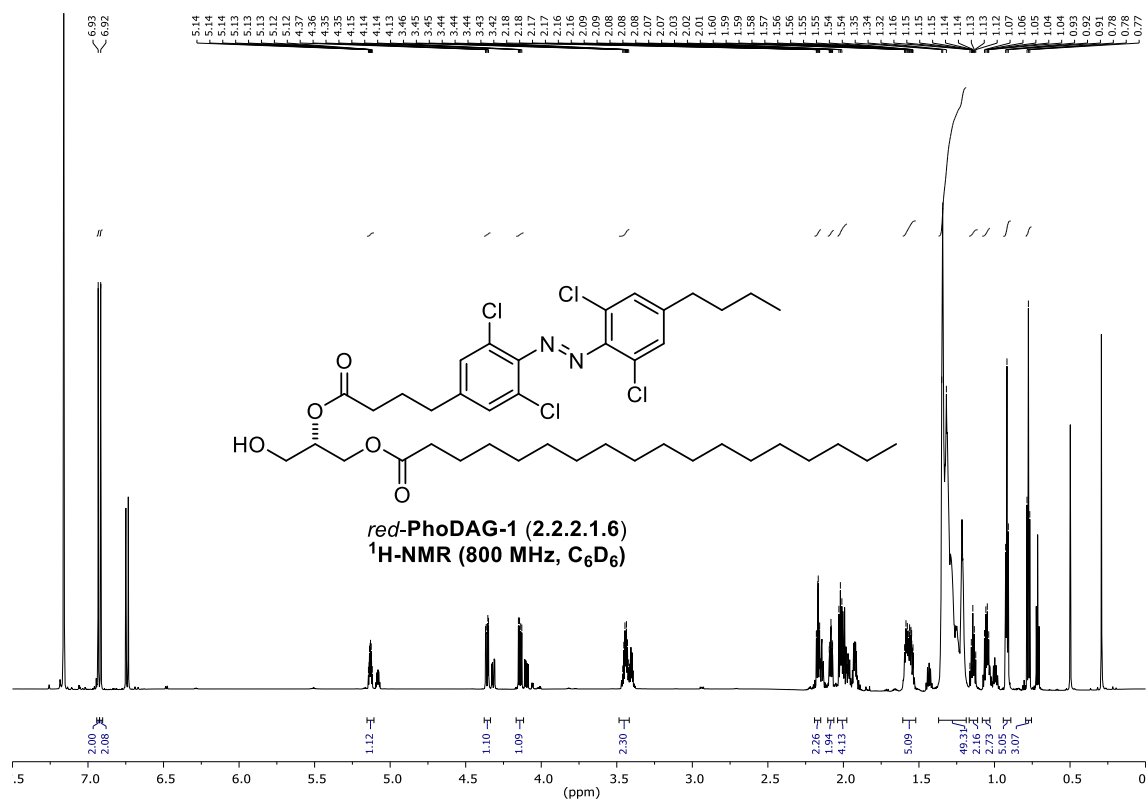


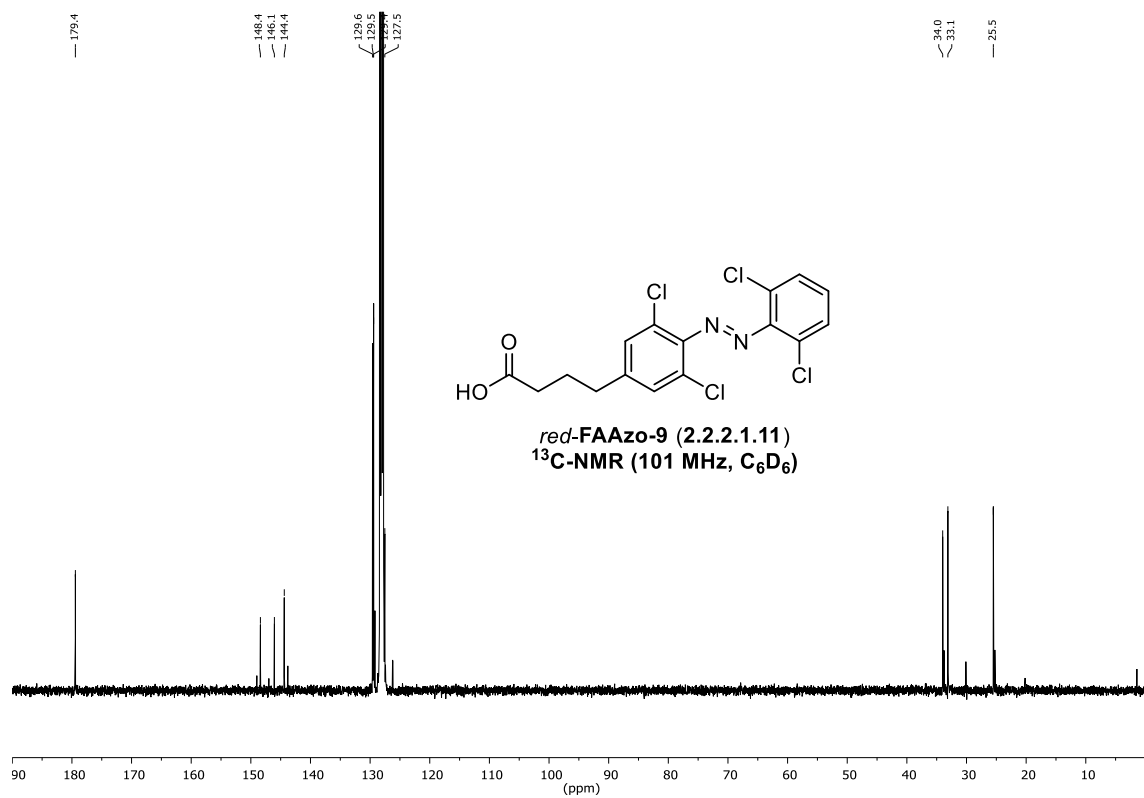
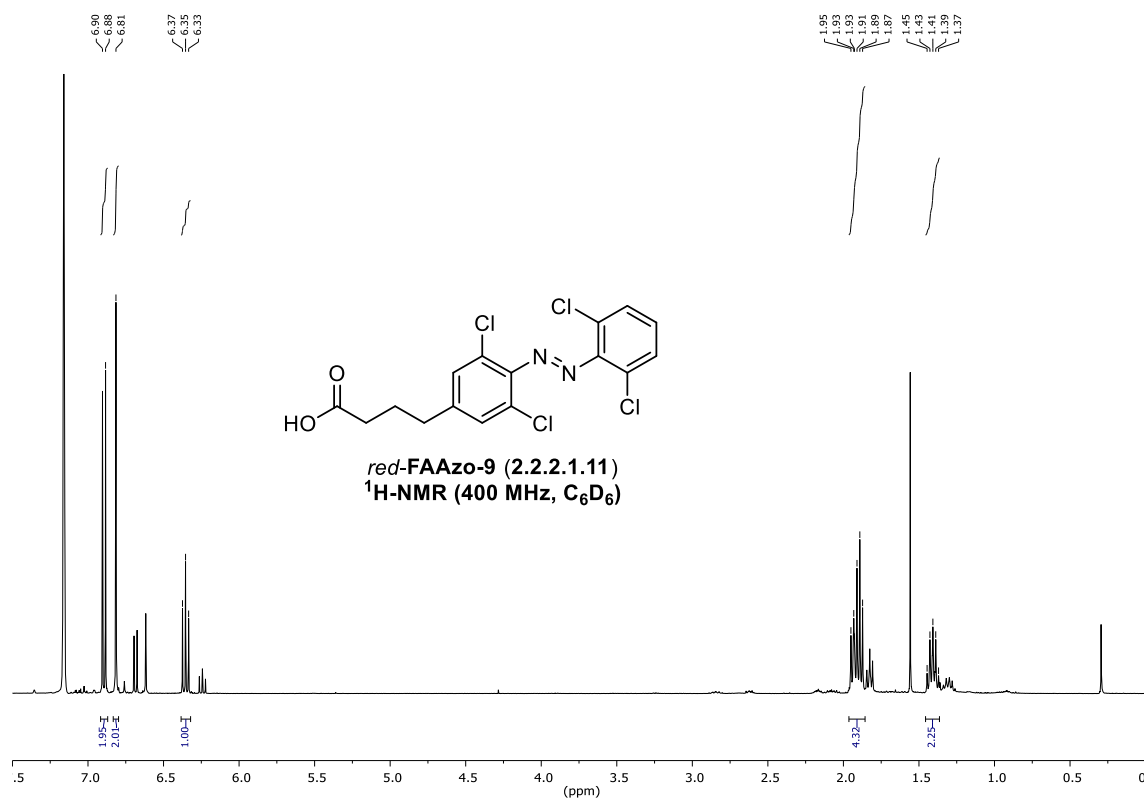
methyl 3'-((2-cyclopentyl-1-oxoisindolin-5-yl)diazenyl)-[1,1'-biphenyl]-4-carboxylate
(2.1.3.9)



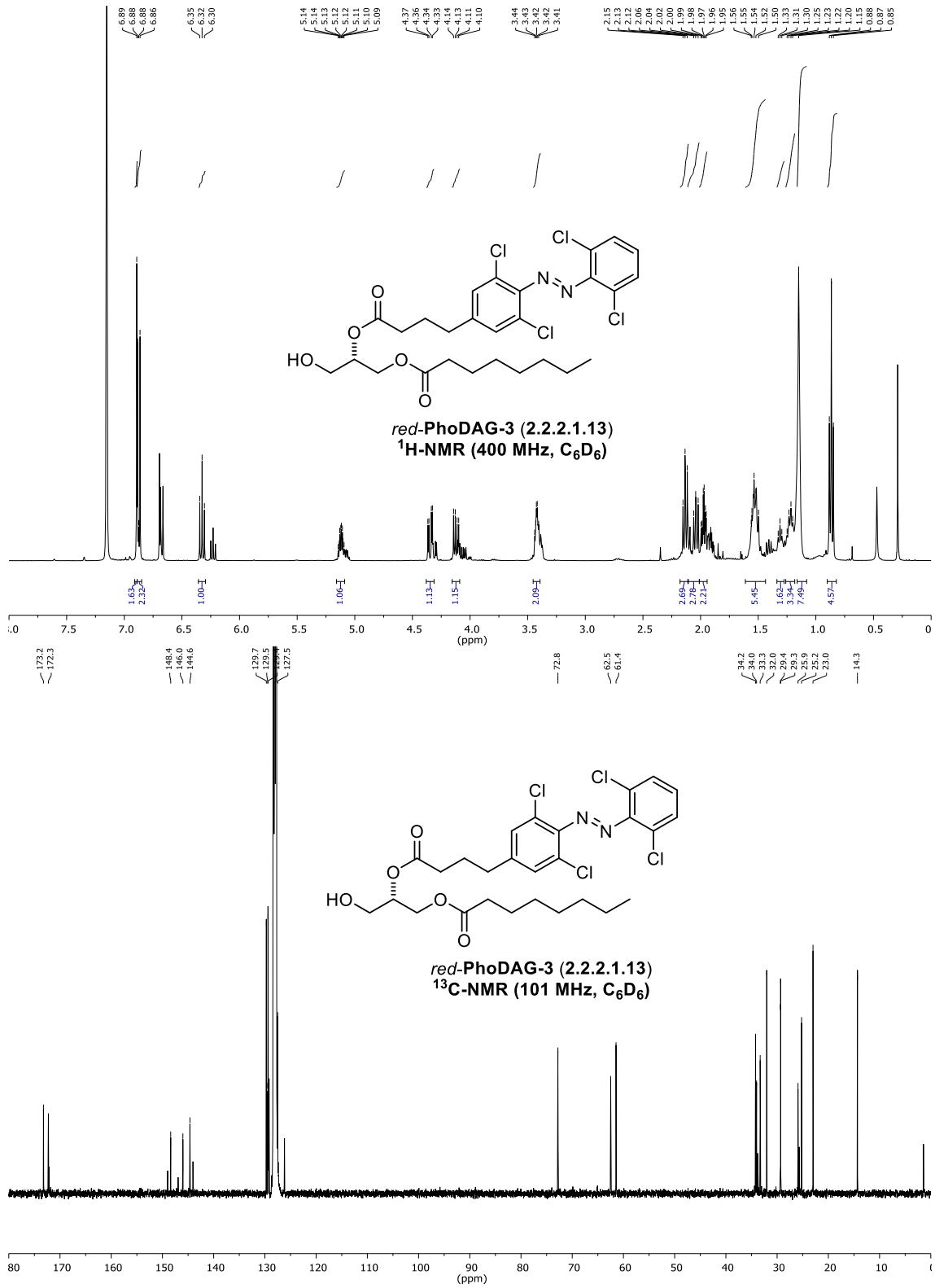
3'-((2-cyclopentyl-1-oxoisindolin-5-yl)diazenyl)-[1,1'-biphenyl]-4-carboxylic acid
(2.1.3.3)

(S)-2-((4-(4-((4-butyl-2,6-dichlorophenyl)diazenyl)-3,5-dichlorophenyl)butanoyl)oxy)-3-hydroxypropyl stearate (*red-PhoDAG-1*, 2.2.2.1.6)

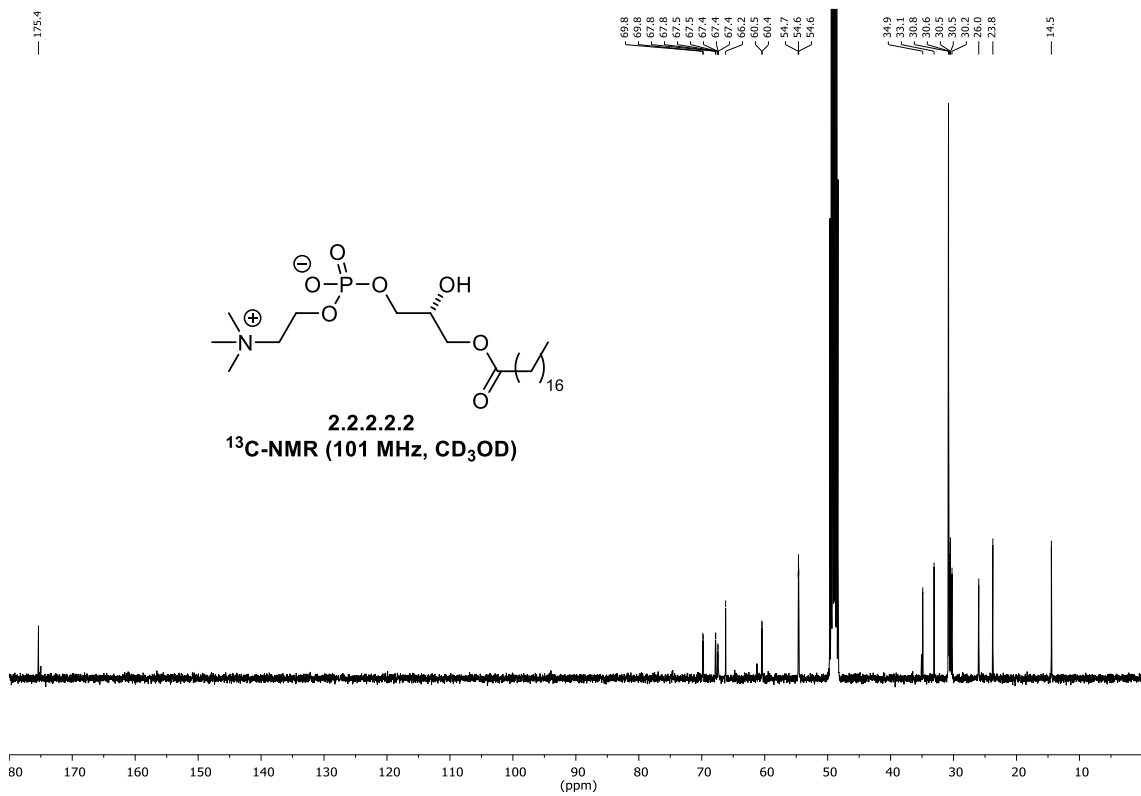
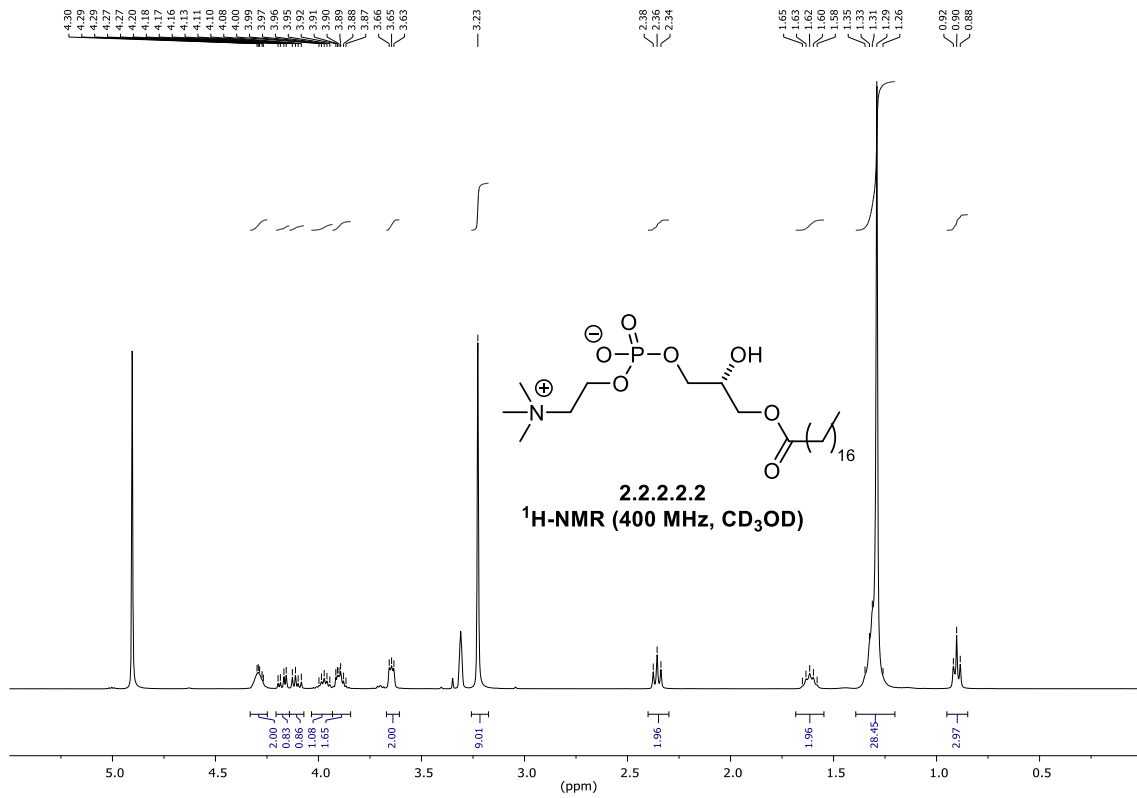


4-(3,5-dichloro-4-((2,6-dichlorophenyl)diazenyl)phenyl)butanoic acid (*red*-FAAzo-9, 2.2.2.1.11)

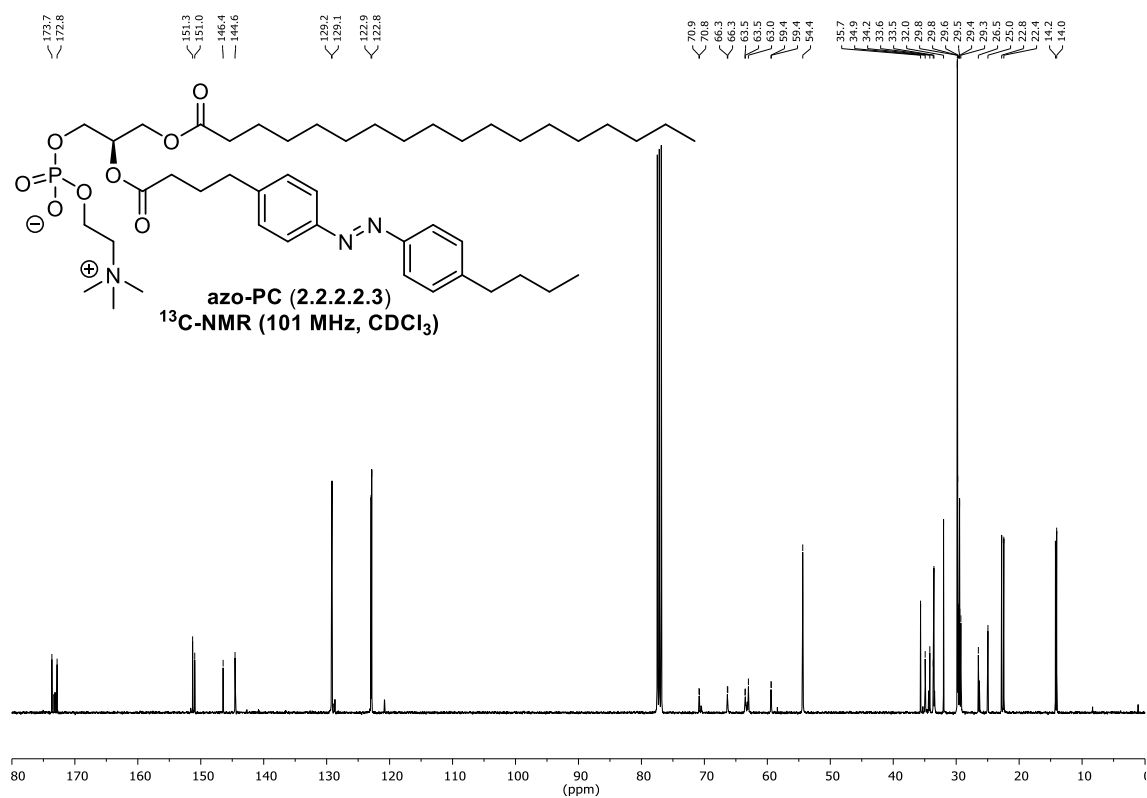
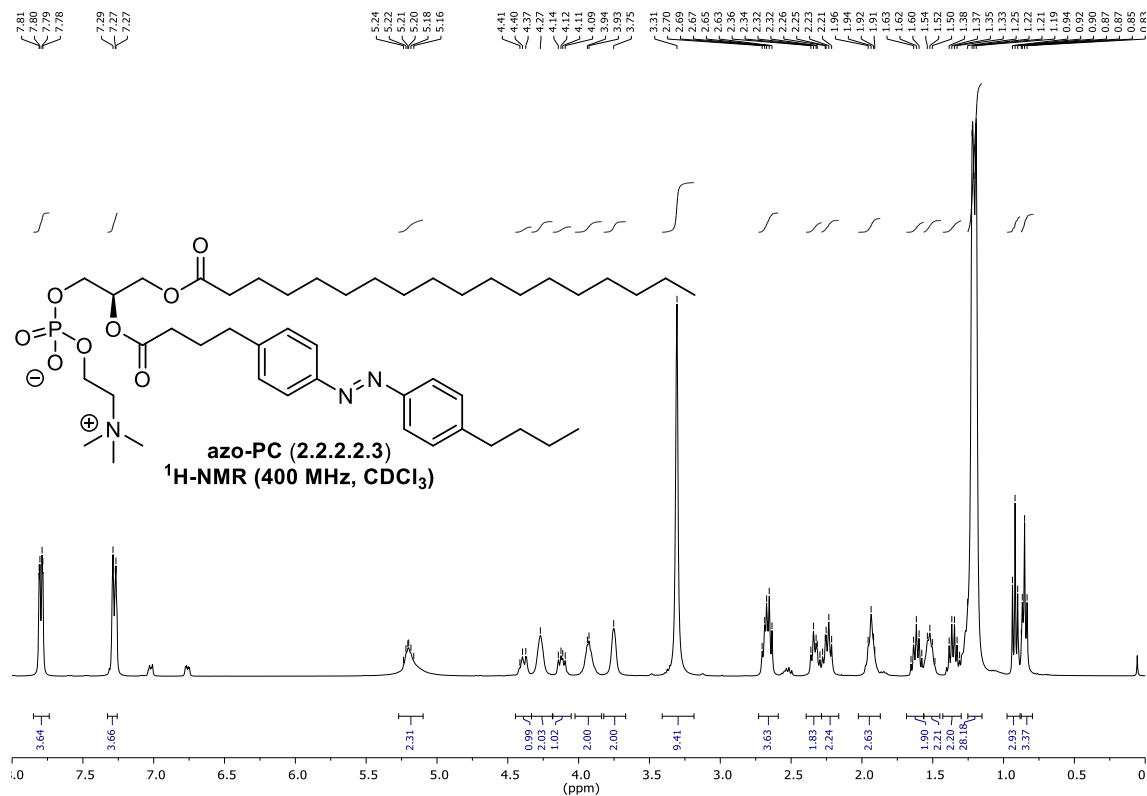
(S)-2-((4-(3,5-dichloro-4-((2,6-dichlorophenyl)diazenyl)phenyl)butanoyl)oxy)-3-hydroxypropyl octanoate (*red-PhoDAG-3*, 2.2.2.1.13)

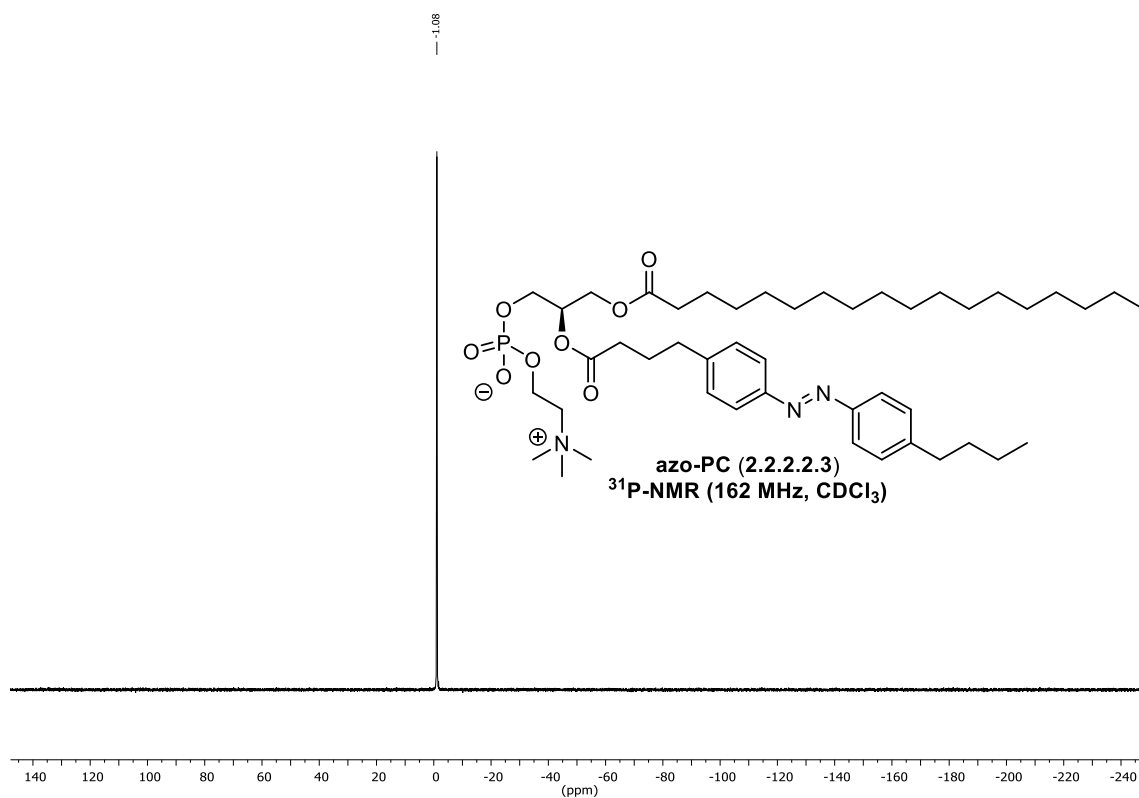


(*R*)-2-hydroxy-3-(stearoyloxy)propyl (2-(trimethylammonio)ethyl) phosphate
(2.2.2.2.2)

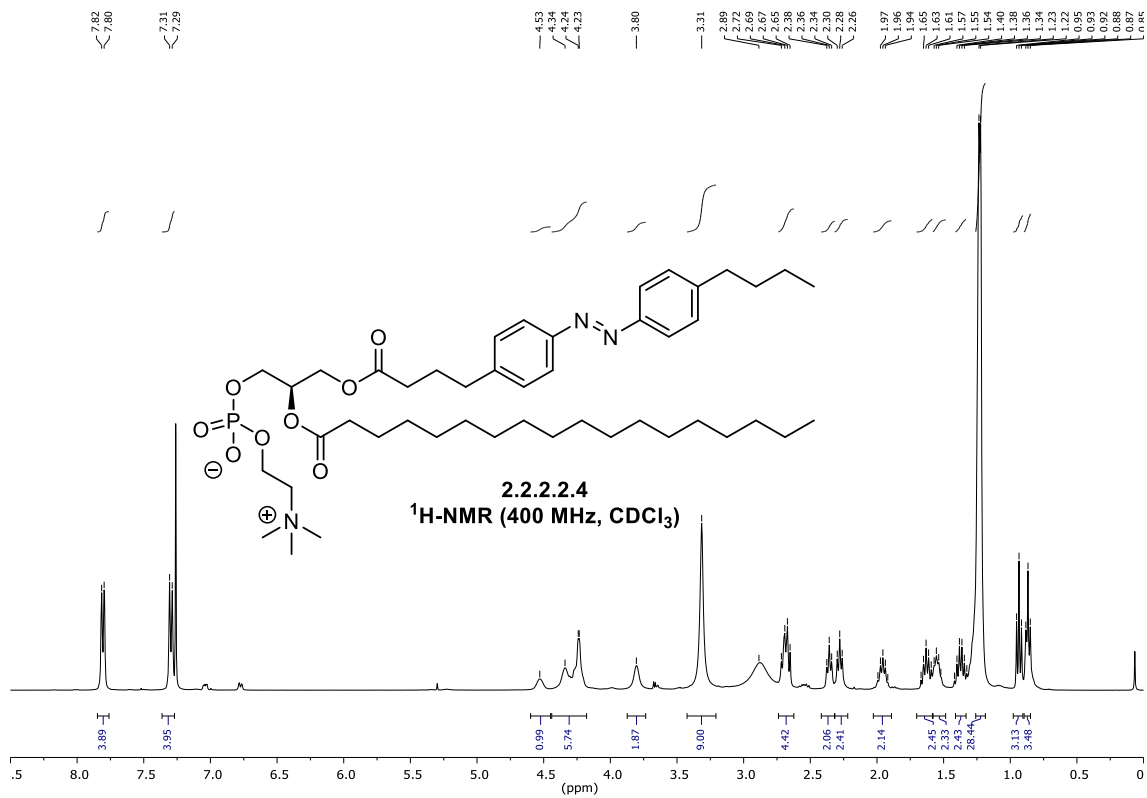


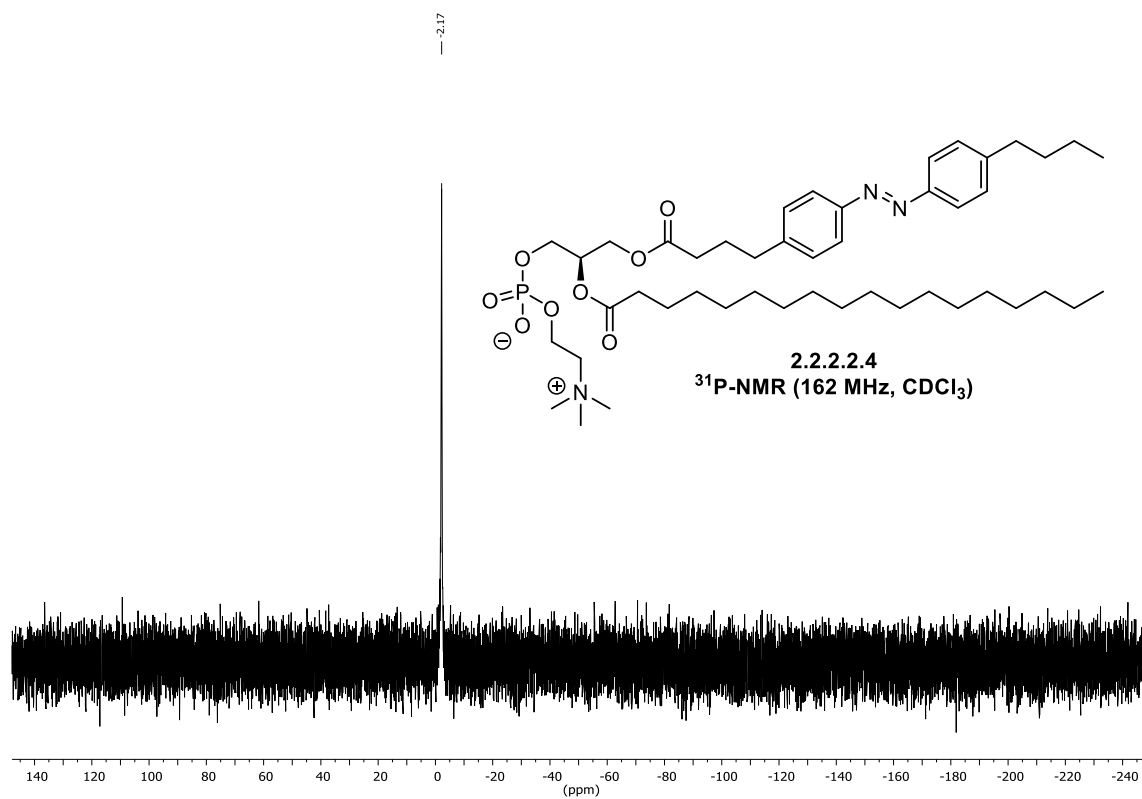
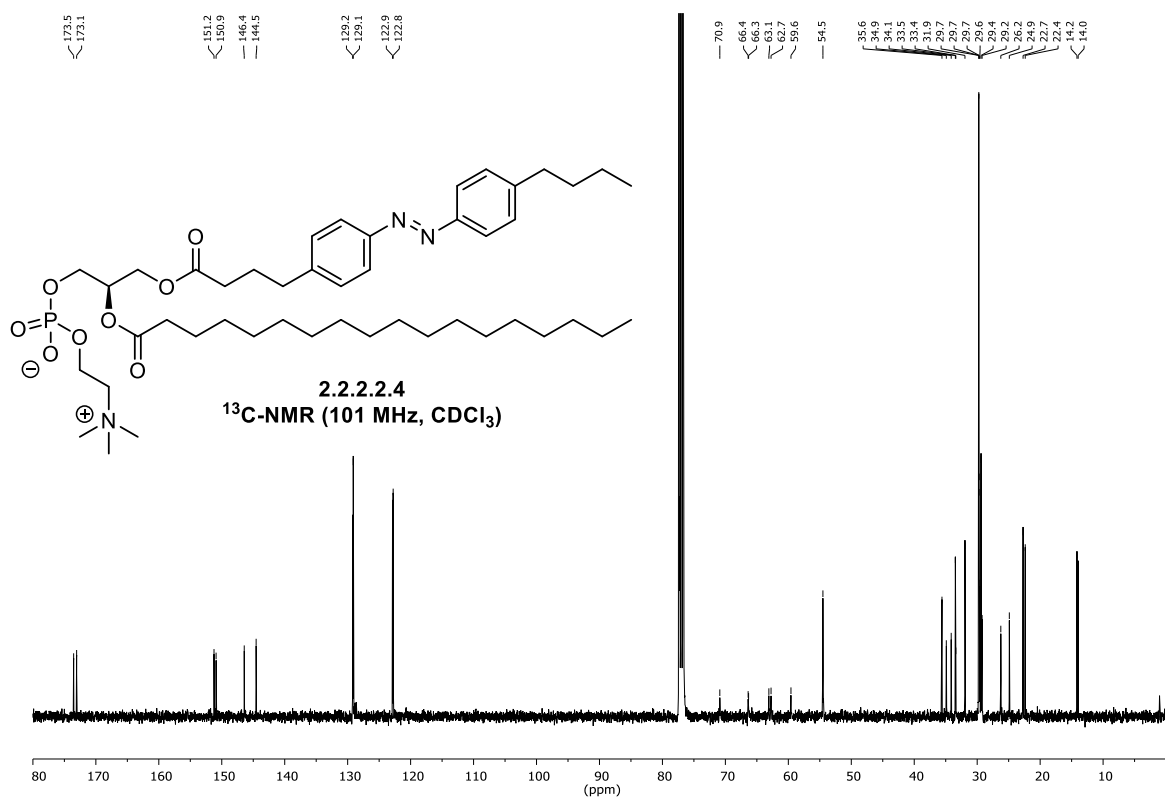
(*R*)-2-((4-(4-((4-butylphenyl)diazenyl)phenyl)butanoyl)oxy)-3-(stearoyloxy)propyl (2-(trimethylammonio)ethyl) phosphate (azo-PC, 2.2.2.2.3)



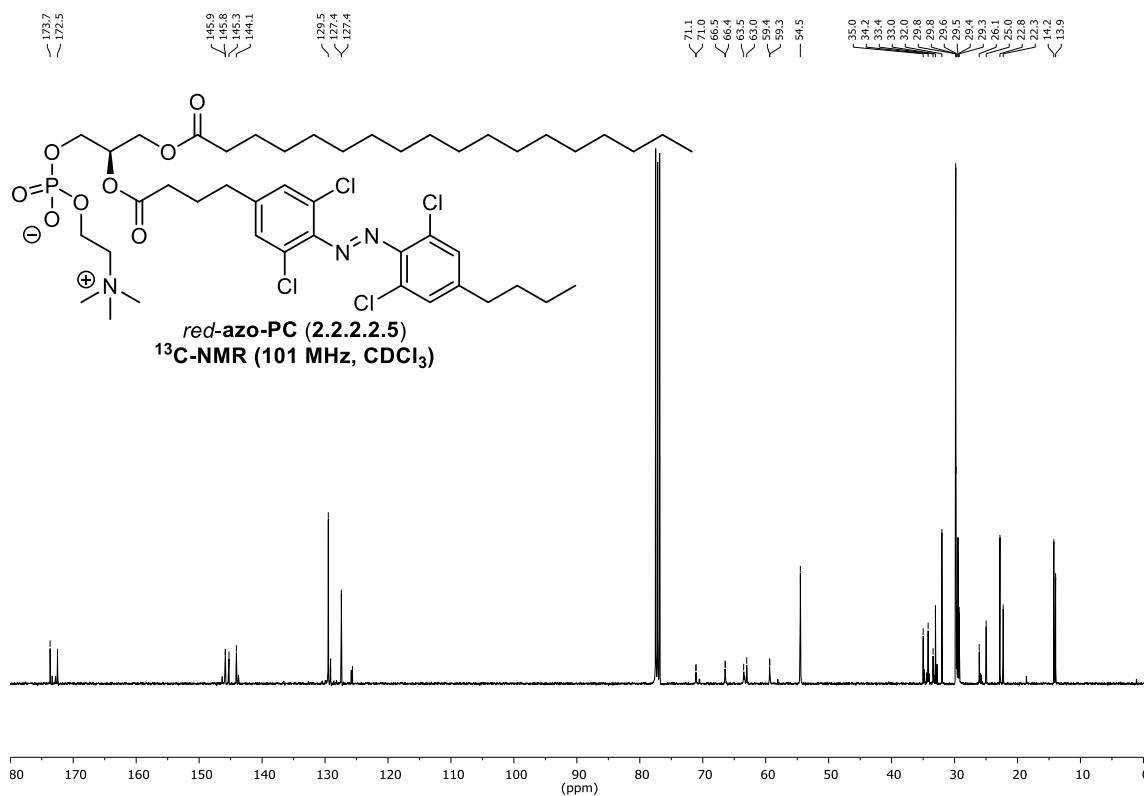
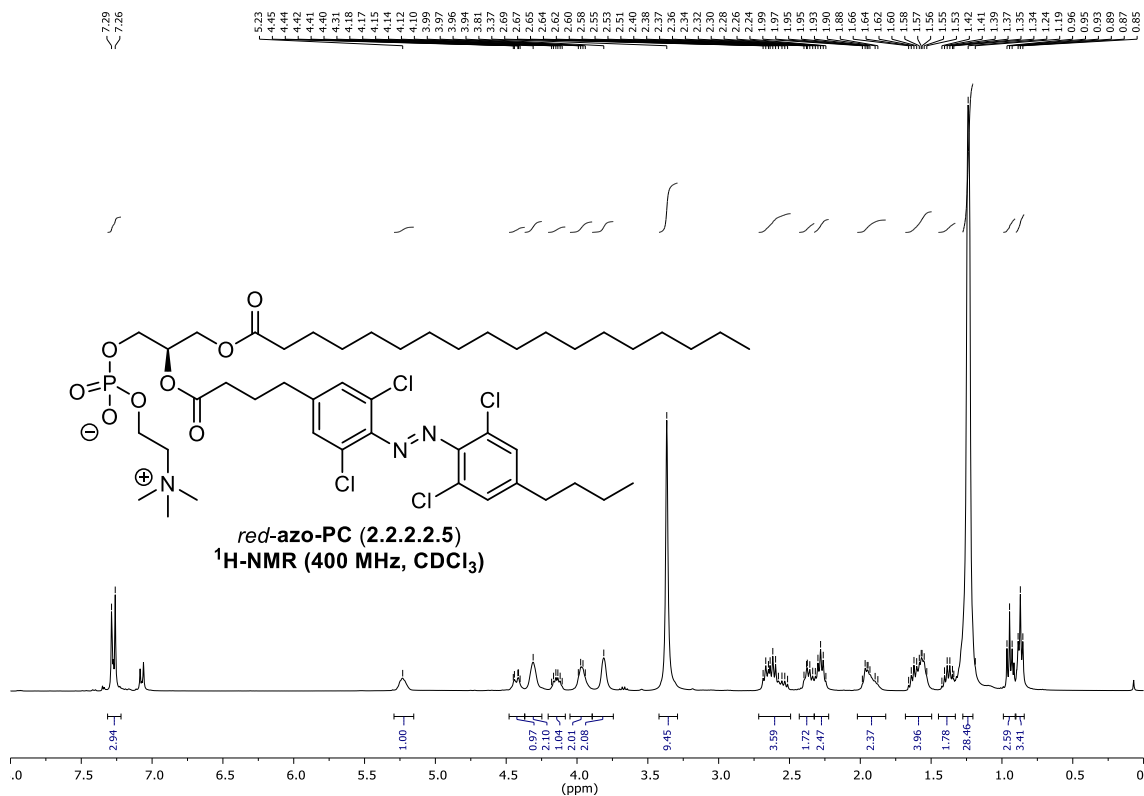


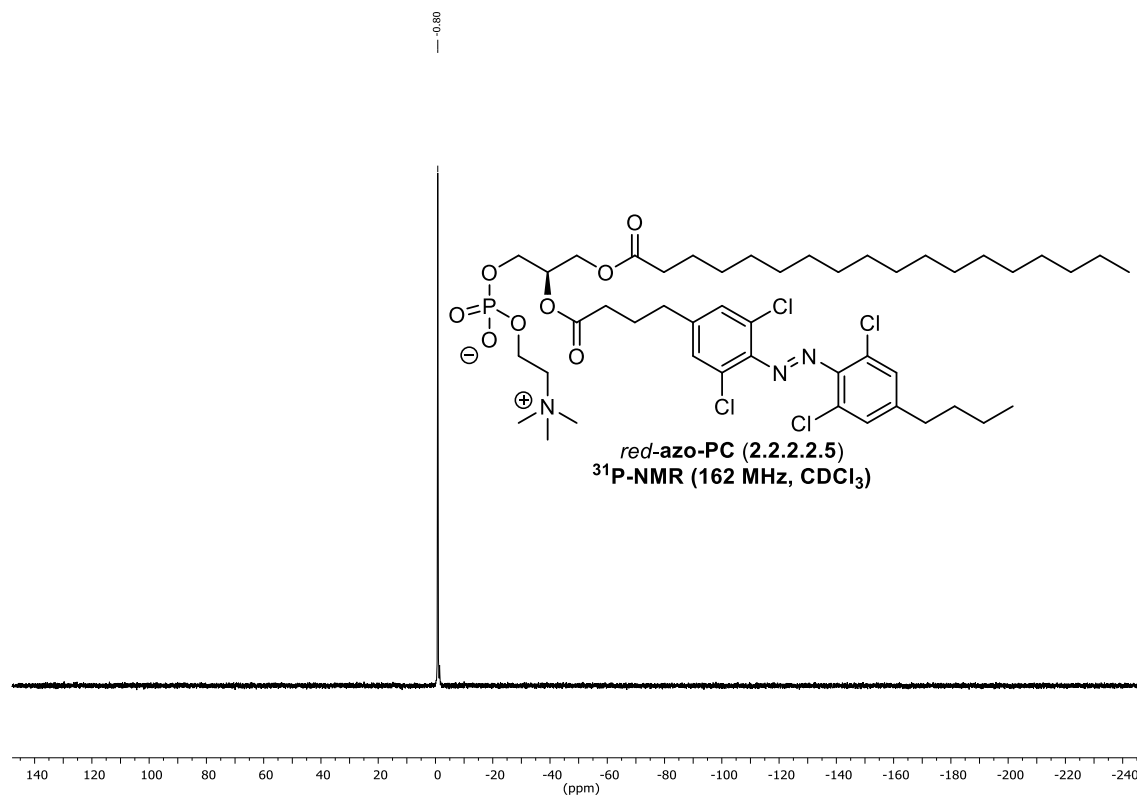
(R)-3-((4-(4-((4-butylphenyl)diazenyl)phenyl)butanoyl)oxy)-2-(stearoyloxy)propyl (2-(trimethylammonio)ethyl) phosphate (2.2.2.2.4)



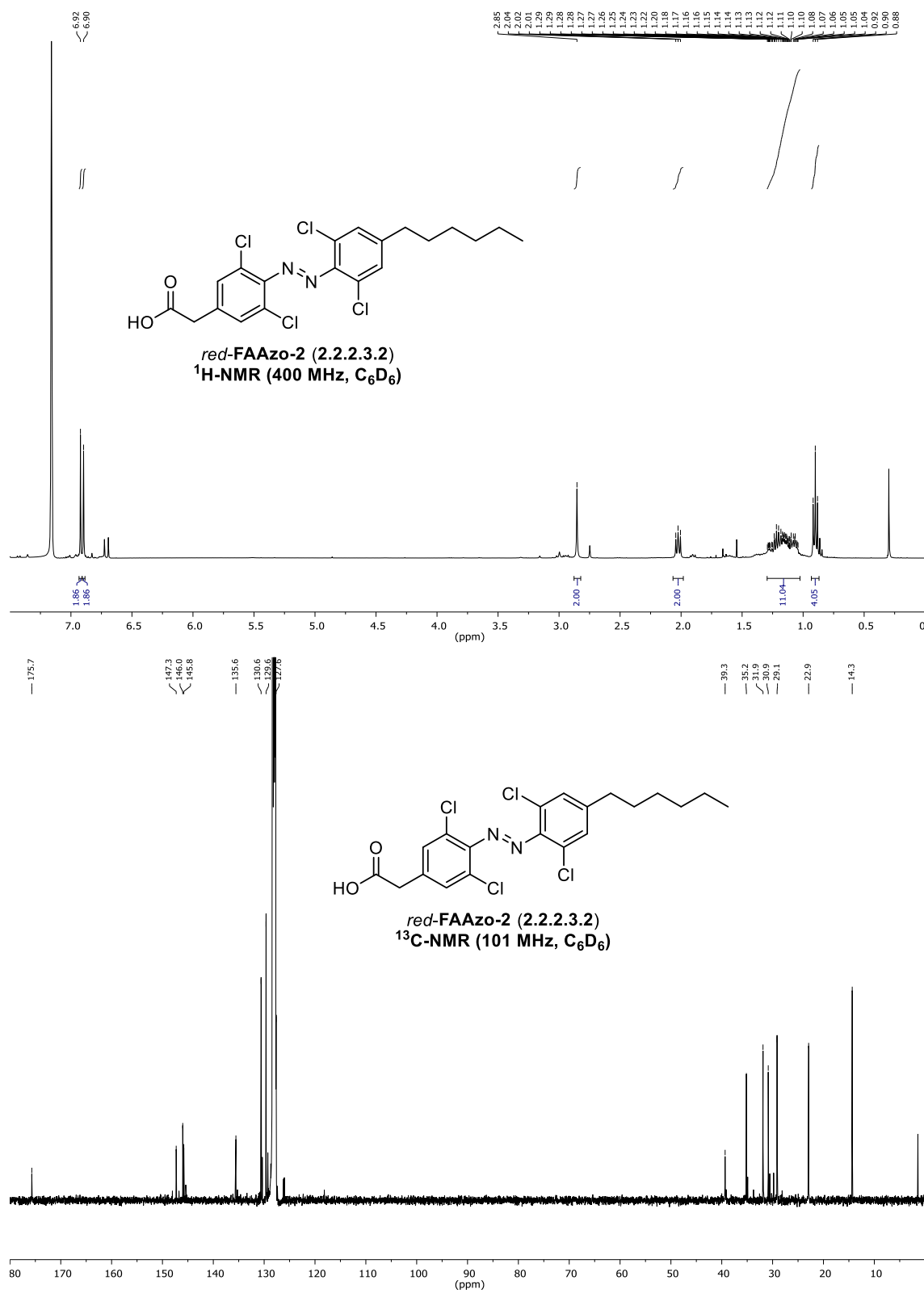


(*R*)-2-((4-(4-((4-butyl-2,6-dichlorophenyl)diazenyl)-3,5-dichlorophenyl)butanoyl)oxy)-3-(stearoyloxy)propyl 2-(trimethylammonio)ethyl phosphate (*red-azo-PC*, 2.2.2.2.5)

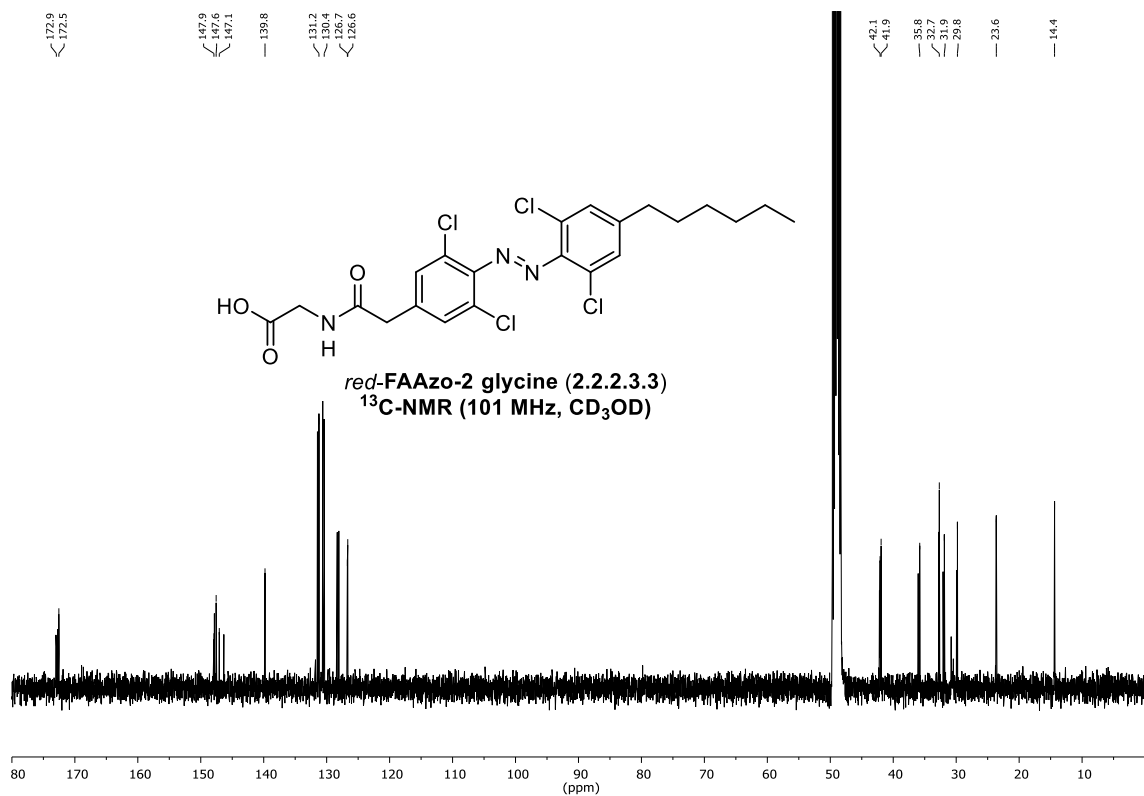
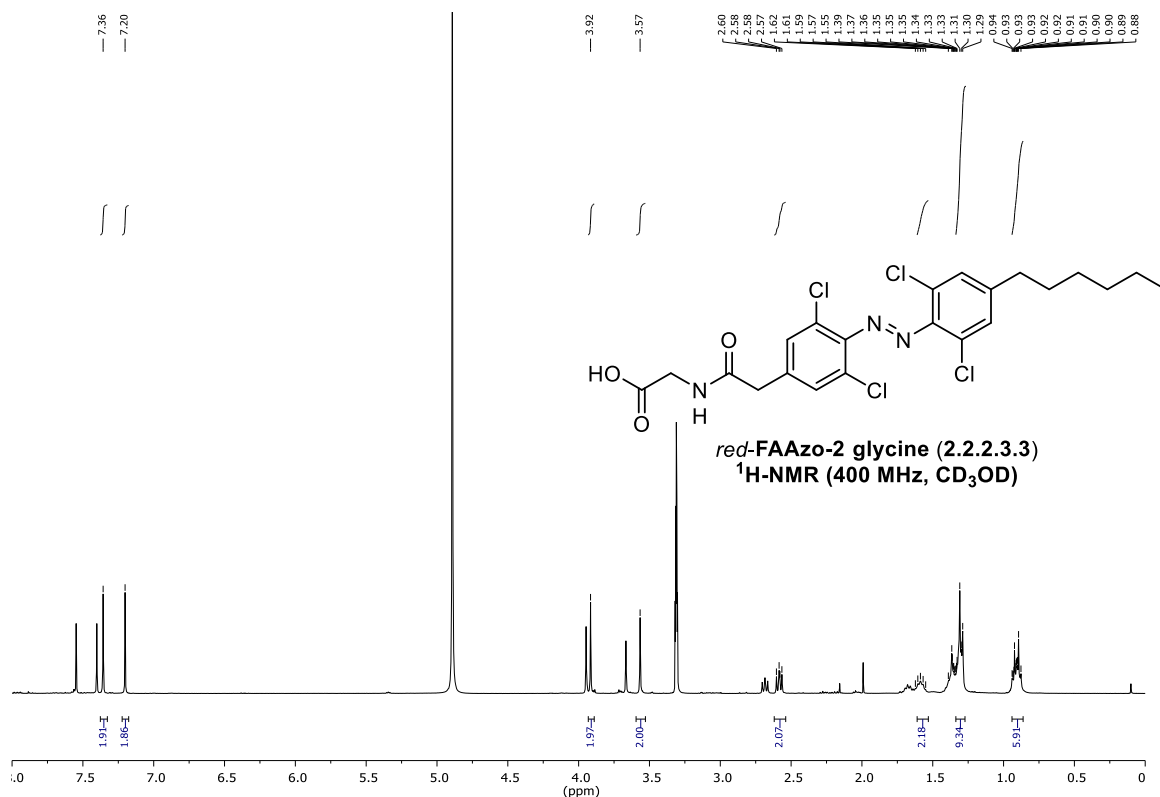




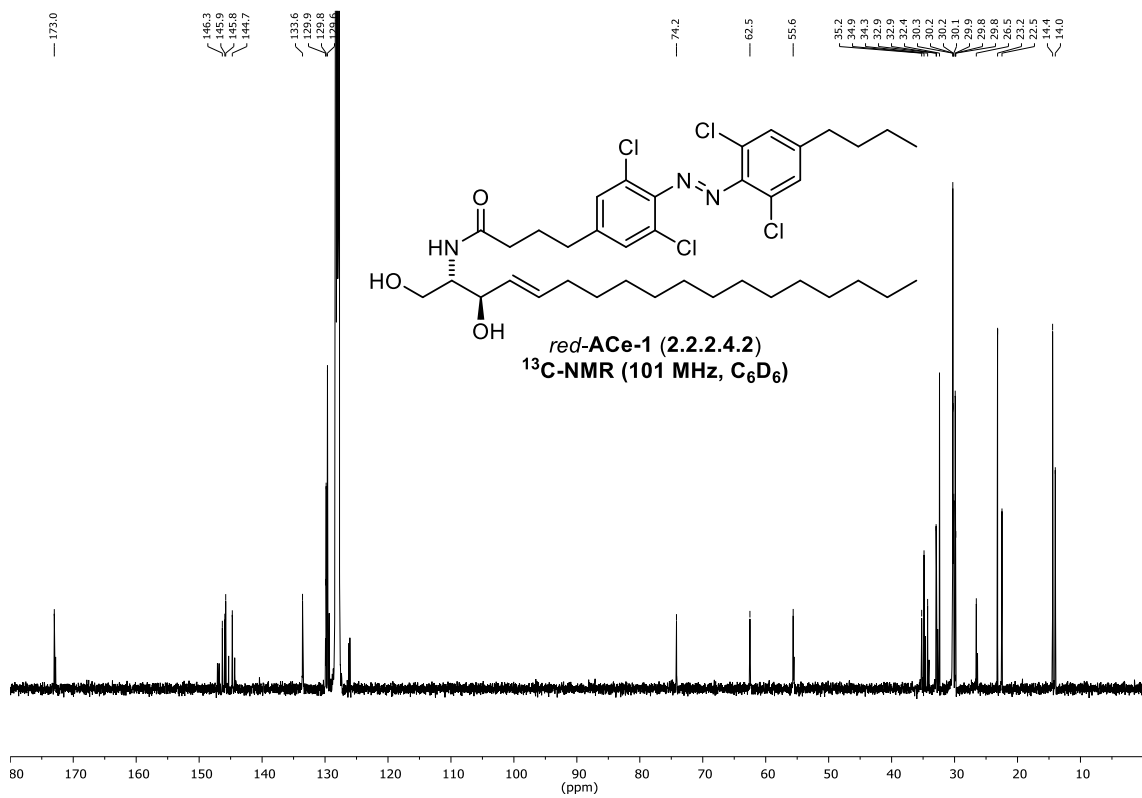
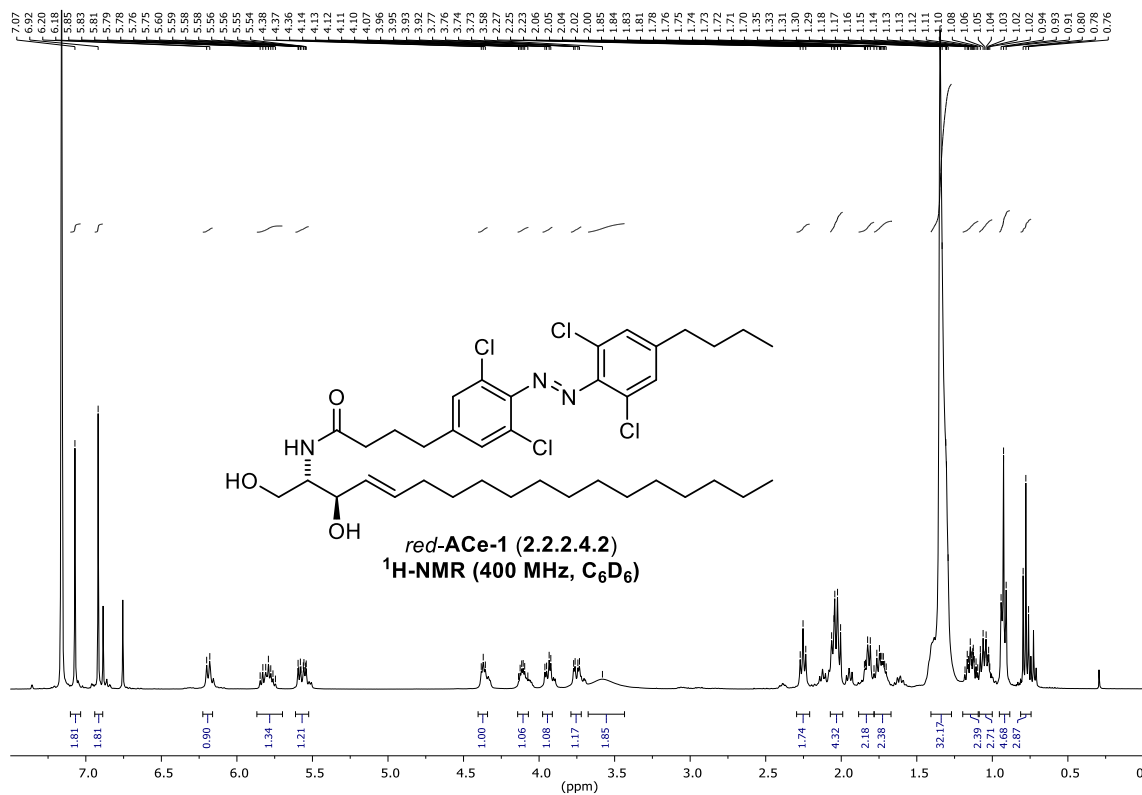
2-(3,5-dichloro-4-((2,6-dichloro-4-hexylphenyl)diazenyl)phenyl)acetic acid (*red-FAAzo-2*, 2.2.2.3.2)



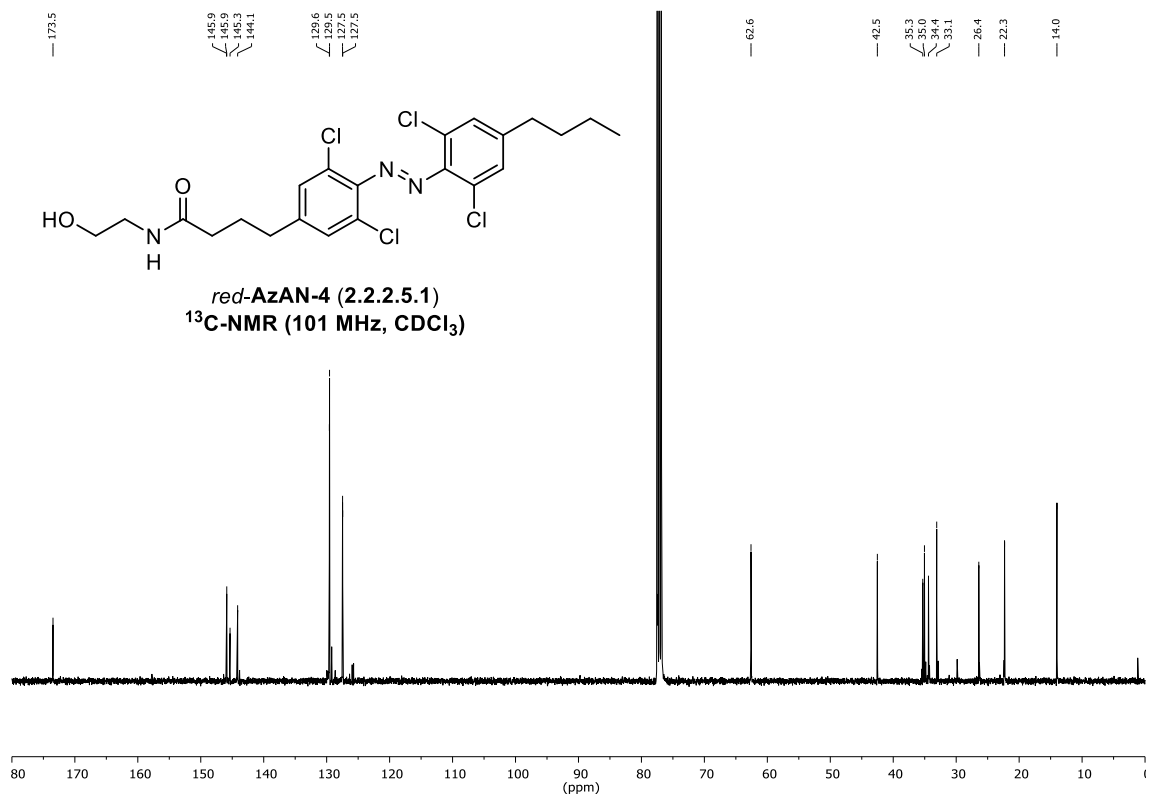
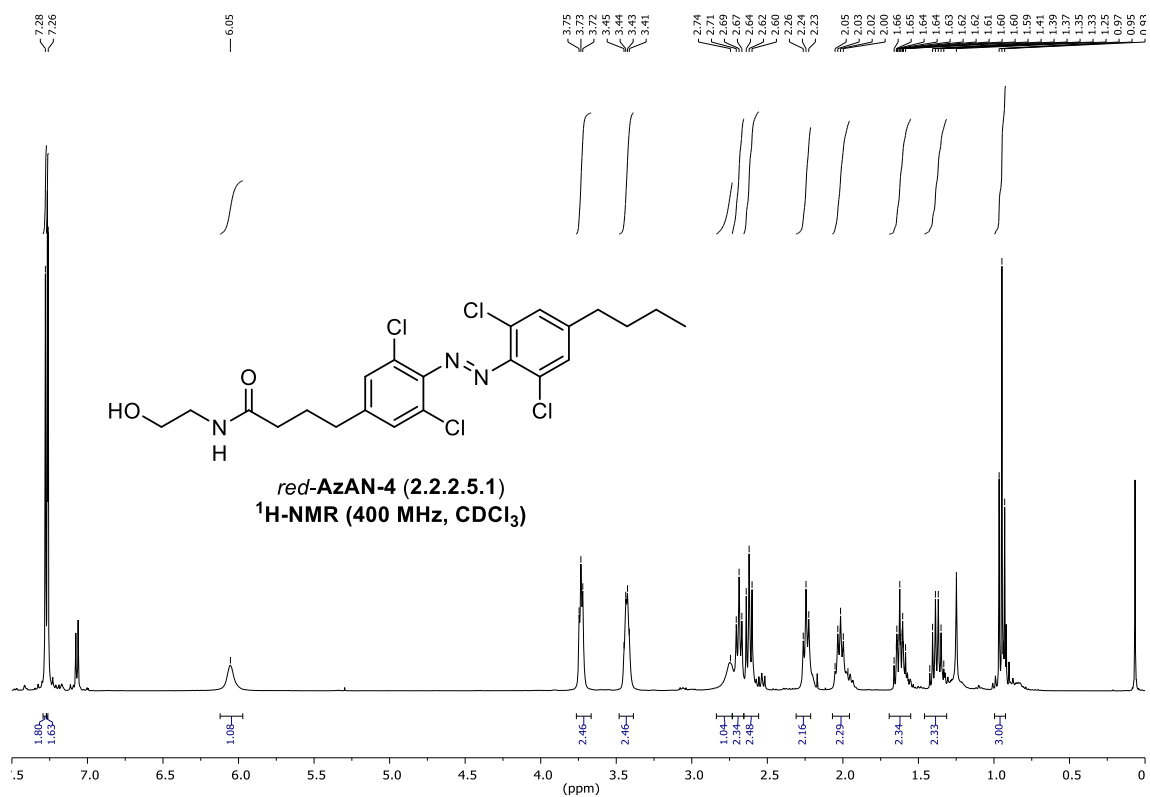
2-(3,5-dichloro-4-((2,6-dichloro-4-hexylphenyl)diazenyl)phenyl)acetyl)glycine (*red*-FAAzo-2 glycine, 2.2.2.3.3)



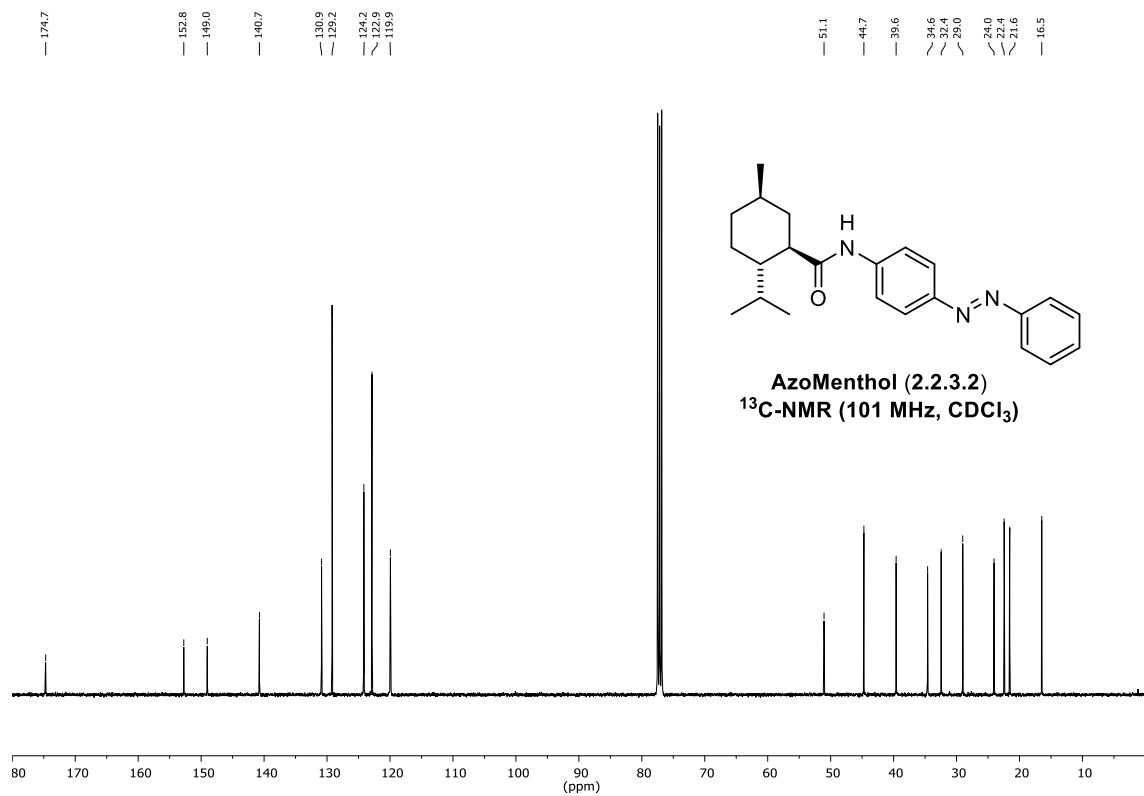
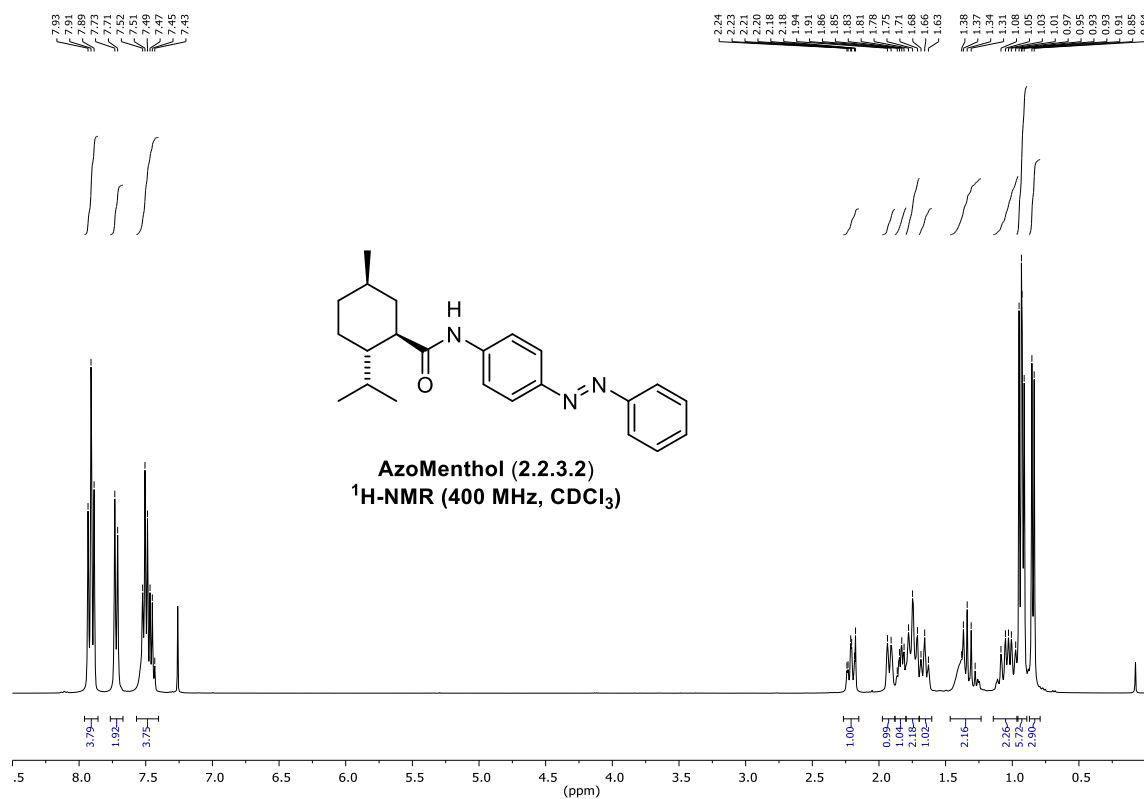
4-(4-((4-butyl-2,6-dichlorophenyl)diazenyl)-3,5-dichlorophenyl)-N-(2-hydroxyethyl)butanamide (*red-ACe-1*, 2.2.2.4.2)



4-(4-((4-butyl-2,6-dichlorophenyl)diazenyl)-3,5-dichlorophenyl)-N-(2-hydroxyethyl)butanamide (*red-AzAN-4*, 2.2.2.5.1)



(1*R*,2*S*,5*R*)-2-isopropyl-5-methyl-*N*-(4-(phenyldiazenyl)phenyl)cyclohexane-1-carboxamide (AzoMenthol, 2.2.3.2)



4.2 X-Ray Data

(3*aR*,4*R*,5*S*,6*S*,7*S*)-4,6-bis(benzyloxy)-2',2'-dimethyl-3*a*,4,6,7-tetrahydro-3*H*-spiro[benzo[*c*]isoxazole-5,4'-[1,3]dioxolan]-7-yl phenylcarbamate (1.2.3.6)

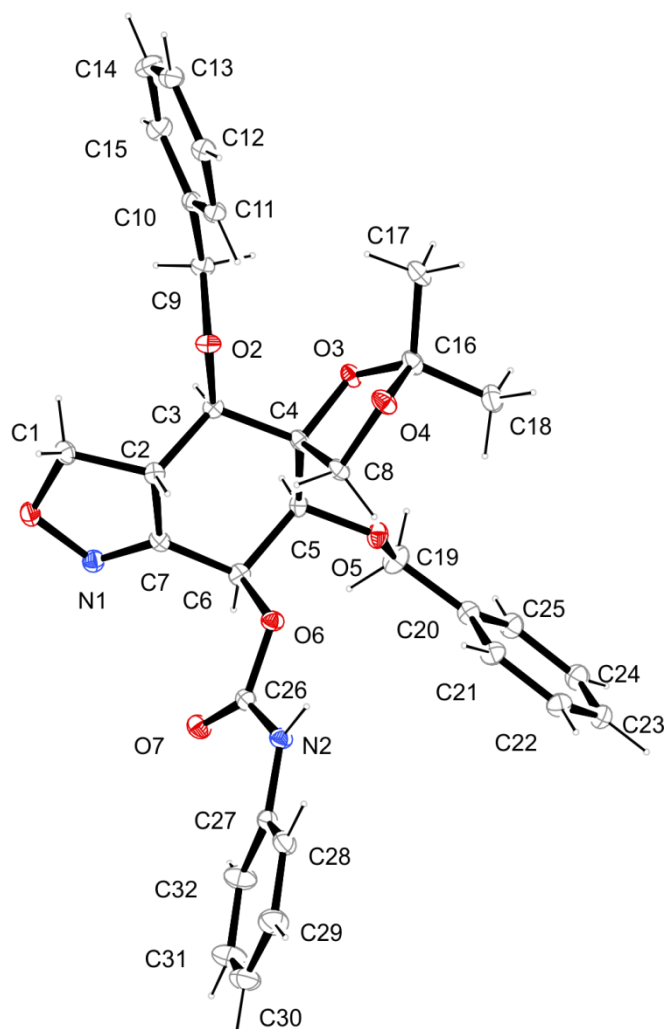


Figure 1. ORTEP of the molecular structure of (3*aR*,4*R*,5*S*,6*S*,7*S*)-4,6-bis(benzyloxy)-2',2'-dimethyl-3*a*,4,6,7-tetrahydro-3*H*-spiro[benzo[*c*]isoxazole-5,4'-[1,3]dioxolan]-7-yl phenylcarbamate (1.2.3.6)

Table 1. Crystallographic data for 1.2.3.6

net formula	C ₃₂ H ₃₄ N ₂ O ₇
<i>M_r</i> /g mol ⁻¹	558.61
crystal size/mm	0.100 × 0.020 × 0.020
<i>T</i> /K	100.(2)
radiation	MoK α

diffractometer	'Bruker D8 Venture TXS'
crystal system	monoclinic
space group	'C 1 2 1'
$a/\text{\AA}$	39.467(2)
$b/\text{\AA}$	6.2098(3)
$c/\text{\AA}$	11.8739(6)
$\alpha/^\circ$	90
$\beta/^\circ$	99.8859(16)
$\gamma/^\circ$	90
$V/\text{\AA}^3$	2866.9(2)
Z	4
calc. density/ g cm^{-3}	1.294
μ/mm^{-1}	0.092
absorption correction	Multi-Scan
transmission factor range	0.8308–0.9585
refls. measured	25552
R_{int}	0.0528
mean $\sigma(I)/I$	0.0422
θ range	3.144–26.363
observed refls.	4914
x, y (weighting scheme)	0.0339, 1.5227
hydrogen refinement	C-H: constr, N-H: refall
Flack parameter	–0.4(5)
refls in refinement	5659
parameters	376
restraints	1
$R(F_{\text{obs}})$	0.0401
$R_w(F^2)$	0.0890
S	1.075
shift/error $_{\text{max}}$	0.001
max electron density/ e \AA^{-3}	0.696
min electron density/ e \AA^{-3}	–0.220

(*S*)-4-((*S,E*)-1-(benzyloxy)-3-nitroallyl)-4-((*R*)-1-(benzyloxy)allyl)-2,2-dimethyl-1,3-dioxolane (1.2.3.7)

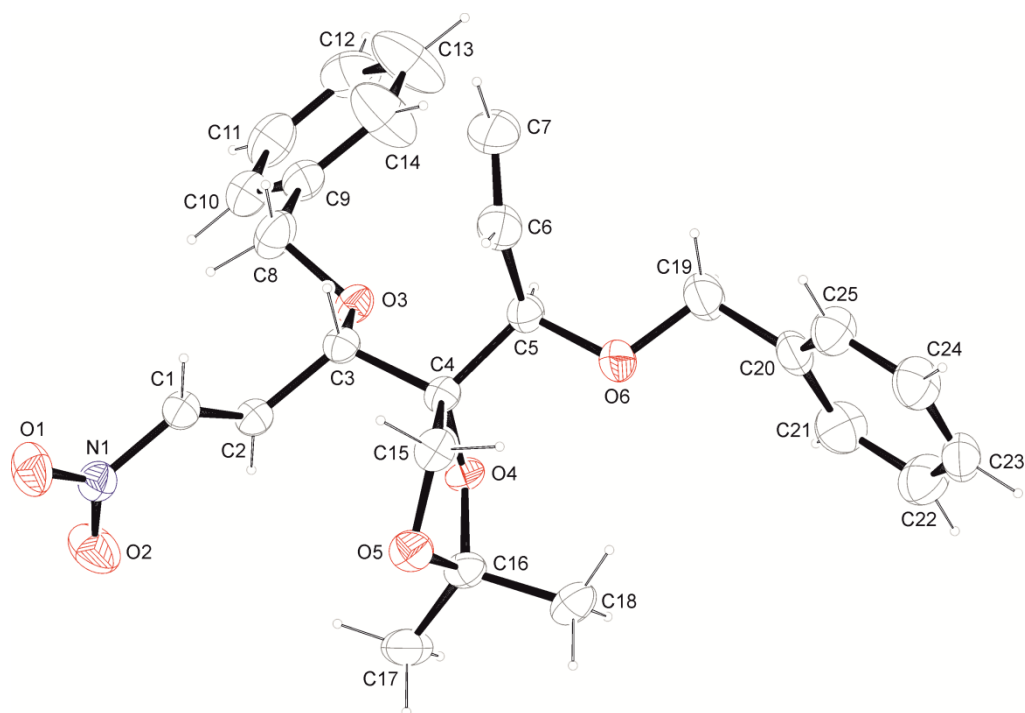


Figure 1. ORTEP of the molecular structure of (*S*)-4-((*S,E*)-1-(benzyloxy)-3-nitroallyl)-4-((*R*)-1-(benzyloxy)allyl)-2,2-dimethyl-1,3-dioxolane (**1.2.3.7**).

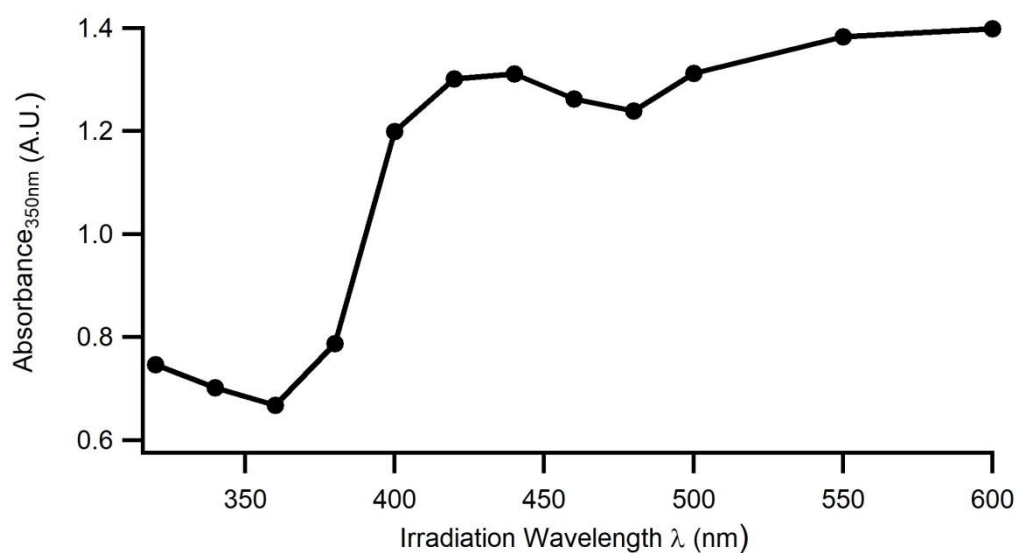
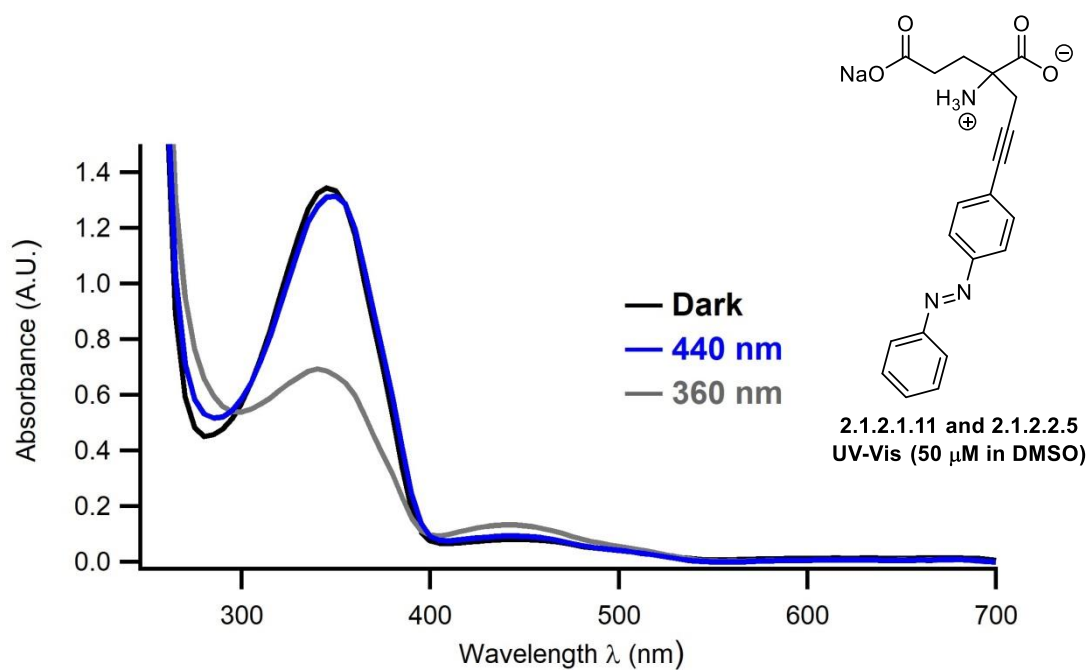
Table 1. Crystallographic data for **1.2.3.7**

net formula	C ₂₅ H ₂₉ NO ₆
<i>M_r</i> /g mol ⁻¹	439.49
crystal size/mm	0.100 × 0.030 × 0.030
<i>T</i> /K	153(2)
radiation	MoK α
diffractometer	'Bruker D8 Venture TXS'
crystal system	monoclinic
space group	'P 21'
<i>a</i> /Å	5.4618(2)
<i>b</i> /Å	22.7390(12)
<i>c</i> /Å	9.8018(5)
α /°	90
β /°	99.336(2)

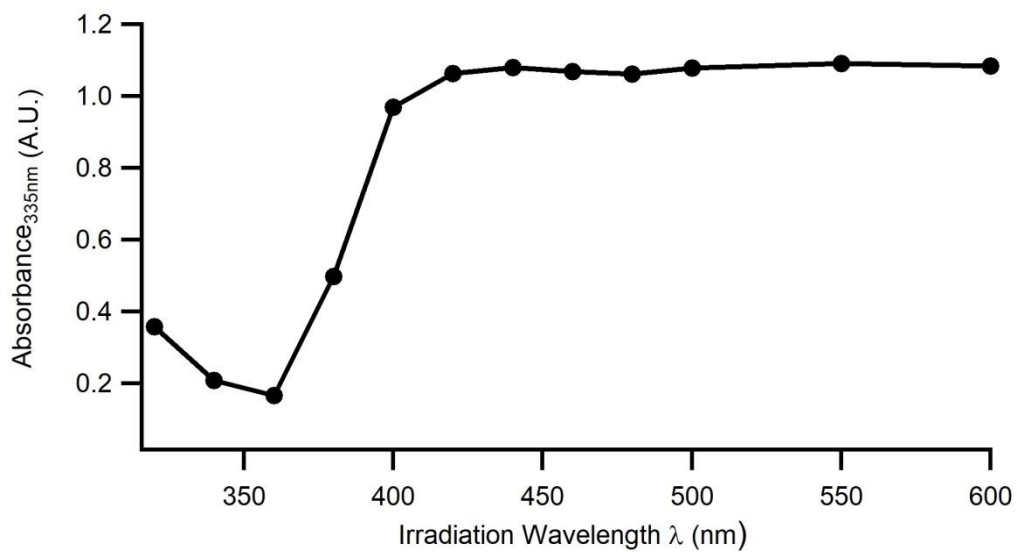
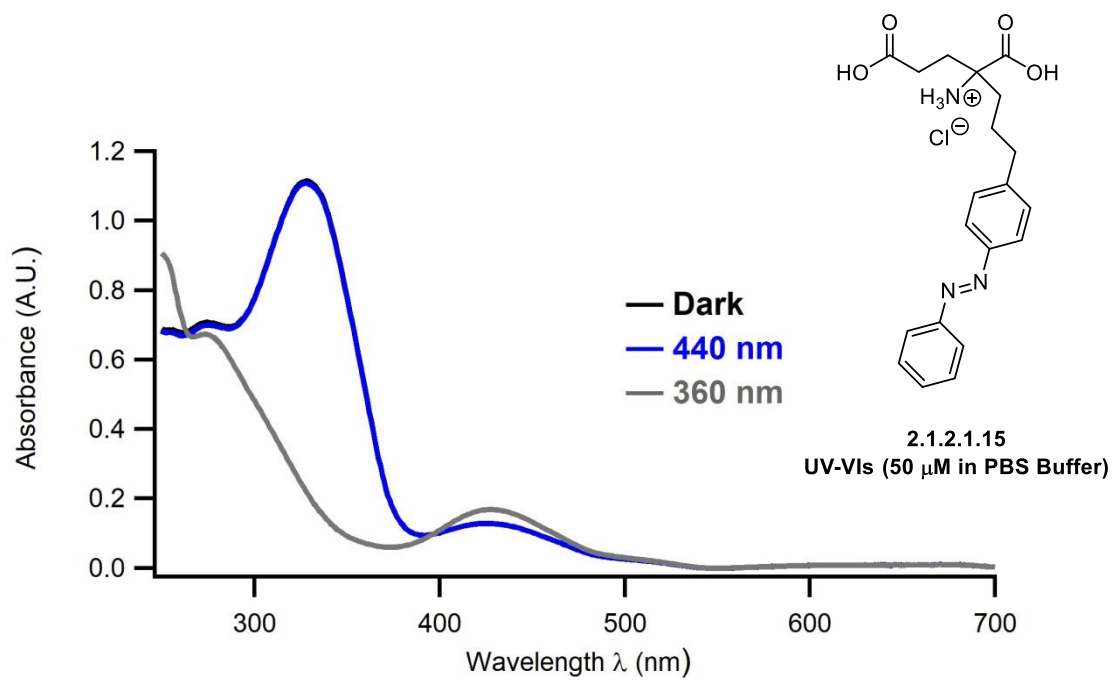
$\gamma/^\circ$	90
$V/\text{\AA}^3$	1201.22(10)
Z	2
calc. density/g cm ⁻³	1.215
μ/mm^{-1}	0.087
absorption correction	multi-scan
transmission factor range	0.8730–0.9590
refls. measured	20473
R_{int}	0.0318
mean $\sigma(I)/I$	0.0303
θ range	3.415–27.482
observed refls.	4943
x, y (weighting scheme)	0.0375, 0.1954
hydrogen refinement	constr
Flack parameter	0.4(2)
refls in refinement	5474
parameters	291
restraints	1
$R(F_{\text{obs}})$	0.0344
$R_w(F^2)$	0.0842
S	1.053
shift/error _{max}	0.001
max electron density/e \AA^{-3}	0.171
min electron density/e \AA^{-3}	-0.161

4.3 UV-Vis Data

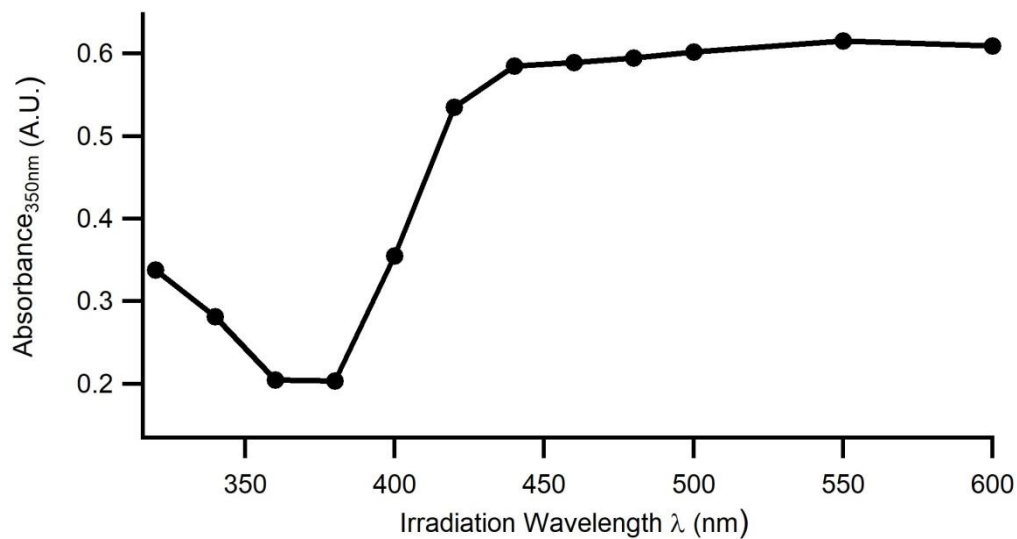
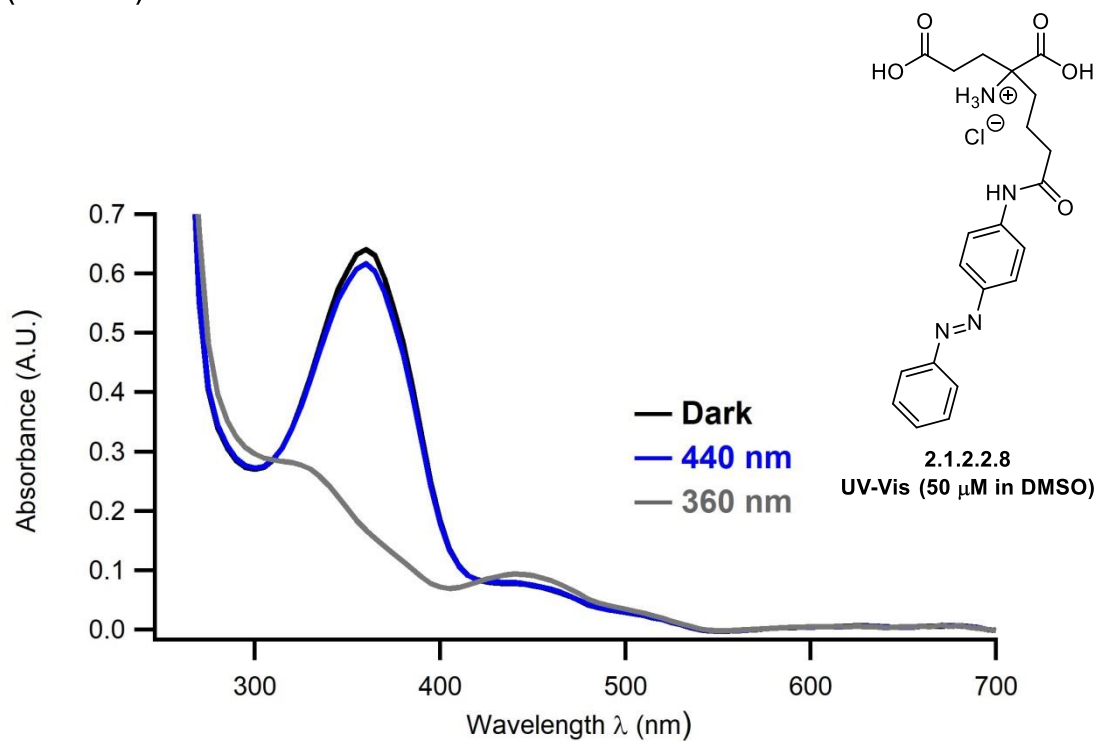
sodium 2-ammonio-2-(3-(4-(phenyldiazenyl)phenyl)prop-2-yn-1-yl)pentanedioate
(2.1.2.1.11 and 2.1.2.2.5)



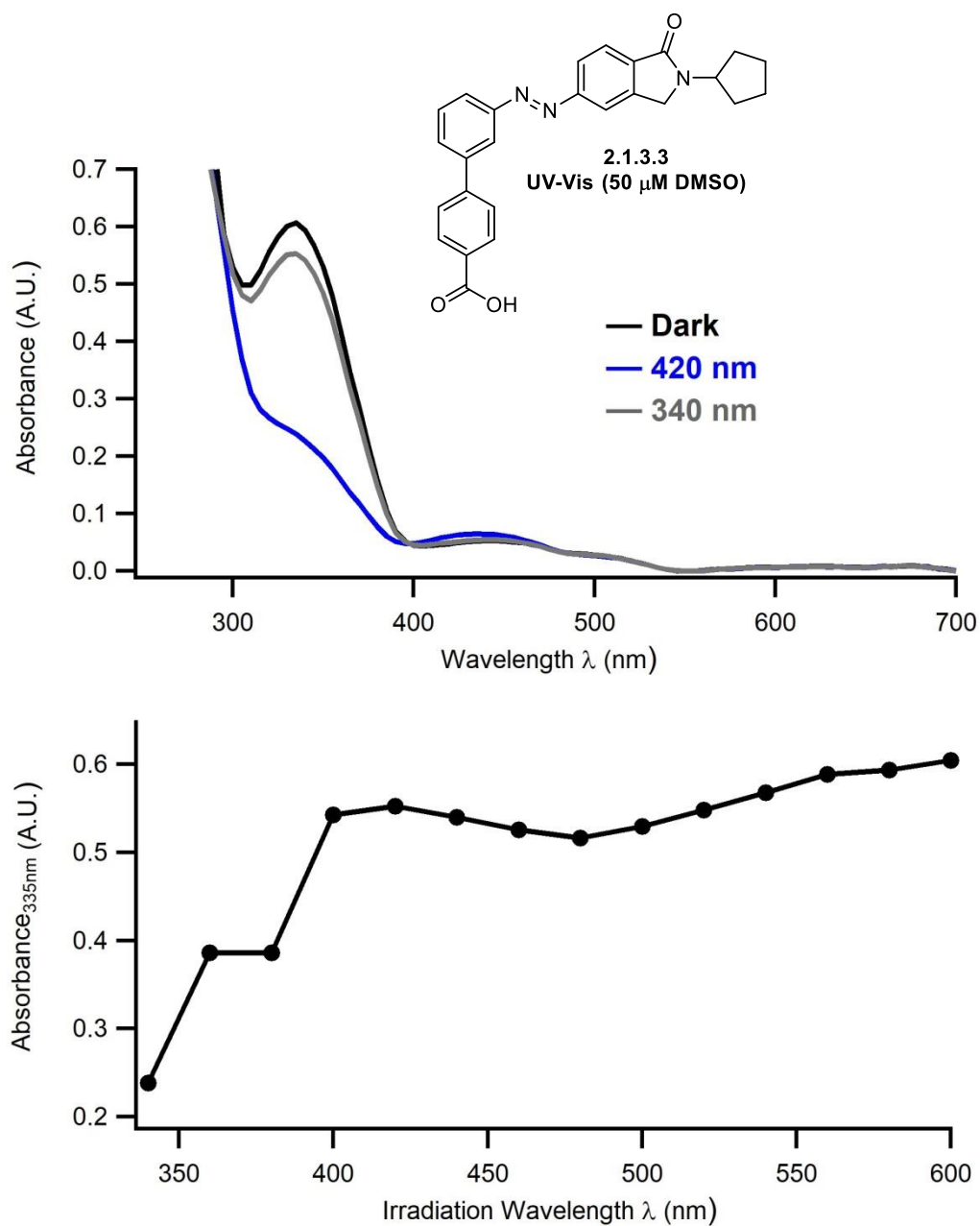
1,3-dicarboxy-6-(4-(phenyldiazenyl)phenyl)hexan-3-aminium chloride (2.1.2.1.15)



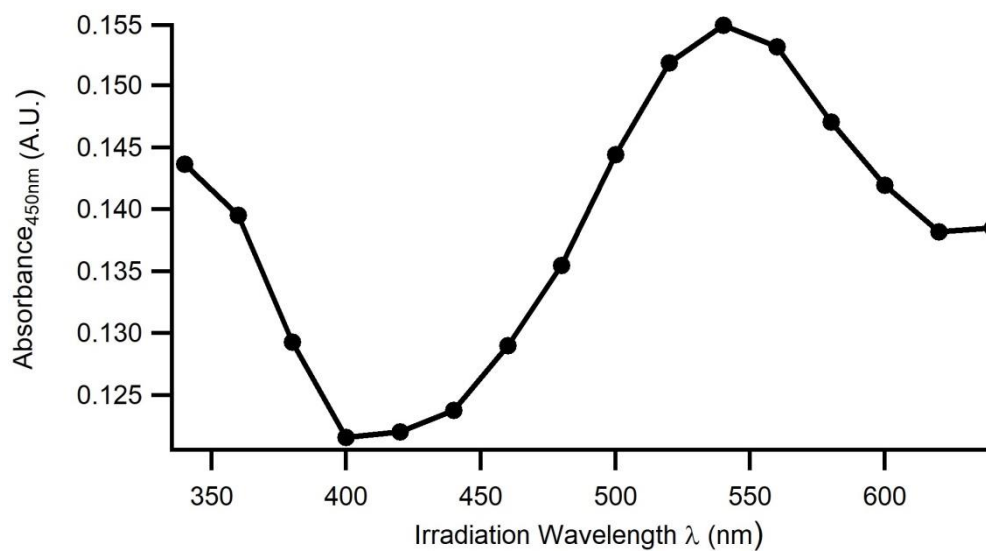
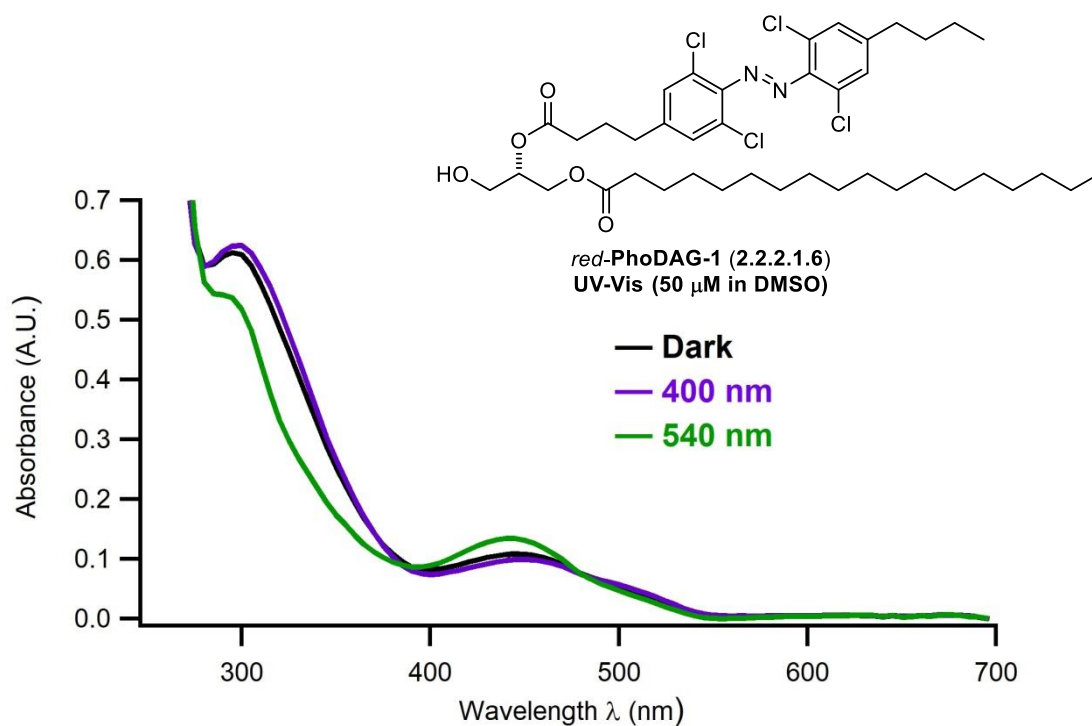
1,3-dicarboxy-7-oxo-7-((4-(phenyldiazenyl)phenyl)amino)heptan-3-aminium chloride
(2.1.2.2.8)



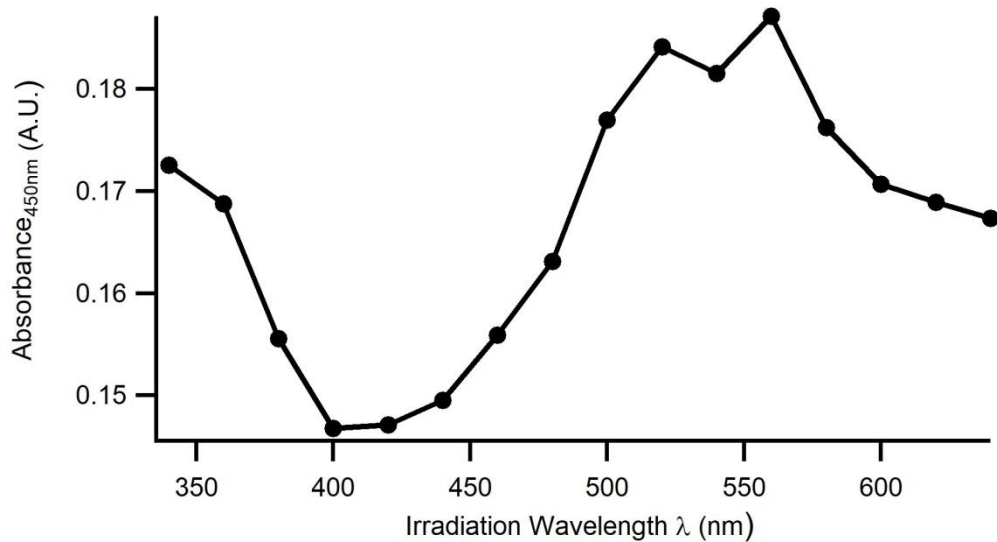
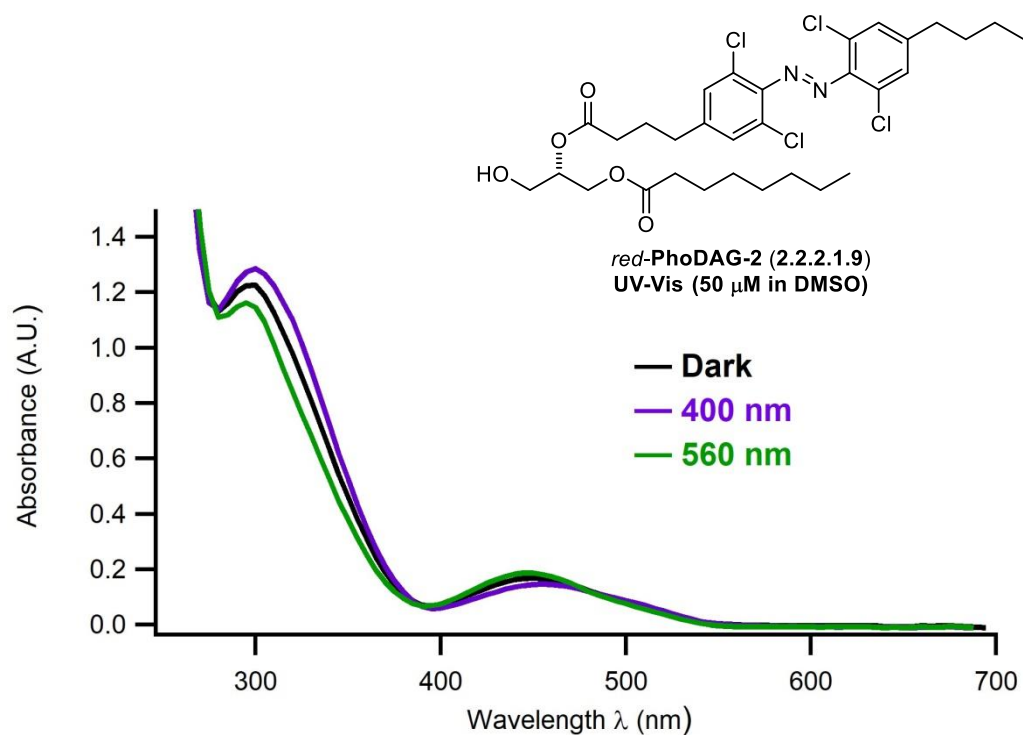
3'-((2-cyclopentyl-1-oxoisindolin-5-yl)diazenyl)-[1,1'-biphenyl]-4-carboxylic acid
(2.1.3.3)



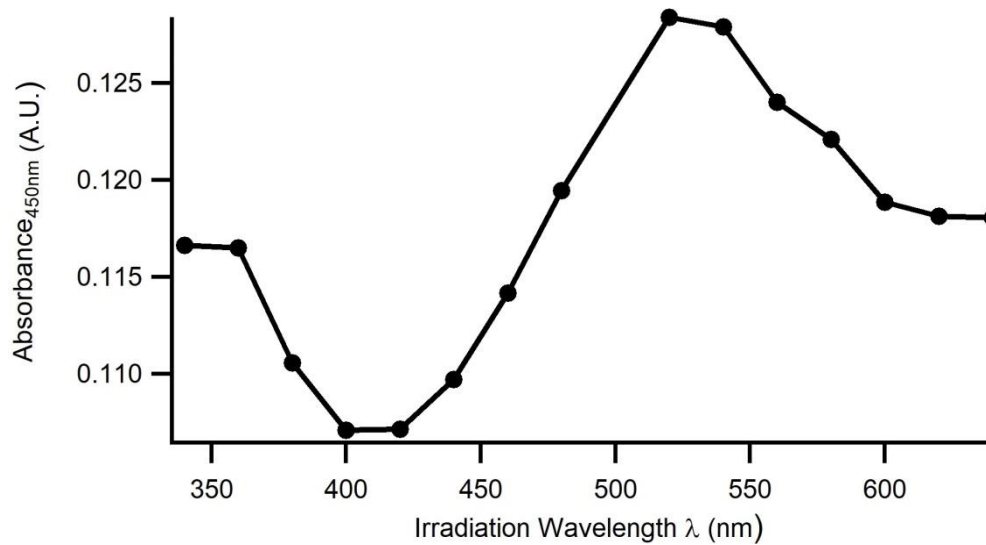
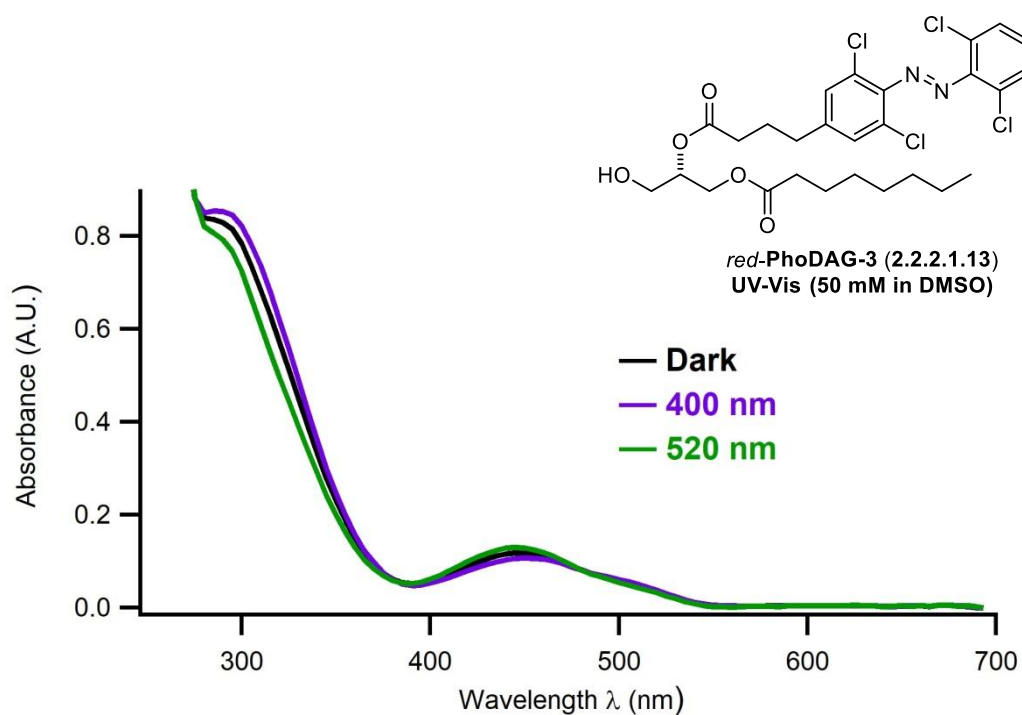
(S)-2-((4-(4-((4-butyl-2,6-dichlorophenyl)diazenyl)-3,5-dichlorophenyl)butanoyl)oxy)-3-hydroxypropyl stearate (*red*-PhoDAG-1, 2.2.2.1.6)



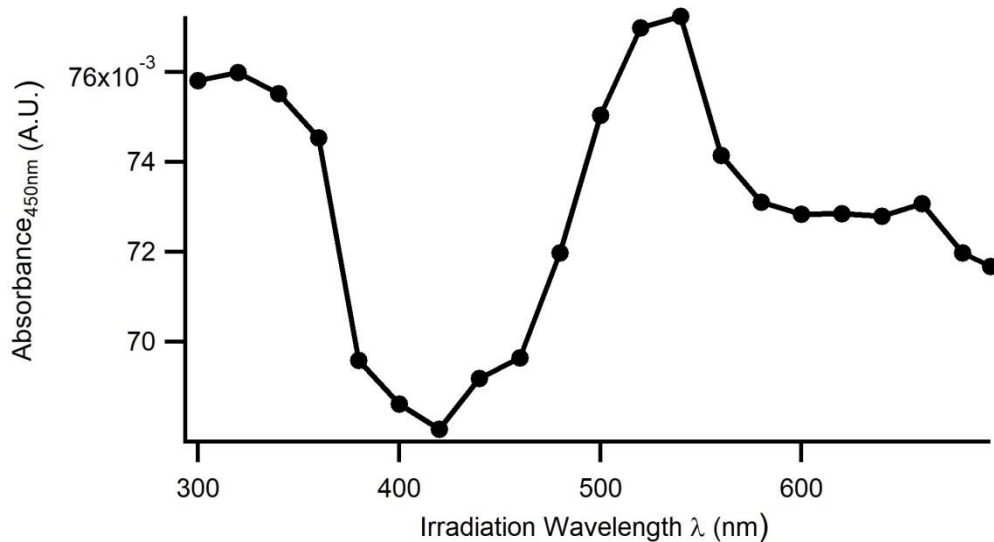
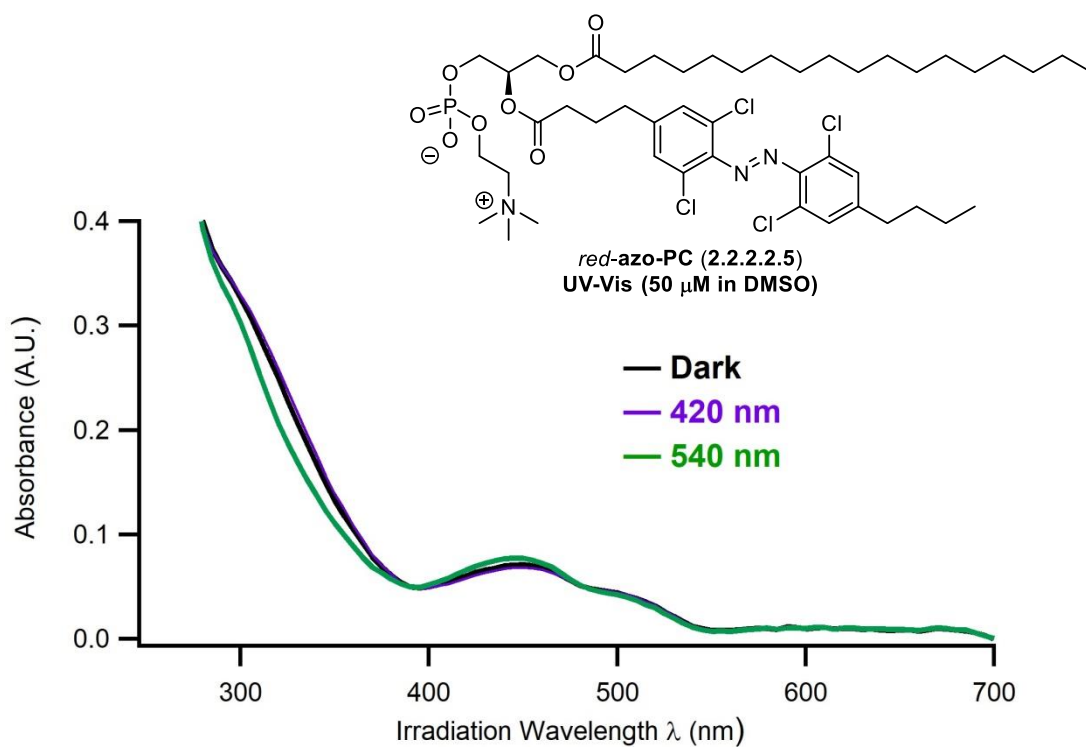
2-((4-(4-((4-butyl-2,6-dichlorophenyl)diazenyl)-3,5-dichlorophenyl)butanoyl)oxy)-3-hydroxypropyl octanoate (*red*-PhoDAG-2, 2.2.2.1.9)



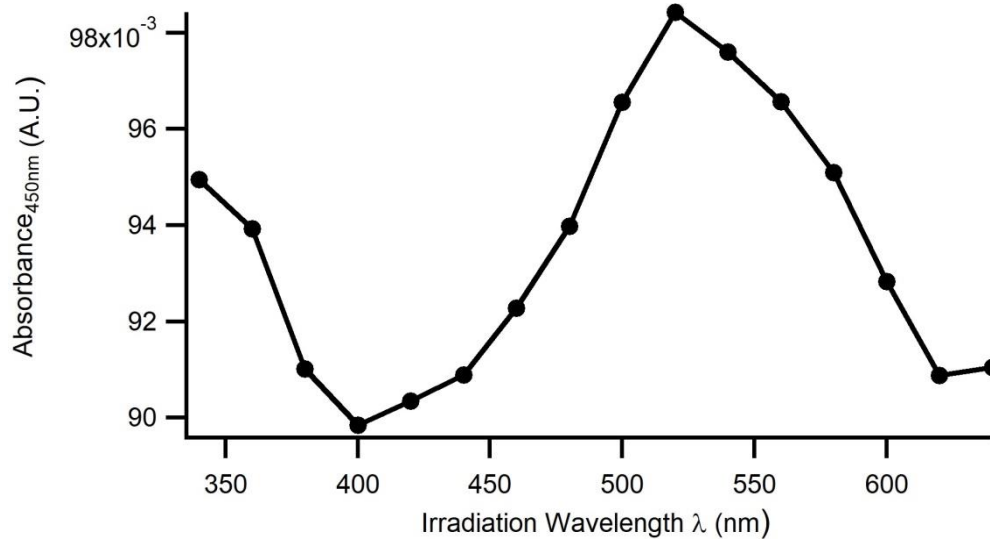
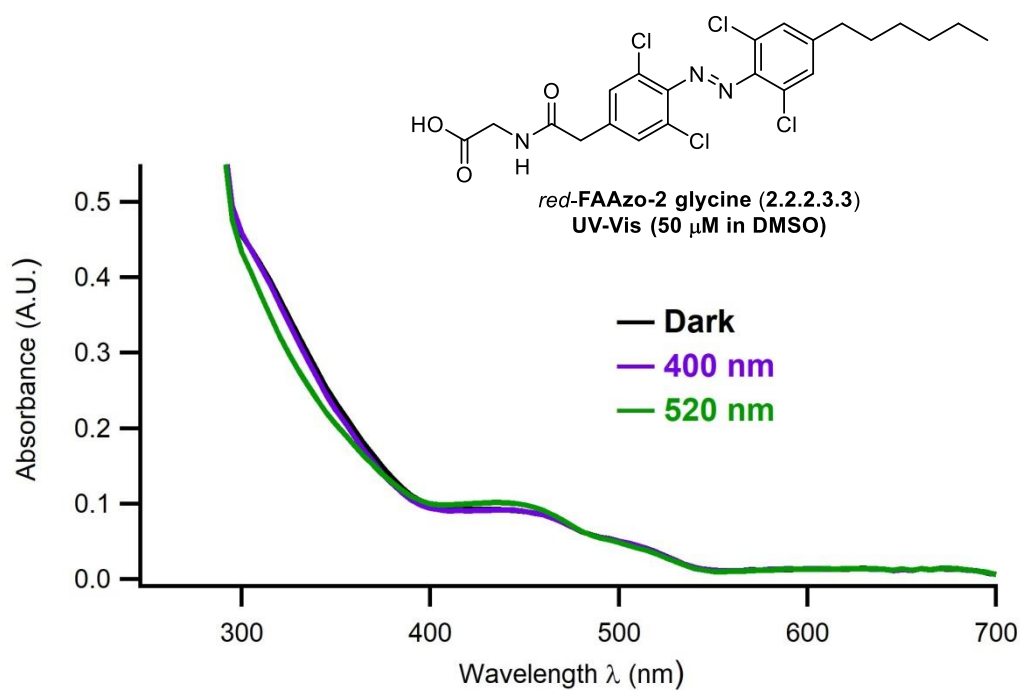
(S)-2-((4-(3,5-dichloro-4-((2,6-dichlorophenyl)diazenyl)phenyl)butanoyl)oxy)-3-hydroxypropyl octanoate (*red*-PhoDAG-3, 2.2.2.1.13)



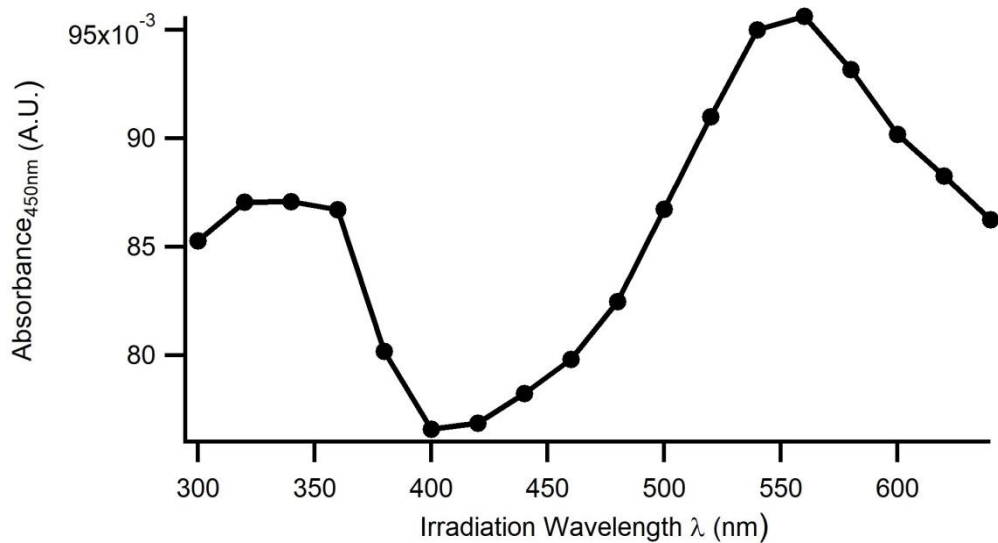
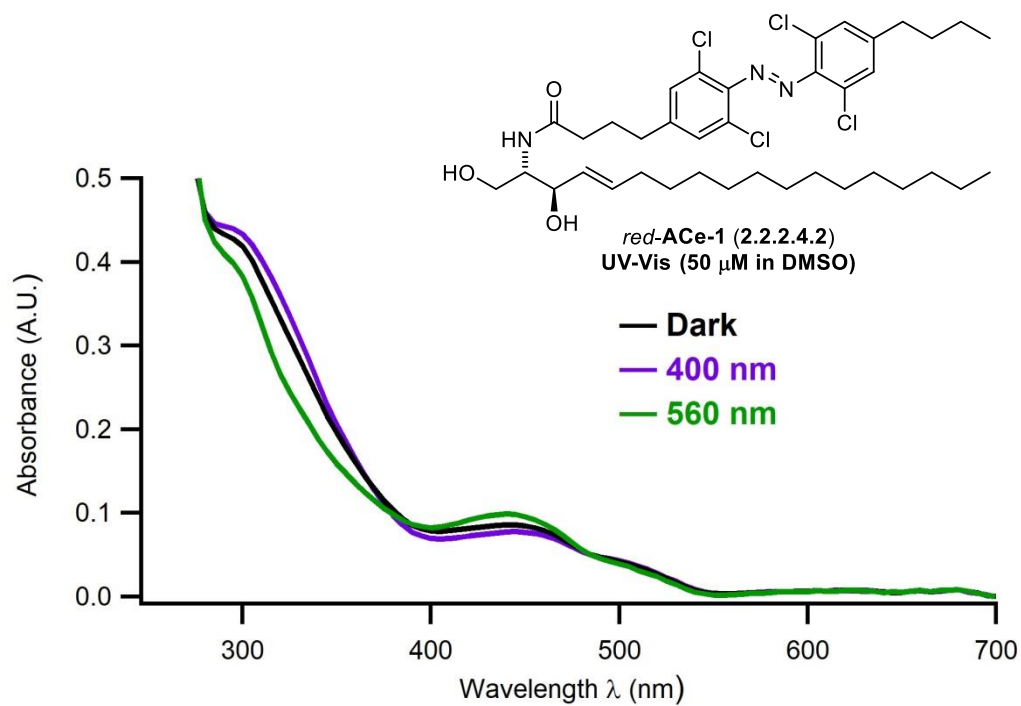
(*R*)-2-((4-(4-((4-butyl-2,6-dichlorophenyl)diazenyl)-3,5-dichlorophenyl)butanoyl)oxy)-3-(stearoyloxy)propyl (2-(trimethylammonio)ethyl) phosphate (*red-azo-PC*, 2.2.2.2.5)



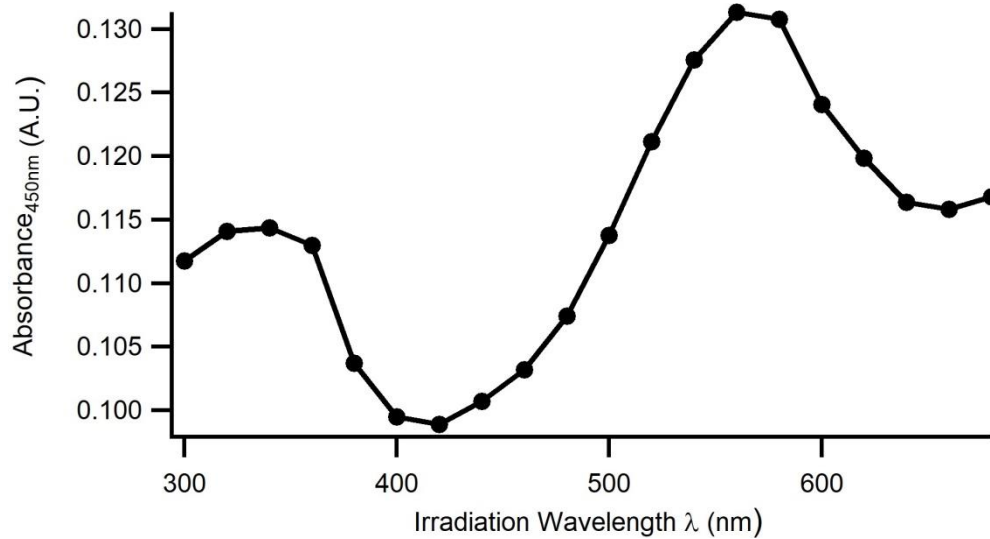
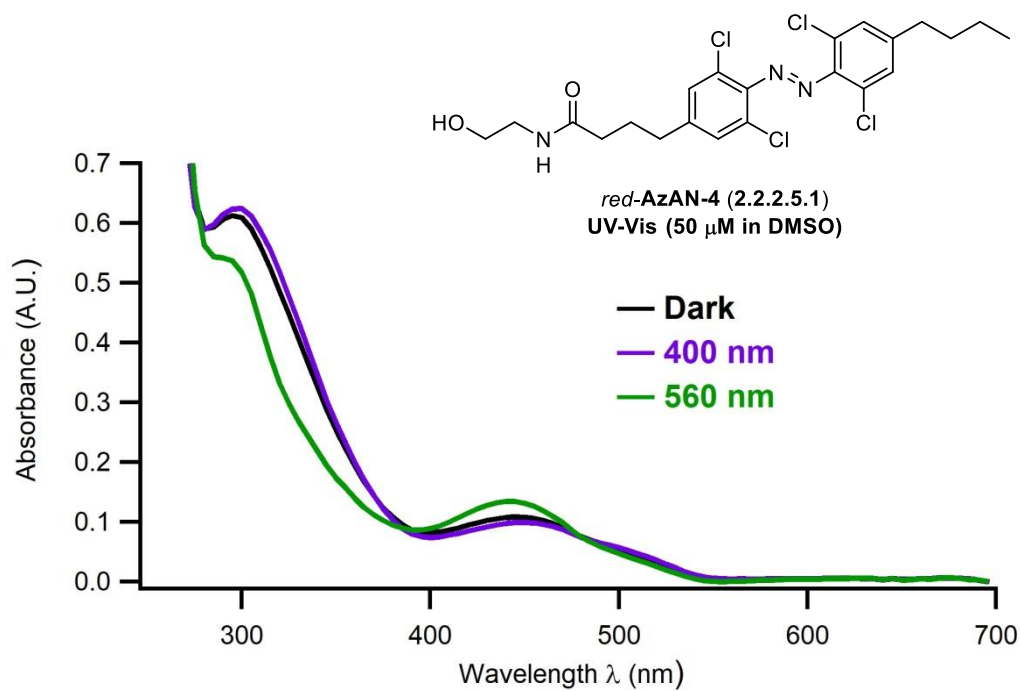
2-(3,5-dichloro-4-((2,6-dichloro-4-hexylphenyl)diazenyl)phenyl)acetyl)glycine (red-FAAzo-2 glycine, 2.2.2.3.3)



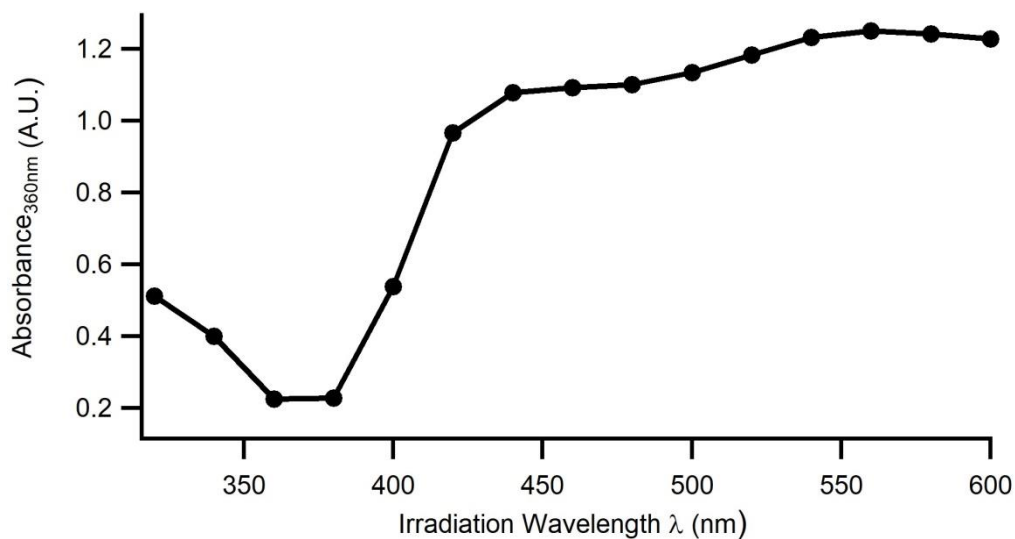
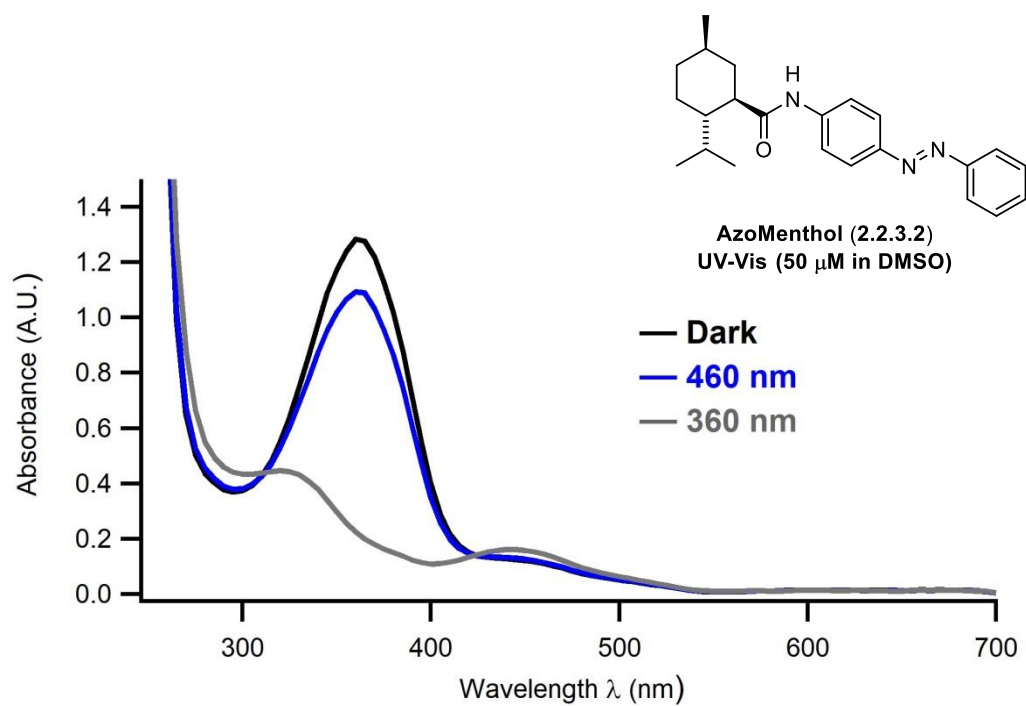
4-(4-((4-butyl-2,6-dichlorophenyl)diazenyl)-3,5-dichlorophenyl)-N-(2-hydroxyethyl)butanamide (*red-ACe-1*, 2.2.2.4.2)



4-(4-((4-butyl-2,6-dichlorophenyl)diazenyl)-3,5-dichlorophenyl)-N-(2-hydroxyethyl)butanamide (*red-AzAN-4*, 2.2.2.5.1)



(1*R*,2*S*,5*R*)-2-isopropyl-5-methyl-*N*-(4-(phenyldiazenyl)phenyl)cyclohexane-1-carboxamide (AzoMenthol, 2.2.3.2)



5 References

- (1) T. N. U. Simidu; D. F. Hwang; Y. Shida; K. Hashimoto *Appl. Environ. Microbiol.* **1987**, *53*, 1714
- (2) Saito, T.; Noguchi, T.; Harada, T.; Murata, O.; Hashimoto, K. *Nippon Suisan Gakk.* **1985**, *51*, 1175.
- (3) Hanifin, C. T. *Mar. Drugs* **2010**, *8*, 577.
- (4) Catterall, W. A.; Goldin, A. L.; Waxman, S. G. *Pharmacol. Rev.* **2005**, *57*, 397.
- (5) Tahara, Y. *Biochem. Z.* **1911**, *10*, 255.
- (6) Yokoo, A. *J. Chem. Soc. Jpn* **1950**, *71*, 590.
- (7) Woodward, R. B. *Pure Appl. Chem.* **1964**, *9*, 49.
- (8) Goto, T.; Kishi, Y.; Takahashi, S.; Hirata, Y. *Tetrahedron* **1965**, *21*, 2059.
- (9) Tsuda, K.; Ikuma, S.; Kawamura, M.; Tachikawa, R.; Sakai, K.; Tamura, C.; Amakasu, O. *Chem. Pharm. Bull.* **1964**, *12*, 1357.
- (10) Furusaki, A.; Tomiie, Y.; Nitta, I. *Bull. Chem. Soc. Jpn.* **1970**, *43*, 3332.
- (11) Kishi, Y.; Aratani, M.; Fukuyama, T.; Nakatsubo, F.; Goto, T.; Inoue, S.; Tanino, H.; Sugiura, S.; Kakoi, H. *J. Am. Chem. Soc.* **1972**, *94*, 9217.
- (12) Kishi, Y.; Fukuyama, T.; Aratani, M.; Nakatsubo, F.; Goto, T.; Inoue, S.; Tanino, H.; Sugiura, S.; Kakoi, H. *J. Am. Chem. Soc.* **1972**, *94*, 9219.
- (13) Kishi, Y.; Nakatsubo, F.; Aratani, M.; Goto, T.; Inoue, S.; Kakoi, H. *Tetrahedron Lett.* **1970**, *11*, 5129.
- (14) Kishi, Y.; Nakatsubo, F.; Aratani, M.; Goto, T.; Inoue, S.; Kakoi, H.; Sugiura, S. *Tetrahedron Lett.* **1970**, *11*, 5127.
- (15) Chau, J.; Ciufolini, M. A. *Mar. Drugs* **2011**, *9*, 2046.
- (16) Nicolaou, K. C. C., J. S., *Classics in Total Synthesis III*. Wiley-VCH: 2011.
- (17) Walker, J. R.; Novick, P. A.; Parsons, W. H.; McGregor, M.; Zablocki, J.; Pande, V. S.; Du Bois, J. *Proc. Natl. Acad. Sci.* **2012**, *109*, 18102.
- (18) Yu, F. H.; Catterall, W. A. *Genome Biol.* **2003**, *4*, 207.
- (19) Chen, R.; Chung, S.-H. *Biochem. Biophys. Res. Commun.* **2014**, *446*, 370.
- (20) Rosker, C.; Lohberger, B.; Hofer, D.; Steinecker, B.; Quasthoff, S.; Schreibmayer, W. *Am. J. Physiol. Cell Physiol.* **2007**, *293*, C783.
- (21) Fozzard, H. A.; Lipkind, G. M. *Mar. Drugs* **2010**, *8*, 219.
- (22) Payandeh, J.; Scheuer, T.; Zheng, N.; Catterall, W. A. *Nature* **2011**, *475*, 353.
- (23) Noguchi, T.; Arakawa, O. *Mar. Drugs* **2008**, *6*, 220.
- (24) Venkatesh, B.; Lu, S. Q.; Dandona, N.; See, S. L.; Brenner, S.; Soong, T. W. *Curr. Biol.* **2005**, *15*, 2069.
- (25) Hashiguchi, Y.; Lee, J. M.; Shiraiishi, M.; Komatsu, S.; Miki, S.; Shimasaki, Y.; Mochioka, N.; Kusakabe, T.; Oshima, Y. *J. Evol. Biol.* **2015**, *28*, 1103.
- (26) Yotsu-Yamashita, M.; Okoshi, N.; Watanabe, K.; Araki, N.; Yamaki, H.; Shoji, Y.; Terakawa, T. *Toxicon* **2013**, *72*, 23.
- (27) Yotsu-Yamashita, M.; Sugimoto, A.; Terakawa, T.; Shoji, Y.; Miyazawa, T.; Yasumoto, T. *Eur J Biochem* **2001**, *268*, 5937.
- (28) Jal, S.; Khora, S. S. *J. Appl. Microbiol.* **2015**, *119*, 907.
- (29) Bane, V.; Lehane, M.; Dikshit, M.; Riordan, A.; Furey, A. *Toxins* **2014**, *6*, 693.
- (30) Hanifin, C. T.; Brodie, E. D.; Brodie, E. D. *Toxicon* **2002**, *40*, 1149.
- (31) Pires, O. R.; Sebben, A.; Schwartz, E. F.; Morales, R. A. V.; Bloch, C.; Schwartz, C. A. *Toxicon* **2005**, *45*, 73.
- (32) Noguchi, T.; Arakawa, O. *Mar. Drugs* **2008**, *6*, 220.
- (33) Matsumura, K. *Nature* **1995**, *378*, 563.
- (34) Brodie, E.; Brodie Jr, E. *Evolution* **1990**, *44*, 651.

- (35) Williams, B.; Brodie, E. J. *Chem. Ecol.* **2004**, *30*, 1901.
- (36) Sheumack, D.; Howden, M.; Spence, I.; Quinn, R. *Science* **1978**, *199*, 188.
- (37) Copyright © 2014 by Brocken Inaglory. The photograph was obtained from the URL: https://commons.wikimedia.org/wiki/File:Puffer_Fish_DSC01257.JPG (active as of May 2018) and is licensed under the Creative Commons Attribution-Share Alike 3.0 License (<https://creativecommons.org/licenses/by-sa/3.0/deed.en>). It is used here in its unmodified form.
- (38) Copyright © 2012 by Shubham Chatterjee. The photograph was obtained from the URL: https://commons.wikimedia.org/wiki/File:Tachypleus_gigas.JPG (active as of May 2018) and is licensed under the Creative Commons Attribution-Share Alike 3.0 Unreported License (<https://creativecommons.org/licenses/by-sa/3.0/deed.en>). It is used here in its unmodified form.
- (39) Copyright © 2013 by Sylke Rohrlach. The photograph was obtained from the URL: [https://commons.wikimedia.org/wiki/File:Blue-ringed_octopus_\(Hapalochlaena_maculosa\),_Parsley_Bay,_Sydney,_NSW.jpeg](https://commons.wikimedia.org/wiki/File:Blue-ringed_octopus_(Hapalochlaena_maculosa),_Parsley_Bay,_Sydney,_NSW.jpeg) (active as of May 2018) and is licensed under the Creative Commons Attribution-Share Alike 3.0 License (<https://creativecommons.org/licenses/by-sa/3.0/deed.en>). It is used here in its unmodified form.
- (40) Copyright © 2015 by Connor Long. The photograph was obtained from the URL: https://en.wikipedia.org/wiki/File:Taricha_torosa,_Napa_County,_CA.jpg (active as of May 2018) and is licensed under the Creative Commons Attribution-Share Alike 3.0 License (<https://creativecommons.org/licenses/by-sa/3.0/>). It is used here in its unmodified form.
- (41) Copyright © 2011 by Brian Gratwicke. The photograph was obtained from the URL: https://commons.wikimedia.org/wiki/File:Atelopus_limosus_female_02.jpg (active as of May 2018) and is licensed under the Creative Commons Attribution 2.0 Generic License (<https://creativecommons.org/licenses/by/2.0/deed.en>). It is used here in its unmodified form.
- (42) Copyright © 2010 by Mark A. Wilson. The photograph was obtained from the URL: https://commons.wikimedia.org/wiki/File:Thamnophis_sirtalis_sirtalis_Wooster.jpg (active as of May 2018) and was released into the public. It is used here in its unmodified form.
- (43) Mebs, D.; Yotsu-Yamashita, M. *Toxicon* **2012**, *60*, 120.
- (44) Tsuruda, K.; Arakawa, O.; Kawatsu, K.; Hamano, Y.; Takatani, T.; Noguchi, T. *Toxicon* **2002**, *40*, 131.
- (45) Yotsu-Yamashita, M.; Mebs, D.; Kwet, A.; Schneider, M. *Toxicon* **2007**, *50*, 306.
- (46) Yotsu, M.; Iorizzi, M.; Yasumoto, T. *Toxicon* **1990**, *28*, 238.
- (47) Do, H. K.; Kogure, K.; Simidu, U. *Appl. Environ. Microbiol.* **1990**, *56*, 1162.
- (48) Yasumoto, T.; Yasumura, D.; Yotsu, M.; Michishita, T.; Endo, A.; Kotaki, Y. *Agric. Biol. Chem.* **1986**, *50*, 793.
- (49) Noguchi, T.; Jeon, J.-K.; Arakawa, O.; Sugita, H.; Deguchi, Y.; Shida, Y.; Hashimoto, K. *J. Biochem.* **1986**, *99*, 311.
- (50) Lee, M.-J.; Jeong, D.-Y.; Kim, W.-S.; Kim, H.-D.; Kim, C.-H.; Park, W.-W.; Park, Y.-H.; Kim, K.-S.; Kim, H.-M.; Kim, D.-S. *Appl. Environ. Microbiol.* **2000**, *66*, 1698.
- (51) Noguchi, T.; Arakawa, O.; Takatani, T. *Comp. Biochem. Physiol., Part D: Genomics Proteomics* **2006**, *1D*, 153.
- (52) Yotsu-Yamashita, M.; Gilhen, J.; Russell, R. W.; Krysko, K. L.; Melaun, C.; Kurz, A.; Kaufenstein, S.; Kordis, D.; Mebs, D. *Toxicon* **2012**, *59*, 257.
- (53) Hanifin, C. T. *Mar. Drugs* **2010**, *8*, 577.
- (54) Yotsu-Yamashita, M.; Mebs, D.; Yasumoto, T. *Toxicon* **1992**, *30*, 1489.
- (55) Pettit, R. K. *Mar. Biotechnol.* **2011**, *13*, 1.
- (56) Mosher, H. S. *Ann. N. Y. Acad. Sci.* **1986**, *479*, 32.
- (57) Teramoto, N.; Yotsu-Yamashita, M. *Mar. Drugs* **2015**, *13*, 984.
- (58) Yasumoto, T.; Yotsu-Yamashita, M. *Toxin Rev.* **1996**, *15*, 81.
- (59) Kudo, Y.; Yasumoto, T.; Konoki, K.; Cho, Y.; Yotsu-Yamashita, M. *Mar. Drugs* **2012**, *10*, 655.
- (60) Yasumoto, T.; Yotsu, M.; Endo, A.; Murata, M.; Naoki, H. *Pure Appl. Chem.* **1989**, *61*, 505.

- (61) Pires, O. R.; Sebben, A.; Schwartz, E. F.; Bloch, C.; Morales, R. A. V.; Schwartz, C. A. *Toxicon* **2003**, *42*, 563.
- (62) Pires, O. R.; Sebben, A.; Schwartz, E. F.; Largura, S. W. R.; Bloch, C.; Morales, R. A. V.; Schwartz, C. A. *Toxicon* **2002**, *40*, 761.
- (63) Khora, S. S.; Yasumoto, T. *Tetrahedron Lett.* **1989**, *30*, 4393.
- (64) Luo, X.; Yu, R. C.; Wang, X. J.; Zhou, M. J. *Food Addit. Contam. A* **2012**, *29*, 117.
- (65) Arakawa, O.; Noguchi, T.; Shida, Y.; Onoue, Y. *Fish Aquatic Sci.* **1994**, *60*, 769.
- (66) McNabb, P.; Selwood, A. I.; Munday, R.; Wood, S. A.; Taylor, D. I.; MacKenzie, L. A.; van Ginkel, R.; Rhodes, L. L.; Cornelisen, C.; Heasman, K.; Holland, P. T.; King, C. *Toxicon* **2010**, *56*, 466.
- (67) Rodríguez, P.; Alfonso, A.; Otero, P.; Katikou, P.; Georgantelis, D.; Botana, L. M. *Food Chem.* **2012**, *132*, 1103.
- (68) Silva, M.; Azevedo, J.; Rodriguez, P.; Alfonso, A.; Botana, L. M.; Vasconcelos, V. *Mar. Drugs* **2012**, *10*, 712.
- (69) Zaman, L.; Arakawa, O.; Shimosu, A.; Onoue, Y. *Toxicon* **1997**, *35*, 423.
- (70) Yotsu, M.; Hayashi, Y.; Khora, S. S.; Sato, S. i.; Yasumoto, T. *Biosci. Biotechnol. Biochem.* **1992**, *56*, 370.
- (71) Jang, J.-H.; Lee, J.-S.; Yotsu-Yamashita, M. *Mar. Drugs* **2010**, *8*, 1049.
- (72) Yotsu-Yamashita, M.; Abe, Y.; Kudo, Y.; Ritson-Williams, R.; Paul, V.; Konoki, K.; Cho, Y.; Adachi, M.; Imazu, T.; Nishikawa, T.; Isobe, M. *Mar. Drugs* **2013**, *11*, 2799.
- (73) Ritson-Williams, R.; Yotsu-Yamashita, M.; Paul, V. J. *Proc. Natl. Acad. Sci.* **2006**, *103*, 3176.
- (74) Nishikawa, T.; Asai, M.; Ohyabu, N.; Yamamoto, N.; Isobe, M. *Angew. Chem. Int. Ed.* **1999**, *38*, 3081.
- (75) Kotaki, Y.; Shimizu, Y. *J. Am. Chem. Soc.* **1993**, *115*, 827.
- (76) Jang, J.; Yotsu-Yamashita, M. *Toxicon* **2006**, *48*, 980.
- (77) Yotsu-Yamashita, M.; Goto, A.; Nakagawa, T. *Chem. Res. Toxicol.* **2005**, *18*, 865.
- (78) Kim, Y.; Brown, G.; Mosher, F. *Science* **1975**, *189*, 151.
- (79) Yang, L.; Kao, C. Y. *J. Gen. Physiol.* **1992**, *100*, 609.
- (80) Kudo, Y.; Yamashita, Y.; Mebs, D.; Cho, Y.; Konoki, K.; Yasumoto, T.; Yotsu-Yamashita, M. *Angew. Chem. Int. Ed.* **2014**, *53*, 14546.
- (81) Rodríguez, I.; Alfonso, A.; Alonso, E.; Rubiolo, J. A.; Roel, M.; Vlamis, A.; Katikou, P.; Jackson, S. A.; Menon, M. L.; Dobson, A.; Botana, L. M. *Sci. Rep.* **2017**, *7*, 40880.
- (82) Satake, Y.; Adachi, M.; Tokoro, S.; Yotsu-Yamashita, M.; Isobe, M.; Nishikawa, T. *Chem. Asian J.* **2014**, *9*, 1922.
- (83) Yotsu-Yamashita, M.; Sugimoto, A.; Takai, A.; Yasumoto, T. *J. Pharmacol. Exp. Ther.* **1999**, *289*, 1688.
- (84) Kao, C. Y. *Ann. N. Y. Acad. Sci.* **1986**, *479*, 52.
- (85) Kao, C. Y.; Yasumoto, T. *Toxicon* **1985**, *23*, 725.
- (86) Kao, C. Y. *Toxicon* **1982**, *20*, 1043.
- (87) Yang, L.; Kao, C. Y. *J. Gen. Physiol.* **1992**, *100*, 609.
- (88) Yang, L.; Kao, C. Y.; Yasumoto, T. *Toxicon* **1992**, *30*, 635.
- (89) Wu, B. Q.; Yang, L.; Kao, C. Y.; Levinson, S. R.; Yotsu-Yamashita, M.; Yasumoto, T. *Toxicon* **1996**, *34*, 407.
- (90) Yotsu-Yamashita, M.; Urabe, D.; Asai, M.; Nishikawa, T.; Isobe, M. *Toxicon* **2003**, *42*, 557.
- (91) Botana, L. M.; Hess, P.; Munday, R.; Nathalie, A.; DeGrasse, S. L.; Feeley, M.; Suzuki, T.; van den Berg, M.; Fattori, V.; Garrido Gamarro, E.; Tritscher, A.; Nakagawa, R.; Karunasagar, I. *Trends Food Sci. Technol.* **2017**, *59*, 15.
- (92) Yotsu-Yamashita, M.; Yamagishi, Y.; Yasumoto, T. *Tetrahedron Lett.* **1995**, *36*, 9329.
- (93) Kao, C. Y.; Yeoh, P. N.; Goldfinger, M. D.; Fuhrman, F. A.; Mosher, H. S. *J. Pharmacol. Exp. Ther.* **1981**, *217*, 416.

- (94) Rosker, C.; Lohberger, B.; Hofer, D.; Steinecker, B.; Quasthoff, S.; Schreibmayer, W. *Am. J. Physiol.* **2007**, *293*, C783.
- (95) Kudo, Y.; Cho, Y.; Konoki, K.; Yotsu-Yamashita, M.; Yasumoto, T.; Mebs, D. *Angew Chem Int Ed Engl* **2016**, *55*, 8728.
- (96) Yasumoto, T.; Yotsu, M.; Murata, M.; Naoki, H. *J. Am. Chem. Soc.* **1988**, *110*, 2344.
- (97) Nozomi, U.; Keita, S.; Yuta, K.; Ken-ichi, O.; Yuko, C.; Keiichi, K.; Toshio, N.; Mari, Y. Y. *Chem. Eur. J.* **2018**, *24*, 7250.
- (98) Shimizu, Y.; Kobayashi, M. *Chem. Pharm. Bull.* **1983**, *31*, 3625.
- (99) Kudo, Y.; Yasumoto, T.; Mebs, D.; Cho, Y.; Konoki, K.; Yotsu-Yamashita, M. *Angew. Chem. Int. Ed.* **2016**, *128*, 8870.
- (100) Kurosawa, E. *Bull. Chem. Soc. Jpn.* **1961**, *34*, 300.
- (101) Ohyabu, N.; Nishikawa, T.; Isobe, M. *J. Am. Chem. Soc.* **2003**, *125*, 8798.
- (102) Ichikawa, Y.; Isobe, M.; Bai, D.-L.; Goto, T. *Tetrahedron* **1987**, *43*, 4737.
- (103) Nishikawa, T.; Urabe, D.; Isobe, M. *Angew. Chem. Int. Ed.* **2004**, *43*, 4782.
- (104) Ebata, T.; Matsushita, H. *J. Syn. Org. Chem. Jpn* **1994**, *52*, 1074.
- (105) Nishikawa, T.; Asai, M.; Ohyabu, N.; Yamamoto, N.; Fukuda, Y.; Isobe, M. *Tetrahedron* **2001**, *57*, 3875.
- (106) Asai, M.; Nishikawa, T.; Ohyabu, N.; Yamamoto, N.; Isobe, M. *Tetrahedron* **2001**, *57*, 4543.
- (107) Nishikawa, T.; Asai, M.; Isobe, M. *J. Am. Chem. Soc.* **2002**, *124*, 7847.
- (108) Adachi, M.; Imazu, T.; Sakakibara, R.; Satake, Y.; Isobe, M.; Nishikawa, T. *Chem. Eur. J.* **2014**, *20*, 1247.
- (109) Nishikawa, T.; Urabe, D.; Yoshida, K.; Iwabuchi, T.; Asai, M.; Isobe, M. *Chem. Eur. J.* **2004**, *10*, 452.
- (110) Nishikawa, T.; Urabe, D.; Yoshida, K.; Iwabuchi, T.; Asai, M.; Isobe, M. *Org. Lett.* **2002**, *4*, 2679.
- (111) Adachi, M.; Sakakibara, R.; Satake, Y.; Isobe, M.; Nishikawa, T. *Chem. Lett.* **2014**, *43*, 1719.
- (112) Carreira, E. M.; Du Bois, J. *J. Am. Chem. Soc.* **1994**, *116*, 10825.
- (113) Hinman, A.; Du Bois, J. *J. Am. Chem. Soc.* **2003**, *125*, 11510.
- (114) Akai, S.; Seki, H.; Sugita, N.; Kogure, T.; Nishizawa, N.; Suzuki, K.; Nakamura, Y.; Kajihara, Y.; Yoshimura, J.; Sato, K.-i. *Bull. Chem. Soc. Jpn.* **2010**, *83*, 279.
- (115) Sato, K.-i.; Akai, S.; Shoji, H.; Sugita, N.; Yoshida, S.; Nagai, Y.; Suzuki, K.; Nakamura, Y.; Kajihara, Y.; Funabashi, M.; Yoshimura, J. *J. Org. Chem.* **2008**, *73*, 1234.
- (116) Sato, K.-i.; Akai, S.; Sugita, N.; Ohsawa, T.; Kogure, T.; Shoji, H.; Yoshimura, J. *J. Org. Chem.* **2005**, *70*, 7496.
- (117) Chau, J.; Xu, S.; Ciufolini, M. A. *J. Org. Chem.* **2013**, *78*, 11901.
- (118) Mendelsohn, B. A.; Ciufolini, M. A. *Org. Lett.* **2009**, *11*, 4736.
- (119) Xu, S.; Ciufolini, M. A. *Org. Lett.* **2015**, *17*, 2424.
- (120) Ciufolini, M. A.; Braun, N. A.; Canesi, S.; Ousmer, M.; Chang, J.; Chai, D. *Synthesis* **2007**, *2007*, 3759.
- (121) Maehara, T.; Motoyama, K.; Toma, T.; Yokoshima, S.; Fukuyama, T. *Angew. Chem. Int. Ed.* **2017**, *56*, 1549.
- (122) Bulow, L.; Naini, A.; Fohrer, J.; Kalesse, M. *Org. Lett.* **2011**, *13*, 6038.
- (123) Kiyooka, S.; Kaneko, Y.; Komura, M.; Matsuo, H.; Nakano, M. *J. Org. Chem.* **1991**, *56*, 2276.
- (124) Tsubuki, M.; Okita, H.; Honda, T. *Heterocycles* **2006**, *67*, 731.
- (125) Ishikawa, T.; Shimizu, Y.; Kudoh, T.; Saito, S. *Org. Lett.* **2003**, *5*, 3879.
- (126) Reeve, W.; Erikson, C. M.; Aluotto, P. F. *Can. J. Chem.* **1979**, *57*, 2747.
- (127) Bordwell, F. G.; Bartmess, J. E.; Hautala, J. A. *J. Org. Chem.* **1978**, *43*, 3107.
- (128) Phan, T. B.; Mayr, H. *Can. J. Chem.* **2005**, *83*, 1554.
- (129) Bug, T.; Lemek, T.; Mayr, H. *J. Org. Chem.* **2004**, *69*, 7565.
- (130) Lemek, T.; Mayr, H. *J. Org. Chem.* **2003**, *68*, 6880.
- (131) Diethelm, S.; Carreira, E. M. *J. Am. Chem. Soc.* **2015**, *137*, 6084.

- (132) Gopalakrishnan, R.; Kozany, C.; Gaali, S.; Kress, C.; Hoogeland, B.; Bracher, A.; Hausch, F. *J. Med. Chem.* **2012**, *55*, 4114.
- (133) Lee, H. J.; Lim, C.; Hwang, S.; Jeong, B. S.; Kim, S. *Chem. Asian J.* **2011**, *6*, 1943.
- (134) Chakraborty, C.; Vyavahare, V. P.; Dhavale, D. D. *Tetrahedron* **2007**, *63*, 11984.
- (135) Mercadante, M. A.; Kelly, C. B.; Bobbitt, J. M.; Tilley, L. J.; Leadbeater, N. E. *Nat. Protoc.* **2013**, *8*, 666.
- (136) Cartmell, J.; Adam, G.; Chaboz, S.; Henningsen, R.; Kemp, J. A.; Klingelschmidt, A.; Metzler, V.; Monsma, F.; Schaffhauser, H.; Wichmann, J.; Mutel, V. *Br. J. Pharmacol.* **1998**, *123*, 497.
- (137) Schweitzer, C.; Kratzeisen, C.; Adam, G.; Lundstrom, K.; Malherbe, P.; Ohresser, S.; Stadler, H.; Wichmann, J.; Woltering, T.; Mutel, V. *Neuropharmacology* **2000**, *39*, 1700.
- (138) Cai, S.-L.; Song, R.; Dong, H.-Q.; Lin, G.-Q.; Sun, X.-W. *Org. Lett.* **2016**, *18*, 1996.
- (139) Sheffler, D. J.; Pinkerton, A. B.; Dahl, R.; Markou, A.; Cosford, N. D. P. *ACS Chem. Neurosci.* **2011**, *2*, 382.
- (140) Schoenberger, M.; Damijonaitis, A.; Zhang, Z.; Nagel, D.; Trauner, D. *ACS Chem. Neurosci.* **2014**, *5*, 514.
- (141) Bonnefous, C.; Vernier, J.-M.; Hutchinson, J. H.; Gardner, M. F.; Cramer, M.; James, J. K.; Rowe, B. A.; Daggett, L. P.; Schaffhauser, H.; Kamenecka, T. M. *Bioorganic Med. Chem. Lett* **2005**, *15*, 4354.
- (142) Dhanya, R. P.; Sidique, S.; Sheffler, D. J.; Nickols, H. H.; Herath, A.; Yang, L.; Dahl, R.; Ardecky, R.; Semenova, S.; Markou, A.; Conn, P. J.; Cosford, N. D. *J. Med. Chem.* **2011**, *54*, 342.
- (143) Sidique, S.; Dhanya, R.-P.; Sheffler, D. J.; Nickols, H. H.; Yang, L.; Dahl, R.; Mangravita-Novo, A.; Smith, L. H.; D'Souza, M. S.; Semenova, S.; Conn, P. J.; Markou, A.; Cosford, N. D. P. *J. Med. Chem.* **2012**, *55*, 9434.
- (144) Frank, J. A.; Yushchenko, D. A.; Hodson, D. J.; Lipstein, N.; Nagpal, J.; Rutter, G. A.; Rhee, J.-S.; Gottschalk, A.; Brose, N.; Schultz, C.; Trauner, D. *Nat. Chem. Biol.* **2016**, *12*, 755.
- (145) Leinders-Zufall, T.; Storch, U.; Bleyemehl, K.; Mederos y Schnitzler, M.; Frank, J. A.; Konrad, D. B.; Trauner, D.; Gudermann, T.; Zufall, F. *Cell Chem. Biol.* **2018**, *25*, 215.
- (146) Pernpeintner, C.; Frank, J. A.; Urban, P.; Roeske, C. R.; Pritzl, S. D.; Trauner, D.; Lohmüller, T. *Langmuir* **2017**, *33*, 4083.
- (147) Fasoli, E.; Arnone, A.; Caligiuri, A.; D'Arrigo, P.; de Ferra, L.; Servi, S. *Org. Biomol. Chem.* **2006**, *4*, 2974.
- (148) Frank, J. A.; Franquelim, H. G.; Schwille, P.; Trauner, D. *J. Am. Chem. Soc.* **2016**, *138*, 12981.
- (149) Dong, M.; Babalhavaeji, A.; Samanta, S.; Beharry, A. A.; Woolley, G. A. *Acc. Chem. Res.* **2015**, *48*, 2662.
- (150) Samanta, S.; Beharry, A. A.; Sadovski, O.; McCormick, T. M.; Babalhavaeji, A.; Tropepe, V.; Woolley, G. A. *J. Am. Chem. Soc.* **2013**, *135*, 9777.
- (151) Pacher, P.; Bátkai, S.; Kunos, G. *Pharmacol. Rev.* **2006**, *58*, 389.
- (152) Wang, H.; Siemens, J. *Temperature (Austin)* **2015**, *2*, 178.
- (153) Frank, J. A.; Moroni, M.; Moshourab, R.; Sumser, M.; Lewin, G. R.; Trauner, D. *Nat. Commun.* **2015**, *6*, 7118.
- (154) Senaratne, P. A.; Orihuela, F. M.; Malcolm, A. J.; Anderson, K. G. *Org. Process Res. Dev.* **2003**, *7*, 185.
- (155) Cunningham, D.; Gallagher, E. T.; Grayson, D. H.; McArdle, P. J.; Storey, C. B.; Wilcock, D. *J. J. Chem. Soc., Perkin Trans. 1* **2002**, 2692.
- (156) Västilä, P.; Pastor, I. M.; Adolfsson, H. *J. Org. Chem.* **2005**, *70*, 2921.
- (157) Bülow, L.; Naini, A.; Fohrer, J.; Kalesse, M. *Org. Lett.* **2011**, *13*, 6038.
- (158) Krasovskiy, A.; Knochel, P. *Synthesis* **2006**, 2006, 0890.
- (159) Shinji, C.; Maeda, S.; Imai, K.; Yoshida, M.; Hashimoto, Y.; Miyachi, H. *Bioorg. Med. Chem.* **2006**, *14*, 7625.

- (160) Uehling, D. E.; Shearer, B. G.; Donaldson, K. H.; Chao, E. Y.; Deaton, D. N.; Adkison, K. K.; Brown, K. K.; Cariello, N. F.; Faison, W. L.; Lancaster, M. E.; Lin, J.; Hart, R.; Milliken, T. O.; Paulik, M. A.; Sherman, B. W.; Sugg, E. E.; Cowan, C. *J. Med. Chem.* **2006**, *49*, 2758.
- (161) Fasoli, E.; Arnone, A.; Caligiuri, A.; D'Arrigo, P.; de Ferra, L.; Servi, S. *Org. Biomol. Chem.* **2006**, *4*, 2974.